United States
Consumer Product Safety Commission

September 2023

CPSC Staff[1] Statement on: Literature Review on Nanomaterials – Carbon Nanotubes, Nano Silver, and Nano Titanium Dioxide

The report titled, "Literature Review on Nanomaterials – Carbon Nanotubes, Nano Silver, and Nano Titanium Dioxide," is a literature review and analysis of available toxicological information performed by the contractor Toxicology Excellence for Risk Assessment (TERA) under Task Order 20 of Contract CPSC-D-12-0001.

Nanomaterials are defined as materials/particles that range from 1 to 100 nanometers (nm) in any external dimension. Because of unique chemical and physical properties, nanomaterials are used in manufacturing products, including machinery, electronics, cleaning products, and personal care products, to allow them to have better performance qualities.[2]

CPSC staff selected three nanomaterials for this review, Carbon Nanotubes (CNTs), Nano Silver (Nano-Ag), and Nano Titanium Dioxide (Nano-TiO_2), because these nanomaterials are reported as those most commonly used in consumer products.

- Due to their distinctive electrical, mechanical, and thermal properties, CNTs are used to make lightweight, but strong products, including sporting goods equipment, textiles and shoes, and transparent electrodes for computers and electronics.
- Due to its antimicrobial properties, Nano-Ag is used in products, including spray disinfectants, hair dryers, soaps and dish detergents, cooking utensils, food preservative film, filters for air and water purification systems, household appliances, textiles, clothes, shoes, and personal care products.
- Due to its unique whitening and photochemical properties, Nano-TiO_2 is used in products, including air filtration and purification systems, household products and home improvement products (*e.g.*, paints).

TERA searched primary (*e.g.,* PubMed, Web of Science, TOXLINE) and secondary (*e.g.*, national and international government and professional society websites, peer-reviewed panel reports) sources for the period of 2010-2016 for pertinent literature. A third-tier search was performed to fill gaps by expanding the keyword list for reviewing references cited in primary literature. TERA located more than 17,000 reports, of which 170 were relevant to hazard determinations; an additional 440 reports were supportive for the derivation of a health risk value. Criteria for the

[1] This statement was prepared by the CPSC staff, and the attached report was produced by Toxicological Excellence for Risk Assessment for CPSC staff. The statement and report have not been reviewed or approved by, and do not necessarily represent the views of, the Commission.
[2] The report reviews consumer products under CPSC's jurisdiction pursuant to the Consumer Product Safety Act. Staff notes that CPSC also has jurisdiction of other products under other statutes administered by CPSC, such as the Federal Hazardous Substances Act.

relevant studies included information on physico-chemical characterization, use of appropriate dose levels, relevance of the test method for the specified route of exposure (*i.e.*, inhalation, dermal, oral), and demonstration of a dose-response relationship.

For each nanomaterial, relevant information on exposure-induced health effects was reviewed to derive an acceptable daily intake (ADI)[3]. The information on toxicological studies and areas of needed research for the three nanoparticles is summarized below.

1. CNTs

The surveyed literature suggests that physico-chemical properties of CNTs, including diameter and length, appear to be correlated with CNT-induced toxic effects. Long, single-walled carbon nanotubes (SWCNTs) were more potent in inducing fibrogenic effects than short SWCNTs. Multi-walled carbon nanotubes (MWCNTs) dispersed as semi-rigid fibers are more likely to induce fibrogenic effects in epithelial and mesothelial membranes compared to thin-walled, curly MWCNTs. Cobalt contamination of CNTs may enhance CNT-induced toxicity.

Limited toxicokinetic data indicate that a small amount of SWCNTs may enter the blood stream following oral exposure. Inhaled and instilled SWCNTs are deposited in the respiratory tract and absorbed in the pulmonary lymph nodes. Inhaled MWCNTs are poorly cleared from the lung with small amounts of MWCNTs distributing to the liver, the kidney, and the spleen. MWCNT particles were also found in the brain, possibly transported via the olfactory bulb during inhalation exposures.

The identified studies indicate that both SWCNTs and MWCNTs exhibit relatively low toxicity by oral exposure. Repeat inhalation of MWCNTs exhibited granulomatous changes and epithelial hyperplasia in the airways and the lungs as well as neutrophilic inflammation observed in bronchoalveolar lavage fluid (BALF). A thick-walled, semi-rigid fiber-like MWCNT (MWNT-7) is classified as 'possibly carcinogenic in humans' (Group 2B) by the International Agency for Research on Cancer (IARC), while both SWCNTs and MWCNTs other than MWNT-7 are not classifiable (Group 3). Overall, mutagenicity studies presented mixed results in both *in vitro* and *in vivo* tests. Ames assays predominantly elicited negative results; *in vitro* micronucleus (MN) assays predominantly elicited positive results; two *in vitro* chromosomal aberration assays elicited negative results. *In vivo* MN or comet assays elicited negative results for SWCNTs. In contrast, *in vivo* comet assays elicited positive results for MWCNTs.

Both SWCNTs and MWCNTs have been shown in published studies to induce oxidative stress, the primary mechanism of CNT toxicity. CNTs are known to disrupt the membranes of macrophages, frustrating phagocytosis and destabilizing lysosomes. Other toxicological modes of action could be volumetric overload of alveolar macrophages, leading to failed clearance of particles; chromosomal aberrations, including aneuploidy and micronuclei formation; inflammation; and fibrosis. TERA proposed ADI values for MWCNTs from a short-term inhalation study (14-day) and a long-term inhalation study (2-year) are 0.15 μg/m^3/d and 15 ng/m^3/d, respectively.

Well-planned toxicokinetic studies with robust repeat-dose protocols would broadly improve the confidence of future hazard assessments for CNTs. There are limited dose-response toxicity data for determining an exposure limit for CNTs. There are no repeat-dose oral or inhalation studies for SWCNTs. Some toxicity data for MWCNTs are available for certain MWCNT variants (*e.g.*, morphological). There are no carcinogenicity studies of low-diameter, tangled MWCNT variants. Furthermore, there are no developmental and reproductive toxicology (DART) inhalation studies available for MWCNTs.

[3] Acceptable daily intake (ADI) is an estimate of the amount of a substance that an individual can be exposed to on a daily basis, over a lifetime, without presenting an appreciable risk to their health.

2. Nano-Ag

Coatings are used to decrease agglomeration and to modify dissolution of Nano-Ag particles. Because physico-chemical properties are associated with Nano-Ag toxicity, information on coatings is important in interpreting toxicity studies. Coatings can result in different surface charges and thus influence cell-nanoparticle interactions. The collected literature showed that particle size is associated with Nano-Ag biological activities; smaller particles generate more cytotoxic effects when similar doses as mass unit are used. Silver toxicity can result from the direct action of silver ions (ionic silver, Ag^+) which is released from Nano-Ag.

Following oral exposure, studies demonstrated that most Ag was found in feces, and Nano-Ag levels in the blood were very low, suggesting that absorption through the gastrointestinal tract is poor (*i.e.*, low bioavailability). However, Ag^+ may be more bioavailable compared to Nano-Ag particles. Several studies reported that Ag can translocate to non-respiratory regions following inhalation exposure to Nano-Ag particles.

Oral subchronic studies in rats present a No-Observed-Adverse-Effect Level (NOAEL)[4] of 30 mg/kg, based on liver toxicity. Inhalation subchronic studies in rats demonstrated that the lung and the liver are the primary target organs with a NOAEL of 133 $\mu g/m^3$. Dermal application of Nano-Ag to guinea pigs caused skin, liver, spleen, kidney and bone toxicities and generated a Lowest-Observed-Adverse-Effect Level (LOAEL)[5] of 100 µg/mL. Rodent studies reported that Nano-Ag particles can cross the blood-testes and the blood-brain barrier from intravenous exposure.

Research has shown that Nano-Ag particles induced DNA damage in *in vitro* comet and micronuclei (MN) assays in human cell lines. An *in vitro* human cell study indicates that cells exposed to Nano-Ag particles generated DNA adducts that may be associated with reactive oxygen species (ROS) production. An *in vivo* study in rats also showed DNA damage measured by the comet assay in blood cells. However, most *in vivo* MN assays generated negative results. Chromosome aberration assays with Nano-Ag particles produced mixed results.

The mechanism of Nano-Ag toxicity is not completely understood. Ag^+ is considered the toxic form of Ag particles. Ag^+ was significantly more toxic than Nano-Ag particles to human dermal cell lines. Size and coating can also influence the cytotoxicity of Nano-Ag particles. Smaller and coated Nano-Ag particles may induce higher toxicities, by reducing agglomeration, than larger and uncoated particles. Nano-Ag particles can move from extracellular space into cells. After the cellular translocation, Ag can bind to DNA and proteins, leading to additional cellular activities, such as oxidative stress, DNA damage, cell cycle arrest, and apoptosis through an inflammatory signaling pathway.

A 90-day rodent oral exposure study resulted in the TERA proposed ADI of 0.1 mg/kg/d. No long-term inhalation and dermal studies were available to determine ADI values for these routes of exposure.

Derivation of more reliable ADIs for Nano-Ag particles remains challenging because of the lack of information on toxicokinetic and toxicodynamic data, human studies, different organ-specific toxicity, robust repeat-dose studies, and chronic exposure toxicity, including DART studies.

3. Nano-TiO_2

The limited number of available human and animal studies indicate that Nano-TiO_2 particles are absorbed to a small extent from the lungs and the gastrointestinal tract and distributed to the liver,

[4] The No-Observed-Adverse-Effect Level (NOAEL) is the greatest concentration or amount of a substance at which no detectable adverse effects occur in an exposed population.

[5] The Lowest-Observed-Adverse-Effect Level (LOAEL) is the lowest level of a substance that has been observed to cause harm in an exposed population.

kidneys, spleen, and brain. Nano-TiO_2 particles do not appear to effectively penetrate intact skin in humans and animals. Oral exposure to Nano-TiO_2 elicited alterations in immune/inflammatory responses, apoptosis, and oxidative stress in animal studies. The survey literature also showed that inhalation exposure to Nano-TiO_2 elicited minimal bronchiolo-alveolar hyperplasia, as well as minimal irritation and inflammation in airways. There is a lack of epidemiological data for evaluating chronic and carcinogenic potential for Nano-TiO_2.

Mutagenicity studies presented mixed results in *in vitro* and *in vivo* tests. Most Ames assays elicited negative results. *In vitro* MN studies and comet assays elicited predominantly positive results. *In vivo* MN studies elicited predominantly negative results. *In vivo* comet assays generated conflicting results. Some studies reported the formation of oxidized bases in DNA after Nano-TiO_2 treatment.

Although the mode of action (MOA) for Nano-TiO_2 toxicity is not well understood, its toxic effects include sustained inflammation, impairment of cellular defense mechanisms, production of ROS, oxidative DNA damage, cell proliferation, apoptosis, necrosis, depletion of antioxidants and ROS scavengers, and/or gene mutations.

TERA proposed long-term oral and inhalational ADI values are 0.7 µg/kg/d and 30 µg/m^3/d, respectively.

TERA determined that derivation of ADIs for Nano-TiO_2 is challenging because of high uncertainty with a lack of reliable dose-response data. In addition, there is a lack of epidemiological data to understand whether TiO_2 dust can increase respiratory disease or lung cancer mortality rates in exposed industrial workers. More detailed information is needed to further understand how physicochemical properties of Nano-TiO_2 particles influence their toxicity. Although limited studies reveal that a small amount of Nano-TiO_2 is absorbed via respiratory and gastrointestinal tracts, information on their translocation rates to other organs and toxicokinetics is uncertain. There are significant uncertainties in cardiovascular, immune, neurological, and DART toxicity endpoints of Nano-TiO_2. The WHO IARC Working Group classified TiO_2 as a Group 2B (possibly carcinogenic to humans) chemical. However, limited human and animal studies are available to understand the carcinogenicity of Nano-TiO_2. For the observed toxicity of Nano-TiO_2, the exact mechanisms and pathways of Nano-TiO_2-induced toxicity are not clear. In particular, understanding of human exposure to Nano-TiO_2 during use of consumer products is lacking.

TERA

INDEPENDENT
NON-PROFIT
SCIENCE
FOR PUBLIC HEALTH
PROTECTION

Literature Review on Nanomaterials – Carbon Nanotubes, Nano Silver, and Nano Titanium Dioxide

Task Order 20
Contract Number
CPSC-D-12-0001

06/28/2018
FINAL REPORT
Volume 1

Prepared by:
Toxicology Excellence for Risk Assessment (TERA):

Authors:

Patricia M. McGinnis
Evan A. Frank
Raymond G. York
Julie A. Skare
Chijioke G. Onyema
Michael L. Dourson

Contact:
Patricia McGinnis mcginnis@tera.org

CONTENTS

AUTHORS AND CONTRIBUTORS

Patricia M. McGinnis, Ph.D., DABT
Evan A. Frank, Ph.D.
Raymond G. York, Ph.D., DABT, FATS
Julie A. Skare, Ph.D.
Chijioke G. Onyema, MPH
Michael L. Dourson, Ph.D., DABT. FATS

LIST OF TABLES

LIST OF FIGURES

ABBREVIATIONS

α-HDBH	Alpha-hydroxybutyrate dehydrogenase
β-NAG	Beta-N-acetylglucosaminidase
γ-GT	Gamma-glutamyl transferase
3-HB	3-Hydroxybutyrate
AA	Atomic Absorption
ACGIH	American Conference of Governmental Industrial Hygienists
ACP	Acid phosphatase
ACF	Aberrant crypt foci
AChE	Acetylcholinesterase
ADI	Acceptable daily intake
AES	Atomic emission spectrometry
Ag	Silver
Ag+	Ionic silver
Ag^0	Reduced silver
$AgNO_3$	Silver nitrate
Ag NP	Silver nanoparticle
AgOAc	Silver acetate
AHR	Airway hyperreponsiveness
AKP	Alkaline phosphatase
Al	Aluminum
$Al(OH)_3$	Aluminum hydroxide
ALP	Alkaline phosphatase
ALT	Alanine aminotransferase
A*prt*	Adenosine phosphoribosyl transferase
AST	Aspartate aminotransferase
ASTM	American Society for Testing and Materials
ATP	Adenosine triphosphate
ATSDR	Agency for Toxic Substances and Disease Registry
AUC_{24hr}	Area under the curve at 24 hours
AUC_{IV}	Area under the curve after intravenous administration
AUC_{oral}	Area under the curve after oral administration
BALF	Bronchoalveolar lavage fluid
BET	Brunauer-Emmett-Teller
BMD	Benchmark dose
BSA	Bovine serum albumin
BUN	Blood urea nitrogen
bw	Body weight

ºC	degree Celsius
C_3H_6	Propene
Ca	Calcium
CalEPA	California EPA
CAS	Chemical Abstract Service
CASRN	Chemical Abstract Service Registry Number
CAT	Catalase
CBMN	Cytochalasin B micronucleus assay
CDC	Centers for Disease Control and Prevention
CED	Critical Effect Dose/Concentration
CHO	Chinese hamster ovary
cm^2	square centimeter
cm^3	cubic centimeter
CMC	Carboxymethyl cellulose
CMD	Count median diameter
CNT	Carbon nanotube
CO	Carbon monoxide
Co	Cobalt
COOH	Carboxylic acid
COOH-fMWCNT	Carboxylate-functionalized multi-walled carbon nanotube
CPSA	Consumer Product Safety Act
CPSC	Consumer Product Safety Commission
CR	Creatinine
Cr	Chromium
CRP	C-reactive protein
Cu	Copper
d	day
dia	diameter
d/wk	days per week
D	Dimension
DART	Developmental and Reproductive Toxicology
DLS	Dynamic light scattering
DMBA	Dimethylbenz[a]anthracene
DMH	1,2-dimethylhydrazine
DNA	Deoxyribonucleic acid
DPI	Diphenyleneiodonium
DPPC	Dipalmitoylphosphatidylcholine
DTPA	Diethylentriaminepentaacetic dianhydride
DWNT	Double-walled nanotube
DWCNT	Double-walled carbon nanotube
E2	Estradiol
ECHA	The European Chemicals Agency
EF	Energy filtering
EFSA	European Food Safety Authority
ELISA	Enzyme-linked immunosorbent assay
EMBASE	Excerpta Medica Database

EMT	Epithelial-mesenchymal transition
Endo III	Endonuclease III
ENP	Engineered nanoparticle
EPA	Environmental Protection Agency
ETSA	Extrathoracic surface area
f	Functionalized
F1	First filial generation
F2	Second filial generation
fCNT	Functionalized carbon nanotube
FDA	U.S. Food and Drug Administration
Fe	Iron
FeTiO3	Ilmenite
FISH	Fluorescence *in situ* hybridization
fMWCNT	Functionalized multi-walled carbon nanotube
FOB	Functional observational battery
fpg	Formamidopyrimidine-DNA-glycosylase
FSH	Follicle-stimulating hormone
g/kg	gram per kilogram
g/cm^3	gram per cubic centimeter
g/m^3	gram per cubic meter
g/mL	gram per milliliter
GC-MS/MS	Gas chromatography tandem-mass spectrometry
GD	Gestation day
GI	Gastrointestinal
GLP	Good Laboratory Practice
GPC	Glycerophosphocholine
GPX	Glutathione peroxidase
GSD	Geometric standard deviation
GSH	Reduced Glutathione
GSSG	Oxidized Glutathione
H&E	Hematoxylin and eosin
h	hour(s)
H&E	Hematoxylin and eosin
h/d	hours per day
H_2O	Water
H_2O_2	Hydrogen peroxide
H_2SO_4	Sulfuric acid
HB	Hemoglobin
HDF	Human dermal fibroblasts
HDL	High-density lipoprotein
HC	Health Canada
HCT	Hematocrit
HEC	Human equivalent concentration
HEK	Human epidermal keratinocytes
HHS	U.S. Department of Health and Human Services
HNO_3	Nitric oxide

HPLC-MS/MS	High performance liquid chromatography tandem-mass spectrometry
hOGG1	8-oxoguanine DNA glycosylase-1
HPLC-MS	High performance liquid chromatography mass spectrometry
HPMC	Hydroxypropyl methylcellulose
HPRT	Hypoxanthine phosphorybosyl transferase
HSDB	Hazardous Substances Data Bank
Hsp	Heat shock protein
HYP	Hydroxyproline
IARC	International Agency for Research on Cancer
IC75	Inhibitory concentration where viability is reduced by 75%
ICP-AES	Inductively coupled plasma atomic emission spectroscopy
ICP-MS	Inductively coupled plasma mass spectrometry
ICP-OES	Inductively coupled plasma optical emission spectrometry
IEP	Isoelectric point
IgE	Immunoglobulin E
IgM	Immunoglobulin M
IL	Interleukin
IL-1	Interleukin-1
IL-1R	Interleukin-1 receptor
IL-1α	Interleukin-1 alpha
IL-1β	Interleukin-1 beta
IL-4	Interleukin-4
IL-5	Interleukin-5
IL-6	Interleukin-6
IL-10	Interleukin-10
IL-12	Interleukin-12
IL-18	Interleukin-18
IL-33	Interleukin-33
INF-γ	Interferon gamma
IP	Intraperitoneal
IPRL	Isolated perfused rat lung
IRIS	Integrated Risk Information System
ISO	International Organization for Standardization
IT	Intratracheal
IV	Intravenous
JRC	Joint Research Centre
K	Potassium
kDa	kilodaltons
L/hr	Liter per hour
La	Lanthanum
LALN	Lung-associated lymph node
LC_{50}	Median lethal concentration
LD_{50}	Median lethal dose
LDH	Lactate dehydrogenase
LDL	Low-density lipoprotein
LH	Luteinizing hormone

LOAEC	Lowest observed adverse effect concentration
LOAEL	Lowest observed adverse effect level
LOD	Limit of detection
LOEL	Lowest observed effect level
LPS	Lipopolysaccharide
m^2/g	square meter per gram
MAPK	Mitogen-activated protein kinase
MCH	Mean corpuscular hemoglobin
MCHC	Mean corpuscular hemoglobin concentration
MCP-1	Monocyte chemoattractant protein-1
MCV	Mean corpuscular volume
MDA	Malondialdehyde
MEF	Mouse embryo fibroblast
µg	microgram
µg/g	microgram per gram
µg/animal	microgram per animal
µg/plate	microgram per plate
µg/mL	microgram per milliliter
µg/mouse	microgram per mouse
µg/mouse/day	microgram per mouse per day
$\mu g/cm^2$	microgram per square centimeter
µg/kg/d	microgram per kilogram per day
µg/kg bw/day	microgram per kilogram of body weight per day
$\mu L/cm^2$	microliter per square centimeter
µm	micrometer
Mg	Magnesium
mg	milligram
mg/cm^2	milligram per square centimeter
mg/g	milligram per gram
mg/kg	milligram per kilogram
mg/kg bw	milligram per kilogram of body weight
mg/kg bw/d	milligram per kilogram of body weight per day
mg/kg bw/week	milligram per kilogram of body weight per week
mg/kg/d	milligram per kilogram per day
mg/L	milligram per liter
mg/m^2	milligram per square meter
mg/m^3	milligram per cubic meter
mg/mL	milligram per milliliter
mg/mouse	milligram per mouse
mg/mouse/day	milligram per mouse per day
mg Ti/kg	milligram of Titanium per kilogram
MIF	Macrophage migration inhibitory factor
MIP-1α	Macrophage inflammatory protein 1-alpha
ml	Milliliter
mL/kg	milliliter per kilogram
mL/kg bw	milliliter per kilogram of body weight

mM	millimolar
mm	millimeter
MMAD	Mass median aerodynamic diameter
MMP1	Matrix metalloproteinase-1
MN	Micronucleus
Mn	Manganese
MnSOD	Manganese-containing superoxide dismutase
MOA	Mode/mechanism(s) of action
MPO	Myeloperoxidase
MPPD	Multiple Path Particle Deposition
MPV	Mean platelet volume
MRI	Magnetic Resonance Imaging
mRNA	Messenger ribonucleic acid
MS	Mass spectrometry
MTT	3-(4,5-dimethylthiazol-2-yl)-2,5-diphenyltetrazolium bromide
mV	millivolts
MWNT	Multi-walled nanotube
MWCNT	Multi-walled carbon nanotube
Na	Sodium
NAC	N-acetylcysteine
NaCl	Sodium chloride
NADPH	Nicotinamide adenine dinucleotide phosphate
nano-Ag	nano-Silver
nano-TiO2	nano-Titanium dioxide
ncTiO2	Non-coated titanium dioxide
NCE	Normochromic erythrocyte
NF	Nanofiber
NF-kB	Nuclear factor kappa-light-chain-enhancer-of activated B cells
ng	nanogram
ng/g	nanogram per gram
ng/kg/bw	nanogram per kilogram of body weight
ng/L	nanogram per liter
ng/mouse	nanogram per mouse
NH4-fMWCNT	Amine-functionalized multi-walled carbon nanotube
NHDF	Normal human dermal fibroblasts
Ni	Nickel
NICNAS	National Industrial Chemicals Notification and Assessment
Scheme NIH	National Institutes of Health
NIOSH	National Institute for Occupational Safety and Health
NK	Natural killer
NLRP3	(NOD)-like receptor protein 3
NNI	National Nanotechnology Initiative
NM	Nanomaterial
NMR	Nuclear Magnetic Resonance
nm	nanometer
nm^2	square nanometer

nm^3	cubic nanometer
NO	Nitric oxide
NO_2	Nitrogen dioxide
NOAEC	No observed adverse effect concentration
NOAEL	No observed adverse effect level
NOEL	No observed effect level
NP	Nanoparticle
NQO1	NADPH oxidoreductase 1
NR	Not reported
NSCEP	National Service Center for Environmental Publications
NTP	National Toxicology Program
nV	Nanovolt
O	Oxygen
o	Oxidized
OECD	Organisation for Economic Co-operation and Development
OEHHA	Office of Environmental Health Hazard Assessment
OGG1	8-oxoguanine DNA glycosylase-1
OH	Hydroxide
OH-fSWCNT	Hydroxyl functionalized single-walled carbon nanotube
o-MWCNT	Oxidized multi-walled carbon nanotube
OPA	Oropharyngeal aspiration
OSHA	Occupational Safety and Health Administration
P4	Progesterone
p	Pristine
particles/cm^3	particles per cubic centimeter
PBS	Phosphate-buffered saline
PBPK	Physiologically based pharmacokinetic model
PCE	Polychromatic erythrocyte
PCR	Polymerase chain reaction
PDGF	Platelet-derived growth factor
PDI	Polydispersity Index
PDMS	Polydimethylsiloxane
PEG	Polyethylene glycol
PEI	Polyethylene imine
PEP	Printer-emitted nanoparticles
PET	Positron emission tomography
pg	Pigment-grade
pH	Potential of hydrogen
PKcs	Protein kinase C's
PMN	Polymorphonuclear neutrophil
PND	Postnatal day
POD	Point of departure
PP	Peyer's patches
ppm	Parts per million
PTT	Partial thromboplastin time
PVP	Polyvinylpyrrolidone

QSAR	Quantitative structure-activity relationship
RBC	Red blood cell
RDDR	Regional Deposited Dose Ratio
REACH	Registration, Evaluation, Authorisation and Restriction of Chemicals
Redox	Reduction-oxidation
REL	Reference exposure level
RfD	Reference dose
RNA	Ribonucleic acid
ROS	Reactive oxygen species
RT-PCR	Real-time polymerase chain reaction
RTECS	Registry of Toxic Effects of Chemical Substances
SAEC	Small airway epithelial cells
SC	Subcutaneous
SCE	Sister chromatid exchange
SD	Standard deviation
SE	Standard error
SEM	Scanning electron microscopy
SHE	Syrian hamster embryo
SiO_2	Silicon dioxide
SMA	Styrene-co-maleic anhydride
SMART	Somatic mutation and recombination test
SOD	Superoxide dismutase
SP-D	Surfactant protein D
SPR	Surface plasmon resonance
sTiO2	Silicone-coated titanium dioxide
SWNT	Single-walled nanotube
SWCNT	Single-walled carbon nanotube
t1/2	half-life
tau-MWCNT	Taurine functionalized multi-walled carbon nanotube
TEM	Transmission electron microscopy
TERA	Toxicology Excellence for Risk Assessment
TGF	Transforming growth factor
TGF-β	Transforming growth factor beta
THF	Tetrahydrofurane
Th	T-helper cell
Th1	Type 1 T helper cell
Th2	Type 2 T helper cell
TI	Tail intensity
Ti	Titanium
TiO2	Titanium dioxide
TNOS	Total nitric oxide synthase
TNF	Tumor necrosis factor
TNF-α	Tumor necrosis factor-alpha
TOXLINE	Toxicology Information Online
TOXNET	Toxicology Network
TSCA	Toxic Substances Control Act

TWA	Time-weighted average
TWNT	Triple-walled nanotube
TWCNT	Triple-walled carbon nanotube
U.S.	United States
U.S. EPA	U.S. Environmental Protection Agency
UA	Uric acid
UF	Uncertainty factor
uf	Ultrafine
uo	Ultra-oxidized
UV	Ultraviolet
UV-Vis	Ultraviolet-visible spectroscopy
VEGF	Vascular Endothelial Growth Factor
wt	weight
wt%	weight percent
wk	week(s)
w/v	weight per volume
w/w	weight per weight
WBC	White blood cell
WHO	World Health Organization
WT	Wild-type
Zn	Zinc

1 INTRODUCTION

Nanomaterials represent a broad range of materials that are being used in a wide variety of products. For the purpose of this report, nanomaterials are defined as materials/particles that range from 1 to 100 nanometers (nm) in any external dimension. Although nanomaterials may have the same chemical composition as their non-nanomaterial versions, nanoscale materials can differ substantially in their structure, physical and chemical properties, and potentially in their behavior in the environment and in the human body. These properties also vary significantly between different forms of the same nanomaterial. The use of nanomaterials has been reported in various products purchased by the American public. These products include cosmetics, cleaning products, personal care products, sporting goods, textiles and clothing, electronics, food and beverages, home and garden products, and sunscreens.

The United States (U.S.) Consumer Product Safety Commission (CPSC) is currently evaluating information on nanomaterials in consumer products to determine if there are any potential safety and health risks to the public. Under the Consumer Product Safety Act (CPSA) enacted in 1972, a consumer product is any article or component part produced or distributed for sale to consumer, or for their personal use in household, school, recreation or otherwise. It does not include any article that is not customarily produced or distributed for sale or use to the consumer, tobacco and tobacco products, motor vehicles or motor vehicle equipment, pesticides, firearms and ammunition, aircraft, boats, drugs, cosmetics or food (CPSC, 2011). This report focuses on the use of three nanomaterials in consumer products.

This report, prepared by Toxicology Excellence for Risk Assessment (TERA) for CPSC, summarizes the recent relevant toxicological data (2010 to 2016) on three specific types of nanomaterials: carbon nanotubes (CNTs) (including the two distinct forms single-walled [SWCNTs] and multi-walled [MWCNTs]), silver nanoparticles (nano-Ag or Ag NP), and titanium dioxide nanoparticles (nano-TiO2 or TiO2 NP). It is a follow-up report to a report compiled by Versar (2012) that reviewed the toxicologic literature prior to 2010 with the goal to derive potential acceptable daily intake values (ADIs) to aid in identification of possible health hazards for use in risk evaluations for the three nanomaterials. The objective of this report is similar to the earlier report, that is, to derive ADI for the three nanomaterials for oral, inhalation and dermal routes, if there are sufficient high quality data to do so.

TERA's research approach is described in Section 2. TERA research focused on worldwide primary literature, from 2010 to 2016 in English. TERA also screened secondary sources such as books and government reports for information. It is acknowledged that this report is not comprehensive, that is, all the literature on the three nanomaterials is not covered in this report. TERA was selective with the priority to identify relevant, high-quality studies so as to derive ADIs. These include studies addressing the toxicology of the three nanomaterials via oral, inhalation and dermal routes for various durations of exposure: acute, repeat-dose intermediate (or subchronic), long-term (or chronic), and for various endpoints: systemic toxicity, carcinogenicity, developmental and reproductive toxicity, genotoxicity and mechanism of action. It should be noted that for the purpose of this review, data were generally not considered for exposures to forms of these nanomaterials that are typically used in products not covered under CPSC's regulatory authorities. The rationale for this decision is that nanomaterial types differ

greatly by manufacturing method even for the same material composition. For similar reasons, U.S. Environmental Protection Agency (EPA) has regulated each manufacturing process for MWCNTs as a separate entity under the Toxic Substances Control Act (TSCA). Therefore, an ADI developed to be applied to CPSC-regulated product uses should primarily consider the nanomaterial forms and manufacturing processes used for CPSC consumer products.

Section 3 provides an overview of use of the nanomaterials in consumer products and how the nanomaterials could be released from the consumer product(s), thereby exposing the product users. Exposure to nanomaterials depends on the properties of the nanomaterial in the consumer product (such as chemical entity, shape of the nanomaterial in the product, concentrations of the nanomaterial in the product, and application of the product), how the nanomaterial is released from the product (such as by abrasion, chemical or thermal decomposition of the composite matrix) as well as exposure media (air, water, dust) and routes (inhalation, ingestion or via the skin) and exposure conditions. Reports of complete exposure assessments related to use of CPSC regulated products that measured the amount ingested, total dermal exposure, or conducted an exposure assessment based on air concentrations in homes are summarized, if available. The three nanomaterials are used in a variety of products:

- CNTs are used in CPSC-regulated products due to their electrical, mechanical, and thermal properties that are useful in developing lightweight, strong building materials and computers. Products reported to contain CNTs include: sporting goods equipment (e.g., tennis rackets, bicycles), textiles and shoes, and transparent electrodes for computers and electronics.
- Nano-Ag has been reported to be used in a number of consumer products including spray disinfectants, hair dryers, soaps and dish detergents, cooking utensils, food preservative film, filters for air and water purification systems, household appliances, textiles, clothes, shoes, and personal care products.
- Nano-TiO2 has been used in various products including air filtration and purification systems, household products and home improvement products.

For each of the nanomaterials, Sections 4, 5 and 6 (for CNTs, nano-Ag and nano-TiO2, respectively) cover the following:

- Physical/chemical properties, including groupings that may affect ADI derivation (e.g., single vs. multiwalled carbon nanotubes; crystalline state; functionalization);
- Toxicokinetics of the nanomaterial;
- Toxicity data, with a focus on high quality *in vivo* studies using environmentally relevant routes, as discussed above. For each key study, the significance of the study is summarized (e.g., whether it informs on the mechanism of action) and uncertainties are highlighted. The lowest observed adverse effect level (LOAEL)/no observed adverse effect level (NOAEL) is identified for each study as appropriate, and dosimetry modeling is conducted, to the degree feasible and appropriate. For the oral route, standard allometric adjustments are applied;
- For each nanomaterial or subset of nanomaterials, the database was evaluated to determine the adequacy of the data for development of ADIs for oral, inhalation, and/or dermal exposure for acute (up to two weeks) and chronic exposures. The report focuses

on the critical effect(s) for each exposure route/duration, rather than developing a weight of evidence for each endpoint. When supported by the data for a given duration/route, an ADI was derived, including identification of the critical effect(s), identification of the point of departure, and application of appropriate uncertainty factors; and
- Research needs and data gaps for each nanomaterial.

In Sections 4, 5, and 6, the focus was on high quality studies that included best practice documentation of nanomaterial characteristics, including, but not limited to:

- Physico-chemical characteristics,
- Concentration of the nanomaterials,
- Particle size and shape,
- Particle number and distribution,
- Purity of the nanomaterial,
- Use of proper controls, and
- Documentation of analysis (e.g., standard test methods were used from such standard organizations as ASTM International (ASTM) or the International Organization for Standardization (ISO)); instruments were calibrated; measurement protocols are discussed and cited.

Studies that used other routes are addressed only to the degree that they provide information not fully covered by the other routes. Similarly, some studies of lesser quality or of forms not used in CPSC products were reviewed in this report if they informed database coverage or potential mode of action. *In vivo* mechanistic or gene expression studies are characterized to the degree that they inform a mode of action determination or otherwise inform the derivation of an ADI, but highly specialized studies using endpoints with questionable or remote relevance to standard toxicity endpoints are not included. Similarly, in vitro studies are addressed only to the degree that they inform the broader mechanistic issues related to the sufficiency for deriving an ADI via any of the environmentally-relevant routes. However, both *in vivo* and *in vitro* genotoxicity studies using standard test methods are summarized, since *in vitro* studies are part of the overall weight of evidence determination for genotoxicity. To the degree appropriate, the text summarizes those studies from the Versar report (2012) that are relevant to the new assessment.

In reviewing the literature, the following were considered:

- The effect that physico-chemical properties have on exposure and toxicity,
- Whether dose levels were appropriate/relevant,
- Relevance of the test method for the specified route of exposure,
- Whether the study demonstrates a dose-response relationship for the nanomaterial, and
- For studies on consumer products, whether the study determines the concentration of the nanomaterial in the product, the amount of nanomaterial released from the consumer product and the conditions that cause such release as well as the characteristics of the released nanomaterials.

For each of the three nanomaterials addressed in the report, the text addresses the data related to both the unmodified (a.k.a., undecorated or "pristine") form of the nanomaterial, as well as

functionalized/coated versions that would likely be used in consumer products (as appropriate for CPSC). To the degree possible based on the available data, whether toxicity differs for different forms of each nanomaterial was determined, and whether there are appropriate groups (e.g., whether certain functionalizations or sizes) that should be evaluated together. The focus of the ADIs was for the unmodified or pristine form of the nanomaterial.

Research needs for each of the three nanomaterials were considered, particularly those that would influence the derivation of the ADI.

References for the report are listed in Section 7.

Appendices include summary tables for data and studies that form the basis for conclusions drawn in the related sections, and are presented in an accompanying volume.

1.1 Characterization of Nanomaterials

1.1.1 Minimum Consistent Characterization

The physical and chemical properties vary widely for each nanomaterial. Furthermore, the form of the nanomaterial to which people may ultimately be exposed from use of CPSC products may vary from the form added to the product because of transformations or filtering that happens as the nanomaterial is emitted from the product. Thus, the appropriate physicochemical characterization of nanomaterials used in toxicity testing is essential for data interpretation in relation to the material properties, inter-comparisons between studies and conclusions drawn regarding human health risk from potential exposures related to consumer product use. The dependence of nanomaterial behavior on physical and chemical properties includes assessing a range of properties such as shape, crystal structure, particle size distribution, agglomeration state, surface area, surface chemistry, surface charge and porosity. Information for physical and chemical properties for each nanomaterial is presented in the section for that nanomaterial.

Appropriate and rigorous physicochemical characterization of nanomaterials used in toxicity testing is essential for data interpretation in relation to the material properties, intercomparisons between studies, and conclusions drawn regarding hazard (Oberdorster et al., 2005 [as cited in Versar, 2012]; Card and Magnuson, 2010; Castranova, 2011; Powers et al., 2006; 2013; EFSA, 2011; Pettit and Lead, 2013; OECD, 2016a). The U.S. EPA (2007; as cited in Versar, 2012]) reported that understanding the physical and chemical properties of nanomaterials is a requirement in the evaluation of all routes of toxicological exposure and hazard. Chemical properties such as vapor pressure, boiling point, molecular weight, and other properties usually included for discrete chemical substances may not be important for some nanomaterials. However, physical and chemical properties relevant to nanomaterial toxicity include properties such as shape, crystal structure, particle size distribution, agglomeration state, surface area, surface chemistry, surface charge and porosity of the nanomaterial (Oberdorster et al., 2005; U.S. EPA, 2007). In addition, solubility and dissolution rates related to toxicity testing or fate in exposure pathways may be critical in assessing toxicity specific to the nanoscale characteristics of the nanomaterial as used in products (OECD, 2016a).

1.1.2 Variation in Characteristics

A main difference between nano- and micron- sized particles is the much greater surface area of a given volume or mass of nanoparticles (NP) compared to an equivalent volume or mass of the same type of micron-sized particles. To illustrate, a 5-nm nanoparticle (assuming it is a sphere and with volume = $4/3\pi r^3$) would have a volume of almost 65 nm^3, whereas, a 0.5 micron particle (100 times bigger) would have a volume of approximately 65,000,000 nm^3 (U.S. EPA, 2010a). Therefore, one million 5-nm particles would equal the volume of a 500-nm sized particle. The surface area of a 5-nm particle (assuming it is a sphere and with surface area = $4\pi r^2$) would equal approximately 80 nm^2, whereas the surface area of a 0.5 micron particle is approximately 800,000 nm^2. Multiplying the surface area of the 5-nm particle by one million (the number of 5- nm nanoparticles needed to equal the volume of a 500-nm particle) yields a total surface area of approximately 80,000,000 nm^2, which is 100-fold greater than the surface area of the 0.5 micron particle. For some nanomaterials, the difference in surface area per unit mass is particularly important for toxicity studies to accurately characterize the nanomaterial physical characteristics.

2 Technical Approach/Literature Review Strategy

A three-tiered literature search strategy was employed to identify high quality studies for each of the three nanomaterials under review (Figure 1). Tier 1 involved online searching for primary sources of literature from scholarly and peer reviewed journals that report original research on the nanomaterials of interest, including documentation of methodology and results. The Tier 2 literature search was conducted in websites and databases considered to be secondary authoritative sources (i.e., sources that did not present original data or primary research reports but were compendia or reviews of literature on the nanomaterials), in reports from government, professional societies, international agencies, or peer review panel reports. Tier 3 comprised gap-searching of the primary literature using new keywords not used in Tier 1, as well as identification and retrieval of suggested references for each nanomaterial from the Versar peer review report (TERA, 2013) and tree-searching by TERA authors.

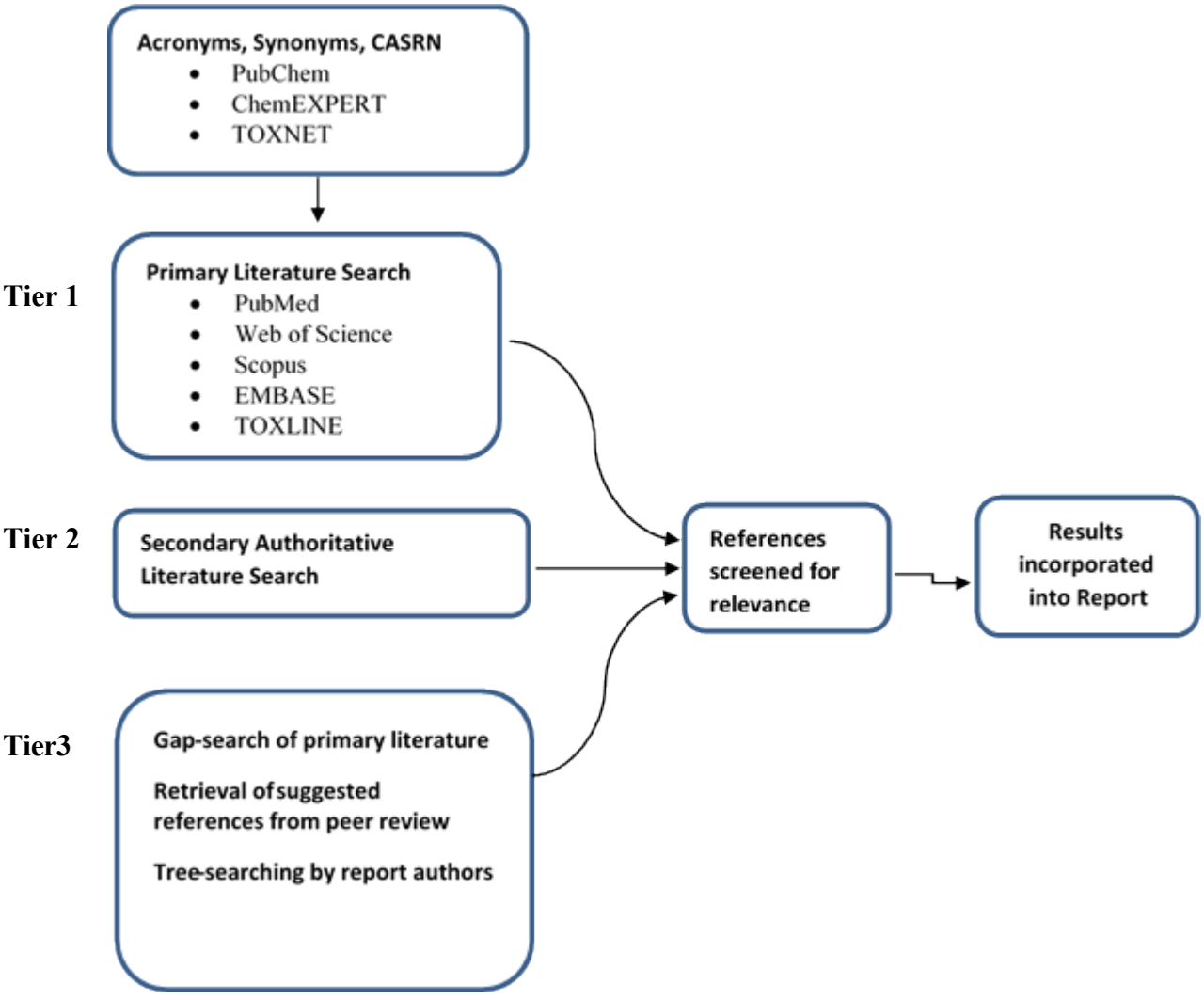

Figure 1: Three-tiered search strategy for nanomaterial information

2.1 Tier 1, Primary Literature Search

In order to perform the primary literature search for the selected nanomaterials, TERA's first step was to compile a comprehensive list of acronyms, synonyms, and Chemical Abstracts Service Registry Numbers (CASRNs) for each nanomaterial using online databases such as PubChem, ChemEXPERT, and TOXNET (Figure 1). Each of these acronyms, synonyms and CASRNs were then searched individually for primary literature in each of the five databases. The acronyms, synonyms, and CASRNs (identifiers) that either returned no results or returned conflicting results were eliminated. For example, assume that the CASRN for a generic nano-metal is the same CASRN number as its elemental form, did not return any search results in one database, returned a total of only four search results in two databases (none of which had any information on the nano metal), and returned numerous results in the two remaining databases (such as EMBASE and TOXLINE). If in the latter two databases, many of the references only made cursory mention of the metal and had little to no information on the nano metal, then the CASRN for the nano metal would be removed as a search term.

TERA compiled a list of common critical effects/toxicological endpoints of interest. The selected list of acronyms, synonyms, and CASRNs (where applicable) for each nanomaterial, together with the critical effects/toxicological endpoints of interest, was used to develop appropriate search strings (as shown in Table 1).

Table 1: Search Strings for each Nanomaterial and Critical Effects/Toxicological Endpoints of Interest

	Search string name	Search strings for primary literature
1	**Carbon nanotubes**	buckytube OR "carbon nanotube" OR "carbon nanotubes" OR CNT OR CNTs OR "cylindrical fullerene" OR "single walled carbon nanotube" OR "single walled carbon nanotubes" OR SWNT OR SWNTs OR SWCNT OR SWCNTs OR "double walled carbon nanotube" OR "double walled carbon nanotubes" OR DWNT OR DWNTs OR DWCNT OR DWCNTs OR "multi walled carbon nanotube" OR "multi-walled carbon nanotubes" OR MWNT OR MWNTs OR MWCNT OR MWCNTs OR "triple walled carbon nanotube" OR "triple walled carbon nanotubes" OR TWNT OR TWNTs OR TWCNT OR TWCNTs
2	**Nanosilver**	nanosilver OR "nano silver" OR nano-silver OR "silver nano" OR "silver nanoparticle" OR "silver nanoparticles"
3	**Nano titanium dioxide**	titania OR "titanium dioxide" OR "titanium(IV) oxide" OR TiO2 OR TiO2-NP* OR "nano TiO2" OR nano-TiO2 OR nano-anatase OR rutile OR anatase OR brookite OR 13463-67-7 OR 1317-80-2 OR 1317-70-0
4	**Critical effects/Toxicological endpoints**	assessment OR "adverse effects" OR "health effects" OR toxic OR toxicity OR toxicant OR toxicological OR toxicology OR endpoint OR "critical effects" OR "point of departure" OR NOEL OR NOAEL OR LOEL OR LOAEL OR genotoxic OR genotoxicity OR genotoxicology OR genotoxicological OR reproductive OR developmental OR carcinogen OR carcinogenic OR carcinogenicity OR acute OR subacute OR ames OR cytotoxic OR cytotoxicity OR cytotoxicology OR chronic OR subchronic OR sensitization OR "dose response" OR embryotoxic OR embryotoxicity OR "embryo toxicity" OR embryotoxicology OR hepatotoxic OR hepatoxicity OR hepatoxicology OR irritation OR lethality OR "mechanism of action" OR "margin of exposure" OR "mode of action" OR neurotoxic OR neurotoxicity OR neurotoxicology OR neurotoxicological OR pharmacokinetics OR poison OR "case study" OR "case studies"

The literature search was conducted in the following five databases: PubMed, Web of Science, Scopus, EMBASE, and TOXLINE. A combination of the search string for each nanomaterial and the search string for the critical effects/toxicological endpoints was used to search each database with appropriate search filters applied. Search filters are standardized strategies present within the database designed to limit search results by increasing the specificity of the literature search. Search filters differ between databases. Examples of search filters that were applied include "document type," "publication types" and "publication years." The publication years searched in the five databases were from 2010 to 2016. Although Tier 1 was focused on the identification of primary sources of literature for each of the nanomaterials, some secondary authoritative literature, such as systematic reviews and book chapters, were also identified. The results of the literature search for each nanomaterial in each database, with a complete list of the search filters that were applied, are documented in Tables 2 through 4. The search results for each nanomaterial from all five databases were downloaded, combined and saved in an EndNote library, making a total of three EndNote libraries, one for each nanomaterial.

Thereafter, the appropriateness of the search strings used, search filters applied, and the methodology adopted for the primary literature search were reviewed by TERA toxicologists, a nano-expert, and CPSC staff.

Table 2: Primary Literature Search Results for Carbon Nanotubes using Combination String Searches with Filters

Database	String Combination	# Hits
PubMed	Carbon nanotubes + Critical effect/toxicological endpoint **Date search conducted:** 11-04-2016 SEARCH FILTERS APPLIED: **Entrez Date[a]:** 01-01-2010 – 12-31-2016 **Languages:** English **Subjects:** Toxicology **Species:** Humans, other animals	1,514
Total obtained after removal of duplicates		1,499
Web of Science	Carbon nanotubes + Critical effect/toxicological endpoint **Date search conducted:** 11-04-2016 SEARCH FILTERS APPLIED: **Timespan:** 2010 – 2016 **Languages:** English **Web of Science Categories:** Toxicology, environmental sciences, pharmacology pharmacy, public environmental occupational health **Document Types:** Article, proceedings paper, review, book chapter	1,774
Total obtained after removal of duplicates		1,773
Scopus	Carbon nanotubes + Critical effect/toxicological endpoint **Date search conducted:** 11-04-2016 SEARCH FILTERS APPLIED: **Published:** 2010 – 2016 **Language:** English **Document Type:** Article, article in press, book, book chapter, review **Source Type:** Journals, book, book series **Subject Areas:** Environmental science, pharmacology, toxicology and pharmaceutics	1,406
Total obtained after removal of duplicates		**1,399**

Database	String Combination	# Hits
EMBASE	Carbon nanotubes + Critical effect/toxicological endpoint **Date search conducted:** 11-04-2016 SEARCH FILTERS APPLIED: **Publication years:** 2010 – 2016 **Date added to EMBASE:** 1-1-2010 –12-31-2016 **Diseases:** Acute toxicity, drug cytotoxicity, genotoxicity, granuloma, inflammation, liver toxicity, lung toxicity, neoplasm, neurotoxicity, side effect, toxicity **Drugs:** Carbon nanotube, multi walled nanotube, nanomaterial, nanoparticle, single walled nanotube **Floating Subheadings:** Adverse drug reaction, drug concentration, drug dose, drug toxicity, pharmacology, side effect **Publication Types:** Article, article in press, chapter, review **Study Types:** Animal experiment, animal model, human, *in vitro* study, non-human	369
Total obtained after removal of duplicates		366
TOXLINE	Carbon nanotubes + Critical effect/toxicological endpoint **Date search conducted:** 11-04-2016 SEARCH FILTERS APPLIED: **Publication Date:** 01-01-2010 – 12-31-2016 **Subject:** biomarkers, environmental monitoring, occupational exposure, mutagens, mutagenicity tests, administration, inhalation, environmental exposure	98
Total obtained after removal of duplicates		**98**
Total All Databases		**5,161**

[a]Date citation added to the database

Table 3: Primary Literature Search Results for Nanosilver using Combination String Searches with Filters

Database	String Combination	# Hits
PubMed	Nanosilver + Critical effect/toxicological endpoint **Date search conducted:** 12-15-2016 SEARCH FILTERS APPLIED: **Entrez Date[a]:** 01-01-2010 – 12-31-2016 **Languages**: English **Subjects:** Toxicology **Species:** Humans, other animals	1,097
Total obtained after removal of duplicates		1,097
Web of Science	Nanosilver + Critical effect/toxicological endpoint **Date search conducted**: 12-15-2016 SEARCH FILTERS APPLIED: **Timespan:** 2010 – 2016 **Languages:** English **Web of Science Categories:** Toxicology, public environmental occupational health **Document Types:** Article, proceedings paper, review, book chapter	808
Total obtained after removal of duplicates		782
Scopus	Nanosilver + Critical effect/toxicological endpoint **Date search conducted:** 12-15-2016 SEARCH FILTERS APPLIED: **Published:** 2010 – 2016 **Language:** English **Document Type:** Article, article in press, book, book chapter, review **Source Type:** Journals, book, book series **Subject Areas:** Pharmacology, toxicology and pharmaceutics	682
Total obtained after removal of duplicates		**653**

Database	String Combination	# Hits
EMBASE	Nanosilver + Critical effect/toxicological endpoint **Date search conducted:** 12-15-2016 SEARCH FILTERS APPLIED: **Publication years:** 2010 – 2016 **Date added to EMBASE:** 01-01-2010 – 12-31-2016 **Diseases:** Acute toxicity, chronic toxicity, developmental toxicity, drug cytotoxicity, genotoxicity, immunotoxicity, inflammation, liver toxicity, lung toxicity, neoplasm, neurotoxicity, reproductive toxicity, toxicity **Drugs:** Metal nanoparticle, nanomaterial, nanoparticle, silver nanoparticle **Floating Subheadings**: Adverse drug reaction, drug dose, drug toxicity, oral drug administration, pharmacology, side effect, topical drug administration **Publication Types:** Article, article in press, chapter, review **Study Types:** Animal experiment, animal model, human, *in vitro* study, *in vivo* study, non-human	432
Total obtained after removal of duplicates		414
TOXLINE	Nanosilver + Critical effect/toxicological endpoint **Date search conducted:** 12-15-2016 SEARCH FILTERS APPLIED: **Publication Date:** 01-01-2010 – 12-31-2016 **Subject:** mice, toxicity tests, rats, dose-response relationship, drug, rats, sprague-dawley, rats, wistar; lung; risk assessment, toxicity tests, acute; liver, animals, humans	583
Total obtained after removal of duplicates		**576**
Total All Databases		**3,602**

[a]Date citation added to the database

Table 4: Primary Literature Search results for Nano Titanium Dioxide using Combination String Searches with Filters

Database	String Combination	# Hits
PubMed	Nano titanium dioxide + Critical effect/toxicological endpoint **Date search conducted:** 11-10-2016 SEARCH FILTERS APPLIED: **Entrez Date**[a]: 01-01-2010 – 12-31-2016 **Languages:** English **Subjects:** Toxicology **Species:** Humans, other animals	1,185
Total obtained after removal of duplicates		1,162
Web of Science	Nano titanium dioxide + Critical effect/toxicological endpoint **Date search conducted:** 11-10-2016 SEARCH FILTERS APPLIED: **Timespan:** 2010 – 2016 **Languages:** English **Web of Science Categories:** Toxicology, environmental sciences, pharmacology pharmacy, public environmental occupational health **Document Types:** Article, proceedings paper, review, book chapter	2,110
Total obtained after removal of duplicates		2,069
Scopus	Nano titanium dioxide + Critical effect/toxicological endpoint **Date search conducted:** 11-10-2016 SEARCH FILTERS APPLIED: **Published:** 2010 – 2016 **Language:** English **Document Type:** Article, article in press, book, book chapter, review **Source Type:** Journals, book, book series **Subject Areas:** Environmental science, pharmacology, toxicology and pharmaceutics	1,723
Total obtained after removal of duplicates		**1,686**

Database	String Combination	# Hits
EMBASE	Nano titanium dioxide + Critical effect/toxicological endpoint **Date search conducted:** 11-10-2016 SEARCH FILTERS APPLIED: **Publication years:** 2010 – 2016 **Date added to EMBASE:** 01-01-2010 – 12-31-2016 **Diseases:** Acute toxicity, chronic toxicity, drug cytotoxicity, genotoxicity, granuloma, immunotoxicity, liver toxicity, lung toxicity, membrane damage, neoplasm, nephrotoxicity, neurotoxicity, reproductive toxicity, toxicity **Drugs:** Titanium dioxide, titanium dioxide nanoparticle **Floating Subheadings:** Adverse drug reaction, drug concentration, drug dose, drug toxicity, pharmacology, side effect **Publication Types:** Article, article in press, chapter, review **Study Types:** Animal experiment, animal model, human, *in vitro* study, non-human	313
Total obtained after removal of duplicates		312
TOXLINE	Nano titanium dioxide + Critical effect/toxicological endpoint **Date search conducted:** 11-10-2016 SEARCH FILTERS APPLIED: **Publication Date:** 01-01-2010 – 12-31-2016 **Subject**: mice, toxicity tests, rats, dose-response relationship, drug, environmental pollutants, mutagens, rats, sprague-dawley, risk assessment, toxicity tests, acute; environmental monitoring, administration, inhalation; inhalation exposure, biomarkers	348
Total obtained after removal of duplicates		**342**
Total All Databases		**5,679**

[a]Date citation added to the database

2.2 Tier 2, Secondary Authoritative Sources (Websites)

The purpose of Tier 2 was to identify secondary sources of literature from websites of reputable and authoritative agencies or organizations throughout the world that could have reports or other information of relevance to this project. From a list of 49 websites that have been identified as potentially useful from previous projects conducted by TERA, 29 websites that were deemed to be of potential relevance to the current task were selected. In addition, three websites (i.e., the European Food Safety Authority (EFSA), the U.S. Food and Drug Administration (FDA), and the National Nanotechnology Initiative (NNI)) were included in the list, making a total of 32 authoritative websites. The complete list of the 32 websites that were searched in Tier 2 is found in Appendix A. Hazardous Substance Data Bank (HSDB) (2017a,b,c) reported no CASRN for the three nanomaterials of interest to this project. Each website was searched using the most common name(s) for each nanomaterial (i.e., carbon nanotubes, nano-titanium dioxide, and nano-silver). The website, the total number of results obtained, as well as the number of results that were saved because they were considered potentially relevant are documented in Table 5. The majority of these websites returned numerous search results that were not relevant to the project and were not considered further. There are two factors predominantly responsible for the prevalence of irrelevant search results:

1. Most of these websites lack the function to restrict search results to specific publication years, and
2. In many instances, search results comprise all documents containing a mention of each half of a nanomaterial name (e.g., search results for carbon nanotubes consisting of all documents containing the words "carbon" and "nanotubes") irrespective of whether they appear as a phrase or in isolation within these documents.

This search returned over 3,000 hits of which only 24 were considered relevant to the scope of the project and were used for research.

Table 5: Search Results from Secondary Authoritative References

Website	Keyword[a]	# of Hits	Potentially Relevant[b]
Australia (Dept. of Health): http://www.nicnas.gov.au/home	Nano silver	73	-
	Nano titanium dioxide	23	1
	Carbon nanotubes	248	-
Canadian Centre for Occupational Health and Safety – RTECS: http://www.ccohs.ca/search.html	Nano silver	29	-
	Nano titanium dioxide	78	-
	Carbon nanotubes	116	-
Environment Canada: http://www.ec.gc.ca/default.asp?lang=En&n=ECD35C36	Nano silver	2	-
	"Titanium dioxide"	14	-
	"Carbon nanotubes"	6	-
Health Canada: http://www.hc-sc.gc.ca/index-eng.php	Nanosilver	4	1
	Nano titanium dioxide	10	1
	Carbon nanotubes	7	-
Environment Canada (Risk Management Reports - Final Assessments): http://www.ec.gc.ca/lcpe-cepa/default.asp?lang=En&xml=09F567A7-B1EE-1FEE-73DB-8AE6C1EB7658	Nanosilver	16	-
	Nano titanium dioxide	12	-
	Carbon nanotubes	35	-
ECHA: https://echa.europa.eu/	Nanosilver	17	-

Website	Keyword[a]	# of Hits	Potentially Relevant[b]
	"Nano titanium dioxide"	59	-
	"Carbon nanotubes"	77	-
Denmark EPA: http://eng.mst.dk/topics/chemicals/consumers--consumer-products/danish-surveys-on-consumer-products/	Nanosilver	9	1
	"Titanium dioxide"	12	2
	"Carbon nanotubes"	5	1
	Nanomaterials[c]		5
ACGIH: http://www.acgih.org/	Silver/"Nano silver"/Nanosilver	-	-
	"Titanium dioxide"	9	-
	"Carbon nanotubes"	2	-
CPSC: http://www.cpsc.gov/	Nano silver	4	-
	Nano titanium dioxide	8	-
	Carbon nano tubes	117	-
Federal Docket: http://www.regulations.gov/#!home	Nanosilver	42	-
	"Titanium dioxide"	463	-
	"Carbon nanotubes"	96	-
National Service Center for Environmental Publications: http://www.epa.gov/nscep/	Nanosilver	19	-
	Titanium dioxide	168	-
	Carbon nanotubes	45	-
OSHA: https://www.osha.gov/dts/chemicalsampling/toc/toc_chemsamp.html	Nanosilver	8	-
	"Titanium dioxide"	65	-
	"Carbon nanotubes"	20	-
HSDB: http://toxnet.nlm.nih.gov/newtoxnet/hsdb.htm	Nanosilver	4	1
	"Titanium dioxide"	63	1
	"Carbon nanotubes"	27	1
NTP: http://ntp.niehs.nih.gov/index.cfm	Nanosilver	5	1
	"Titanium dioxide	86	-
	"Carbon nanotubes"	40	-
OEHHA: https://oehha.ca.gov/	"Nano silver"	2	-
	"Titanium dioxide"	100	-
	"Carbon nanotubes"	3	-
USA-CA (Draft Assessments): http://www.ec.gc.ca/lcpe-cepa/default.asp?lang=En&xml=6892C255-5597-C162-95FC-4B905320F8C9	Nanosilver	17	-
	"Titanium dioxide"	38	-
	"Carbon nanotubes"	35	-
ATSDR: http://www.atsdr.cdc.gov/substances/index.asp	Nanosilver	25	-
	"Titanium dioxide"	Over 240	2
	"Carbon nanotubes"	Over 160	1
	Nanomaterials[c]		1
EPA SCIENCE INVENTORY: http://cfpub.epa.gov/si/	Nanosilver	13	1
	"Titanium dioxide"	43	-
	"Carbon nanotubes"	50	-
IARC: http://monographs.iarc.fr/ENG/Monographs/PDFs/index.php	"Nano silver"	2	-
	"Titanium dioxide"	205	-
	"Carbon nanotubes"	14	-
EFSA: http://www.efsa.europa.eu/en/press/news/170118-0	Silver/"Nano silver"/Nanosilver	-	-
	Titanium dioxide	8	1
	Carbon nanotubes/"Carbon	-	-

Website	Keyword[a]	# of Hits	Potentially Relevant[b]
	nanotubes"		
	Nanomaterials[c]		1
FDA: http://www.fda.gov/	Nano silver	15	-
	Nano-titanium	4	-
	Carbon nanotubes	23	-
Nano.gov: https://www.nano.gov/	Nanosilver	6	1
	Titanium dioxide	6	-
	Carbon nanotubes	34	1
Total		**3,186**	**25**

[a]Keyword represents the nanomaterial name (exactly as it appears in the table, with or without quotation marks) that either returned the most relevant search results/documents for the nanomaterial of interest, or returned search results where other variations of the nanomaterial name did not. Some of the websites of these secondary authoritative sources are programmed in such a way that employing the quotation marks designation ("") in a search phrase ensures specificity of search results

[b]Fact sheets, human health hazard assessments/reviews, reports, and other publications on the nanomaterial of interest or nanomaterials in general before 2010 were not considered "potentially relevant."

[c]This word was not used as a keyword for the literature search. However, results that pertained to nanomaterials generally, rather than to a specific nanomaterial, and were considered potentially relevant were documented in this row.

2.3 Tier 3, Gap-Search

There were several steps used to search for "missing" information or address potential "gaps" identified by the authors or by the Versar peer reviewers (2012). Missing information/potential gaps, as used here, refer to additional keywords that were not used in the initial primary literature search, suggested references for all three nanomaterials from the peer review report, and references identified through tree-searching, as explained in detail below.

The first step of the third tier involved gap-searching of the primary literature using additional keywords that were not used during the initial primary literature search (Tier 1) to confirm whether additional studies of potential relevance were available. The additional keywords were included only in the "critical effects/toxicological endpoints" search string and can be found in Table 6.

Table 6: Additional Keywords for Gap-Search[a]

Search string name	Search strings for primary literature
Critical effect/Endpoint	assessment OR "adverse effects" OR "health effects" OR toxic OR toxicity OR toxicant OR toxicological OR toxicology OR endpoint OR "critical effects" OR "point of departure" OR NOEL OR NOAEL OR LOEL OR LOAEL OR genotoxic OR genotoxicity OR genotoxicology OR genotoxicological OR reproductive OR developmental OR carcinogen OR carcinogenic OR carcinogenicity OR acute OR subacute OR ames OR cytotoxic or cytotoxicity or cytotoxicology OR chronic OR subchronic OR sensitization OR "dose response" OR embryotoxic OR embryotoxicity OR "embryo toxicity" OR embryotoxicology OR hepatotoxic or hepatoxicity or hepatoxicology OR irritation OR lethality OR "mechanism of action" OR "margin of exposure" OR "mode of action" OR neurotoxic OR neurotoxicity OR neurotoxicology OR neurotoxicological OR pharmacokinetics OR poison OR "case study" OR "case studies" OR **oral** OR **dermal** OR **inhalation** OR **"acceptable daily intake"**

[a]Additional keywords are emboldened

Using the same methodology of combining the search string for each nanomaterial with the search string for the critical effects/toxicological endpoints (with the additional keywords), two of the five databases (TOXLINE and EMBASE) were searched again, using the same search filters that were applied in the Tier 1 literature search. These databases were chosen because they returned the most relevant literature from the initial searches as deemed by the toxicologist(s) screening the searches.

The gap-search results from the aforementioned databases were downloaded and combined with the initial EndNote libraries for those two databases for each nanomaterial. Duplicate results were deleted in order to get the actual number of "new" references that were retrieved. The numbers of additional references obtained as a result of the gap-search for each nanomaterial are shown in Tables 7, 8, and 9.

Table 7: Gap-Search Results for Carbon Nanotubes

Title	Date Search Conducted + Final Result
Initial search conducted	11-4-2016
Gap-search conducted	01-14-2017
Date range used for both initial search and gap-search	(01-01-2010 – 12-31-2016)
Number of new references obtained from gap-search	81[a]

[a]This number was obtained by combining the initial and gap-search results from two databases (EMBASE and TOXLINE), followed by the removal of duplicates

Table 8: Gap-Search Results for Titanium Dioxide

Title	Date Search Conducted + Final Result
Initial search conducted	11-10-2016
Gap-search conducted	01-15-2017
Date range used for both initial search and gap-search	(01-01-2010 – 12-31-2016)
Number of new references obtained from gap-search	116[a]

[a]This number was obtained by combining the initial and gap-search results from two databases (EMBASE and TOXLINE), followed by the removal of duplicates

Table 9: Gap-Search Results for Nanosilver

Title	Date Search Conducted + Final Result
Initial search conducted	12-15-2016
Gap-search conducted	01-16-2017
Date range used for both initial search and gap-search	(01-01-2010 – 12-31-2016)
Number of new references obtained from gap-search	80[a]

[a]This number was obtained by combining the initial and gap-search results from two databases (EMBASE and TOXLINE), followed by the removal of duplicates

The second step of Tier 3 involved the identification and retrieval of references suggested by the peer reviewers of the Versar report (2012). It was anticipated that these references might provide additional insight, particularly on the toxicokinetics of nanomaterials.

The third step that was employed in Tier 3 of the literature search strategy involved the identification of potentially relevant references either cited in the reference sections from primary literature or through tree-searching by toxicologists reviewing the nanoparticle literature, followed by subsequent retrieval and review of the identified references for screening.

2.4 Screening Literature Searches

2.4.1 Relevant Literature

Literature retrieved through the above methods were screened for high quality, relevant studies primarily on the basis of whether the experimental data was relevant and reported in a format that could provide a dose or concentration as a point of departure (POD) from which an ADI could be derived. High quality studies were considered those that include best practice documentation of nanomaterial characteristics, including, but not limited to:

a. physico-chemical characteristics,
b. concentration of the nanomaterials,
c. particle size and shape,
d. particle number and distribution,
e. purity of the nanomaterial,
f. use of proper controls, and
g. documentation of analysis (e.g., standard test methods were used from such standard organizations as ASTM or ISO); instruments were calibrated; measurement protocols were discussed and cited.

Further, studies were deemed to be potentially relevant to an ADI, or were otherwise considered toxicologically relevant information, if they met the following criteria:

1) The study was in English.
2) The study measured *in vivo* (humans, mouse, rat, hamster, rabbit, guinea pig, dog, or primate) responses to a form of the nanomaterial relevant to CPSC. Nanomaterial preparations specific to cosmetic, food, drug, transportation, or other applications not regulated by the CPSC were excluded.
3) The study used a route of administration relevant to likely exposure by way of CPSC-regulated articles, which included oral, inhalation, or dermal routes. Studies using intratracheal instillation (IT), oropharyngeal aspiration (OPA), intraperitoneal injection (IP), subcutaneous injection (SC) or intravenous injection (IV administration) were not considered appropriate for providing dose-response toxicity information or serving as the basis of the ADI calculation/derivation, but were considered potentially relevant to inform toxicity if the database of oral, inhalation or dermal studies were limited (see Section 2.3.2).
4) The study measured toxicity endpoints relevant to an ADI. These included any form of systemic toxicity, portal of entry toxicity (e.g., lung inflammation from inhalation exposure), but excluded eye and skin irritation, and skin sensitization, as these are usually acute studies that examine only portal of entry effects and not systemic toxicity.
5) The study reported effects from which a dose-response could be informed, which was considered to be two or more dose levels plus a control. Studies reporting only one exposure dose were considered relevant for demonstrating a NOAEL/LOAEL if they were performed according to a specific OECD Test Guidance/Guideline.
6) Studies investigating genotoxicity or mutagenicity were considered relevant, other criteria notwithstanding.

2.4.2 Potentially Relevant Literature

Studies that did not meet the above criteria but were considered to be potentially informative to some aspect of this assessment were placed into a "potentially helpful/relevant" folder. The criteria used to select these studies were not strict, but in general studies were deemed "helpful" if they contributed information to the following subjects:

1) Absorption, distribution, metabolism, or excretion of nanomaterials,
2) The impact of physicochemical variability on nanomaterial toxicity,
3) The biological mode-of-action of nanomaterial toxicity,
4) Hazard characterization of nanomaterials using routes of exposure (e.g., IV) not directly relevant to CPSC-regulated articles,
5) The use of nanomaterials in CPSC-regulated product groups, their release from such articles, or assessment of consumer exposure to nanomaterials through such articles,
6) Epidemiological association of nanomaterial exposures with effects in humans,
7) Approaches for risk assessment of nanomaterials, and
8) Authoritative reviews of literature, as deemed appropriate.

These screening criteria initially resulted in the following number of "relevant" and "potentially helpful" studies for each nanomaterial (Table 10):

Table 10: Number of Studies identified after Screening

Nanomaterial Name	Studies "Relevant to ADI"	"Potentially Helpful" Studies
Carbon nanotubes	43	136
Nano-titanium dioxide	67	205
Nanosilver	60	103

The screened groups of "relevant to ADI" and "potentially helpful" publications for each nanomaterial were further reviewed for completeness by an outside expert who was selected on the basis of having an extensive background in the toxicology, commercial uses, risk assessment, and environmental exposure of these nanomaterials.

3 USE AND EXPOSURE IN CONSUMER PRODUCTS

3.1 Overview

Literature available prior to 2010 has been summarized in Versar (2012). The scientific consensus on consumer exposure from this period is limited by a lack of both experimentation and systematic assessment of consumer exposure potential. At the time of the Versar review, there was a great deal of uncertainty regarding release or emission of added NP from products. Versar (2012) summarized a systematic review by Wijnhoven (2009) that laid out factors expected to contribute to consumer exposure risk arising from the addition of nanomaterials to products. These factors included: 1) properties of the nanomaterial, 2) properties of the product and prevalence of the product use, and 3) route of exposure. An expert panel convened by the Dutch National Institute for Public Health and the Environment reached the conclusion that nano-enabled products outside of the food-and-drug purview were not likely to result in high-level exposures except where free particles were used, such as in adhesives, cleaning products, and paints/coatings (Versar, 2012). An EPA assessment (U.S. EPA, 2010b) on potential routes of exposure to nanosilver stated that exposure route was highly dependent on specific products and uses. This echoes the points made by Wijnhoven (2009), and it may be noted that detailed volume and use information on nanomaterial-containing products would be very valuable. This information may be difficult to retrieve in the many cases where it may be proprietary to private manufacturers.

Consumer exposure studies published from 2010 to 2017 continue to discuss and develop frameworks for identifying the likelihood of nanomaterial exposure to consumers through consumer products. In the recent literature retrieved, a majority of consumer exposure assessments for nanosized TiO2 and nanosilver have been for cosmetic or food-related products (Vance et al., 2015) and neither application is under CPSC regulatory purview. Many of the consumer exposure scenarios studied for CNTs are relevant to the CPSC, with the exception of biomedical, therapeutic, and automotive/aeronautical applications. Increasing emphasis has been placed on determining conditions under which these nanomaterials may be released from a product at any point during the product life cycle, thus creating a potential for consumer exposure. Extent of release will depend on how a nanomaterial is incorporated into products, as nanomaterials may be securely entrained in some applications but freestanding (i.e., loose particles not bound in matrices or aggregates) in others (Nowack et al., 2013; David et al., 2015; Harper et al., 2015). It will also depend on the composite in which the nanomaterial is used, as release from some composites are more likely under some use conditions than others (Kingston et al., 2014).

Routes of exposure that are anticipated to be of importance to use of consumer products are oral and inhalation routes. Regarding the possibility of exposure by way of dermal routes, Filon et al. (2016) reviewed the dermal absorption of NPs and agglomerates in occupational settings. Metal NPs were thought to present a higher risk of skin absorption relative to larger graphene-based mega-molecules. This was not due to the intrinsic nature of the NP so much as the tendency of metal NPs to shed metal ions depending on conditions. Solid NPs smaller than 45 nm in diameter may penetrate the epidermis, but only exceedingly small particles (less than 1 nm) are capable of being systemically absorbed through intact skin. Dermal absorption of NPs from products, therefore, appears unlikely.

Research into nanomaterial release from products has only recently begun to make progress in characterizing the effects of weathering and consumer use stresses, which can include abrasion, heat, ultraviolet (UV)/sunlight exposure, and chemical reactions (Froggett et al., 2014; Harper et al., 2015). Several attempts have been made to model weathering of nanomaterial-containing products (Wohlleben and Neubauer, 2016). As recently as 2011, a nearly total lack of nanomaterial release information was acknowledged in a critical review by a German Federal Environment Agency and German Federal Institute for Risk Assessment working group on the carcinogenic potential of nanomaterials in consumer products, focusing primarily on CNTs and TiO2 NPs (Becker et al., 2011). The goal of the review was to assess whether nanomaterials in products presented a cancer hazard to humans based on the available data on NP carcinogenicity and NP release from products. The group concluded that no reliable conclusions could be drawn regarding release of nanomaterials from products at that time and highlighted the need for data specific to release.

The Danish Environmental Protection Agency published a detailed effort to assess consumer exposure to nanomaterials (Danish EPA, 2015a). The assessment was specific to products intended for the European and Danish markets, but provides some insight to exposure assessment strategies for nanomaterials. The report noted that consumer exposure assessment tools developed for nanomaterials are, so far, limited to qualitative judgements that may allow for risk prioritization of exposure scenarios but not determination of concrete risk. The report developed a well-supported assessment of consumer use scenarios and developed quantitative estimates of exposure to a variety of nanomaterials in these. These analyses were specific to products in the European market, but may provide some insight into consumer exposure risks from analogous North American products. Other international organizations have compiled and reviewed consumer exposure information to nanomaterials (http://nanoportal.gc.ca/default.asp?lang=En&n=57FB12B0-1&printfullpage=true).

Several reviews have been published that further develop the scientific discussion of consumer-level exposure to CNTs and other nanomaterials. Nowack et al. (2013) reviewed possible scenarios of CNT release from various polymer-based product applications, including sports equipment, electronics, car tires, and textiles. In general, potential for release was considered to be low at all stages of product life cycles, including injection molding, machining, consumer use, incineration, and disposal in landfills. Possible exceptions included CNTs incorporated into car tires and textiles. Mitrano et al. (2015) reviewed possible transformations of CNTs and several other nanomaterials during the life cycle of nano-enabled products, arguing that anticipation of these transformations based on product use and environmental conditions is necessary to design relevant toxicity tests. Caballero-Guzman and Nowack (2016) reviewed strategies to incorporate nanomaterial release data into material flow analysis of nano-enabled products. The review, which was not exclusive to CNTs, noted that only 36% of product categories (not individual products) have been investigated and few relevant scenarios have been studied. Erdely et al. (2016) reviewed the implications of exposure assessment science for risk assessment of CNTs in general, stressing that toxicity testing should be informed as to what form of NPs are anticipated in real-life exposure scenarios. Mackevica and Foss Hansen (2016) reviewed literature relevant to consumer exposure assessment of nanomaterials in products, asking whether the available data could satisfy requirements for exposure assessment under Registration, Evaluation,

Authorisation and Restriction of Chemicals (REACH). The authors concluded that less than half the retrieved exposure data was documented in a form that could be used under REACH, and most studies did not characterize particles released from products, and that REACH guidelines concerning hazardous substance release from products are not easily adapted to the unique situation of nanomaterials. Taken together, these reviews place emphasis on using knowledge of nanomaterial type, composite type, product life cycle and use to identify consumer exposure risks. Further, high-priority scenarios should ideally be reflected in the design of toxicity studies.

3.2 Consumer Exposure to CNTs

Due to their range of unique properties, CNTs are utilized in diverse applications including construction and civil engineering, electronics, and biomedicine. MWCNTs make up the majority of CNT usage by volume. MWCNTs are used in roles such as flame retardants, electrical conduction, structural reinforcement, and nanomanipulation/engineering. Product groups, many of which are considered consumer products, incorporating or expected to incorporate MWCNTs include reinforced composites, additives to polymers, textiles, filters, cables, lithium ion batteries, photovoltaic cells, paints, inks, and developing biomedical products (Versar, 2012; De Volder et al., 2013). Most current product applications use CNT powders either dispersed in solids (most common) or deposited as thin films surface-bound to a product. CNTs are rarely found in freestanding form in consumer products (Vance et al., 2015). SWCNTs are typically used for demanding electrical applications, for example as transistors or superconductors. These applications for SWCNTs remain in development (De Volder et al., 2013).

In response to the growing need to model nanomaterial release from products, numerous studies have investigated the extent and character of particles released in simulated weathering scenarios. Most of the nanomaterial research of this kind conducted outside of food and drug applications have focused on CNT-enabled products. Schlagenhauf et al. (2012) investigated abrasion of CNT-containing epoxy and found free-standing CNTs among abraded particles, but could not quantify the level of free CNTs at that time. Wohlleben et al. (2013) developed a CNT-containing polyurethane polymer and tested it in degradation scenarios that included abrasion, machining, and outdoor weathering (UV exposure). The analysis detected no free CNTs released under any of the conditions tested. After an extended period of wear in these experiments, entangled CNTs previously suspended within the polymer were exposed from the degraded polymer surface. The report noted that the softness of the polymer enhanced the embedding of CNTs in the material, even in abraded particles. This suggests that CNTs complexed with soft materials have less potential to be shed as freestanding CNT particles compared to CNTs incorporated into hard matrices.

Ging et al. (2014) studied simulated outdoor weathering of CNT polymer nanocomposites and tested the toxicity of weathered particles in a *Drosophila* model. This species was selected for ease of studying developmental effects. The authors simulated weathering by subjecting CNT-containing epoxy surfaces to repeated cycles of UV and humidity exposure. Weathered surfaces featured bared CNT fibers and agglomerates, but release of particles was not quantified. These weathered CNT-containing surfaces exhibited no toxicity when micronized into fine particles and exposed in Drosophila larvae, while a comparable dose of free CNTs inhibited growth and

survival. Jiang et al. (2014) studied particle release from a SWCNT-containing polystyrene polymer under abrasion and thermal degradation conditions. Abrasion produced micron-sized particles with protruding SWCNTs and SWCNTs agglomerates. Heat treatment of the composites at 100°C for 10 days did not change particle release, but 350°C for 1 hr enhanced SWCNT release, generating released SWCNTs in the form of clusters or rope-like bundles. The high heat treatment resulted in the loss of almost half the weight of the polymer sample, suggesting that CNTs were released as the polymer was burned away. The study concluded that SWCNT incorporation modestly improved abrasion resistance, but that high heat decreased abrasion resistance and could liberate agglomerates of intact CNTs by burning away surrounding matrices.

Grieger et al. (2015) reviewed a risk ranking algorithm estimating risk of nanomaterial release from nano-enabled materials used in U.S. Army equipment. CNTs were ranked highly due to inhalation risks during research and development scenarios, which presumably may involve CNT use and handling more typical of occupational settings involving manufacture or machining of CNTs. Schlagenhauf et al. (2015a, b) characterized and quantified CNT release from epoxy materials as a result of abrasion in combination with UV light or immersion in water. Abrasion processes released free-standing CNTs from only one specific epoxy formula containing 1% w/w MWCNTs (a composition considered to be typical of CNT-containing polymers). The authors estimated that 0.004% (w/w) of the abraded nano-epoxy material released into the submicron size fraction would be in the form of free-standing MWCNTs, suggesting a low rate of release for CNTs not still entrained in abraded polymer particles. An additional component of this study tested the toxicity of abraded particles containing CNTs and found they did not cause greater toxicity than CNT-free epoxy in human airway and macrophage *in vitro* tests. Kim et al. (2016) reported on methods for quantifying CNT release from barrier fabrics and polyurethane foam. In general, free CNTs were not generated from weathering these composites. Sotiriou et al. (2016) studied release of nanomaterials from thermoplastic polymers following thermal decomposition. The group found minimal, but detectable, nanomaterial release. Wohlleben et al. (2016) investigated the effect of chemical and mechanical weathering on model elastomers, tested in a scenario of nanofiber-enabled car tires. Considerable release was only observed when aging stresses were combined. Overall, these studies indicate that significant levels of CNT exposure from composites are predictable and limited to a narrow range of scenarios. These scenarios appear most likely to involve combinations of weathering stresses (e.g., heat and abrasion); release potentials may be reduced or eliminated through combinations of material choices and use restrictions.

In most cases of consumer product use observed so far, amounts of free CNTs released to direct exposure pathways (e.g., inhalation from use of the product) will likely be negligible, as released CNTs often remain embedded in the composite matrix (i.e., polymer) and freestanding particles are not likely to be released at rates that would result in meaningful exposure concentrations in most situations. The experimental data suggest that conservative assumptions should be used where applications involve combinations of stresses, especially where high heat is a condition. In addition, even low rates of free-standing CNT release may be a concern where continuous release over time may result in accumulation of free CNTs in dusts on surfaces in homes and other consumer environments.

3.3 Consumer Exposure to Nanosilver

Nanosilver (or silver nanoparticles, Ag NP) is one of the most commonly used nanomaterials in consumer products. Most of the applications utilize nanosilver's inherent antimicrobial properties. Nanosilver-enabled consumer applications are most commonly seen when disinfectant or antibacterial properties are needed in spray disinfectants, medical products not regulated by the FDA, hair dryers, soaps, cooking utensils, filters of air and water purification systems, household appliances (refrigerators and washing machines), electronics (computer hardware, mobile phones), textiles, clothing, shoes, and toys (Versar, 2012). Silver NPs in consumer products are usually found moderately to well-dispersed and are used suspended in solids, coated on surfaces, reactively bound to matrices (e.g., textiles), or in freestanding form (Dallas et al., 2011). Silver NPs are known to be present in over 400 consumer products (not necessarily all under CPSC purview) and is occasionally used in combination with nano-TiO2 in the same product. Silver NPs are most commonly found suspended in liquids and are also common as surface coatings (Vance et al., 2015).

Studies retrieved addressing consumer exposure to Ag NP released from products were largely focused on food-related and medical applications, while only a few were considered relevant to CPSC. Overall conclusions from these studies were that a significant fraction of Ag NP release from surfaces and solids was in the ionic form, and that heat increased the rate of release overall. Nanosilver in liquids can be found as particles or dissolved ions, the ratio of which can vary widely among different product formulas. A recurring challenge in estimating consumer exposure risk is inconsistency in manufacturer reporting of whether products contain nanosilver and in what form (Quadros and Marr, 2010). Exposure of consumers to nanosilver via products is expected to occur predominately from inhalation of freestanding Ag NPs in sprays (http://toxnet.nlm.nih.gov/newtoxnet/hsdb.htm). The risk of nanosilver exposure to consumers is of particular interest due to the prevalence of nanosilver use in products and, in particular, in products meant for use in the home and around children (Tulve et al., 2015). The available studies are summarized below.

Quadros and Marr (2010) reviewed the uses and anticipated release of Ag NPs in consumer products, indicating disinfectant and deodorant sprays as having the highest potential for aerosolization of this NP. Heat was considered a significant factor for NP release, especially from coatings. Fourteen percent of inventoried nanosilver-containing products were estimated to present the potential for aerosolization of silver NPs during use.

Schafer et al. (2013) reported on a conference held at the German Federal Institute for Risk Assessment which covered several aspects of nanosilver toxicology and human exposure, including exposure through consumer products. Most Ag-containing products identified and discussed were microbiocidals, which generally contained more micron-scale, than nano-scale, particles. Biocidal effects are due to dissolved ions from the surface of the particle. A presenter at the conference reported functionalization of textiles with nanosilver where 0.75% (w/w) nanosilver incorporation was effective at inhibiting bacterial growth. Details relating to release were not presented, but the information in the review indicated that the nanosilver concentration in textiles may be substantially higher than those in topical antibacterial creams. Riebeling et al. (2016) used the *in silico* Multiple Particle Path Deposition (MPPD) model to estimate lung deposition of NPs from antibacterial spray products with the goal of identifying consumer

exposure situations that could lead to lung overload. Lung overload is a mechanism that produces lung toxicity when phagocytic clearance mechanisms in the lung are volumetrically overwhelmed and is associated with the high surface area of NPs (Oberdorster et al., 1994). The study presented dosimetric modeling of nanosilver regional doses based on nanosilver spray product information from Quadros and Marr (2010) and concluded overload was unlikely in the context of consumer exposure to sprays.

Nazarenko et al. (2014) estimated quantitative exposure to NP aerosols through nanotechnology-enabled spray products, one of which was a nanosilver spray. Transmission Electron Microscopy (TEM) of the captured spray particles showed silver NPs, mostly in agglomerated clusters in the 50-100 nm range. The quantitative estimate of nanosilver dose to the respiratory tract was derived from the size-distributed mass fractions measured during a 1-minute simulated use. The size-distributed mass fractions of particles captured from the nanosilver spray were not statistically distinguishable from those captured from a particle-free silver (Ag) spray used as a control. It was unclear whether this discrepancy in the expected size distribution is due to inaccurate labeling of products, non-homogeneity of product samples, or an artifact of the methods.

von Goetz et al. (2013) analyzed release of nanosilver from plastic food containers containing different simulated foodstuffs, including water, olive oil, and solutions of acetic acid or ethanol. Significant release of nanosilver into contents was observed only following storage of acidic foodstuff in new containers. About 12% of released silver was in NP forms, with the remainder being ions. The authors note that the level of total consumer exposure to silver (all forms) via this ingestion route would be low compared to the background level of total silver in the general population.

Tulve et al. (2015) published a detailed review and assessment of nanosilver-containing consumer products, focused on the U.S. market and potential exposure to children. Children's products incorporating Ag NPs included wipes, breast milk storage bags, stuffed toys, toothbrushes, and plastic dishware. The assessment characterized the forms and characteristics of Ag particles in a wide variety of products. The silver particles ranged from micron to nanoscale in size and included free silver ions (Ag+); particles and Ag+ were distributed heterogeneously throughout product matrices. Freestanding Ag NPs in sprays were distributed between agglomerated and dispersed states. A basic formula for estimating exposure of the user (children) to Ag on a mg/kg bw basis was proposed. Presumably, some of this Ag would be in an ionic state and some portion would be ingested or absorbed as nano- or micron-scale particles. More detailed release simulations may allow for better characterization of exposure risk to consumers, particularly considering the extent of nanosilver use in products meant for very young children.

3.4 Consumer Exposure to TiO2

Nanosized TiO2 is used in air filtration and purification systems, motor vehicle coatings, cleaning products, paints, and various other household products (Versar, 2012). Titanium dioxide NPs are often incorporated into products to make use of their photochemical qualities. They are found mostly in coatings and suspended in liquids. Although nanosilver far exceeds nano-TiO2 in number of applications (inventoried products), nano-TiO2 is produced in far more

volume due to its use in paints and coatings (e.g., Pigment White 6), which are applied to a wide variety of surfaces (Vance et al., 2015). Food grade TiO2 (E171) is also widely used, for example, to whiten frostings and gum, and is reported to contain approximately 30% particle size below 100 nm by weight (Weir et al., 2012). TiO2 (P25 Aeroxide®) is a common sunscreen ingredient and most of the available literature addressing consumer exposure is specific to this use as well as its use in cosmetic products. Use of TiO2 in food, sunscreen and cosmetics are not under CPSC regulatory jurisdiction.

There were few available resources specifically addressing non-FDA regulated products with TiO2. Overall, the greatest risk of consumer exposure to TiO2 NPs appears to be via inhalation of freestanding NPs, for example as present in wet paints, ink toners, and spray-on self-cleaning coatings (Pirela et al., 2015). Nanoparticle release from dried paints and coatings appears to be negligible relative to levels expected to be hazardous (Al-Kattan et al., 2013; 2014) and TiO2 NPs are thought to be firmly entrained in these matrices (Olabarrieta, 2012; Shandilya et al., 2014). However, extended weathering experiments have nonetheless documented the release of free-standing TiO2 NPs from coatings (Shandilya et al., 2015). Nanoparticles may leach from surfaces when not entrained in coatings or other non-porous polymers, as is seen in the case of textiles (Windler et al., 2012) and cement (Bossa et al., 2017). TiO2 NPs are also found in antimicrobial sprays and similar products. There are also a number of products containing both TiO2 and Ag NPs (Vance et al., 2015). Product categories featuring significant volumes of nano-TiO2 are discussed below.

Paints, coatings, and printer inks/toners containing nanosized TiO2 are sources of freestanding NPs which could be aerosolized and inhaled. Pirela et al. (2015) investigated physicochemical and morphological characteristics of NPs released from toner cartridges used in consumer-level laser printers. NPs released from the use of different printer toners resulted in peak emissions of between 3000 and 1.3 x 10^6 particles/cm^3, ranging from 49 to 208 nm in size and variously dispersed and in small agglomerates. TiO2 NPs are used in this product category, but metals only accounted for up to 2 to 3% of the composition. The study concluded that considerable differences existed between NPs characterized in their native post-synthesis state (as usually studied in toxicity assays) and post-usage. This may create uncertainty with regard to what may be considered a safe level of consumer exposure when health reference levels are derived from published toxicity data. The author notes that concentrations up to and over 1 million particles per cm^3 have been documented by other investigators during the use of high-speed laser printers utilizing NP-enabled toners.

A study by Al-Kattan et al. (2013) measured release of NPs from nanoTiO2-containing building paints during simulated weathering (UV, rainwater extended storage), concluding that NP release was negligible over the anticipated use lifetime and that NPs were tightly bound within the solid paint matrix. This reflects the view that hardened paints and coatings present little risk of exposure to free-standing TiO2 NPs, but this conclusion may be premature. Shandilya et al. (2015) used simulated weathering consisting of UV and water spray cycles meant to simulate 7 months of weathering. An 80-µm layer of coating containing 1.1% nano-TiO2 applied to a masonry brick was used. Cracks in the coating were observed after 4 months and the surface was discontinuous after 7 months. Titanium (Ti) was not detected in water runoff from the coating, but the brick itself readily degraded. The authors indicated that the data are consistent

with contraction of the coating layer with increased weathering, causing cracks and inconsistencies in the coating, but firmly retaining the TiO2 NPs within the coating. However, when weathered surfaces were abraded it was found that longer-weathered surfaces shed higher amounts of Ti and free-standing NPs were observed among abraded particle aerosols. The authors considered this unusual as NPs in hardened coatings are thought to be tightly bound, but is consistent with the perspective that combinations of weathering stresses increase the likelihood of matrix degradation and NP release.

The release of TiO2 nanoparticles from textiles was investigated during sweating (von Goetz et al., 2013) and washing (Windler et al., 2012). In the Windler investigation, six nanoTiO2-containing textile products (none of which listed nanoTiO2 as an ingredient) were subjected to up to 10 wash cycles in a laundry machine. Textiles contained between 0.2 and 0.8% Ti content by weight, which was assumed to be in TiO2 form. Repeated washings caused small, non-significant decreases in Ti content, with the exception of two textiles that shed 23-32% of product Ti content over 10 washes. TiO2 NPs were shed mostly as agglomerates of a few hundred nm to over 1µm in size. Textiles lost less than 0.07% of their Ti content in the first wash cycle, except for one example which lost 3.4% Ti. The high-loss example included TiO2 for its antimicrobial properties rather than for pigment purposes.

Bossa et al. (2017) conducted an experimental study of NP release from hardened nanoTiO2-containing cement pastes. Leeching of Ti in soluble and NP forms was quantified over a 7 day leaching period in pure water. TiO2 released into water was detected only in NP form and NPs were free-standing. The study found a maximum release rate of 33.5±5.1 mg Ti (corresponding to 0.04% of initial NP content) per m^2 of hardened cement surface over 168 h of leeching in water (estimated to represent two years of aging in product use). The leaching occurred as a result of increased porosity of the hardened cement and dissolution of the cement matrix into water. The rate of nano-TiO2 loss appeared to plateau with time.

3.5 Summary

There are a wide variety of uses for the three nanomaterials discussed in this report. Some of these applications involve high volume-use of nanomaterials, such as TiO2 NPs used in paint pigment. Scenarios involving high volumes of freestanding NPs (e.g., spraying NP-containing paints) appear to present the highest potential for consumer exposure. Carbon nanotubes are rarely found as freestanding particles in material released from products, thus the overall potential for significant exposure for consumer uses appears minimal. Long-term exposure potential from accumulation in dusts in homes has not been explored in the reviewed studies. In the cases of nanosilver and nanoTiO2, many nanomaterial-enabled products are intended for the home and are used by adults and children. Examples include construction materials, glass coatings, textiles, disinfectant sprays, cleaners, self-cleaning spray coatings, air and water filters, and food containers. Nanosilver in particular is widely used in home products, including many children's products such as wipes, toys, toothbrushes, and plastic dishware. Caution would therefore be prudent regarding, for example, assumptions about nanosilver exposure and absorption in adults vs. children. Absorption of nanoparticles and ionic metals in infants and small children may differ from that estimated for adults. It should also be noted that nanosilver-containing products may release silver predominantly in the ionic form as opposed to NPs. Dissolved ionic silver may exhibit different absorption and distribution behavior compared to Ag

NPs, and relative toxicities may be different between these forms.

A significant challenge in estimating consumer exposure to nanomaterials in various products is incomplete or unreliable information regarding the actual content of NPs and their form and manner of incorporation. Manufacturers frequently do not fully describe these particulars and information may only be available in the imprecise language of advertising. Furthermore, manufacturers may be reluctant to clearly disclose or label where nanomaterials are used in products due to public perception about nanotechnology safety (Vance et al., 2015).

Regarding NP release from products, peer-reviewed studies focused on consumer-level exposure from the use of nanomaterial-enabled products emphasize the following: 1) consumer exposure to high-aspect-ratio macromolecular particles (i.e., length many times greater than diameter, as with CNTs and other graphenes) is primarily a function of incorporation into a stable matrix, and 2) the use of metal NPs (such as silver) introduces exposure to both nanoscale and ionic (dissolved) metals, and 3) combinations of weathering and stresses/stressors potentiate the release of freestanding NPs (CNT, Ag, TiO2) from surrounding matrices, especially when heat stress is involved.

4 TOXICITY DATA FOR CNTS

4.1 Physical and Chemical Properties of CNTs

As briefly summarized in Versar (2012), literature prior to 2010 reflects an appreciation of the importance of physicochemical characteristics in determining the toxicity of CNTs. However, literature from this period lacked empirical data investigating factors leading to biological entrapment and toxicity of CNTs. Expert opinion at that time held the expectation that properties including shape, crystal structure, particle size distribution, agglomeration state, surface area, surface chemistry, surface charge, and porosity would be relevant to the toxicity of most nanomaterials, including CNTs (Oberdorster et al., 2005).

4.1.1 Experimental Toxicology Studies

The body of experimental work testing the impact of physicochemical variation on the toxicity of CNTs and other nanomaterials has continued to grow. Apart from single-walled vs. multi-walled, which are being addressed separately in this report, characteristics of CNTs include diameter, length, purity (particularly with regard to trace metal contaminants), surface area, surface modification (pristine vs. functionalized or oxidized[1]), presence of defects in the CNT molecular configuration, surface coating by dispersants, and morphology/agglomeration. There have been a number of experimental studies contributing to the evidence of certain physicochemical features of CNTs as determinants of toxicity. Although the observed norms and available technical guidance regarding documentation of physicochemical characterization have improved greatly (ISO, 2012), the published results of many experiments remain difficult to interpret and generalize. In some scenarios, it is apparent that certain physicochemical features of CNTs are reproducibly associated with specific toxic outcomes.

On balance, the most consistent distinction is that CNT diameter and length are generally correlated with toxic effects, (i.e., fibrosis of the lung following aspiration or instillation bolus exposures to CNTs) (Manke et al., 2014; Xu et al., 2014; Poulsen et al., 2015). With regard to fiber diameter, high-diameter "thick" MWCNTs (greater than 40 to 50 nm) are semi-rigid and experimental preparations are often dispersed as individual fibers, while lower-diameter "thin" MWCNTs (less than 20 to 30 nm) or SWCNTs are curly and almost always form tangled, amorphous agglomerates of some kind. There is consistent evidence that simple acid-based functionalization (carboxylation) as it increases the solubility, it decreases the inflammatory potential of CNTs (Lee et al., 2015; Hamilton et al., 2013; Silva et al., 2014). As of yet, the data demonstrating functionalization effects on toxicity potential are largely limited to carboxylated examples; there is some evidence that other functional groups may have the opposite effect on

[1]raw: "As-delivered" CNTs that have not been washed to remove impurities.
pristine: Unmodified CNTs with no surface decoration or functionalization. Synonyms: unmodified, undecorated
purified: CNTs processed to remove metal contaminants, usually by acid treatment (common) or high heat (less common). Acid treatment may introduce oxidation and acid-functionalization of the CNT surface. Synonyms: acid-treated, acid-washed, oxidized functionalized: CNTs modified with functional groups. The chemical process normally involves acid treatment, so functionalized CNTs may be assumed to be purified

biocompatibility (Zhang et al., 2010). A review of the experimental literature since 2010 is provided below.

4.1.1.1 SWCNT

Manke et al. (2014) tested the effect of fiber length on the fibrogenic potential of SWCNTs using *in vitro* fibroblast cultures, showing that long SWCNTs (~12.31 μm) were more potent than short (~1.13 μm) in inducing collagen production and transforming growth factor beta (TGF-ß) in fibroblasts. The long SWCNTs were also more fibrogenic when measured in a follow-up mouse lung 90 day pharyngeal aspiration study.

Lee et al. (2015) tested the immunotoxicity of carboxylic acid (COOH)-functionalized SWCNTs in the spleen of mice following IV exposure. The independent variable was degree of carboxylation of the nanotube surface. Increased carboxylation of the CNT surface decreased the level of cytotoxicity, proliferation, and inflammation induced in the spleen; this was attributed to greater dispersion of the CNTs in biological media.

Fujita et al. (2015) tested toxicity differences between SWCNTs aggregated as long, thick bundles (400 to 600 nm diameter, 1.5 to 1.7 μm length) and shorter, thinner bundles (130 to 170 nm diameter, 0.36 to 0.51 μm length) *in vivo* and in rat alveolar macrophage cultures. The different dispersions were obtained from the same stock using different-sized pore filters and were stabilized using 1% albumin. Rats were exposed to 1.8 mg/kg bw IT (one-time exposure) and observed for up to 90 days. Long, thick- or short, thin-bundled SWCNTs caused similar responses in rat lungs, but the thin-bundled SWCNTs induced more cells in bronchoalveolar lavage fluid (BALF), predominantly neutrophils. In rat alveolar macrophage cultures, thick-bundled MWCNTs induced significantly more intracellular reactive oxygen species (ROS) release as well as of macrophage inflammatory protein 1-alpha (MIP-1α).

Park et al. (2016) tested whether acid-treatment purification of a raw (unpurified) SWCNT stock would affect immune system or reproductive toxicity in a mouse model following instillation in the lung. Acid treatments are typically used to remove metal contamination from raw CNT materials, although it is not clear whether the treatment used in this study had other effects such as oxidation/functionalization. For animal exposures, SWCNT were delivered via a single IT dose in Pluronic F127 surfactant; BALF and lung histology were analyzed 90 days post-exposure. Although the study hypothesis addressed iron (Fe) contamination as a variable, the starting level of metal contamination reported for the unpurified SWCNT was already quite low (0.12% Fe, <0.03% other metals), leaving only a small 0.1% difference in iron contamination between the raw and purified samples. The purified SWCNTs nonetheless induced less lactate dehyrogenase (LDH) in BALF than unpurified SWCNTs, however, the purified SWCNTs appeared to cause slightly more total cell accumulation in BALF. Both SWCNT types (purified and unpurified) decreased the pregnancy rate, with a greater decrease seen following exposure to unpurified SWCNTs.

4.1.1.2 MWCNT

Zhang et al. (2010) reported on the development of an 80-member CNT library of surface-functionalized CNT variants built on a common MWCNT precursor that had a mean diameter of

40 nm. The purpose was to identify biocompatible variants on the basis of their functional groups. The variants were tested for protein binding, cytotoxicity (*in vitro* viability), and immunotoxicity (nitric oxide response in macrophages). Certain functional groups were identified as being significantly less biocompatible than others based on experimental results. These commonly included unsubstituted aromatic ring moieties, which were associated with higher protein binding affinity for hemoglobin (HB), carbonic anhydrase, and chymotrypsin. The most favorable biocompatibility scores went to variants featuring a specific monochlorinated aromatic ring moiety that was associated with lower protein binding affinity.

Kim et al. (2011a) tested the effect of MWCNT aspect ratio on genotoxicity using Ames, chromosome aberration, and *in vivo* micronuclei tests. The authors tested two MWCNTs of identical diameter but different lengths. It was found that the longer MWCNTs caused greater genotoxicity in the assays compared to the shorter variant.

Murphy et al. (2011) tested clearance of MWCNTs of varying lengths from the pleural cavity of mice following intrapleural injection of a 0.5% albumin suspension. Longer MWCNT examples were poorly cleared compared to shorter variants.

Tabet et al. (2011) tested the effects of surface coating on MWCNT toxicity using *in vitro* and *in vivo* tests. MWCNTs were tested as either pristine or 50/50 wt% coated with acid- or polystyrene-based polymer. In both test systems, *in vitro* macrophages and mouse lungs (wherein MWCNTs were delivered via IT), acid-based coating increased MWCNT-induced cytotoxicity, oxidative stress, and inflammation compared to pristine MWCNTs, while the polystyrene-based coating decreased toxic effects.

Muhlfeld et al. (2012) compared the effects of a 10 µg dose of either long, thick (mean 13 µm length, ~85 nm diameter, semi-rigid fibers)) or short, thin (1 to 5 µm length, ~15 nm diameter, tangled agglomerates) MWCNTs administered to mice via OPA in a 0.5% albumin suspension. Both MWCNT types caused inflammation, but only short MWCNTs caused an increase in septal wall thickness 28 days following exposure. Long MWCNTs were also reported to cause type II pneumocyte hypertrophy, but type II pneumocyte hyperplasia and granulomatous inflammation (typically seen following MWCNT exposure in the lung) were not seen after exposure to either material. The increase in septal wall thickness was examined by TEM and appeared to be due to a fibrotic response, running against the general principle that fiber length and diameter are associated with fibrosis. The authors noted that unlike the long MWCNTs, the short MWCNTs used contained 1.79% Fe and were shown to produce ROS based on electron resonance data, suggesting that the fibrotic reaction could be tied to iron-induced oxidative stress. The surface area of the short MWCNTs, although not reported, was also presumably much higher than the long, thicker-walled example.

Bussy et al. (2012) performed a study testing the effects of ultrasonic shortening on the inflammatory effects of MWCNT in murine macrophages *in vitro*. MWCNTs subjected to sonication were shorter (4.8 µm mean length, 37.5 nm diameter) than the unsonicated particles (9.5 µm mean length, 42 nm diameter) and were affected by molecular defects, chemical oxidation, and accumulation of iron on the surface. These shortened MWCNTs induced higher levels of cytokine and oxidative stress responses than the unsonicated CNTs. One possible

explanation given by the authors was the presence of defects induced by sonication, which was documented by X-ray diffraction data. Molecular defects in the π-hybridized nanotube surface had been shown by Muller et al. (2008) to augment the inflammatory potential of MWCNTs. While this explanation was not specifically tested, experimentation with iron chelators ruled out iron accumulation as the cause of increased toxicity by sonicated MWCNTs. The extent of molecular defects induced by sonication varies between different materials and preparations.

Fenoglio et al. (2012) tested MWCNT diameter as a factor in acute lung toxicity (via IT administration) using animal and *in vitro* models. Effects of two MWCNT types with similar characteristics apart from diameter (9.4 vs. 70 nm) were assessed using BALF analysis in rats and *in vitro* tests for cytotoxicity, uptake, and oxidative stress in murine alveolar macrophages. Both MWCNT types were taken up into cells, but low diameter CNTs caused more *in vitro* cytotoxicity than thicker-diameter as well as more LDH and cell accumulation in BALF samples. The authors note that the thick-diameter MWCNTs underwent acid-based purification, while low-diameter was heat-purified. We note that these purification treatments could plausibly have skewed results if the acid-purified MWCNTs underwent functionalization, which would be expected to lead to lower toxicity.

Wang et al. (2012) conducted a study on the effect of dispersants on MWCNT toxicity. A MWCNT material (20 to 30 nm diameter) was dispersed in aqueous media using either bovine serum albumin (BSA) or pluronic F108, a non-ionic polyalkene oxide surfactant. Following OPA lung exposure in mice, pluronic-dispersed MWCNTs caused less fibrosis and induced less interleukin-1 beta (IL-1ß) than BSA-dispersed MWCNTs. The authors determined through functional inhibition experiments that the decreased toxicity of pluronic-dispersed MWCNTs was due to decreased cell uptake and increased stability of lysosomes.

Hamilton et al. (2013a) conducted a study of unpurified, purified, and carboxylated forms of three different MWCNT size variants in THP-1 human monocytes and seven-day exposures in mice using single-dose OPA. Diameters ranged from 16 to 32 nm, lengths ranged from 760 to "too long to measure" nm, and surface areas ranged from 140 to 217 m^2/g. Contaminants of unpurified MWCNTs included iron (0.51 to 0.85%) and nickel (0.47 to 1.19%). Purified MWCNT were generated using dilute nitric acid and COOH-MWCNTs were generated using concentrated nitric and sulfuric acids. All MWCNTs had similar tangled morphologies. Marked differences in *in vivo* lung inflammation and *in vitro* inflammasome activation were not apparent, and physicochemical differences between variants were themselves not extensive, but the authors nonetheless found positive correlations between MWCNT size and toxicity where long, narrow CNTs were more toxic than shorter ones. Carboxylation of the MWCNTs sharply attenuated inflammasome activation in monocytes *in vitro* (this variable was not tested *in vivo*).

Hamilton et al. (2013b) conducted an additional study using *ex vivo* alveolar macrophages and human THP-1 cells exposed to unpurified MWCNTs, purified MWCNTs, and COOH-functionalized MWCNTs prepared from the same material. Purified MWCNTs were prepared using sonication in a hydrochloric acid bath, and COOH-MWCNTs were generated from purified CNTs using concentrated nitric acid (no further details were given). Scanning electron microscopy (SEM) showed the MWCNT variants to be 20 to 30 nm in diameter and had a tangled morphology that precluded measurement of length. Detailed analysis of defects showed

that purified MWCNTs carried the lowest extent of defects in the tube structure. Results from exposure of mouse alveolar macrophages and human THP-1 cells to albumin-dispersed MWCNTs showed that unpurified MWCNTs induced the greatest toxicity, purified slightly less, and carboxylation again attenuated toxicity to levels approximating controls.

Lee et al. (2013) tested impacts on pulmonary surfactant following administration of short (0.94 μm mean length) or long (3.4 μm mean length) MWCNTs derived from the same starting material (44 nm diameter). Wistar rats were exposed to a single dose of 0.2 mg via IT and BALF was analyzed up to 1-year post-exposure. As in similar studies, markers of inflammation in BALF were slightly higher following exposure to long as compared to short MWCNTs. Levels of surfactant protein D (SP-D) were increased in BALF less than 7 days following short MWCNT exposure, and to a lesser extent after long MWCNT exposure. Surface tension values in BALF were decreased following MWCNT exposures, but long MWCNTs decreased surface tension to a greater extent compared to short MWCNTs. This was in contrast to the greater SP-D increases following short MWCNT exposure, but the authors acknowledged that surface tension is also affected by BALF total protein (inconclusive differences measured between short vs long groups) and surfactant proteins B & C (not measured).

Yu et al. (2013) exposed mice to 100 μg one-time doses of either pristine (untreated) or acid-treated MWCNTs (12.5 nm mean diameter) via IT and analyzed markers of autophagolysosome accumulation in lung tissue after 6 months. Pristine MWCNTs caused significantly increased markers of both autophagy and cell proliferation in lung tissue compared to levels observed from acid-treated MWCNT exposure. Epithelial hyperplasia and adenoma/adenocarcinoma were also seen following MWCNT exposure, and these were more pronounced in pristine MWCNT-exposed animals.

Ohba et al. (2014) tested the difference in toxicity between two MWCNT variants, a 'long' (8 μm length, 150 nm diameter, as stiff, semi-rigid fibers) and a 'short' (3 μm length, 15 nm diameter, as tangled agglomerates). MWCNTs dispersed in Pluronic F68-supplemented medium were administered by microsprayer to the upper trachea of rats on days 1, 4, and 7 in 0.3 ml doses of 250 μg/mL MWCNTs. Long MWCNTs caused loss of ciliated epithelium and short MWCNTs caused granulation of tissue on day 8 post-exposure. A later study (Xu et al., 2014) by a related group from the same institution, explored the extent to which size differences of the aforementioned MWCNTs played a role in early markers of mesothelial disease expected to be induced by exposure. Following 24 weeks of biweekly exposures (0.5 ml/dose of 250 μg/mL in Pluronic F68 vehicle) via tracheal microspraying, the long, stiff MWCNTs translocated to the parietal pleura and were associated with fibrosis, mesothelial cell proliferation, and inflammatory cytokines recovered in pleural lavage. The short, tangled MWCNTs did not cause pleural fibrosis, proliferation, or significant inflammation in pleura, but induced higher levels of inflammatory cytokines in lung tissue than the long MWCNTs. The different effects of these MWCNT examples may be linked to their contrasting morphology, where the longer, thicker example consists of stiff fibers and the shorter, thin-walled example forms tangled, globular agglomerates.

Silva et al. (2014) conducted a study testing three similar MWCNT types (20 to 30 nm diameter) in both intratracheal and inhalation exposures in rats. One MWCNT variant was delivered

unpurified (4.5% Ni, 0.76% Fe), another was purified using acid washing, and a third was carboxylated using concentrated acid. Animals were exposed by IT (single dose) or inhalation (single 6h exposure) and BALF and lung histology analyzed 21 days following exposure. A thermogravimetric method was used to determine lung burden. The intratracheal dose was 200 μg, while the retained inhaled dose was 380 μg. The study results suffer from what appears to be a high level of background pathology in the rat lungs; however, the results are generally consistent with the view that purified MWCNTs are more biocompatible than unpurified, while functionalization with carboxyl groups exhibit less toxicity compared to unmodified MWCNTs. Another effect that was apparent and related to material properties was that dispersion of MWCNTs in an albumin- and phosphocholine-supplemented medium prior to aerosolization (in effect creating a coating) attenuated lung pathology and BALF macrophage levels compared to water-dispersed MWCNTs.

Taylor et al. (2014) tested whether aluminum oxide coating would influence the toxicity of MWCNTs, and whether *in vitro* methods showing a difference were predictive of similar responses *in vivo*. MWCNTs (~50 nm diameter, 0.5 to 40 μm length) were coated with aluminum oxide nanoparticles, which increased the fiber diameter by ~20 nm. The coating potentiated the production of IL-1ß by THP-1 human monocytes and primary human monocytes *in vitro*, but decreased release of interleukin-6 (IL-6), tumor necrosis factor (TNF), and Th1-promoting cytokine osteopontin. *In vivo*, aluminum oxide coating decreased CNT-induced fibrosis 28 days following aspiration exposure, but did not significantly affect inflammatory markers in BALF, as compared to uncoated CNTs.

Esposito et al. (2015) performed a modified quantitative structure-activity relationship (QSAR) study using an 80-member library of surface-functionalized MWCNTs and tested these materials for protein binding to four proteins, as well as cytotoxicity and induction of nitric oxide (NO) in macrophages (this library is different from that used in Zhang et al., 2010, summarized above). The aim of the study was to inferentially identify detailed interactions between CNT functional groups and the biological milieu. The study built on the work of previous QSAR studies that have associated specific molecular groups with toxicity and used this preexisting knowledge to investigate the differences in toxicity (binding activity) between functional groups decorating MWCNTs in different conformations (i.e., various peptide-like and branched-chain molecules). The study found that protein binding and *in vitro* immunogenicity were increased by functional groups that had an extended conformation perpendicular to the MWCNT surface, such as large branched-chain molecules. Cytotoxicity (decreased cell viability) varied widely among examples and the most cytotoxic subgroup of MWCNTs were those decorated with functional groups in collapsed, tight conformations, where the presence of hydrophobic moieties encouraged folding into a closed structure. These different outcomes could plausibly reflect differing modes of action due to physicochemical differences.

Poulsen et al. (2015) tested two MWCNT types, a small variant (11 nm diameter, 0.85 μm length, 87% pure) and a large variant (67 nm diameter, 4.05 μm length, 97% pure) in a toxicogenomics study of mouse lung tissue with exposure via IT. BALF, lung histology, deoxyribonucleic acid (DNA) damage, oxidative stress, and global gene transcription were evaluated up to 28 days post-exposure. The two MWCNT types caused similar inflammatory responses as measured in BALF, but large MWCNTs caused a greater prevalence of eosinophils

at 28 days post-exposure. Large MWCNTs appeared to cause significant alveolar septal fibrosis, while limited fibrosis was observed following exposure to small MWCNTs. Large MWCNTs also produced bronchoalveolar granulomas in the lung, while small MWCNTs caused smaller foci and diffuse alveolar hyperplasia and septal thickening. The effects of exposure on gene expression were measured using microarrays to quantify transcript abundance and results were presented as activation status of biological functional pathways, as indicated by the gene changes and their direction. Both MWCNT types had similar effects on functional pathways, except that large MWCNTs upregulated pathways involved in fibrosis. This was consistent with apical endpoints, and underscores the link between semi-rigid morphology and fibrosis as seen in experimental models.

The relative toxicities of 10 MWCNT variants of varying dimensions and functional groups in a mouse model of lung exposure were tested by Poulsen et al. (2016). MWCNTs were delivered via IT and changes were assessed in BALF collected up to 92 days post-exposure. Inflammatory markers in BALF were most accurately predicted by surface area. Genotoxicity, also measured in BALF cells, was negatively associated with surface area and positively associated with MWCNT diameter. Increasing functionalization by hydroxyl and carboxyl groups decreased the extent of inflammation.

4.1.2 Meta-analyses and Assessments

In addition to the above experimental work, recent literature includes several assessments and meta-analyses of primary results examining the implications of physicochemical variation in CNTs. In one such analysis, Birch et al. (2013) assessed the relationship between particle surface area and other physicochemical properties in a set of MWCNT and SWCNT examples obtained from commercial sources. This was performed because surface area was recognized as a significant predictor of toxicity for some nanomaterials. However, the measured surface area of CNTs may be much higher than the effective surface area because of agglomeration. In many cases, the surface area specified by the manufacturer (which is often used for investigators' report of material characteristics) may not reflect the toxicologically active surface area of the material because this information often does not reflect the degree of aggregation or agglomeration that determines the effective surface area directly related to toxicity in experiments. The assessment found that the number of walls, diameter, impurities, and surface coating/functionalization all affected the effective (measured) surface area.

Two other recent analyses have attempted to build statistical associations between physicochemical properties of CNTs and toxicity. Gernand and Casman (2014) reported on a meta-analysis of 17 CNT toxicity studies (nine single-walled and 11 multi-walled) from 2004 to 2011 focusing on lung toxicity measured *in vivo* following inhalation, IT or OPA exposure. Associations between test material characteristics and toxicity endpoints measured in BALF (numbers of macrophages and neutrophils, level of LDH and total protein) were assessed using regression tree and random forest methods. These predictive models are considered ideal for quantitative association assessments that must rely on sparse data sets. In the analysis of CNTs, the highest-scoring physicochemical predictor of inflammatory responses in BALF was metal impurities, specifically cobalt (other metals, such as iron, were not correlated). Diameter, which ranged from 1 to 35 nm, was slightly correlated with the protein level in BALF, and length (reported as ranging from hundreds of nm to 100 μm) was slightly negatively correlated with

LDH (cell damage marker) levels. The size of CNT aggregates was positively associated with leukocytic response and negatively correlated with LDH (i.e., cell damage). The data were not sufficient to evaluate a relationship between mass median aerodynamic diameter (MMAD) and toxicity. The findings regarding the influence of cobalt at common MWCNT-borne levels on toxicity, are significant considering that a number of toxicity studies have used material with cobalt trace contamination (Ma-Hock et al., 2009a; Pauluhn, 2010), but overall the results of the study do not agree with the principle that length and diameter contribute to toxicity. Wang et al. (2014) included original experimental data in an analysis of a relationship between nanomaterial physicochemistry and toxicity using a principal component analysis. Toxicity of a panel of nanomaterials was assessed in *in vitro* tests for cytotoxicity, apoptosis induction, hemolysis, and mitochondrial stress. Although only one CNT example was tested, together with results from various metal nanowires, the data supported length as a determinant of toxicity for fiber nanoparticles in general.

4.1.3 Summary

For the most part, it is not conclusively known how variation in given physicochemical aspects relates to toxicity. Quantitative analyses of physicochemical profile and toxicity have made progress, but prediction of toxicity based on intrinsic properties remains difficult beyond some basic generalizations supported by data reviewed here. It may be suggested that thick-walled (>50 to 60 nm diameter) MWCNTs dispersed as semi-rigid fibers are more likely to induce fibrogenic effects in epithelial and mesothelial membranes compared to thin-walled, curly MWCNTs, and that fiber length is also a factor for this outcome. The differences in toxic effects may relate to MWCNT morphology, where thicker-walled variants are usually high-aspect-ratio particles and thin-walled form tangled, amorphous agglomerates hundreds of nm to μm in diameter that are not fiber-like. This would appear to relate the case of MWCNTs to the historical understanding that fiber shape and rigidity are fundamental to the fibrogenic toxicity associated with other insoluble fiber examples, such as amphibole asbestos (Donaldson et al., 2006). The tangled agglomerated variants are often shown to have greater inflammatory effects than the non-agglomerated variants (Fenoglio et al., 2012; Hamilton et al., 2013; Ohba et al., 2014). A tangled-form MWCNT was also reported to be fibrogenic in one *in vivo* study (Muhlfeld et al., 2012), but this was based only on an increase in septal wall thickness and fibrosis (collagen deposition) was not specifically assessed. Poulsen et al. (2015) similarly found that tangled-type MWCNTs increased septal wall thickness but only long, semi-rigid MWCNTs caused pronounced interstitial deposition of collagen as evaluated using histochemical staining. Poulsen et al. (2016) identified thick-walled, semi-rigid MWCNT variants as genotoxic compared to tangled variants. This study also correlated surface area with inflammatory markers in BALF, and high surface area is intrinsic to thin-walled variants adopting the tangled morphology.

Simple acid functionalization (oxidation of the CNT surface with –OH and –COOH groups) is consistently observed to markedly attenuate inflammatory effects *in vivo* and *in vitro*, which appears to be due to the intrinsic solubility of these variants compared to unfunctionalized CNTs. More elaborate functional groups may have a variety of effects on toxicity (Zhang et al., 2010; Esposito et al., 2015) that may be difficult to predict, although solubility in general appears to promote biocompatibility.

One meta-analysis raises a concern that metal impurities may factor into toxicity results in ways not previously appreciated, specifically that low levels of cobalt contamination previously presumed inert may account for a significant portion of CNT-induced toxicity (Gernand and Casman, 2014). This finding seems to have implications for efforts to measure CNT dose-response toxicity, as quantification of CNT-entrained Co in tissue (via ICP-MS) is considered one of the few accurate ways to measure CNT burden in tissue (Pauluhn, 2010). However, the assessment is limited by the low number of studies in this case, and the association could reflect some other quality common to commercial MWCNTs manufactured using a cobalt catalyst. In general, this study disagreed with the premise of CNT length and diameter being modifiers of toxicity, which runs against the general consensus found in other studies. This may reflect the importance of particle morphology (e.g., bundled vs. amorphous and tangled), and if so, attempts to assume simple relationships between a given metric (e.g., length) and toxicity without considering that final morphology of CNT particles may fail to consistently predict toxicity. Other properties, such as surface defects and oxidation state, have also been shown to influence toxicity in experimental literature (Muller et al., 2008; Li et al., 2013; Jiang et al., 2017). One aspect that is not well-captured is the extent to which defects in the CNT surface may be introduced by dispersing MWCNTs in suspension via sonication. Defects following sonication are documented in some cases and not found in others, and in many studies is not characterized at all. This carries more implication for studies using CNTs in suspension, as sonication is rarely used in preparations of CNTs as aerosols.

The summarized work supports the importance of fiber diameter, length, trace metals, and agglomeration/morphology as modifiers of toxicity in some way. In this report, diligence was applied to documenting CNT diameter, length, surface area, contaminants (purity), and agglomeration in data tables and summaries. Most investigators report these metrics in some form and their relevance to toxicity has good experimental support. Emphasis has also been placed on testing nanomaterials in a form that is consistent with the physical conditions in which they are thought to present a hazard (Pettitt and Lead, 2013), as well as characterizing test materials in the same form used for experimentation (i.e., post-processing).

Experimental studies often use bolus exposures (instillation or aspiration of liquid particle suspensions into the lung or pleura) instead of inhalation exposure for evaluation of lung effects. Studies have shown that the use of dispersants in suspension media can have a considerable effect on CNT toxicity, and some surfactant dispersants used in toxicology studies can attenuate cellular toxicity by stabilizing interactions with cell membranes (Wang et al., 2012; Silva et al., 2014). The MMAD is an important factor for inhalation toxicity of particles, but is not applicable to bolus exposures in suspensions. These methodology differences cause uncertainty in applying the results of the above work to meaningful conclusions about CNT inhalation toxicity. For the current assessment, documentation of diameter, length, surface area, contaminants, and agglomeration are considered core characterization for key studies. Inhalation studies should also document MMAD and the geometric standard deviation (sigma g). The toxicological differences between thick-walled semi-rigid MWCNTs and thin-walled agglomerate-forming variants can only be ascertained with data from well-documented testing of representatives from both groups. Dose-response data for thick-walled CNTs (which are usually 60 nm or greater, but might be conservatively assumed to be MWCNT of greater than 30 to 40 nm diameter) are needed as a minimum because investigation of only thin-walled MWCNT may

underestimate the ability of thick-walled CNTs to cause lung remodeling and fibrosis at comparable doses.

4.2 Toxicokinetics of CNT

4.2.1 Single-walled CNT

4.2.1.1 Oral Exposure

No oral exposure studies in humans were found in Versar (2012) or in recent literature.

Prior to 2010, only one study was published addressing kinetics of SWCNT by the oral route (Versar, 2012). Wang et al. (2004) administered radiolabeled hydroxyl-SWCNT (OH-SWCNT, diameter of ~1.4 nm, mean length of 340 nm) to male KM mice (5/group) by gavage. OH-SWCNTs were detected primarily in stomach, bone, kidney, and lung on orders of 10's to over 100 ng per gram of tissue. Lesser amounts of OH-SWCNTs were found in the blood/skin, heart, liver, spleen, intestine, muscle, or brain.

No studies published after 2010 addressing biokinetics of SWCNT by the oral route were identified. Available studies found no evidence of systemic toxicity following exposure via the oral route.

4.2.1.2 Inhalation Exposure

No studies specifically addressing SWCNT biokinetics in humans or animals following inhalation exposure could be found in the literature, either before (Versar, 2012) or after 2010. Some information can be gleaned from studies designed for other purposes.

In a study examining respiratory toxicity one year following a five-day inhalation exposure to 5 mg/m^3 SWCNTs, Shvedova et al. (2014) (Table 10) observed SWCNT in tracheobronchial lymph nodes of mice, indicating the possibility of extrapulmonary transit of SWCNT from lungs. The SWCNT were fibers 1 to 4 nm in diameter (1 to 3 μm length) and mostly aggregated into bundles and ropes around 65 nm in diameter. One other inhalation study (Morimoto et al., 2012) was not informative regarding SWCNT kinetics.

Sturm (2016) conducted an *in silico* assessment of SWCNT and MWCNT deposition in the human lungs by assuming a stochastic structure of the bronchial network where particle transport takes place along randomly selected paths. Particle deposition in the entire lungs was approximated by using the aerodynamic/thermodynamic diameter concept and related empirical deposition formulae. Deposition was modeled for SWCNT variants of diameter from 5 to 10 nm and up to 10 μm long. The authors found a significant dependence of CNT regional deposition on the size of the particles and breathing conditions affecting flow rate in the model. Based on the modeling, the authors concluded that extremely small-diameter CNTs (~1 nm) are primarily filtered in the extrathoracic airways, intermediate diameter CNTs (~10 nm) exhibit a preference to deposit in the alveoli, and large diameter CNTs (~100 nm MWCNTs) are marked by minimal

deposition. SWCNT length was described by aspect ratio in results, and total deposition of 1:1 vs. 1:1000 aspect ratio SWCNTs did not differ by more than 18% of inhaled particles for a given diameter group. The modeling treated CNTs as dispersed fibers and did not appear to account for agglomeration. The conclusions could, therefore, be considered informative for dispersed or tightly bundled SWCNTs, but may not accurately predict the deposition of tangled agglomerates and non-fibrous aggregates.

4.2.1.3 Lung Instillation of SWCNTs

Matthews et al. (2013) examined the extent of pulmonary translocation of SWCNTs from lung airways of rats. SWCNTs (1.2 to 1.5 nm diameter, 2 to 5 μm in length) and polyethylene glycol (PEG)-conjugated SWCNTs (4 to 5 nm diameter, 0.5 to 0.6 μm length) were used. These investigators used an ex vivo isolated perfused rat lung (IPRL) model that retains the intact lung architecture to evaluate upper limits of potential translocation of SWCNTs. Doses (100 μg) of SWCNTs were instilled into the airways of the IPRL and the pulmonary translocation of SWCNTs to a modeled circulatory compartment was quantified based on SWCNT-bound nickel (Ni). Results showed a small increase in Ni in the circulatory compartment, but this result was not statistically significant. The authors concluded that SWCNT translocation from the airways across an intact pulmonary barrier into what would be the systemic circulation would be no greater than 0.05% of the instilled dose over 90 minutes, which was the limit of detection (LOD) for this method. Using this as a theoretical maximum, further pharmacokinetic simulation incorporating a term for mucociliary clearance estimated that over a 14-day post-exposure period the maximum approximate cumulative pulmonary translocation from rat lung would be less than 0.15% of a 100 μg deposited dose.

Metabolism of SWCNT may take place through degradation by hypochlorite that is generated by neutrophil myeloperoxidase (MPO), as demonstrated by Kagan et al. (2010). Shvedova et al. (2012) used *in vivo* knockout models to demonstrate that MPO-deficient mice had several fold higher lung burdens of SWCNTs compared to wild type mice 28 days following a 40 μg exposure via instillation in saline suspension. Other peroxidases have been shown to be capable of degrading SWCNT as well (Vlasova et al., 2011). This suggests degradation in the lung as a significant clearance mechanism for SWCNTs.

4.2.1.4 Dermal Exposure

No studies assessing SWCNT absorption through human or animal skin were found. A recent critical review (Filon et al., 2016) observed that rigid nanoparticles less than 45 nm in cross-sectional size have the ability to penetrate skin. SWCNTs are, in general, non-rigid particle fibers, and individual fibers and small agglomerates may be less than 45 nm in cross-sectional size. However, the dimensions of the fibers make it unlikely that significant penetration of SWCNTs will occur in contact with unbroken skin. Although very small agglomerates or truncated fibers could conceivably permeate the epidermis, the possibility of significant systemic absorption of SWCNTs through dermal exposure is not likely.

4.2.1.5 Other Routes of Exposure

Principi et al. (2016) exposed male and female MITO-Luc and CD1 mice (aged 6 to 8 weeks;

9/group), to 0.16 mg/kg, 1.6 mg/kg, or 6.4 mg/kg of SWCNTs (1.2 nm diameter, 2 to 5 μm length) via the tail vein, either once or once every 3 weeks for 9 weeks. Specifically, these investigators monitored and traced the accumulation of SWCNTs in different organs and the subsequent biological responses. SWCNTs accumulated in the lungs, spleen, kidneys and liver. A dose- and time-related accumulation in the liver was associated with increases in metabolic markers associated with liver damage.

4.2.1.6 Summary

Data on toxicokinetics of SWCNTs are limited. Absorption of SWCNTs via the oral route appears to be minimal, although there is evidence that a small amount of individual fibers and small aggregates may enter the bloodstream following oral exposure. Very little data are available for assessing the potential for systemic absorption of particles through skin, although the risk of significant exposure through this route is anticipated to be relatively low. Inhaled and instilled SWCNTs deposit in the respiratory tract, and absorption is largely limited to the lung-associated lymph nodes (LALN). SWCNTs in circulation become entrained in liver, kidneys, and spleen. Experimental data informative of SWCNT lung clearance is limited, but one study in mice (Shvedova et al., 2012) reported ~80% clearance of a 40 μg dose of SWCNTs 28 days following OPA. The results of that study also suggested metabolism of SWCNTs by neutrophil MPO and other peroxidases is possible and may be a significant mechanism of clearance from the lung. Data on excretion of SWCNTs were not available.

4.2.2 Multi-walled CNTs

Several studies have been conducted in humans and experimental animals investigating the biokinetics of MWCNT. These studies range from theoretical, to ex vivo, to *in vivo*. Comparisons among species and nanoparticle types are difficult due to physicochemical variation among test materials. MWCNTs vary in diameter; thin-walled (less than ~30 nm diameter) MWCNTs usually have a tangled morphology, while thick-walled are rigid fibers.

4.2.2.1 Oral Exposure

No studies investigating MWCNTs biokinetics by the oral route were located by the original report (Versar, 2012). Morphology of MWCNTs is expected to affect tissue translocation. Thicker MWCNTs (greater than 40-50 nm diameter) individually dispersed as semi-rigid fibers may passively penetrate barriers, whereas thin MWCNTs (<less than ~30 nm diameter) usually have a curly morphology and are tangled into amorphous agglomerates that are not expected to translocate in the absence of an active mechanism.

In literature reviewed after 2010, no studies specifically designed to evaluate MWCNT localization following oral exposure were found. Two studies investigating toxicity via the oral route inform the biokinetics. Golokhvast et al. (2013) exposed mice to MWCNTs (18 to 20 nm diameter, length not reported, surface area of 130 m^2/g, Fe 0.21%, Co 0.12%) in food at 500 mg/kg/d for 6 consecutive days. MWCNTs in the form of 10 to 20 μm aggregates were observed in epithelial cell cytoplasm and nuclei in the small and large intestine starting at day 2. MWCNTs were not observed in the spleen or kidneys. Systemic toxic effects were minimal, but

included lymphoid hyperplasia in the gastrointestinal (GI) wall and spleen. Awasthi et al. (2013) exposed mice via the "oral route" to up to 100 mg/kg bw (single dose) MWCNTs (diameter 20 to 30 nm, length 5 to 50 µm, acid-washed and HNO3/H2SO4-oxidized) and examined livers up to 28 days later. Although mild inflammatory effects were observed in the liver, CNT particles were not observed in hematoxylin and eosin (H&E)-stained liver (at 63x objective magnification).

The limited available oral biokinetic data do not show evidence of systemic absorption/uptake of MWCNTs via oral exposure. However, the available data are not quantitative and the materials tested in these studies are limited to thin-walled fibers that are usually present as agglomerates. The likelihood of systemic absorption following exposure to thick-walled, semi-rigid MWCNT variants cannot be gauged from the current data.

4.2.2.2 Inhalation Exposure

Studies available prior to 2010 informing MWCNT biokinetics following inhalation exposure are limited to two toxicity studies (Ellinger-Ziegelbauer and Pauluhn, 2009; Ryman-Rasmussen et al., 2009a; as reviewed in Versar, 2012). Both of these studies showed that MWCNTs accumulated in lungs and slowly translocated to LALN over a period of months.

The toxicokinetics of inhaled MWCNTs is further explored in several toxicity studies published after 2010, as well as in studies specific to CNT biodistribution. The results reported in post-2010 toxicity studies are consistent with the earlier studies, in that MWCNTs accumulate in the lung and slowly translocate to lymph nodes, with little distribution to other tissues.

Pauluhn (2010) exposed rats to MWCNT (~11 nm diameter, length uncertain, delivered as micronized dust-like aggregates 2 to 4 µm in size with a MMAD of 2.84 µm, geometric standard deviation [GSD] = 2.04) via nose-only inhalation for 13 weeks. MWCNT lung burden and localization were determined by quantification of trace Co that the manufacturing process used to initiate/catalyze MWCNT growth. It is known that some proportion of the Co remains attached to the initiating terminus of the MWCNTs. MWCNTs manufactured by this process contained 0.53% Co; it was determined that 0.115% by weight consisted of attached, non-leachable Co that therefore could be used as a surrogate marker for MWCNT disposition in the body. Cobalt was quantified in left lung lobes and LALN at weeks 8, 13, 17, 26, and 39. Lung elimination half-times of Co were 151, 350, 318, and 375 days following exposure to 0.1, 0.4, 1.5, and 6 mg/m^3, of MWCNTs, respectively. Cobalt was detected in LALN following exposure to 1.5 and 6 mg/m^3.

Pauluhn and Rosenbruch (2015) further studied the impact of agglomeration/aggregation on tissue distribution of the above MWCNT stock following inhalation. The specific focus was on the comparative inhalation dosimetry and kinetics to better understand the cause of putative differences in pulmonary toxicity from exposure to dry, undispersed and dispersed (wetted) formulas of MWCNTs. 'Dry' aerosols were generated from a dust of micronized bulk CNTs, while wet aerosols were produced from nebulization of a CNT suspension "rigorously dispersed" in 2.9% aqueous sodium carboxymethyl cellulose (CMC), which is a commonly used dispersant preparation for nanomaterial studies. Rats were nose-only exposed to dry- and CMC-dispersed CNT aerosols for 6 h at 25 to 30 mg/m^3. Time-course changes of MWCNT retained in the lung

were measured using an optical method for quantifying elemental and total carbon in digested tissues during a post exposure period of 3 months. The initially deposited pulmonary dose of MWCNTs was three times higher following CMC-dispersed MWCNTs when compared with those of dry-dispersed at essentially similar inhalation chamber concentrations. The elimination half-time of dry- and CMC-dispersed MWCNTs was 87 and 46 days, respectively.

Umeda et al. (2013) exposed rats to MWCNTs (88 ± 5 nm mean diameter, 5.0 ± 4.5 μm length, surface area 24 to 28 m^2/g) via whole-body inhalation at 0, 0.2, 1, or 5 mg/m^3 for two weeks. Unprocessed CNTs were aerosolized into particles with an MMAD of ~1.3 μm and a GSD of 2.4 μm at 0.2 mg/m^3 to 3.4 μm at 5 mg/m^3. Deposition of CNTs, assessed using conventional microscopy of tissue sections, was confined mostly to the lung. CNTs were observed in the nasal cavity and bronchiolar lymphoid tissue only in rats exposed to 5 mg/m^3. After a 4-week post-exposure recovery, CNTs were seen in the bronchiolar lymphoid tissue of rats exposed to 1 mg/m^3, while rats exposed to 5 mg/m^3 showed CNTs in peritracheal (mediastinal) lymph nodes.

In a study investigating major routes of exposure following addition of MWCNTs (9.5 mean diameter, 1.5 μm mean length, surface area of 250-300 m^2/g) to bedding material of mice, Albini et al. (2015) found that CNT accumulation occurred primarily in the lungs, brain, and liver, with a small number of aggregates observed in the intestine and kidneys. Based on this, the authors concluded that the respiratory tract appeared to be the main route of entry, with little absorption occurring via the oral route, although it is not clear how this determination was made by the authors.

In Pothmann et al. (2015), rats were exposed to MWCNTs (~12 nm diameter, ~ 1 μm mean length, 225.6 m^2/g surface area, micronized/ball-milled from bulk) via inhalation (MMAD of 1.62 to 2.30 μm, GSD of 4.67 and 2.47, respectively) to doses of 0.05, 0.25 and 5 mg/m^3 for 90 days with a 90-day recovery period. Although lung burdens of CNTs were only estimated qualitatively as a part of histological examination, the CNT burdens in lung tissue at 0.05 and 0.25 mg/m^3 appeared to be lower after the 90-day recovery period compared to immediately after exposure. Lung burdens following 5 mg/m^3 exposure did not appear to decrease substantially during the 90-day recovery.

Kasai et al. (2015) exposed rats to MWCNTs (same characteristics as Umeda et al., 2013, above) via whole-body inhalation at concentrations of 0, 0.2, 1, or 5 mg/m^3 for 13 weeks. The MMAD of the aerosols was ~1.5 μm with a GSD between 2.5 and 3.0. CNTs were observed throughout the respiratory tract at all exposure concentrations. Higher concentrations (1 and 5 mg/m^3) increased the incidence of deposited CNTs being observed following exposure, especially in bronchiolar lymphoid tissue and mediastinal lymph nodes. In a follow-up study (Kasai et al., 2016) rats were exposed to the same MWCNT source and preparation methods for a 2-year period. The findings regarding deposition were similar, with single CNTs and aggregates observed in the lungs and mediastinal lymph nodes in a concentration-related manner. Only very small amounts of CNTs were seen outside of the respiratory tract and lymph nodes; however, CNTs and aggregates were observed in the spleen and liver. Single CNT fibers were also found in the kidneys, olfactory bulb, and brain. Lung burdens were measured using a semiquantitative manual counting process, and were similar in males and females on a body-weight basis.

Several studies published after 2010 have specifically assessed MWCNT distribution following inhalation exposure. Two studies (Mercer et al., 2013; Albini et al., 2015) have used semiquantitative light-microscopy counting methods to assess extrarespiratory distribution of inhaled MWCNT. These studies found that after lung and lymph nodes, the highest observed levels of particles were in the brain followed by lesser amounts in the kidney and liver. It is not known how translocation of freestanding CNTs and small aggregates to the brain occurs, but absorption and retrograde axonal transport though the olfactory nerves and transport of phagocytized CNTs in migrating microglia were suggested as possibilities (Albini et al., 2015). A third study undertook an *in silico* modeling of fiber deposition in human airways (Sturm, 2016).

Mercer et al. (2013) conducted inhalation exposure studies of mice to determine if MWCNTs (49 ± 13 nm width, 3.86 ± 1.94 length, 0.32% iron [Fe], surface area not reported) distribute to the tracheobronchial lymphatics, parietal pleura, respiratory musculature and/or extrapulmonary organs. Specifically, four groups of male C57BL/6 J mice were exposed in a whole-body inhalation system to either 0 or 5 mg/m^3 MWCNT aerosol for 5 h/d for 4 times/week for 3 weeks. Two groups of mice (one control and one exposed) were sacrificed after 1 day and two groups of mice (one control and one exposed) were sacrificed after day 336 of exposure. Lungs, lymph nodes and extrapulmonary tissues were preserved. MWCNT material in tissue was visualized using an enhanced darkfield microscopy method and particles/fibers were counted. Tracheobronchial lymph nodes were found to contain 1.08 and 7.34 percent of the lung burden at 1 day and 336 days post-exposure, respectively. Agglomerates of MWCNTs accounted for approximately 54% of lung burden. In contrast, only singlet MWCNTs were observed in the diaphragm, chest wall, liver, kidney, heart and brain. On average, there were 15,371 and 109,885 fibers per gram in organs outside of the lung at 1 day and 336 days post-exposure, respectively.

Albini et al. (2015) investigated the main routes of entry following environmental exposure to MWCNTs (9.5 mean diameter, 1.5 µm mean length, surface area of 250 to 300 m^2/g). These investigators developed a novel CD1 mouse model to represent a surrogate of a workplace exposure to MWCNTs, and traced the localization of MWCNTs and their possible role in inducing a number of immune responses. Specifically, these investigators exposed 40 male CD1 mice (6 to 8 weeks of age) to 1.5 g MWCNT/80 g litter by adding the dry MWCNT into the wood shaving cage litter. The MWCNTs were "gently mixed with litter without dispersing aggregates." The normal behavior of the experimental animals then allowed for dermal, oral and inhalation exposure, similar to what would be expected in an industrial setting. Following 1 to 5 weeks of continuous environmental exposure, investigators observed that MWCNTs, as compact aggregates at least several µm in diameter, rapidly enter and disseminate in the mice, initially accumulating in the lungs and brain and later reaching the liver and kidney. Minimal MWCNT material was observed in the GI tract, suggesting that oral exposure was not a significant route of entry in this model.

Sturm (2016) conducted an *in silico* assessment of CNT deposition in human lungs by assuming a stochastic structure of the bronchial network where particle transport takes place along randomly selected paths. Deposition was modeled for SWCNT variants of diameter from 5 to 10 nm and up to 10 µm long, and for MWCNTs of diameter 50 to 100 nm and up to 100 µm long.

This investigator found a significant dependence of CNT deposition on both diameter and aspect ratio of the particles. For example, extremely small-diameter CNTs (~1 nm) are primarily filtered in the extrathoracic airways, intermediate diameter CNTs (~10 nm) exhibit a preference to deposit in the alveoli, and large diameter CNTs (~100 nm) are marked by minimum deposition. This modeling did not appear to account for agglomeration and modeled CNT particles as dispersed fibers, suggesting that these results may be informative for thick-walled, semi-rigid MWCNTs (~100 nm). Semi-rigid MWCNTs are more frequently found as dispersed fibers, while thinner variants are tangled agglomerates and aggregates. No data on metabolism or excretion were reported.

4.2.2.3 Lung Exposure via Instillation of Suspensions

Two recent studies investigated biokinetics of semi-rigid and tangled MWCNTs using lung exposure (transtracheal spraying) to MWCNTs in suspension. These studies established that semi-rigid MWCNTs may translocate to tissues that are not reached by agglomerated, tangled fibers. Both MWCNT forms exhibit poor lung clearance. Importantly, studies using the intratracheal route did not observe CNTs in brain tissues (Shinohara et al., 2016), in contrast to tissues from inhalation studies (Mercer et al., 2013; Albini et al., 2015; Kasai et al., 2016). This is consistent with the hypothesis that CNT distribution to the brain happens by way of axonal retrograde transport through the olfactory epithelium following inhalation exposure, because administration that bypasses the nasal cavity does not appear to be associated with distribution to the brain.

Xu et al. (2014) exposed rats to various MWCNTs for a period up to 24 weeks to determine whether the size and shape of MWCNT impact deposition and lesion development in the pleura and lung. Two different MWCNT examples were chosen for this study: a larger sized needle-like MWCNT (MWCNT-L; length = 8 um, diameter = 150 nm), and a smaller sized MWCNTs (MWCNT-S; length = 3 um, diameter = 15 nm), which forms aggregates. Both suspensions were administered to the rat lung once every 2 weeks for 24 weeks by transtracheal intrapulmonary spraying. In contrast to MWCNT-S, MWCNT-L was found to translocate into the pleural cavity, deposit in the parietal pleura, and induce fibrosis and patchy parietal mesothelial proliferation lesions.

Shinohara et al. (2016) administered MWCNTs (mean diameter 48 nm, mean length 2.5 μm) in 0.5 mg/ml Triton-X solution to rats at one dose of 0, 0.20 or 0.55 mg via IT instillation and investigated the pulmonary burden after 1, 3, 7, 28, 91, 175 and 364 days of instillation. Analysis of lung burden suggested that approximately 30% of administrated MWCNTs may have been cleared by bronchial ciliary motion within 24 h of administration of either 0.20 or 0.55 mg. However, pulmonary MWCNT burden did not decrease significantly over 364 days after instillation, suggesting that MWCNTs were not readily cleared from the lung. TEM showed that alveolar macrophages internalized the MWCNTs and that the MWCNTs were retained in the lung for at least 364 days after instillation. MWCNTs were not detected in the liver or brain within the 364-day study period.

4.2.2.4 Dermal Exposure

No studies were identified in humans or animals assessing MWCNTs toxicity by the dermal

route. Filon et al. (2016) provides a general literature review of dermal absorption of nanomaterials, including carbon fibers, fullerenes, quantum dots, and metal NPs. MWCNTs were not specifically addressed, however significant uptake of MWCNTs through skin and systemic exposure is not considered likely given the evidence presented for other nanoparticle examples.

4.2.2.5 Other Routes of Exposure

Al-Jamal et al. (2012) studied how functionalization of a MWCNT material affected distribution in mice. MWCNTs were 20 to 30 nm in diameter and 0.5 to 2 μm in length and were functionalized with diethylentriaminepentaacetic dianhydride (DTPA) in low- and intermediate-degree functionalization variants (the experiment did not appear to use controls). ^{111}Inidium was used as a radiotracer and the dispersed radiolabeled-MWCNT were imaged up to 24 h following IV administration. DTPA-CNTs primarily accumulated in the liver and spleen, with intermediately functionalized CNT accumulating less in the liver and more so in the spleen and lung compared to lightly functionalized variants.

4.2.2.6 Summary

Based on the limited data available for the oral biokinetics of different forms of MWCNTs, oral exposure is not expected to result in systemic absorption. This is consistent with the conclusions of a 2013 review by the Danish EPA. The difficulty in accurately identifying and quantifying CNTs in tissues was noted as a challenge in generating robust absorption data (Danish EPA, 2013).

Generally, it is thought that biopersistent insoluble fibers are not well cleared from the lung (Lippmann, 1990). Data informing lung clearance of MWCNTs indicate that MWCNTs are poorly cleared from the lung. These data include a quantitative study reporting a 151-day half-time following a 90-day inhalation exposure to 0.1 mg/m^3 MWCNTs, the lowest concentration used in the study (Pauluhn, 2010). Other lung studies focused on toxicity have reported MWCNT material evident in the lung following post-exposure recovery periods of up to 1 year (Mercer et al., 2013; Pauluhn and Rosenbuch, 2015; Pothmann et al., 2015; Shinohara et al., 2016). The aforementioned studies also indicate that MWCNTs in the lung slowly migrate to lung-associated lymph nodes over time, with small amounts of material distributing to the liver, kidney, and spleen. One study (Xu et al., 2014) presented evidence that long, semi-rigid MWCNTs may migrate to the pleura and are poorly cleared, while a shorter, agglomerated variant did not reach the pleura. Data from experiments using agglomerated, tangled (thin-walled) MWCNTs indicate that lung clearance of this variety of MWCNT diminishes as a function of dose. The slower clearance of these agglomerates at high doses is presumably due to volumetric overloading of macrophages, as has been demonstrated by Pauluhn (2010). MWCNT were also found in brain tissue, possibly due to exposure of the olfactory epithelium to inhaled MWCNT. No data on excretion of MWCNTs was available.

Although data are limited (especially for low doses), MWCNT fibers that are inhaled should be considered to have very long half-lives in the lower lung, and are expected to gradually migrate to lymph nodes. There is some evidence that significant clearance of SWCNTs from the lung may occur by way of metabolism by peroxidases (Shvedova et al., 2012). MWCNTs are

reported to be labile to peroxidase activity (Russier et al., 2011; Zhao et al., 2011), but experimental data relating to MWCNT clearance by this mechanism are not available. Regardless, the prolonged residence of MWCNTs in the lung indicates that clearance by any mechanism should be assumed to happen at a slow rate. Accumulation in the brain has also been reported following inhalation although the number of studies remains limited. Those particles would plausibly be persistent in this compartment due to their properties and the lack of a clearance mechanism. Overall, a conservative assumption would be that daily exposures to MWCNTs are largely cumulative with regard to total dose, and that a relatively slow clearance rate should be assumed for estimating total dose.

4.3 Acute and Short-Term Toxicity

4.3.1 Single-walled CNT

No SWCNT human data for acute toxicity via the oral, inhalation or dermal routes were located in the recent literature.

4.3.1.1 Oral Exposure

In literature published prior to 2010, limited testing in animals indicated that nonfunctionalized CNTs have a low potential for toxicity following acute oral exposure. Administration of single, oral, 1,000-mg/kg doses of three types of SWCNTs (differing in iron content and lengths) to male Swiss mice produced no deaths, no body-weight changes, no changes in serum biochemistry variables or hematological variables, and no histological changes in several tissues including the stomach, intestines, brain, liver, and kidneys within 14 days after exposure (summarized in Versar, 2012).

In the more recent literature, Matsumoto et al. (2012) investigated SWCNT toxicity in Crl:CD (Sprague-Dawley) rats according to OECD Test Guideline 423 (Acute Oral Toxicity). The SWCNT material is identified as a principal sample in the OECD Sponsorship Programme on the Testing of Manufactured Nanomaterials (Principal 1, Nikkiso SWCNTs) and is characterized in related documentation. The SWCNTs are described as "around 2 nm" in diameter and present as tangled bundles when dispersed in 5% gum acacia in water. Surface area was not provided. Purity was ">95%" but appears to be heavily contaminated with iron (greater than 43,700 parts per million [ppm] Fe) based on OECD documentation. Three female rats were given 50 mg/kg bw SWCNTs subdivided into four gavage doses of 12.5 mg/kg at 1 hr intervals (50 mg/kg total dose) and observed for 14 days for changes in body weight and clinical observations. No body weight changes or clinical signs were evident in the treated rats.

Zhao et al. (2014) exposed Kunming mice (10/group, sex not specified) to SWCNTs with a mean diameter of 1.1 nm and lengths between 0.5 and 100 μm under OECD Test Guideline 401 (for acute oral toxicity). The only endpoint reported was mortality. No deaths were observed at a dose of 5000 mg/kg. The NOAEL of the study was 5000 mg/kg.

The limited available literature indicates that SWCNTs have a low toxicity by way of oral exposure.

4.3.1.2 Inhalation Exposure

Shvedova et al. (2008) reported that short-term SWCNT inhalation exposure was associated with signs of pulmonary inflammation in BALF and/or histological lesions (e.g., epithelial hyperplasia, granulomas, or fibrosis) in bronchoalveolar, alveolar, or subpleural regions of the respiratory tract of female C57Bl/6 mice. A target concentration of 5 mg/m^3 of unpurified SWCNTs (containing 17.7% iron) via whole-body inhalation at 5 hours/day for 4 consecutive days caused minor changes in breathing patterns (elevated breathing frequency). BALF and histology indicated signs of inflammation including leukocyte accumulations, granuloma formation, and epithelial hypertrophy. This study is summarized in Table 11.

In a subsequent study, Shvedova et al. (2014) used a similar exposure model (as Shvedova et al., 2008) in female C57Bl/6 mice with a 1-year post exposure recovery. SWCNTs were 99.7% pure with 0.23% iron content, 1 to 4 nm in diameter, 1 to 3 μm in length, with a surface area of 1040 m^2/g. SWCNTs were agglomerated as ropes and formed bundles up to 65 nm in diameter. Female C57Bl/6 mice (5/group) were exposed to 5 mg/m^3 via whole-body inhalation at 5 hours/day for 4 consecutive days followed by a 1-year post-exposure period. Endpoints included lung histology, BALF analysis, and determination of collagen in lung homogenates. Histopathology of lungs of exposed mice showed fibrosis, pneumonia, and granulomatous lymphadenitis (swelling of tracheobronchial lymph nodes) in all animals following the 1-year recovery. A 2.5-fold increase in lung collagen was also observed. BALF analysis showed sustained elevations of neutrophils, macrophages, and lymphocytes as well as increased LDH. In another group, a SWCNT dose estimated to be equivalent to inhaled was given by bolus (oropharyngeal aspiration), and the authors concluded that inhaled SWCNTs induced more severe inflammatory and fibrogenic effects in the lung than aspirated SWCNT.

Overall, data for acute inhalation of SWCNTs indicate that exposure to SWCNTs can cause lung inflammation persisting up to 1-year post-exposure accompanied by granulomatous changes, epithelial hyperplasia, and increased collagen deposition. The available studies only used very high SWCNT exposure concentrations and are inadequate for demonstrating dose-response or providing a reliable LOAEL or POD dose.

Table 11. Summary of Toxicity to SWCNT via Acute Inhalation

Species and study type (n/sex/group)	Exposure (report concentrations, frequency, duration)	Particle characteristics[a]	NOAEC (mg/m^3)	LOAEC (mg/m^3)	Responses at the LOAEC	Comments	Reference
C57BL/6 mice 12 F/group whole-body exposure	0 or 5 mg/m^3 5 h/d for 5 d; pulmonary toxicity assessed at 1, 7, and 28 d after last exposure	SWCNT: 0.8–1.2 nm dia and 0.1–1 µm length; 82% pure, 17.7% Fe, 0.16Co, 0.049Cr, and 0.046% Ni. Surface area and morphology not reported. MMAD of aerosol = ~4.2µm	None	5	Increases in polymorphonuclear neutrophils (PMN) and macrophage counts, protein content, LDH activity in BALF at 1, 7, and 28 d. Increased proinflammatory and fibrogenic cytokines (TNF-α, IL-6, and TGF-β) in BALF at 1, 7, and 28 d after exposure. Alveolar wall collagen increased with increasing time after exposure.	Aerosols generated by acoustically fluidized powder feeder and knife mill. Histology of respiratory tract showed pulmonary inflammation, bronchiolar epithelial cell hypertrophy, and "green-brown" foreign material in lung interstitium, within macrophages, or freestanding in alveoli; material was most frequently aggregated near bronchoalveolar junctions.	Shvedova et al., 2008[b]
C57Bl/6 mice 6F/group whole-body exposure	0 or 5 mg/m^3 5 h/d for 4 d; pulmonary toxicity assessed at 1 yr post exposure	SWCNTs, 1-4 nm dia, 1-3 µm in length, 99.7% pure, surface area of 1040 m^2/g, agglomerated into ropes and bundles up to 65 nm	None	5	Increased macrophages, neutrophils, and lymphocytes in BALF. Fibrosis, pneumonia, and granulomatous lymphadenitis observed in lung histology. 2.5-fold collagen increase in lung homogenates.	An estimated equivalent dose of SWCNTs via OPA induced less severe inflammatory and fibrogenic effects.	Shvedova et al., 2014

[a] NT characterization data are stated, if reported: source, diameter and length, surface area, purity and impurities, and state of aggregation; shape (bundles, tangles, ropes)

[b] As reviewed in Versar (2012)

4.3.1.3 Dermal Exposure

There are no studies of systemic toxicity via the dermal route of exposure for SWCNTs either in the recent available literature or literature prior to 2010 (Versar, 2012).

4.3.1.4 Other Routes of Exposure

Numerous studies using either IT or OPA administration of SWCNTs are available. Those published prior to 2010 are summarized in Versar (2012). In general, exposure-related toxicity data by these routes are not appropriate for identifying a POD dose due to the non-realistic nature of the total doses, dose rates, deposition, and preparation of suspensions. In the current report, only those IT and OPA from Versar (2012) or recent literature searches that report dose-related toxicity (i.e., three or more doses plus control) and that may inform hazard characterization or uncertainty factors are presented in Appendix B. Acute toxicity studies wherein SWCNTs were administered by IP or IV routes were not considered relevant to exposure from non-food/drug consumer products and are not covered in this section.

Overall, studies of SWCNT toxicity by IT or OPA agree with the results of acute SWCNT inhalation studies, which exposed animals to relatively high concentrations of SWCNTs for short time periods (less than 1 week). The findings demonstrate that SWCNT accumulations in the lungs cause inflammation evident in BALF and lung histology that is persistent up to several months following exposure. Granuloma/granulomatous foci, epithelial hypertrophy/hyperplasia, and increased lung collagen are long-lived lung changes that may be induced by SWCNTs in the lung.

4.3.2 Multi-walled CNTs

No human data for acute toxicity of MWCNTs via oral, inhalation or dermal routes were located in the recent literature.

4.3.2.1 Oral Exposure

In a study published prior to 2010, no changes in serum biochemistry or hematological variables were observed in CD-1 mice within 30 days of administration of single oral doses of 1, 2.5, or 5 mg/kg of acid-functionalized MWCNTs (Carrero-Sanchez et al., 2006). For a more detailed description, see Versar (2012).

Matsumoto et al. (2012) investigated MWCNT toxicity in Crl:CD (Sprague-Dawley) rats according to OECD Test Guideline 423 (Acute Oral Toxicity) in a single-dose tolerance study. The MWCNTs are described as “around 30 nm” in diameter and present as tangled agglomerates when dispersed in 5% gum acacia in water. Surface area was not provided or measured. Purity was reported as “>98%”. Three female rats were given 200 mg/kg bw MWCNTs spread across four gavage doses (200 mg/kg total dose) in 1 hr intervals and observed for 14 days for changes in body weight and clinical observations. No body weight changes or clinical signs were evident in the treated rats.

Awasthi et al. (2013) investigated liver toxicity of MWCNTs in an acute oral study in mice with

a 28-day post-exposure observation. MWCNTs were 20 to 30 nm in diameter and reported to be 5 to 50 μm in length. Surface area and purity were not reported; an acid-washing step included in processing would be expected to minimize trace metals and impurities. Swiss albino mice (24/group, all male) were "orally exposed" to 0, 60, or 100 mg/kg bw MWCNTs in a single bolus dose and observed for 28 days. Body weights were monitored, and livers were examined histologically and antioxidant response (superoxide dismutase [SOD] and catalase [CAT] activity) measured. No body weight changes were observed in treated animals relative to controls. The authors reported inflammation, spot necrosis, and coagulation at both dose levels, but further stated that "no significant changes in liver histology" were induced by the lower dose. Both doses decreased antioxidant enzyme activity in the liver. Taken together, the authors interpreted the responses as "slight hepatotoxicity" in the high-dose group.

Golokhvast et al. (2013) investigated the effects of short-term daily CNT exposure on the GI tract of mice. MWCNTs with 18 to 20 nm diameter and surface area of 130 m^2/g were used. Metal contaminants were iron (0.21%), cobalt (0.12%), and very low amounts of aluminum. Initial aggregates were coiled wires 30 to 50 μm in size. Sonication was used to disperse materials, but post-processing material analysis was not conducted. Male CBA mice (30 per treatment) were exposed to 0 or 500 mg/kg/d CNTs in diet for 6 consecutive days. Kidneys and GI tract sections were collected daily (5 mice/daily group) for examination on days 1 through 6. From day 2 post-exposure, uptake of MWCNTs into epithelial cells was observed in the small and large intestine and was accompanied by mucus hypersecretion. No CNTs were observed in kidney tissues. Generalized lymphoid hypertrophy was seen in the lamina propria of the GI mucosa, but no pronounced toxic effects were associated with oral CNT exposure. CNT particles observed in tissue (visualized via TEM) were present as globular aggregates 10 to 20 μm in size.

The available studies for acute oral exposure to MWCNTs, albeit limited in endpoints examined, species and numbers of animals studies, indicate that MWCNTs exhibit low toxicity by the oral route.

4.3.2.2 Inhalation Exposure

Short-term inflammation in BALF and/or histological lesions (e.g., epithelial hyperplasia, granulomas, or fibrosis) were observed in bronchoalveolar, alveolar, or subpleural regions of the respiratory tract in male Wistar rats exposed to aerosols of MWCNTs at concentrations greater than or equal to 2 mg/m^3 (Ma-Hock et al., 2009a) or 11 mg/m^3 (Ellinger-Ziegelbauer and Pauluhn, 2009); and in male C57BL/6 mice exposed to aerosols of MWCNT at 1 and 30 mg/m^3 (Ryman-Rasmussen et al., 2009a) or 100 mg/m^3 (Ryman-Rasmussen et al., 2009b). The aforementioned studies (reviewed by Versar, 2012) are summarized in Table 12 along with literature available after 2010.

Three recent short-term inhalation studies were located for MWCNTs. Umeda et al. (2013) investigated MWCNT toxicity in a 2-week inhalation study in rats. MWCNTs were 88 nm in mean diameter with a surface area of 24 to 28 m^2/g and a carbon purity of 99.8%. Mean length was 5.0 μm. MWCNT aerosols were characterized by SEM post-exposure. F344 rats of both sexes were exposed via whole-body inhalation to MWCNT at 0, 0.2, 1, or 5 mg/m^3 for 6 h/d, 5 d/week, for 2 weeks. One cohort (5 M/5 F/exposure level) was necropsied at the end of the study

and another cohort (5M/5F/exposure level) was examined at 4-weeks post-exposure. Clinical observations and organ histology were recorded in addition to BALF analysis. The no observed adverse effect concentration (NOAEC) for the study was 0.2 mg/m^3 and the lowest observed adverse effect concentration (LOAEC) was 1 mg/m^3 based on goblet cell hyperplasia of the nasal cavity and nasopharynx and mild neutrophil accumulation in BALF. Both of these effects were reversible following the 4-week recovery period.

Ma-Hock et al. (2013) tested the toxicity of MWCNTs in a 28-day inhalation study in rats. The study was designed as a comparison study between MWCNTs, graphene, graphite nanoplatelets, and high-surface area carbon black. MWCNTs were 15 nm in mean diameter, 161 m^2/g in surface area, and greater than 99% pure. MWCNT agglomerates were fibrilles ranging from 100 nm to 1 µm diameter and amorphous bundles up to 20 µm across. Density of agglomerates was 0.39 g/mL. Male Wistar rats (11 M/group) were exposed to MWCNT at 0, 0.1, 0.5, or 2.5 mg/m^3 for 6 h/d for 5 consecutive days via nose-only inhalation. Measured concentrations were 0, 0.15, 0.57, and 2.86 mg/m^3, respectively. The MMAD at the LOAEC was 1.3 µm with a GSD of 3.7. BALF was collected on days 7 and 28 and analyzed for cytology and cytokines. Increases in measured BALF endpoints were greatest at the 7-day time point and somewhat abated (30-60% abated at the LOAEC) at the 28-day time point. Histology was described for a limited number of lung samples. Interstitial microgranulomatous foci and mild alveolar epithelial cell hyperplasia were observed on study day 4 after exposure to 2.5 mg/m^3 MWCNTs, but toxicologic pathology did not appear to be quantitatively scored. The NOAEC is considered to be 0.1 mg/m^3 and the LOAEC was 0.5 mg/m^3 based on critical effects of neutrophil accumulation and increased LDH, alkaline phosphatase (ALP), and several cytokines measured in BALF.

Pothmann et al. (2015) investigated MWCNT toxicity in a short-term inhalation study in rats. The MWCNTs were 12 nm in diameter, with a surface area of 225.6 m^2/g, and the major contaminants were aluminum (3.0%) and iron (2.7%). MWCNTs were ball-milled to increase dustiness and were delivered as compact aggregates in the size range of hundreds of nm to up to several microns in diameter. MWCNTs were administered to Wistar rats (5 M/5 F per group) via nose-only inhalation at 0, 0.05, 0.25, or 1.25 mg/m^3 (6 h/d) for 5 days and were sacrificed either 24 hours or 28 days post-exposure. The MMAD at the LOAEC was 1.84 µm with a GSD of 1.84. BALF were analyzed and lung histology was examined. BALF cytology revealed no significant changes following MWCNT exposure except for the 1.25 mg/m^3 concentration, which caused a very small increase in neutrophils following the 5-day exposure. Exposure to 1.25 mg/m^3 also caused a small increase in gamma-glutaminase in BALF following 5 days exposure. Although significant inflammatory cell infiltration was not seen at any dose, BALF showed a clear dose-related increase in the levels of total protein following the 5 day exposure as well as the 28-day recovery. Histology of lungs showed minimal bronchiolar cell hypertrophy and slight increases in macrophage infiltration in the group exposed to 1.25 mg/m^3. These changes remained present following the 28-day recovery. The NOAEC for the study was 0.25 mg/m^3 and the LOAEC was 1.25 mg/m^3 based on a critical effect of bronchiolar hypertrophy. Total protein increases were evident in BALF below this dose, but in the absence of increases of any other inflammatory markers (leukocytes, LDH) this does not appear to be an adverse effect.

Table 12. Summary of Acute and Short-term Inhalation Toxicity to MWCNTs

Species and study type (n/sex/group)	Exposure (report concentrations, frequency, duration)	Particle characteristics[a]	NOAEC (mg/m^3)	LOAEC (mg/m^3)	Responses at the LOAEC	Comments	Reference
C57BL/6 mice 6 M/group whole-body exposure	0, 0.3, 1, or 5 mg/m^3, 6 h/d for 7 or 14 d; BALF samples and lungs collected the day after the last exposure.	MWCNTs, >95% pure, 97.9% C, 2.1% oxidized C; 0.5% Ni and 0.5% Fe. 10–20 nm dia and 5–15 µm length; 100 m^2/g surface area; MMADs were 0.7–1 µm (~2 GSD) for low and 1.8 µm (~2.5 GSD) for the highest concentration.	5	None	Histology of lungs sampled within 24 hours after the last high-concentration (5 mg/m^3) exposure were reported to be nondistinguishable from control lungs. BALF samples collected the day after 14 d of exposure showed no exposure-related change in counts of macrophages, PMNs, or lymphocytes.	Aerosols were generated by mechanical agitation using a jet mill coupled to a dry chemical screw feeder. Lack of lung response may be due to relatively low tested concentrations or insufficient observation time to develop lung responses.	Mitchell et al., 2007[b]

Species and study type (n/sex/group)	Exposure (report concentrations, frequency, duration)	Particle characteristics[a]	NOAEC (mg/m^3)	LOAEC (mg/m^3)	Responses at the LOAEC	Comments	Reference
Wistar rats 6 males/group nose-only	0, 11, or 241 mg/m^3 for 6 h; pulmonary toxicity assessed on post-exposure d 7, 28, and 90. Acid-treated MWCNT only assessed at 11 mg/m^3	Pristine and acid-treated MWCNTs, Baytubes®, containing 0.53 and 0.12% Co, respectively. 10–16 nm dia, length not specified; 253 mg^2/g surface area; MMADs ranged from 1.9 to 2.9 µm, GSD 1.6–2.6. Aerosols were generated by a Wright-Dust Feeder.[b]	None	11	Increases in total cell and PMN counts, soluble collagen content, and LDH activity in BALF samples at 7 d after exposure at 11 mg/m^3, and at all time points after exposure to 241 mg/m^3. Increased lung weights at 7- and 90-d sacrifices in both exposure groups. Lung histology at 90 d after exposure to 11 mg/m^3 pristine MWCNT: 6/6 with minimal enlarged foamy macrophages; Response to acid-treated MWCNT was slightly more severe: 4/6 with minimal and 2/6 with slight/mild enlarged foamy macrophages, and 2/6 with minimal focal septal thickening.	Responses in BALF samples greater in rats exposed to pristine MWCNT, compared with acid-treated MWCNT. In contrast, histological responses more severe with acid-treated MWCNT. Results suggest metal contaminants may contribute to the initial (i.e., within 7 d) inflammatory response. Histological responses at 90 d to 241 mg/m^3 included: 6/6 with hypercellularity of bronchioalveolar tissue (vs. 0/6 in control); 6/6 with focal septal thickening (vs. 1/6); and 6/6 with focal increase in septal collagen (vs. 0/6), indicative of a fibrotic response.	Ellinger-Ziegelbauer and Pauluhn, 2009[b]

Species and study type (n/sex/group)	Exposure (report concentrations, frequency, duration)	Particle characteristics[a]	NOAEC (mg/m^3)	LOAEC (mg/m^3)	Responses at the LOAEC	Comments	Reference
C57BL/6 mice; 10M/group nose-only	0, 1, or 30 mg/m^3 for 6 h; lung tissue collected at 1 d, and 2, 6, 14 wks after exposure.	MWCNTs, 94% pure containing 5.5% Ni; 30–50 nm dia, 0.3–50 µm length; reported MMADs were 164 and 183 nm for the low and high concentrations, respectively. Aerosols appeared to be agglomerated with individual tube lengths ranging from <100 nm to >10 µm[b]	None	1	Lesions 1 d after exposure: increased incidence of pleural mononuclear cell aggregates with higher incidence after 30 mg/m^3 exposure. Subpleural fibrosis observed in 1/10, 1/10, and 3/10 mice at 2, 6, and 14 wks after exposure to 1 mg/m^3 (not found in controls at any time). After exposure to 30 mg/m^3, subpleural fibrosis found in 9/10, 6/10, and 1/10 mice at 2, 6, and 14 wks.	Subpleural fibrotic lesions progressed in initial time points after exposure, but appeared to resolve by 14 wks after exposure to the high concentration. Aerosols were generated from aqueous suspensions in 1% pluronic F-68.	Ryman-Rasmussen et al., 2009a[b]
Wistar rats 5 M/group head-nose inhalation	0, 2, 8, or 30 mg/m^3, 6 h/d for 5 d. BALF samples collected 3 and 28 d after last exposure.	MWCNTs, 90% pure, 10% metal oxide (9.6% aluminum oxide with traces of Fe and Co); 5–15 nm dia and 0.1–10 µm length; 250–300 mg^2/g surface area; MMADs between 0.5 and 1.3 µm; GSDs between 3.1 and 5.4; 77.4–86.3% mass of particles had aerodynamic size <3 µm[b]	None	2	Increases in total cell counts (principally PMNs), total protein content, and enzyme activities (LDH, β-NAG, ALP, and γ-GT) in BALF samples, 3 and 21 d after last exposure. Histology showed diffuse or focal histiocytosis, particle-laden macrophages, and broncheoalveolar hypertrophy and hyperplasia. Histological changes were not resolved in rats 3 wks after the last exposure.	Aerosols were generated by a brush generator. BALF fluid samples collected from 5 rats/group; histology of respiratory tract on 3 rats/group. Other effects at 8 mg/m^3: increased lung weight, small alveolar septal granulomas. Additional effects at 32 mg/m^3 included decreased body weight gain, increased upper respiratory tract irritation, minimal to mild diffuse pulmonary histiocytosis, and minimal infiltration with neutrophils.	Ma-Hock et al., 2009a[b]

Species and study type (n/sex/group)	Exposure (report concentrations, frequency, duration)	Particle characteristics[a]	NOAEC (mg/m^3)	LOAEC (mg/m^3)	Responses at the LOAEC	Comments	Reference
Wistar rats 5-6 M/group nose-only inhalation	0, 0.1, 0.5, or 2.5 mg/m^3, 6 h/d for 5 days. BALF analyzed 7 and 28 d after the start of exposure.	Arkema; mean dia of 15 nm; surface area of 161 m^2/g; >99% pure; fibrils ranging from 100 nm to 1µm in dia and amorphous bundles up to 20 µm across. MMAD at the LOAEC was 1.3 µm with a GSD of 3.7	0.1 (measured as 0.15)	0.5 (measured as 0.57)	Neutrophil accumulation and increases in ALP and proinflammatory cytokines measured in BALF	Study designed as a comparison study between different carbon nanomaterials and only measured BALF endpoints. The responses were strongest at 7 d but still present at 28 d.	Ma-Hock et al., 2013
F344 rats 5M/5 F/group whole-body inhalation	0, 0.2, 1, or 5 mg/m^3, 6 h/d, 5 d/wk for 2 wks. BALF samples and histology analyzed at the end of study and after 4 wks post-exposure.	Hodogaya Chemical Co.; mean dia of 88 ± 5 nm, mean length of 5.0 ± 4.5 µm; surface area of 24-28 m^2/g; 99.8% pure; morphology not given. MMAD at 1 mg/m^3 was 1.2 with a GSD of 3.4	0.2	1	Goblet cell hyperplasia of the nasal cavity and mild neutrophil accumulation in BALF. Both effects were reversible following the 4-wk recovery period.	Deposition of CNT in the alveolar spaces at all doses. Deposition in the airways only at 1 and 5 mg/m^3. After the 4-wk recovery, there was no change from this deposition pattern but increased migration of CNT into lymph was seen at this time.	Umeda et al., 2013
Wistar rats 5M/5F/group nose-only inhalation	0, 0.05, 0.25, or 1.25 mg/m^3, 6 h/d for 5 d. BALF samples and lung histology analyzed at the end of study and after 4 wks post-exposure.	MWCNTs, 3.0% Al, 2.7% Fe, mean dia of 12.1 nm, mean length of 1.07 ± 1.10 µm, surface area of 225.6 m^2/g. Bulk MWCNTs were ball-milled to increase dustiness. MMAD at 1.25 mg/m^3 was 1.84 µm with a GSD of 1.84	0.25 (measured as 0.26 ± 0.03)	1.25 (measured as 1.30 ± 0.03)	Bronchiolar hypertrophy, increased BALF total protein	Critical effects remained following 28-day post exposure recovery	Pothmann et al., 2015

[a] NT characterization data are stated, if reported: source, diameter and length, surface area, purity and impurities, and morphology/state of aggregation (bundles, tangles, ropes)

[b] As reported in Versar (2012)

4.3.2.3 Dermal Exposure

No studies of systemic toxicity by the dermal route for MWCNTs were available either in the recent literature or prior to 2010 (Versar, 2012).

4.3.2.4 Other Routes of Exposure

Numerous studies using either IT or OPA of MWCNTs have been conducted. Those available prior to 2010 are summarized in Versar (2012). In general, effects in the lung following exposure by these methods are similar to those seen following inhalation and consist of an initial inflammatory reaction that is poorly-resolving and progresses to epithelial lesions and fibrosis. The current report summarizes IT and OPA studies that report dose-response toxicity (i.e., three or more doses plus control) that may inform hazard characterization or uncertainty factors. However, in general, toxicity data by IT and OPA are not appropriate for identifying a POD dose for ADIs by the oral, inhalation or dermal routes due to the total doses, dose rates, deposition, and preparation of suspensions used. Exposures delivered as a bolus in suspensions result in non-realistic tissue deposition/absorption and total doses are frequently too high and delivered too quickly to be relevant to inhalation toxicity on a dose-response basis. Appendix C lists these studies (entries prior to 2010 are taken from Versar, 2012).

Overall, dose-response studies using IT or OPA administration of MWCNTs indicate that MWCNTs delivered to the lungs as a bolus may cause inflammation evident in BALF at the lower end of most dose ranges used (as low as 5 μg MWCNTs). This inflammation continues for up to several months, and is more persistent with increasing doses. Significant pathology, in the form of granulomatous inflammation and epithelial hyperplasia is evident at doses in the range of 20 μg. Significant septal thickening and collagen increases are associated with higher doses, from 40-80 μg. Lung function has been shown to be affected by these exposures at 4 mg/kg bw (~80 μg assuming a 20 g mouse). Studies have documented hepatotoxicity (Kupffer cell hypertrophy, vascular degeneration) following bolus lung exposure to MWCNTs and high doses have been reported to affect the heart (exacerbated reperfusion injury and depressed coronary flow). These results overall agree qualitatively with those seen in high-dose inhalation exposures.

There are toxicity studies of MWCNT administered by IP and IV routes available that were not considered relevant to exposure from use of non-food/drug consumer products, and are not covered herein.

4.4 Repeat-Dose and Subchronic Toxicity

4.4.1 Single Walled CNT

There were no systemic toxicity repeat-dose or subchronic studies in humans via oral, inhalation or dermal routes located in the recent literature.

4.4.1.1 Oral Exposure

There are no repeat-dose studies of SWCNTs in animals by the oral route available prior to 2010. Matsumoto et al. (2012) investigated SWCNT toxicity in Crl:CD (Sprague-Dawley) rats

according to OECD Test Guideline 407 (Repeated Dose 28-Day Oral Toxicity Study in Rodents). The SWCNTs are an OECD principal material ("Nikkoso SWCNT", OECD, 2016b) described as "around 2 nm" in diameter and present as tangled bundles when dispersed in 5% gum acacia in water. Surface area was 878 m^2/g according to OECD data, but length was not provided. Purity was ">95%" but appears to be heavily contaminated with iron (greater than 43,700 ppm Fe) based on documentation of this material by OECD. Twenty rats/group (10 M/10 F) were administered 0, 0.125, 1.25, or 12.5 mg/kg bw-day by gavage for 28 days. The highest dose was based on physical limits of the amount of SWCNTs deliverable by gavage. Clinical observations, organ histopathology, blood biochemistry, and hematology were recorded. No significant toxicological effects were seen at any dose. The 28-day NOAEL for this study is 12.5 mg/kg/day (highest dose tested).

4.4.1.2. Inhalation Exposure

There are no repeat-dose studies of SWCNTs by the inhalation route available prior to 2010. Morimoto et al. (2012) exposed rats to SWCNT in a 28-day inhalation study. SWCNTs were 99.9% pure, 3 ± 1.1 nm in mean diameter, and had a surface area of 1064 ± 37 m^2/g. SWCNTs were dispersed via ultrasonication in 1% Tween-80 (surfactant) aqueous medium prior to aerosolization. Male Wistar rats (5/group) were exposed to 0, 0.03, or 0.13 mg/m^3 SWCNTs at 6 h/d, 5 d/wk for 4 weeks. The exposure was followed by a 3, 30, or 90-day recovery period. As aerosols, SWCNT were agglomerated into ropes. The geometric mean length of the SWCNT aerosol agglomerates was 0.7 μm with a GSD of 1.7. The geometric mean width of the agglomerates was 0.2 μm with a GSD of 1.7. Lungs were analyzed by histology, protein levels of pro-inflammatory cytokines and heme oxygenase were measured in lung homogenates, and BALF was analyzed. No treatment-related effects were seen in these endpoints and no sign of inflammation was present in the lung.

4.4.1.3 Dermal Exposure

No studies investigating systemic toxicity from repeated dermal exposure to SWCNTs were available in the recent literature or prior to 2010 (Versar, 2012).

4.1.1.4 Other Routes of Exposure

Relevant repeat-dose toxicity studies via IT or OPA exposure to SWCNT were not located. Single doses of SWCNT given as a bolus instillation are thought to model repeated exposures in the lung due to the poor clearance of SWCNT; dose-response studies of this kind are summarized in Appendix B. Studies of repeated IP or IV exposure to SWCNTs were not considered relevant to consumer products within CPSC purview.

4.4.2 Multi-walled CNTs

4.4.2.1 Oral Exposure

No repeat-dose studies of MWCNTs by the oral route were available prior to 2010. More recently, Matsumoto et al. (2012) investigated MWCNT toxicity in Crl:CD (Sprague-Dawley) rats according to OECD Test Guideline 407 (Repeated Dose 28-Day Oral Toxicity Study in

Rodents). The MWCNTs are described as "around 30 nm" in diameter and present as tangled agglomerates when dispersed in 5% gum acacia in water. Surface area was not provided or measured. Purity was reported as ">98%". Twenty rats/group (10 M/10 F) were administered 0, 0.5, 5.0, or 50 mg/kg/d by gavage for 28 consecutive days. The highest dose was selected based on the maximum amount of MWCNTs that the authors were able to suspend in the volume of medium that could be given by gavage. Clinical observations, histopathology, and blood chemistry were recorded. No significant toxicological effects were seen at any dose. The 28-day NOAEL for this study is considered 50 mg/kg/d (highest dose tested).

4.4.2.2 Inhalation Exposure

In studies published prior to 2010 and reviewed in Versar (2012), the toxicity of repeat-dose inhaled MWCNTs to the respiratory tract and concentration-response relationships have been examined in two 13-week studies of Wistar rats exposed to aerosols of two different types of MWCNTs (Pauluhn, 2010; Ma-Hock et al., 2009a). Li et al. (2007, 2009) carried out 30- and 60-day inhalation studies using an unconventional repeat-dose exposure regimen wherein Kumming mice were exposed to MWCNTs every other day. These studies are summarized in Table 13. Detailed documentation of the 13-week studies by Pauluhn (2010) and Ma-Hock (2009a) are available in Versar (2012).

Two studies of intermediate or subchronic duration were located in the recent literature investigating repeated exposure to MWCNTs by inhalation. One study (Pauluhn, 2010) appears in the searches of both the original report (Versar, 2012) and the current report, and is included in the summaries here for completeness. Pauluhn (2010) investigated toxicity of MWCNT (Baytubes®) in a 13-week inhalation study in rats. MWCNTs were 10 nm in diameter, 253 m^2/g in surface area, and greater than 98.6% pure with Co being the major contaminant (0.46 to 0.53% Co). Bulk density was 0.16 g/cm^3. The MWCNTs as obtained in bulk-stock form were compact aggregates on the order of several hundred μm. These were micronized (finely ground), which decreased bulk density to 0.11 g/cm^3 and decreased particle size to ~1 to 3 μm, but did not affect the primary morphology of the densely aggregated MWCNTs. HsdCpb:WU Wistar rats (50 M/10 F per group) were exposed via nose-cone inhalation to 0, 0.1, 0.4, 1.5, or 6 mg/m^3 for 6 h/d, 5 d/wk for 13 weeks. The MMAD varied with concentration; at the LOAEC (for increased lung weights, neutrophils, alveolar hypercellularity, and septal thickening) the MMAD was 3.05 μm with a GSD of 1.98. Lung histopathology and BALF and lung/lymph node burdens (Co measured as index for CNTs in lung lobes and lymph nodes, n = 6) were assessed up to 39 weeks after the start of exposure. Full clinical observations, including general hematology, clinical pathology, and urinalysis (OECD-compliant) were performed at week 13. Clinical signs of toxicity, mortality, body temperature, body weights, and food and water consumption were monitored and were not affected during the 13-week exposure. In BALF samples collected at 13 weeks, MWCNT exposures at concentrations of 0.4 mg/m^3 and above caused increases in neutrophils recovered. Lung and lung lymph node weights were increased at 13 weeks in the groups exposed to the 0.4 mg/m^3 concentration and higher. Histopathology analysis revealed that exposure to 0.4 mg/m^3 caused septal thickening, bronchoalveolar hypercellularity, leukocytic infiltration, and focal increases in collagen staining. Lesions caused by concentrations greater than 0.4 mg/m^3 increased in severity, and included pleural thickening and widespread increased collagen staining. The post-exposure recovery periods, ranging up to 26 weeks of recovery, showed levels of bronchoalveolar cellularity and leukocyte infiltration

decreasing to non-significant levels in the 0.4 mg/m^3 exposure group, while septal thickening and focal collagen staining did not decrease. This was true in the higher exposure groups as well, where inflammatory and repair-related responses (cell infiltration and hypercellularity) subsided in post-exposure periods, but remodeling responses (increased septal/pleural thickening and collagen) appeared more long-lived. The half-lives of Co in the lung were 151, 350, 318, and 375 days at 0.1, 0.4, 1.5, and 6 mg/m^3, respectively. Cobalt was also detected in hilar lymph nodes at 6 months post-exposure in the groups exposed to 1.5 or 6 mg/m^3 (n=6 males/concentration, kept as satellite groups). The NOAEC was 0.1 mg/m^3, the LOAEC was 0.4 mg/m^2, based on critical effects of increased lung weight, neutrophil accumulation (in BALF), bronchoalveolar hypercellularity, and alveolar septal thickening.

Pothmann et al. (2015) investigated MWCNT toxicity in a 13-week inhalation study in rats. The MWCNTs were 12 nm in diameter, with a surface area of 225.6 m^2/g; the major contaminants were aluminum (3.0%) and iron (2.7%). MWCNTs were ball-milled to increase dustiness and were delivered as compact aggregates from the nanometer range up to several microns in diameter. MWCNTs were administered to Wistar rats (10 M/10 F per group) via nose-only inhalation at 0, 0.05, 0.25, or 5.0 mg/m^3 (5 h/d, 5 d/wk) for 90 days. An additional arm of the study exposed rats (10 M/10 F per group) to 0, 0.05, 0.25, or 5.0 mg/m^3 for 90 days (as above) with a 90-day recovery period. The MMAD varied with concentration; at the LOAEC (for effects of neutrophilic inflammation and epithelial lesions) of 0.25 mg/m^2, the MMAD was 1.62 μm with a GSD of 4.67. Antemortem endpoints measured included functional observations, clinical examination, blood chemistry, hematology, urinalysis, and estrous cycle. Postmortem endpoints included organ histology and BALF analysis. Cells recovered in BALF were increased following exposure to 0.25 mg/m^3 MWCNTs, with the increases due to neutrophil accumulation. Total BALF cell numbers generally did not decrease significantly following the 90-day recovery and, in fact, increased in the 5.0 mg/m^3 group. Cytokines measured in BALF included IL-1ß, interleukin 1 alpha (IL-1α), TNF, and interleukin 5 (IL-5). IL-1α and ß levels were not affected following the 90-day exposure to 0.25 and 5.0 mg/m^3, but were increased following the 90-day recovery. IL-5 was also detected following the 90-day recovery, but the levels appeared spurious and not related to exposure concentration. TNF showed the most consistent response in both males and females and was increased at exposure to 0.25 and 5.0 mg/m^3. Lung weights for both sexes were increased following the 90-day exposure to 5.0 mg/m^3. In lung histology, alveolar macrophage increases were present (severity of 'minimal') following exposure to 0.25 mg/m^3.

Exposure to 5.0 mg/m^3 additionally caused leukocytic infiltration and interstitial inflammation at levels ranging from minimal to moderate, and bronchiolar cell hyperplasia and lymphoid infiltrates at a level of 'minimal'. Exposure to 0.25 mg/m^3 caused minimal increases in eosinophilic globules of the nasal cavity, squamous metaplasia of the larynx, and increased lymphocytes in tracheobronchial lymph nodes. Histopathological effects were not significantly decreased following the 90-day recovery. The NOAEC for this study was 0.05 mg/m^3 (0.06 mg/m^3 measured) and the LOAEC was 0.25 mg/m^3 (0.28 mg/m^3 measured), based on accumulations of neutrophils, IL-1ß, and TNF in BALF, and lesions of the nasal and laryngeal epithelia.

Kasai et al. (2015) tested toxicity of MWCNTs in a 13-week inhalation study in rats. MWCNTs

were 90.7 nm in mean diameter (measured). Mean length was 5.7 µm, with 48.7% of tubules greater than 5 µm. Surface area was 24 to 28 m^2/g and carbon purity was greater than 99.6%. MWCNTs were delivered in the form of individual, dispersed fibers based on SEM images. OECD Test Guideline 413 for subchronic inhalation toxicity was followed for this study. Aerosol generation used a cyclone sieve method. F344 rats (10 M/10 F/group) were exposed via whole-body inhalation to concentrations of 0, 0.2, 1, or 5 mg/m^3 MWCNTs for 6 h/d, 5 d/wk over 90 days. The MMAD varied with concentration; at the LOAEC (for effects of granulomatous inflammation and cell damage markers in BALF) of 0.2 mg/m^3, the MMAD was 1.5 µm with a GSD of 2.7. A full array of toxicity endpoints (clinical observations, blood chemistry, hematology, histological examination, and BALF analysis) was measured. All exposure levels caused adverse changes in the lungs. Total protein, LDH, and ALP were increased in BALF at all doses and increases were concentration-related. Neutrophils and lymphocytes were increased following exposure to 1 or 5 mg/m^3 MWCNTs. Exposure to 1 or 5 mg/m^3 also caused granulomatous inflammation and focal fibrosis of the lung in nearly all animals, with lesions present at an average grade of 'slight' or 'slight' to 'moderate' in 1 and 5 mg/m^3 groups, respectively. At 0.2 mg/m^3, 1/10 of the lungs showed granulomatous inflammation. MWCNTs also caused goblet cell hyperplasia and eosinophilic globules in nasal epithelium and nasopharynx, with all animals affected following exposure to 1 or 5 mg/m^3; grades were 'slight' to 'slight to moderate', respectively. Exposure to 0.2 mg/m^3 caused eosinophilic globules in the nasal cavity in 2/10 males and goblet cell hyperplasia in 1/10 male. Histological findings in females were similar to those in males, but only one female showed any histopathological changes in the respiratory tract (eosinophilic globules in the nasal cavity) in the 0.2 mg/m^3 group. In addition, females were less affected with regard to granulomatous inflammation of the lung (4/10 affected at 1 mg/m^3 as opposed to 8/10 in males). The LOAEC was 0.2 mg/m^3 (lowest concentration tested) based on granulomatous inflammation and increased LDH, ALP, and total protein recovered in BALF. There was no NOAEC. An estimation of MWCNT lung burden was carried out after the 13-week exposure using a hydrocarbon adsorption-desorption method on the digested left lung lobe. The lung burdens of CNTs at the LOAEC were 3.23 µg/left lung in males and 2.30 µg/left lung in females. MWCNT burdens were consistently 1.4 to 1.6 times higher in males compared to females at all dose levels.

Table 13. Summary Intermediate Duration and Subchronic Inhalation Toxicity to CNTs

Species and study type (n/sex/group)	Exposure (report concentrations, frequency, duration)	Particle characteristics[a]	NOAEC (mg/m^3)	LOAEC (mg/m^3)	Responses at the LOAEC	Comments	Reference
Kunming mice 9 F/30-d and 60-d exposure groups whole-body exposure	0 or 32.61 mg/m^3 6 h/d for 5 d in an 8d period, 10 d in a 16-d period, and 15 d in a 24-d period (Li et al., 2007). Other groups exposed for 15 d in 30 d and 30 d in 60 d (i.e., every other day) (Li et al., 2009[b]).	MWCNT, 95% pure, <0.2% La and Ni; surface area 280 m^2/g.[b]	None	32.61	In 24-, 30-, and 60-d mice, the principal lung pathology reported to be proliferation and thickening of the alveolar walls. No incidence data reported. In 60-d mice (but not 30-d mice), BALF samples showed increased activities of ALP, ACP, and LDH.	During 90-min exposure periods (four during exposure days), concentrations decreased from about 80 to 13 mg/m^3. The reported concentration is an average. Constant concentrations were apparently not attained. Histology data were only described qualitatively. Collected data are not useful for describing dose-response relationships.	Li et al., 2009[b]; 2007[b]
Wistar rat 10/sex/group head –nose exposure	0, 0.1, 0.5, or 2.5 mg/m^3, 6 h/d, 5 d/wk for 90 d	MWCNT, 90% pure, 10% metal oxide (9.6% aluminum oxide with traces of Fe and Co); 5–15 nm dia and 0.1–10 µm length; 250–300 mg^2/g surface area; MMADs between 0.7 and 2.0 µm; GSDs between 2.1 and 4.1; 77.4–86.3% mass fractions of particles had aerodynamic size <3 µm[b]	None	0.1	Lung lesions: minimal diffuse histiocytosis (8/10 vs. 0/10 in control); Mediastinal lymph node lesions: granulomatous inflammation (2/10 vs. 0/10) Other lesions at 0.5 and 2.5 mg/m^3: granulomatous inflammation, diffuse neutrophilic inflammation, and intraalveolar lipoproteinosis in lung; lymphoreticular hyperplasia in lymph node; and particles in macrophages in lymph nodes.	Incidence and severity of lung and lymph node lesions increased with increasing concentration. No exposure-related changes in hematological or serum chemistry variables. Comprehensive examination of other tissues and organs in control and high-concentration rats revealed no exposure-related increased incidence of lesions. Aerosols were generated by brush generator.	Ma-Hock et al., 2009a[b]

Species and study type (n/sex/group)	Exposure (report concentrations, frequency, duration)	Particle characteristics[a]	NOAEC (mg/m^3)	LOAEC (mg/m^3)	Responses at the LOAEC	Comments	Reference
Wistar rats 50 M and 10 F/group nose only exposure	0, 0.1, 0.4, 1.5, or 6 mg/m^3 6 h/d, 5 d/wk for 13 wks. Pulmonary toxicity assessed 1 d, and 4, 13, and 26 wks after exposure.	Pristine MWCNT, Baytubes®, containing 99.1% C, 0.8% O, and 0.53% Co; 10 nm dia. and 200–300 nm length; 257 m^2/g surface area; MMADs ranged from 2.74–3.05 µm (GSDs 1.98–2.14). Aerosols of micronized MWCNT were generated by a Wright Dust Feeder.	0.1	0.4	BALF samples through post-exposure wks 3 or 13 showed increased PMN counts, soluble collagen and protein and, γ-GT activities. Lung lesions: particle laden macrophages at d 1 and wk 13; alveolar interstitial thickening or hypercellularity at bronchio-alveolar junction at all sampling dates after 13 wks of exposure; focal-widespread inflammatory cell influx at 1 d after exposure; focally increased collagen staining in terminal bronchiole at all sampling dates.	Severity scores for lung lesions with significantly increased incidences reported. Number of lesions and their severity increased with increasing exposure. More pronounced and sustained changes in more BALF variables were observed at 1.5 and 6 mg/m^3 (e.g., increased total cell counts and activities of LDH and β-n-acetyl glucosaminidase). Additional lung lesions observed at 1.5 and 6 mg/m^3 at all sampling dates: pleural thickening (6 mg/m^3 only), increased collagen staining in terminal bronchioles. Upper respiratory tract lesions observed on d 1 after exposure included goblet cell hyperplasia and/or metaplasia, eosinophilic globules, and focal turbinate remodeling at 1.5 and 6 mg/m^3.	Pauluhn, 2010

Species and study type (n/sex/group)	Exposure (report concentrations, frequency, duration)	Particle characteristics[a]	NOAEC (mg/m^3)	LOAEC (mg/m^3)	Responses at the LOAEC	Comments	Reference
Wistar rats 10 M/10 F per group nose-only exposure	0, 0.05, 0.25, or 1.25 mg/m^3, 5 h/d for 5 d/wk for 13 wks.	MWCNTs, 3.0% Al, 2.7% Fe, mean dia of 12.1 nm, mean length of 1.07 ± 1.10 µm, surface area of 225.6 m^2/g. Bulk MWCNT were ball-milled to increase dustiness. MMAD at 0.25mg/m^3 was 1.62 µm with a GSD of 4.67.	0.05 (measured as 0.06)	0.25 (measured as 0.28)	Accumulation of neutrophils and increases in IL-1ß and TNF in BALF and metaplastic lesions of the nasal and laryngeal epithelia	Endpoints included clinical exam, blood chemistry, urinalysis, estrous cycle, organ histology, and BALF analysis. Effects at the LOAEC were not reversed following a 90-day post exposure recovery period investigated in additional groups (10 M/10 F per group), with the exception of BALF neutrophils, which were somewhat abated	Pothmann et al., 2015
F344 rats 10 M/10 F whole body exposure	0, 0.2, 1, or 5 mg/m^3, 6 h/d for 5 d/wk for 13 wks.	MWCNT, >99.6% pure, mean dia of 90.7 nm, mean length of 5.7 µm, surface area of 24-28 m^2/g. MWCNT were delivered dispersed as individual fibers. MMAD at 0.2 mg/m^3 was 1.5 µm with a GSD of 2.7.	None	0.2	Increased alkaline phosphatase, LDH, and total protein in BALF, and granulomatous inflammation of the lung	This study was done according to OECD 413. Endpoints included clinical exam, blood chemistry, hematology, organ histology, and BALF analysis. Lung burdens were estimated on digested lung using a hydrocarbon adsorption-desorption method. The lung burden of CNTs at the LOAEC was 3.23 µg/left lung in males and 2.30 µg/left lung in females. MWCNT burdens were consistently 1.4 to 1.6 times higher in males than females at all doses	Kasai et al., 2015

[a] NT characterization data, if reported: source, diameter and length, surface area, purity and impurities, and state of aggregation; shape (bundles, tangles, ropes)

[b] As reviewed in Versar (2012)

4.4.2.3 Dermal Exposure

No studies investigating systemic toxicity from repeat-dose dermal exposure in animals were available either in the recent literature or in literature prior to 2010 (Versar, 2012).

4.4.2.4 Other Routes of Exposure

Repeat-dose studies relevant to an ADI derivation (i.e., dose-response) using IT or OPA exposure to MWCNTs were not located. Single doses of MWCNT instilled as a bolus are thought to model repeated exposures in the lung due to low clearance rates of MWCNT burdens, and adequate dose-response studies of this kind are summarized in Appendix C. As there are adequate studies by the inhalation route, studies of IP and IV exposures were not considered to contribute additional relevant information.

4.4.2.5 Summary

Overall, the data reflect that both SWCNTs and MWCNTs exhibit low repeat-dose/subchronic toxicity by the oral route, although data is limited to experimentation with one formula each for SWCNTs and MWCNTs (dispersed in 5% gum acacia) in one species (rat) (Matsumoto et al., 2012). The absence of clinical, histological, or blood biochemical effects at the highest doses used in the study (exposures to 12.5 mg/kg/d SWCNT or 50 mg/kg/d for 28 consecutive days) suggest that adverse health effects at lower levels are very unlikely. These high doses were used based on the physical limits of what could be prepared for gavage so testing at the guideline dose limit of 1000 mg/kg/d was not possible.

Data for repeated inhalation exposure to SWCNT is limited to one study (Morimoto et al., 2012). No treatment-related lung effects or inflammation were observed after exposing rats to low concentrations (maximum 0.13 mg/m^3) of surfactant-coated SWCNTs over a 28-day exposure duration. Dose-response toxicity following repeat inhalation to SWCNTs is not well-characterized. In dose-response studies using IT or OPA administration to rats and mice, bolus lung exposures in the range of 0.2 mg/kg bw SWCNTs were sufficient to cause inflammatory responses as measured in BALF (see Appendix B).

Studies of repeat inhalation of MWCNTs showed granulomatous changes and epithelial hyperplasia in the airways and lungs accompanied by signs of neutrophilic inflammation in BALF at LOAECs in the range of 0.1 to 0.4 mg/m^3 over 90-d exposures to MWCNTs. While several well-documented studies agree on these effect levels, the well-characterized data are limited to exposures in rat.

4.5 Chronic Toxicity

4.5.1 Single-walled CNTs

No studies of chronic toxicity from SWCNT exposure by oral, inhalation or dermal routes in humans or animals were available either prior to 2010 (Versar, 2012) or in the recent literature.

4.5.2 Multi-walled CNTs

Only one study of MWCNT exposure by inhalation in the rat is available for assessment of chronic MWCNT exposure; no oral or dermal studies are available.

Kasai et al. (2016) documented chronic MWCNT toxicity by inhalation in a rigorous and Good Laboratory Practices (GLP)-compliant 2-yr carcinogenicity study in rats according to OECD Test Guideline 451. MWCNTs were 90.7 nm in mean diameter (measured). Mean length was 5.7 μm, with 48.7% of tubules greater than 5 μm. Surface area was 24 to 28 m^2/g and carbon purity was greater than 99.6%. MWCNTs were delivered in the form of individual, dispersed fibers as visualized by SEM. F344 rats (50 M/50 F/group) were exposed via whole-body inhalation to 0, 0.02, 0.2, or 2.0 mg/m^3 MWCNT at 6 h/d, 5 d/wk for 104 weeks. Aerosol particle size and morphology were monitored weekly by SEM. The MMAD was 1.3 μm with a GSD of 2.9. Non-neoplastic adverse effects and lesions were documented via clinical observations, hematology, blood biochemistry, organ histology, and BALF analysis. MWCNT exposure caused no adverse changes in urinary, hematological, or blood biochemical endpoints and did not cause changes in any organs apart from lungs and associated tissues. The incidence of non-neoplastic lesions in lungs and associated tissues are given in Table 14. MWCNT exposure for 104 weeks increased lung weights in males at concentrations starting at 0.2 mg/m^3 and in females at doses starting at 0.02 mg/m^3. Lung histology reflected a trend of increasing incidence of the following adverse effects, beginning at the lowest exposure level (0.02 mg/m^3): bronchiolo-alveolar hyperplasia, alveolar hyperplasia, macrophage accumulation, focal fibrosis, and granulomatous inflammation. These effects were statistically significant in males at 0.2 mg/m^3, and focal fibrosis and granulomatous inflammation were present in over 80% of males and females at this concentration. Mesothelial hyperplasia in the pleura was increased in males at 2.0 mg/m^3, and focal fibrosis of the pleura was significantly increased in both males and females at this concentration. In BALF, a trend toward increased macrophage and neutrophil numbers was seen at all exposure levels in both males and females, but this increase was statistically significant only in the 2.0 mg/m^3 group. Significant increases in total protein, LDH, and ALP were measured in BALF in males and females exposed to 0.2 mg/m^3 MWCNT. For non-neoplastic adverse effects, the authors considered 0.02 mg/m^3 as the LOAEC based on increased lung weight in females; there was no NOAEC in this study. MWCNT lung burdens were also estimated using an SEM-enabled counting method. The lung burdens at the LOAEC in males and females were 10.0 and 8.1 μg/lung, respectively.

Table 14. Non-neoplastic Lesions in Lung and Pleura in Rats exposed to MWCNT for 104 weeks

	Male				Female			
Exposure Concentration (mg/m^3)	0	0.02	0.2	2.0	0	0.02	0.2	2.0
Number of Animals in Group	50	50	50	50	50	50	50	50
Lung Weights (mg) ± SD	131±10	134±12	151**±13	237**±31	90±21	94**±10	114**±27	187**±18
Lung								
Bronchiolo-alveolar hyperplasia	2 (1.5)	6 (1.3)	13*(1.2)	22**(1.0)	3(1.3)	3(1.0)	8(1.1)	12*(1.1)
Atypical hyperplasia	0	0	1(1.0)	10**(1.3)	0	0	0	14*(1.1)
Alveolar hyperplasia	0	2(1.0)	13**(1.0)	41**(1.0)	1(1.0)	1(1.0)	6(1.0)	41**(1.1)
Bronchiolar hyperplasia	0	0	4(1.0)	8**(1.0)	0	0	4(1.0)	26**(1.0)
Alveolar macrophage accumulations	2(1.0)	7(1.0)	5(1.0)	48**(2.0)	2(1.0)	6(1.0)	9(1.0)	48**(1.8)
Focal fibrosis (alveoli)	0	2(1.0)	43**(1.0)	48**(1.8)	0	3(1.0)	44**(1.0)	49**(1.2)
Granulomatous inflammation	0	5(1.0)	42**(1.0)	50**(1.9)	0	3(1.0)	45**(1.0)	50**(1.8)
Pleura								
Simple mesothelial hyperplasia	3(1.0)	3(1.0)	7(1.0)	12*(1.0)	3(1.0)	2(1.0)	6(1.0)	10(1.0)
Focal fibrosis (parietal face)	0	0	2(1.0)	6*(1.0)	0	0	0	3(1.0)
Focal fibrosis (ventral face)	0	2(1.0)	4(1.0)	19**(1.1)	0	2(1.0)	2(1.0)	20**(1.0)
Mediastinal inflammation	15(1.0)	18(1.0)	21(1.0)	26*(1.0)	17(1.0)	17(1.0)	16(1.0)	19(1.0)
Diaphragm inflammation	0	0	1(1.0)	1(1.0)	0	1(1.0)	1(1.0)	1(1.0)

[a]Values indicate number of animals bearing lesions; values in parentheses are average severity grade (4-point grading system).
*p ≤ 0.05, **p ≤ 0.01, Chi-square Test except for lung weights, evaluated with Dunnett's test.
Source: Kasai et al., 2016

In summary, no chronic studies are available for SWCNT exposure by the oral, inhalation or dermal routes. Only one study using one MWCNT example material in the rat is available for assessment of chronic MWCNT exposure by inhalation; no oral or dermal studies are available. The LOAEC for chronic toxicity data in rat (0.2 mg/m^3) is supported by the subchronic inhalation studies showing similar epithelial and granulomatous lesions with LOAECs in this

range (see Table 14).

4.6 Reproductive and Developmental Toxicity

4.6.1 Single-walled CNTs

There is a lack of information regarding human exposure to SWCNT and reproductive or developmental outcome. Versar (2012) reported that no standard mammalian tests of reproductive or developmental toxicity had been located for CNTs. More recently, developmental and reproductive studies of CNTs were reviewed by Ema et al. (2016). Four developmental and/or reproductive toxicity studies of SWCNTs were located in the recent search of literature since 2010 (Philbrook et al., 2011; Pietroiusti et al., 2011; Campagnolo et al., 2013; Huang et al., 2014), but none used standard guideline protocols with an environmentally relevant exposure route (such as oral or inhalation). Administration of SWCNTs in developmental/reproductive toxicity studies was restricted to mice and to a single dose or to a few days during gestation; there was one study by oral gavage and three studies by IV administration (Pietroiusti et al., 2011; Philbrook et al., 2011; Campagnolo et al., 2013; Huang et al., 2014). The studies had design, method and analysis limitations: did not use standard guideline protocols, had limited characterization of the nanotubes that was difficult to compare across studies, may have used only one dose level, and/or administered the SWCNTs via parenteral routes. Furthermore, the studies used SWCNTs with differing surface modifications (described by the authors as functionalizations) and chemical treatments (oxidization), and some did not report results for SWCNTs alone. The studies by Campagnolo et al. (2013), Huang et al. (2014), and Pietroiusti et al. (2011), examined external but not skeletal or visceral anomalies. Table 15 summarizes these studies.

4.6.1.1 Oral Exposure

Philbrook et al. (2011) investigated the effect of ingested hydroxyl-functionalized SWCNTs (OH-fSWCNTs) on reproduction and development in CD-1 mice in a non-guideline protocol. Comparison of fSWCNTs with non-functionalized SWCNTs was not provided in the study. The purchased OH-fSWCNTs measured 1 to 2 nm in diameter and 5 to 30 μm in length, and were greater than 90% pure; 75 μm graphite particles at 99.9% pure were used as a control material. The pregnant mice were gavaged with a single 0, 10 or 100 mg/kg suspension of OH-fSWCNTs on gestation day (GD) 9 and sacrificed on GD 19. At termination, all fetuses were counted, weighed, length determined, and examined for external defects. Fetuses were stained with Alcian blue and alizarin red S for visualization of cartilage and bone, respectively. Placentas, livers and kidneys were removed and histopathologically examined from sacrificed fetuses. Clinical observations and changes in maternal weight (GD 9 to GD 19) were statistically similar across all treatment groups; no other maternal effects were reported. Fetal length, weight and viability were also similar across treatment groups. This study is limited in that data analyses were conducted on fetuses rather than by litter, as is more appropriately performed, thereby limiting interpretation of results. There were significantly higher percentages of resorbed implantations, percent total fetuses with gross defects, and skeletal abnormalities in fetuses exposed to 10 mg/kg, but not 100 mg/kg, OH-fSWCNTs. The statistical analyses were based on accumulated gross morphological and skeletal defects using Fisher's Exact test on a fetal, and not on a litter, basis as the unit of analysis. The percentage of total non-viable fetuses were

increased relative to controls (3.2 vs. 0.8), albeit not statistically significantly, and the percentage of fetuses with skeletal defects (mainly limb and vertebral) was significantly higher at 10 mg/kg OH-fSWCNTs.

4.6.1.2 Other Routes of Exposure

There were no reproductive and developmental toxicity studies located for SWCNTs by inhalation or dermal exposure.

Three studies using IV injection evaluated developmental endpoints in pristine or functionalized SWCNT; these studies are listed in Table 15 and described in Appendix D.

4.6.1.3 Summary

There was only one study administering OH f-SWCNTs by the oral route and this study included exposure only on one day of organogenesis (GD 9) in the mouse (Philbrook et al., 2011). Comparison between functionalized and non-functionalized SWCNT was not provided in the study; graphite particles were used as a control due to similarity in chemical structure. The developmental effects were not dose-related (10 mg/kg of OH f-SWCNT had more severe findings than 100 mg/kg), and the statistical analysis must be viewed with caution (as it did not use the litter as the experimental unit). There were three studies using IV administration of SWCNTs (Pietroiusti et al., 2011; Campagnolo et al., 2013; Huang et al., 2014) that produced abortions, fetal malformations and placental damage, demonstrating transplacental passage of the nanoparticles and adverse developmental outcome. However, these studies had limitations: they did not use standard guideline protocols, often had limited characterization of the carbon nanotubes, and/or used only one dose level. Although these studies, taken together, suggest the potential for adverse developmental effects should the SWCNTs become systemically distributed, the limitations of the database preclude definitive conclusions as to the developmental and reproductive toxicity of SWCNTs.

Table 15. Developmental and Reproductive Studies of SWCNTs

Species	SWCNT	Route	Day	Dose	NOAEL	LOAEL	Findings	Reference
CD-1 mice (10-12/gp)	OH-fSWCNTs –D: 1-2 nm x 5-30 µm >90-99.9% pure	Single oral gavage	GD 9	0, 10 or 100 mg/kg	ND[a]	ND[a]	↑ % resorbed implantations, % total fetuses with gross defects, and % skeletal abnormalities in 10 mg/kg but not 100 mg/kg group; study limited by data analyses not performed on a per litter basis	Philbrook et al., 2011
CD-1 mouse (16–23/gp)	p-SWCNTs; o-SWCNTs; uo-SWCNTs	IV	GD 5.5	0, 0.01, 0.1, 0.3, 3, or 30 µg/mouse			↑ incidence of miscarriage at 30 µg of p-, o-, and uo-SWCNTs; Malformed fetuses at 3 µg of p-SWCNTs, 30 µg of o-SWCNTs, and 0.3 µg of uo-SWCNTs	Pietroiusti et al., 2011
CD-1 mouse (5-18/gp)	PEG-SWCNTs L: 86 nm	IV	GD 5.5	0, 0.1, 10, or 30 µg/mouse			One fetus with external malformations at 30 µg on GD 5.5 and five fetuses with malformations in after multiple injections (30 µg total). ↓ size and vascularization of the placentas of malformed fetuses	Campagnolo et al., 2013
			GDs 5.5, 8.5, and 11.5	0 or 10 µg/mouse/day				
p53+/- mouse (4–6/gp)	fPEG-NH4-SWCNTs D: 1-2 nm x 0.5–2 µm)	IV	GDs 10.5, 12.5, and 15.5	0 or 2 mg/kg/d			No effect on maternal or fetal body weight, or incidence of fetal defects	Huang et al., 2014

[a] NOAEL and LOAEL cannot be determined due to study limitations
PEG = polyethylene glycol; f = functionalized; p = pristine; o = oxidized; uo = ultra-oxidized

4.6.2 Multi-walled CNTs

There is no information regarding human exposure to MWCNT and reproductive or developmental outcome. For MWCNTs, eight reproductive and developmental studies in animals were available in the recent literature (Bai et al., 2010; Lim et al., 2011; Fujitani et al., 2012; Ivani et al., 2012; Hougaard et al., 2013; Huang et al., 2014; Qi et al., 2014; Wang et al., 2014). Versar (2012) reported that no standard mammalian tests of reproductive or developmental toxicity had been located for CNTs. Routes of exposure included oral gavage, IT,

and IP and IV injection. Of the eight studies, two were via oral gavage, one in rats (Lim et al., 2011) and one in mice (Wang et al., 2014); the remaining six studies used parenteral routes of administration and several strains of mice (Bai et al., 2010; Fujitani et al., 2012; Ivani et al., 2012; Huang et al., 2014; Qi et al., 2014). Only one study investigated male reproductive toxicity (Bai et al., 2010). None of the studies utilized a standard guideline testing approach, and the studies often used a relatively small number of animals, only one dose level, and/or provided limited and differing types of characterization of the MWCNTs. While the majority of studies were via IT, IV, and/or IP routes and are not generally directly relevant to human exposure via oral, inhalation or dermal exposure, they inform the potential for adverse reproductive and/or developmental effects given the limited database. Table 16 summarizes these studies and, for the two oral studies, the associated NOAELs and LOAELs.

4.6.2.1 Oral Exposure

Lim et al. (2011) investigated MWCNT fetotoxicity in pregnant BALB/c rats in a developmental study via the oral route. The MWCNTs were commercially available, 10 to 15 nm in diameter and approximately 20 nm in length, and "95% carbon and approximately 5% iron" (presumed to be manufacturer-reported). MWCNTs were sonicated in 1% carboxymethylcellulose buffer and administered by gavage to pregnant Sprague-Dawley rats (n =12/group) on GD 6 to 19. Doses were 0, 40, 200, or 1000 mg/kg/d at 20 ml/kg. Pregnant mice were monitored for mortality, morbidity, appearance, and behavior. Postmortem endpoints on GD 20 were organ weights, oxidative stress markers in maternal liver homogenates, uterine content parameters, and skeletal and visceral examination of the fetuses. Significant decreases in maternal absolute and relative thymus weights (approximately -27 and -23%, respectively) occurred at 1,000 mg/kg and were considered treatment-related, showing a clear dose-response. No treatment-related effects were seen in the exposed fetuses.

CD-1 mice were orally gavaged with carboxylated MWCNTs at 0, 22 or 65 mg/kg/d during gestation and lactation (GD 0 through postnatal day [PND] 21) in a perinatal developmental and reproductive study as part of a Bisphenol A investigation (Wang et al., 2014). COOH-fMWCNT alone, at two different dose levels, had no adverse effects on maternal reproductive endpoints, embryo-fetal development, male offspring growth and organ weights, or serum hormone levels (follicle stimulating hormone [FSH], testosterone and leutinizing hormone [LH]) of only male offspring at PND 35. Comparison of fMWCNTs with non-functionalized MWCNTs was not provided in the study.

4.6.2.2 Other Routes of Exposure

There were no developmental or reproductive toxicity studies by the inhalation or dermal route for MWCNTs located in the recent literature search.

The male reproductive toxicity of water soluble carboxylate-functionalized MWCNTs (COOH-fMWCNTs) or amine-functionalized MWCNTs (NH4-fMWCNTs) was studied (Bai et al., 2010). Male mice were IV injected at 0 (vehicle) or 5 mg/kg/d once or five times, every third day with one of the types of MWCNTs. Partially damaged seminiferous tubules and reductions in tubule thickness were observed on day 15 for both fMWCNTs. Neither fMWCNT changed hormone levels (testosterone, FSH and LH) or sperm parameters (concentration, motility,

morphology and acrosome integrity), or had adverse effects on reproductive performance evaluated on days 15 or 60, relative to control. Labeled COOH-fMWCNTs were found to cross the blood–testicle barrier and induce transient histopathological changes in the testes, but not in sperm parameters or male reproductive parameters.

Fujitani et al. (2012) conducted a developmental study wherein 0 (vehicle), 2, 3, 4, or 5 mg/kg MWCNTs by a single IP injection of 3, 4, or 5 mg/kg MWCNT or by a single IT were administered to pregnant CD-1 mice on GD 9; average size of MWCNT was 90 nm (range 70 to 110 nm as described in Sakamoto et al., 2009). For IP, maternal (decreased body weight) and fetal toxicity (decreased fetal weight and increased early resorptions) were observed at all doses, but no statistically significant increases were found in the incidence of individual types of malformations. For IT, maternal toxicity was observed at 4 and 5 mg/kg and fetal growth was inhibited at 5 mg/kg. The incidence of dams with fetuses with external and skeletal defects was higher at 4 and 5 mg/kg, with significant increases in the incidences of fetuses with short or absent tails and with fusion of the ribs, or vertebral bodies, and arches.

Pregnant NMR1 mice were IP injected with MWCNTs at 0, 1.0 or 10 mg/mouse/day on GD 0 and 3 in a postnatal behavioral study (Ivani et al., 2012). Adverse behavioral effects (forced swimming test) were increased at 1.0, but not at 10 mg/mouse/day (i.e., responses were not dose-related).

Hougaard et al. (2013) IT instilled female C57BL/6 mice with MWCNTs at 0 or 67 µg/mouse/d on GD 8, 11, 15 and 18 (total dose 268 µg/mouse). Time to deliver first litter was delayed by an average of 5 days. No effects were observed for gestation and litter parameters, offspring behavior or daily sperm production.

Developmental toxicity was examined for amine-functionalized MWCNTs (NH4-fMWCNT) with outer diameters of 8, 20, or 50 nm; all had a length of 0.5 to 2 µm (Huang et al., 2014). Pregnant heterozygous p53 +/- knockout mice were IV injected with 0 (vehicle) or 5 mg/kg/d on GDs 10.5, 12.5, and 15.5. Only the 50 nm MWCNTs increased the incidence of brain defects and decreased survival of fetuses at termination (GD 17.5). A back-cross mating caused brain defects in half of the p53-/- fetuses but not in p53+/+ and p53+/- with injection on GD 10.5. Injection on GD 15.5 decreased body weight of p53+/+ fetuses. Larger sized (50 nm) MWCNTs crossed the blood-placenta barrier, reduced fetal weights and induced brain deformities, whereas single-walled and smaller sized multi-walled carbon nanotubes caused no or less fetotoxicity.

The abortifacient effect of oxidized MWCNTs (o-MWCNT) was studied in a developmental study in pregnant Kunming mice IV injected with 0 or 20 mg/kg/d, starting on GD 7 and continuing daily until abortion or parturition occurred (Qi et al., 2014). Higher abortion rate and decreased maternal body weight gain were observed in mice injected from GD 7 until abortion or parturition. The observed delay in fetal growth and increased fetal death based on 99mTC labeling seemed to be associated with placental dysfunction caused by o-MWCNTs.

4.6.2.3 Summary

In total, there were two developmental and reproductive studies for MWCNT using the oral route of exposure (Lim et al., 2011; Wang et al., 2014). The Lim et al. (2011) rat study covered

organogenesis and had appropriately spaced dosages (0, 40, 200, or 1000 mg/kg/d). The only findings were a decrease in maternal absolute and relative thymus weights at 1000 mg/kg/d with no adverse fetal findings. The other oral study (perinatal study) in mice was part of a Bisphenol A investigation (Wang et al., 2014) and used two dose levels (22 or 65 mg/kg/d) of functionalized MWCNTs (COOH-MWCNT) with exposure throughout gestation and lactation. There were no adverse effects on maternal reproduction, embryo-fetal development, offspring growth and organ weights, or serum hormone levels of male offspring.

The six studies using parenteral routes of administration were all conducted in mice and showed that MWCNTs could damage seminiferous tubules (Bai et al., 2010); produce adverse maternal and fetal toxicity (Fujitani et al., 2012); behavioral effects (Ivani et al., 2012); delayed mating (Hougaard et al., 2013); brain defects (Huang et al., 2014); and be an abortifacient (Qi et al., 2014) once the CNTs enter the blood stream.

It is difficult to draw definitive conclusions regarding the developmental and reproductive hazards (including male reproductive toxicity) of SWCNTs and MWCNTs as there are no published standard or guideline studies. The limited data herein suggest MWCNTs are more of a developmental hazard than SWCNTs. Furthermore, the larger diameter CNTs are more of a reproductive and developmental hazard than smaller diameter CNTs. This is consistent with the general observation that MWCNT examples with diameters in the range of 50-100 nm have a semi-rigid fiber morphology that is more toxic than other MWCNT forms (see Sec. 4.1). There is insufficient data to draw conclusions between toxicity of functionalized and non-functionalized CNTs.

Table 16. Developmental and Reproductive Studies of MWCNTs

Species	MWCNT[a]	Route	Day	Dose	NOAEL[b] mg/kg/d	LOAEL[b] mg/kg/d	Findings	Reference
CD-1 mice (10/gp)	fCOOH-MWCNT inner/outer dia: ~20 nm/30 nm x ~0.5–2.0 µm	Oral gavage	GDs 0–21 and until weaning	0, 22 or 65 mg/kg/d	65== maternal 65== develop-mental	None None	No effect on maternal body weight, behavior, or reproduction. No effect on litter size, sex ratio of pups, or body or organ weight, or serum levels of malondialdehyde, FSH, LH, or testosterone of male offspring.	Wang et al., 2014
Sprague-Dawley rat (12/gp)	CM-95 by Hanwha Nanotech (Incheon, Republic of Korea) MWCNT M-95; dia 10–15 nm x ~20 µm 95% carbon; 5% iron	Oral gavage	GDs 6–19	0, 8, 40, 200 or 1000 mg/kg/d	200-maternal 1000-develop-mental	1000-maternal None develop-mental	↓ Maternal thymus weight at 1000 mg; no effect on fetal growth, viability, or morphological development	Lim et al., 2011
CD-1 mouse (6–16/gp)	MWCNT-7 - dia: 90 nm x 27.5% longer than 5 µm	Single IP	GD 9	0, 2, 3, 4, or 5 mg/kg			↓ Maternal BW, ↓ litter size and fetal weight at all doses; ↑ Maternal spleen weight at ≥ 2 mg; resorption rate at ≥ 4 mg; fetuses with malformations ≥ 2 mg.	Fujitani et al., 2012
		Single IT		0, 3, 4, or 5 mg/kg			↓ Maternal BW at 4 and 5 mg; fetal BW at 5 mg; ↑ Maternal lung weight at 5 mg; fetuses with malformations at 4 and 5 mg	
NMR1 mouse (10/gp) female	MWCNT dia: 30 nm x 10 µm; Surface area: 270 m^2/g, 95%	IP	GDs 0 and 3	0 or 1 and 10 µg/mouse/d			↑time in forced swimming test at 1 µg. No deaths or changes in toxicity or reproductive parameters. No external malformations or changes in developmental landmarks, reflexes, or behavior in the open field or Morris water maze	Ivani et al., 2012
C57BL/6 mouse (30/group) female	MWCNT-400, dia: 10 nm, length: 295 nm	IT	One day preconception	0 or 67 µg/mouse/d			↑ time to delivery; pathologic changes in mononuclear infiltration and bronchiole edema and ↑ Kupffer cells. No effect on maternal BW or gesta-tional or litter parameters.	Hougaard et al., 2013

Species	MWCNT[a]	Route	Day	Dose	NOAEL[b] mg/kg/d	LOAEL[b] mg/kg/d	Findings	Reference
BALP/c mouse (4-8/gp) male	fCOOH-MWCNT dia: 20–30 nm x 0.5–2.0 mm)	IV	Once every 3 days; 5 times over 13 days.	0 or 5 mg/kg/d			Transient histopathological changes in testes after multiple injections of both fMWCNTs; transient increased levels of MDA in testes after multiple injections of fCOOHs.	Bai et al., 2010
	fNH4-MWCNT dia: 20–30 nm x 0.5–2.0 µm							
p53+/- mouse (4–6/gp) female	fPEG-NH4-MWCNT 8 dia:<8 nm x 0.5–2 µm); PEG-NH4-20 dia: 20–30 nm x 0.5–2 µm); PEG-NH4-50 dia: ~50 nm x 0.5–2 µm)	IV	GDs 10.5, 12.5, and 15.5	0 or 2 mg/kg/d			↓ Maternal BW and ↓ fetal BW after injection of fPEG-NH4-20 and 50; ↑ Fetal brain deformity after injection of fPEG-NH4-50.	Huang et al., 2014
	PL-PEG-NH4-MWCNT-50		GD 15.5	0, 2 or 5 mg/kg			↓ Survival rate of postnatal offspring at 5 mg	
	PL-PEG-NH4-MWCNT-50		GD 15.5	0 or 5 mg/kg			↑ Fetal brain defect (50% of p53-/- fetuses) after injection on GD 10.5; ↓ Body weight of p53+/+ fetuses after injection on GD 15.5; ↓ Brain defect in p53-/- fetuses after co-injection of NA on GD 10.5	
Kunming mice (10/gp) female	o-MWCNTs dia:10–30 nm x 1–2 µm, purity >96%,	IV	GD 7 to abortion or parturition	0 or 20 mg/kg/d			↑ Abortion rate ↓ Maternal body weight gain	Qi et al., 2014
			GDs 4, 11, and 15				↓ Progesterone in maternal sera at GDs 7, 14, and 18 ↑ Estradiol in maternal sera at GDs 7 and 14	
			GDs 9–11				↑ Placental ROS in first-time pregnant mice ↓ Placental VEGF in first- and second-time pregnant mice	

[a]Detailed characterization information is provided for nonfunctionalized CNTs administered by routes relevant to human exposure as follows 1. Source 2. Diameter and length 3. Surface area 4. Purity and impurities 5. State of aggregation; shape (bundles, tangles, ropes)
[b]NOAEL and LOAEL determined only for oral studies because this route is relevant to human exposure
FSH = follicle-stimulating hormone; LH = luteinizing hormone; MDA = malondialdehyde; VEGF = vascular endothelial growth factor

4.7 Carcinogenicity

4.7.1 Single-walled CNTs

No studies in humans or animals are available for SWCNT carcinogenicity by any route, either in the recent literature or prior to 2010 (Versar, 2012).

4.7.2 Multi-walled CNTs

Only one study examining potential carcinogenicity by the inhalation route was located in the recent literature searched. Earlier reports (Versar, 2012) did not locate any carcinogenicity studies for MWCNTs.

Kasai et al. (2016) investigated the carcinogenic potential of MWCNTs in rats in a 2-yr GLP-compliant bioassay according to OECD Test Guideline 451. MWCNTs were 90.7 nm in mean diameter (measured). Mean length was 5.7 µm, with 48.7% of tubules greater than 5 µm. Surface area was 24 to 28 m^2/g and carbon purity was greater than 99.6%. MWCNTs were delivered in the form of individual, dispersed fibers as visualized by SEM. F344 rats (50 M/50 F/group) were exposed via whole-body inhalation to 0, 0.02, 0.2, or 2.0 mg/m^3 MWCNTs for 6 h/d, 5 d/wk for 104 weeks. Aerosol particle size and morphology were monitored weekly by SEM. The MMAD was 1.3 µm with a GSD of 2.9. Survival rates over the 104-week exposure were at least 72% (males) and 68% (females) in all groups, and no differences in survival rates or body weights were seen in MWCNT-exposed groups vs. controls. No differences from controls were observed in urinary, hematological, or blood biochemical analyses. Postmortem tumor surveillance was carried out via histology of the nasal cavity, nasopharynx, larynx, trachea, lungs, bone marrow, lymph nodes (including LALN), thymus, spleen, heart, tongue, salivary gland, esophagus, stomach, small intestine, large intestine, liver, pancreas, kidneys, urinary bladder, pituitary gland, thyroid, parathyroid, adrenal glands, testis, epididymis, seminal vesicle, prostate, ovaries, uterus, vagina, mammary gland, brain, spinal cord, peripheral nerve, olfactory bulb, eye, Harderian gland, muscle, bone, and diaphragm. Tumors caused by MWCNT exposure were limited to the lung and pleura; incidences are given in Table 17. The incidence of bronchiolo-alveolar carcinomas was increased in males following exposure to 0.2 and 2.0 mg/m^3 (8/50 and 10/50, respectively), and in females exposed to 2.0 mg/m^3 (5/50). The incidence of bronchiolo-alveolar adenomas was increased in males at 0.2 and 2.0 mg/m^3 (13/50 and 16/50, respectively) and in females at 2.0 mg/m^3 (11/50). Adenosquamous carcinoma in the lung was found in 1/50 male and 1/50 female in the 2.0 mg/m^3 groups. One incidence each of poorly differentiated adenocarcinoma and squamous carcinoma in the lung were also found in the female 2.0 mg/m^3 group. Although not statistically significant, the latter three tumor types were noted to be extremely rare as background lesions. Bronchiolo-alveolar carcinomas were accompanied by fibrous proliferations, which the authors note as not being seen in spontaneous background tumors occurring in controls. Pleural mesothelioma was not observed at any exposure level, but mesothelial hyperplasia and focal fibrosis was seen in the pleura following exposure to 2.0 mg/m^3 in both sexes. The authors concluded that 0.02 mg/m^3 was the NOAEC for carcinogenicity. The LOAEC for carcinogenesis was 0.2 mg/m^3 based on a statistically significant increase in the incidence of bronchiolo-alveolar carcinoma in males. The lung burden at this concentration, estimated using visual counting of fiber particles in tissue sections, was 152.4 µg/lung.

Table 17. Tumor Incidence in Rats exposed to MWCNT for 104 weeks (Kasai et al., 2016)

	Male				Female			
Exposure Level (mg/m^3)	0	0.02	0.2	2.0	0	0.02	0.2	2.0
Number of Animals in Group	50	50	50	50	50	50	50	50
Lung								
Bronchiolo-alveolar carcinoma	1	1	8*	10**	0	1	0	5**
Adenosquamous carcinoma	0	0	0	1	0	0	0	1
Poorly differentiated adenocarcinoma	0	0	0	0	0	0	0	1
Squamous carcinoma	0	0	0	0	0	0	0	1
Total carcinoma	1	1	8*	11**	0	1	0	8**
Bronchiolo-alveolar adenoma	1	1	7*	5	3	1	4	3
Total lung tumors	2	2	13*	16**	3	2	4	11*
Peritoneum								
Malignant mesothelioma	0	3	1	1	0	0	0	0

[a]Values indicate number of animals bearing lesions. *$p \leq 0.05$, **$p \leq 0.01$, Fisher Exact Test.

4.7.3 Summary

Overall, the carcinogenicity of SWCNTs and MWCNTs is challenging to predict due to the limited number of long-term studies. No studies are available for SWCNTs and only one well-documented study has been published for MWCNTs. The study uses inhalation of MWCNTs in both sexes of F344 rat and reports increased adenomas and carcinomas at 0.2 mg/m^3. The tumor incidence was significant in males at 0.2 mg/m^3 and was significant in females at the high dose of 2.0 mg/m^3.

Considering the data are limited to one species (rat), it should be noted that tumorigenesis secondary to lung overload (volumetric overwhelming of alveolar macrophage-mediated clearance) is often considered to be a rat-specific phenomenon (Oberdorster, 1996). This is significant because lung overload was considered by Pauluhn (2010) to be a principal mode of action of MWCNT toxicity in rodents. However, the MWCNT variant used in Kasai et al. (2016) (commonly known as "MWNT-7" or "Mitsui-7") is a thick-walled, semi-rigid fiber-like variant of MWCNT, while Pauluhn's MWCNTs were thin and densely aggregated. Fiber-like CNTs are toxicologically distinct from agglomerated forms (Arts et al., 2015). Pauluhn (2010) used bulk density to extrapolate data from airborne concentrations of carbon black inducing overload in the F344 female rat (Elder et al., 2005) to MWCNTs. The density of MWNT-7 is comparable to the density of carbon black (~2 g/cm^3, manufacturer data), so following the example of Pauluhn (2010) would lead to a hypothesis that MWNT-7 may cause overload at concentrations between 1 and 7 mg/m^3 based on results from Elder et al. (2005). Using Pauluhn's (2010) results concluding that overload in a 90-day exposure was reached in the F344 rat at a concentration of 0.4 mg/m^3 MWCNTs (density = 0.1-0.3 g/cm^3), overload would be

predicted to occur at a concentration of 4.0 mg/m^3 MWNT-7, adjusting for bulk density. Both of these estimates indicate that overload may be occurring in the current study at the high concentration of 2.0 mg/m^3, but that it is rather unlikely to be the principal mechanism of tumorigenesis as this would be at the far low end of the estimated range of overload conditions, and tumors are observed below this dose (in males).

Overall, it is likely that carcinogenicity of inhaled MWCNTs in Kasai et al. (2016) occurs through a morphology-dependent paradigm intrinsic to semi-rigid, high-aspect-ratio biopersistent fibers where fiber morphology frustrates clearance mechanisms of the lung, damaging phagocytic macrophages and prolonging residency (Oberdorster, 2002: Hirano et al., 2008). Reflecting this perspective, an IARC working group in 2014 specifically classified MWNT-7 as 'possibly carcinogenic in humans' (Group 2B), while both SWCNTs and MWCNTs other than MWNT-7 were not classifiable (Group 3) (Grosse et al., 2014).

4.8 Mechanistic Data

4.8.1 Mutagenicity/Genotoxicity Studies Overview

Results of short-term tests to assess the mutagenicity/genotoxicity of CNTs published prior to 2011 have been previously reviewed by Versar (2012) and are presented in Appendix E (Tables E-1 and E-2). Data for both types of CNTs (SWCNTs and MWCNTs) were cited in Versar (2012) in support of the general observations made about CNT mutagenicity/genotoxicity. The Versar review noted that CNTs have not induced mutations in most *in vitro* studies. Both SWCNTs and MWCNTs showed negative results for mutagenicity in standard Salmonella typhimurium strains (three studies). Two out of three *in vitro* mammalian cell mutagenicity studies were negative, although one of the negative studies involved only a single test concentration. In the study showing positive results, a MWCNT test material purified to lower metal catalyst residues induced an increase in mutation frequency at the adenosine phosphoribosyl transferase (Aprt) locus in mouse embryonic stem cells. Another study of MWCNTs found no increase in mutation frequency at the hypoxanthine phosphorybosyl transferase (HPRT) locus in Chinese hamster lung cells treated with MWCNTs.

The Versar review (2012) noted that *in vitro* studies of both SWCNTs and MWCNTs induced genotoxicity in a number of mammalian cell types, including human cells. Nearly all of the nine micronucleus (MN) assays for both SWCNTs and MWCNTs were positive, with the exception of one assay with equivocal results for SWCNTs. In the comet assay three of five studies of SWCNTs were positive, and two were negative. The two negative studies involved testing of a single concentration. All four comet assays of MWCNTs were positive. Five studies (two with SWCNTs and three with MWCNTs) evaluated DNA repair as measured by induction of γ-H2AX foci or induction of DNA repair enzymes, and all were positive. *In vitro* chromosomal aberration assays were limited to two studies of MWCNTs and showed no evidence of an increase in chromosomal aberrations, although in one study polyploidy was induced.

Three *in vivo* studies, one with SWCNTs administered by oral gavage and two with MWCNTs administered by IP or by IT, have shown that these materials are associated with genotoxicity in a number of tissues (liver, lungs, bone marrow, and peripheral lymphocytes). Endpoints evaluated include MN and DNA damage as measured by the Comet assay, oxidative DNA

damage, and chromosomal aberrations. SWCNTs were evaluated in two other studies employing endpoints that are less commonly used for evaluation of *in vivo* genotoxicity. These studies showed mitochondrial DNA damage in aortic tissue after pharyngeal aspiration and increased K-ras mutations in lung after inhalation exposure.

Several factors were mentioned in Versar (2012) as potentially contributing to the potential for genotoxicity of CNTs. These include length, diameter, surface charge, metal content, presence or absence of functional groups, and degree of agglomeration or dispersibility in aqueous media. However, the available data were considered inadequate to determine the relative importance of these factors or to characterize their interactions. Although the molecular modes of action by which CNTs induce genotoxicity are uncertain, the Versar review noted that the involvement of ROS associated with inflammatory responses and direct interaction with DNA have been proposed.

Numerous additional mutagenicity/genotoxicity studies of CNTs (both SWCNTs and MWCNTs) have been published demonstrating both *in vitro* and *in vivo* genotoxicity, with experimental evidence for *in vivo* genotoxicity clearer for MWCNTs. Less data are available to evaluate the mutagenic potential of these materials, since *in vitro* studies in mammalian cells have produced conflicting results and there are insufficient data from *in vivo* studies. The mutagenic/genotoxic mode of action of CNTs appears to be complex and may differ for different endpoints. These data are summarized separately for SWCNT and MWCNT in Appendix E.

A large number of both *in vitro* and *in vivo* mutagenicity/genotoxicity studies on SWCNTs and MWCNTs have been recently conducted. An extensive review of these studies is presented in Appendix E (Section E.1 and Tables E-3 and E-4). CNTs have not induced mutations in most *in vitro* studies. Both SWCNTs and MWCNTs have shown negative results for mutagenicity in standard *S. typhimurium* and *E. coli* WP2uvrA strains. It has been suggested that the lack of a mutagenic response in bacteria may be due to a lack of cell uptake. However, Clift et al. (2013) reported that SWCNTs, MWCNTs, and other nanofibers did penetrate bacterial cells based on visualization with electron microscopy, suggesting mutagenicity is not dependent on uptake. Few *in vitro* mutagenicity studies in mammalian cells have been published. Only one *in vitro* study measuring SWCNT mutagenicity in mammalian cells was found in the recent literature (Manshian et al., 2013). SWCNTs of varying lengths were tested in an HPRT mutation assay, where SWCNTs of 1 to 3 µm length increased mutation frequencies dose-dependently but longer (5 to 30 µm) or shorter (400 to 800 nm) did not. The intermediate-length SWCNTs also caused ROS increases and oxidative stress responses. All SWCNT examples were described as high-purity, so metal contamination does not appear to account for the differences in mutagenicity and oxidative stress induction. No recent in vitro mutagenicity studies in mammalian cells were found for MWCNTs, although one earlier study summarized in Versar (2012) reported Aprt mutations induced by MWCNT in mouse embryonic stem cells.

No *in vivo* mutagenicity studies of SWCNTs have been identified beyond the study reporting K-ras mutations in lung after inhalation exposure summarized in Versar (2012). One *in vivo* mutagenicity study of MWCNTs in transgenic mice reported an increase in mutation frequency in the lung after repeated intratracheal doses, suggesting that exposure sufficient to result in mutations can be achieved *in vivo* under certain conditions. Two *in vivo* somatic mutation and recombination tests (SMART) in *D. melanogaster* with MWCNTs have been published and

neither showed evidence of an increase in somatic mutation. Systemic uptake appeared to be very low, and the lack of mutagenic response may be attributable to lack of exposure.

In vitro genotoxicity studies have been conducted using the chromosomal aberration assay, the MN assay and/or the comet assay. *In vitro* chromosomal aberration assays have produced mixed results for both SWCNTs and MWCNTs, with roughly half the studies showing negative results and half showing a positive response. In studies where a positive response has been observed, clastogenicity and/or aneuploidy have been reported for both SWCNTs and MWCNTs. *In vitro* MN assays in cells from a variety of mammalian species have shown predominantly positive results for both SWCNTs and MWCNTs. Notable exceptions to this are two studies that reported no increase in MN frequency for SWCNTs and/or MWCNTs (Lindberg et al., 2013; Catalan et al., 2016). Both of these studies were conducted in a human bronchial epithelial cell line. However, other investigators have observed a significant dose-related increase in mitotic spindle damage in this same cell line along with an increase in aneuploidy with both SWCNTs and MWCNTs. Given adequate dose levels, SWCNTs and MWCNTs are capable of producing DNA damage in most of the cell lines evaluated, including human cell lines, when tested in comet assays. None of the *in vitro* comet assays with SWCNTs employed a fgp-modified assay to determine if oxidative DNA damage was induced. However, one publication found an increase in malondialdehyde DNA adducts after SWCNT treatment in two human cell lines established from the lung (Lindberg et al., 2013), suggesting capacity for oxidative DNA damage. Four *in vitro* comet fgp-modified assays with MWCNTs found no evidence of oxidative DNA damage in human cell lines established from the lung; the same human cell lines showing an increase in malondialdehyde DNA adducts associated with SWCNTs found a dose-related decrease in these adducts after MWCNT treatment.

With respect to *in vivo* genotoxicity potential, two older studies discussed in Versar (2012) reported some evidence of genotoxicity (oxidative DNA adducts in lung and liver after oral gavage and mitochondrial DNA damage in aortic tissue after pharyngeal aspiration) associated with SWCNTs. However, more recent *in vivo* genotoxicity studies of SWCNTs have been limited to three bone marrow MN assays in animals dosed by oral gavage and one comet assay in lung after intratracheal administration, and none of these studies reported evidence of genotoxicity (Naya et al., 2011, 2012a; Ema et al., 2013; Kim et al., 2015). *In vivo* genotoxicity study results with MWCNTs present a different picture. Six *in vivo* comet assays produced results that clearly showed an increase in DNA damage either in the lung following inhalation or intratracheal instillation or in bone marrow or lymphocytes following IP injection. The results in one study that showed a positive comet response in the lung after inhalation of semi-rigid MWCNTs, but not tangled MWCNTs, are consistent with the consensus that semi-rigid fibers are generally more toxic (as noted in Section 4.1). Both SWCNTs and MWCNTs have demonstrated genotoxicity *in vitro* and *in vivo*, although the experimental evidence for *in vivo* genotoxicity is clearer for MWCNTs. Less data are available to evaluate the mutagenic potential of these materials, since *in vitro* studies in mammalian cells have produced conflicting results and data is insufficient from *in vivo* studies. *In vivo* studies involving all routes of exposure, including oral, inhalation, IP and IV routes have been included in this report for completeness. However, the IP and IV routes of exposure are generally not recommended for risk assessment for consumer products without specific scientific justification.

The mutagenic/genotoxic mode of action of CNTs appears to be complex and may differ for different endpoints. While oxidative stress may be associated with mutagenic capacity, it may not be the primary factor involved in chromosomal damage. Modes of action involving both direct interaction with chromosomes (either the DNA or mitotic spindle) are likely more important for the observed clastogenic effects and induction of aneuploidy. The induction of ROS may, in some cases, be related to the presence of metal catalyst impurities. Oxidative stress associated with inflammatory responses that are unrelated to metal catalyst has also been proposed. The degree of agglomeration and formation of tangles and bundles for both SWCNTs and MWCNTs can also influence exposure, the outcome for both *in vitro* and *in vivo* tests, and further complicate an understanding of mutagenicity/genotoxicity as a possible mode of action.

4.8.2. Mode of Action of CNTs

4.8.2.1 Introduction

A review of literature prior to 2010 (Versar, 2012) summarized *in vitro* studies investigating mechanisms of CNT toxicity in cultured animal and human cells. Hypotheses tested in these studies addressed mechanisms of CNT-effects including cellular uptake, growth arrest, cell lethality, induction of apoptosis, induction of proinflammatory Nf-κB, AP-1, and p38/mitogen-activated protein kinase (MAPK) pathways, and activation of immune cells to secrete inflammatory mediators. The report noted that the majority of cell culture cytotoxicity studies demonstrated cellular uptake of CNTs with ensuing toxic effects, but some studies reported low or no toxicity following CNT uptake.

The literature published since 2010 is more richly populated in both *in vitro* and *in vivo* mechanistic studies modeling CNT toxicity, mostly germane to lung effects following inhalation exposure. CNT toxicity mechanisms have been investigated using an extensive array of endpoints, with most efforts addressing pulmonary inflammation, lung fibrosis, and carcinogenicity. Immune system toxicity (local to the lungs) and cardiotoxic effects have also been documented and explored on a mechanistic basis. The nature of the toxicity varies based on physicochemical characteristics, and studies demonstrating this are discussed in Section 4.1.

Recent literature has seen broad improvements in documentation of critical information such as physicochemical characteristics of CNT test articles. However, there are a large number of published mechanistic studies that inadequately report critical information, are of poor quality in general, or contribute little to existing knowledge. Several reviews of CNT toxicological mechanisms are available summarizing the body of published literature (Dong and Ma, 2015; Shvedova et al., 2012; Vietti et al., 2016). Although some insightful data have been published, the critical biological interactions are only speculation at this time and are complicated by what are likely multiple possible modes of action. In addition, physicochemical variation among CNT materials and preparations severely hampers cross-examination of data. There is widely acknowledged difficulty extrapolating mode-of-action information from experimental CNT exposures to real-world scenarios. Many studies investigating toxicity mechanisms utilize experimental designs that are non-standard and the format for reporting data varies widely. Even for many studies of moderately good quality, documentation of effects cannot be clearly compared to standardized toxicity testing identifying critical effects and effect levels. Differences in reporting formats, in addition to other variables such as test article formulation,

make it challenging to determine whether mechanisms identified in experiments have a causal relationship to toxicity in test animals and real-world scenarios.

The conclusions that can be drawn regarding mechanisms of toxicity of SWCNTs and MWCNTs include mode-of-action information generalizable to non-specific ultrafine particles as well as mechanisms that may be specific to CNTs. Much of the literature addressing mechanisms of CNT toxicity do not address SWCNTs and MWCNTs separately, instead focus on specific adverse effects (most of which are common to both forms).

4.8.2.2 Molecular Mechanisms Initiating CNT Toxicity

There are competing hypotheses as to what molecular interactions fundamentally initiate the *in vivo* toxic effects of CNTs. Several possible modes-of-action are common to SWCNTs and MWCNTs, while others are variant-specific. As noted in Section 4.1, different physicochemical variants may act as toxicologically distinct entities. This appears especially true for MWCNTs, due to the more diverse range of fiber morphologies and secondary structures. There are no well-demonstrated "receptors" mediating toxicity from SWCNTs or MWCNTs, but macrophage scavenger receptors have been shown to be instrumental in uptake of CNTs into cells (Hirano et al., 2012; Keka et al., 2014).

4.8.2.3 Oxidative Stress

Both SWCNTs and MWCNTs have been shown to induce oxidative stress, and numerous authors consider oxidative stress to be a primary mechanism of CNT toxicity (Rodriguez-Yanez et al., 2013; Liu et al., 2013; Dong and Ma, 2016). At the same time, it is remains unclear whether oxidative stress is an initiating mechanism, obligatory downstream event, or simply correlated with CNT toxicity. Several early CNT toxicity studies initially attributed oxidative stress-mediated adverse effects to CNTs, but the effects were later found to be caused by catalytic metal contamination, principally iron, rather than the CNT particles themselves (Pulskamp et al., 2007; Ge et al., 2012). By nature of their surface chemistry, SWCNTs and MWCNTs are capable of both generating and absorbing free radicals (Fenoglio et al., 2006; Galano, 2008; Crouzier et al., 2010), meaning that CNTs could plausibly induce oxidative stress as well as act in an antioxidant capacity.

SWCNTs have been shown to induce oxidative stress in cell culture-based experiments (Azad et al., 2013; Wang et al., 2012) and in rodents (Shvedova et al., 2012). Unpurified SWCNT material commonly contains high amounts of iron, but induction of oxidative stress by SWCNTs has been documented in both the presence and absence of iron. Shvedova et al. (2012) reviewed evidence identifying molecular initiating events of SWCNT toxicity, focusing primarily on oxidative stress. Numerous studies had, at the time, identified oxidative stress in cells as a consequence of exposure to various CNT types in a variety of exposure models. The primary goal of the review was to define the role of oxidative stress as a toxic initiating event, a downstream obligatory mechanism of toxicity, or an incidental byproduct of cellular responses. The authors profiled peroxidized lipid species following four days of whole-body inhalation exposure to 5 mg/m^3 SWCNTs containing high amounts of iron (17.7%/weight). Profiling was conducted using lipidomic methods (tandem MS). Despite the presence of iron, a known catalyst for the generation of hydroxyl radicals, lipidomic profiles did not reflect widespread non-specific

oxidation. Results detected the presence of oxidized lipid species in a specific profile that several other studies had associated with release of cytochrome c to the cytoplasm, suggesting mitochondrial toxicity as a source of redox stress. This restricted pattern of lipid peroxidation was also associated with widespread apoptosis of lung cells, suggesting that oxidative effects and apoptosis induction were secondary to a shared cause. These findings are consistent with mitochondrial stress being an upstream event. However, antioxidants such as vitamin E have been shown to inhibit SWCNT cytotoxicity *in vitro*, including loss of mitochondrial membrane potential (Wang et al., 2012). It remains unknown whether oxidative stress is an initiating or downstream event in SWCNT toxicity and it is possible that oxidative stress effects following SWCNT exposure are induced by multiple mechanisms.

MWCNTs have been shown to cause oxidative stress *in vitro*. This is true for both thick, semi-rigid MWCNTs (Palomaki et al., 2011) and thin, tangled MWCNTs (He et al., 2011; Alarifi and Ali, 2015; Srivastava et al., 2011). Similarly to SWCNTs, studies often identified mitochondrial stress as a mechanistic event in MWCNT toxicity. Again, it is not known whether oxidative stress following MWCNT exposure is initiated by reactive surface chemistry of the MWCNT itself or by disruption of mitochondria. A recent comparison study of SWCNTs and a thin-walled MWCNT variant (diameter of 5.5 nm) concluded that both caused toxicity to mitochondria (loss of membrane potential, decreased mitochondrial adenosine triphosphate (ATP), and release of cytochrome c, but SWCNTs were more toxic than the thin MWCNTs (Ghanbari et al., 2017). It has been suggested that the relatively low toxicity of OH-functionalized MWCNTs (vs. unfunctionalized) may be due to reduced toxicity to mitochondria (Liu et al., 2014). Beyond intrinsic reactivity and mitochondrial disruption, a third possible mechanism of CNT-induced oxidative stress is destabilization of phagolysosomes (see Section 4.8.2.4). A loss of lysosomal integrity causes release of reactive contents, including free radicals (Palomaki et al., 2011).

4.8.2.4 Frustrated Phagocytosis and Destabilization of Lysosomes

As non-specific unopsonized particles, CNTs and their agglomerates are taken up by immune cells (principally macrophages) and subject to processing in phagolysosomes. This process induces NADPH oxidase and generates free radicals to be utilized in the breakdown of phagocytosed material. Because of their shape and aspect ratio, CNTs are known to disrupt the membranes of macrophages (Hirano et al., 2008; Nagai et al., 2011), frustrating phagocytosis and destabilizing the phagolysosome and causing the release of lysosomal free radicals and cathepsins. These events are known to contribute to induction of inflammasome assembly, which allows for the maturation of IL-1ß. This mode of action may be specific to the semi-rigid morphology of thicker, larger-diameter MWCNT variants, as semi-rigid or "needle-like" MWCNTs were shown to destabilize lysosomes and induce inflammasome maturation, while a thin-walled, tangled variant produced less-pronounced effects (Palomaki et al., 2011). Oxidative stress is considered to be a requirement for activation of the inflammasome and maturation of IL-1 cytokines (Martinon, 2010; Rabolli et al., 2016), with lysosomal cathepsins being a co-stimulatory inducer of this process. The argument that semi-rigid fiber morphology is intrinsic to this mode of action is further supported by the use of crocidolite asbestos as a comparison test article. Palomaki et al. (2011; 2015) showed not only that asbestos had a similar effect on inflammasome maturation, but that the protein profile secreted by exposed macrophages was similar between semi-rigid MWCNTs and asbestos. This was in contrast to the protein profile

secreted after exposure to tangled MWCNTs. Inflammasome maturation is likely to be of importance for adverse effects including acute inflammation caused by CNT exposure, but its role in longer-lived responses associated with eosinophilic or Th2-type (allergic) inflammation may be more complex (Girtsman et al., 2014; Arnoldussen et al., 2015). The IL-1/inflammasomal signaling axis has been shown to be critical for lung remodeling and fibrosis in other toxicological models of progressive lung disease (Gasse et al., 2007; Cassel et al., 2008).

4.8.2.5 Volumetric Overload of Alveolar Macrophages

The capacity of alveolar macrophages to clear poorly-soluble particulates from the lower lung is limited by the volume of material that may be carried in a given cell at once. Alveolar macrophages loaded beyond this limit are inhibited in their mobility, leading to failed clearance and persistence of particles in the lung (Morrow, 1988; Oberdorster et al., 1992; Tran et al., 2000). Cytotoxicity and inflammation may ensue in these cases due to the prolonged residence of activated macrophages. The possible mechanisms of macrophage immobility include competition for actin mobilization between phagocytic and cell migratory demands and the induction of chemotactic factors as a consequence of excessive activation by repeated cell-particle interactions (Morrow, 1988). The rat is known to be a sensitive species in toxicity occurring by the overload mode of action, especially with regard to tumorigenesis following high level exposures to otherwise inert insoluble dusts. Guideline two-year carcinogenicity studies are generally conducted in the F344 rat. Overload-induced tumorigenesis is considered specific to that species and is not used as a critical effect for human risk estimates (McCunney, 1996).

CNTs may cause overloading because they are resistant to breakdown after uptake into alveolar macrophages, and may accumulate to overload volumes in the cell. Pauluhn (2010) considered lung overload to be a principal mechanism of lung toxicity from exposure to thin-walled, tangled MWCNTs. These CNTs generally form amorphous agglomerates in suspensions and aerosols. Although the MWCNT primary structure is fundamentally fibrous, the particulates they form are amorphous and may not share the same mode of action as rigid fibers. Pauluhn argued that the low density of MWCNTs is a driving factor in toxicity in the rat lung because exposure dose on the basis of mass will result in a higher volumetric dose relative to inert reference materials such as carbon black. This argument contends that tangled MWCNTs caused toxicity through an inert dust-like mechanism rather than a fiber-related or nanostructure-specific mechanism. Pauluhn's experimentation supports this hypothesis, but is limited to the rat.

Lung overloading effects other than tumorigenesis do generally occur in other species, and cause disease in humans (e.g., coal worker's pneumoconiosis) (McCunney, 1996). MWCNTs are biopersistent and whether they cause overload effects in humans will be dependent on whether exposure levels are sufficiently high. Given the available data, the initiating mechanisms of toxicity by thin-walled tangled MWCNT variants may include lung overload in some exposure scenarios and may not include it in others. Mechanistic studies summarized in this report indicate that MWCNTs can potentially elicit a host of effects that do not appear to be related to an overload-based reaction. Given that the relevant dose-response data are limited to a sensitive species (rat), it is difficult to say whether *in vivo* studies have demonstrated toxicity of tangled MWCNTs below the overload threshold dose. A variety of dose-response curves have been published using bolus instillation (IT or OPA) studies in mice, but these are generally not useful for estimating effect-levels in true inhalation exposures. Overload response is considered a high-

dose phenomenon and may not be of concern in exposure scenarios pertaining to consumer products.

4.8.2.6 Disruption of Chromosomes by Fiber Structures

Although results are somewhat mixed, several *in vitro* studies have documented chromosomal aberrations, including aneuploidy and micronuclei formation, in cells exposed to SWCNTs and MWCNTs (Sargent et al., 2009; Sargent et al., 2012; Catalan et al., 2012; Siegrist et al., 2014). A more thorough accounting of genotoxicity studies is given in Appendix E. Based on detailed microscopy localizing CNT fibers within microtubule-chromosomal assemblies in these studies, the mechanism of the effects appears to be disruption of the mitotic spindle as a result of CNT fiber morphology. Interestingly, COOH-fSWCNTs or MWCNTs were reported to be more potent inducers of chromosomal aberrations than unfunctionalized forms (Patlolla et al., 2010; 2016). As discussed in Section 4.1, COOH-functionalization is associated with sharply attenuated toxicity by a wide variety of endpoints, however, chromosomal disruption may be an exception to this.

4.8.2.7 Pathways Mediating the Apical Lung Effects of CNT Exposure

4.8.2.7.1 Inflammation and Granulomatous Pathology

Inflammation assessed in BALF and tissue pathology are the most common, and often most sensitive, effects of exposure to SWCNTs or MWCNTs. BALF collected from exposed animals shows accumulation of neutrophils, increases in macrophage number, increased protein content, and elevated levels of cytokines and chemokines. Lung pathology exhibits accumulation of hypertrophic macrophages ("foamy" macrophages), infiltration of neutrophils, irregular interstitial expansions of lymphoid tissue, and granulomatous formations ranging from small alveolar foci to well-formed granulomas (Pauluhn, 2010; Pothmann et al, 2015; Kasai et al., 2015). Mild inflammation of upper airways was also present in rodent studies. The form of inflammation induced by CNTs is generally neutrophilic (rather than eosinophilic), implying a Th1-biased immune environment which might be expected to result from an unresolved acute inflammatory response. The alveolar macrophage is thought to be particularly instrumental in signaling the onset of inflammation (Frank et al., 2015). TNF is principally produced by macrophages and is a powerful regulator of neutrophilic inflammation. The inflammatory cascades initiated by SWCNTs or MWCNTs have been shown to be mediated by the Nf-κB, AP-1, p38 MAPK, and NLRP3 inflammasome pathways (Bhattacharya et al., 2013; Dong and Ma, 2015).

The maturation of IL-1ß, one of the most potent inflammatory mediators, is regulated at multiple levels and requires assembly of the inflammasome. Palomaki et al. (2011) investigated whether inflammasome assembly and IL-1ß maturation in human primary macrophages differed between tangled MWCNTs, semi-rigid MWCNTs, and crocidolite asbestos. Results demonstrated that semi-rigid MWCNTs and asbestos activated secretion of IL-1β from LPS-primed macrophages, but tangled MWCNTs did not. NLRP3 activation induced by asbestos and MWCNTs was dependent on reactive oxygen species production and cathepsin B activity, both of which are associated with loss of lysosomal integrity. IL-1ß is a key inflammatory mediator that is produced by cells of all types in response to cellular damage; signaling through its receptor (IL-

1R) broadly activates Nf-κB- and MAPK-dependent responses in lymphocytes, fibroblasts, and epithelial cells (Dinarello, 1996). The role of IL-1R signaling in MWCNT-induced inflammation was investigated by Girtsman et al. (2014) in wild-type (WT) and IL-1R−/− mice. Their results suggested that MWCNT-induced acute pulmonary inflammation was dependent on IL-1R signaling. Additionally, wild-type mice demonstrated significant increased airway resistance 24 hours post-exposure to MWCNTs, but this was blocked in the IL-1R−/− mice. In contrast, by 28 days post-exposure to MWCNTs, the inflammatory response that was initially absent in IL-1R−/− mice was elevated in comparison to the WT mice. Rydman et al. (2015) reported similar findings using IL-1R knockout mice. The biological significance of the delayed response is not known, but these data indicate that IL-1R signaling plays a role in the regulation of MWCNT-induced pulmonary inflammation. This indicates that upstream triggers of inflammasome assembly (oxidative stress, potassium influx, lysosomal leakage) could be events that MWCNTs cause, with oxidative stress being commonly demonstrated (as reviewed in Shvedova et al. 2012).

PPARγ was shown to be a negative modifier of granuloma formation following exposure to MWCNTs (Huizar et al., 2013). Barna et al. (2013) identified the Twist1 transcription factor as a possible mediator of granuloma formation 60 days following MWCNT exposure via instillation. Based on the results of the study, Twist1 was considered a possible target of the inhibitory actions of PPARγ.

Overall, the induction of inflammation by SWCNTs and MWCNTs is a process involving many downstream mediators. Because inflammation involves extensive cross-talk between different signaling pathways, it is difficult to link specific signaling events to distinct inflammatory outcomes beyond differentiation of broad types of signaling environments (e.g., Th1- versus Th2-based). In the case of CNTs, a key characteristic of inflammatory responses is that episodes tend to be poorly-resolving. This is presumably intrinsic to the CNT biopersistence. The data suggest that different physicochemical variants of CNTs induce many of the same inflammatory signaling pathways, with some differences. At this time, the data indicate that semi-rigid MWCNTs have particular potency in the induction of inflammasome/IL-1R signaling compared to tangled variants. This inflammasome and signaling induction is suspected to be due to disruption of lysosomal membranes, possibly demonstrating a commonality between semi-rigid MWCNT and crocidolite asbestos.

4.8.2.7.2. Fibrosis

In general, CNTs that are thicker and semi-rigid are observed to cause long-lived inflammation and interstitial fibrosis often local to granulomatous inclusions of MWCNT deposits. Thin-walled tangled MWCNTs may cause diffuse interstitial fibrosis at high exposures, but are generally less fibrogenic on a mass basis than semi-rigid CNTs. Fibrosis is characterized by deposition of excess collagen synthesized by myofibroblasts. Vietti et al. (2016) developed an extensive review in drafting an adverse outcome pathway model mapping key mechanistic events underpinning lung fibrosis, which was developed in the context of CNT exposure. The authors mapped key biological events in the pathogenesis of lung fibrosis by cell type, individually addressing fibroblasts, macrophages, and lung epithelial cells and their responses to CNTs. In the resulting event pathway model, activation of p38 MAPK, NF-κB, and inflammasome pathways in those cell types give rise to cytokines and growth factors well known

to be instrumental in progressive fibrosis. *In vitro* evidence supports the relationships posited between CNT exposures and the downstream key signaling events, but not enough is known about how the interactions of CNTs with cells lead to activation of those signaling pathways. The review by Vietti et al. (2016) is noteworthy as an in-depth review of how effects of CNTs may cause fibrosis, and discusses both SWCNTs and MWCNTs.

Cellular differentiation from mesenchymal cells to myofibroblasts and subsequent collagen deposition is stimulated via multiple overlapping mechanisms, with TGF-ß and platelet-derived growth factor (PDGF) being two principal mediators. Several studies have shown that these mediators can be induced by exposure to SWCNTs and MWCNTs based on *in vitro* (Azad et al., 2013; Guo et al., 2012; He et al., 2011; Hussain et al., 2014; Lin et al., 2012; Manke et al., 2014; Mishra et al., 2015) and *in vivo* data (Dong et al., 2015; Khaliullin et al., 2015; Park et al., 2011; Wang et al., 2013). These inflammatory mediators were also elevated in sputum samples collected from workers from a MWCNT manufacturing plant (Fatkhutdinova et al., 2016). In the above studies, SWCNTs and MWCNTs stimulated the activity of myofibroblasts indirectly through primary effects on epithelial and macrophage cells; however, some studies also found that myofibroblasts are stimulated by direct exposure to CNTs themselves. Elevated inflammatory mediators commonly accompanied fibrosis-related endpoints. Inflammation generally plays a key role in driving fibrosis. IL-1R signaling is involved in the progression of fibrosis (Gasse et al., 2007), but the obligatory events mediating this relationship in disease are not well-demonstrated. The IL-17A/Th17 T-cell signaling axis has been suggested to play a role linking inflammation to the progression of fibrosis (Wilson et al., 2010).

Experimental evidence has shown that the de-differentiation of epithelial cells to mesenchymal cells (termed epithelial-mesenchymal transition, EMT) is a downstream mechanism leading to fibrosis. Several studies have shown that SWCNTs and MWCNTs can induce EMT or associated markers *in vivo* and *in vitro* (Chang et al., 2012; Chen et al., 2014a; Wang et al., 2015a; Polimeni et al., 2016). Chen et al. (2014a) showed that between two thin-walled MWCNTs, a 'long' MWCNT example (5 to15 μm) induced EMT and collagen deposition in C57Bl/6 mice, but a 'short' MWCNT (350 to 700 nm) did not. EMT caused by MWCNT exposure is mediated by the TGF-ß/p-Smad2 pathway, and TGF-ß can also signal through Akt/GSK-3ß (Polimeni et al., 2016).

4.8.2.7.3 Carcinogenesis

Evidence that SWCNTs or MWCNTs cause tumorigenesis in the lung is limited. This assessment found only one carcinogenesis guideline study with inhalation exposure to MWCNTs. This study observed increased incidence of total lung tumors in F344 rats following two years of inhalation exposure (Kasai et al., 2016). Sargent et al. (2014) demonstrated that inhaled MWCNTs acted as tumor promotors in the presence of a primary carcinogen in B6C3F1 mice.
Tumors were increased when measured 17 months following co-administration of methylcolanthrene and MWCNTs. The mechanism(s) by which MWCNTs induce or promote tumor growth are not known, but may involve multiple mechanisms related to those discussed above.

Because aneuploidy and chromosomal aberrations can be induced by MWCNTs, it is thought that interference with mitotic structures may be a mode-of-action linking MWCNTs to

carcinogenesis. Another possible mechanism could be EMT of lung epithelial cells, as de-differentiation of cells during EMT is a known paradigm of carcinogenic transformation for adenocarcinomas in general (Theiry, 2002). Inflammation can contribute to transformation, but the knowledge regarding this is incomplete (Mantovani et al., 2008). Nagai et al. (2011) showed that thicker, semi-rigid MWCNTs (~50 nm mean diameter), but not thin, tangled MWCNTs induced peritoneal mesotheliomas following IP instillation in rats (all MWCNTs were of comparable length). Semi-rigid MWCNTs penetrated the membranes of mesothelial and macrophage cells *in vitro* and decreased cell viability relative to tangled MWCNT. This study also tested a very thick-walled MWCNT with a mean diameter of 150 nm, and this was less toxic and less tumorigenic than the variants of ~50 nm diameter. Overall, multiple mechanisms may contribute to MWCNT toxicity and physicochemical variants may differ widely in their tumorigenic potential.

The carcinogenicity of SWCNTs is not known. No studies were located that tested SWCNTs as either a complete carcinogen or as a tumor promoter.

4.8.2.7.4 Impairment of Pulmonary Function in Mice

Limited studies have documented impaired pulmonary function in mice following exposure to MWCNTs (Wang et al., 2011a). Limited but compelling evidence exists that this effect is mediated by a Th2 immune signaling axis involving IL-33 and mast cells. The main limitation in the data supporting this mode of action is that all work was carried out in the C57Bl/6 inbred mouse strain. Inbred mouse strains can display responses unique to that strain and C57Bl/6, in particular, display strain-specific bias in T-helper cell-mediated responses (Schulte et al., 2008). Thus, it is difficult to know whether these results are applicable outside of this specific animal model.

Katwa et al. (2012) tested pulmonary function changes in mice following IT exposure to MWCNTs (12-25 nm diameter, "several microns" length). MWCNTs were administered, at 4 mg/kg bw, to wild-type, mast cell-null (c-Kit-/-), and IL-33 receptor-null (ST2-/-) C57Bl/6 mice. MWCNT-induced inflammation was markedly attenuated in transgenic mice lacking either mast cells or the IL-33 receptor. Pulmonary resistance was increased by MWCNT exposure in wild-type, but not mast cell-deficient animals. IL-33 receptor-deficiency also attenuated the increase in lung resistance. Responses to MWCNTs were restored by adoptive transfer of intact mast cells, but not IL-33 receptor-deficient mast cells. The study also documented an increased myocardial infarction risk following MWCNT exposure in an ischemia-reperfusion injury model, which was also dependent on mast cells with intact IL-33 receptor expression.

Beamer et al. (2013) tested the hypothesis that instillation of MWCNTs impair pulmonary function in C57Bl/6 mice due to the development of IL-33-dependent Th2-associated inflammation. Findings included elevated levels of IL-33 (likely originating from airway epithelial cells) in the lavage fluid, of airway hyperresponsiveness (AHR), of eosinophil recruitment, and production of Th2-associated cytokines and chemokines. MWCNT exposure also resulted in the recruitment of innate lymphoid cells. Collectively, these data suggested to the investigators that MWCNTs induce epithelial damage that releases IL-33, which in turn promotes innate lymphoid cell recruitment and the development of an IL-13-dependent inflammatory response.

4.8.2.8 Conclusions

A great deal of work has been published investigating mechanisms contributing to SWCNT and MWCNT toxicity in the lung, pleura, or surrogate tissues (i.e., peritoneal cavity). Given the volume of available studies and their relative usefulness for the purposes of this assessment, only a review of the major mechanisms potentially involved in the mode-of-action for CNTs has been presented. The body of work addressing mode-of-action is inconsistent in many respects and the physicochemical diversity of CNTs continues to present challenges in developing a consistent hypothesis. Protocols from different laboratories are not well-harmonized and the question of whether experimental exposures and dose-rates usefully approximate real-world exposure scenarios continues to be an issue.

The available body of work suggests that SWCNTs and MWCNTs may induce toxicity through multiple mechanisms, and some mechanisms may be specific to physicochemical characteristics. Reviewing the mechanistic data, oxidative stress is frequently observed as an upstream event. It is not clear whether the measurement of oxidative stress endpoints reflects a true initiating mechanism or a downstream event. Although both SWCNTs and MWCNTs can be intrinsically active in both generating and absorbing free radicals, it is not known whether CNTs are reactive in this way in the biological milieu of the lung. Oxidative stress could be an event downstream of frustrated phagocytosis or mitochondrial destabilization. Evidence to this point is mixed, but suggests that oxidative stress may play different mode-of-action roles respective to different physicochemical forms. Phagocytosis by alveolar macrophages is likely to be a key factor in several initiating mechanisms of toxicity by various CNT forms, however, MWCNTs are also shown to have the ability to penetrate cells in the absence of a phagocytic (i.e., actin-dependent) uptake mechanism (Ursini et al., 2016).

The downstream pathways mediating adverse effects of CNT exposure are also varied, but exhibit extensive cross-talk. The complexity of cross-signaling among inflammatory, fibrotic, and tumorigenic processes makes it difficult to distinguish whether mechanisms are truly obligatory. Investigations may show a partial attenuation of toxic responses following ablation of a given mechanism, suggesting that multiple event pathways contribute to the overall toxic response. These include Nf-κB, p38 MAPK, NLRP3 inflammasome/IL-1R, AP-1, TGF-ß/Smad-2, PPARγ, and IL-33/ST2 pathways. It is possible that pathways may work synergistically to produce outcomes, or that various signaling axes compete to bias the microenvironment of the lung to one outcome over another. Different physicochemical groups, further differentiated by differing formulations in various laboratories, could activate the same signaling pathways through different initiating mechanisms. These kinds of challenges make it difficult to describe a well-defined mode-of-action at this time, even for a specific physicochemical grouping. There is some evidence indicating that a semi-rigid fiber morphology may be linked to disruption of lysosomal membranes and activation of the inflammasome.

4.9 Derivation of ADI

4.9.1 Single-walled CNT

4.9.1.1 Oral Exposure

Data were not available to support 14-day or chronic ADIs for SWCNTs. The only repeat-dose oral study was Matsumoto et al. (2012) that demonstrated a 28-day NOAEL of 12.5 mg/kg/d in male and female rats. The SWCNT used was an OECD reference material (OECD, 2016) and was delivered as a sonicated suspension. The morphology of the SWCNT was not assessed by electron microscopy but roped assemblages were evident by light microscopy. No treatment-related adverse effects were found in blood biochemistry or histology, including the liver. In the absence of a LOAEL, a NOAEL at this relatively low dose level is not considered appropriate for quantitative determination of risk for either short-term or chronic exposure scenarios.

The reproductive and developmental toxicity of SWCNTs by the oral route is not clear. Philbrook et al. (2011) exposed pregnant mice to up to 100 mg/kg bw OH-SWCNTs. Fetal effects (resorbed implantations, gross defects, skeletal abnormalities) were increased in one exposed group, but were not dose-related (i.e., effects were seen at a low but not a high dose). This study, along with three others using IV administration of SWCNTs in pregnant mice, suggests the potential for developmental effects, but the results are inconclusive for deriving an ADI for oral exposure.

4.9.1.2 Inhalation Exposure

Available data were insufficient to derive a 14-day inhalation ADI for SWCNTs. Only one study investigated repeat-dose SWCNT exposure. Morimoto et al. (2012) exposed rats to up to 0.13 mg/m^3 over 28 days without seeing adverse effects in the lung, but left lung lobes were the only tissue evaluated and other respiratory tract tissues were not examined. In general, reporting in this study was insufficient for supporting an ADI.

No studies were located assessing reproductive and developmental toxicity of SWCNTs by the inhalation route. As summarized above, the data available for reproductive and developmental toxicity by oral and IV routes suggests the potential for developmental toxicity, but the data are inconclusive and do not contain useful dose-response information for derivation of an ADI.

4.9.1.3 Dermal Exposure

No studies investigating systemic exposure to SWCNTs by the dermal route are available. Due to the shape and size of SWCNT particulates, absorption by the dermal route is expected to be negligible (refer to Section 4.2.1.4).

4.9.2 Multi-walled CNTs

Inhalation is expected to be the most sensitive route of exposure to MWCNT particles. MWCNTs are fibrous, but are found principally as either tangled agglomerates of thin-diameter MWCNTs or semi-rigid fibers in the case of thicker-diameter MWCNTs. The principal effects of MWCNT inhalation exposure are inflammatory and regenerative responses of the respiratory

tract that may progress to remodeling, fibrosis, and tumorigenesis at sufficient exposure levels. The severity of effects is related to MWCNT particle morphology.

4.9.2.1 Oral Exposure

There were no recent studies located that were suitable for 14-day or chronic ADIs by the oral route. Matsumoto et al. (2012) reported no adverse changes in oral 28-day exposures to up to 50 mg/kg/d in rats. The absence of an adverse effect level (LOAEL), the inability to estimate a threshold, and the use of a NOAEL from a database with only one study, results in information not considered sufficiently robust to derive an ADI. MWCNTs are expected to have relatively low level of toxicity by the oral route.

4.9.2.2 Inhalation Exposure

Two studies provide toxicity information for short-term and chronic ADI values. These studies were conducted by the same group of investigators using identical test materials and exposure methods. The material used was a semi-rigid MWCNT variant commonly known as MWNT-7 or Mitsui-7. The MWCNTs were documented predominantly as individual fibers during inhalation exposures. On balance, it was deemed best to use mg/m^3 as the dose metric as alternative metrics are not clearly related to toxicity for this nanomaterial form.

While it is expected that dispersed, semi-rigid MWCNTs are more toxic by weight than tangled, agglomerated MWCNT (see Section 4.1), whether this ADI is applicable to exposure to tangled or agglomerated MWCNTs cannot be determined from available data. Two other repeat-dose studies (Pauluhn, 2010; Pothmann et al., 2015) were available, but both studies used ground dust-like MWCNTs that were not considered by TERA to be sufficiently potent examples for determination of an adverse effect level. Ma-Hock et al. (2009a) obtained 90-day inhalation toxicity data for tangled, loosely agglomerated MWCNTs in rats that suggested a LOAEL of 0.1 mg/m^3 based on critical effects of mild histiocytosis and granulomatous inflammation and was reviewed previously in Versar et al. (2012). There was no NOAEL in Ma-Hock et al. (2009a); however, based on the nature and severity of the adverse findings compared with those of semi-rigid fibers, it is unlikely that the tangled, agglomerated MWCNTs would be more toxic and have a LOAEL less than those identified for semi-rigid fiber MWCNTs in the derived ADIs.

MWCNT examples with variations in other physicochemical qualities (e.g., coatings, functionalization, molecular defects, etc.) are generally not expected to be more toxic than the material used in the principal study. Variations involving unique coatings, complex functionalizations, or outstanding departure from the morphological forms discussed above may still warrant individual attention before applying the derived ADIs.

4.9.2.3 Dermal Exposure

No studies were located assessing systemic effects after dermal exposure to MWCNTs. Absorption of MWCNT fibers and particulates is expected to be negligible (see Section 4.2 for pharmacokinetic information on MWCNTs).

4.9.2.4 Short-Term Inhalation ADI (14-day)

4.9.2.4.1 Principal Study and Critical Effect

A short-term ADI may be derived from a 14-day inhalation study in rats, exposed 6 hours/day for 5 days, reported by Umeda et al. (2013). The most sensitive adverse effect observed was goblet cell hyperplasia occurring in the nasal cavity and nasopharynx of males at 1.0 mg/m^3. The use of incidence data for modeling dose response was explored using benchmark dose modeling (BMDS 2.7, U.S. EPA), but the data were deemed unsuitable due to the distribution of the response data and the limited group sizes (n = 5). The 14-day NOAEC for goblet cell hyperplasia of the nasal cavity and nasopharynx in males was 0.2 mg/m^3. Therefore, a NOAEC approach was used for derivation of the ADI.

Adjustment to Human-Equivalent Exposure

Adjustment of intermittent exposure in rats to continuous exposure was undertaken by adjusting exposure duration. Exposure duration was adjusted from experimental intermittent (H = hours/d and D = d/wk) to continuous exposure (24h/d, 7d/wk) using the following equation:

$NOAEC_{Continuous} = NOAEC_{Experimental} \times H/24 \times D/7$

Using values from the principal study gives the following:

$NOAEC_{Continuous} = 0.2\ mg/m^3 \times 6h/24 \times 5d/7$

$NOAEC_{Continuous} = 0.036\ mg/m^3 = 36\ \mu g/m^3$

Cross-species dosimetric adjustment of the experimental NOAEC to a human equivalent concentration (HEC) was undertaken by calculating the regional deposited dose ratio (RDDR) between rat and human (U.S. EPA, 1994), using extrathoracic surface area (ETSA) as a normalizing factor and minute volume (Ve) and regional deposition fraction (Fr) in the following equation:

$$RDDR = \frac{ETSA_{Human} \times Ve_{Rat} \times Fr_{Rat}}{ETSA_{Rat} \times Ve_{Human} \times Fr_{Human}}$$

Fr values for the extrathoracic regions were calculated in MPPD v3.04 software using the reported MMAD (1.3 µm, GSD = 2.7) and aspect ratio values (aspect ratio = 57 based on reported length/diameter), as well as manufacturer-reported density of 2.1 g/cm^3 for this MWCNT variant as documented by other authors (Kobayashi et al., 2010; refer to Appendix C). Breathing scenarios were whole-body exposure and oro-nasal normal augmented breathing for the rat and human models, respectively. ETSA and Ve values for rat and human were calculated in MPPD, using a 180g default body weight for the rat and resulting default breathing and tidal volumes. Plugging these values into the RDDR equation gave the following:

$$RDDR = \frac{436.7\ cm^2 \times 169\ mL/min \times 0.20}{8.8\ cm^2 \times 7.5\ L/min \times 0.55}$$

RDDR = 0.41

The RDDR was multiplied by the duration-adjusted NOAEC ($NOAEC_{Continuous}$) to give the HEC:

36 $\mu g/m^3$ x 0.41 = $NOAEC_{HEC}$

$NOAEC_{HEC}$ = 14.8 $\mu g/m^3$

Uncertainty Factors

Uncertainty in the 14-day ADI was accounted for using uncertainty factors (UFs) for inter-individual variation, animal-human extrapolation, and database completeness. No UFs were needed to account for study duration or presumed no-effect dose extrapolation because the POD is a no-effect concentration taken from a 14-day study.

A UF of 10 was used to account for inter-individual variation in responses to inhaled MWCNTs. This UF is needed to protect sensitive human subpopulations such as those with preexisting lung disease.

A UF of 3 was used to account for toxicodynamic differences between rat and human. Toxicokinetic differences are addressed above in the respiratory tract dosimetry adjustments. A UF of 3 was used to account for database completeness. This was motivated by the following limitations in available data: 1) suitable data were available in only one species (rat), whereas the critical effect(s) in multiple species provides higher certainty and confidence; and, 2) information on possible developmental toxicity following MWCNT inhalation is limited. Data from IT exposure (Hougaard et al., 2013) suggests little or no developmental toxicity following lung exposure to high levels of MWCNTs, but no inhalation data are available.

ADI = $NOAEC_{HEC}$ /UFs = (14.8 $\mu g/m^3$) / (100) = 0.15 $\mu g/m^3$

4.9.2.5 Long-Term Inhalation ADI

4.9.2.2.1 Principal Study and Critical Effect

The study best supportive of a chronic inhalation ADI for MWCNTs is the 2-yr carcinogenicity study in rats by Kasai et al. (2016; Table 12). This study is preferred as the principal study because it is a guideline chronic duration study and utilizes a well-standardized semi-rigid form of MWCNTs. This MWCNT variant is the same as that used in the 14-day inhalation study by Umeda et al. (2013), and other experimental particulars beyond duration (i.e., strain, exposure protocol, apparatus) are also generally identical to the earlier study. Data for the incidence of lesions in the lung were reported. Bronchiolo-alveolar hyperplasia and alveolar hyperplasia were

increased in males at an exposure concentration of 0.2 mg/m^3. Focal fibrosis and granulomatous inflammation occurred in both sexes at a concentration of 0.2 mg/m^3. The authors noted that goblet cell hyperplasia occurred in the nasal cavity and nasopharynx following 2-yr exposure to concentrations as low as 0.02 mg/m^3, the lowest dose tested. The incidence for these effects were not given. Because these hyperplastic changes in the nasal region were the most sensitive effects in the 14-day study above (Umeda et al., 2013) using identical conditions, goblet cell hyperplasia of the nasal cavity/nasopharynx was considered the most sensitive adverse effect in the 2-yr study. The authors report that the low concentration of 0.02 mg/m^3 caused this effect in females. The lack of incidence data precluded the use of benchmark dose modeling. The goblet cell hyperplasia in females was considered to be a no-adverse-effect-concentration for the following reasons: 1) goblet cell hyperplasia is a relatively mild effect that may be considered adaptive in many scenarios as opposed to adverse and, 2) the authors report this effect occurred in females only, implying a low or possibly spurious result given that females are expected to be less sensitive than males. The NOAEC from this study was therefore 0.02 mg/m^3.

Adjustment to Human-Equivalent Exposure

Adjustment of intermittent exposure in rats to continuous exposure was undertaken by adjusting exposure duration. Exposure duration was adjusted from experimental (H = hours/d and D = d/wk) to continuous exposure (24h/d, 7d/wk) using the following equation:

$NOAEC_{Continuous} = LOAEC_{Experimental} \times H/24 \times D/7$

Using values from the key study gives the following:

$NOAEC_{Continuous} = 0.02\ mg/m^3 \times 6h/24 \times 5d/7$

$NOAEC_{Continuous} = 0.0036\ mg/m^3 = 3.6\ \mu g/m^3$

The RDDR was used to adjust the experimental concentration to an HEC. The animal strain, test material, exposure methods, and target species were all identical to the related 14-day study by Umeda et al., (2013), and the calculations used to find the RDDR are also the same as those given above in the derivation of the 14-day ADI. The RDDR was 0.41.

The RDDR was multiplied by the duration-adjusted NOAEC ($NOAEC_{Continuous}$) to give the HEC:

$3.6\ \mu g/m^3 \times 0.41 = NOAEC_{HEC}$

Uncertainty Factors

Uncertainty in the long-term ADI was accounted for using UFs for inter-individual variation, animal-human extrapolation, and database completeness. No UFs were needed to account for study duration or presumed no-effect dose extrapolation because the POD is a no-effect concentration taken from a chronic 2-yr study.

A UF of 10 was used to account for inter-individual variation in responses to inhaled MWCNTs.

This UF is needed to protect sensitive human subpopulations such as those with preexisting lung disease.

A UF of 3 was used to account for toxicodynamic differences between rat and human. Toxicokinetic differences were addressed above in the respiratory tract dosimetry adjustments.

A UF of 3 was used is account for database completeness due to the following limitations in available data: 1) suitable data were available in only one species (rat); and, 2) information on possible developmental toxicity following MWCNT inhalation is limited. Data from IT exposure (Hougaard et al., 2013) suggests little or no developmental toxicity following lung exposure to high levels of MWCNTs, but no inhalation data are available.

4.9.2.5.2 Long Term ADI for Semi-Rigid MWCNT Fibers

The long-term ADI for MWCNT for semi-rigid fibers was determined by dividing the $NOAEC_{HEC}$ by the UFs:

$ADI = NOAEC_{HEC} / UFs = (1.5\ \mu g/m^3) / (100) = 0.015\ \mu g/m^3 = 15\ ng/m^3$

4.10 Research Needs for CNTs

4.10.1 General Research Needs

Derivation of an ADI for SWCNTs and MWCNTs remains challenging due to the limited availability of well-conducted dose-response studies with robust repeat-dose protocols. Broad obstacles exist in harmonization of protocols between laboratories and wide physicochemical variability among CNT test articles. Some CNTs appear to act similarly to high-aspect-ratio insoluble fibers, while others form agglomerates with pharmacokinetics and toxic effects similar to insoluble dusts. There has been some progress in developing strategies to group CNTs into toxicologically similar families based on physicochemical characteristics, but these are not yet reconciled with inconsistencies in the published experimental record. Improved harmonization and a more robust body of data informing toxicokinetics and effects of toxicologically distinct physicochemical subgroups of CNTs are general research needs that would broadly improve the confidence of future risk assessment for these nanomaterials.

There were no repeat-dose studies available for any functionalized variants of either SWCNTs or MWCNTs by the inhalation route. Functional groups generally increase the solubility of CNTs and unmodified, uncoated MWCNTs and SWCNTs are expected to be as, or more, toxic than functionalized or coated forms. For most consumer product exposure scenarios, ADIs for unmodified, uncoated CNTs should be conservatively applicable to functionalized or coated forms. CNT formulations with exotic coatings or elaborate functional groups may require additional consideration as to whether the ADIs are appropriate and may be applied.

Dose-response toxicity data appropriate for determination of an exposure limit for CNTs is generally sparse, especially for specific subgroups of CNT variants. Dermal exposure is not expected to result in a significant level of absorption for either multi-walled or single-walled forms, so a lack of dose-response toxicity data for the dermal route is not a significant data gap

for this assessment.

4.10.2 Specific Needs for SWCNTs

There are no well-standardized repeat-dose oral or inhalation studies for SWCNTs, and no ADI derivation was feasible for this form. Oral exposure does not appear to cause significant toxicity at relatively high doses, but dose-ranges from published studies that investigated oral toxicity of SWCNTs are nonetheless too low to be used practically for ADI determination. These data would be helpful, if only to establish a definitive ADI for exposure by the oral route. Sufficiently well-reported studies assessing repeat-dose toxicity of SWCNTs via inhalation were not available. Developmental and Reproductive Toxicology (DART) information for CNTs is limited at this time, especially for SWCNTs. Concerning dermal, oral, and inhalation routes, only one DART study was available for SWCNTs, investigating DART toxicity of OH-functionalized SWCNTs in mice by the oral route. The only other studies found were three IV studies. The developmental toxicity of SWCNTs is suspected to be substantially different between injected and environmentally relevant routes.

Determination of short-term (14-day) and chronic ADIs for SWCNTs require additional data in the following areas:

- Subacute (14-28 days exposure) repeat-dose oral toxicity at dose levels approaching 1000 mg/kg/d (authors in Matsumoto et al., 2012 suggest reaching this dose level may be technically difficult);
- Subchronic or chronic/carcinogenicity repeat-dose oral toxicity;
- Subacute (14-28 days exposure) repeat-dose inhalation toxicity;
- Subchronic or chronic/carcinogenicity repeat-dose inhalation toxicity; and,
- Developmental and reproductive toxicity by oral and inhalation routes

4.10.3 Specific Needs for MWCNTs

Toxicity data for MWCNTs is partially complete for some MWCNT variants, but lacking for others. Broadly, MWCNTs are found either as semi-rigid fibers (higher diameter) or tangled agglomerates (lower diameter, less than 30 nm). Repeat-dose toxicity data for semi-rigid fiber-like MWCNTs is available for up to 2 years (chronic/lifetime) exposure in the rat. This affords some ability to characterize the hazard for semi-rigid MWCNTs, but data in an additional species would improve confidence in the assessment. There are two 90-day toxicity studies for low-diameter MWCNTs; both of these use micronized (non-dispersed) MWCNTs delivered as compact aggregates. There is uncertainty as to whether compact MWCNT aggregates are an appropriate test material as the basis for an ADI because a dispersed form (loose, tangled agglomerates) is suspected to be more potent. There are no carcinogenicity studies of low-diameter, tangled MWCNT variants. In general, semi-rigid MWCNTs are expected to be more toxic than tangled, agglomerated MWCNTs. Data that provide further detail and context to this assumption may support the use of semi-rigid fiber ADIs for MWCNTs, in general, if it can be conclusively shown that adverse effect doses for semi-rigid fibers reliably fall below those for tangled agglomerates. Conversely, additional toxicity data for tangled, agglomerated MWCNTs may allow for a relatively less-restrictive ADI value for this particular MWCNT form.

The only DART studies found for MWCNT exposure by the relevant routes were two oral studies, one of which used thin-walled, tangled MWCNTs while the other used COOH-fMWCNTs. Six further DART studies using IT, IP or IV exposure were located in the published literature. The body of DART data for MWCNTs lack an oral study using thick-walled, semi-rigid MWCNTs, which is an important data gap because semi-rigid MWCNTs translocate more readily than tangled MWCNT, as shown in Sections 4.1 and 4.2 of this report. Results of one of the above studies using the IV route (Huang et al., 2014) also suggested that semi-rigid MWCNTs (diameter of 50 nm in this case) translocated across the placenta. No DART studies by the inhalation route were found for MWCNTs or any variants thereof.

Determination of short-term (14-day) and chronic ADIs for MWCNTs require additional data in the following areas:

- Subacute (14-28 days exposure) repeat-dose oral toxicity at dose levels approaching 1000 mg/kg/d (as for SWCNTs, authors in Matsumoto et al., 2012 suggest reaching this dose level may be technically difficult);
- Subchronic or chronic/carcinogenicity repeat-dose oral toxicity; and,
- Developmental and reproductive toxicity by oral and inhalation routes, in particular for semi-rigid fiber-like MWCNTs.

5 Toxicity Data for Nanosilver

5.1 Physical and Chemical Properties of Nano Ag

Typical physical and chemical properties for chemical substances (such as molecular weight, solubility, boiling point, melting point) may not be associated with toxicity as much as other physicochemical properties unique to nanomaterials (including particle size, hydrodynamic size, surface area, aggregation/agglomeration state, and environmental characteristics). This section addresses the physicochemical properties of silver nanoparticles (Ag NPs) and the potential association of those properties to Ag NP toxicity.

5.1.1 Functionalization (Surface Coatings)

The surface of Ag NPs in solution establishes a double layer of charge that prevents aggregation of the NPs. Capping (coating) Ag NPs with citrate, dextran, peptides, sugars, tannic acid, or polyvinylpyrrolidone (PVP) stabilizes the NP to various degrees (Radziuk et al., 2007). Citrate weakly associates with the surface of the Ag NP and is often used because it is readily displaced by a range of other molecules including thiols, amines, polymers, antibodies, and proteins that provide longer-term stability. Tannic acid is a multidentate capping ligand that can be displaced by many thiol-containing molecules and is often used where high particle concentrations are required. PVP is a polymer that binds strongly to the Ag NP surface and provides greater stability than citrate or tannic capping agents, because it is more difficult to displace (Aldossari et al., 2015). Therefore, different kinds of coatings are used to decrease agglomeration (Chappell et al., 2011) and dissolution of Ag NPs (Yang et al., 2012; Zook et al., 2012) and to modify their biological activity, such as in a therapeutic drug delivery system (Yang et al., 2012; Chappell et al., 2011; Theodorou et al., 2015). Because biological effects of Ag NPs are often dependent on their coating (Powers et al., 2011; Yang et al., 2012; Suresh et al., 2012), coatings should be described in the interpretation of any toxicity study.

5.1.2 Particle Size

Nanoparticles have unique characteristics due to their small size (1 to 100 nm). Size-dependency has been found to have profound influence over Ag NP biologic activities (Teeguarden et al., 2007; Johnston et al., 2010; Powers et al., 2010, 2011; Trickler et al., 2010). Smaller particles have been shown to be more cytotoxic when dose is expressed on a mass basis. This is hypothesized to be from the greater reactive surface area of the smaller nanoparticles relative to larger particles (Liu et al., 2010), suggesting that surface area is a more meaningful dose metric than mass. However, Ag NPs of the same size with different chemical compositions show different toxicities (Liu et al., 2010), indicating that evaluation of Ag NPs should first group the NP toxicity data based on chemical composition.

In addition to larger reactive surface area (Johnston et al., 2010), smaller Ag NP toxicity has been associated with higher cellular uptake (Choi and Hu, 2008). Higher uptake and larger surface area can facilitate faster dissolution and release of silver ions (Ag^+), thought by some researchers to be the toxic silver form. A major challenge is to distinguish precisely what portion of any observed toxicity is from the Ag^+ form and what portion is from the Ag NP form (McShan et al., 2014). Smaller particle size is not necessarily correlated with more Ag^+ (Yang

et al., 2012), and as described above, coatings and interactions with biomolecules can influence dissolution rate.

5.1.3 Hydrodynamic Size

Hydrodynamic size can be measured by Dynamic Light Scattering (DLS) and is defined as the size of a hypothetical hard sphere that diffuses in solution in the same fashion as that of the particle being measured (Volker et al., 2013). In reality, NPs in solution are non-spherical, dynamic (tumbling), and solvate, a process by which solvent molecules surround and interact with the nanoparticles. The hydrodynamic diameter is that of a sphere that has the same translational diffusion coefficient as the particle being measured, assuming a hydration layer surrounding the particle or molecule. The DLS value of Ag NPs will typically be greater than the physical size obtained by TEM. When a dispersed Ag NP moves through a liquid medium, a thin electric dipole layer of the solvent adheres to its surface. This layer influences the movement of the NP in the medium. The hydrodynamic diameter gives information on the behavior in solution of the inorganic core along with any coating material and the solvent layer attached to the NP as it moves under the influence of Brownian motion. While estimating size by TEM, this hydration layer is not present; hence, TEM provides information only about the inorganic Ag core (Stensberg et al., 2011).

5.1.4 Surface Area

Particle size and surface area of nanoparticles are related variables (see Section 5.1.2). As previously stated, surface area is considered one of the main factors in Ag NP toxicity (Johnston et al., 2010); however, this characteristic is not always assessed in biological studies. There are no widely available methods to measure surface area in solution or in complex matrices; although approaches based on nuclear magnetic resonance (NMR) have general applicability. The standard approach is to estimate the surface area in solution based on the dry state. Using dispersity, a way to calculate objects that have an inconsistent size, shape or mass distribution, it may be possible to estimate surface area from particle primary size and size *in situ* in exposure media (Liden, 2011). For highly poly-dispersed samples, it is difficult to separate the effects of different size fractions of the Ag NPs (Kaegi et al., 2011; Powers et al., 2010). All NPs have surface area to volume ratios that are extremely high (see Table 18). Pal et al. (2007) estimated a 109-fold increased surface area as the size of a spherical NP was reduced from 10 μm to 10 nm.

Table 18. Ag NP Surface Area

Diameter (nm)	Surface area (nm^2)	Volume (nm^3)	Ratio Surface Area: Volume
10	314	523	0.60
20	1260	4190	0.30
30	2830	14,100	0.20
40	5013	33,500	0.15
50	7850	65,500	0.12
60	11,300	113,000	0.10
70	15,400	180,000	0.09
80	20,100	268,000	0.08
90	25,400	382,000	0.07
100	31,400	523,600	0.06

Source: https://nanocomposix.com/pages/silver-nanoparticles-physical-properties

Many of the physical properties of Ag NPs, such as solubility and stability, are determined by the nature of the NP surface. The Ag NP's small size, large surface area, and, thus, large surface reactivity, give these particles the ability to bind to receptors and proteins on cell membranes (Lynch and Dawson, 2008). While high surface area to volume ratios are important for applications such as catalysis, there are other properties of Ag NPs that may impact reactivity *in vivo*, as described in the sections that follow.

Interactions between Ag NPs and proteins that form a protein layer or protein corona on the NP surface (see Section 5.1.8) are governed by a number of specific and nonspecific forces, such as hydrogen bonds and interactions such as van der Waals, electrostatic charge, steric and solvation forces (Saptarshi et al., 2013). Surface ligands of Ag NPs also determine the interactions between particles and receptors. Ag NPs in a biological system are likely to adsorb to protein surfaces, causing changes of particle properties and biological activity (Saptarshi et al., 2013). The adsorbed proteins may undergo structural changes, as well as function and reactivity alterations, thereby affecting particle interactions with receptors and other proteins (Brown et al., 2010). The higher affinity of Ag to thiol groups also contributes to the binding of Ag NPs with sulfur-containing protein membranes (Colman et al., 2013).

5.1.5 Aggregation/Agglomeration Status

Agglomerates are a collection of weakly bound (by van der Waals forces or simple physical entanglement) NPs where the resulting external surface area is similar to the sum of the surface areas of the individual components (Reidy et al., 2013). Aggregates are comprised of strongly bonded (covalent bonds) or fused particles where the resulting external surface area may be significantly smaller than the sum of calculated surface areas of the individual components. These definitions are based on ISO terminology (TS 27687: 2008).

Preventing Ag NP aggregation can be difficult, depending on the use or application. As stated previously, agglomeration can be decreased with coating/capping treatment (Chappell et al., 2011). Ag NPs are either charged-stabilized or sterically stabilized. Typically, Ag NPs with Zeta potentials > +20 mV or < -20 mV have sufficient electrostatic repulsion to remain stable in solution. The Zeta potential (see 5.1.9) is a measure of the NP stability.

5.1.6 Shape

Ag NPs can be synthesized in a huge variety of forms and shapes (spheres, rods, bars, wires, triangles, cubic, pyramid, bipyramids, stars, prisms, lattice planes, plates, flower-like, dendritic, and irregular morphology), which are often found together in different proportions (Glover et al., 2011; Khodashenas and Ghorbani, 2015; Zhang et al., 2016). Directionally dependent shapes are formed in the presence of a stabilizing polymer that preferentially binds to one crystal face and results in one crystal direction growing faster than the others (Khodashenas and Ghorbani, 2015). However, even what is characterized as "spherical" Ag NPs can have a range of shapes and sizes depending on synthesis and handling conditions.

Since shape (e.g., spherical, rod shaped, and truncated triangular) has been shown to affect anti-

microbial properties (Pal et al., 2007), it is plausible that different shapes could impact mammalian toxicity. Moreover, the shape of NPs plays an important role in deciding the efficiency of cellular uptake, including phagocytosis by macrophages (Champion and Mitragotri, 2009). The shape of Ag NPs can be an important factor in their toxic properties and needs to be fully described in any NP toxicity study.

5.1.7 Silver Ions (Ag+ Release)

The outermost electrons of an atom determine the physical properties of the matter. Remove one electron from a Ag atom and Ag ion (Ag+) is formed. Ionic Ag (Ag+) is not the same as metallic Ag, Ag particles or colloidal Ag. Colloidal Ag is made up of tiny nanoparticles of metallic Ag. Ag+ has no surface area, is highly reactive, easily gets inside cells, and forms complexes with both inorganic and organic molecules (Reidy et al., 2013). Liu et al. (2010) hypothesized that ionic Ag+ might be the form that transports Ag within the body and from which some nanosilver may be reformed in body tissues. Ag+, which flows from Ag NPs when oxidized, is what makes Ag toxic, not the Ag NPs themselves, to bacteria (Williams, 2012). The mechanism of Ag NP toxicity is uncertain; Ag and Ag NP translocation intracellularly and throughout the body are not completely understood (see also Sections for Toxicokinetics and Mechanism of Action).

An important factor in assessing kinetics and toxicity of Ag NPs is that the concentration of Ag in organs measured using inductively coupled plasma-mass spectrometry (ICP-MS) does not distinguish between ionic and nano Ag forms (Reidy et al., 2013).

5.1.8 Protein Corona

The protein adsorption layer (protein corona) that forms on the surface of colloidal Ag NPs plays an important role in the physical and chemical interactions of Ag NPs with biological systems. Characteristics of the protein corona affect exposure to Ag NPs and the response of cells and organisms (McShan et al., 2014). Formation of a protein corona and resultant bioavailability and uptake of Ag NPs is only one type of NP-protein interaction that is biologically relevant. Nanoparticles were shown to affect the conformation of some proteins bound to their surface, which may lead to denaturation of those bound proteins or may increase the protein's stability/activity by immobilization at surfaces (Lynch and Dawson, 2008).

5.1.9 Zeta Potential

Zeta potential is the electrokinetic potential in colloidal dispersions (McNaught and Wilkinson, 1997). It is the potential difference between the dispersion medium and the stationary layer of fluid attached to the dispersed particle. It is widely used for quantification of the magnitude of the charge and is often the only available way to characterize electrical double-layer properties. Double layer refers to two parallel layers of charge surrounding a nanoparticle. The first layer, the surface charge (either positive or negative), consists of ions adsorbed onto the particle due to chemical interactions. The second layer is composed of ions attracted to the surface charge via the Coulomb force, electrically screening the first layer. The Zeta potential is a key indicator of the stability of colloidal dispersions. The magnitude of the Zeta potential indicates the degree of electrostatic repulsion between adjacent, similarly charged particles in a dispersion. For

nanoparticles that are small enough, a high Zeta potential will confer stability (i.e., the solution or dispersion will resist aggregation). When the potential is small, attractive forces may exceed this repulsion and the dispersion may break and agglomerate. Typically, Ag NPs with Zeta potentials either greater than 20 nV or less than -20 nV have sufficient electrostatic repulsion to remain stable in solution and not aggregate. However, the Zeta potential is highly responsive to other biomolecules or contaminants in solution as well as to the solution pH.

Coatings/cappings can result in different surface charges (Suresh et al., 2012) and thus influence nanoparticle interactions (Choi and Hu, 2008); and since toxicity may change with vehicles (Chappell et al., 2011), Zeta potential should be measured in the dosing vehicle and reported in toxicity studies. In some studies, no impact of Zeta potential on toxicity was found (Yang et al., 2012). On the other hand, Suresh and coworkers (2012) reported a direct correlation between the cytotoxicity of dispersed Ag NPs and their overall surface charge and/or surface coating. Positive surface charges on Ag NPs allow them to stay for a longer time in the blood stream compared to negatively-charged NPs (Zhang et al., 2016).

Colloids with high Zeta potential (negative or positive) are electrically stabilized while colloids with low Zeta potentials tend toward aggregation/agglomeration as outlined in Table 19 below.

Table 19. Zeta Potential and Stability of Colloid

Zeta potential [mV]	Stability behavior of the colloid
0 to ±5	Rapidly aggregate
±10 to ±30	Incipient instability
±30 to ±40	Moderate stability
±40 to ±60	Good stability
≥ ±61	Excellent stability

Source: O'Brien et al. (1990)

5.1.10 Crystalline Structure and Porosity

The crystal structure and porosity of engineered Ag NPs are noted primarily in medical and cosmetic literature (Bandyopadhyay et al., 2012), not subjects of this report. However, crystalline structure and porosity may have a role in Ag NP toxicity. Bhol and Schechter (2007) reported the anti-inflammatory activity of nanocrystalline silver (NPI 32101) in the rat. Rats treated intra-colonically or orally with nanocrystalline silver showed significantly reduced colonic inflammation. Mice treated with crystalline Ag NPs by both routes showed rapid healing of ulcerative colitis and improved appearance, in a dose-related manner.

5.1.11 Contaminants

The impact of different contaminants, which may be present in Ag NPs, their coatings and suspensions, has been rarely studied. According to Samberg et al. (2011), the way in which Ag NP suspensions are prepared can influence their toxic properties. Unmodified Ag NPs, synthesized by base reduction, contained formaldehyde and were much more toxic than "washed" Ag NPs (synthesized in the same way, but washed 20 times in phosphate buffer, which decreased the content of formaldehyde).

5.1.12 Other Characteristics

The Ag NP surface is dynamic and strongly influenced by the local environment (Volker et al., 2013). High salt environments will collapse the electrical double layer and cause nanoparticle aggregation (see Section 5.1.1). Highly acidic or basic solutions can increase the dissolution rate of the Ag NP into an ionic form (Ag+) that can then attach to surfaces or re-deposit onto existing Ag NPs, changing the Ag NP average diameter and size distribution parameters (*i.e.*, cause aggregation). Depending on the form (*e.g.,* coated, colloidal), Ag NPs solutions can be susceptible to light (especially ultraviolet), undergoing oxidation, and therefore, must be stored in the dark to lessen the variability in ultraviolet–visible (UV–Vis) spectroscopy measurement values (Gorham et al., 2014).

Plasmonic metal nanoparticles, including gold, silver, and platinum, are highly efficient elements at absorbing and scattering light (Evanoff and Chumanov, 2005). By changing nanoparticle size, shape, and composition, the optical response can be tuned from the UV through the visible to the near-infrared regions of the electromagnetic spectrum (Evanoff and Chumanov, 2005). By shifting the absorption and scattering, the color of nanoparticle dispersions and films can also be tuned. For example, solutions of Ag NPs are yellow due to the plasmon resonance in the blue region of the spectrum (red and green light is unaffected).

Another property of Ag at the nanoparticle level is a phenomenon known as a surface plasmon resonance (SPR). Ag NPs, at specific wavelengths of light, can drive the conduction electrons in the metal to collectively oscillate (Evanoff and Chumanov, 2005). When these resonances are excited, absorption and scattering intensities can be up to 40 times higher than identically-sized particles that are not plasmonic. The brightness and tunability of plasmonic of the Ag NP optical properties makes them highly useful in numerous applications, such as molecular detection and solar energy materials.

5.1.13 Preparation (Synthesis)

Numerous methods for the synthesis of Ag NPs have been reported in the literature (Khodashenas and Ghorbani, 2015; Zhang et al., 2016). Traditional methods involve solution-phase synthesis techniques and are based on various modifications of using reducing agents of different Ag salts. Silver nitrate ($AgNO_3$) is often used as a precursor in the synthesis of different forms of Ag NPs. Aggregation can be inhibited by thick electrical double layers that form around metal nanoparticles in low-ionic-strength suspensions. For high ionic strength or organic-phase suspensions, capping agents such as self-assembled monolayers, surfactants, polymers, and dendrimers (Evanoff and Chumanov, 2005) can be used to protect the particles from aggregation. Ag NPs can also be capped after synthesis with desired molecules to facilitate their transfer into nonpolar phases or to tailor their surface chemistry. Non-traditional synthesis methods include: high-temperature reduction in porous solid matrices, vapor-phase condensation of a metal onto a solid support, laser ablation of a metal target into a suspending liquid, photoreduction of Ag+, and electrolysis of a Ag salt solution (Evanoff and Chumanov, 2005). The biological activity of Ag NPs depends on many factors, including the type of reducing agents used for the synthesis of Ag NPs; these may be determinants of cytotoxicity (Zhang et al., 2016).

5.1.14 Summary

Physical and chemical properties of Ag NPs, including: surface chemistry, size, size distribution, shape, particle morphology, particle composition, coating/capping, agglomeration, dissolution rate, particle reactivity in solution, efficiency of ion release, cell type, and type of reducing agents used for synthesis, are factors that can influence cytotoxicity. Therapeutic approaches take advantage of synthesized Ag NPs in shapes, such as spherical, rod, octagonal, hexagonal, triangle, and flower-like. Characterization of shape is a crucial factor for the determination of cytotoxicity (Zhang et al., 2016). Previous studies support the assertion that smaller size particles cause greater toxicity than larger particles, due to their larger surface area. Ag NP toxicity depends on chemical and/or biological coatings on the nanoparticle surface. Ag NP surface charges can determine the toxic response in cells. For instance, positive surface charge of Ag NPs gives them a longer half-life in the blood stream than negatively-charged Ag NPs (Choi et al., 2011).

5.2. Toxicokinetics

5.2.1 Oral Exposure

No human data for toxicokinetics of Ag NPs via oral exposure were presented in Versar (2012) nor were any data found in the search of the recent literature.

Park et al. (2011) investigated the bioavailability, tissue distribution, blood concentration, and excretion of functionalized citrate-coated Ag NPs (size, 7.9 ± 0.95 nm). Male Sprague-Dawley rats were treated by a single aqueous solution via oral or IV administration of either 1 or 10 mg/kg bw Ag NPs. Ag concentration in blood tissues was determined as a surrogate for Ag NPs at 10 min, and at 1, 2, 4, 8, 24, 48, and 96 h after treatment. Ag concentration in the liver, lungs, and kidneys was also measured at 24 and 96 h after treatment. Excretion of Ag via feces and urine was determined at 24 h after treatment. After oral administration, most Ag was found in feces, and the blood concentration was very low, suggesting that absorption through the gastrointestinal tract was poor. In contrast, the Ag concentration in blood was significantly elevated at 10 mins after rats were injected in the tail vein with 1 mg/kg bw Ag NP. An elevated Ag concentration in blood was also seen in rats treated with 10 mg/kg bw Ag NPs, but unlike for the lower dose, this concentration remained elevated during the experimental period. On the basis of the values of AUC_{oral}/AUC_{IV}, the bioavailability of orally administered Ag NPs was 1.2 percent in the group treated with 1 mg/kg bw Ag NPs and 4.2 percent in the group treated with 10 mg/kg bw Ag NPs. ICP-MS analyses revealed oral administered Ag NPs accumulation in the liver, lungs, and kidneys. Following oral exposure, Ag NP levels in the urine were extremely low compared to the levels in the feces. When rats were injected IV with Ag NPs, these particles were also detected in feces at 24 hours after treatment, suggesting biliary secretion.

Park (2013) measured blood levels, tissue distributions, and excretion of Ag in male Sprague-Dawley rats (n = 5) up to 24 h after a single oral administration of Ag NPs or silver ions (Ag^+) in deionized water. The AUC_{24hr} of Ag^+ was 3.81 ± 0.57 µg/d/mL when rats were treated with a single dose of 20 mg/kg bw, whereas that of Ag NPs was 1.58 ± 0.25 µg/d/mL. Tissue distribution of Ag in liver, kidneys, and lungs was higher when Ag^+ was administered, compared to Ag NPs. Orally administered Ag NPs were predominantly excreted through feces, suggesting

low bioavailability.

Bergin et al. (2016) compared the effects from acute administration of two different coatings (PVP- or citrate-stabilized) and sizes (nominal median hydrodynamic diameters of 20 and 110 nm) of manufactured Ag NPs to male C57BL/6NCrl mice, using doses of 0.1, 1 or 10 mg/kg/d administered in aqueous solution by oral gavage for 3 days. Silver acetate was used as ionic silver control, and given at the same doses. The authors found no toxicity and no significant tissue accumulation for Ag NPs. Between 70.5 percent and 98.6 percent of the administered Ag NP dose was recovered in feces and particle size and coating differences had no significant influence on percent recovered. Less than 0.5% of the administered Ag NP dose was cumulatively detected in the liver, spleen, intestines, or urine at 48 h. In contrast, Ag+ was detected in the liver, spleen and kidney of mice at marginally higher levels than those observed with Ag NPs, suggesting that Ag+ may be more bioavailable.

Park and coworkers (2010) conducted a 14-day, oral gavage repeat-dose toxicity study in six-week old male and female ICR mice (5/sex/group) using 22, 42, 71, or 323 nm purchased Ag NPs in a 1.0 mg/kg/d dose. The control group received deionized water only. The Ag NPs (22 nm, 42 nm, and 71 nm) significantly accumulated, measured by ICP-MS, after 14 days in the brain, lung, liver, kidney, and testes, while large-sized NPs (323 nm) were not detected in those tissues. This study demonstrated that smaller-sized Ag NPs were more easily absorbed and translocated by the gastrointestinal tract than larger micron-size particles.

Van der Zande et al. (2012) exposed rats to a 28-day oral exposure of 20 nm non-coated Ag NP, or functionalized <15 nm PVP-coated Ag NPs (for both coated and non-coated NPs, Ag dose of 90 mg/kg), or $AgNO_3$ (Ag of 9 mg/kg), or carrier solution only, containing the stabilizing agent Tween. Dissection was performed at day 29, and after a wash-out period of 1 or 8 weeks. Ag was present in all examined organs with the highest levels in the liver and spleen for all Ag treatments. Silver concentrations in the organs were highly correlated to the amount of free Ag+ in the Ag NP suspension, indicating that mainly Ag+, and to a much lesser extent Ag NPs, crossed the intestines in the Ag NP-exposed rats. In all groups Ag was cleared from most organs after 8 weeks after dosing, but remarkably not from the brain and testes. Ag NPs were detected by ICP-MS, in Ag NP exposed rats, but, also in $AgNO_3$ exposed rats, thereby, demonstrating the formation of nanoparticles from Ag+ *in vivo* that are probably composed of Ag salts.

Lee et al. (2013) investigated the clearance of tissue Ag concentrations following oral Ag NP exposure. Sprague-Dawley rats were assigned to three groups: control (0.9% citrate), low dose (100 mg/kg), or high dose (500 mg/kg), and exposed daily to two different sizes of Ag NPs (average diameter 10 and 25 nm) over 28 days. The rats were allowed to recover for four months. Regardless of Ag NP size, the Ag content in most tissues gradually decreased during the four-month recovery period, indicating tissue clearance of the accumulated Ag. The exceptions were Ag concentrations in the brain and testes, which did not clear after the four-month recovery period. The results indicated that the size of the Ag NPs did not affect their tissue distribution. Furthermore, biological barriers, such as between the blood and the brain, and the blood and the testes, seemed to play an important role in the Ag clearance from these tissues.

Hendrickson et al. (2016) orally gavaged male Sprague-Dawley rats with commercially available

12 nm non-coated Ag NPs, for a single exposure and for repeated exposures over 30 days. The daily doses in distilled water were 2000 mg/kg or 250 mg/kg for single and multiple administrations, respectively. Single and multiple administrations resulted in Ag accumulation in the liver, kidneys, spleen, stomach, and small intestine. After both single- and repeated-dose exposures, the highest Ag contents were detected in the liver (0.87 ± 0.37 mg/kg of organ) and kidneys (0.24 ± 0.02 mg/kg of organ). The concentrations of Ag detected in tissues were far smaller than the administered doses, indicating Ag is efficiently excreted from the animal. Overall, the authors concluded that Ag NPs were absorbed to a small extent from the gastrointestinal tract and accumulated in the organs of rats.

Kim et al. (2008) conducted a 28-day oral toxicity study in male and female Sprague-Dawley rats following OCED Test Guideline 407 and GLPs. Six-week-old rats were divided into four groups (10/sex/group) and gavaged daily with 0 (CMC vehicle control), 30, 300, or 1000 mg/kg/d with purchased Ag NPs (60 nm); dosing volume was 10 mL/kg. The method(s) used to determine the characteristics of the test material was not reported, and no information about the possible agglomerization of particles in the suspension was reported. After 28 days of treatment the tissue distribution of Ag NPs showed a dose-related accumulation of Ag content in all tissues examined. In addition, a gender-related difference in the accumulation of Ag was noted in the kidneys, with a two-fold higher concentration in females than in males.

Kim et al. (2010a) subsequently conducted a repeat-dose 90 day oral toxicity study with a different rat strain. The purchased Ag NPs (56 ± 1.46 nm) were orally gavaged to male and female F344 rats over a period of 13 weeks following OECD Test Guideline 408 and GLPs. Five-week-old rats were divided into four groups (10/sex/group): 0 (CMC vehicle control), 30, 125, or 500 mg/kg/d. Count median diameter and geometric standard deviation of the particles in suspension were determined by TEM, but no mention was made of possible agglomerization of the particles in the administered suspensions (as discussed in Versar, 2012). After 90 days of exposure, clinical chemistry, hematology, organ weight, histopathology, and Ag distribution were studied. A dose-related accumulation of Ag occurred in all tissues examined, including the testes. As in the earlier and shorter-term study, a gender-related difference in the accumulation of Ag was noted in the kidneys, with a two-fold higher level in females compared to males.

Jimenez-Lamana et al. (2014) carried out a comprehensive study on bioavailability of orally administered Ag NPs (Collargol with average diameter of 15 nm) for short-term to subchronic exposures (between 30 and 81 days) in weanling male Sprague-Dawley rats. The Ag uptake was monitored in the liver and kidneys, as well as in the urine and feces. Significant accumulation of Ag was found in both organs, the liver being the principal target. A significant (~50 percent) fraction of Ag was found in the feces, whereas the fraction excreted via urine was negligible. Intact Ag NPs were found in the feces. ICP-MS analysis revealed Ag NPs were able to penetrate into the liver, in contrast to the kidneys where they were retained in the cortex. Ag speciation analysis in kidney cytosols showed Ag-metallothionein complex as the major species. In the liver the majority of ionic Ag released by the oxidation of Ag NPs was bound to high-molecular proteins.

Boudreau et al. (2016) evaluated particulate and ionic forms of Ag as well as particle size for differences in Ag accumulation, distribution, morphology, and toxicity when administered daily by oral gavage to Sprague Dawley rats for 13 weeks. Seven-week-old rats (10 rats per sex per

group) were randomly assigned to treatments of either Ag NPs (10, 75, and 110 nm) at 9, 18, or 36 mg/kg, or silver acetate (AgOAc) at 100, 200, and 400 mg/kg, or controls (2 mM sodium citrate or water, respectively). Differences in the distributional pattern and morphology of Ag deposits (by TEM) were seen in rats exposed to Ag NPs as compared to control and AgOAc treated mice. Specifically, Ag NPs appeared predominantly within cells, while AgOAc had an affinity for extracellular membranes. Significant dose-related and inversely Ag NPs size-related accumulations were also detected in tissues by ICP-MS. Furthermore, sex differences in Ag accumulations were noted for a number of tissues and organs, with accumulations being significantly higher in female rats, especially in the kidney, liver, jejunum, and colon.

Kim et al. (2009) investigated the gender specific accumulation of Ag NPs in kidneys of Fischer 344 rats through a detailed histopathological study by Ag-enhancement staining after 90-day oral exposure to Ag NPs (52.7 to 70.9 nm, average 60 nm, and at least 99.98 percent pure). The vehicle control was 0.5 percent CMC. Female rats showed a higher accumulation of Ag NPs in all kidney regions, including cortex, outer medulla, and inner medulla. In particular, the glomerulus in the cortex contained a higher accumulation in females than males. The Ag NPs were also preferentially accumulated in the basement membranes of the renal tubules in the cortex, middle and terminal parts of the inner and outer medulla. In addition, Ag NPs were detected in the cytoplasm and nuclei of interstitial cells in the inner medulla of the kidney.

Hong et al. (2014) conducted a combined repeat-dose reproductive/developmental toxicity study using manufactured functionalized 7.9 ± 0.95 nm citrate-coated Ag NPs, using male and female Sprague-Dawley rats. The rats (10/sex/group) were orally gavaged with 0 (distilled water control), 62.5, 125, or 250 mg/kg/d Ag NPs. Males were dosed once a day for 42 days (14 days before mating, 14 days during mating and 14 days post-mating until necropsy) and females were dosed up to 52 days (2 weeks before mating, during mating and gestation and during 4 days of lactation). The average quantity of Ag in the livers of treated rats (1117.55 ± 381.68 ng/g) was increased 34-fold compared to the level in control rat livers (33.54 ± 15.25 ng/g). Ag levels in the lung and kidneys were also significantly increased. Distribution of Ag to fetal tissues was not measured.

5.2.2 Inhalation Exposure

No human data for toxicokinetics of Ag NPs via inhalation exposure were presented in Versar (2012), nor were any data found in the search of the recent literature. Versar located several rat studies providing evidence that Ag is distributed to extra-respiratory tissues following inhalation exposure to Ag NPs (Sung et al., 2009; Ji et al., 2007a; Takenaka et al., 2001).

Smulders et al. (2015) investigated Ag engineered nanoparticle (ENP) lung distribution; local concentration; co-localization with other elements such as Fe, Cu and S; and, speciation (formation of new and distinct molecular structures) after lung exposure. Analysis of the ENPs by DLS showed a polydisperse suspension with 3 populations: 130 nm (11 percent in number), 506 nm (89 percent in number), and 5180 nm (0.1 percent in number). The particles were negatively charged. Inductively coupled plasma optical emission spectroscopy (ICP-OES) measurements showed impurities of Ca (216.8 mg/g), Fe (23.8 mg/g) and Cu (0.6 mg/g). Aged paint containing Ag ENPs and paints without ENPs (control) were administered via OPA into male BALB/c mice (20 µg/aspiration) once a week for 5 weeks and mice were sacrificed either 2

or 28 days post-final treatment (Smulders et al., 2014). The lung, liver, kidney, spleen, and heart tissue were harvested, and Ag concentrations were determined. Biodistribution experiments showed distribution of Ag outside the lung after aspiration to respectively pristine Ag ENPs. The authors found that approximately a quarter of all macrophages in the lumen of the airways contained these Ag ENPs. High local concentrations of Ag were also detected in the lung tissue, probably phagocytized by macrophages. The largest portion of these particles was dissolved and bound to thiol-containing molecules. Increased concentrations of Fe and Cu observed in the Ag-rich spots suggest that these molecules are metallothioneins.

5.2.3 Dermal Exposure

Human studies indicate that absorption of Ag from Ag NPs can occur (discussed in Versar, 2012). No recent literature of absorption, distribution, metabolism or elimination in humans or animals was identified.

5.2.4 Parenteral Exposure

See also discussion of Park et al. (2011) in the oral section of this chapter.

Ashraf et al. (2015) IV administered a water-based suspension of functionalized radio-labeled dextran-coated Ag NPs (dextran–Ag NPs) or non-coated Ag NPs into male rabbits at a concentration of 1 mCi/ml of ^{99m}Tc (containing almost 200 µg/ml of Ag NPs) with a size range of 5.6–43.8 nm (maximum occurrence frequency at size 7.53 nm). *In vivo* tissue uptake of nanoparticles revealed that Ag NPs and dextran–Ag NPs mainly accumulated in the liver/spleen region, but that uptake of dextran–Ag NPs were delayed in the liver, thus functionalization enhanced blood retention time.

Xue et al. (2012) evaluated the biokinetics of IV administered Ag NPs in ICR mice exposed to different dosages of Ag NPs (7.5, 30, or 120 mg/kg). Biokinetics and tissue distribution of Ag NPs were evaluated at a single dose of 0 (saline control) or 120 mg/kg bw in both male and female mice. The highest Ag levels were observed in the spleen, followed by liver, lungs and kidneys. The elimination half-lives and clearance of Ag NPs were 15.6 hours and 1.0 mL/hour/g (presumed to be of creatinine) for male mice and 29.9 hours and 0.8 mL/hour/g (presumed to be of creatinine) for female mice. These results indicated that Ag NPs could be distributed extensively to various tissues in the body, but primarily to the spleen and liver. Furthermore, there appeared to be gender-related differences in the biokinetic profiles in blood and distribution in lungs and kidneys.

Dziendzikowska et al. (2012) IV administered a single dose of 0 (0.9 percent NaCl solution) or 5 mg/kg bw Ag NPs (nominal diameters of 20 and 200 nm) to male Wistar rats. Biological material was sampled 1, 7 and 28 days after injection. Ag NPs were shown to distribute from the blood to the main organs and the concentration of Ag in tissues was significantly higher in rats treated with 20 nm Ag NPs as compared with 200 nm Ag NPs. The highest concentration of Ag was measured in the liver after 24 hours. After 7 days, a high level of Ag was observed in the lungs and spleen. The Ag concentration in the kidneys and brain increased during the experiment and reached the highest concentration after 28 days. In the urine, the highest concentration of Ag NPs was observed at 1 day after the injection; this urine level was

maintained for 14 days and then decreased. The Ag fecal level peaked within 2 days after Ag NP administration.

Tang et al. (2009) studied the distribution and accumulation of Ag NPs in rats after a single SC injection of 62.8 mg/kg bw. Particles were spherical and electron-dense, with a 50 to100 nm diameter. Results indicated that these particles were distributed to the blood and then throughout the body. Ag accumulation occurred especially in the kidneys, liver, spleen, brain and lungs.

Recordati et al. (2016) IV injected male CD-1 (ICR) mice with commercially available functionalized Ag NPs of different sizes (10 nm, 40 nm, or 100 nm), either citrate- or PVP-coated, at a single dose of 0 (control) or 10 mg/kg bw. An equivalent dose of Ag+ was administered as silver acetate. For all particle sizes, regardless of their coating, the highest Ag concentrations were found in the spleen and liver, followed by lung, kidney, and brain. Ag concentrations were significantly higher in the spleen, lung, kidney, brain, and blood of mice treated with 10 nm Ag NPs than those treated with larger particles. In mice treated with silver acetate, Ag concentrations were significantly lower in the spleen and lung, and higher in the kidney than in mice treated with 10 nm Ag NPs. The authors concluded that administration of the smallest (10 nm) Ag NPs resulted in enhanced Ag tissue distribution compared to larger NPs (40 and 100 nm), while coatings had no relevant impact. Distinctly different patterns of tissue distribution were observed after silver acetate (Ag+) administration.

Lankveld et al. (2010) studied blood kinetics and tissue distribution of 20, 80 and 110 nm Ag NPs in male Wistar rats up to 16 days after IV injections (tail vein), once daily for 5 consecutive days. Distribution of Ag NPs was monitored starting immediately after the first injection and continued for the duration of the study. Following both the first and repeated IV injections of 0 (phosphate buffer control) or any sized particle, Ag NPs disappeared rapidly from the blood and distributed to all organs evaluated, including the liver, lungs, spleen, brain, heart, kidneys and testes. The 20 nm particles distributed mainly to the liver, followed by the kidneys and spleen, whereas the larger particles distributed mainly to the spleen followed by the liver and lung. In the other organs evaluated, no major differences in concentrations were observed among the different sized particles. Repeated administration resulted in accumulation in the liver, lung and spleen, indicating that these organs may be potential target organs for toxicity after repeated exposure. A physiologically-based pharmacokinetic (PBPK) model that describes the kinetics of Ag NPs was developed. Model parameter values were estimated by fitting to data. No clear relation between parameter values and corresponding particle sizes was apparent.

Wen et al. (2016) conducted intranasal instillation of commercially available functionalized PVP-coated Ag NPs in neonatal Sprague-Dawley rats at doses of 0 (aqueous solution), 1 or 0.1 mg/kg/d for 4 or 12 weeks, respectively. A 4-week recovery was added after the 12-week exposure. Parallel exposures using $AgNO_3$ for Ag+ were performed for the comparative studies. Dose-related Ag accumulation occurred for both Ag NPs and Ag+ groups, but relatively higher Ag accumulations were observed in Ag+ groups. The highest Ag concentration was in the liver at week 4, while it shifted to the brain after a 12-week exposure. The time course revealed a uniquely high concentration and retention of Ag in the brain, implying chronic intranasal instillation caused brain-targeted Ag accumulation. These findings provided substantial evidence of potential neuronal effects from the intranasal administration of Ag NPs or Ag colloid-based products.

5.2.5 Physiologically-Based Pharmacokinetic Model (PBPK)

Bachler et al. (2013) developed a PBPK model for Ag+ and Ag NPs. The structure of the model was established on the basis of toxicokinetic data from IV studies. The authors validated the model structure for both Ag forms by reproducing exposure conditions (dermal, oral, and inhalation) of *in vivo* experiments and comparing simulated and experimentally assessed organ concentrations. In all of the cases examined, the model successfully predicted the distribution of Ag+ and 15 to 150 nm Ag NPs, which were not coated (functionalized) with substances designed to prolong the circulatory time. Furthermore, the results of the model indicated that particle size and coating had minor influences on distribution. The authors stated that it is more likely that Ag NPs are directly stored as insoluble salt particles, than dissolved into Ag+; and that compartments of the phagocytic system play a minor role at exposure levels that are relevant for human consumers.

See also Lankveld et al. (2010) in the parenteral part of this section for a brief description of a PBPK model.

5.2.6 Transplacental Transfer

Austin et al. (2012) injected laboratory synthesized Ag NPs (average diameter 50 nm) into the tail vein of pregnant CD-1 mice, 6-12/group, on GD 7, 8, and 9 at dose levels of 0 (citrate buffer control), 35, or 66 μg Ag/mouse. Mice were killed on GD 10 and Ag content was monitored. Ag was significantly increased in the spleen, lung, tail (IV site), visceral yolk sac, endometrium and extra-embryonic tissues on GD 10, and non-significantly increased in the embryo. These results show that once Ag NPs reach the bloodstream, they enter maternal tissues, extra-embryonic tissues, and to a limited extent, the embryo.

Austin et al. (2016) also examined the distribution of Ag in pregnant mice and embryos/fetuses following IV injections of 10 nm Ag NPs or soluble silver nitrate ($AgNO_3$) at dose levels of 0 (citrate buffer control) or 66 mg Ag/mouse on GDs 7, 8 and 9. For the visceral yolk sac, mean Ag concentration following $AgNO_3$ treatment was approximately two-fold of that following Ag NP treatment (4.87 ng Ag/mg tissue vs. 2.31 ng Ag/mg tissue). For all other tissues examined, mean Ag concentrations following either Ag NPs or $AgNO_3$ treatment were not significantly different from each other (2.57 or 2.84 ng Ag/mg tissue in maternal liver and 1.61 or 2.50 ng Ag/mg tissue in maternal spleen, respectively). Ag accumulation in embryos/fetuses was negligible; with concentrations ranging from 0.03 ng Ag/mg tissue (embryos) to 2.57 ng Ag/mg tissue (maternal liver) at GD 10, and 0.02 ng Ag/mg tissue (fetuses) to 0.896 ng Ag/mg tissue (maternal liver) at GD 16. Most embryos appeared small for their age (GD 10) compared to the controls. Thus, IV injection of 10 nm Ag NPs to pregnant mice resulted in notable Ag accumulation in maternal liver, spleen and visceral yolk sac, and may have affected embryonic growth.

Melnik et al. (2013) conducted a quantitative assessment of Ag NP transfer through the placenta and breast milk in Wistar rats using ^{110m}Ag-labeled (34.9 ± 14.8 nm diameter) PVP-functionalized Ag NPs. Preparations were administered to three controls, three low-dose and four high-dose pregnant rats by gavage on day 20 of gestation at dosages of 0 (water control), 1.69, or 2.11 mg/kg/d ^{110m}Ag NPs. On days 10 to 11 of lactation, another unexposed group of

five female rats, nursing nine pups each, received 2.11 mg/kg/d ^{110m}Ag NPs. The average level of accumulation in the visceral yolk sac in fetuses was 0.085 to 0.147 percent of the administered dose, which was comparable to the accumulation of the labeled Ag NPs in the liver, blood, and muscle of the dams. The total accumulation of labeled Ag NPs into the milk exceeded 1.94 ± 0.29 percent of the administered dose over a 48-hour period of lactation; at least 25 percent of this amount was absorbed into the gastrointestinal tract of rat pups.

Fatemi et al. (2013) gavaged pregnant Wistar rats (45/group) with 0 (deionized water) or 25 mg/kg/d manufactured Ag NPs (20 ± 4 nm), daily from GD 9 to delivery. After parturition, a number of effects were monitored, including the amount of Ag in the brain of the pups one day after birth. Ag concentration in the brains of pups (on PND 1) born by mothers exposed to Ag NPs were statistically significantly higher than the Ag content in pups of unexposed mothers. Results indicate that the Ag NPs transferred transplacentally to the fetal brain and produced oxidative stress and apoptosis (glutathione, glutathione peroxidase, malondialdehyde, and caspase 8 and 9 levels measured) in the brain of offspring.

Wang et al. (2013) exposed 5-10 male and female BALB/c mice/group to Ag NPs at 0 (Phosphate-buffered saline [PBS] vehicle), 22, or 108 µg/kg every 2 days for 4 weeks premating, via IP and IV routes of administration. On GD 14.5, embryos from 3 to 5 dams/group were collected. The results showed that Ag NPs were predominantly localized in the liver and spleen in adult mice for both administration methods and doses. Compared to IP administration, Ag NPs were quickly removed and excreted from the body after IV administration. The accumulation of Ag NPs in livers caused hepatic toxicity for both doses and routes of administration Furthermore, the results of Ag NP tissue distribution in male mice revealed that Ag NPs could pass through the blood-testes barrier, resulting in localization in testes when IV administered (the IP route was not tested). Ag NP retention lasted for more than 4 months, and the Ag content in the major recipient organs decreased in a time-dependent manner. Ag NPs crossed the placental barrier and accumulated in fetuses.

5.2.7 Summary

Toxicokinetic studies in rats and mice are available for oral exposure, although the form of Ag is not always identified in the tissues. Studies on the transformation of Ag NP to other forms of Ag in human or animal tissues are not available.

In general with oral exposure, absorption of Ag NP through the gastrointestinal tract in rats was poor, indicated by high levels of Ag NP found in feces. Systemically absorbed Ag NPs accumulated in several organs and were slowly cleared with the exception of the brain and testes. Gender-related differences have been noted in the kidneys and liver, with females accumulating almost twice the amount of Ag as males. Excretion of Ag NPs levels in the urine was low.

Tissue concentrations of orally-administered Ag in the liver, kidneys, and lungs were higher for the ionic form (Ag+) (administered as Ag acetate) than for Ag NPs. Orally administered Ag NPs were predominantly excreted through feces, again suggesting low bioavailability. Coating differences (functionalization) and particle size had no significant influence on Ag recovery in the feces from oral exposure; between ~70 to 99 percent of the administered Ag NP dose was

recovered. Less than 0.5 percent of the administered Ag NP dose was cumulatively detected in the liver, spleen, intestines, or urine at 48 hours. In contrast, Ag was detected at marginally higher levels in the liver, spleen and kidney of mice administered Ag+ than in mice administered Ag NPs, suggesting that Ag+ may be more bioavailable. Small-sized Ag NPs (22 nm, 42 nm, and 71 nm) administered orally, significantly accumulated after 14 days in the brain, lung, liver, kidney, and testes, while large-sized Ag NPs (323 nm) were not detected in those tissues, demonstrating that smaller-sized Ag NPs were more easily absorbed via the gastrointestinal tract and translocated than the larger micron-size particles. With longer duration oral exposure (greater than 28 days), Ag content in organs was correlated with the Ag concentration in the Ag NP, and was cleared from most organs, except for the brain and testes.

Toxicokinetic studies via inhalation or dermal exposure in humans or animals were not available in the recent literature search. Biodistribution experiments of engineered Ag NP following OPA showed distribution of Ag in the lung tissue as well as to organs outside the lung.

Intravenously administered (acute and repeated) Ag NPs showed accumulation mainly in the liver and spleen regions in laboratory animals, with smaller diameter particles distributing faster. Particles were detected in feces at 24 hours after treatment, suggesting biliary secretion.

Numerous studies indicate that Ag NPs or Ag+ that reach the bloodstream, also enter maternal tissues, extra-embryonic tissues, breast milk, and to a limited extent, the embryo.

5.3 Acute and Short-term Toxicity

5.3.1 Oral Exposure

No case reports or other acute toxicity information for Ag NPs by the oral route in humans was located in the literature search conducted for this project.

Maneewattanapinyo et al. (2011) conducted an acute oral toxicity study in 18 male and female (10 to 12 weeks old) CD-1 (ICR) mice divided into 3 mice/sex/group of a colloidal Ag NP synthesized by the investigators following OECD Test Guideline 425. The Ag NPs were spherical (TEM), having a primary particle diameter of 10 to 20 nm with Ag+ concentration less than 0.04 percent. Gavage administration of colloidal Ag NPs in distilled water was at a single limit dose of 5,000 mg/kg bw and produced no mortality or acute toxic signs throughout the 24-hour observation period and 14-day post-treatment period. Percentage of body weight gain, hematological and blood chemistry analyses showed no significant difference between control and treatment groups. No gross lesions or histopathological changes were observed. The results indicated that the median lethal dose (LD_{50}) of colloidal Ag NPs is greater than 5,000 mg/kg bw.

Kim et al. (2013a) evaluated the acute oral toxicity of commercially manufactured Ag NPs according to OECD Test Guideline 423 and conducted following GLPs. The Ag NPs dispersed in 1 percent citric acid had an average particle size of 10.0 nm (TEM), with a mean surface area of 3.18×10^2 mm^2/particle. Three female 7-week old Sprague-Dawley rats were given a single dose of up to 2000 mg/kg in a four-step process and observed for abnormal clinical signs and mortality. Rats were administered a single dose by oral gavage at each step. The first step was a

single gavage at 300 mg/kg at 10 mL/kg; with no animal deaths, the second step was a single gavage at 300 mg/kg to the same rats. As the second step produced no moribund animals or mortality, the third step was a single gavage at 2000 mg/kg. Finally, as the third step produced no moribund animals or mortality, the fourth step was another single gavage of 2000 mg/kg. The time course of the steps and administration of the material was not apparent from the report. The rats were observed daily for 14 days. There were no dead animals or abnormal signs observed, no significant differences in body weights during 14 days after administration, and no abnormal gross findings at necropsy. The LD_{50} was determined to be greater than 2000 mg/kg/d by oral gavage.

These studies evaluate the acute toxicity of oral exposure in rats to commercially produced Ag NPs in accordance with OECD Acute Test Guidelines and GLPs. The LD_{50} was determined to be the greater than 5,000 mg/kg bw.

5.3.2 Inhalation Exposure

No case reports or other acute toxicity information by the inhalation route in humans was located in the literature search conducted for this project.

Versar (2012) did not identify any acute studies in animals via the inhalation route.

Sung et al. (2011) conducted a four-hour acute whole-body inhalation toxicity study of Ag NPs following OECD Test Guideline 403 and GLP using seven-week-old male and female Sprague-Dawley rats. Rats were divided into four exposure groups (five/sex/group): dried and filtered fresh-air control, low-concentration (0.94×10^6 particles/cm^3, 76 µg/m^3), middle-concentration (1.64×10^6 particles/cm^3, 135 µg/m^3), and high-concentration (3.08×10^6 particles/cm^3, 750 µg/m^3). The particles were generated as described in Ji et al. (2007a,b) and Jung et al. (2006). A full necropsy was conducted two weeks after exposure. Lung function was measured twice per week after the initial 4-hour exposure. No significant mortality, body weight changes, feed consumption value changes or clinical changes were found during the 2-week observation period. Pulmonary function tests (4/group) indicated no significant difference between the control and the exposed groups. The median lethal concentration (LC_{50}) for Ag NPs was higher than 3.1×10^6 particles/cm^3 (750 µg/m^3).

Kwon et al. (2012) investigated the acute pulmonary toxicity of Ag NPs in 5-week-old male C57BL/6 mice (10/group) using nose-only exposure chambers. Acute pulmonary toxicity and body distribution of inhaled laboratory-generated Ag NPs were evaluated in mice exposed for 6 hours. The Ag NPs were generated as described in Jung et al. (2006) and had a geometric mean diameter of 20.30 nm. Whole lung BALF analysis, Western blotting, histopathological changes, and Ag burdens in various organs (brain, heart, lung, liver, spleen, and testes) were determined. The mean concentration, total surface area, volume and mass concentrations were respectively maintained at 1.09×10^{10} nm^2/cm^3, 2.72×10^{11} nm^3/cm^3, and 2854.62 µg/m^3 during exposures. Inhalation of Ag NPs caused mild pulmonary toxicity (evaluated by total protein, lactate acid dehydrogenase, and cytology assays) with distribution of Ag in various organs; however, the Ag burdens decreased rapidly at 24-hours post-exposure in the lung. In summary, single inhalation exposure of 1.93×10^7 particles/cm^3 Ag NPs caused mild pulmonary toxicity associated with activation of the MAPK signaling pathway indicating immunotoxicity, and

would be considered the LOAEC (only concentration tested).

Braakhuis et al. (2014) determined the lung burden, tissue distribution, and the induction of and recovery from adverse effects after short-term inhalation exposure to 15 nm (generated in the laboratory) and 410 nm (commercially purchased) Ag NPs. Twelve male Fisher 344 rats/group were nose-only exposed to clean air, 15 nm (179 $\mu g/m^3$) or 410 nm (167 $\mu g/m^3$) Ag NPs for 6 hours per day, for four consecutive days. Six rats/group were necropsied at 24 hours and the remaining 6/group after 7 days. The 179 $\mu g/m^3$ (15 nm) Ag NP dose resulted in a 175-fold increase in neutrophils and a two-fold increase of cellular damage markers in the lungs, a five-fold increase in pro-inflammatory cytokines in the lungs, and a 1.5-fold increase in total glutathione in the lungs at 24 hours after exposure indicating moderate pulmonary toxicity. These signs of toxicity disappeared by 7 days after exposure. No toxic effects were observed after exposure to 167 $\mu g/m^3$ of the larger (410 nm) NPs. The results show a clear size-dependent effect after inhalation of similar mass concentrations of 15 nm and 410 nm Ag NPs.

Braakhuis and coworkers (2016) researched a suitable dose metric to describe the effects of agglomerated Ag NP toxicity after a short-term nose-only inhalation exposure. Male Fisher 344 rats (3/group) were exposed for 45 min, 90 min, 3 hours, or 6 hours to different concentrations (ranging from 41 to 1105 mg silver/m^3) of 18, 34, 60 or 160 nm Ag NPs for four consecutive days and sacrificed at 24 hours or 7 days after exposure. The 18 nm (range 15 to 20 nm), 34 nm (range 30 to 35 nm), and 60 nm (range 60 to 65 nm) agglomerates were generated in the laboratory. The PVP-coated 160 nm Ag NPs consisted of three to five agglomerated 80 nm Ag NPs (commercially purchased) that fused into a single spherical particle when heated in an oven. The particle characteristics are summarized in Table 20.

Table 20. Ag NP Characteristics in Braakhuis et al. (2016)

Agglomerate size count median diameter (nm)[a]	Mean Mass ($\mu g/m^3$)[a]	Mean Particle number (#/cm^3)[a]	Mean Surface Area (nm^2/cm^3)[a]
18.1 (1.24)	438 (130)	1.3×10^7 (4.0×10^6)	1.4×10^{10} (4.1×10^9)
34.5 (1.3)	325 (50)	6.6×10^6 (1.0×10^5)	5.4×10^9 (9.0×10^8)
60.3 (1.32)	341 (21)	3.6×10^5 (2.1×10^4)	3.2×10^9 (4.1×10^8)
160 (1.55)	1109 (46)	5.3×10^4 (1.7×10^3)	1.4×10^9 (4.1×10^9)

[a]Values in parentheses are geometric standard deviations

There were no alterations in clinical observations, body and organ weights, feed and water intake, or feces and urine production. Hematology and BALF, pro-inflammatory cytokines, and oxidative stress analyses were performed at necropsy. There was a concentration-related increase in cell counts and pro-inflammatory cytokines in the BALF, indicative of pulmonary toxicity. The authors selected the total cell number, the number of neutrophils, and the level of IL-1β and MCP-1 in the lung fluid after the exposure period to determine the most suitable dose metric for Ag NPs because these were significantly affected. The data were analyzed using: (1) the external Ag concentration in air during exposure, (2) the internal lung dose of Ag, and (3) the alveolar dose as calculated using the exposure concentration and an internal lung dose model. For each of the parameters, graphs were produced and all showed that when the particle surface area that reaches the alveoli is used as a dose metric, the dose-response curves of the various particle sizes almost completely overlap. Using software, the critical effect concentration (CED)

was calculated that induced a 20 percent response. Based on exposure concentration, the CED_{20} of the different sized Ag NPs do not overlap when expressed as mass or particle number. When expressed as surface area, the critical effect concentrations were closer to each other, but did not overlap. The same was true for the lung internal dose; mass and particle numbers resulted in different CED_{20} for the different particle sizes, while surface area moved them towards each other. Based on the alveolar dose, however, the CED_{20} of the different particle sizes overlapped when the dose was expressed as surface area. Therefore, in the alveoli, particle surface area seems the best dose metric to describe the effect of Ag NPs on the total cell number, the number of neutrophils and the level of IL-1β and MCP-1 after short-term inhalation. The authors concluded that the alveolar dose expressed as particle surface area is the most suitable dose metric to describe the toxicity of Ag NPs by inhalation.

Inhalation studies evaluated the acute toxicity of inhalation exposure in rodents to commercially- or laboratory-produced Ag NPs. One whole-body study in rats was in accordance with OECD Acute Test Guidelines and GLPs; the LC_{50} for Ag NPs in that study was higher than 3.1×10^6 particles/cm^3 (750 μg/m^3). Nose-only inhalation studies in mice and rats using laboratory generated Ag NPs caused transient mild to moderate pulmonary toxicity.

5.3.3 Dermal Exposure

Versar (2012) described two case studies of treatment of humans with burns with dressing containing Ag NPs. In one study, a patient developed argyria-discoloration after 6 days and elevation of serum levels of liver enzymes indicative of hepatotoxicity**;** these returned to normal after the dressing was removed (Trop et al., 2006). A second case study of 30 burn patients treated with the same dressing for 3 to 19 days reported increased serum Ag levels that were not significantly correlated with changes in serum liver enzyme levels, but were marginally correlated with HB, platelet count, and eosinophil count (Vlachou et al., 2007).

Maneewattanapinyo et al. (2011) conducted an acute dermal toxicity study in guinea pigs with colloidal Ag NPs synthesized by the investigators following OECD Test Guideline 434. The Ag NPs were spherical (TEM), having a primary particle diameter of 10 to 20 nm with free Ag+ concentration less than 0.04 percent. The guinea pigs were randomly divided into three groups containing three animals each in the following manner: group 1, distilled water (vehicle control); group 2 and group 3 received 50 and 100,000 ppm of colloidal Ag NPs in 2 mL, respectively. The test substance was applied to a 7 x 10 cm rectangle area of shaven skin and occluded for 24 hours. All animals were observed for signs of toxicity at 1, 3, 7 and 14 hours. At 1, 3, and 7 days after exposure a skin biopsy was conducted for histopathological evaluation. No gross abnormalities or microscopic changes during the 14-day post-treatment observation period were noted in the skin of the guinea pigs exposed to 0, 50 or 100,000 ppm doses of colloidal Ag NPs.

Kim et al. (2013a) evaluated the dermal toxicity of commercially manufactured colloidal Ag NPs according to the OECD Test Guideline 404 and GLPs. The average particle size was 10.0 nm (TEM) with a mean surface area of 3.18×10^2 mm^2/particle. In the acute dermal toxicity study, the dose groups consisted of 0 and 2000 mg/kg, with 5 male and 5 female Sprague-Dawley rats in each group. The skin was shaven, and the test substance applied and the site occluded for 24 hours. The animals were observed twice daily over 15 days for any signs of irritation and toxicity. The Ag NPs did not induce any abnormal clinical signs, mortality, or abnormal gross

findings in any of the treated groups at necropsy.

In summary, human and animal studies evaluated the acute toxicity of dermal exposure to commercially- or laboratory-synthesized Ag NPs. Wound patients treated with AgNP-containing burn dressings developed argyria-discoloration after 6 days as well as elevation of serum levels that are indicative of hepatotoxicity. An acute dermal guinea pig study in accordance with OECD Acute Test Guidelines and GLPs showed no gross abnormalities or microscopic changes after 14 days following one-day exposures up to 100,000 ppm. Similarly, a rat study showed no abnormal clinical signs, mortality or gross findings.

5.4 Repeat-Dose and Subchronic Toxicity

5.4.1 Oral Exposure

No human data for oral exposure to Ag NPs were reviewed in Versar (2012).

A human study of nanoscale Ag was conducted using commercial 10- and 32-ppm colloidal Ag solutions (consisting of both silver ions and Ag NPs) in a single-blind, controlled, cross-over, intent-to-treat, design (Munger et al., 2014). Thirty-six healthy subjects consumed daily a 10 ppm Ag particle aqueous solution and were evaluated at 3, 7 and 14 days; and 24 healthy subjects consumed daily a 32 ppm Ag particle solution and were evaluated at 14 days. All underwent metabolic measures, blood counts, urinalysis, sputum induction, and chest and abdomen magnetic resonance imaging (MRI) prior to and after treatment. Serum and urine Ag content were determined. The Ag NPs were in the form of zero-valent elemental Ag particles, coated with silver oxide, with manufacturer's claims for 10 ppm to have a particle size ranging between 5 to 10 nm and the 32 ppm to have a mean particle size of 32.8 nm, and range of 25 to 40 nm. The average daily ingestion of this elemental Ag colloid formulation was estimated to be 100 μg/day for 10 ppm, and 480 μg/day for 32 ppm Ag. No clinically important changes in metabolic, hematologic, or urinalysis measures were identified. No morphological changes were detected in the lungs, heart or abdominal organs. No significant changes were noted in pulmonary ROS or pro-inflammatory cytokine generation.

Munger et al. (2015) subsequently investigated whether orally ingested commercially available colloidal Ag nanoproduct interfered with select cytochrome P450 enzymes. A prospective, single-blind, controlled *in vivo* human study using simultaneous administration of standardized probes for P450 enzyme classes CYP1A2, CYP2C9, CYP2C19, CYP2D6 and CYP3A4 was conducted. The reduced Ag (Ag^0) NP size averaged 32.8 nm, with a size range of 25 to 40 nm, and was consumed orally for 14 days with an estimated dose of 480 μg/day. Both Ag and Ag+ characterizations were fully described (Munger et al., 2014). Ingestion of a commercial colloidal Ag nanoproduct produced detectable Ag in human serum after 14 days of dosing. This Ag, however, elicited no demonstrable clinically significant changes in metabolic, hematologic, urinary, physical findings or cytochrome P450 enzyme inhibition or induction activity.

Three repeat-dose oral animal studies (Kim et al., 2008; Kim et al., 2010a; Jeong et al., 2010) were reviewed in Versar (2012). These studies by Kim and coworkers (cited in Versar, 2012) are included in Table 21 along with other more recent studies. Jeong et al. (2010) did not have adequate reporting and is excluded from further discussion.

Kim et al. (2008; as described in Versar, 2012) reported increased ALP activity in males and increased cholesterol in female Sprague-Dawley rats receiving 300 mg/kg/d AgNPs by oral gavage, indicating slight liver damage. At 1000 mg/kg/d, males showed changes in blood biochemistry (increased ALP, total cholesterol and decreased total protein) and hematology (increased mean corpuscular volume [MCV]). Females showed increased ALP and cholesterol, and increased red blood cells (RBCs), hematocrit (HCT) and HB at both 300 and 1000 mg/kg/d and increased active partial thromboplastin time (sec) at 1000 mg/kg/d. Increased incidence of bile duct hyperplasia in male and female rats was observed at 1,000 mg/kg/d. For this study, 300 and 30 mg/kg/d are considered the LOAEL and NOAEL, respectively based on minimal liver toxicity.

Kim et al. (2010a; as discussed in Versar, 2012) conducted a 90-day oral toxicity study of Ag NPs in five-week-old F344 rats following OECD Test Guideline 408. Groups of 10 rats/sex were exposed by daily gavage to suspensions of commercial Ag NPs in 0.5 percent aqueous CMC at doses of 0 (vehicle control), 30, 125, or 500 mg/kg/d for 90 days; dose volume was 10 mL/kg. The test material was purchased and reported to be 99.98 percent pure. Count median diameter and GSD of the particles in suspension were 56 nm and 1.46, respectively, by TEM. Tissue samples were analyzed for Ag content. At the highest dose level, total cholesterol was significantly increased in males and females, and ALP activity was significantly increased in females. Histopathological examination showed a significantly increased incidence for pigmentation in the villi of the intestine of high-dose males (8/10) and females (5/10), relative to their respective controls (0/10, 0/10). There was a statistically significant dose-related increase in the Ag concentration of all tissue (testes, liver, kidneys, brain, lungs, and blood) samples from the groups exposed to Ag NPs. Overall, the results indicate a NOAEL of 125 mg/kg/d and a LOAEL of 500 mg/kg/d based on evidence for minimal liver toxicity and yellow pigmentation in intestinal villi.

Park et al. (2010a) treated CD-1 (ICR) mice (5/sex/group) with purchased Ag NPs (22, 42, 71, or 323 nm) at 0 (distilled water) or 1 mg/kg for 14 days by gavage administration. Absolute or relative organ weights were not different between the control and the Ag NP-treated groups. An increased distribution of natural killer cells and B cells were observed only in the group treated with the small Ag NPs (22, 42, and 71 nm), and not in the group treated with the large (323 nm) Ag NPs. TGF-β has various functions in cells including cell growth and differentiation, apoptosis, cell motility, extracellular matrix production, and cellular immune responses. TGF-β levels were significantly increased in groups treated with small-sized Ag NPs, but not with large-sized Ag NPs. In addition, B cell distribution was increased by the small-sized Ag NPs, but not in large-sized-Ag NPs, as determined by phenotype analysis.

In the same study, Park et al. (2010a) treated CD-1 (ICR) mice (6/sex/group) with 42 nm Ag NPs at 0 (distilled water), 0.25, 0.50 or 1.00 mg/kg/d (doses provided by authors) for 28 days by oral gavage. Body weights were collected weekly and blood collected from 3 mice for cellular aspartate aminotransferase (AST), alanine aminotransferase (ALT), ALP, creatinine, and blood urea nitrogen (BUN). Histopathology was conducted on the kidneys, livers, and small intestines of the control and treated groups. The concentrations of cytokines and Immunoglobulin E (IgE) in the serum were determined by enzyme linked immunosorbent assay (ELISA) kits. The 28-day repeated-dose toxicity study of 42 nm Ag NPs adversely impacted the liver and kidney in the 1.00 mg/kg/d group, when determined by blood chemistry and histopathological analysis.

Specifically, the levels of ALP and AST in serum were significantly increased in both male and female mice in the 1 mg/kg treated group. The level of ALT was increased in only female mice but not in male mice treated with 1 mg/kg Ag NPs. The pro-inflammatory cytokines IL-1, IL-6, IL-4, IL-10, IL-12, and TGF- β were increased in a dose-related manner. Serum levels of B lymphocytes and IgE were also increased. Slight cell infiltrations were observed in the cortex of the kidneys in both male and female mice, but there were no other histopathological changes. For the 28-day repeat dose study, the NOAEL was 0.50 mg/kg/day and the LOAEL was 1.00 mg/kg/d based on the significantly increased ALP, AST, and ALT levels.

Hadrup et al. (2012a) conducted 14- and 28-day toxicity studies using 14 nm Ag NPs coated with PVP and an equimolar dose of ionic silver (Ag+) in the form of silver acetate in four-week-old Wistar rats. In the 14-day study, six males/group received 0 (11.5 mg/mL PVP vehicle control), 4.5, or 9.0 mg/kg/d (administered in two daily 4.5 mg/kg/d doses) of Ag PVP-coated NPs at 10 mL/kg by oral gavage. In the 28-day study, ten females and six males/group received 0 (11.5 mg/mL PVP vehicle control); eight females/group received 2.25 or 4.5 mg/kg/d; and ten females and six males/group received 9.0 total mg/kg/d Ag PVP-coated NPs at 10 mL/kg by oral gavage. Ten females and six males/group received orally 9 mg Ag acetate/kg/d for 28 days. Clinical, hematological and biochemical parameters, organ weights, macro- and microscopic pathological changes were evaluated for both the 14- and 28-day studies. For the PVP-coated Ag-NPs groups, no toxicological effects were reported. For Ag acetate, lower body weight gain, increased plasma ALP, decreased plasma urea and lower absolute and relative thymus weight were recorded. These findings indicate toxicity at 9 mg/kg/d Ag+, but not at an equimolar Ag NP dose.

Shahare and coworkers (2013) treated Swiss albino male mice with Ag NPs and evaluated effects on the small intestinal mucosa. Ag NPs from 3 to 20 nm were administered orally by gavage at a dose of 0 (deionized water), 5, 10, 15 or 20 mg/kg/d for 21 days. The Ag NPs were laboratory-synthesized and TEM imaging confirmed the size of particles (average diameter was 10.15 nm) and the shape, which was either oval or spherical. Clinical observation, body weights and feed consumption values were collected. At necropsy, only the small intestines were collected and processed. There was a significant decrease in the body weight of mice in all Ag NP-treated groups. It was found that Ag NPs at all doses damaged the epithelial cell microvilli as well as intestinal glands. The LOAEL is considered 5 mg/kg/d based on changes in body weight and microvilli damage.

A subchronic study was initiated to assess the impact of size and dose of commercially available Ag NPs on gut microbiota and gut-associated immune responses (Williams et al., 2014). Three sizes (10, 75 and 110 nm) of citrate-stabilized Ag NPs in 2 mM sodium citrate/ 0.1 percent CMC, were orally gavaged for 13 weeks to male and female Sprague-Dawley rats (10/sex/group) at equal volumes (9, 18, or 36 mg/kg/d). Silver acetate was dissolved in 0.1 percent CMC and dosed at 100, 200 or 400 mg/kg by the same study design, to provide silver ions (Ag+) as a different form of silver. The Ag NP exposures changed the ileum mucosal microbial populations, and intestinal gene expression of the gut microbiota towards more Gram-negative bacteria. DNA-based analyses showed exposure to 10 nm Ag NPs and low-dose Ag+ (100 mg/kg/day silver acetate), modulated the gut-associated immune response and the overall homeostasis of the intestinal tract.

Boudreau et al. (2016) evaluated commercially available Ag NPs of different particle sizes, ionic forms of Ag, as well as Ag accumulation, distribution, morphology, and toxicity in tissues when administered daily by oral gavage for 13 weeks. The Ag NPs and silver acetate (AgOAc) were each 99 percent pure suspended in a sodium citrate/CMC suspension. Seven week-old Sprague-Dawley rats (10 rats/sex/group) were administered 10, 75, or 110 nm spherical Ag citrate-coated NPs at 9, 18, or 36 mg/kg/d; and silver acetate (Ag+) at 100, 200, or 400 mg/kg/d. Controls received 2 mM sodium citrate or water. At termination, complete necropsies were conducted, and histopathology, hematology, serum chemistry, micronuclei, and reproductive system analyses were performed. Ag accumulation and distribution were determined (refer to Section 5.2.1). In rats exposed to Ag NPs, no significant changes occurred in body weight or in feed and water consumption values, relative to controls. The blood, reproductive system, and genetic tests were also similar to controls. The NOAEL was 36 mg/kg/d for 10, 75, or 110 nm citrate-coated Ag NPs. Increased incidence and severity of lesions were detected in rats exposed to AgOAc (400 mg/kg) and included mucosal hyperplasia in the small and large intestine, as well as, thymic atrophy or necrosis.

Garcia et al. (2016) assessed the effects of an oral 90-day subchronic exposure to PVP-coated Ag NPs in rats. The study also assessed if oral PVP-Ag NP exposure can alter the levels of various metals (Fe, Mg, Zn and Cu) in tissues. Commercially obtained, 99.95 percent pure, PVP-Ag NPs averaged 20 to 30 nm in size. Adult male Sprague-Dawley rats (12/group) were orally gavaged with 0 (0.9 percent saline), 50, 100 or 200 mg/kg/d of PVP-Ag NPs at 4 mL/kg. TEM indicated the average particle size was 15.16 ± 2.21 nm and particles were spherical in shape; agglomerations were not observed. Body weights, feed consumption values, Ag metal accumulation in the liver, kidney, spleen, thymus, brain, and ileum, Ag urine and feces excretion, biochemical and hematological assessment, as well as histopathological changes and subcellular distribution were measured. After 90 days, PVP-Ag NPs were found within hepatic and ileum cells in treated animals. The major tissue concentration of Ag was found in the ileum. All tissues of PVP-Ag NPs-exposed animals showed increased levels of Ag in comparison with the control group. No adverse effects in liver, kidney, biochemical markers or hematological or histopathological changes were reported in treated animals. The NOAEL was 200 mg/kg/d, the highest dose tested.

Qin et al. (2017) treated male and female Sprague-Dawley rats (10/sex/group) with repeated oral gavage administration of synthesized PVP-coated Ag NPs. Effects were compared with animals treated with an equivalent dose of $AgNO_3$. Specifically, 100 male and female rats were orally administered particulate or ionic forms of silver (Ag+), separately, at doses of 0.5 or 1 mg/kg/d for 28 days. The size distribution of each dose of the synthesized Ag NPs was 28.21 nm (12.3 percent), 32.67 nm (18.1 percent), 37.84 nm (16.9 percent), 43.82 nm (11.7 percent), 91.28 nm (3.6 percent), 105.7 nm (3.6 percent), and 122.4 nm (3.5 percent). The total concentration of Ag in the Ag NP stock solution was 778.0 µg/mL and the dissolved Ag+ content was 56.6 µg/mL. Results revealed no significant adverse effects of Ag NPs and $AgNO_3$ at doses up to 1 mg/kg/d for clinical observations, body weights, organ weight, food utilization values, and histopathological examination. Differences in hematological and plasma biochemical parameters were observed for the Ag NPs and $AgNO_3$ treated groups compared to the controls. For male rats treated with Ag NPs, RBC count increased and platelet count decreased significantly in the 1.0 mg/kg/d group; AST increased significantly in both Ag NP treatment groups; these parameters were unaffected in male rats treated with $AgNO_3$. In female rats treated with Ag

NPs, RBC count increased in the 0.5 mg/kg/d group; platelet count decreased in both 0.5 and 1 mg/kg/d groups; and white blood cell (WBC) count increased in the 1.0 mg/kg/d group. RBC count increased in female rats treated with 0.5 mg/kg/d $AgNO_3$, which was the only hematological and plasma biochemical parameter affected in females treated with $AgNO_3$. Ag distribution pattern in organs of rats treated with Ag NPs was similar to that of $AgNO_3$ treated rats, showing liver and kidneys were the main target organs followed by testes and spleen. The total Ag content in organs was significantly lower in the Ag NPs treated rats than those in the $AgNO_3$ treated rats.

Table 21. Summary of Toxicity to Ag NPs via Oral Repeated Exposure

Species and Group Size (n/sex/group)	Exposures duration	Particle characteristics Mean (SD)[a]	NOAEL (mg/kg/d)	LOAEL (mg/kg/d)	Responses at the LOAEL	Comments	References
Sprague-Dawley rats 10/sex/group 6 weeks old	0, 30, 300, or 1000 mg/kg/d (10 mL/kg) 28 days gavage	commercial Ag NP; average particle diameter = 60 nm (52.7-70.9 nm); 99.98% pure; suspension in 0.5% CMC	30	300	Liver toxicity: increased blood levels of ALP in males; increased total cholesterol in females	OECD TG 407 + GLPs	Kim et al., 2008[b]
F344 rats 10/sex/group	0, 30, 125, 500 mg/kg/d 90 days gavage	median diameter = 56 nm (1.46 SD); 99.98% pure; 0.5% CMC	125	500	Minimal liver toxicity; pigmentation in intestinal villi.	OECD TG 408 + GLPs	Kim et al., 2010a[b]
ICR mice 5-6/sex/group	0 or 1 mg/kg/d 14-day study gavage 0, 0.25, 0.5 or 1 mg/kg/d 28 day study gavage	22, 42, 71 or 323 nm (14 day) 42 nm (28 days)	None 0.5	1 1	Increase natural killer cells and B cells (22, 42, 71 nm) Adverse impact on liver and kidney (increase ALP, ALT, AST)	22, 42, and 71 nm were distributed to organs while 323 nm were not	Park et al., 2010a
Wistar rats 6-10/sex/group	0, 2.25, 4.5, or 9 mg/kg/d 28 days gavage	PVP-coated 14 nm	9	None	----	Comparable dose of Ag+ ↓ BW and urea; ↑ ALP and thymus weights; 14 day study also conducted	Hadrup et al., 2012a
Swiss albino mice male 5/group	0, 5, 10, 15 or 20 mg/kg/d 21 days gavage	Oval or spherical; mean particle size diameter = 10.15 nm; range 3 to 20 nm	None	5	↓ in BW at 10 mg/kg/d; damage to epithelial cell microvilli and intestinal glands	Only small intestine mucosa evaluated; loss of microvilli reduce Ag absorptive capacity at higher dosages	Shahare et al., 2013
Sprague-Dawley	9, 18, or 36	10, 75 and 110 nm of	None	9	Changed the ileum		Williams et

Species and Group Size (n/sex/group)	Exposures duration	Particle characteristics Mean (SD)[a]	NOAEL (mg/kg/d)	LOAEL (mg/kg/d)	Responses at the LOAEL	Comments	References
rats 10/sex/group	mg/kg/d Ag NPs Silver acetate 13 weeks gavage	citrate-stabilized 100, 200 or 400 mg/kg	None	100 mg/kg/d silver	mucosal microbial populations, and intestinal gene expression of the gut microbiota towards more Gram-negative bacteria.		al., 2014
Sprague-Dawley rats 10/sex/group	0, 9, 18, or 36 mg/kg/d 13 weeks gavage	Spherical Ag citrate-coated nanoparticles; particle size = 10, 75, or 110 nm; 99% pure	36 for all sizes	None	----	Dose and size-dependent accumulations in tissues (see toxicokinetics)	Boudreau et al., 2016
Sprague-Dawley rats 12 /sex/group	0, 50, 100, 200 mg/kg/d 90 days gavage	PVP-Ag NPs; average particle size = 15.16 ± 2.21; spherical; 99.95% pure	200	None	----		Garcia et al., 2016
Sprague-Dawley rats 10/sex/group	0, 0.5 or 1 mg/kg/d 28 days	Synthesized PVP-coated Ag NPs; multiple particle sizes: 28.21 (12.3%), 2.67 (18.1%), 37.84 (16.9%), 43.82 (11.7%), 91.28 (3.6%), 05.7(3.6%), and 122.4 nm (3.5%)	0.5	1	----	↑ AST and ↑ in red blood cell counts, ↓ platelet count	Qin et al., 2017

[a] NT characterization data are stated, if reported: source, diameter and length, surface area, purity and impurities, and state of aggregation; shape (bundles, tangles, ropes)
[b] As reviewed in Versar (2012)

5.4.2 Inhalation Exposure

Four inhalation studies were reviewed in Versar (2012) and are summarized in Table 22. There were no repeat dose subchronic studies via inhalation in the recent available literature.

Ji et al. (2007a; as cited in Versar, 2012) conducted a 28-day whole body inhalation toxicity study of uncoated Ag NPs in eight Sprague-Dawley rats following OECD Test Guideline 412. Groups of ten rats per sex were chamber exposed to fresh air or three concentrations of Ag NPs for 6 h/d, 5 d/wk for four weeks. Ag NPs were generated by evaporation/condensation using a ceramic heater. Marginally increased incidences of cytoplasmic vacuolation in the liver of females at 3.5 and 61 µg Ag/m^3 were reported, but cytoplasmic vacuolation in males was not increased. The highest exposure level in this study, 61 µg Ag/m^3, was designated as a NOAEC.

Hyun et al. (2008; as cited in Versar, 2012) evaluated the rats from the 28-day inhalation study by Ji et al., (2007a) for histological effects in the lungs and nasal cavity, as well as for histochemical changes in mucins in the goblet cells of the nasal respiratory mucosa. No histopathological changes were found in the lungs or nasal cavity or meaningful histochemical changes in the nasal mucosa, indicating a NOAEC of 61 µg Ag/m^3, the highest exposure concentration.

Sung et al. (2008, 2009; as reviewed in Versar, 2012) conducted a 90-day whole body inhalation study of Ag NPs that followed OECD Test Guideline 413, and was designed to identify possible adverse effects not detected in the 28-day study (Hyun et al., 2008; Ji et al., 2007a). Groups of ten male and ten female 8-week-old Sprague-Dawley rats were chamber-exposed to fresh air or one of three concentrations of Ag NPs for 6 h/d, 5 d/wk for 13 weeks. The lungs and liver were target organs for inhaled Ag NPs in rats. Both functional and inflammatory changes were observed in the lungs with statistically significant decreases in tidal volume, minute volume, and/or peak inspiration flow in males at 515 µg Ag/m^3 (Sung et al., 2008). There were no consistent exposure-related changes in lung function endpoints in female rats. BALF cell counts were not significantly increased in either sex; however, BALF inflammatory markers were significantly increased in females at 515 µg Ag/m^3. Alterations in both sexes showed increased incidences of minimal severity chronic alveolar inflammation, alveolar macrophage accumulation, and a mixed cell perivascular infiltrate. Exposure-related histopathological effects were observed in the liver, where incidences of minimal bile duct hyperplasia were significantly increased in both sexes at 515 µg Ag/m^3. The results indicate that 515 and 133 µg Ag/m^3 were the LOAEC and NOAEC, respectively, in this study for increased incidences of male and female rats with lung lesions and liver lesions.

Table 22. Summary of Toxicity of Ag NPs via Inhalation Repeat Exposure

Species and Group Size (n/sex/group)	Exposure and Duration (µg/m^3)	Particle Characteristics Mean (SD)[a]	NOAEC (µg/m^3)	LOAEC (µg/m^3)	Responses at the LOAEC	Comments	References
Sprague-Dawley rat 10/sex/group	0, 0.5, 3.5, or 61 6 h/d, 5 d/wk 4 weeks whole body	11.93 (0.22), 12.40 (0.15), 14.77 nm (0.11)	61	**None**		OECD 412; GLPs; near ACGIH Ag dust limit of 100 µg/m^3	Ji et al., 2007a[b]
Sprague-Dawley rat 10/sex/group	0.5, 3.5, or 61 6 h/d, 5 d/wk 4 weeks	13-15 nm	61	None			Hyun et al., 2008[b]

Species and Group Size (n/sex/group)	Exposure and Duration (µg/m^3)	Particle Characteristics Mean (SD)[a]	NOAEC (µg/m^3)	LOAEC (µg/m^3)	Responses at the LOAEC	Comments	References
Sprague-Dawley rat 10/sex/group	49, 133 or 515; 6 h/d, 5 d/wk; 13 weeks whole body	Geometric mean diameters = 18.12 (1.42), 18.33 (1.12), and 18.93 nm (1.59)	133	515	Decrease in tidal volume, minute volume, and/or peak inspiration flow in males; increase in BALF inflammatory markers in females. Increased incidence of minimal severity chronic alveolar inflammation, alveolar macrophage accumulation, and a mixed cell perivascular infiltrate in both sexes. Increased incidence of minimal bile duct hyperplasia in both sexes.	OECD 413; GLPs. Follow-on study to Hyun et al. (2008) above	Sung et al., 2008: 2009[b]

[a] NT characterization data are stated, if reported: source, diameter and length, surface area, purity and impurities, and state of aggregation; shape (bundles, tangles, ropes)
[b] As reviewed in Versar (2012)

5.4.3 Dermal Exposure

Three studies via dermal exposure are available. One study is cited in Versar (2012) and two more recent studies are described here.

Samberg et al. (2010; cited in Versar, 2012) evaluated dermal toxicity of washed or unwashed commercial Ag NPs (average diameters of 20 or 50 nm, purchased suspended in deionized water) in pigs topically exposed for 14 days. Sites on the back skin of female weanling pigs (n = 2; 20 to 30 kg) were dosed with 500 µL of suspension concentrations ranging from 0.34 to 34 µg/mL for 14 days. Lesions occurred in layers under the stratum corneum, which the authors attributed to Ag+ flux into the lower layers from the particles in the stratum corneum. TEM showed particles only on the surface of the stratum corneum or in the superficial layers of the stratum corneum. The porcine dermal NOAEL was 34 µg/mL.

Korani et al. (2011) dermally applied colloidal nanosilver (less than 100 nm by TEM) to the shaved backs of male Hartley albino guinea pigs (six/group) in a 13-week subchronic study. Exposure was 5 d/wk to 0, 100, 1000, or 10,000 µg/mL of colloidal nanosilver. A 100 µg/mL solution of $AgNO_3$ served as a positive control. Weekly clinical observations and histopathologic examination of the skin (application site), liver and spleen (three/group) were conducted. There were no deaths. Similar skin inflammatory responses were recorded in all treatment groups compared to the vehicle control group. All observed adverse skin responses were dose- and time-related. In the $AgNO_3$ group, a reduced thickness of the epidermis and papillary layer was observed, which was accompanied by an increase in Langerhans cells. In the 10,000 µg/mL group, degenerative muscle fibers with acidophilic cytoplasm were surrounded by macrophages, and in particular, the increased levels of macrophages were located in the endomysium along with other signs of skin inflammation. In the $AgNO_3$ and nanosilver groups, destruction of hepatocyte cords was reported; in the test groups this pattern was magnified by increased nanosilver concentrations. Overproduction of Kupffer cells and degeneration of hepatocytes increased with increasing nanosilver concentrations. In the spleen, $AgNO_3$ treatment caused thinner red capsules, inflammation, and white pulp hypertrophy. In the 1000 µg/mL colloidal nanosilver group, splenic changes were red pulp inflammation and white pulp atrophy. White pulp hypertrophy was a specific response to $AgNO_3$, but not to any Ag NP dose. The dermal LOAEL was 100 µg/mL for colloidal nanosilver in guinea pigs based on histopathologic abnormalities in the skin, liver, and spleen in all test groups.

Korani and coworkers (2013), as per OECD Test Guideline 411, dermally applied Ag NPs to male Hartley albino guinea pigs (12/group) and analyzed Ag NP tissue levels, morphological changes and pathological abnormalities. The sizes of the Ag NPs were less than 100 nm (TEM). Guinea pigs were exposed to concentrations of 0, 100, 1000 or 10,000 ppm Ag NPs or the positive control, $AgNO_3$, for 13 weeks. A close correlation between dermal exposure and tissue levels of Ag NPs was found and tissue uptakes occurred in dose-related manner, with the highest levels observed in the kidney, followed in decreasing levels by muscle, bone, skin, liver, heart, and spleen. Severe proximal convoluted tubule degeneration and distal convoluted tubule were seen with histopathological examination in the kidneys of the 1000 and 10,000 ppm groups. Separated lines and narrow marrow space were determined as two major signs of bone toxicities observed in all three dose levels of Ag NPs. Increased dermal dose of Ag NPs caused cardiocyte deformity, congestion and inflammation. All Ag NP doses gave comparable results for several

endpoints measured in heart, bone and kidney, but differed in tissue concentrations and the extent of histopathological changes. Ag+ could be detected in different organs after dermal exposure compared to control and Ag NP treatment groups

The cytotoxicity of Ag NPs has been demonstrated in human epidermal keratinocytes as well as their inflammatory effect and penetration into *in vivo* porcine skin. The systemic toxicity of Ag NPs via dermal application has also been demonstrated, with Ag NPs found in the skin, liver, and spleen of guinea pigs after dermal application resulting in slight damages to these tissues/organs. The dermal LOAEL was 100 µg/mL for Ag NPs (less than100 nm) in guinea pigs based on histopathologic abnormalities in the skin, liver and spleen in all test groups.

5.4.4 Other Routes of Exposure

To avoid limited systemic exposure due to the cellular barriers present in the lung and GI tract, the IV administration of nanosilver was used to evaluate its potential systemic toxicity. De Jong et al. (2013) determined the systemic toxicity of commercially available Ag NPs using different sizes (20 nm and 100 nm) in a 28-day repeated dose toxicity study, OECD Test Guideline 407, in male and female Wistar rats using the tail vein for IV route of administration. The physico-chemical characteristics were 21.0 ± 2.6 and 107 ± 7.6 in average diameter; size range from 12.4 to 27.9 and 99.8 to 128.4 nm; surface area 1.40 x 10^3 and 3.62 x 10^4 nm^2; and Zeta potential of -40.8 and -38.7 mV for the 20 and 100 nm Ag NPs, respectively. Doses were 0 (phosphate buffer), 0.0082, 0.025, 0.074, 0.22, 0.67, 2.0, or 6.0 mg/kg/d of the 20 nm Ag NPs and 0 (phosphate buffer) or 6.0 mg/kg/d of the 100 nm Ag NPs. Treatment groups ranged in size with 2 to 4 rats of each sex per dose. Treatment up to 6 mg/kg bw was well-tolerated by the animals. Reduced relative body weight gain for the male and female rats was observed during the treatment with both 20 nm and 100 nm Ag NPs. Large increases in spleen size and weight occurred and were attributed to increased cell number. Both T and B cell populations showed an increase in absolute cell number, whereas the relative cell numbers remained constant. At histopathological evaluation, brown and black pigment indicating Ag NP accumulation was noted in the spleen, liver, and lymph nodes. Liver damage was indicated by increased ALP, ALT, and AST levels, but was not confirmed by histopathology. Hematology also showed a decrease in several red blood cell parameters. Almost complete suppression of natural killer cell activity in the spleen occurred at high doses. Other immune parameters affected were decreased interferon, interleukin and TNF-α production; increased serum Immunoglobulin M (IgM), IgE and blood neutrophilic granulocytes.

5.4.5 Summary

No clinically important changes in metabolic, hematologic, or urinalysis measures, and no morphological changes were detected in the lungs, heart or abdominal organs of healthy humans orally daily administered colloidal Ag solutions of both silver ions and Ag NPs up to 14 days, though Ag was detected in the serum. The average daily ingestion of this elemental Ag colloid formulation was estimated to be 100 µg/day for 10 ppm, and 480 µg/day for 32 ppm Ag.

Study reports indicate that in animals, Ag NPs are distributed to multiple organs. Using uncoated, commercially available Ag NPs (56 to 60 nm), a NOAEL and LOAEL of 30 mg/kg and 300 mg/kg, respectively, based on liver toxicity; increased blood levels of ALP in males and

increased total cholesterol in females have been reported for a 28-day oral gavage toxicity study using rats. With a longer duration of 90 days of gavage administration, a NOAEL of 30 mg/kg and LOAEL of 125 mg/kg were obtained in rats based on significant decreases in the body weight of male rats after four weeks of exposure, and significant dose-dependent changes in ALP, cholesterol, liver bile-duct hyperplasia (with or without necrosis), fibrosis, and pigmentation.

Subchronic inhalation exposure to Ag NPs showed that lung and liver tissues were the target organs in rats. Both functional and inflammatory changes were observed in the lungs with statistically significant decreases in tidal volume, minute volume, and/or peak inspiration flow. Liver toxicity consisting of minimal bile duct hyperplasia was significantly increased in both sexes at 515 μg Ag/m^3 after 13 weeks of exposure; in addition, functional and inflammatory changes were observed in the lungs with statistically significant decreases in tidal volume, minute volume, and/or peak inspiration flow in males. The NOAEL was 133 μg/m^3 after 13 weeks of exposure. Shorter term exposure of 61 μg/m^3 for 28 days did not have any significant health effects.

Dermal application of high dosages (100, 1000 and 10,000 ppm) of Ag NPs for 13 weeks to guinea pigs caused signs of kidney and bone toxicities. The dermal LOAEL was 100 μg/mL for Ag NPs in guinea pigs based on histopathologic abnormalities in the skin, liver and spleen.

5.5 Chronic Toxicity

No human studies were found that reported adverse health effects with chronic exposure to Ag NPs.

Laboratory animal studies were not located in the current literature search on the possible systemic toxicity with chronic (lifetime) exposure to Ag NPs by any route of exposure, nor were any studies identified in Versar (2012).

The National Toxicology Program selected Ag NPs for chronic toxicity testing. To date, those studies have not been completed; however, short-term toxicity and toxicokinetic studies have been published (NTP, 2017). The U.S. EPA Oral Reference Dose (RfD) assessment for Ag (CASRN 7440-22-4) on EPA's Integrated Risk Information System (IRIS) is based on argyria, a cosmetic effect, which is bluish-gray pigmentation to the skin and mucous membranes, and argyrosis, which is bluish-gray pigmentation to the eyes. It is not considered an adverse human health effect (U.S. EPA, 2017a). Ag NPs are not included in IRIS. The risk assessment for nano Ag by the Danish EPA (2015b) also considered argyria as the critical effect following oral exposure to Ag; no relevant long-term studies were identified. The risk assessment was based on the presumed mechanism that the Ag NP surface continually releases Ag+ in the body, which accumulates and causes argyria.

NIOSH (2015) did not develop a Recommended Exposure Limit (REL) for Ag NPs; no studies that reported adverse health effects to Ag NPs or evaluated specific Ag particle size or solubility effects on human health were found. The few studies that investigated health effects with long-term exposures to chronic Ag dust and fumes in workers reported argyria. Exposure to high levels of Ag in the air can result in breathing problems, lung and throat irritation, and stomach

pains. Skin contact with Ag can cause mild allergic reactions including rashes, swelling, and inflammation in some people (NIOSH, 2015).

5.6 Reproductive and Developmental Toxicity

Human data regarding reproductive and developmental outcomes from exposure to Ag NPs were not found in the literature search conducted for this project.

No standard *in vivo* mammalian tests of reproductive or developmental toxicity were located for Ag NPs in an earlier search of the literature (Versar, 2012).

From 2010 to 2016, standard mammalian tests of reproductive or developmental toxicity and a reproductive/developmental toxicity screening study (Hong et al., 2014), as well as several standard subchronic studies that examined reproductive organs (Kim et al., 2008, 2010a) were located for Ag NPs by the oral route of administration (Yu et al., 2014; Charehsaz et al., 2016). In addition, one standard inhalation subchronic repeat-exposure mammalian toxicity test with examination of reproductive organs (Sung et al., 2009) was also located. However, no guideline (nonscreening) studies of developmental toxicity or of reproductive function were located for either route.

Transfer of Ag NPs into breast milk, placenta, testes, brain, fetuses, and pups was reported in non-guideline studies for oral exposure (Loeschner et al., 2011; Philbrook et al., 2011; Lee et al., 2012a; Hadrup et al., 2012b; Fatemi et al., 2013; Melnik et al., 2013; Miresmaeili et al., 2013; Sleiman et al., 2013; Thakur et al., 2014; Mathias et al., 2015; Lafuente et al., 2016; Charehsaz et al., 2016). In addition, studies using IV (Lankveld et al., 2010; Austin et al., 2012; Castellini et al., 2014), IP (Mahabady, 2012; Rezazadeh-Reyhani et al., 2015), and subcutaneous (Lankveld et al., 2010; Rashno et al., 2014; Ghaderi et al., 2015; Tabatabaei et al., 2015, Fatemi Tabatabaie et al., 2017) routes of exposure provide some confirming evidence of Ag NP systemic transfer after oral absorption.

Hormone levels for male reproductive regulation following IV administration of Ag NP have been studied (Gromadzka-Ostrowska et al., 2012; Garcia et al., 2014; Dziendzikowska et al., 2016; see Appendix F). While studies by the IV route may indicate a potential hazard (with alterations in LH and testosterone), their relevance to oral, inhalation or dermal toxicity for Ag NPs is uncertain.

Developmental abnormalities that have been observed following *in vitro* exposure have been discussed in Versar (2012); *in vitro* studies are not further reviewed in this report due to the large number of available *in vivo* studies.

5.6.1 Oral Exposure

5.6.1.1 Reproductive Toxicity

No studies of reproductive function were located for uncoated Ag NPs, although several systemic toxicity studies evaluated effects on reproductive organs. Studies are compiled in Table 23.

A combined repeated-dose reproduction/developmental toxicity screening study using citrate-coated Ag NPs was conducted in male and female Sprague-Dawley rats (Hong et al., 2014). The citrate-capped Ag NPs were manufactured with reported size of the Ag NPs estimated to be 7.9 ± 0.95 nm based on TEM. The particle size was confirmed in the authors' laboratory. Zeta potential of Ag NPs in water (10 ppm) was calculated to be –17.55 ± 4.16 mV (average ± standard deviation). The suspension of Ag NPs for oral administration was prepared by diluting the stock Ag NP (20 percent w/v) with distilled water and adjusting for the volume of 10 mL/kg bw of the rats. Formulations of 62.5, 125 and 250 mg/kg were freshly prepared daily prior to use. Suspensions were routinely stable in solution during the experiments. The size distribution of the Ag NPs in suspension was measured using a submicron particle size analyzer (NICOMPTM) and energy-filtering (EF) TEM using a LIBRA120 apparatus. EF-TEM images were obtained for Ag NPs dispersed in ethanol. The rats (10/sex/group) were orally gavaged with 0 (vehicle control), 62.5, 125, or 250 mg/kg/d Ag NPs. Males were dosed once a day for 42 days (14 days before mating, 14 days during mating and 14 days post-mating until necropsy) and females were dosed up to 52 days (2 weeks before mating, during mating and gestation and during 4 days of lactation). Five or more rats of each gender were also maintained for 14 days in two recovery groups: vehicle control and high-dose groups. The study was performed based on OECD Test Guideline 422 and GLPs. The high dose of 250 mg/kg/d for the 52-day treatment was selected based on a preliminary dosage test, in which only salivation was shown in a few pregnant rats during a treatment period of seven days. Clinical signs including mortality, motility, general appearance and autonomic activity were recorded daily. Individual body weights were measured weekly during pre-mating, mating and recovery periods. During the pregnancy and lactation periods, body weights were measured at day GDs 0, 3, 6, 9, 12, 15, 18, and 20 for pregnant rats, and day of delivery, and day 4 postpartum for the offspring. Feed consumption values were measured during the pre-mating, pregnancy, lactation and recovery periods. Regularity and length of the estrus cycle, mating index, fertility index, pregnancy rate, gestation length, live and dead pups, sex, and external anomalies of live pups were observed and recorded. Delivery rate, sex rate, survival rate at day 4 postpartum and body weight of live pups on day 0 and day 4 postpartum, were also recorded. During the lactation period, nursing behaviors of dams and viability of pups were observed. Functional observations, urinalysis (glucose, bilirubin, ketone, specific gravity, blood, pH, protein, urobilinogen, nitrite and leukocytes), hematology (prothrombin time and activated partial thromboplastin time), serum biochemistry, absolute and relative organ weights (including pituitary gland, ovaries, testes, epididymis, seminal vesicles or uterus) and histopathology (vehicle control and 250 mg/kg/d groups only) were evaluated in five animals of each sex from each main group. Corpora lutea and implantation sites were counted in all females and pre- and post-implantation losses were calculated. The functional observations and neurobehavioral evaluation for five males of each group were conducted on the day before final treatment and for five females after separating their pups on lactation day 4. Auditory response, pupillary reflex, hot-plate test, rotarod performance test, and passive-avoidance test were performed on offspring. No deaths were observed in any of the groups. There were no statistically significant changes in weight gain or feed consumption values in any of the treatment groups during the pre-mating and mating periods in male rats, or in females during the pre-mating, gestation and lactation periods. Absolute and relative weights of testes, pituitary gland, seminal vesicles and epididymis in the treated groups showed no significant differences from the control group. There was no evidence of toxicity for reproduction and developmental endpoints, including mating, fertility,

implantation, delivery and fetal development. The NOAEL for reproductive/developmental toxicity was 250 mg/kg/d, the highest dose tested.

As part of a biodistribution study, Park and coworkers (2010a) conducted a 14-day, oral gavage repeat-dose toxicity study in six-week old male and female CD-1 (ICR) mice (five/sex/group) using purchased Ag NPs in a 1.0 mg/kg/d dose. The control group received deionized water only. Ag NPs (from a US chemical company) were suspended with sonication in 99.8 percent Tetrahydrofurane, Fluka (THF). The suspension was stirred, deionized water added and the THF evaporated until it was completely replaced by deionized water. The total Ag NP suspension was filtered by using different pore sizes of polycarbonate isopore filters and the size distribution was analyzed by dynamic light scattering (DLS; Japanese instrument). The average diameters of Ag NPs prepared by differential filtration were 22 nm, 42 nm, 71 nm, and 323 nm, respectively. THF was not detected in the suspension of Ag NPs. There were no treatment-related changes in body weights or in the ratio of organ to body weights after 14 days. The small-sized Ag NPs (22 nm and 42 nm) significantly accumulated in a size-dependent pattern after 14 days in the brain, lung, liver, kidney, and testes, while large-sized NPs (323 nm) were not detected in those tissues. This study demonstrated that smaller-sized Ag NPs were more easily absorbed via the gastrointestinal tract and translocated to the testes than the larger micron-size particles.

A 28-day oral repeat dose toxicity study was conducted in male and female Sprague-Dawley rats following OCED Test Guideline 407 and GLPs (Kim et al., 2008). Four-week-old rats were divided into four groups (10/sex/group) and gavaged daily with 0 (0.5 percent CMC) vehicle control, 30, 300, or 1000 mg/kg/d Ag NPs, and dosing volume was 10 mL/kg. The Ag NPs (52.7 to 70.9 nm; average 60 nm) were purchased and were at least 99.98 percent pure. After 28 days of treatment, clinical chemistry, hematology, organ weight, histopathology (including testes, ovaries, uterus, epididymis, seminal vesicle, thyroid gland, and prostate), and Ag distribution were measured. There were no treatment-related findings in clinical observation, body weights, feed consumption values, or absolute and relative reproductive organ weights. The NOAEL for reproductive toxicity was 1000 mg/kg/d, the highest dose tested.

Kim et al. (2010a) subsequently conducted a repeat-dose oral toxicity study over 90 days with a different rat strain. Ag NPs (CAS No. 7440-22-4) were purchased and were at least 99.98 percent pure. Count median diameter and geometric standard deviation of Ag NPs in 0.5 percent aqueous CMC, analyzed by TEM, were 56 nm and 1.46, respectively. The Ag NPs were orally gavaged daily to male and female F344 rats over a period of 13 weeks following OCED Test Guideline 408 and GLPs. Five-week-old rats were divided into four groups (10/sex/group): 0 (CMC vehicle control), 30, 125, or 500 mg/kg/d Ag NP. After 90 days of exposure, clinical chemistry, hematology, organ weight and histopathology (including testes, ovaries, uterus, epididymis, seminal vesicle, thyroid gland, prostate), and Ag distribution were studied. There was a significant decrease in the body weight of male rats in the 500 mg/kg/d dose group after 4 weeks of exposure and for the 125 mg/kg/d male rats at week 10, although there were no significant changes in feed or water consumption values for either treatment group. Dose-related increases were found in the relative weight of the left and right testes (significance reached for the left testes) at 500 mg/kg/d of Ag NPs. There were no significant differences in the relative weights of the other reproductive organs (prostate, uterus, and ovary) in the males or females. A dose-related accumulation of Ag occurred in all tissues examined, including the testes. The NOAEL for general toxicity was 30 mg/kg/d, based on liver toxicity at 125 mg/kg/d and

increased testicular weight at 500 mg/kg/d. The LOAEL for reproductive toxicity was 125 mg/kg/d.

5.6.1.2 Male Reproductive Toxicity

In a male reproductive toxicity study, the effect on spermatogenesis of 0 (distilled water), 25, 50, 100, or 200 mg/kg/d Ag NP doses was evaluated. The Ag NPs (70 nm) were dissolved in PBS and then orally gavaged twice daily (every 12 hours) for 48 days (one spermatogenesis cycle) at their final concentrations (Miresmaeili et al., 2013). Reproductive toxicity was evaluated in 45-day old male Wistar rats (8 rats/group) using the acrosome reaction assay to evaluate sperm viability, the ability of sperm to fuse with the oocyte membrane, and the degenerative acrosome reaction that occurs in immotile sperm. In the acrosome reaction assay, there was no significant difference in dead sperm cells with or without acrosome reaction in any treatment group compared with controls. There was a significant difference between the control group live sperm with and without intact acrosome reaction (11.00 ± 0.00 vs. 24.25 ± 3.68 live sperm). There was a significant reduction in the number of spermatogonia cells in the 200 mg/kg/d group. The 50, 100, and 200 mg/kg/d groups showed a significant reduction in the number of primary spermatocytes, spermatids, and spermatozoa. There were no significant differences between groups for Sertoli cell number and seminiferous tubule diameter. The reproductive NOAEL was 25 mg/kg/d and the LOAEL is considered 50 mg/kg/d based on the dose-related negative effects on the spermatogenesis process (decreasing percentages of primary spermatocytes, spermatids and spermatozoa).

A 90-day male reproductive toxicity study in rats was conducted with PVP-coated Ag NPs (0.2 wt percent PVP; with an average size 20 to 30 nm, obtained as dry powder [Ag, 99.95 percent, PVP coated]) to determine if harmful effects on epididymal sperm could be induced (Lafuente et al., 2016). The PVP-Ag NPs were dispersed by sonication and were freshly prepared daily just before treatment. The morphological characteristics of the PVP-Ag NPs were analyzed by TEM and were reported to have an average particle size of 25.24 ± 3.25 nm; 75 percent of the particles had a core size less than 30 nm (15.6 ± 2.21 nm), while the remaining 25 percent of the particles had core sizes ranging from 30 to over 100 nm. The morphology of the PVP-Ag NPs was analyzed on carbon film-coated Cu grids in contact with PVP-Ag NPs in 0.5 percent aqueous CMC. To reduce the risk of possible artifact formation, all TEM samples were prepared and analyzed on the same day in which the grids were prepared. The size of 200 particles was determined with a particle analysis tool to establish size distributions using the Image J software (Version 1.48). Male Sprague-Dawley rats (6/group) were gavaged daily with 0 (0.9 percent saline), 50, 100, or 200 mg/kg/d PVP-coated Ag NPs at a volume of 4 mL/kg according to OECD Test Guideline 408. Clinical signs and mortality of the rats were observed daily; body weights and feed intake were recorded weekly. Sperm count, motility, morphology, viability, and a histological evaluation of testes and epididymis were evaluated at the end of treatment. There were no treatment-related differences in body weight, body weight gain or feed consumption values. There was an increase, albeit not significant, in epididymis and testes weights at 100 and 200 mg/kg/d. Sperm count, sperm motility and viability from treated rats did not show any significant differences in the epididymal sperm compared to that of the control group. The authors point out that after Ag NP treatment, a downward trend (72, 71, 77 and 65 percent, at 0, 50, 100, or 200 mg/kg/d, respectively; no statistical trend test was conducted) occurred in sperm viability. The decrease at 200 mg/kg, which could be due to low PVP-coated

Ag NP absorption, was not significant. High doses of PVP-coated Ag NPs showed higher numbers of abnormal sperm. Histopathological examination of the testes did not reveal any significant changes. The reproductive NOAEL was 100 mg/kg/d and the LOAEL was 200 mg/kg/d based on abnormal sperm.

In a study designed to examine male reproductive effects, weaned male Wistar rats (10/group), were orally gavaged with a suspension of manufactured 60 nm Ag NPs at low dosages of 0 (vehicle not provided), 15, or 50 µg/kg/d (0.015 or 0.050 mg/kg/d), using a volume of 0.25 mL/kg, from PNDs 23 through 53 and sacrificed on PND 53 or 90 (Sleiman et al., 2013). Pup growth was assessed by daily weighing, and puberty was measured on the day of preputial separation. Spermatogenesis was assayed at necropsy on PNDs 53 or 90 by measuring sperm count in the testes and epididymis and examining the morphology and morphometry of seminiferous epithelium; testosterone and estradiol blood levels were assayed at sacrifice. Body weights at PND 90 were not statistically different, but growth was reduced in the 50 µg/kg/d group. Ag NP exposure produced a delay in puberty. Total and daily sperm production was reduced in the 50 µg/kg/d on PND 53 and significantly reduced in both treatment groups on PND 90. Decreased sperm reserves in the caput, corpus and cauda of the epididymis and significantly diminished sperm transit time through the segments of the epididymis occurred at PND 53 for both treatment groups. Morphometric analysis of the seminiferous tubules did not reveal marked alterations in epithelial height or in luminal or tubular diameters for either the 15 or 50 µg/kg dosages. At PND 53, the groups treated with Ag NPs at 15 and 50 µg/kg/d showed quantitative reduction in epithelial height, tubular and luminal diameters, but at PND 90 the values were similar to control. The morphology of the seminiferous epithelium was markedly altered by discontinuity and disorganization of seminiferous epithelium, cellular debris in the lumen, and sloughing of the germinal cells from the epithelium into the tubular lumen at both dose levels. The weight of testes, epididymis (caput, corpus, and cauda), seminal vesicles, and ventral prostate were not significantly different at the timepoints, except for the weight of the cauda of the epididymis at PND 53 (significantly decreased) in both groups. Testosterone and estradiol serum concentrations did not reveal any significant alterations at PNDs 53 or 90. The data demonstrate that prepubertal exposure to Ag NPs altered reproductive development in prepubertal male Wistar rats, as evidenced by impairment in spermatogenesis and a lower sperm count in adulthood, supporting a reproductive LOAEL of 0.015 mg/kg/d, the lowest dose tested.

Weanling male Wistar rats were orally gavaged daily with 0 (water), 15, or 30 µg/kg/d (0.015 or 0.030 mg/kg/d) Ag NP solution at a volume of 0.25 mL/100g bw from PNDs 23 to 58 and sacrificed at day 102 to evaluate male reproductive toxicity (Mathias et al., 2015). The Ag NP suspension particles were 60 nm in diameter. To evaluate whether dilution of the Ag NP solution affected NP stability, the mean particle size and polydispersity index (PDI) were analyzed by DLS. The Ag NPs were 86.1 nm when measured by DLS in solution (20 µg/mL), 86.1 nm for the 6 µg/mL dilution (15 µg/kg bw), and 87.0 nm for the 12 µg/mL dilution (30 µg/kg bw). The PDI were measured as 0.330, 0.330 and 0.346 for the commercial, 6 and 12 mg/mL solutions, respectively. Balanopreputial separation was evaluated starting at PND 33 and continued daily until complete. The animals were weighed daily from PNDs 23 to 59 and then every other day from days 59 to 120. A determination of the sexual partner preference was performed at day 90 and sexual behavior was evaluated at day 95. At sacrifice, reproductive hormones and the cauda of the epididymis were collected; sperm acrosome integrity, plasma membrane integrity, mitochondrial activity, and morphology were evaluated. Ag NPs reduced

the acrosome and plasma membrane integrities, significantly reduced the mitochondrial activity, and significantly increased morphological abnormalities of the sperm in both treatment groups. Ag NP exposure significantly delayed the onset of puberty, although no changes in body growth were observed in either treatment group. The animals did not show changes in sexual behavior or serum hormone (FSH, LH, testosterone and estradiol) concentrations. Based on alterations in sperm parameters and delay in the onset of puberty, the reproductive LOAEL was considered 0.015 mg/kg/d, the lowest dose tested.

In a study designed to examine male reproductive effects, male Wistar rats (8/group) were orally gavaged for 90 consecutive days with 0 (double distilled water) or 20 µg/kg/d (0.020 mg/kg/d) of synthesized (5 to 20 nm diameter particle size) Ag NPs (Thakur et al., 2014). Preparation of 5 $\times 10^3$ mol/L of Ag NPs was conducted via citrate-reduction. Ultraviolet-visible (UV-Vis) absorption along with TEM were used to study the particle's size, morphology and diameter of the Ag NPs in an aqueous dispersion. The rats were monitored daily for clinical signs of toxicity and weighed weekly until sacrificed. The testes tissue was processed for histology and examined by light microscopy. The testes of the treated rats showed disorganization in appearance and different degrees of atrophy in the seminiferous tubules. The germinal epithelium also appeared disorganized, with loss of spermatogenic cells, especially spermatocytes and spermatids, and exfoliation of the germ cells. The seminiferous tubular lumens were more thickened with fibrous connective tissue, and showed severe atrophy and loss of epithelium, with only Sertoli cells and spermatogonia present. Sperm were absent; the spermatogenic cells showed degeneration and/or necrosis. The Sertoli cell nuclei were necrotic and dislocated from the basal membrane portion, while their cytoplasm contained severe vacuolization and an accumulation of lysosomal bodies containing Ag NPs. Lysosomal bodies containing NPs were also noted near deformed elongated spermatids. Spermatids appeared with high vacuolation and dense bodies, and large populations of developing spermatids showed acrosomal changes (sub-acrosomal swelling and perturbed integrity of the membranes). Many apoptotic spermatids had vacuolated and collapsed nuclear membranes. Elongated spermatids had deformed tail and head with increased sub-acrosomal space. These deformed elongated spermatids were phagocytized by Sertoli cells, which resulted in engulfed spermatids and residual bodies in the cytoplasm of Sertoli cells. Ag NPs were found accumulated in the Sertoli cells cytoplasm. The reproductive LOAEL was considered 0.020 mg/kg/d, the only dose tested.

Table 23. Summary of Reproductive Toxicity to Ag NPs via Oral Exposure

Species (n/sex/group)	Exposure concentrations frequency, duration	Particle characteristics[a]	NOAEL (mg/kg/d)	LOAEL (mg/kg/d)	LOAEL Response	Comments	Reference
Male and female ICR mice 5/sex/group	0 (deionized water) or 1 mg/kg/d by gavage; 14 days	Purchased 22, 42, 71 or 323 nm	1	None	No effect on reproductive organ weights or histopathology.	Non-guideline	Park et al., 2010a
Male and female Sprague-Dawley rats 10/sex/group	0 (0.5% CMC), 30, 300, or 1000 mg/kg/d by gavage; 28 days	Purchased 60 nm	1000	None	No effect on reproductive organ weights or histopathology	OECD 407/GLP study	Kim et al., 2008
Male and female F344 rats 10/sex/group	0 (0.5% CMC), 30, 125, or 500 mg/kg/d by gavage; 90 days	Purchased 56 ± 1.46 nm	125	500	Significant ↓ in male body weights; and significant ↑ in relative left testes weight	OECD 408/GLP study	Kim et al., 2010a
Male Wistar rats 8/group	0 (distilled water), 25, 50, 100, or 200 mg/kg/d by gavage; 2x/day for 48 days	Synthesized 70 nm	25	50	Significant ↓ in spermatogonia, spermatocytes and spermatids at 50, 100, and 200 mg/kg/d	Non-guideline; twice/day dosing; no difference in testes weight	Miresmaeili et al., 2013
Male Wistar weanling rats 10/group	0 (not given), 15, or 50 µg/kg/d (0.015 or 0.050 mg/kg/d) by gavage; daily PND 23-53	Purchased 60 nm	None	0.015	Significant ↓ in sperm production at 50 µg/kg/d and ↓ sperm reserves at 15 and 50 µg/kg/d	Non-guideline; low dosages	Sleiman et al., 2013
Male Wistar rats 8/group	0 (double distilled water) or 20 µg/kg/d; (0.020 mg/kg/d) daily by gavage; 90 days	Synthesized 5-20 nm	None	0.020	Adverse testicular histopathological findings	Non-guideline	Thakur et al., 2014
Male and female Sprague-Dawley rats 10/sex/group	0 (distilled water), 62.5, 125, or 250 mg/kg/d by gavage; 42 days males and 52 days females	Manufactured 7.9 ± 0.95 nm citrate-coated	250	None	No effect on reproductive organ weights or histopathology.	OECD 422/GLP study	Hong et al., 2014

Species (n/sex/group)	Exposure concentrations frequency, duration	Particle characteristics[a]	NOAEL (mg/kg/d)	LOAEL (mg/kg/d)	LOAEL Response	Comments	Reference
Male Wistar weanling rats 10/group	0 (water), 15, or 30 µg/kg/day (0.015, 0.030 mg/kg/d) by gavage; daily PND 23-58	Purchased 60 nm; measured 86.1 nm	None	0.015	Significant ↓ acrosome integrity and onset of puberty; significant ↑ abnormal sperm at 15 and 30 µg/kg/d; delay in puberty.	Non-guideline; no effect on body growth	Mathias et al., 2015
Male Sprague-Dawley rats 6/group	0 (0.9% saline), 50, 100, or 200 mg/kg/d by gavage; 90 days	Purchased PVP-coated 25.24 ± 3.25 nm	100	200	Non-significant ↑ in epididymis and testes weights at 100 and 200; and ↓ sperm viability; significant ↑ in abnormal sperm at 200 mg/kg/d	OECD Guideline 408	Lafuente et al., 2016

[a]Particle characteristics described in text

5.6.1.3 Developmental Toxicity

The effect of oral administration of Ag NPs on the development of the CD-1 mouse (4 to 6 weeks old) was investigated by Philbrook and coworkers (2011). The purchased Ag NPs were untreated and supplied as 20 nm (99.8 percent pure). TEM analysis showed that the Ag NPs "were well-dispersed, but more heterogeneous in size." When measured in distilled water, particle size range was 24 to 47 nm (average size 35.3 ± 5.8 nm), and when measured in tragacanth gum (vehicle), the sizes ranged from 144 nm to 260 nm (average size 220 ± 21.1 nm). The developmental success of CD-1 mice (12 to 18 litters) was evaluated after a single 5 mL/kg oral gavage dose to dams of 0.2 percent, 2.0 percent, and 20 percent w/v suspension in a 0.5 percent tragacanth gum aqueous solution at 0 (distilled water), 10, 100, or 1000 mg/kg Ag NPs, only on GD 9. Dams were weighed and then euthanized on GD 19 and each uterus was examined for resorptions. All fetuses (210, 177, 146, and 147 in the four dose groups, respectively) were counted, weighed, measured for length and examined for any external morphological defects. Placentas, fetal livers and fetal kidneys were processed, stained with H&E, and the sections examined histopathologically. Fetuses were skinned, eviscerated and the skeletons stained with Alcian Blue and Alizarin Red S for cartilage and bone visualization, respectively. There was no indication of maternal toxicity (including the dams' behavior and body weights) after Ag NP treatment during the 10-day post-exposure period. Litter size, maternal weight gain from GD 9 to GD 19 and mean fetal weights and lengths also did not differ from the control group. There was a significant increase in the number of non-viable fetuses obtained from dams exposed to 10 mg/kg Ag NPs; at the 100 or 1000 mg/kg concentrations, this effect was not apparent. There was no increase in the number of external, visceral or skeletal defects in fetuses prenatally exposed to Ag NPs. "Limited" TEM analysis identified the presence of Ag NP in the fetal liver and fetal kidneys. This latter finding indicates transplacental exposure occurred by the oral route from a single exposure.

Both Ag NPs and ionic Ag+ were investigated for potential developmental toxicity (Charehsaz et al., 2016). Pregnant female Sprague-Dawley rats (10/group) were dosed by gavage (4 mL/kg) with 0, 0.2, 2.0, or 20 mg/kg/d of synthesized Ag NPs (average 55 nm in hydrodynamic diameter by TEM) or 20 mg/kg/d $AgNO_3$ suspensions for Ag+, from GD 7 to 20. On the second day after parturition, dams and pups were sacrificed and Ag level measured by atomic absorption (AA) in several maternal and pup organs. Hepatotoxicity, oxidative stress parameters in the brain and liver, and histopathology of the maternal brain, heart, lungs, liver, kidneys, spleen, ovaries, and uterus, as well as the brain, heart, liver, lung, and kidney from one pup/litter, were also evaluated. No treatment-related effects were found for gestational indices including length of pregnancy, maternal weight gain, number of implantations, fetal resorptions, birth weight, sex distribution, litter size, and offspring weights at any dose level of Ag NPs or Ag+. Relative weights of the heart, uterus and brain were significantly reduced at 20 mg Ag NPs in the dams. Maternal weight gain was lower in dams receiving $AgNO_3$, indicating Ag+ exerts a higher toxicity compared to the Ag NP form. Tissue content of Ag, including breast milk, was higher in all treated groups compared to control dams and pups, indicating transfer of Ag across the placenta and blood-brain barriers of both silver forms. Biochemical analysis of two biomarkers of hepatotoxicity, ALT and AST, showed no significant differences between groups. Some minimal adverse responses were observed in histopathological analysis of liver. Interleukin 6, which acts as both a pro-inflammatory cytokine and an anti-inflammatory myokine, was slightly increased by both forms of Ag. Oxidative stress was induced in dams and their offspring as

indicated by induction of SOD activity after dosing with $AgNO_3$. Histopathological examination of brain tissue revealed a high incidence of hippocampal sclerosis in dams treated with Ag NPs or ionic Ag+.

Pregnant Sprague-Dawley rats (11/group) were gavaged daily with 0 (0.5 percent CMC), 100, 300, or 1000 mg/kg/d Ag NP suspensions with a dose volume of 10 mL/kg on GD 6 through 19 and Cesarean-sectioned on GD 20 (Yu et al., 2013). The Ag NPs were commercially available with a particle size listed as 7.5 ± 2.5 nm and measured by TEM as 6.45 ± 2.55 nm. Dams were examined daily throughout the gestation period for clinical signs; individual body weights and feed consumption values were measured on GD 0, 6, 9, 12, 15, 17, and 20. At Cesarean section, the number of corpora lutea and the status of all implantation sites (i.e., live and dead fetuses, early and late resorptions, and total implantations) were counted; all fetuses were examined for signs of embryotoxic and teratogenic effects. Examinations of hepatic oxidant/antioxidant balance and serum biochemistry to measure oxidative stress were also added to the routine developmental toxicity endpoints. No treatment-related clinical signs were observed and no significant differences in body weight or feed consumption values were observed between the four groups. At the scheduled autopsy, no treatment-related gross findings were observed in dams of any group. Absolute brain weights in all treatment groups increased significantly compared to vehicle controls; all other absolute and relative organ weights (pituitary, adrenals, liver, spleen, kidneys, heart, ovaries) were not significantly different. Overall, pregnancy rates were comparable across all dosage groups, ranging from 72.7 to 100 percent. There were no completely resorbed litters in any group and the number of corpora lutea, implantations, post-implantation loss rates, fetal deaths, litter size, gender ratio of live fetuses, fetal body weights, and placental weights in the treatment groups were not statistically different from the controls. The pre-implantation loss rate in the 1000 mg/kg group was significantly higher than the controls. Some external and visceral malformations and variations were observed in fetuses from treated groups; however, the incidences of these findings were comparable between the groups. Only one case of a skeletal malformation (i.e., short 13^{th} rib) was observed in the 1000 mg/kg group. Although some types of skeletal variations, including incomplete ossification of the parietal bones that form the central side and upper back part of the skull, incomplete ossification of the inter-parietal, wavy ribs, short supernumerary ribs, full supernumerary ribs, misshapen sternebrae, misaligned sternebrae, bipartite ossification of the sternebrae, dumbbell ossification of the sternebrae, unossified thoracic centrum, bipartite ossification of the thoracic centrum, and dumbbell ossification of the thoracic centrum were found in the treatment groups, no significant differences in the number of fetuses with developmental variations or in the number of litters with affected fetuses were observed between the groups. No significant difference was observed between the treatment groups and controls regarding any of the serum biochemical parameters examined in pregnant dams. Treatment with Ag NPs caused a significant decrease in liver catalase and glutathione reductase activities at greater than or equal to 100 mg/kg/d and a reduction in glutathione content at 1000 mg/kg/d in maternal liver tissues. The results show that repeated oral doses of Ag NPs during pregnancy caused oxidative stress in hepatic tissues at greater than or equal to 100 mg/kg/d, but did not cause developmental toxicity at doses of up to 1000 mg/kg/d. The NOAEL of Ag NPs is considered to be less than 100 mg/kg/d for dams (maternal toxicity) and 1000 mg/kg/d for developmental toxicity.

Fatemi et al. (2013) examined adverse effects of manufactured Ag NPs (20 ± 4 nm) in the brain of male pups from pregnant Wistar rats (45/group) that were orally gavaged with 0 (deionized

water) or 25 mg/kg/d from GD 9 to delivery. After parturition, one male from each litter was sacrificed and the brain removed for determination of the amount of Ag, malondialdehyde, glutathione, and glutathione peroxidase (GPX) activity to measure oxidative stress. Pup body weights and relative brain weights (n=16) were significantly reduced in the Ag NP-exposed neonates. Histopathological examination of the Ag NP-exposed brains (8/group) revealed a significant increase in microvacuolar structures indicating brain damage. A significant decrease in GPX activity and glutathione levels and a significant increase in malondialdehyde levels were observed in the brains of pups. In total, these findings suggest that Ag NPs may act as a developmental toxicant.

The studies are compiled in Table 24.

Table 24. Summary of Developmental Toxicity of Ag NPs via Oral Gavage Exposure

Species n/sex/group	Exposure concentration, frequency, duration	Particle characteristics	NOAEL (mg/kg/d)	LOAEL (mg/kg/d)	LOAEL Responses	Comments	Reference
Pregnant CD-1 mice 12-18 litters	0, 10, 100, or 1000 mg/kg/d GD 9 only	Purchased 35.3 ± 5.8 nm; ranged 24-47 nm	1000	None	None	Non-guideline; only dosed GD 9	Philbrook et al., 2011
Pregnant Wistar rats 45/group	0, 25 mg/kg/d GDs 9 to delivery	Purchased 20 ± 4 nm	None	25	↓ pup and brain wts; ↑ micro- vacuolization in pup brains	Non-guideline; only 1 dosage	Fatemi et al., 2013
Pregnant Sprague-Dawley rats 11/group	0, 100, 300, or 1000 mg/kg/d GDs 6 to 19	Purchased 7.5 ± 2.5 nm	None	100	↓ brain weight	Preimplantation loss was ↑ at 1000 mg/kg/d but had no effect on litter size	Yu et al., 2013
Pregnant Sprague-Dawley rats 10/group	0, 0.2, 2.0, or 20 mg/kg/d Ag NPs or 20 mg/kg/d $AgNO_3$ GDs 7 to 20	Synthesized 55 nm	2.0 NPs None	20 NPs 20 $AgNO_3$ (for Ag+)	↓ maternal body weight; no embryo/fetal effects	Non-guideline	Charehsaz et al., 2016

5.6.2 Inhalation Exposure

No data regarding inhalation exposure in humans and reproductive or developmental outcome were located in the recent literature search. The reproductive studies in animals via inhalation exposure are shown in Table 25.

5.6.2.1 Reproductive Toxicity

This 90-day subchronic inhalation toxicity study (OECD Test Guideline 413) of Ag NPs used eight-week-old male and female Sprague-Dawley rats, divided into four groups (10/sex/group): clean air (dried and filtered) control, low concentration (0.6×10^6 particles/cm^3, 49 μg/m^3), middle concentration (1.4×10^6 particles/cm^3, 133 μg/m^3), and high concentration (3.0×10^6 particle/cm^3, 515 μg/m^3) (Sung et al., 2009). The animals were exposed to Ag NPs generated by the investigators (average diameter 18 to 19 nm; surface areas were 1.08 to 6.61 x 10^9 nm^2/cm^3) for 6 h/d, 5 d/wk, for 13 weeks in a whole-body inhalation chamber. Clinical observations, body weight and feed consumption values were recorded weekly. At necropsy, blood samples were collected for hematology and clinical chemistry tests, and the organ weights (testes, epididymis, seminal vesicle, prostate, uterus and ovaries) were measured and evaluated histopathologically. There were no treatment-related effects on the weights of the reproductive organs. Sperm parameters and estrus cycling were not measured. The NOAEC for reproductive effects was 515 μg/m^3, the highest concentration tested, as no adverse effects on reproductive organ weights were reported.

Table 25. Summary of Reproductive Toxicity of Ag NPs via Inhalation

Species (n/sex/ group)	Exposure, frequency, duration	Particle characteristics	NOAEC (μg/m^3)	LOAEC (μg/m^3)	LOAEC Responses	Comments	Reference
Male and female SD rats 10/sex/ group Whole body exposure	0, 49, 133, or 515 μg/m^3 6 h/d, 5 d/wk, 90 days	Synthesized 18 to 19 nm; surface area = 1.08 to 6.61x109 nm^2/cm^3	515 (repro effects)	None	Reproductive function not evaluated	OECD TG 413	Sung et al., 2009

5.6.2.2 Developmental Toxicity

No studies were located via the inhalation route of exposure to evaluate developmental toxicity.

5.6.3 Dermal Exposure

No studies were located using the dermal route of exposure to evaluate reproductive or developmental toxicity.

5.6.4 Other Routes of Exposure

There are several reproductive and developmental toxicity studies by the oral route relevant to inform ADI derivation for consumer products containing Ag NPs. There is a paucity of studies by inhalation or dermal routes. There are numerous Ag NP toxicity studies by parenteral routes. Many of these studies have limitations in the animal number, dosing period, dosage level, and number of groups. However, they may provide some insight into the mechanism of action, target tissues, and transplacental biokinetics and transfer across blood brain and blood-testes barriers in potentially susceptible populations for adverse reproductive and developmental effects of Ag NPs, and thus are briefly addressed in Appendix F.

5.6.5 Summary

No standard *in vivo* mammalian guideline tests of reproductive toxicity were located for Ag NPs in the search of recent literature. However, an oral reproductive/developmental toxicity screening study (Hong et al., 2014), as well as several oral standard subchronic studies (Kim et al., 2008, 2010a) that evaluated some reproductive endpoints were published (Yu et al., 2014; Charehsaz et al., 2016). In addition, one standard inhalation subchronic repeat-exposure mammalian toxicity test with reproductive endpoints (Sung et al., 2009) was located. It has been reported that Ag NPs cross the blood-testes and blood-brain barrier in mice (Lankveld et al., 2010) and rats (Asare et al., 2012). Further, Ag NPs produce significant severe effects on seminiferous tubules, Sertoli cells and sperm production in rats orally gavaged with 50 to 200 mg/kg/d of synthesized Ag NPs (70 nm) for 48 days and at a much lower dose (0.020 mg/kg/d) for 90 days with synthesized (5 to 20 nm) Ag NPs (Miresmaeili et al., 2013; Thakur et al., 2014).

It is not likely that humans would be exposed to NPs from consumer products via parenteral routes such as IV, SC or IP routes. However, these routes may provide insight if there are data gaps for more common routes, as is the case for the inhalation or dermal routes for Ag NPs. These studies are discussed in Appendix F. Subcutaneous or IV studies may provide an indication of potential reproductive/developmental effects should there be dermal exposure to damaged skin. These routes also provide information as to kinetics, such as transfer across the blood-brain barrier, blood-testes barrier, and transplacental transfer.

Several IV, IP and SC developmental studies fill data gaps for developmental neurobehavioral testing and indicate neurochemical alterations. These endpoints were not evaluated via the oral or inhalational routes.

5.7 Carcinogenicity

Laboratory animal studies were not located in the recent literature search on the possible carcinogenicity of Ag NPs by any route of exposure. The National Toxicology Program selected Ag NPs for carcinogenicity testing, however, these studies have not been conducted.

According to the criteria of the U.S. EPA (U.S. EPA, 2010b, 2017b), silver (CASRN 7440-22-4) is not classifiable as a human carcinogen (Group D). Ag NPs have not been considered for assessment in IRIS.

5.8 Mechanistic Data

5.8.1 Mutagenicity/Genotoxicity Studies

Results of short-term tests to assess the mutagenicity/genotoxicity of Ag NPs published prior to 2012 have been reviewed by Kim and Ryu (2013). While no *in vitro* or *in vivo* mutagenicity studies were identified in this review, there were ten publications describing results of *in vitro* genotoxicity studies of Ag NPs in cells derived from mammalian species and two *in vivo* genotoxicity studies in rats. A brief summary of the Kim and Ryu (2013) review is provided here as this review covered a broader range of studies than the review prepared by Versar (2012). The inclusion criteria for studies (i.e., study quality or test material characteristics), were not provided in the Versar (2012) nor in Kim and Ryu (2013). Ag NPs induced DNA damage in the *in vitro* comet assay in five studies using six different human cell lines. Formation of micronuclei (MN) was also induced by Ag NPs in two *in vitro* studies involving three different human cell lines. An enhanced level of γH2AX, which forms at the sites of DNA double strand breaks, was observed in three studies involving two human cell lines and two mouse cell lines. In the studies in mouse cell lines, expression of Rad51, a DNA damage repair protein, was also measured and found to be increased. One study reported increased formation of bulky DNA adducts in cells from a human cell line exposed to Ag NPs. The level of adducts was decreased by pretreatment with N-acetylcysteine (NAC), an antioxidant, suggesting the involvement of ROS in DNA adduct formation. As for the two *in vivo* genotoxicity studies in rats, one showed an increase in DNA damage measured by the comet assay in blood cells after IV injection of Ag NPs at 5-day intervals over a 32-day period, while the other showed no significant increase in MN in the bone marrow after inhalation exposure for 90 days (6 h/d). In the inhalation study there was no evidence of target tissue toxicity suggesting that the lack of a MN response may have been due to inadequate target tissue exposure.

In their review Kim and Ryu (2013) addressed the influence of Ag NP physicochemical characteristics on genotoxicity potential. Characteristics such as coating and surface charge, NP size, release of Ag+ ions, and agglomeration/aggregation may all play a role, but the influence of these parameters is not fully understood. Ag NPs are often coated to promote stability and dispersibility, resulting in surface polarity that prevents agglomeration. Only a few *in vitro* studies discussed in this review addressed the effect of coating on Ag NP-induced cytotoxicity, and only one of them specifically addressed genotoxicity. In that study, polysaccharide-coated Ag NPs induced more extensive DNA damage as measured in a γH2AX assay compared with uncoated Ag NPs of equivalent size. Given the broad variety of coating agents used and the different surface chemistries imparted by these agents, no conclusions can be drawn from the studies reviewed by Kim and Ryu (2013). NP size is an important factor, and smaller-sized Ag NPs may contribute to greater cytotoxicity and genotoxicity by allowing greater penetration of the mammalian cell membrane. Smaller size also affords a larger particle surface area (i.e., m^2/g), for interaction with cellular organelles and constituents. One study reviewed by Kim and Ryu (2013) supported the greater genotoxicity of PVP-coated 5 nm Ag NPs in a comet assay when compared with PVP-coated 20 and 50 nm Ag NPs. Ag+ ions are released by the surface oxidation of Ag NPs in the presence of water and studies have demonstrated Ag^+ genotoxicity. However, the genotoxicity of Ag NPs in an *in vitro* MN study was only partially eliminated by cysteine, a strong Ag+ ligand, indicating that the genotoxicity of Ag NPs was not fully accounted for by Ag+ release.

Kim and Ryu (2013) concluded that a variety of *in vitro* and *in vivo* models indicate that Ag NPs induce genotoxicity as well as oxidative stress and apoptosis, although specific mechanisms that account for these effects are unclear. The physicochemical characteristics discussed above complicate the interpretation of study results and the elucidation of Ag NP-specific modes of action for genotoxicity. Ag NP preparation methods, particularly procedures related to the coating and dispersion of Ag NPs, may differ across studies conducted by different research groups, making it not entirely feasible to compare data from one study with another. Further evaluation of studies since 2012, confirms that it is essential to develop evaluation methods that accommodate the unique physicochemical characteristics inherent to Ag NPs and to attempt to standardize and harmonize experimental procedures related to the study of Ag NP-induced toxicity, including genotoxicity.

Numerous additional *in vitro* and *in vivo* mutagenicity/genotoxicity studies of Ag NPs have been published since 2012. These are summarized below and reviewed in Appendix G.

5.8.1.1 Summary

A large number of both *in vitro* and *in vivo* mutagenicity/genotoxicity studies on Ag NPs have been conducted. Bacterial mutagenicity assays have typically shown negative results. However, the lack of uptake by bacterial cells, as well as the significant antibacterial properties of silver, suggests that bacterial mutagenicity tests such as the Ames test are not well-suited for the evaluation of Ag NP mutagenicity. Although Ag NPs have shown mixed results in several mammalian cell mutagenicity assays, the data suggest that at least some Ag NPs are mutagenic in these test systems. Small size and citrate-coated Ag NPs appear to have greater mutagenic potential. Results of only two *in vivo* mutagenicity assays have been published, and they both suggest a lack of *in vivo* mutagenicity for the Ag NPs evaluated under the test conditions used in those studies. However, the data are too limited to make definitive conclusions concerning the overall *in vivo* mutagenicity of Ag NPs as a class of materials.

Genotoxicity studies, both *in vitro* and *in vivo*, have typically been conducted using the chromosome aberration assay, the MN assay or the comet assay. Four i*n vitro* chromosome aberration assays with Ag NPs have produced mixed results. The reason for the differing results is unclear. None of these studies compared Ag NPs varying in particle size or coating in the same test system, thus precluding an evaluation of the influence of these characteristics on clastogenicity.

In vitro MN assay results were reported in 18 publications. Most of these studies involved human cell lines as a test system. Positive results were reported in 15 of them, one study showed positive results in one cell line but not another, and two studies showed negative results. The study showing a difference in response between two cell types also demonstrated that MN assay methodology can influence study outcomes (Sahu et al., 2014a,b; Sahu et al., 2016a,b; discussed in Appendix G). One of the studies showing negative results was conducted in a human bronchial epithelial cell line; positive results were reported by another group of investigators in the same cell line. The difference in results remains unexplained. A few *in vitro* MN studies have evaluated Ag NPs differing in size and coating under the same experimental conditions. Most of these studies showed that small (10 to 20 nm) Ag NPs and citrate-coated Ag NPs were more potent than PVP-coated Ag NPs in inducing genotoxicity. While one study showed 100

nm Ag NPs gave a greater response than 10 nm Ag NPs, there was evidence of agglomeration of the 10 nm Ag NPs and this is likely to have influenced the findings (Souza et al., 2016).

Numerous *in vitro* alkaline comet assays have been conducted in a wide variety of human cell lines and primary cell cultures as well as animal cell lines. With very few exceptions these have shown positive results. One study reported negative results in two types of normal human cells when Ag NPs were tested at non-cytotoxic concentrations. However, other studies have shown positive comet responses at non-cytotoxic concentrations. The negative study utilized an unconventional scoring method for scoring comet results. Given the large number of positive studies, this negative study can be given little weight. Five modified comet assays designed to detect specific oxidative DNA damage have been published and four have shown a positive response. Although these studies suggest that some Ag NPs have the capacity to induce oxidative DNA damage *in vitro*, further study of the characteristics of Ag NPs that are associated with this capacity is warranted as the one negative study did not support oxidative DNA damage as a mode of action for Ag NP genotoxicity.

When ROS has been measured in MN or comet assays, most have shown an increase in ROS accompanying the positive genotoxicity response. However, one study showed that, while ROS was increased by all three Ag NPs evaluated, the ROS responses across three different cell lines did not correlate with increases in percent tail DNA. The role of ROS in the mode of action of Ag NP-induced DNA damage also requires further evaluation. Likewise, the role of release of Ag+, either extracellularly or intracellularly, in the mode of action of Ag NP genotoxicity is not clear.

The experimental evidence suggests that Ag NPs of diverse characteristics are capable of inducing DNA damage *in vitro* as measured by the comet assay. Consistent with the *in vitro* MN results, some studies have reported that small size and citrate coating are associated with greater potency in the comet assay. However, one study showed comparable effects on percent tail DNA with Ag NPs ranging in size from 10 to 75 nm that were either citrate-coated, PVP-coated, or uncoated (Gliga et al. (2014). Further study of the effect of particle characteristics as well as other factors that may influence the outcome of these assays with Ag NPs, such as dosing regimens, effect of dispersion method on aggregation, cell culture conditions, assay methodology, and vehicle used would be useful.

In vivo Ag NP genotoxicity has been evaluated using the MN assay or the comet assay. *In vivo* studies involving all routes of exposure, including oral, inhalation, IP and IV routes have been included in this report for completeness. However, the IP and IV routes of exposure are generally not recommended for risk assessment for consumer products without specific scientific justification. Five positive MN studies indicate genotoxic potential for Ag NPs following exposure by the oral, IP, or IV routes. However, negative results have also been reported in one IV study and one IP study. The lack of a MN response in the negative studies does not appear to be explained by inadequate target tissue exposure. Further study of the factors that may influence the outcome of *in vivo* assays with Ag NPs, such as dosing regimens, Ag NP characteristics such as particle size and coating, effect of dispersion method on aggregation, assay methodology, vehicle used, and route-specific differences in biokinetics and protein corona surrounding the NP would be useful.

Ag NPs have been shown to cause DNA damage *in vivo* in the comet assay in bone marrow following exposure by either the oral or IP routes in three studies. Negative results in an IV study evaluating bone marrow may have been attributable to inadequate target tissue exposure. An analysis of the Ag NP test material characteristics on the outcome of the *in vivo* comet assays in bone marrow was not undertaken, given the small number of studies, varying routes and durations of exposure.

Among 10 *in vivo* MN studies in rats or mice, one study showed an increase in MN formation and one study was negative despite evidence of cytotoxicity to the bone marrow. The remaining studies were also negative. A lack of evidence of target tissue cytotoxicity, indicating lack of adequate exposure may be the explanation for some of these eight negative studies, but cytotoxicity in the target tissue was not evaluated in all of these studies. Time of sacrifice after exposure could also explain the lack of a MN response in at least one study. Numerous *in vivo* comet assays have also been conducted looking for DNA damage in various target organs after exposure via various routes (oral, IV, inhalation, IT). These studies have given conflicting results. As with the *in vivo* MN assays, negative results are not adequately explained by a lack of evidence of target organ exposure or target organ toxicity.

5.8.2 Mechanism of Action

The causative agent and the mechanism of action for the toxicity of Ag NPs are not known. Research has been directed at discerning whether the NPs themselves cause toxicity or whether Ag ions dissociated from the Ag NP may be the toxic moiety. Similarly, several events have been postulated to be involved in the adverse outcome pathway for Ag NPs: interaction with cellular proteins, ROS, inflammation, cell death and genotoxicity. The role of coatings, aggregation, and NP size, while thought by some to contribute to toxicity, has not been teased-out of the milieu of factors that influence the cascade of events leading to Ag NP toxicity.

Ag NPs have many recent applications for antimicrobial activity (Chen and Schluesener, 2008; Johnston et al., 2010; Wang et al., 2015b). However, this application is regulated by the U.S. EPA and the FDA and is not within the jurisdiction of CPSC. Therefore, the mechanism of action for antimicrobial activity is not considered in this report.

5.8.2.1 Physicochemical Form of Silver and Toxic Moiety

Ionic silver (Ag+) is considered the toxic form of Ag by many researchers in the nanomaterial field. The dissolution of Ag+ from Ag NPs within cells and in close proximity to cells in aqueous environments has been proposed to be one mode of action of toxicity of Ag NPs; however, contribution to toxicity from the NPs (themselves) have also been proposed (Hwang et al., 2008; Liu et al., 2010).

Recent studies, summarized below, support that the ionic form of Ag is likely more cytotoxic (on a mass basis) than Ag NPs. In addition, NP characteristics such as coating(s) and smaller size, influence cellular toxicity in human and animal cells *in vitro*. Because Ag NPs shed Ag+, the release of Ag+ and resistance of NPs to dissolution may be a factor influencing NP toxicity. From a regulatory standpoint, products labelled as containing Ag NPs in solution frequently contain high concentrations of Ag+ (U.S. EPA, 2010b).

The comparative *in vitro* cytotoxicity of Ag NPs and Ag+ has been examined in studies with mammalian cells, including human mesenchymal stem cells (Greulich et al., 2009; Hackenberg et al., 2011a), human monocytic cells (Foldbjerg et al., 2009, 2011), human HEPG2 hepatoma cells (Kawata et al., 2009; Kim et al., 2009), human HeLa S3 cells (Miura and Shinohara, 2009), human intestinal cells (Bohmert et al., 2014), human lung A549 cancer cells (Chairuangkitti et al., 2013; Foldbjerg et al., 2011; Hatipoglu et al., 2015); human liver HepG2 and mouse liver primary cells (Faedmaleki et al., 2014); human Jurkat T cells (Eom and Choi, 2010); human dermal fibroblasts (HDF) and epidermal keratinocytes (Galandakova et al., 2016); rat alveolar macrophages (Carlson et al., 2008); rat adrenal medulla pheochromocytoma cells (Powers et al., 2010, 2011); mouse spermatogonia stem cells (Braydich-Stolle et al., 2010), mouse bone marrow mast cells (Aldossari et al., 2015); mouse RAW264.7 peritoneal cells (Park et al., 2010b); and mouse L929 fibroblast cells (Kumar et al., 2015). The results suggest that mammalian cytotoxic responses to Ag NPs are dependent on particle physical and chemical characteristics and are similar, although not identical, to responses to Ag+, especially for Ag NPs with smaller average diameters (less than ~30 nm). Additional studies of mammalian cells exposed to Ag NPs, but not Ag+, provide supporting results (Arora et al., 2009, 2008; Rosas-Hernandez et al., 2009; Hsin et al., 2008; Hussain et al., 2006, 2005; Versar, 2012).

Key findings from historical, as well as more recent, literature following exposure to either Ag NPs or Ag+ include increased levels of ROS (Foldbjerg et al., 2009, 2011; Kim et al., 2009; Carlson et al., 2008; Hussain et al., 2006, 2005; Liu et al., 2010; Lim et al., 2012b; Ahmad et al., 2012; Chairuangkitti et al., 2013; see also review in Versar, 2012), induction of oxidative stress management genes (Kim et al., 2009; Miura and Shinohara, 2009; Bouwmeester et al., 2011; Huo et al., 2015; Chen et al., 2016), increased percentage of apoptotic cells (Foldbjerg et al., 2009; Miura and Shinohara, 2009; Hsin et al., 2008; Kumar et al., 2015), and attenuation of Ag-induced cytotoxic effects by NAC (a glutathione precursor, ligand for Ag+, and ROS scavenger) (Kawata et al., 2009; Kim et al., 2009; Hsin et al., 2008; McShan et al., 2014). Across a number of studies, Ag+ from either silver nitrate or silver acetate was consistently more potent than Ag NPs in inducing apoptosis and ROS (Foldbjerg et al., 2009; Kim et al., 2012b) and reducing cell viability (Greulich et al., 2009; Kim et al., 2009; Miura and Shinohara, 2009; Carlson et al., 2008), while silver carbonate was less potent as Ag NPs in decreasing cell viability (Kawata et al., 2009).

The potential toxicity of Ag NPs was compared to the effects of Ag+ using normal primary HDF and normal human epidermal keratinocytes in serum-free culture (Galandakova et al., 2016). Besides the effect of Ag NPs and Ag+ on cell viability, the inflammatory response and DNA damage in Ag NPs and Ag+-treated cells were examined. Ag+ was significantly more toxic than Ag NPs both on normal dermal fibroblasts and epidermal keratinocytes. Non-cytotoxic concentrations of Ag NPs and Ag+ did not induce DNA strand breaks and did not affect inflammatory markers, except for a transient increase in IL-6 levels in Ag+–treated dermal fibroblasts.

Comfort and coworkers (2014) found Ag+ dissolution disrupted epidermal growth factor signal transduction even after the removal of the excess NPs, suggesting that intracellular Ag+, not NPs themselves, is the toxic moiety.

The role of coatings and optimum size of Ag NPs that affect toxicity is an ongoing subject of

research. Results from studies of mouse spermatogonia stem cells showed that size and coating can influence the cytotoxicity of Ag NPs (10 to 130 nm) (Braydich-Stolle et al., 2010). Smaller Ag NPs (10 to 15 nm) and higher concentrations (greater than 10 µg Ag/mL) of either hydrocarbon- or polysaccharide- coated Ag NPs significantly impaired mitochondrial function and inhibited cell proliferation. Ahamed et al. (2008) reported that exposure to 25nm Ag NPs, with either coating, induced apoptosis, and, decreased mitochondrial function in cultured mouse embryonic stem cells and fibroblasts.

Ag NP seeds (NPs with 8 to 15 nm hydrodynamic sizes that fuse together) were the major source of cytotoxicity and genotoxicity in HDF and human lung cancer (A549) cell lines with exposure to spherical Ag NPs synthesized from silver nitrate (Hatipoglu et al., 2015). The Ag NPs seeds, having reactive surfaces, tend to release Ag+ ions. The formation of larger Ag NPs effectively decreased the toxicity.

Powers et al. (2011) noted that significant differences were found in potencies and differentiation outcomes that depended both on particle size and coating when *in vitro* neurodevelopmental endpoints were measured in PC12 cells from pheochromocytoma rat adrenal medulla. None of the effects reflected simple physical attributes of NPs, as equivalent concentrations of silica NPs had no detectable effects.

Using bone marrow derived from mouse mast cells and Ag NPs of varying physicochemical properties, Aldossari and coworkers (2015) tested whether Ag NPs' (spherical 20 nm and 110 nm suspended in either PVP or citrate) physicochemical properties can influence mast cell degranulation and osteopontin production. Mast cell responses were found to be dependent on the physicochemical properties of the Ag NPs. Mast cell degranulation was not dependent on Ag NPs dissolution, but was prevented by tyrosine kinase inhibitor pretreatment.

5.8.2.2 Cellular Translocation

Physiological differences in the portal of entry for oral, inhalation or dermal routes of exposure likely have a role in local intracellular translocation as well as toxicity from Ag NPs. The small size and extremely large surface area of Ag NPs affects the adhesion of the NPs so that they make strong contact with the surface of cells and alter membrane properties (Wong and Liu, 2010). Limited research was available regarding how Ag NPs are moved from the extracellular space into cells and if disruption of the membrane surface facilitates intracellular translocation. A handful of *in vitro* and *in situ* studies have attempted to explore these differences.

The cytotoxicity of Ag NPs on intestinal cells was investigated using Caco-2 cells (a continuous cell line of heterogeneous human epithelial colorectal adenocarcinoma cells) (Bohmert et al., 2014). The authors found that Ag NPs only partially aggregate as a result of an artificial digestive process. Small differences in cell viability between digested and undigested particles were reported, suggesting that Ag NPs overcome the gastrointestinal juices in their particulate form without forming large quantities of aggregates. The authors concluded that the Ag NPs likely reach the intestinal epithelial cells *in vivo* after ingestion with only a slight reduction in their cytotoxic potential.

The cytotoxicity of commercially available Ag NPs on human epidermal keratinocytes (HEKs)

was investigated by Samberg et al. (2010) using eight different unwashed/uncoated particle sizes (20 to 80 nm particle diameter), washed/uncoated (20 to 80 nm), and carbon-coated (25 and 35 nm). Localization of all Ag NPs was visualized in cytoplasmic vacuoles. Each of the unwashed Ag NPs elicited a significant increase in interleukins and TNF-α concentrations.

De Matteis et al. (2015) showed that intracellular release of Ag+ in living cells occurred after Ag NP internalization from *in situ* particle degradation by the acidic lysosomal environment. The toxicity of Ag+ is addressed in the previous section.

5.8.2.3 Interaction with Cellular Proteins

Toxicity of Ag NPs has been proposed to involve Ag binding to DNA and proteins, leading to interference with cellular functions (Jung et al., 2008; Greulich et al., 2009; Al Gurabi et al., 2015; see Versar, 2012).

The dissolution of Ag NPs releases Ag+ ions which can interact with sulfur-containing cellular proteins (Volker et al., 2013). This interaction of dissolved Ag+ ions with thiol groups on cytoplasmic proteins may lead to impaired function or inactivation of enzymes, with effects including disruption of mitochondrial respiration (Pal et al., 2007; Lee et al. 2012b).

Park et al. (2010b) studied purchased Ag NPs (less than 150 nm; 68.9 ± 30.3 nm; Zeta potential of -0.91 mV) in cell cultures of mouse peritoneal macrophages (RAW264.7). They reported decreased intracellular glutathione levels, increased nitric oxide secretion, increased protein and gene levels of TNF-α, and increased gene expression of matrix metalloproteinases. Ag NPs were observed in the cytosol of the activated cells, but were not observed in the dead cells.

Using prepared rat liver microsomes and purchased Ag NPs (particle size of less than 100 nm diameter, with a specific surface area of 5 m^2/g), Kulthong et al. (2012) demonstrated a strong inhibition of rat hepatic cytochrome P450 enzymes CYP2C and CYP2D activities.

The *in vitro* toxicity of Ag NPs was investigated in comparison to silver nitrate in J774.1 murine airway macrophage cells (Arai et al., 2015). The cells were exposed to various concentrations of $AgNO_3$ or (20, 60 or 100 nm diameter) Ag NPs. Ag was mainly bound to metallothioneins and to high molecular weight proteins in $AgNO_3$- and Ag NPs-exposed cells. The Ag NPs were apparently transported to lysosomes and were co-localized with lysosomes in cells, and were gradually dissolved in the macrophages, causing milder inflammatory stimulation in the mouse lung compared to $AgNO_3$.

5.8.2.4 Oxidative Stress and Inflammation

ROS are reactive chemical species containing oxygen (peroxides, superoxide, hydroxyl radical, and singlet oxygen) that can be generated outside the cell, in medium, or inside the cell causing cell damage and disruption of cellular function (Liu et al., 2010; Skalska et al., 2016). The impact of ROS on cell cycle progression has been known for over a decade (Boonstra and Post, 2004) and the impact depends on the amount and duration of ROS exposure. Various ROS species are regularly in flux as a part of the normal reduction-oxidation (redox) balance in the cell. Oxidative stress is a state of redox imbalance consisting of an increased ratio of ROS to antioxidants and a number of changes in cell signaling and function.

Signs of oxidative stress have been reported in human cell lines in response to both Ag NPs and ionic silver and suggest oxidative stress and apoptosis as pathways of cytotoxicity (Foldbjerg et al., 2011, 2009; Greulich et al., 2009; Kawata et al., 2009; Kim et al., 2009; Miura and Shinohara, 2009; reviewed in Versar, 2012). Results from *in vitro* studies using animal cells showed oxidative stress in various cell types (see discussion in Versar, 2012). Recent studies investigating oxidative stress-related endpoints are summarized below. Overall, published results support that both Ag NPs and ionic silver induce oxidative stress and at least some of their cytotoxic effects are mediated by redox-sensitive mechanisms. These chiefly include mitochondrial toxicity (mitochondria being a major sensor of redox stress) and activation of ROS-inducible signaling.

Eom and Choi (2010) investigated the effects of Ag NPs on human Jurkat T cells, using oxidative stress-related endpoints. Jurkat cells are immortalized human T lymphocytes that are used to study T cell signaling and expression of various chemokine receptors and their ability to produce interleukin 2. The effect of Ag+ was used as a comparator with that of Ag NPs, as it was anticipated that Ag+ would be released from Ag NPs and responsible for their toxicity. Cell viability tests indicated high sensitivity of Jurkat T cells when exposed to Ag NPs compared to Ag+; however, both Ag NPs and Ag+ induced similar levels of cellular ROS during the initial exposure period. After 24 hours, cytotoxicity was increased with exposure to Ag NPs compared to Ag+, which suggested to the authors that oxidative stress was an indirect cause of the observed cytotoxicity of Ag NPs. The authors' hypothesized/concluded that Ag NP exposure activates p38 MAPKSs that are responsive to stress stimuli, such as cytokines, through a prototypical proinflammatory signaling pathway, causing DNA damage, cell cycle arrest and apoptosis.

The *in vitro* toxic effects of Ag NPs on A549 cells were mediated via both ROS-dependent (cytotoxicity) and ROS-independent (cell cycle arrest) pathways. Chairuangkitti et al. (2013) evaluated the *in vitro* mechanisms of Ag NP (spherical primary particle size 40 to 90 nm; hydrodynamic diameter 182.7 ± 13.0 nm; and specific surface area of 5.0 m^2/g) toxicity in relation to the generation of ROS in A549 cells. In a concentration- and time-related response, Ag NPs caused ROS formation in the cells, a reduction in their viability, a reduction in mitochondrial membrane potential, an increase in the proportion of cells in the cell cycle sub-G1 (apoptosis) population, S phase arrest, and down-regulation of the cell cycle associated proliferating protein that helps synthesize DNA during replication. Pretreatment of the A549 cells with an antioxidant, NAC, decreased some of these effects.

After 24-hour exposure of human cell lines A431 or HT-1080 (derived from human skin carcinoma and fibrosarcoma, respectively) to Ag NPs, signs of oxidative stress occurred (Arora et al., 2008). In HepG2 human hepatoma cells, 24-hour exposure to Ag NPs (average diameter 5 to 10 nm; agglomerates 100 to 300 nm) or silver nitrate decreased mitochondrial function and membrane integrity, increased ROS generation, increased the expression of two genes for oxidative stress management proteins, and caused DNA damage (Kim et al., 2009). TEM indicated Ag NPs within the cells following 24 hours of exposure.

Carlson et al. (2008) showed in rat alveolar macrophages that oxidative stress played a contributory role in the cytotoxicity of Ag NPs and ionic silver, and that the *in vitro* cytotoxic potency of Ag NPs declined with increasing particle diameter and degree of agglomeration.

Earlier studies with BRL3A rat liver cells (Hussain et al., 2005) and PC-12 rat cells derived from pheochromocytoma cells (Hussain et al., 2006) similarly showed oxidative stress with Ag NPs. Mitochondrial function and membrane integrity were decreased and ROS levels were increased following exposure to uncoated Ag NPs with average diameters of 15 or 100 nm. Mouse NIH3T3 fibroblast cells exposed for 24 hours to Ag NPs showed increased ROS and increased percentage of apoptotic cells (Hsin et al., 2008). Commercial Ag NPs (average diameter 29 nm) altered gene expression in the caudate, frontal cortex, and hippocampus of three genes known to be involved in either oxidative metabolism or protection from oxidative stress in the brain of male C57BL/6N mice (Rahman et al., 2009).

5.8.2.5 Cell Death and Genotoxicity

Ag NPs inhibit growth in cells and arrest cell cycle. Li et al. (2014) found Ag NPs could penetrate intracellular and nuclear membranes and denature DNA and ribonucleic acid (RNA), inhibiting replication, in mouse bone marrow and liver cells. According to Wong and Liu (2010), silver ions can also interact with phosphorus-containing compounds (e.g., DNA) interfering with replication processes and decreasing the number of cells over time.

Park et al. (2010b) studied purchased Ag NPs (less than 150 nm; 68.9 ± 30.3 nm; Zeta potential of -0.91 mV) in cell cultures of mouse peritoneal macrophages (RAW264.7). They reported increased subG1 fraction, which indicated cellular apoptosis as well as changes in proteins and enzymes with NPs observed in the cytosol of the activated cells.

Several researchers have concluded that smaller-sized NPs have a greater ability to induce apoptosis than larger size NPs. Kim et al. (2012b) examined the size-dependent cellular toxicity of Ag NPs using three different characteristic sizes (~10, 50, or 100 nm) against several cell lines including an osteoblast precursor cell line derived from mouse skull (MC3T3-E1) and pheochromocytoma of a rat adrenal medulla (PC-12). The 10 and 100 nm NPs were purchased, and the 50 nm were prepared by the investigators. Cytotoxicity was determined based on cell viability, intracellular ROS generation, LDH release, ultrastructural changes in cell morphology, and up regulation of stress-related genes. Adverse effects were size- and dose-dependent. Ag NPs stimulated apoptosis in the MC3T3-E1 cells and induced necrotic cell death in the PC-12 cells.

Faedmaleki et al. (2014) investigated the cytotoxic effects of Ag NPs (20 to 40 nm in diameter) on cancerous human liver HepG2 cells and normal primary Swiss albino mouse liver cells. The Ag NPs were 44 times stronger in inhibiting growth of cancerous cells (HepG2 cell line) compared to normal primary liver cells.

Using flow cytometry, Kumar and coworkers (2015) evaluated cytotoxicity (as cell necrosis and apoptosis) of three different size Ag NPs (10, 100, or 200 nm) at different mass concentrations (1, 25, or 50 µg/mL) in mouse L-929 fibroblast cells. Cell necrosis and apoptosis in Ag NP-exposed fibroblasts depended on dose, exposure time, and particle size, with decreases in cell viability; the 10 nm Ag NPs were significantly more toxic than larger-sized particles.

5.8.2.6 Summary

Data indicate the most likely modes-of-action of Ag NPs are mediated by oxidative stress and genotoxic pathways. The initiating mechanism of toxicity is not known, but may involve direct interaction of Ag NPs and ionic silver with proteins. Silver can react with thiol groups in proteins and also with DNA. These interactions can denature proteins; induction of unfolded protein responses to Ag NPs were demonstrated *in vitro* and in mice using IT instillation (Huo et al., 2015).

Ag NPs and ionic silver are growth-arresting in normal and carcinomatous human cells with smaller Ag NPs being more toxic than larger particles. For both NP and ionic forms of silver, both mitochondria and DNA appear to be cellular targets of toxicity. Loss of mitochondrial homeostasis can be either a downstream or upstream cause of oxidative stress. Silver ions could induce oxidative stress either by depleting thiol-based antioxidants (reduced glutathione [GSH]) or through denaturation of mitochondrial membrane pore-forming proteins. DNA is also damaged by oxidative stress and excess ROS species, and this may be a mechanism by which oxidative stress contributes to growth arrest in response to Ag NP exposure.

Ag NPs were shown to induce both necrosis and apoptosis in experimental systems. Apoptosis may be induced as a result of unfolded protein responses, oxidative stress, or DNA damage. A combination of these responses appears to be involved in toxicity of Ag NPs.

5.9 Derivation of ADI

5.9.1 Oral Exposure

A human study of nanoscale Ag was conducted using commercial 10 and 32 ppm colloidal Ag solutions (consisting of both ionic Ag and Ag NPs) in a single-blind, controlled, cross-over, intent-to-treat, design (Munger et al., 2014). Thirty-six healthy subjects consumed 10 ppm and were evaluated at three to 14 days; 24 healthy subjects consumed 32 ppm Ag solution and were evaluated at 14 days. The average daily ingestion of elemental Ag colloid formulation was estimated by the authors to be 100 μg/day for 10 ppm Ag, and 480 μg/day for 32 ppm Ag. No significant changes were reported in metabolic, hematologic, or urinalysis measures; morphology of the lungs, heart or abdominal organs; and, in pulmonary reactive oxygen species or pro-inflammatory cytokine generation. Munger et al. (2015) subsequently investigated whether orally ingested commercially available colloidal Ag nanoproduct interfered with select cytochrome P450 enzymes in a prospective, single-blind, controlled *in vivo* human study. The reduced Ag (Ag^0) NP (size averaged 32.8 nm, with a size range of 25 to 40 nm) was consumed orally for 14 days and the dose was estimated to be 480 μg/day. No demonstrable clinically significant changes in metabolic, hematologic, urinary, physical findings or cytochrome P450 enzyme inhibition or induction activity was reported. Despite being studies with humans, these studies are not suitable for the ADI as colloidal Ag solution (comprised of both ionic Ag and Ag NPs) was administered.

Acute oral studies in animals are of too short duration to support a short term (14-day) or long term ADI.

There are nine repeat dose animal studies; all exposures were gavage administration. Two studies are in mice (two strains of mice used in each study) and seven studies in rats (Wistar, Sprague-Dawley and Fischer 344). Duration of treatment in the studies in mice are 14 to 21 days, whereas duration in rats is 28 to 90 days. The particles vary with PVP-coated, citrate-stabilized, synthesized and commercially purchased, and include Ag NPs (sizes 22 to 323 nm); one study includes a group treated with silver acetate. The two most robust studies are those using 98 to 99 percent pure Ag NPs of similar size and following OECD Test Guidelines and GLPs for 28 or 90 consecutive days (Kim et al., 2008; Kim et al., 2010a, respectively). The method used to determine the characteristics of the test material was not reported, and no information about possible agglomerization of particles in the suspension was reported for the 28-day study. Liver toxicity, increased ALP, and increased total cholesterol are identified as effects at the LOAEL of 300 (NOAEL is 30) mg/kg/d in the 28-day study. Count median diameter and geometric standard deviation of the particles in suspension were determined by TEM in the 90-day study, but no mention was made of possible agglomerization of the particles in the administered suspensions (as discussed in Versar, 2012). The 90-day study identifies minimal liver toxicity and pigmentation in intestinal villi as critical effects with a NOAEL of 125 and LOAEL of 500 mg/kg/d.

No human or animal studies were found with chronic exposure to Ag NPs.

There are several relevant reproductive and developmental toxicity studies by the oral route relevant to inform the ADI which indicate potential maternal toxicity and adverse male reproductive effects. There is one developmental study in mice and three developmental studies in rats (in two strains); none of the studies appear to be Guideline or GLP studies and one study used only one dose level. Ag NPs were purchased or synthesized and varied between 7.5 to 55 nm. The two multiple dose rat developmental studies (with differing NOAEL/LOAELs) indicate decreases in maternal organ and body weights but no embryo or fetal toxicity.

Of nine reproductive toxicity studies, eight are in three strains of rats; four of these are OECD guideline studies and employ purchased/manufactured Ag NPs, of approximately 7 to 60 nm; NPs are PVP- or citrate-coated in two studies. While some of these studies indicate no effect on reproductive organ weight or histopathology, other studies indicate impacts on male reproductive organs and sperm viability. LOAELs for the OECD guideline studies range from 200 to 500 mg/kg/d; whereas NOAELs in those studies vary from 100 to 1000 mg/kg/d. The reproductive toxicity findings and overlapping NOAEL/LOAELs appear to be related to differences in dose selection and use of coatings. The range of reproductive effects is similar to that of the systemic toxicity range.

5.9.2 Inhalation Exposure

Acute inhalation studies in animals, designed to determine LC_{50}, are of too short duration (up to 6 hours) to support a 14-day ADI.

No human studies were found with inhalation exposure to Ag NPs. There were no repeat dose subchronic or chronic duration animal studies via inhalation in the recent available literature.

Laboratory animal studies were not located in the current literature search on possible systemic

toxicity with chronic (lifetime) exposure to Ag NPs by any route of exposure, nor were any studies identified in Versar (2012). No studies were located via the inhalation route of exposure to evaluate developmental toxicity or carcinogenicity.

Four inhalation studies in earlier literature from 2007-2009 (reviewed in Versar, 2012) were conducted in Sprague-Dawley rats; all the studies were whole body exposure to Ag NPs of 12 to 19 nm, with two studies of four-week duration and two studies of 13 weeks duration. Three were OECD guideline and GLP studies. Both four-week studies reported NOAEC of 61 $\mu g/m^3$ and no LOAEC. In the 13-week studies, functional alterations and inflammation in the lung and hyperplasia in the bile duct were reported at the LOAEC of 515 $\mu g/m^3$; the NOAEC was 133 $\mu g/m^3$. In the 13-week systemic toxicity studies, reproductive organ weights were not altered (reproductive function was not evaluated) at 515 $\mu g/m^3$ (NOAEC; no LOAEC).

5.9.3 Dermal Exposure

Human and animal studies evaluated the acute toxicity of dermal exposure to commercially- or laboratory-synthesized Ag NPs. The human studies used burn dressings on wounds with bandages containing Ag NPs; patients developed argyria-discoloration after 6 days and elevation of serum liver protein levels indicative of hepatotoxicity. An acute dermal guinea pig study in accordance with OECD acute test guidelines and GLPs showed no gross abnormalities or microscopic changes after 14 days following one-day exposures up to 100,000 ppm.

Three studies via repeated dermal exposure are available; one study was in pigs for 14 days duration and two studies of 13 weeks duration in guinea pigs. Samberg et al. (2010; cited in Versar, 2012) evaluated dermal toxicity of washed or unwashed commercial Ag NPs (average diameters of 20 or 50 nm) in pigs topically exposed for 14 days. Lesions occurred in layers under the stratum corneum, which the authors attributed to Ag ion (Ag+) flux into the lower layers from the particles in the stratum corneum. The dermal NOAEL was 34 µg/mL (the highest dose tested).

The two guinea pig studies considered the LOAEL as 100 µg/mL; no NOAELs were identified. Korani et al. (2011) dermally applied nanosilver (less than 100 nm by TEM) to guinea pigs for five d/wk for 13 weeks at 0, 100, 1000, or 10,000 µg/mL. A 100 µg/mL solution of $AgNO_3$ served as a positive control. The dermal LOAEL was based on histopathologic abnormalities in the skin, liver, and spleen in all test groups. Subsequently, in an OECD guideline study, Korani and coworkers (2013) compared the tissue levels of Ag NPs in guinea pigs after dermal application of 0, 100, 1000 or 10,000 ppm Ag NPs or the positive control, $AgNO_3$, for 13 weeks. The sizes of the NPs were less than 100 nm (TEM). The three different Ag NP concentrations gave comparable results for several endpoints measured in heart, bone and kidney. The dermal LOAEL was based on histopathologic abnormalities in the skin, liver and spleen.

No human or animal studies were located in the current literature search on possible systemic toxicity with chronic (lifetime) dermal exposure to Ag NPs, nor were any studies identified in Versar (2012). Laboratory animal studies were not located in the recent literature search on the possible carcinogenicity of Ag NPs or on the evaluation of reproductive or developmental toxicity by the dermal route.

5.9.4 Toxic Moiety and the ADI

The mechanism of Ag NP toxicity is uncertain; Ag+ and Ag NP translocation intracellularly and within the body are not completely understood. There is uncertainty as to what is the toxic moiety of Ag NPs.

Many researchers in the nanomaterial field consider ionic silver (Ag+) as the toxic form of Ag and suggest that intracellular ionic Ag, not the NPs themselves, is responsible for the apparent NP toxicity. The dissolution of Ag+ from Ag NPs within cells and in close proximity to cells in aqueous environments has been proposed to be one mode of action of toxicity of Ag NPs; however, contribution to toxicity from the NPs (themselves) has also been proposed. Higher uptake and larger surface area of Ag NPs can facilitate faster dissolution and release of Ag+. A major challenge is to distinguish precisely what portion of any observed toxicity is from the Ag+ form and what portion is from the Ag NP form (McShan et al., 2014). Smaller particle size is not necessarily correlated with more Ag+ (Yang et al., 2012), suggesting that coatings and interactions with biomolecules can influence dissolution rate.

Studies on the transformation of Ag NPs to other forms of Ag in human or animal tissues are not generally available. Liu et al. (2010) hypothesized that ionic Ag+ might be the form that transports Ag within the body and from which some nanosilver may be reformed in body tissues. Van der Zande et al. (2012) exposed rats to a 28-day oral (gavage) exposure of non-coated Ag NP, PVP-coated Ag NPs or $AgNO_3$. Silver concentrations in examined organs were highly correlated to the amount of free Ag+ in the Ag NP suspension, indicating that mainly Ag+, and to a much lesser extent Ag NPs, passed the intestines in the Ag NP-exposed rats. Ag NPs were detected by ICP-MS in Ag NP exposed rats, and, also in $AgNO_3$ exposed rats, thereby, demonstrating the potential formation of nanoparticles from Ag+ *in vivo* (probably composed of Ag salts).

Recent *in vitro* and *in vivo* studies support that the ionic form of silver is likely more cytotoxic (on a mass basis) than Ag NPs (Reidy et al., 2013). In addition, Ag NP characteristics such as coating(s) and smaller size, influence cellular toxicity in human and animal cells *in vitro*, making it difficult to tease out the toxic moiety. Because Ag NPs shed ionic silver, the release of ionic silver and resistance of NPs to dissolution may be a factor influencing NP toxicity.

Several animal studies indicate toxicity at doses of Ag+ forms, but not at an equimolar Ag NP dose (e.g., Hadrup et al., 2012a). Qin et al. (2017) demonstrated the total Ag content in organs were significantly lower in Ag NP-treated rats than that of $AgNO_3$ treated rats. Both Ag NPs and ionic Ag+ were investigated for potential developmental toxicity (Charehsaz et al., 2016). Because maternal weight gain was lower in dams receiving $AgNO_3$, the authors concluded that Ag+ exerts a higher toxicity compared to the Ag NP form.

In contrast, Gliga et al. (2014) showed that Ag+ release by the Ag NPs in culture medium was not correlated with cytotoxicity but that intracellular release of Ag+ may be involved in the cytotoxic mode of action of Ag NPs. This study also suggested that the genotoxicity of Ag NPs was not fully accounted for by Ag+ release. Thus, the role of Ag+ release, either extracellularly or intracellularly, in the mode of action of Ag NP mutagenicity/genotoxicity is not clear. On a cautionary note, products labelled as containing Ag NPs in solution frequently contain high

concentrations of Ag+, with the amounts not specified (Reidy et al., 2013).

When there are robust studies in the database, the NOAEL and LOAEL (or NOAEC/LOAEC) are the administered dose/concentration of Ag NPs, regardless of the toxic moiety or mechanism of action. Whether the observed adverse effects are attributable to the Ag NP itself or to complete dissolution of the Ag NP to Ag+, the estimation of the LOAEL is the same-administered dose.

The uncertainty that Ag NPs may not be the toxic moiety complicates the determination of dose-response assessment for derivation of the ADI. In cases where data are limited, a series of important questions are raised. For example, if there are not sufficient robust studies to determine the NOAEL/LOAEL for Ag NPs, could one use information from other studies employing Ag+? In fact, answers to questions regarding the toxic moiety become the driver in determining an ADI or safe dose/concentration, such as: Are the observed responses in studies attributable to the Ag NPs or to Ag+, or to some combination of the two? What is the relationship of administered Ag NP to Ag+, particularly if the latter is the potential ultimate toxicant? What is the relative toxicity of Ag NP and Ag+ (i.e., which is more toxic)? What is the rate of dissolution, if dissolution occurs? If the Ag NP partially dissolves to Ag+, how is the LOAEL determined from the administered dose? What is the appropriate dose metric for the observed effect(s)? Can risk assessments for Ag be cross-walked to the assessment of Ag NPs and be protective of human health?

At this time, there are no clear answers to many of these questions and further research is needed (see Section 5.10). For this assessment of ADIs, we have simplistically assumed that Ag NPs are the toxic moiety, they remain intact and that further research is needed before information on other forms of Ag can inform the derivation.

5.9.5 Short-term Oral ADI (14-day)

5.9.5.1 Principal Study and Critical Effect

Short-term studies in humans are available (Munger and coworkers, as described in Section 5.4.1); however, these studies used an elemental Ag colloid formulation and the dose of Ag NPs is unknown, limiting applicability of these data to derivation of the ADI.

The most robust study of appropriate duration is the 28-day study in Sprague-Dawley rats using 98 to 99 percent pure commercial Ag NPs (average particle diameter of 60 nm) and following OECD Test Guideline 407 and GLPs (Kim et al., 2008, cited in Versar, 2012). Doses administered were: 0, 30, 300, or 1000 mg/kg/d. Liver toxicity, increased blood ALP in males, and increased total cholesterol in females are identified as adverse effects at the LOAEL of 300, and the NOAEL is 30 mg/kg/d.

Developmental studies of Ag NP are non-guideline, but the two multiple dose rat developmental studies (with differing NOAEL/LOAELs) indicate maternal toxicity. There is uncertainty as to reproductive effects caused by Ag NP, as some studies indicate no effect and other studies indicate impacts on male reproductive organs and sperm viability, although findings may be related to differences in dose selection and use of coatings. The range of LOAELs for the OECD

guideline reproductive studies is similar to that of the systemic toxicity range. Studies by parenteral routes indicate that Ag NPs may cross the blood-testes barrier and produce severe adverse male reproductive effects. Developmental studies using parenteral routes indicate severe adverse developmental effects.

A traditional NOAEL/LOAEL approach has been taken for derivation of the ADI. Another approach would be to conduct a benchmark dose (BMD) on three endpoints (i.e., ALP, cholesterol, and liver toxicity) from Kim et al. (2008, as cited in Versar, 2012). Incidence data from the original study is needed to conduct benchmark modeling.

5.9.5.2 Adjustment to Human-Equivalent Exposure

No duration adjustment is needed as exposure was for 28-consectuve days. The study duration of 28 days is longer than the 14 days for the short-term ADI, most likely leading to a conservative value.

5.9.5.3 Uncertainty Factors

Uncertainty in the 14-day ADI was accounted for using UFs for animal-human extrapolation, inter-individual variation, and database completeness. No UFs were needed to account for study duration or presumed no-effect dose extrapolation because the POD is a no-effect concentration taken from a 28-day study.

An UF of 3 was used to account for extrapolation from rat to human, primarily for toxicokinetic differences. Although the toxic moiety is uncertain, it is likely similar across mammals. Therefore, an uncertainty factor for toxicodynamic differences between species is not needed as significant differences between mammalian species is not likely to occur at the cellular level with metals (that is, the interaction of Ag, Ag+ or Ag NPs at the cellular level is likely not to vary significantly).

An UF of 3 was used to account for inter-individual variation and sensitive subpopulations in response to ingested Ag NPs. The critical effect is liver toxicity, which occurs in both sexes of rats. While there is likely to be some variability between individuals, the data suggests that the variability in response is not likely sex-related. It is anticipated that it would occur primarily in those persons with preexisting liver disease.

An UF of 10 was used to account for database completeness. This UF was motivated by the following limitations in available data: 1) The method(s) used to determine the characteristics of the test material was not reported; however the authors reported methods in a subsequent 90-day study; 2) only one suitable robust study was available in only one species (rat), although other studies (one in rats and one in mice) report liver toxicity as the critical effect; 3) the database is limited to gavage studies; 4) pertinent data are limited to Ag NP average size of 60 nm; and, 5) information on possible developmental toxicity via oral route is limited. Data from parenteral studies suggest potential reproductive and/or developmental toxicity.

$$\text{ADI} = \text{NOAEL/UF} = (30 \text{ mg/kg/d}) / (100) = 0.3 \text{ mg/kg/d}$$

5.9.6 Long-Term Oral ADI

5.9.6.1 Principal Study and Critical Effect

The most robust study of appropriate duration for a long-term ADI is Kim et al. (2008, reviewed in Versar, 2012), a consecutive 90-day study in Sprague-Dawley rats using 98 to 99 percent pure commercial Ag NPs (average particle diameter of 56 nm) and following OECD Test Guideline 408 and GLPs. Doses administered were: 0, 30, 125, and 500 mg/kg/d. Minimal liver toxicity and pigmentation in intestinal villi were identified as critical effects with a NOAEL of 125 and LOAEL of 500 mg/kg/d. A traditional NOAEL/LOAEL approach has been taken for derivation of the ADI. Another approach would be to conduct a benchmark dose (BMD) on three endpoints (i.e., ALP, cholesterol, and liver toxicity) from Kim et al. (2008, as cited in Versar, 2012). Incidence data from the original study is needed to conduct benchmark modeling.

Although not OECD or GLP guideline studies, two multiple dose rat developmental studies (with differing NOAEL/LOAELs) indicate maternal toxicity. There is uncertainty as to reproductive effects caused by Ag NPs as some studies indicate no effect and other studies indicate impacts on male reproductive organs and sperm viability, although findings may be related to differences in dose selection and use of coatings. The range of LOAELs for the OECD guideline reproductive studies is similar to that of the systemic toxicity range. Studies by parenteral routes indicate that Ag NPs may cross the blood-testes barrier and produce severe adverse male reproductive effects. Developmental studies using parenteral routes indicate severe adverse developmental effects.

5.9.6.2 Adjustment to Human-Equivalent Exposure

No duration adjustment is needed as exposure was for 90 consecutive days.

5.9.6.3 Uncertainty Factors

Uncertainty in the long-term ADI was accounted for using UFs for subchronic to chronic duration, animal to human extrapolation, inter-individual variation, and database completeness. No UFs were needed to account for presumed no-effect dose extrapolation because the POD is a no-effect concentration taken from a 90-day study.

An UF of 10 was used to extrapolate from a 90-day subchronic duration study to a long-term (such as several years or lifetime). This UF contrasts with the 28-day study where the NOAEL is lower than in this 90-day study. Differences in doses used in the studies (0, 30, 300, and 1000 mg/kg/d for the 28-day; whereas, 0, 30, 125 and 500 for the 90-day study) likely contribute to the NOAEL difference. However, because studies are limited to determine the underlying rationale for the NOAEL/LOAEL difference, a 10-fold UF is applied conservatively to protect public health.

An UF of 3 was used to account for extrapolation from rat to human, primarily for toxicokinetic differences. Although the toxic moiety is uncertain, it is likely similar across mammals. Therefore, an uncertainty factor for toxicodynamic differences between species is not needed as significant differences between mammalian species is not likely to occur at the cellular level with metals (that is, the interaction of Ag, Ag+ or Ag NPs at the cellular level is likely not to vary

significantly).

An UF of 3 was used to account for inter-individual variation and sensitive subpopulations in response to ingested Ag NPs. The critical effects are liver toxicity and gastrointestinal alterations, which occur in both sexes of rats. While there is likely to be some variability between individuals, the data suggests that the variability in response is not likely sex-related. It is anticipated that it would occur primarily in those persons with preexisting liver or gastrointestinal disease.

An UF of 10 was used to account for database completeness. This was motivated by the following limitations in available data: 1) this is the only suitable robust study of four in rats (the only species tested at this duration); and, 2) information on possible developmental toxicity via oral route is limited. Data from parental studies suggest potential reproductive and/or developmental toxicity.

ADI = NOAEL/UF = (125 mg/kg/d) / (1000) = 0.125 (or 0.1) mg/kg/d

Other oral assessments of chronic exposure are based on Ag and not Ag NPs (EPA, 2017a; Danish EPA, 2015a; NIOSH, 2015). A risk assessment on nano Ag by the Danish EPA (2015b) considered argyria as the critical effect following oral exposure to silver; no relevant long-term studies were identified. The risk assessment was based on the presumed mechanism that the Ag NP dissolves in solution, continually releasing Ag+, which accumulate and cause argyria.

5.9.7 Short-term Inhalation ADI (14 days)

Available data are insufficient to derive a 14-day ADI for the inhalation route. There are two four-week studies in Sprague-Dawley rats; one was according to OECD Test Guideline 412 and GLP (Ji et al., 2007a; Hyun et al., 2008; as reviewed in Versar, 2012) and both studies were performed by the same laboratory. Both studies report a NOAEC of 61 μg/m^3 (the highest dose tested) and no LOAEC.

5.9.8 Long-term Inhalation ADI

Available data are insufficient to derive a long-term ADI for the inhalation route. The inhalation database is comprised of one 13-week study (Sung et al. [2008, 2009]; as reviewed in Versar, 2012) conducted by the same group of investigators as the shorter-term inhalation studies (in Section 5.9.7). Functional alterations and inflammation in the lung and hyperplasia in the bile duct were reported at the LOAEC of 515 μg/m^3; the NOAEC was 133 μg/m^3. The study follows OECD Test Guideline 413 and GLP, but uses a unique strain of rat bred by the investigators, making the reproducibility of the study results questionable.

The only study evaluating reproductive endpoints was a 13-week systemic toxicity study (Sung et al., 2009), in which reproductive organ weights were not altered (reproductive function was not evaluated) at 515 μg/m^3 (NOAEC; no LOAEC).

5.9.9 Short-term Dermal ADI (14 days)

Available data are insufficient to derive a 14-day ADI for the dermal route. One dermal study of commercial Ag NPs was conducted in pigs for 14 days duration (Samberg et al. 2010; cited in Versar, 2012). The dermal NOAEL was 34 µg/mL (the highest dose tested); no LOAEL was identified.

5.9.10 Long-Term Dermal ADI

5.9.10.1 Principal Study and Critical Effect

Available data are insufficient to derive a long-term ADI for the dermal route. No human or animal studies were located in the current literature search on the possible systemic toxicity with chronic (lifetime) dermal exposure to Ag NPs, nor were any studies identified in Versar (2012). No studies were located using the dermal route of exposure to evaluate reproductive or developmental toxicity.

Two dermal studies in guinea pigs (Korani et al., 2011; Korani et al., 2013) conducted by the same laboratory considered the LOAEL as 100 µg/mL; no NOAELs were identified following exposure to guinea pigs of nanosilver (less than 100 nm by TEM) for five days/week for 13 weeks at 0, 100, 1000, or 10,000 µg/mL. A 100 µg/mL solution of $AgNO_3$ served as a positive control. Although no incidence data were reported, the dermal LOAEL was based on histopathologic abnormalities in the skin, liver, and spleen in all test groups. Subsequently, in an OECD test guideline study, Korani and coworkers (2013) compared the tissue levels of Ag NPs in guinea pigs after dermal application of the same concentration and size Ag NPs, with the same positive control, for 13 weeks (presumably for 5 d/wk, although not specified in the report). The three different Ag NP concentrations gave comparable results for several endpoints measured in heart, bone and kidney. No incidence data were reported; however, the dermal LOAEL of 100 µg/mL was based on histopathologic abnormalities in the skin, liver and spleen. While the data may be amenable to the determination of an ADI, the uncertainty in the long-term value based on a LOAEL from this subchronic study in an incomplete database is extremely large and confidence in the ADI would be very low.

5.10 Research Needs and Data Gaps

5.10.1 General Research Needs

Derivation of ADIs for Ag NPs remains challenging, with generally high uncertainty due to a paucity of studies, particularly of chronic duration. The existent studies are limited by lack of reliable, quantitative dose-response data.

The association of the physicochemical properties of Ag NPs with their toxicity is an area needing further study. Physical and chemical properties of Ag NPs are factors that influence cytotoxicity. Understanding the mechanism and the magnitude by which these factors may alter toxicity requires further research. Further study of the factors that may influence the outcome of *in vivo* assays with Ag NPs, such as dosing regimens, Ag NP characteristics such as particle size

and coating, effect of dispersion method on aggregation, assay methodology, vehicle used, presence of contaminants, and protein corona surrounding the NP would be useful.

There is a lack of human data for toxicokinetics of Ag NPs via oral, inhalation and dermal exposure, particularly for rate and extent of absorption. Toxicokinetic studies in animals are available for oral, inhalation and parenteral exposures, but the form of Ag in tissues is not routinely identified and the primary method of oral exposure is by gavage, which may not be relevant with consumer oral exposures. Route-specific differences and rates in biokinetics is an important area for research. Studies on the transformation of Ag NPs to other forms of Ag in human or animal tissues are not available. Some studies in animals via oral exposure to Ag NPs have noted gender differences in distribution between males and females, with females accumulating more than males; this line of research should be pursued. Distribution of Ag reported by parenteral routes of exposure have not been corroborated by oral, inhalation or dermal routes leaving a gap in scientific knowledge. Similarly, numerous studies indicate that Ag NPs or Ag+ that reach the bloodstream, also enter maternal tissues, extra-embryonic tissues, breast milk, and to a limited extent, the embryo. Kinetic studies related to transfer across the blood-brain barrier, blood-testes barrier, and transplacental transfer are generally lacking.

Robust, repeat-dose, multi-dose studies with Ag NPs are lacking in more than two species for oral and inhalation routes (mice and rats), and dermal route (pigs and guinea pigs). Many of the existing studies have limitations in the animal number, dosing period, dosage level, and number of groups.

No chronic duration systemic toxicity studies, carcinogenicity studies, or robust developmental or reproductive studies, in humans or animals were located, making it challenging to derive ADIs with high confidence.

Much of the genotoxicity data are too limited to make definitive conclusions concerning the overall *in vivo* mutagenicity of Ag NPs as a class of materials. Often differing results are reported; the reason is unclear. Further study of the factors that may influence the outcome of *in vivo* assays with Ag NPs, such as dosing regimens, Ag NP characteristics such as particle size and coating, effect of dispersion method on aggregation, assay methodology, vehicle used, and route-specific differences is needed.

The causative agent (toxic moiety) and the mechanism of action for the toxicity of Ag NPs is not known. Research has been directed at discerning whether the NPs themselves cause toxicity or whether Ag ions dissociated from the Ag NP may be the toxic moiety. Similarly, several events have been postulated to be involved in the adverse outcome pathway for Ag NPs: interaction with cellular proteins, ROS, inflammation, cell death and genotoxicity. The role of coatings, aggregation, and NP size, while thought by some to contribute to toxicity, have not been teased-out of the milieu of possible factors.

Lack of understanding of human exposure from consumer products, particularly via the oral and dermal routes, makes it unknown how applicable the derived ADIs are to consumer scenario.

5.10.2 Specific Research Needs

Determination of ADIs for Ag NPs require additional data in the following areas:

- Studies using the form of Ag NPs used in consumer products (i.e., pure, functionalized)
- Toxicokinetic and toxicodynamic studies in humans and guideline study animal species
- Studies in humans, including sensitive subpopulations of consumers
- Studies on the impact various diseases (e.g., liver, gastrointestinal and skin) have on toxicity of Ag NPs
- Robust multi-dose, characterized Ag NP, short-term and repeat-dose studies of subchronic duration in species other than rat that identify NOAELs and LOAELs
- Chronic duration studies via oral, inhalation, and dermal routes
- Robust developmental and reproductive studies

6 TOXICITY DATA FOR TITANIUM DIOXIDE

6.1 Physical and Chemical Properties of Titanium Dioxide (TiO2)

6.1.1 Introduction

Appropriate and rigorous physicochemical characterization of nanomaterials used in toxicity testing is essential for data interpretation, comparisons between studies, and conclusions regarding hazard (Oberdorster et al., 2005 [as cited in Versar 2012]; Card and Magnuson, 2010; Castranova 2011). The U.S. EPA (2007; as cited in Versar, 2012) reported that understanding the physical and chemical properties of nanomaterials is a requirement in the evaluation of all routes of toxicological exposure and hazard. Chemical properties such as vapor pressure, boiling point, molecular weight, and other properties may not be important for some nanomaterials. Physical and chemical properties relevant to nanomaterial toxicity include properties such as shape, crystal structure, particle size distribution, agglomeration state, surface area, surface chemistry, surface charge and porosity of the nanomaterial (Oberdorster et al., 2005; U.S. EPA, 2007). In addition, solubility in media related to toxicity testing may be critical in assessing toxicity specific to the nanoscale characteristics of the nanomaterial as used in products (OECD, 2016a). Table 26 lists the physicochemical characteristics of commonly manufactured TiO2.

6.1.2 Crystal Structure and Shape

Titanium dioxide (CASRN 13463–67–7), is a noncombustible, white, crystalline, solid, odorless powder (PubChem, 2017). It is highly insoluble in water, hydrochloric acid, nitric acid or alcohol and is generally regarded as an inert substance. Crystalline morphological forms of TiO2 NPs differ in optical and photocatalytic properties. Common TiO2 polymorphs include rutile (CASRN 1317–80–2) and anatase (CASRN 1317–70–0). While both rutile and anatase are tetragonal crystals, rutile has a denser arrangement of atoms. For example, rutile, which is used in sunscreens, is considered to be a more inert morphological form than anatase, which is used in photocatalytic, catalytic, and sensing applications (Rossi et al., 2010). Brookite, an orthorhombic crystal, is a third variant of TiO2, exhibiting photocatalytic activity, and is used in antifogging mirror sprays. Ilmenite is titanium-iron oxide (FeTiO3) and is the main source of mineral TiO2. Most of the available toxicological data for TiO2 in the current literature are on the rutile and anatase forms.

Titanium dioxide has also been produced as engineered nanomaterials, which may be equidimensional crystals or sheets and are composed of either TiO2-rutile or TiO2-anatase. Titanium dioxide NPs can be precisely engineered and highly characterized based on shape, such as nanorods, nanobelts, nanowires, spheres, shells, tubes, fibers; and, functionalization (https://nanocomposix.com/collections/titanium-dioxide-NPs).

The shape of the TiO2 NP may influence biological activity and toxicity. For example, the potency for pulmonary inflammation and damage from exposure was compared following treatment via OPA with nanospheres, or short nanobelts or long nanobelts of varying lengths and widths (Porter et al., 2012). Development of pulmonary fibrosis was noted with the nanobelts but not the nanospheres. Similarly, Silva and coworkers (2013) concluded that the particle shape (TiO2-nanobelts) was the most important physico-chemical property for toxicity (lung

inflammation) by IT.

6.1.3 Particle Size

Titanium dioxide particles are referred to as primary, aggregates or agglomerates. Primary particles are single crystals that are bound by crystal planes. Aggregates and agglomerates are held together by van der Waal's forces.

Commercial application affects the size of the NP. For example, light scattering by TiO2 is maximized in particles that are 0.2 to 0.3 μm in diameter, and most commercial products that are used as pigments have modal primary particle sizes within this range. Non-pigmentary TiO2 is composed of either uncoated manufactured TiO2 (both TiO2-anatase and TiO2-rutile) or ground natural rutile. In general, these products contain coarser particles than pigmentary TiO2 (Linak et al., 2002). Ultrafine TiO2 particles (NPs) range in size from 1 to 150 nm, with a primary particle size of 10 to 50 nm. Primary particles generally form aggregates and agglomerates and are not normally found as discrete particles. In commercial products, the particle size of pigmentary and ultrafine material is approximately equal because of aggregation and agglomeration (American Chemistry Council, 2005).

Due to its high diffraction index and strong light scattering and incident-light reflection capability, TiO2 is used as white pigment. It is these properties, as well as high UV resistance, that make TiO2 the standard white pigment found in white dispersion paints (ASTM, 1988). Since light scattering does not occur to a greater extent in nanoscale particles, the white TiO2 pigments used are almost exclusively rutile modification particles with grain sizes in the μm range. These white pigments are used for their opacity in paints and dyes but also in varnishes, plastics, paper, inks and textiles. Having “E number” E171, these pigments are used as food additives and occur in toothpastes, several cosmetics, and drugs. E numbers are codes for substances that are permitted to be used as food additives for use within Europe. Titanium dioxide pigments for use in plastics constitute the fastest growing market. It is primarily due to the packaging industry’s strong demand that consumption of TiO2 pigments are on the increase (Mackevica and Foss Hansen, 2016).

Nanoscale TiO2 is manufactured for specific applications by using 100x finer particle size than the low μm sized TiO2 pigments and thus have other unique physical properties than those of pigment TiO2. Unlike TiO2 pigments, nanoscale TiO2 are not used as food additives (Winkler, 2003); instead, they are mainly found in high-factor sun protection creams, textile fibers or wood preservatives (Hsu and Chein, 2007). At present, high sun protection factors can only be achieved using nanoscale TiO2 (Wijnhoven et al., 2009).

Titanium dioxide NPs are often synthesized in the investigator’s laboratory and used in various sizes including fine particles with the size of approximately 0.1 to 2.5 μm and nanosize particles with the primary size of less than 0.1 μm. Nanoparticles synthesized in the laboratory may be difficult to reproduce by other investigators and may have little relevance to commercialized forms of TiO2 (which are more standardized) used in consumer products, but are reported in the literature in toxicity and mechanistic studies. The source of the test material (i.e., synthesized by the investigator or commercially purchased, when available) for each citation is noted in the study description.

6.1.4 Surface area

The surface area of the NP is related to its size or mass. Smaller particles have a much greater surface area per unit mass, than larger particles. As surface area per mass of a material increases, a greater amount of the material can come into contact with surrounding materials, affecting reactivity (USNNI, 2017). A benefit of greater surface area, and improved reactivity, in nanostructured materials is that they have greater catalytic function.

Aggregates and agglomerates have much greater total surface area than spheres of the same external diameter, due to the complexity of their structure with adsorbed molecules. Surface areas of nano-TiO2 primary particles, aggregates, and agglomerates can also be expressed as total surface area (or external surface area). The surface area is quantitated utilizing probing gases that do not chemically react with material surfaces. The total surface area of agglomerates or coated NPs is measured by the Brunauer, Emmett, Teller (BET) method (Brunauer et al, 1938).

6.1.5 Coatings

Titanium dioxide products may be coated with additional materials to achieve different properties for commercial applications. With the exception of non-pigmentary TiO2, such as ground rutile and anatase that are used as food additives, all commercially-produced TiO2 is coated. These coatings improve dispersibility, dispersion stability, opacity, durability and gloss. They form a barrier between the TiO2 and organic substances, such as those found in paints, and prevent contact catalysis. Rutile pigments generally contain 1 to 15 percent of coatings and anatase pigments contain 1 to 5 percent of coatings. The most common coatings are composed of oxyhydrates and oxides of aluminum and silicone. Oxides and oxyhydrates of zirconium, tin, zinc, phosphorous, cerium and boron are also used (Linak et al., 2002).

The thickness of coatings is variable, but is generally only a few atom layers thick; and are generally coherent over the surface of the TiO2 particle (American Chemistry Council, 2005), but some TiO2 and titanium hydroxide may be present on the surfaces (Braun, 1997). The thinness of the coatings precludes most techniques of structural analysis and their atomic structure, therefore, remains largely unknown (Braun, 1997). Silica coatings are fluffy, and consist of polymerized silicic acid. Coating with alumina and silica can more than double the surface area (Braun, 1997). The surface area of untreated pigment ranges from 8 to 10 m^2/g. Treated pigment surface areas generally range from 8 to 19 m^2/g and matte-finish pigments (that have high levels of alumina) can extend up to 35 m^2/g. Surface areas of ultrafine products are in the range of 35 to 100 m^2/g (American Chemistry Council, 2005). Coated TiO2 particles and pigments, other than silicone-coated particles, are hydrophilic.

6.1.6 Other Characteristics

Water forms a closed film on the surface of TiO2-containing products due to the hydrophilic properties of nanoscale TiO2 (Kaegi et al., 2008). House paints or tiles containing TiO2 particles are self-cleaning (scaling) and pollutant-degrading (so-called “anti-fog coatings”). The ultra-thin water film on a glass pane coated with a transparent layer of nanoscale TiO2 impedes the formation of water droplets.

Zeta potential describes the electric potential between the surface of a nanomaterial (or associated groups thereon) and the suspension medium. Negatively charged cell membranes can interact more easily with positively charged nanomaterials, making them potentially more toxic than neutral or negatively charged nanomaterials (Cho et al., 2012). Ionic solution strength and pH affect NP dispersion properties. Increasing TiO2 NP surface area results in a decrease in solution pH. At fixed pH, increasing the particle surface area enhances the collision frequency between particles and leads to a higher degree of agglomeration. In addition to the synthesis method of TiO2, the isoelectric point (IEP) is dependent on particle size. The IEP is the pH at which a particular molecule carries no net electrical charge. For anatase TiO2, particles of size 6, 16, 26, 38, 53, and 104 nm, the IEP decreased from 6.0 to 3.8 resulting in changes in dispersion, Zeta potential and hydrodynamic size. The hydrodynamic size gives information on the inorganic TiO2 core along with any coating material and the solvent layer attached to the particle. TiO2 NP IEP was found to be insensitive to particle crystal structure (anatase vs. rutile).

6.1.7 Summary

The biological activity of TiO2 NPs will depend on physicochemical parameters not routinely considered in toxicity screening studies. Physicochemical properties that appear important in understanding the toxic effects of TiO2 NPs are: dissolution rates, (or solubility), particle size and distribution, agglomeration state (mass), shape, crystal structure, chemical composition, surface area, surface chemistry, surface charge, and porosity. Until the mechanism(s) of toxicity are more fully understood, it will be necessary to ensure that TiO2 nanoscale characteristics are measured or can be determined in toxicity screening tests. In as far as it is possible, it is desirable to collect sufficient information to allow retrospective interpretation and comparison of toxicity data in the light of new findings.

Table 26. Physiochemical Characteristics of Some Commonly Manufactured TiO2 (Titania)[a]

TiO2 Name	Use	Shape	Crystal Structure	Coating	Surface Area (mg^2/g)	Primary Diameter Size (nm)	Comment
NM-100 (Bulk comparator)	JRC repository	tetragonal	anatase	uncoated	9.23	---	Tiona AT-1 (non-nano reference)
NM-101 (Hombikat UV 100)	JRC repository	tetragonal	anatase	uncoated	169.5	130	Research grade; largest agglomerates (140 to 150 nm)
NM-102 (PC105)	JRC repository	tetragonal	anatase	uncoated	65.6	140	Research grade; largest agglomerates (140- to 50 nm)
NM-103 (UV TITAN M262)	JRC repository	tetragonal	rutile	PDMS	51.1	95	Research grade; smallest agglomerates (80 to 90 nm)
NM-104 (UV TITAN M212)	JRC repository	tetragonal	rutile	Al-Si	52.4	80	Research grade; smallest agglomerates (80 to 90 nm)
NM-105 (Aeroxide® P25)	JRC repository	sphere	anatase-85% rutile-15%	uncoated	47.0	26.1 ± 1.3	Research grade
E171 (Europe); Synonym for Pigment White 6	Pigmented colorant when used in foods	ortho-rhombic	rutile or anatase	no	10 for anatase	110 ± 17	36% of particles less than100 µm
Pigment White 6 (CI 77891)	Paints	ortho-rhombic	rutile or anatase	no	6.137 for anatase	200 to 350	white pigment and opacifier
AMT-100	Photocatalysis	sphere	anatase	no	100 to 120	6	teeth whitener
AMT-600	Photocatalysis	unknown	anatase	no	52	30	deodorizes, disinfects
TITANIX JA-1	Pigment grade	unknown	anatase	no	9	180	circuit boards
MT-150AW	Cosmetics	spindle	rutile	stearic acid	100 to 120	19.5 by 2.6	lipstick
MP-100	Photoshield	sphere	rutile	no	6	289 to393	sunscreen
TTO S-3	UV-shielding	spindle	rutile	no	12	10 to 20 by 41.2 to 48.9	transparent sunscreen
				$Al(OH)_3$	102		
FTL-100	Reinforcement	needle	rutile	no	12.0	89.8 to 393	mechanical strength
5430MR	Pigment, UV-shielding	sphere	anatase	no	240	15	reagent
Ti-Pure™ R-105	White pigment for PVC windows; Portland cement	unknown	rutile	Al-Si	unknown	200 to 300	UV stabilization of synthetic paper
Nanovation AG Product 1.1	Reference material	irregular spheres	95% anatase 5% rutile	surface organic molecules	117	17	Federal Ministry of Education and Research

TiO2 Name	Use	Shape	Crystal Structure	Coating	Surface Area (mg^2/g)	Primary Diameter Size (nm)	Comment
Evonik Degussa Product 1.2	Reference material	tetragonal	anatase rutile	uncoated	52	272	Dr. Christoph Steinbach, DECHEMA e.V. Theodor-Heuss-Allee 25 60486 Frankfurt a,M. Germany
Evonik Degussa Product 1.3	Reference material	tetragonal	anatase rutile	uncoated	38	42.3	
Evonik Degussa Product 1.4	Reference material	tetragonal	anatase rutile	uncoated	63	33.4	
Evonik Degussa Product 1.5	Reference material	tetragonal	anatase rutile	uncoated	115	12.5	

[a]Source: Compiled from multiple sources cited in above text

6.2 Toxicokinetics of Nano TiO2

Due to the extensive application of TiO2 NPs and their inclusion in many commercial products, the exposure of humans to NPs is possible via oral, inhalation or dermal exposure during contact with consumer products. As a crystalline solid, the metabolic transformation of TiO2 morphological forms (i.e., rutile, anatase, brookite, ilmenite; refer to Section 6.1) in mammalian systems is unlikely and has not been a focus of research (see also Versar, 2012). Similarly, there is little information on the excretion of TiO2. Thus, this section will focus primarily on the absorption and distribution of TiO2 in humans and animals.

6.2.1 Oral Exposure

There are limited human and animal data for the oral ingestion route of exposure to TiO2 NPs. Some sources are intentionally designed components of food products (e.g., TiO2 particles functioning as whiteners), as well as food supplements, flavor enhancers, and other pigments. It should be noted, however, that most of the TiO2 particles consumed in food applications are of the pigment-grade form (i.e., greater than 100 nm) and not in the NP size range (Winkler, 2003). While sources of exposure from TiO2 NPs intentionally added to food or drinks or in pharmaceutical capsules are not within the purview of CPSC, nor within the scope of this project, TiO2 NPs in food and drink containers (or container parts) that may contain pigment-grade TiO2 particles that could leach or otherwise contaminate the food or drink is of concern to CPSC. As discussed in Section 3, nano release is a recent topic of research in the nanomaterial field and these types of data for TiO2 do not appear to be readily available, although they were not specifically searched for this project.

Jones et al. (2015) conducted human *in vivo* and *in vitro* studies on the gastrointestinal absorption of NPs, using TiO2 as a model compound, and to compare NP behavior with that of larger particles. Nine volunteers (four males, five females, age range 30 to 56 years) received a 5 mg/kg single oral dose of a commercially available TiO2 dispersed in water. The sizes (TEM) of the TiO2 were 15 nm (100 percent anatase), 100 nm (95 percent rutile) and ~5 μm (100 percent rutile). Very little TiO2 was absorbed (less than 0.1 percent administered dose) via the gastrointestinal tract. Absorption for the three particle sizes tested was similar. All tested formulations were shown to agglomerate in simulated gastric fluid. Less than 0.02 percent of the dose penetrated a colorectal cell line during *in vitro* testing. This study found no evidence that nanoparticulate TiO2 is more likely to be absorbed in the gut than micron-sized TiO2 particles.

Seven human volunteers with normal intestinal permeability were orally administered capsules of pharmaceutical/food grade TiO2 containing 50 mg anatase for a total of 100 mg (diam 50 to 260 nm) (Pele et al., 2015). Blood samples were collected at 0 (baseline) and from 0.5 to 10 hours post ingestion and analyzed for the presence of reflectant bodies (particles) by dark field microscopy and for total Ti by ICP-MS. Blood analyses implied early absorption of particles; particle uptake started early (i.e., by two hours following ingestion) and peaked later (i.e., six hours following ingestion). The presence of the reflectant NPs in blood roughly mirrored the levels of total Ti by ICP-MS, providing good evidence for the latter being a measure of whole particle (TiO2) absorption. The authors concluded, this pattern of early uptake with a later peak may be explained by some absorption in the proximal small intestine (duodenum/jejunum) with

later Peyer's patch uptake in the more distal small intestine (ileum). This study showed that a fraction of pharmaceutical/food grade TiO2 is absorbed systemically by humans following ingestion. It confirms that at least two areas of particle uptake may exist in the human gut- one proximal and one distal.

Qualitative evidence of oral absorption and distribution to tissues is reported from elevated Ti concentrations in several organs in CD-1 (ICR) mice two weeks after administration of single nonlethal 5 g/kg doses of various commercial TiO2 suspensions (Wang et al., 2007b, as cited in Versar, 2012). Titanium concentrations in tissue samples (ng Ti/g tissue) were determined by ICP-MS. Mean Ti concentrations were elevated in some forms of TiO2 in spleen, kidney, liver and brain, but not RBCs, relative to vehicle-exposed control mice two weeks post-exposure.

Cho and coworkers (2013) observed very low absorption when they administered purchased TiO2 NPs by gavage to six-week old male and female Sprague-Dawley rats for two or 13 weeks (seven d/wk). The TiO2 were 80 percent anatase-20 percent rutile NPs, with a primary size of 21 nm and surface area of 50 ± 15 m^2/g. Eleven rats were assigned to each of four treatment groups: vehicle control (distilled water) and TiO2 NPs at 260.4, 520.8, or 1041.5 mg/kg/d (suspended in distilled water and administered at 10 mL/kg bw). Immediately after gavage, urine and feces samples were collected for 24 hours from five animals/group and analyzed for Ti concentration by ICP-MS. The blood concentrations of TiO2-treated male rats (but not females) showed a shallow, gradual increase of Ti with dose. TiO2-treatment groups showed no significant increase of Ti in sampled organs, low urinary Ti concentration, and high fecal Ti concentrations compared to the vehicle control group, demonstrating TiO2 NPs had extremely low absorption by the oral route.

Tissue distribution and blood kinetics of various TiO2 NP suspensions (NM-100, NM-101, NM-102, NM-103, and NM-104), which differed with respect to primary particle size, crystalline form and hydrophobicity, were investigated in adult male and female Wistar rats, six days after oral gavage for five days (Geraets et al., 2014). The resulting exposure suspension concentration was 2.304 mg/mL TiO2 (per the author, a low and realistic human dose level based on personal care product data from Weir et al., 2012). The European Commission's Joint Research Centre (JRC) characterized standard physico-chemical properties of manufactured nanomaterials of TiO2 with NM-100, included in the series as a bulk comparator (Rasmussen et al., 2014). All TiO2 containing suspensions for the Geraets et al. (2014) study gave reliable agglomerate/aggregate results (between 80 to 150 nm). Suspensions of rutile NM-103 and NM-104 contained the smallest agglomerates/aggregates (80 to 90 nm), whereas the largest were observed with anatase NM-101 and NM-102 (140 to 150 nm). NM-101 and NM-102 showed a bimodal size distribution with another much less frequent distribution of ~1µm. No particles were observed between 3 and10 µm for any of the materials. All liver and spleen tissue samples (NM-101: male and females; NM-102, NM-103 and NM-104: males) contained very low Ti levels (mostly below the LOD of 0.03 µg/g), while all samples of mesenteric lymph node tissue contained amounts above the LOD (0.07 µg/g tissue or 0.11 µg/tissue for the whole node). The results indicated that absorption of TiO2 after oral administration was very low.

In studies designed to evaluate genotoxicity of TiO2 NPs, indirect support for absorption and systemic distribution of TiO2 to femoral bone marrow was found after oral gavage in mice (Sycheva et al., 2011) and rats (Chen et al., 2014b; Grissa et al., 2015).

6.2.2 Inhalation Exposure

6.2.2.1 Deposition and Clearance of NPs

Both fine particles with diameters in the 1 to 2.5 μm range and NPs (with at least one dimension less than 100 nm), can be inhaled and deposited in the oral and nasal cavities, the tracheal/bronchiole region of the lung, and the alveolar region of the lung (Kreyling et al., 2002). In fact, all compartments of the respiratory tract are targeted by both inhaled fine and ultrafine particles; it is only the amount which is deposited in different regions that varies (ICRP, 1994). Figure 2 shows how deposition fraction in humans varies with the diameter of the particulate matter. Little deposition occurs with particles much above 10 microns in diameter. A bi-phasic deposition occurs with lower diameter particles.

Several authors (Geiser et al., 2008; Kreyling et al., 2002; Oberdörster, 1988) have discussed NP deposition and clearance. These are briefly summarized as cited in Versar (2012) below; details of the studies are presented in full in Versar (2012). To reiterate, NPs deposited in the alveolar region of the respiratory tract may be cleared from the alveolar region by: (1) macrophage phagocytosis and mucociliary transport along the tracheobronchial tree to the GI tract, (2) translocation into interstitial tissue, (3) translocation to the lymphatic system, (4) particle dissolution with subsequent absorption into lung cells and transport into the blood (a very limited process for TiO2 particles given the *in vivo* insolubility of TiO2), and (5) translocation of the particles into lung cells from lung surfaces and possible transport into the blood. Clearance from tracheal/bronchiole regions may occur by similar pathways. Nanoparticles deposited in the nasal mucosa also may be subject to particle dissolution and absorption into the blood (again, not likely with insoluble TiO2) or direct translocation into the olfactory bulb of the brain via the olfactory nerve; however, translocation of NPs from the olfactory bulb to other brain regions is poorly studied (Oberdörster et al., 2004).

6.2.2.2 Translocation of Inhaled TiO2 NPs

Approximately 20 percent of TiO2 NPs detected by energy-filtering TEM in alveolar lung regions were located within and beyond the epithelia immediately, or at 24 hours, following one-hour exposure of male WKY/NCRl BR rats to a TiO2 concentration of 0.11 mg/m^3, corresponding to a mean number concentration of 7.3×10^6 (SD 0.5×10^6) $particles/cm^3$ (Geiser et al., 2005; as cited in Versar, 2012). The remaining percentage of detected particles was located on the luminal side of the airways and alveolar epithelium (79.3 ± 7.6 percent), 4.6 ± 2.5 percent within epithelial or endothelial cells, 4.8 ± 4.5 percent within the connective tissue, and 11.3 ± 3.9 percent within the capillaries. The 22 nm aerosol particles were agglomerates of smaller primary particles with estimated diameters of 4 nm.

The observation of particles in alveolar capillaries provides qualitative evidence that translocation to the blood occurred. A subsequent analysis of the data, which related the number of particles in the various lung compartments with compartment size, indicated that particles were preferentially translocated to connective tissues immediately after exposure and to

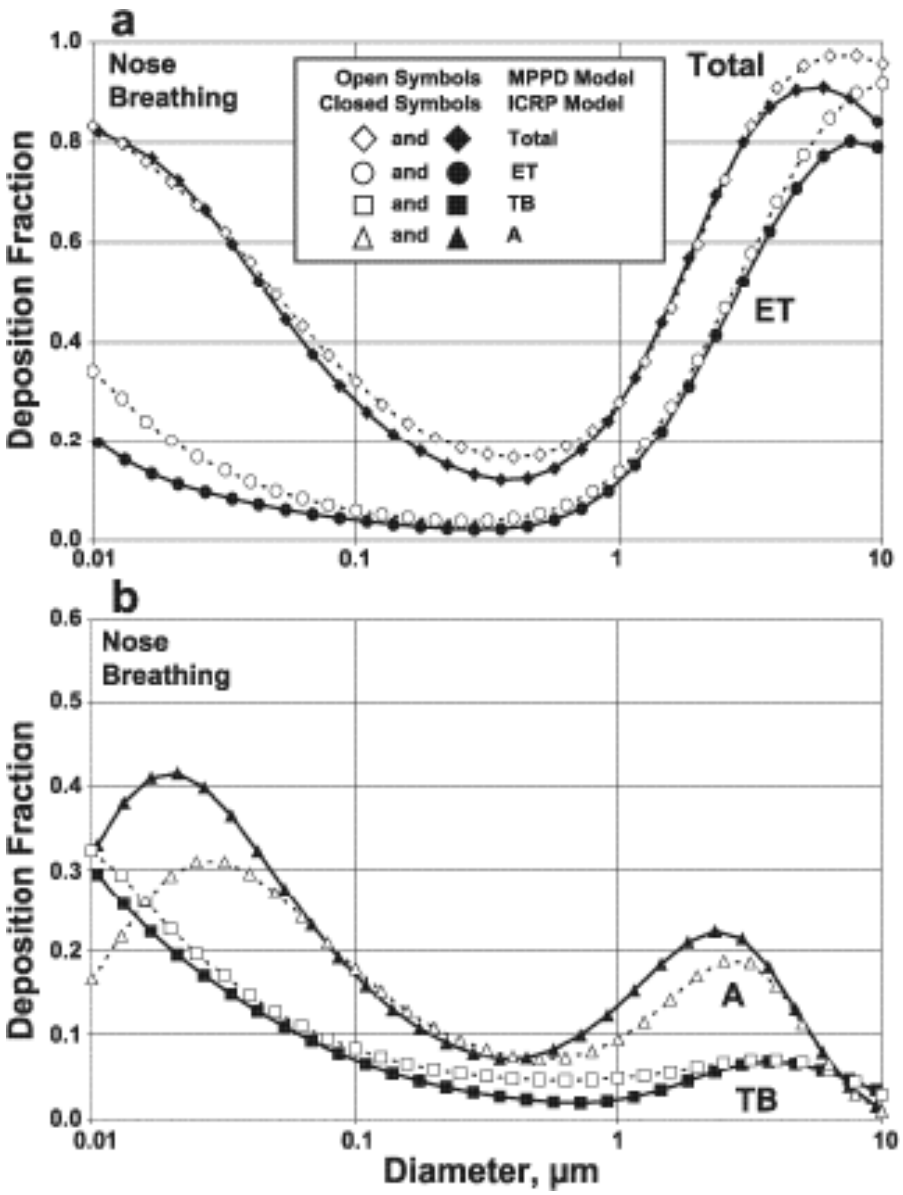

Figure 2. Human deposition patterns
A = alveolar deposition; ET = extrathoracic deposition; TB = tracheal-bronchiolar deposition

the capillary lumen at 24 hours after exposure (Muhlfeld et al., 2007; as cited in Versar, 2012). Particles detected within cells were not membrane bound, suggesting that the particles entered cells via a non-endocytotic mechanism (Geiser et al., 2005). This observation was contrary to other observations of membrane-bound agglomerations of TiO2 particles within human epithelial cells (reported average diameter of primary particles ≈50 nm; crystal structure not specified) (Stearns et al., 2001). The *in vivo* results suggest that, under the low-concentration, low-agglomeration conditions as in the study by Geiser et al. (2005), at least 20 percent of poorly

soluble TiO2 NPs deposited in the peripheral lung are absorbed into lung tissue via a mechanism that may not involve endocytosis. Other studies of the extent or rate of respiratory tract absorption of inhaled TiO2 NPs were not located in the literature searched for Versar (2012) nor for this report.

Uptake of TiO2 NPs by pulmonary macrophages was studied by Rossi et al. (2010; as cited in Versar, 2012). Absorbed NPs are able to cross the pulmonary epithelium (translocate) and reach the interstitium, blood, and other organs, such as the liver, heart, and brain (Oberdorster, 2002). Agglomerations (typically greater than 100 nm in size) of TiO2 particles were observed by light microscopy and TEM in membrane-bound organelles (phagosomes) within pulmonary macrophages of mice (Rossi et al., 2010; as cited in Versar, 2012). The MMADs for the aerosols generated in this study were not reported, but the aerosol aerodynamic size distribution range was reported to be 15.9 nm to 10 µm. Most aerosol particles were reported to show MMAD in the µm size. Containment of the particles within organelles suggests that macrophages may have engulfed the deposited particles via an endocytic mechanism. In contrast, following exposure to aerosols made from silicon dioxide (SiO_2)-coated rutile TiO2 NPs, most particles were observed in the macrophage cytosol, and phagosomes were absent. This observation was interpreted to suggest that the phagosomes were destroyed and the internalized NPs were released to the macrophage cytosol.

6.2.2.3 Lung Deposition and Clearance Kinetics

No studies were located in the literature searched examining lung deposition and clearance kinetics following exposure to nanosized aerosols of TiO2. Several studies have compared lung deposition and clearance in animals exposed by whole body inhalation to aerosols made from TiO2 -fine particles with diameters greater than 100 nm and ultrafine (i.e., nano) particles with diameters less than 100 nm (Bermudez et al., 2004, 2002; Oberdörster et al., 1994; Ferin et al., 1992; all as cited in Versar, 2012). However, regardless of particle size of the starting materials, the MMADs of aerosols used in these studies (about 0.7 to 1.4 µm) were similar and outside of the NP size range. The results indicated that exposure to microsized aerosols made from NPs results in similar lung deposition burdens, but particle size of the starting material affected lung clearance kinetics.

Bermudez et al. (2002, 2004; as cited in Versar, 2012) exposed rats, mice, and hamsters for 13 weeks with a 52-week recovery to 0.5, 2.0, or 10 mg/m^3 in whole-body chambers to aerosols of P25 TiO2 NPs (Bermudez et al., 2004) or to 10, 50, or 250 mg/m^3 of aerosols of fine (pigmentary) particles with similar respective MMADs (and GSDs) (Bermudez et al., 2002; as cited in Versar, 2012). Although MMADs for aerosols generated from nano- and micro-sized TiO2 particles were within the same range, differential effects were observed for the two particle types:

> (1) Similarly sized aerosols (NP or fine particle) showed similar TiO2 lung burdens, but total lung clearance during the 64-week recovery period was slower for NPs ($t_{1/2}$ = 501 days) compared with fine particles ($t_{1/2}$ = 174 days). In addition, a greater proportion of the TiO2 mass in the lungs was in the hilar lymph nodes immediately following NP exposure compared with fine particle exposure (Oberdörster et al., 1994; Ferin et al.,

1992; as cited in Versar, 2012). For both particle types, 93 percent was cleared from the alveolar space within one-year post-exposure. For NPs, a large fraction (44 percent) of the cleared alveolar mass appeared in the interstitial space during the post-exposure period. A smaller fraction appeared in the interstitial space (13 percent) following exposure to fine particle aerosols, which were presumably cleared to a larger extent via the GI tract.

(2) Exposure-dependent TiO2 mass lung burdens were similar between rats and mice, but were approximately two to five-fold lower in hamsters (Bermudez et al., 2004; as cited in Versar, 2012). Total lung retention half-times were longest in the rats and shortest in the hamsters. Similar species differences in lung deposition and lung retention kinetics were noted with aerosols made from fine TiO2 particles (Bermudez et al., 2002; as cited in Versar, 2012).

A few observations in rats following inhalation exposure to aerosols of TiO2 NPs suggest that macrophage-mediated clearance of TiO2 NPs from the alveolar region and from the lung may be dependent on exposure concentration, the degree to which inhaled aerosols are agglomerated, or lung burden, but current understanding is insufficient to describe macrophage-mediated clearance of TiO2 NPs from the lung (Geiser et al., 2008; as cited in Versar, 2012).

In contrast, following exposure of mice to a much higher concentration, light microscopy and TEM showed that particles accumulated primarily in pulmonary macrophages and not in the surrounding lung tissue and that the particles were agglomerated within phagosomes (Rossi et al., 2010; as cited in Versar, 2012). The factors contributing to the apparent differences in these observations are unknown, but could include different exposure concentrations and durations, size of the aerosols, or surface characteristics of the particles.

6.2.2.4 Tissue Distribution Following Inhalation Exposure

No evidence for translocation of TiO2 to the liver, kidney, spleen, or the basal brain (with olfactory bulb) was found in Wistar rats exposed for 6 h/d for 5 days to aerosols made from TiO2 NPs at concentrations of 2, 10, or 50 mg/m^3 (Ma-Hock et al., 2009b; as cited and summarized in Versar, 2012). Dust aerosols in this study were made by dispersing uncoated TiO2 primary particles with average diameters of 25.1 ± 8.2 nm (MMAD 0.7 to 1.1 μm; GSD 2.3 to 3.4). Due to agglomerates generated during the aerosolization process, the concentration of particles less than 100 nm in size was only a small fraction (0.1 to 0.4 percent) of the total particle mass at each exposure concentration. TiO2 NPs were characterized as 86 percent anatase/14 percent rutile, had an uncoated hydrophobic surface, ranged from 13 to 71 nm size, and had a surface area of 51.1 ± 0.2 m^2/g. Thus, the aerosols were similar to those used in the studies by Bermudez et al. (2004) and Ferin et al. (1992). Mean TiO2 mass in lung tissue increased with increasing exposure concentration, and during a 16-day post-exposure period, lung burdens decreased to about 74 to 82 percent of values immediately after exposure. TiO2 was only detected in mediastinal lymph nodes of rats exposed to the highest concentration. Increase in lymph node content during the post-exposure period suggests that translocation to the lymph nodes contributed to the lung clearance. In liver, kidney, spleen, and basal brain, TiO2 could not be detected by inductively coupled plasma-atomic emission spectroscopy (ICP-AES), indicating

that translocation of inhaled TiO2 NPs to non-respiratory tissues appears to be limited. The results suggest that clearance of TiO2 during post-exposure may have occurred predominantly via macrophage-mediated mucociliary transport to the GI or via the lymph system without considerable translocation to the nonrespiratory tract tissues examined. A study limitation is that fecal samples were not collected and analyzed for TiO2.

Ti levels were not detectable in liver, kidney, spleen, and basal brain (with olfactory bulb) from Wistar rats exposed (head/nose) to aerosols of TiO2 NPs at a concentration of 100 mg/m^3, 6 hours/day for 5 days (van Ravenzwaay et al., 2009; as cited in Versar, 2012). The mean TiO2 lung concentration declined over 14 days post exposure; however, concentrations in lymph nodes increased during this time, indicating clearance from the lung to the lymph node. The results indicate that translocation to nonportal-of-entry tissues is limited.

6.2.3 Dermal Exposure

Few studies on dermal absorption or penetration of TiO2 in humans or animals were located in the literature, including those studies with TiO2 in sunscreens.

Pflucker et al. (2001) performed dermal tests with three different types of TiO2 NPs (between 10 and 100 nm). The test emulsions were applied on the forearm of a human volunteer at a concentration of 4 mg emulsion/cm^2 or 160 µg TiO2/cm^2 for 6 hours. Punch biopsies (2 mm in diameter) were examined using TEM and the TiO2 pigments were located exclusively on the outermost layer of the human stratum corneum, indicating very limited dermal absorption.

While an in-depth review of sunscreen and cosmetics are outside the scope of this project, the body of literature with sunscreens report that TiO2 did not penetrate through the skin in either animals (domestic pig, minipig) or humans (Mavon et al., 2007; Kiss et al., 2008; as cited in Versar, 2012; Menzel et al., 2004; Sadrieh et al., 2010; Wu et al., 2009). These studies are consistent and supportive of the Pflucker et al. (2001) study.

No data were located regarding excretion of absorbed TiO2 NPs following dermal exposure, which is not unexpected given that Ti does not appear to penetrate the dermis.

6.2.4 Other Routes of Exposure

Studies of other routes of exposure to TiO2 that have investigated absorption and distribution have been conducted via intranasal instillation, IT, OPA, and abdominal injection. While these studies suggest there is translocation and absorption of Ti into systemic circulation and organs, the relevance of these routes of exposure and high doses to human oral or inhalation exposure is uncertain.

Evidence of translocation of TiO2 to brain regions has been reported from studies of mice given intranasal instillations of aqueous suspensions of rutile or anatase NPs and sacrificed 24 hours after 1, 5, 10, and 15 treatments (Wang et al., 2008a, b; as cited in Versar, 2012). Increased brain Ti concentrations have also been observed in CD-1 (ICR) mice following 14 daily abdominal injections of 5 to 150 mg/kg/d TiO2 NPs (5 nm anatase; agglomeration of particles not characterized) (Ma et al., 2010; as cited in Versar, 2012). It is not known how the particles

are transported to the brain and cross the blood-brain barrier.

Results from IT studies in rats suggest that TiO2 NPs deposited in the lungs are transported into the interstitium and lymph nodes (Sager, 2008a; Ferin et al., 1992; as cited and discussed in Versar, 2012). Fu et al. (2014) reported that following IT of TiO2 NPs in male SD rats, twice per week for four weeks with 0.5 to 32 mg/kg, there was slight congestion in the spleen, deposition in the lymph nodes and alterations in immune function. These observations support translocation and absorption of TiO2 following this route of administration.

6.2.5 Summary

Limited information from human and animal studies indicates that TiO2 NPs are absorbed to a small extent from the lungs and gastrointestinal tract via alveolar macrophages or systemic blood circulation, then distributes to liver, kidneys, spleen and the brain, causing localized effects. The rate of translocation is uncertain. TiO2 NPs, however, can penetrate the blood–brain, blood-testis and blood-placenta barriers.

In humans, there is low absorption following oral exposure. Some absorption apparently occurs in the proximal small intestine as well as uptake via Peyer's patch in the more distal small intestine (ileum). In animals, there is also very low absorption as evidenced by low urinary, and high fecal excretion. Few studies showed systemic distribution to spleen, kidney, liver, brain, lymph nodes and bone marrow following oral exposure in animals.

Available results from animal studies indicate that, following nose-only or whole-body inhalation exposure, TiO2 NPs deposited in the lung can be (1) cleared by macrophage engulfment and translocated to the GI tract via mucociliary transport and swallowed; and, (2) transported from airspace surfaces into the interstitium and lymph tissue, and, with non-overload conditions in the lungs, cleared with slower kinetics than microsized TiO2 particles (Geiser et al., 2008, 2005; Sager et al., 2008a, b; Bermudez et al., 2002, 2004; Oberdörster et al., 1994; Oberdörster, 2002; Hext et al., 2005; Ferin et al., 1992; Leppanen et al., 2011, 2015a, 2015b; Eydner et al,, 2012; Noel et al., 2012; 2013; McKinney et al., 2012; Baisch et al., 2014; Oyabu et al., 2016; Larsen et al., 2016). With overload conditions, alveolar macrophages apparently engulf too large of a volume of particles, become immobile and clearance fails. In general, deposition, clearance and effects are animal species-specific and are not specific for TiO2 versus other poorly soluble low cytotoxic particulates (Bermudez et al., 2002, 2004). Translocation of inhaled TiO2 NPs to non-respiratory tissues appears to be limited.

TiO2 NPs do not appear to penetrate intact skin in humans or animals. No data were located regarding excretion of absorbed TiO2 NPs following dermal exposure, which is not unexpected given that TiO2 does not appear to penetrate the dermis.

Data from other routes of exposure suggest there is translocation and absorption of TiO2 into systemic circulation and organs. One study in mice reported brain Ti following abdominal injections of TiO2 NPs. It is not known how the particles are transported to the brain and cross the blood-brain barrier. However, the relevance of these routes of exposure and how the high doses employed in animal studies relate to human oral or inhalation exposure is not known.

6.3 Acute Toxicity

Versar (2012) reviewed acute toxicity studies of nano TiO2 prior to 2010. The relevant literature since that time is presented in this section. Acute oral studies in humans were not located for TiO2 NP forms relevant to CPSC. Shakeel et al. (2016) recently published a review of studies with laboratory animals by various routes of exposure for further reference.

6.3.1 Oral Exposure

Only two studies (Warheit et al., 2015a; Tassinari et al., 2014) of the acute/short term oral toxicity of TiO2 were found in a search of the literature from 2010 to 2017; these studies are described below and summarized in Table 27. Two older studies (Warheit et al., 2007; Wang et al., 2007, as evaluated in Versar, 2012) are also presented in Table 27.

Warheit et al. (2015a) conducted an acute oral toxicity study with nanoscale TiO2 in accordance with OECD Test Guideline 425. This study was designed as a repeat of the authors' earlier study (Warheit et al., 2007). Fasted female Sprague-Dawley rats were administered a single oral gavage of commercial surface-treated TiO2, with a crystal structure composed of both rutile and anatase (see Table 27), with doses of 0, 175 (1 rat), 550 (1 rat), 1750 (1 rat) or the limit dose of 5000 (3 rats) mg/kg bw. Mortality, clinical signs and body weights were evaluated over a 14-day post-exposure period. No mortality was observed; the oral LD50 was greater than 5000 mg/kg bw.

An acute study explored possible reproductive and endocrine effects of short-term, oral exposure to 0, 1, or 2 mg/kg/d anatase TiO2 NPs in rats (Tassinari et al., 2014). NPs were purchased and characterized to be anatase (Table 27). Male and female Sprague-Dawley rats (7/sex/group, approximately 60 days old) were gavaged suspensions of 0 (ultrapure water), 1, or 2 mg/kg/d TiO2 at 2 ml/100g bw for 5 days. Twenty-four hours after the last treatment, blood samples were collected for testosterone, 17β estradiol, and triiodothyronine measurements. The uterus, ovary, testes, thyroid, spleen and adrenal glands were collected for histopathological examination. Deposition of TiO2 NPs in the spleen was measured by ICP-MS. TEM observations showed that TiO2 NPs were of two morphologies, i.e., spherical (20 to 60 nm) or irregularly shaped (40 to 60 nm). Eighty-seven percent of the large particle (determined by SEM) agglomerates ranged from 30 to 900 nm, with an average diameter of 284 ± 43 nm. The main impurity was Fe. A statistically significant increase of Ti occurred in ovarian and splenic tissue in 2 mg/kg dosed rats. No other differences in Ti levels were reported across treatment groups. There were no treatment-related effects in either sex for clinical observations, body weights, body weight gains, feed consumption values, and absolute and relative target organs between the treated and control groups. Testosterone serum levels were statistically significantly increased at 2 mg/kg compared to control values. 17β Estradiol serum levels did not show any differences among groups. Histological and histomorphometric data of the ovary revealed a significant increase in the incidence of apoptosis in granulosa cells at both 1 and 2 mg/kg/d with respect to the control group. Morphometric analysis did not show any difference among groups. Thyroid histomorphometry showed a statistically significant increase in follicular epithelium height, both at 1 and 2 mg/kg. Triiodothyronine serum levels showed dose-related, statistically significantly decreases both at 1 and 2 mg/kg/d. In the spleen, the white-to-red pulp area ratio was significantly affected at 2 mg/kg, as a consequence of the significantly increased white pulp

area. The LOAEL is considered to be 1 mg/kg/d; there was no NOAEL.

Acute oral toxicity data for TiO2 NPs in humans were not located. Animal oral exposure studies with TiO2 NPs showed biochemical changes. The LD50 in rats was greater than 5000 mg/kg.

Table 27. Summary of Acute and Short-Term Oral Studies to TiO2 NPs

Species and study type (n/sex/group)	Dose (frequency, duration)	Particle characteristics[a]	NOAEL (mg/kg/d)	LOAEL (mg/kg/d)	Responses at LOAEL	Comments	Reference
Sprague Dawley rats females 1/group 3/group	Single gavage dose 0, 175, 550, 1750 5000	commercial surface-treated rutile/anatase TiO2 particles (D50 = 73 nm by number) ultrafine or nanoscale; characterized by multiple methods for surface area and size	None		LD50 greater than 5000 mg/kg	Designed as LD50 study; 14-day post exposure period. Repeat of Warheit et al. (2007) study	Warheit et al., 2015a
Sprague-Dawley rats male and female 7/sex/group	Oral gavage 0, 1, or 2 mg/kg/d for 5 days	gavage suspension; purchased 99% pure anatase; less than 25 nm primary particle size; BET surface area 45 to 55 m^2/g; spherical or irregular shaped; characterized by SEM, TEM	None	1	Significant decrease of triiodothyronine serum levels	Increased incidence of apoptosis in granulosa cells of the ovary. Increase in follicular epithelium height in the thyroid. Endpoints evaluated: body weight, organ weight, feed consumption values, and testosterone, 17β estradiol, and triiodothyronine concentrations	Tassinari et al., 2014
Sprague-Dawley rats females 1/group 3/group	Single dose gavage 0, 175, 550, or 1750 mg/kg 5000 mg/kg	ultrafine TiO2 particles (79% rutile/ 21% anatase) (90% wt titania/7% alumina/1% amorphous silica); median particle size 140 nm in water[b]			At greater than 1750, gray feces observed; LD50 greater than 5000 mg/kg	Sacrificed 2 weeks after dosing; no adverse effects reported	Warheit et al., 2007[b]

Species and study type (n/sex/group)	Dose (frequency, duration)	Particle characteristics[a]	NOAEL (mg/kg/d)	LOAEL (mg/kg/d)	Responses at LOAEL	Comments	Reference
CD-1 ICR mice 10/sex/group	Single gavage 5000 mg/kg/d	nanosized (25 and 80 nm) and fine (155 ± 33 nm) TiO2 particles (greater than 99% pure); crystalline forms not specified[b]		5000	Mortality (not attributed to treatment): increase ALT, ALT/AST ratio, BUN concentration, LDH and α-HBDH, increased relative liver weight in females and increased ALT/AST ratio in males at 25 and 80 nm; brain, kidney, liver lesions in both sexes with 80 nm and fine particles	Sacrificed 2 weeks after dosing	Wang et al., 2007[b]

[a]Particle data presented if available: source, coating, primary particle size, surface area, shape/morphology, mineral form, aggregation, purity
[b]As described in Versar (2012)

6.3.2 Inhalation Exposure

Acute inhalation toxicity data for TiO2 NPs in humans were not located. Acute animal inhalation exposure studies (nose/head-only or whole body) with TiO2 NP (forms relevant to CPSC) showed signs of pulmonary inflammation; no systemic effects were evaluated.

Several acute or short-term inhalation toxicity studies have been published since 2010, and are described in this section and summarized in Table 28. Older studies, while not described herein, are also presented in Table 28 (as summarized in Versar, 2012) for a comprehensive presentation of acute and short-term inhalation toxicity studies for TiO2.

An acute nose-only inhalation study of 5 nm TiO2 aerosols with two distinct sizes (or agglomeration states), smaller or larger than 100 nm, induced mild pulmonary effects in adult male Fisher 344 rats at 7 mg/m^3 (Noel et al., 2012). The investigators hypothesized the larger agglomerates would more likely be phagocytized by macrophages, whereas the smaller agglomerates would escape phagocytosis and cause cytotoxicity. Six groups (6/group) of rats were exposed for 6 hours to 0 (2 groups exposed to clean air, one for each agglomerate size), or the large (2 groups) or small (2 groups) agglomerates at 2 or 7 mg/m^3 mass concentration. The commercially purchased (from a US company) TiO2 (greater than 90 percent anatase and less than 10 percent rutile) had a specific area of 200 to 220 m^2/g, and a greater than 90 percent spherical morphology (and were less than 10 percent rod-shaped). An acute inflammatory response followed the exposure to large agglomerates. Clear trends showing both cytotoxic and oxidative stress effects in BALF, without apparent activation and recruitment of immune cells, was observed for small agglomerates. The lung burden of rats exposed to 2 mg/m^3 was 14.5 µg for the aerosol composed of small agglomerates and 14.1 µg for the aerosol composed of large agglomerates. The lung burden of rats exposed to 7 mg/m^3 was 51.3 µg for the aerosol composed of small agglomerates and 51.5 µg for the aerosol composed of large agglomerates. BALF analyses showed a statistically significant increase in the number of neutrophils for the group exposed to the large agglomerates. The study provides evidence that biological responses to NPs might not depend solely on the dimension of the primary NP, but also on the dimension of the NP agglomerates. Therefore, the characterization of the size distribution of the NP agglomerates in the aerosol is essential for the establishment of adequate and relevant correlations between NP exposure dose and adverse biological effects.

To determine the role of primary NP size and their degree of agglomeration in aerosols on pulmonary effects, the same laboratory conducted a further investigation (Noel et al., 2013). Small NPs are thought to have greater biological reactivity, but their level of agglomeration in an aerosol may also have an impact on pulmonary response. The authors investigated the role of primary NP size and the agglomeration state in aerosols on pulmonary toxicity, through inflammatory, cytotoxic and oxidative stress effects in adult Fisher 344 male rats (6 animals/ group). Three different near spherical sizes of TiO2 NPs (greater than 90 percent anatase and less than 10 percent rutile), with a primary size 5, 10 to 30 or 50 nm, were commercially purchased (U.S.). Small (less than 100 nm) or large agglomerates (greater than 100 nm) were generated at 20 mg/m^3 and rats were exposed once for 6 hrs in nose-only chambers. Compared to two groups of controls (clean air, one for each agglomerate size), BALF showed that large agglomerate aerosols induced an acute inflammatory response, characterized by a significant increase in neutrophils, while small agglomerates aerosols produced significant oxidative stress

damage and cytotoxicity. In addition, for an agglomeration state smaller than 100 nm, the 5 nm particles (specific surface area of 200 to 220 m^2/g) caused a significant increase in cytotoxic effects relative to controls (increased LDH). A greater degree of oxidative damage was seen with the 10, 30 nm, and 50 nm particles. In both small and large agglomerate aerosols, the 10 to 30 nm TiO2 NP size increased BALF inflammatory cytokines relative to controls.

6.3.2.1 Whole Body Inhalation versus Nose-only Inhalation

Nose-only animal inhalation studies have become widely used because of the ability to achieve higher exposure concentrations, less test substance waste, and less oral consumption with preening, than with whole body inhalation exposure. However, a downside of this exposure scenario, when compared with whole body exposure, is the additional stress on the animals from being in a confined space, and the associated increased respiratory and heart rate.

Oyabu et al. (2016) compared the results of exposure via the two inhalation methods (nose-only and whole-body) using the same material under the same exposure conditions (99.5 percent pure commercial spindle-shape rutile-crystalline TiO2 NPs). Based on measurements of deposited amounts and evaluation of histopathology in the lung, they concluded that the results of the two methods were comparable. Both methods exposed F344 rats (5/group; sex not reported) to 0 (fresh air), or the same TiO2 NPs at approximately the same exposure concentration for 6 hours. The concentration in the whole-body exposure chamber was 4.10 ± 1.07 mg/m^3, and for nose-only was 4.01 ± 1.11 mg/m^3. The TiO2 NPs had a primary diameter of 12 nm x 55 nm long, with a specific surface area 121 m^2/g. The particle sizes were 230 and 180 nm, respectively. TiO2 deposited in the lungs after the exposure was 42.6 ± 3.5 µg in the whole-body exposure and 46.0 ± 7.7 µg in the nose-only exposure. The body weights of the two groups were similar with wet lung weights of the nose-only group significantly less than controls, but similar to the whole-body exposure group. The histopathological evaluation showed the same findings in both exposure groups: no infiltration of inflammatory cells in the alveolar space and interstitium, and no fibrosis, leading the authors to conclude there were no differences in effects between the two inhalation methods.

Table 28. Summary of Acute and Short-Term Inhalation Studies to TiO2 NPs

Species and study type (n/sex/group)	Exposure (concentrations, frequency, duration)	Particle characteristics[a]	NOAEC (mg/m^3)	LOAEC (mg/m^3)	Responses at the LOAEC	Comments	Reference
Fisher 344 rats males 6/group; 6 groups total nose-only exposure	Small (less than100 nm) and large agglomerates (greater than100 nm) of 2 or 7 mg/m^3 for 6 hrs; 2 control groups (compressed air)	Greater than 90% anatase/less than10% rutile; 5 nm particle size; TEM greater than 90% spherical/less than 10% rod-shaped; Aerosols: MMAD = 30 and 185 nm (at 2 mg/m^3), 31 and 194 nm (at 7 mg/m^3)	2	7	Increased lung burden of agglomerates; at 7 mg/m^3 acute inflammatory response and; increased neutrophils in BALF with large agglomerates; cytotoxic and oxidative stress effects with small agglomerates	Lung burden similar with small or large agglomerates at both 2 or 7 mg/m^3; lung burden 3 to 4 times greater at higher concentration for both size agglomerates	Noel et al., 2012
Fisher 344 rats males 6/group; 8 groups total nose-only exposure	Small (less than 100 nm) and large agglomerates (greater than100 nm) of 20 mg/m^3 for 6 hrs; 2 control groups (compressed air)	3 types of NPs: (1) 5 nm particle size; greater than 97% anatase/less than 3% rutile; surface area = 200 to 220 m^2/g; TEM greater than 97% spherical/less than 3% rod-shaped, (2) 10 to 30 nm particle size; pure anatase; surface area = 200 to 220 m^2/g; spherical, (3) 50 nm particle size; greater than 80% anatase/less than 20% rutile; TEM greater than 80% spherical/less than 20% rod-shaped	None	20	BALF of large agglomerates found increased neutrophils (inflammatory response); small agglomerates produced oxidative stress (increased LDH activity) and cytotoxicity.	Limited by only one concentration tested	Noel et al., 2013

Species and study type (n/sex/group)	Exposure (concentrations, frequency, duration)	Particle characteristics[a]	NOAEC (mg/m^3)	LOAEC (mg/m^3)	Responses at the LOAEC	Comments	Reference
Sprague-Dawley rats males 3-12/group whole-body exposure	0, 1.5, 3, 6, 10 or 12 mg/m^3 for ultrafine and 0, 3, 6, 12, 15 or 16 mg/m^3 for fine; 4 or 5 hours	25 nm (ultrafine at 4, 6, 10, 19 or 38 µg) and 1 µm (fine at 8, 20, 36, 67 or 90 µg) primary particle sizes[b]	None	38 µg of ultrafine for 5 hours	Impaired vasodilation in the systemic microcirculation of shoulder muscle	Only looked at pulmonary deposition and vasodilation in the systemic microcirculation	Nurkiewicz et al., 2008[b]
Wistar rats males number/group not specified head and nose exposure	0 or (target) 100 mg/m^3 TiO2 (concentration 88 mg/m^3) for 5 h/d for 5 days 0 or 250 mg/m^3 pigmentary TiO2 (274 mg/m^3) for 6 h/d for 6 days	70% anatase/30% rutile; 20 to 30 nm particle size; TEM surface area = 48.6 m^2g; density 4.2 g/cm^3; uncoated, shape not specified Aerosols: MMAD = 1.0 µm (2.2); 0.5% of total particle mass less than100 nm[b] Pigmentary TiO2 99.4% pure rutile; 200 nm size; surface area=6 m^2/g; Aerosol: MMAD = 1µm; 0.05% total particle less than 100 nm[b]	None None	88 (lung) 274 (lung)	Significant changes in BALF parameters (including↑ total cells, lymphocytes and neutrophils; ↑ protein, ↑ enzymatic activities), decreased lung weight immediately after exposure, and histological changes to the lungs, mediastinal lymph nodes, and nasal cavity	Endpoints evaluated included BALF parameters (total and differential cell counts, protein content, and enzyme activity), organ weights, and histological examination of respiratory tract tissues. Sacrificed immediately or 14 days post-exposure Recovery was apparent for most endpoints by 14 days post-exposure Effects same of nano and pigmentary form	van Ravenzwaay et al., 2009[b]
Wistar rats males 5–6 rats/endpoint/ group head and nose	0, 2, 10, or 50 mg/m^3 6 h/d for 5 days	86% anatase/ 14% rutile; 31 to 71 nm particle size (mean 25 nm); surface area = 51.1 m^2/g; uncoated hydrophobic surface, shape assumed spherical if	None	2 (lung)	Changes in BALF (including ↑ total protein, ↑ enzymatic activities), increased cell proliferation in the large/medium bronchi and terminal bronchioli.	Endpoints evaluated included body wts, BALF (total and differential cell counts, protein content, and enzyme activity), rates of cell proliferation and apoptosis in the lung, hematology parameters,	Ma-Hock et al., 2009[b]

Species and study type (n/sex/group)	Exposure (concentrations, frequency, duration)	Particle characteristics[a]	NOAEC (mg/m^3)	LOAEC (mg/m^3)	Responses at the LOAEC	Comments	Reference
exposure		less than 100 nm in size[b] Aerosols: MMAD = 0.8–1.1 µm (GSD 2.3–3.4); 0.1–0.4% of total particle mass less than 100 nm[b]			↑ incidences histological inflammatory lesions in lungs at the two highest concentrations (e.g., diffuse alveolar infiltration with histiocytes, pigment-loaded macrophages in mediastinal lymph nodes). Signs of pulmonary inflammation in BALF and from cell proliferation measures increased in severity at higher concentrations.	organ weights, and histological examination of respiratory tract tissues. Controls received conditioned air. Sacrifices immediately at end of exposure, 3 or 16 days post-exposure. No indication of systemic effects	

Species and study type (n/sex/group)	Exposure (concentrations, frequency, duration)	Particle characteristics[a]	NOAEC (mg/m^3)	LOAEC (mg/m^3)	Responses at the LOAEC	Comments	Reference
BALB/c/Sca mice females 8/group whole body	0 or 10 mg/m^3 for 2 h/d for 3 days	Four types of nano-particles: (1) SiO_2-coated nano rutile TiO2:10 × 40 nm (needle- shaped); surface area = 132 m^2/g; rutile; coated with silica, (2) nano-TiO2 anatase: less than 25 nm, surface area = 222 m^2/g; (3) nano-TiO2 rutile:anatase: 30 to 40 nm; surface area = 23 m^2/g, rutile:anatase 9:1, and (4) nano TiO2 anatase/brookite: ~21 nm, surface area = 61 m^2/g, anatase:brookite 3:1, lab produced. Aerosols: MMADs ~ 100 and ≤ 2 nm for commercial and lab-produced particles, respectively.[b]	None	10 (lung)	Increased neutrophils in BALF. Effects observed for silica- coated rutile TiO2 NPs only. Other test materials induced no signs of pulmonary inflammation under the 2-h/d exposure conditions.	Endpoints evaluated included BALF (differential cell counts and cytokine levels) and expression of mRNAs in lung tissue for gene products involved in inflammatory responses. Concluded that surface-coating was the most likely variable to explain potency difference observed across the test materials. This was supported by citation of unpublished findings that 10 × 40 nm needle-shaped rutile NPs with an alumina coating did not elicit inflammatory responses in an *in vitro* test system.	Rossi et al., 2010[b]

Species and study type (n/sex/group)	Exposure (concentrations, frequency, duration)	Particle characteristics[a]	NOAEC (mg/m^3)	LOAEC (mg/m^3)	Responses at the LOAEC	Comments	Reference
C57BL/6 mice males 24/group	0 or 8.9 mg/m^3 for 4 h/d for 10 days	Anatase; 3.5 nm particle size (mean 25 nm); surface area = 219 m^2/g; O, OH, and H_2O at the surface; shape not specified; marked aggregation Aerosols: MMAD = 120 to 128 nm (GSD 1.6–1.7)[b]	None	8.9 (lung)	Increased numbers of particle-laden alveolar macrophages in the lung tissues (indicative of inflammation)	Endpoints evaluated included body weights, BALF (total and differential cell counts, total protein, cytokine levels) at 1, 2, 3 weeks post-exposure, and histopathological examination of lung tissues at necropsy. Sentinel mice exposed to nebulized water. Mice recovered by week 3 post-exposure.	Grassian et al., 2007a[b]
C57BL/6 mice males 6/group	0.8 or 7.2 mg/m^3 for 4 hours whole body	Anatase; 3.5 nm particle size (mean 25 nm); surface area = 219 m^2/g; O, OH, and H_2O at the surface; shape not specified Aerosols: MMAD = 120 to 128 nm (GSD 1.6–1.7)[b]	0.8	7.3	Increased numbers of total cells and alveolar macrophages in BALF	Endpoints evaluated included body weights, BALF (total and differential cell counts, total protein, cytokine levels), and histopathological examination of lung tissues. Sentinel mice exposed to nebulized water.	Grassian et al., 2007a[b]

C57BL/6 mice males 6/group	0.62 or 7.16 mg/ m^3 for 4 hours	Uncoated anatase/rutile; aerosol; 17.8 nm (no other information)[b]	NR	NR	Increased number of macrophages in BALF	Endpoints evaluated included BALF (macrophage numbers, protein, LDH)	Grassian et al., 2007b[b]

[a] Particle data presented if available: source, coating, primary particle size, surface area, shape/morphology, mineral form, aggregation, purity

[b] As presented or described in Versar (2010)

NR= not reported

6.3.2.2 Whole Body Inhalation versus IT

Acute studies often use bolus methods that deliver NPs at high dose rates that do not reflect likely human exposures. The delivered dose rate is a key determinant of the inflammatory response in the respiratory tract when the deposited dose is constant.

Baisch et al. (2014) exposed adult male Fisher-344 rats (3-5/group) to the same deposited doses of TiO2 NPs (Aeroxide P25) by single IT exposure (high or low dose rate), or via single or repeated low dose rate whole body aerosol inhalation (controls were exposed to saline or filtered air, respectively). Dose rates were determined so that the same deposited dose could be achieved for both methods. The high deposited dose was ~200 μg TiO2 and the lower dose was ~45 μg TiO2. The MPPD was used to calculate the aerosol concentrations to produce the same deposited doses by inhalation exposure. The aerosol exposure of 33 $\mu g/m^3$ was the high single exposure deposited dose; the aerosol exposure of 13 mg/m^3 was for single, low deposited dose and also for repeated inhalation exposures for 4 hrs (for 4 days). BALF neutrophils, biochemical parameters and inflammatory mediator release were quantified at 4, 8, and 24 hours and 7 days after IT instillation. Although the initial lung burdens of TiO2 were the same between the two methods, instillation resulted in greater short-term retention than whole body inhalation. High dose rate NP delivery by IT elicited significantly greater inflammation compared to low dose rate delivery and whole-body inhalation. In addition to inflammatory effects between the two methods, the pattern of regional deposition in the respiratory tract differed between the two methods.

6.3.2.3 Inhalation of Mixtures Containing TiO2

While humans may be exposed to mixtures of substances, it may be difficult in mixture studies to discern which components cause adverse effects. In the following studies, the mixture containing TiO2 NPs was investigated; however, the resultant toxicity cannot be attributed to TiO2 NPs alone.

Pirela et al. (2015) published a detailed physicochemical and morphological characterization of TiO2 printer-emitted NPs (PEPs) that become airborne during printing from 11 toners from major printer manufacturers. The analysis found evidence that respirable TiO2 fibers (less than 1 to 10 μm long) incorporated in the current toner formulations were released into the air during printing.

Pirela and coworkers (2016a, b) conducted *in vitro* and *in vivo* studies on PEPs. The biological responses of a panel of three physiologically relevant human cell lines, specifically, human Small Airway Epithelial Cells (SAECs), macrophages (THP-1 cells), and lymphoblasts (TK6 cells), were investigated with doses (0.5 to 100 μg/mL) corresponding to doses resulting from human inhalation exposures for consumer relevant durations of 8 hr or more (Pirela et al., 2016a). The printer-emitted NPs caused significant membrane integrity damage, an increase in ROS production, and an increase in pro-inflammatory cytokine release in different cell lines at doses equivalent to exposure durations from 7.8 to 1,500 hours. There were differences in methylation patterns that demonstrated the potential effects of PEPs on the overall epigenome following exposure. The authors suggest the *in vitro* findings indicate that laser printer–emitted engineered NPs may be deleterious to lung cells.

The laboratory subsequently tested laser printer-emitted NPs in an *in vivo* murine model (Pirela et al., 2016b). Adult male Balb/c mice were exposed to various doses of PEPs (0.5, 2.5 and 5 mg/kg) by IT. The authors claimed these exposure doses were comparable to those obtained from real world human inhalation exposures ranging from ~14 to 140 hrs of printing. Toxicological parameters evaluated included lung membrane integrity, inflammation, and regulation of DNA methylation patterns. Results showed that while IT of PEPs caused no changes in the lung membrane integrity, there was a pulmonary immune response, indicated by an elevation in neutrophil and macrophage percentage over the vehicle control and lowest dose groups.

6.3.3 Dermal Exposure

No studies of acute or short-term toxicity in humans or in animals of forms of TiO2 relevant to CPSC's jurisdiction were available in the current literature or in previous searches (as cited in Versar, 2012).

6.3.4 Other Routes of Exposure

Acute toxicity studies by parenteral routes were not considered in this report as there are sufficient acute duration studies for the oral and inhalation routes to identify potential hazards.

6.4 Repeat-Dose and Subchronic Toxicity

No studies of repeat-dose or subchronic systemic toxicity in humans for forms of TiO2 relevant to CPSC's jurisdiction were located in the current literature.

6.4.1 Oral Exposure

Seven repeat dose studies in rodents by the oral route with durations less than 100 days have been published since 2010 and are summarized in this section and in Table 29. These studies were designed to look at immunotoxicity (Bettini et al., 2017; Auttachoat et al., 2014; Sheng et al., 2014), neurobehavioral toxicity (Hu et al., 2015), endocrine toxicity (Hu et al., 2015), cardiovascular toxicity (Chen et al., 2015a, b) and systemic toxicity (Warheit et al., 2015a, b). In addition, one study (Duan et al., 2010) reviewed in Versar (2012) is also included in Table 29.

Warheit et al. (2015a) conducted repeat dose 28-day and 90-day oral studies in Sprague-Dawley rats by OECD Testing Guidelines. In the 28-day repeated-dose oral toxicity study (OECD Test Guideline 407), groups of five young adult male Sprague-Dawley rats were administered daily gavage doses of one of two almost identical rutile-type, uncoated, pigment-grade TiO2 test particles (d50 = 173 nm by number) made by different methods and from two different ores, or the water vehicle (controls). A single dose of 24,000 mg/kg/d of test material A (considered "research-grade") or B (considered "commercial-grade) was administered for 28 consecutive days. Body weight, body weight gain, feed consumption values, feed efficiency and clinical observations were evaluated weekly. All animals were evaluated daily for abnormal behavior and appearance; clinical pathology and gross and microscopic pathology examination were evaluated on all rats. There were no adverse effects reported during, or following, the end of the exposure period. The NOAEL was determined to be 24,000 mg/kg/d.

In the 90-day study (OECD Test Guideline 408), Warheit et al. (2015a, b) treated groups of young adult male and female rats with a rutile-type, alumina surface-coated pigment-grade TiO2 test particle (d50 = 145 nm - 21 percent NPs by particle number criteria) by oral gavage for 90 days. Dose levels were 0, 100, 300 or 1000 mg/kg/d in 0.5 percent aqueous methylcellulose with a dose volume of 10 ml/kg bw. Body weight, body weight gain, feed consumption values, feed efficiency and clinical observations were collected for the 90 days. Just before study termination, clinical pathology evaluations were collected after 15 hours in a metabolism cage including blood samples for hematology (RBC, HB, HCT, MCV, mean corpuscular hemoglobin concentration [MCHC], partial thromboplastin time [PTT], red cell distribution width, absolute reticulocyte count, platelet count, WBC count, differential WBC count and activated partial thromboplastin time) and clinical chemistry measurements (aspartate aminotransferase, alanine aminotransferase, sorbitol dehydrogenase, ALP, total bilirubin, urea nitrogen, creatinine, cholesterol, triglycerides, glucose, total protein, albumin, globulin, calcium, inorganic phosphorus, sodium, potassium, chloride, and total bile acids). Anatomic and microscopic pathology evaluations were conducted, however, only on tissues from the 1000 mg/kg/d group. Neurobehavioral evaluation consisted of functional observational battery, motor activity, grip strength, as well as sensory development by touch, sharp auditory stimulus, tail pinch and pupillary constriction. The NOAEL for both male and female rats in this study was 1000 mg/kg/day, the highest dose tested, based on a lack of TiO2 particle-related adverse effects on any in-life, clinical pathology, or anatomic/microscopic pathology parameters.

Bettini et al. (2017) treated a group (11-12/gp) of adult male Wistar rats with TiO_2 reference-grade NM-105 (or P25 Aeroxide®, the referent OECD nanomaterial) or food-grade white pigment (E171 in Europe, mixed nano- and micron-sized particles, of which up to 36% are less than 100 nm) at 10 mg/kg/d through drinking water for 100 days. As food uses are not within CPSC jurisdiction, only the results with NM-105 are discussed. Control rats received water only. TiO2 products were prepared following the generic Nanogenotox dispersion protocol (Jensen et al., 2011). After 7 days, Ti signal (by nanoSIMS) was detected in Peyer's patches (PP) of Ti-treated rats, but not in controls. Dendritic cell frequency significantly increased in PP after 7 days exposure, but had no effect on regulatory T cells after that time. In TiO_2-treated rats, stimulation of immune cells isolated from PP showed a decrease in T helper cells.

To address whether exposure can result in immunosuppressive effects or induce contact hypersensitivity response, Auttachoat et al. (2014) conducted a 28-day oral gavage study in female B6C3F1 mice (8/gp) at doses of 1.25 to 250 mg/kg/d nano-TiO2 in 0.5 percent methylcellulose in a volume of 0.1 ml/10g body weight. The TiO2 was spherical anatase particles, less than 25 nm in diameter, but no characterization was conducted. The oral nano-TiO2 produced no significant effects on innate, humoral, or cell-mediated immune functions or selected organ weights (spleen, thymus, liver, lung, and kidneys with adrenal glands).

Sheng et al. (2014) investigated, in mice, splenic immune dysfunction (neutrophilic cell proliferation, lymph nodule proliferation, splenic apoptosis, disperative replication of white pulp, anemia of red pulp, and macrophage infiltration), the capacity to elicit an immune response, as well as splenic gene expression changes. Doses of 2.5, 5, or 10 mg/kg/day bw anatase TiO2 NPs suspended in 0.5% hydroxypropyl-methylcellulose were administered to CD-1 (ICR) mice (40/gp) by gavage for 90 consecutive days. The surface area of the TiO2 sample was 174.8 m^2/g

and the mean hydrodynamic diameter of the TiO2 NPs in the solvent was 294 nm (range of 208 to 330 nm), with the Zeta potential of 7.57. At necropsy, the spleen was weighed and saved for histopathological evaluation, and blood samples collected. TiO2 NP exposure resulted in dose-dependent increases of adverse spleen indices (absolute spleen wet weight and relative to body weight), immune dysfunction (up-regulation of *NF-kB, TNF-α, MIF, IL-2, IL-4, IL-6, IL-8, IL-10, IL-18, IL-1β, CRP, TGF-β,* and *INF-γ* expressions, and down-regulation of *IkB* expression), severe macrophage infiltration and apoptosis in the spleen, gradual decrease in body weight, and significantly increased spleen Ti content, and marked decreases in hematological parameters (WBC, lymphocytes, neutrophilic granulocyte, RBC, HB, and platelets) at all doses tested. TiO2 NP-treated groups presented significant macrophage infiltration and dispersive replication of white pulp in the spleen. Black or brown agglomerates were observed in the TiO2 NP-exposed mouse spleens. Microarray data also showed significant alterations in the splenic expression of 1041 genes involved in immune/inflammatory responses, apoptosis, oxidative stress, stress responses, metabolic processes, ion transport, signal transduction, cell proliferation/division, cytoskeleton and translation at the high dose of 10 mg/kg/d. The overall NOAEL for this study could not be determined. The LOAEL appeared to be the low dose of 2.5 mg/kg/d.

To examine the role that TiO2 NPs may play in impairment of spatial recognition memory, female ICR mice (20/group) were exposed to TiO2 NPs via gavage administration at 0 (0.5 percent hydroxypropyl methylcellulose), 5, 10 or 50 mg/kg, daily for 60 days and then tested in a Y-maze (Hu et al., 2010). The spherical anatase TiO2 NPs were made in the investigator's laboratory and measured 5 nm with a BET surface area of 174.78 m^2/g. The Y-mazes (a variant of T-maze) are used to study how rodents function with memory and spatial learning through applying various visual cues. After 60 days of treatment and behavioral Y-testing, all animals were weighed and then sacrificed. The liver, spleen, kidneys, lungs, heart, and brain were weighed and part of the brain preserved for histopathological evaluation. Elemental Ti content was analyzed in a portion of each brain and the remainder of the brain homogenized for measurement of enzymatic activities and determination of neurochemicals. Daily behaviors, feeding, drinking and activity in TiO2 NP-treated groups were similar to the control group. Ti content in the mouse brain was significantly increased at doses greater than or equal to 10 mg/kg/d. Relative weight of the liver, kidney, and spleen to body weight, were statistically significantly greater in the 10 and 50 mg/kg TiO2-treated groups than the controls. Relative brain weight decreased gradually with increasing dose, reaching significance at 10 mg/kg/d and greater, indicating the higher doses of TiO2 NPs could cause brain alterations. The adverse effect on the brain was confirmed by impaired spatial recognition memory and significantly increased Ti content in the brain at 10 and 50 mg/kg/d. Brain histopathology reported calcification in neurocytes (result of too much calcium depositing and accumulating in the brain), and proliferation of ependyma and spongiocytes. The content of Ca and Na were higher, whereas the content of Mg, K, Zn and Fe were lower than in the control brain homogenates. Exposure to TiO2 NPs significantly inhibited the activities of Na/K-ATPase, Ca-ATPase, Ca/Mg-ATPase, and promoted the activities of acetylcholinesterase (AChE) and total nitric oxide synthase (TNOS) in the brains of mice at all doses tested. Evaluation of spatial recognition memory indicated that TiO2 NPs increasingly impaired the spatial recognition memory of mice in a dose-related fashion. The authors concluded the TiO2 accumulation in the brain caused brain injury and altered the contents of electrolytes and neurotransmitters. The LOAEL for this study appears to be 10 mg/kg/d; a NOAEL is found at 5 mg/kg/d.

Hu and co-workers (2015) explored the endocrine effects from oral gavage of TiO2 NPs at 0, 64 or 320 mg/kg/d to CD-1 mice (group size not specified), for 7 days per week for 14 weeks. The TiO2 NPs were anatase with a primary size provided by the manufacturer of 15 nm, but the average size measured by TEM was 25.64 ± 6.63 nm. The average hydrodynamic size of TiO2 NPs in PBS measured by DLS was 49.59 ± 0.41 nm. In a range-finding study of absorption, different concentrations of TiO2 NPs were measured following treatment of mice with 0, 0.52, 2.6, 13, 64 or 320 mg/kg/d TiO2 NPs by oral gavage and blood collected from the hearts at 0, 0.5, 1, 2, 4, 6, 9, 12 and 24 hours. Heart blood plasma insulin was measured using a mouse insulin ELISA kit. The results showed that Ti levels cannot be detected after oral administration of 0.52 and 2.6 mg/kg/d, but blood Ti levels increased significantly after 13, 64 and 320 mg/kg/d TiO2 NPs, with peak absorption at 1 hour after oral administration. Therefore, doses of 64 and 320 mg/kg/d of TiO2 NPs were selected to be administered for 14 weeks. Biochemical analyzes included plasma glucose, insulin, triglycerides, free fatty acid, low-density lipoprotein (LDL) cholesterol, high-density lipoprotein (HDL) cholesterol, total cholesterol, TNF-α, IL-6 and ROS-related markers. Results included increases in Ti levels in the liver, spleen, small intestine, kidney and pancreas that increased with dose. There was no significant difference among the body weights in the TiO2 NPs groups after 14 weeks. Biochemical analyses showed that plasma glucose and ROS levels significantly increased in the serum and liver at both doses, indicating that oral administration of TiO2 NPs increases ROS markers, resulting in insulin resistance and increasing plasma glucose levels in mice.

Table 29. Summary of Repeat Dose Oral Exposure Studies of TiO2 NPs

Species Strain and Sex (n/sex/group)	Exposure (doses, route, duration)	Particle characteristics	NOAEL (mg/kg/d)	LOAEL (mg/kg/d)	Responses at the LOAEL	Comments	References
Sprague-Dawley rats males 10/group	0 or 24,000 mg/kg/d, gavage; 28 days	2 nearly identical rutile-type, uncoated, pigmented, d50=173 nm	24,000	none	none	OECD TG 408, GLP conducted; TiO2 commercially available; only one dose tested	Warheit et al., 2015a
Sprague-Dawley rats males & females 10/sex/group	0, 100, 300 or 1000 mg/kg/d, gavage; 92-93 days	1 rutile-type, uncoated, pigmented, d50=145 nm	1000 (males and females)	none	none	OECD TG 425, GLP conducted; TiO2 commercially available	Warheit et al., 2015a
Wistar rats males 11-12/group	0 or 10 mg/kg/d; drinking water; 100 days	Water, E171 or NM-105 (i.e., P25), 30 to 40 nm diam	none	10	Colon inflammation and preneoplastic lesions	E171 is food grade white pigment nanoparticle; non-guideline study; only one dose tested	Bettini et al., 2017
Sprague-Dawley rats males & females 10/sex/group	0, 2, 10, or 50 mg/kg; daily gavage for 30 and 90 days	spherical, anatase crystals; 99.90% purity; average size 24 ± 5 nm; surface area 63.95 m^2/g	none	2 (both 30 and 90 days)	Mild, temporary reduction in heart rate and increased systolic blood pressure at 30 d; decreased LDH, alpha-hydroxybutyrate dehydrogenase, creatine kinase. Increased WBC and granulocytes, increased TNF-α, interleukin 6 at 90 days	Same study described in Cardiovascular Effects below	Chen et al., 2015a
B6C3F1 mice females 8/group	0, 1.25, 3.75, 12.5, 37.5, 125 or 250 mg/kg/d; gavage; 28 days	spherical anatase particles, less than 25 nm in diameter	250	none	none	No significant effects on innate, humoral, or cell-mediated immune functions; non-guideline study	Auttachoat et al., 2014

Species Strain and Sex (n/sex/group)	Exposure (doses, route, duration)	Particle characteristics	NOAEL (mg/kg/d)	LOAEL (mg/kg/d)	Responses at the LOAEL	Comments	References
CD-1 (ICR) mice females 40/group	0, 2.5, 5, or 10 mg/kg/d; gavage; 90 days	Anatase; hydrodynamic diam= 294 nm; surface area =174 m^2/g	none	2.5	Decreased body wt and increased Ti accumulation and spleen damage	TiO2 prepared by lab; non-guideline study	Sheng et al., 2014
CD-1 (ICR) mice males group size not stated	0, 64 or 320 mg/kg/d; gavage; 14 weeks	Anatase; 15 nm; hydrodynamic dia.= 49.59 nm	none	64	Increased ROS markers and induced insulin resistance	No effect on body weight or feed intake	Hu et al., 2015
CD-1 mice females 20/group	0, 5, 10 or 50 mg/kg/d, gavage; 60 days	Spherical anatase, 5 nm in diameter; surface area = 174.78 m^2/g	5	10	Significant increased body wt; decreased relative organ wts	Impairment of spatial recognition memory; non-guideline study	Hu et al., 2010
CD-1 (ICR) mice females 20/group	0, 62.5, 125, or 250 mg/kg every other day; gavage: 30 days	anatase; 5 nm in size; containing 58% titanium, 41% oxygen, 0.2% carbon and 0.1% hydrogen, suspended in 0.5% HPMC K4 M 4 M	31.25 (treatment every other day)	62.5	Decreased body wt gain, increased relative organ wts (liver, kidney, spleen, and thymus), increased serum hepatic enzyme markers, decrease in hematological endpoints	Made by the laboratory	Duan et al., 2010[a]

[a]As cited in Versar (2012)

6.4.1.1 Cardiovascular Effects

A study in male and female Sprague-Dawley rats (10/sex/group) was conducted to determine cardiovascular effects after oral gavage of TiO2 NPs (Chen et al., 2015a). The commercially purchased TiO2 NPs were spherical, anatase crystals with a purity of 99.90 percent. The average size was 24 ± 5 nm and the surface area was 63.95 m^2/g, as measured by BET method. TiO2 NPs were observed in the form of larger particles of 40.9 ± 0.4, 149.3 ± 33.9 nm and 168.1 ± 29.6 nm in ultra-pure water, artificial gastric juice and artificial intestinal juice. After daily gavage administration of TiO2 at 0, 2, 10, or 50 mg/kg in a volume of 1 ml for 30 and 90 days, heart rate, blood pressure, blood biochemical parameters and histopathology of cardiac tissues was assessed to quantify any cardiovascular damage. The doses were designed to mimic typical exposure to children through consumption of sweets containing TiO2 NPs (Weir et al., 2012). Body weights and feed consumption values were collected weekly. Histopathological examination of H&E stained heart tissue was performed by a pathologist blinded to treatment group. Mild and temporary reduction of heart rate and increased systolic blood pressure was observed after daily oral administration for 30 days. There were no adverse clinical observations or treatment-related effects on body weights or feed consumption values at any dose level tested. Injury of cardiac function was indicated after daily oral administration of TiO2 NPs for 90 days by decreased activities of lactate dehydrogenase, alpha-hydroxybutyrate dehydrogenase and creatine kinase. Increased white blood cell count and granulocytes in blood as well as increased concentrations of TNF-α and interleukin 6 in the serum indicated an inflammatory response initiated by TiO2 exposure. Histological analysis of cardiac tissue revealed no obvious pathological changes in TiO2 NP exposed rats compared to the control group. The authors hypothesized that cardiac damage and inflammatory response were the possible mechanisms of the adverse cardiovascular effects from the TiO2 exposure. The study authors suggested that the LOAEL for adverse cardiovascular effects after 30 days or 90 days of oral exposure occurred at the lowest dose of 2 mg/kg.

6.4.1.2 Summary

Seven oral subchronic TiO2 studies in rodents have been published since 2010. Warheit et al. (2015a) conducted repeat-dose OECD TG 28-day and 90-day oral studies in Sprague-Dawley rats. In the 28-day study the NOAEL was determined to be 24,000 mg/kg/d. In the 90-day study the NOAEL for both male and female rats was 1000 mg/kg/d, the highest dose tested. Bettini et al. (2017) treated male Wistar rats with TiO2 reference-grade or food-grade white pigment through their drinking water for 100 days. Alterations in immune function in the colon were noted. Auttachoat et al. (2014) conducted a 28-day oral gavage study in female mice with spherical anatase particles, less than 25 nm in diameter, and found no significant effects on innate, humoral, or cell-mediated immune functions or selected organ weights. Sheng et al. (2014) investigated immune dysfunction of mice with doses of 2.5, 5, or 10 mg/kg/d bw anatase NPs by gavage for 90 consecutive days. Microarray data showed significant alterations in immune/inflammatory responses, apoptosis, oxidative stress, stress responses, metabolic processes, ion transport, signal transduction, cell proliferation/division, cytoskeleton and translation at the 10 mg/kg/d level. Hu et al, (2010) measured spatial recognition memory in mice exposed to 5 nm anatase TiO2 NPs via gavage administration at up to 50 mg/kg/d, for 60 days. Ti content in the mouse brain was significantly increased at 10 mg/kg/d and higher doses, and caused brain injury and altered electrolyte and neurotransmitter levels. Hu and co-workers

(2015) also oral-gavaged mice with 15 nm anatase NPs at doses up to 320 mg/kg/d for 14 weeks. Plasma glucose and ROS levels significantly increased in the serum and the liver at 13 mg/kg/d and higher, indicating increased ROS markers.

6.4.2 Inhalation Exposure

Prior to 2000, several subchronic duration studies were performed according to the same basic exposure protocol by the same research group (Baggs et al., 1997; Janssen et al., 1994; Oberdörster et al., 1994; Ferin et al., 1992). These studies are detailed in Versar (2012) and summarized here in Table 30. Rossi et al. (2010) and Bermudez et al. (2004), also discussed in Versar (2012), are summarized below and in Table 30. The recent literature search conducted for this project, identified three inhalation studies in rats and mice with exposures from 21 days to 13 weeks. These studies are also shown in Table 30 and summarized below.

Rossi et al. (2010; as cited in Versar, 2012) exposed BALB/c/Sca mice via whole-body to TiO2 NPs as an aerosol at 0 or 10 mg/m^3 for 2 h/d for 4 days or for 4 weeks. Three commercially available and one *in situ*-produced form of TiO2 NPs were used; the NP types were differentiated throughout the study by their size and crystalline morphology. The authors concluded that surface coating (rather than surface area, primary or aggregate particle size or shape, or radical formation capacity) was the best correlate for lung inflammation parameters. The results indicate that the only tested exposure concentration, 10 mg/m^3, was a LOAEL for pulmonary inflammation in BALB/c/Sca mice. Other test materials (including aerosols made from uncoated anatase, uncoated rutile/anatase (9:1), and uncoated anatase/brookite (3:1) NPs) did not elicit changes in the examined pulmonary inflammation endpoints.

Bermudez et al. (2004; as presented in Versar, 2010) exposed female CDF (F344)/CrlBR rats, B3C3F1/CrlBR mice, and Lak:LVG (SYR) BR hamsters by whole-body inhalation to nanosized TiO2 (average primary particle size of 21 nm, P25, typically 80 percent anatase:20 percent rutile) as an aerosol at targeted concentrations of 0 (filtered air control), 0.5, 2.0, or 10 mg/m^3 for 6 h/d, 5 d/wk for 13 weeks; animals were observed for up to 1 year post-exposure. Aerosolized particles showed evidence of agglomeration. Increased terminal bronchiolar and alveolar cell replication and histopathological changes in the lungs (including accumulation of particle-laden macrophages, their migration to interstitial regions, and aggregation in subpleural and centriacinar zones with minimal hypertrophy and hyperplasia) support NOAEL and LOAEL values of 0.5 and 2.0 mg/m^3, respectively, for the rats. In mice, changes in increased total and differential BALF cell counts (including increased numbers of macrophages, neutrophils, and lymphocytes), changes in BALF parameters (increased total protein and LDH activity), and histopathological changes in the lungs (including aggregations of particle-laden macrophages in centriacinar sites and their migration to interstitial areas, and perivascular lymphoid proliferation), identify NOAEL and LOAEL values of 2.0 and 10 mg/m^3, respectively. Based on significant increases in neutrophil counts in the BALF and the level of bronchiolar cell replication, NOAEL and LOAEL values of 2.0 and 10 mg/m^3, respectively, are identified in hamsters.

Table 30. Subchronic Toxicity from Repeat Exposure by Inhalation to TiO2 NPs

Species Strain and Sex (n/sex/group)	Exposure (report concentrations, frequency, duration)	Particle characteristics	NOAEC (mg/m^3)	LOAEC (mg/m^3)	Responses at the LOAEC	Comments	Reference
Crl:OF1 mice males 2 groups of 6 mice head only exposure	0 or 30 mg/m^3 for 16 hrs (1 h/d, 4 d/wk for 4 weeks)	Crystal phase anatase+brookite 3:1; 20 nm particle size; mean count diam 130 nm at mass concentrations of 30 $mg/m^{3/}$	none	30	Pulmonary irritation	Sensory and pulmonary irritation also observed in the control group, suggest, irritant effects caused by reaction by-products cannot be ruled out. Irritation and inflammation potencies of the studied TiO2 was low; only one concentration tested	Leppanen et al., 2011
BALB/c mice females 2 groups of 8 mice	0 or 16 mg/m^3 for 16 hrs (1 h/d, 4 d/wk for 4 weeks)	Silica-coated nano-TiO2 rutile; 10 x 40 nm particle size; surface area = 132 m^2/g	none	16	Sensory irritation, airflow limitation, enhanced pulmonary mRNA expression of chemokines and elevated expression of proinflammatory cytokines TNF-α and IL-6	Silica-coated TiO2 NP induced pulmonary and sensory irritation and airflow limitation and pulmonary inflammation Only one concentration tested	Leppenen, 2015b

Wistar rats females 10/group ~10 weeks old Nose-only inhalation exposure	6 h/d for 21 days under OECD 412 GLPs; clean-air, nano- or fine-sized TiO2 at 0, 25/10 (with/without buffer) or 45 mg/m^3 3, 28 and 90-day recovery periods	0, 25/10 (with or without buffer) or 45 mg/m^3 of 2 types of particles: (1) Aeroxide® (P25); 20% rutile/80% anatase 21 nm particle size nanoparticles; surface area = 50 ± 15 m^2/g; MMAD = 0.7 µm, (2) Bayertit T; 99.5% rutile fine particles; 0.3 µm particle size; surface area = 5.2 m^2/g; MMAD = 1.1 µm Calculated lung burdens: Nano: 1238 µg/lung; 59,400 mm^2/lung Fine: 5760 µg/lung; 29,950 mm^2/lung	none	25/10	Lungs of rats treated with nano-sized and fine particles showed minimal inflammatory changes in lungs with both particle sizes; specifically, moderate alveolar infiltration with particle-laden macrophages found at all recovery timepoints. In both treated groups, few particle-laden macrophages seen intra-luminally and sub-epithelially in bronchi and bronchiole. Minimal interstitial infiltration with mononuclear cells and minimal alveolar infiltration with neutrophilic granulocytes also observed in both treated groups. Minimal bronchiolo-alveolar hyperplasia, minimal inflammatory changes in the lungs, leucopenia, and a decrease in β-glucuronidase observed.	Both nano-sized and fine particles elicited similar effects. After 28 and 90 days of recovery, WBC and lymphocyte counts significantly reduced in the nano- and fine-groups. Number of segmented neutrophils reduced in nano-sized treated group.	Eydner et al., 2012

Species Strain and Sex (n/sex/group)	Exposure (report concentrations, frequency, duration)	Particle characteristics	NOAEC (mg/m^3)	LOAEC (mg/m^3)	Responses at the LOAEC	Comments	Reference
BALB/c/Sca mice females 8/group	0 or 10 mg/m^3 for 2 h/d for 4 days; or 4 d/wk for 4 weeks	Four types of nano-particles: (1) SiO_2-coated nano rutile TiO2:10 × 40 nm (needle-shaped); surface area = 132 m^2/g; rutile; coated with silica, (2) nano-TiO2 anatase: less than 25 nm, surface area = 222 m^2/g; anatase, (3) nano-TiO2 rutile/anatase: 30 to 40 nm; surface area = 23 m^2/g, rutile:anatase 9:1, and (4) nano TiO2 anatase/brookite: ~21 nm, surface area = 61 m^2/g, anatase:brookite 3:1, lab produced. Aerosols: MMADs ~ 100 and ≤82 nm for commercial and lab-produced particles, respectively	none	10 (lung)	Increased neutrophils in BALF, increased expression of mRNAs (CXCL1 and TNF-α) associated with inflammatory response in lung tissue. Effects observed for silica- coated rutile TiO2 nanoparticles only. Other test materials (anatase, rutile/anatase, and anatase/brookite) induced no signs of pulmonary inflammation under the 2-h/d exposure conditions used in this study.	Endpoints evaluated included BALF parameters (differential cell counts and cytokine levels) and expression of mRNAs in lung tissue for gene products involved in inflammatory responses. Authors concluded that surface-coating was the most likely variable to explain potency difference observed across the test materials in this study. This was supported by citation of unpublished findings that 10 × 40 nm needle-shaped rutile nanoparticles with an alumina coating did not elicit inflammatory responses in an *in vitro* test system. Short exposure duration Only one concentration tested	Rossi et al., 2010[a]

Species Strain and Sex (n/sex/group)	Exposure (report concentrations, frequency, duration)	Particle characteristics	NOAEC (mg/m^3)	LOAEC (mg/m^3)	Responses at the LOAEC	Comments	Reference
F344 rats males 4–8/group	0 or 23.5 mg/m^3 for 6 h/d, 5 d/wk for 12 wks	Anatase, 20 to 21 nm particle size; surface area = 50 m^2/g; density 4.28; uncoated. Aerosols: MMADs of 0.71 to 0.78 µm (1.7 to 1.9)	none	23.5 (lung)	Variations in BALF (increased total cell and neutrophil counts, increased protein, changes in enzyme activity), increased expression of antioxidant enzymes (lung), and histopathological changes in the lungs (including increased alveolar epithelial thickness and septal fibrosis).	Endpoints evaluated included BALF (total and differential cell counts, total protein, enzyme activity), gene and protein expression of antioxidant enzymes in lungs, and histopathological examination of lung tissues. Animals were observed up to 64 wks post-exposure. Only one concentration tested	Baggs et al., 1997; Janssen et al., 1994; Oberdörster et al., 1994; Ferin et al., 1992[a]

Species and study type (n/sex/group)	Exposure (report concentrations, frequency, duration)	Particle characteristics	NOAEC (mg/m^3)	LOAEC (mg/m^3)	Responses at the LOAEC	Comments	Reference
CDF (F344)/CrlBR rats females 65/group	0 or 10, 50, or 250 mg/m^3 for 6 h/d, 5 d/wk for 13 weeks; recovery groups held additional 4, 13, 26 or 52 weeks (46 weeks for hamsters)	Commercially obtained pigmented rutile; MMAD = 1.36 to 1.44 µm; σ_g = 1.50 to 1.72	10 (rats)	50 (rats)	Inflammation (increases in macrophage and neutrophil numbers and in soluble indices of inflammation in BALF [rats greater than mice, hamsters]) and lung lesions (progressive epithelial and fibroproliferative changes) at 50 mg/m^3 in rats	Rats, mice, and hamsters vary significantly in their lung responses to inhaled pigmented TiO2 particles; rats most sensitive of these species in this experiment. Effects likely related to particle overload.	Bermudez et al., 2002
B3C3F1/CrlBR mice females 73/group			10 (mice)	50 (mice)			
Lak:LVG (SYR)BR hamsters females 73/group			10 (hamsters)	50 (hamsters)			
CDF (F344)/CrlBR rats females 25/group	0 or 0.5, 2.0, or 10 mg/m^3 for 6 h/d, 5 d/wk for 13 wks	P25 from Degussa; ~21 nm; typically 3:1 anatase:rutile; uncoated Aerosols: MMADs of 1.29 to 1.44 µm σ_g of 2.5 to 3.4	0.5	2.0	Decreased body weight gain, increased cell replication, and histopathological changes in the lung (aggregation of particle-laden macrophages, hypertrophy, and hyperplasia of type II alveolar epithelial cells).	Endpoints evaluated included mortality, clinical signs, body weights, BALF parameters (total and differential cell counts, total protein, enzyme activity), cell proliferation in the lungs, and histopathological examination of the lungs. Groups of animals sacrificed immediately after exposure (13 wks), and after post-exposure periods of 4, 13, 26, or 52 (49 for hamsters) wks.	Bermudez et al., 2004[a]
B3C3F1/CrlBR mice females 25/group			2.0	10 (lung)	Changes in BALF parameters (total and differential cell counts, protein content, enzyme activity), increased cell replication, and histo-pathological changes in the lung (aggregation of particle-laden macrophages).		

Species and study type (n/sex/group)	Exposure (report concentrations, frequency, duration)	Particle characteristics	NOAEC (mg/m^3)	LOAEC (mg/m^3)	Responses at the LOAEC	Comments	Reference
Lak:LVG (SYR)BR hamsters females 25/group			2.0	10 (lung)	Body weight loss, increased neutrophils in the BALF and increased bronchiolar cell replication.		

An earlier study by Bermudez et al. (2002; as cited in Versar, 2010) was designed to compare toxicity between CDF (F344)/CrlBR rats, B3C3F1/CrlBR mice, and Lak:LVG (SYR) BR hamsters, exposed by inhalation to pigmented rutile TiO2; MMAD of 1.40 μm. Targeted concentrations for the whole-body inhalation were 0, 10, 50, or 250 mg/m^3 for 6 h/d, 5 d/wk for 13 weeks; recovery animals were observed 4, 13, 26, or 52 weeks post-exposure (46 weeks for the hamsters). Retained lung burdens following exposure were greatest in mice, with rats and hamsters having lower, but similar, lung burdens. Particle retention data indicated pulmonary overload was achieved in both rats and mice at the 50 and 250 mg/m^3 exposure levels; hamsters were better able to clear the pigmented TiO2 particles. Lung histopathology revealed species and concentration-related differences in TiO2 retention patterns. Increases in macrophage and neutrophil numbers from BALF (rats had greater increases than mice and hamsters) indicated lung inflammation in all three species at 50 and 250 mg/m^3. There were significant species differences in responses to inhaled pigmented TiO2 particles. Rats were more likely than either mice or hamsters to develop lung burden overload, as well as a more severe and persistent pulmonary inflammatory response. Rats also were unique in the development of progressive fibroproliferative lesions and alveolar epithelial metaplasia in response to 90 days of exposure to the highest concentration of pigmented TiO2 particles. The NOAEL for this study was 10 mg/m^3. The LOAEL was 50 mg/m^3.

A 21-consecutive day nose-only inhalation study for 6 h/d was conducted by Eydner et al. (2012), with 10 week-old female Wistar rats (10/group) under OECD Test Guideline 412 and GLPs with clean-air, nano- or fine-sized TiO_2 at 0, 25/10 (with/without buffer) or 45 mg/m^3 followed by 3, 28, and 90 day recovery time periods. The TiO2 NPs were commercially available Aeroxide® TiO2 P25; composition was 20 percent rutile and 80 percent anatase with specific surface area of 50 ± 15 m^2/g and MMAD of 0.7 μm; the TiO2 fine particles were commercially available 99.5 percent rutile with a primary particle size of 0.3 μm, a specific surface area of 5.2 m^2/g, and MMAD of 1.1 μm. Lung volume measurements, histology, electron microscopy, hematology, and BALF analyses were conducted and the relative deposition index was calculated. Clinical observations and body weights between groups were similar. The lungs of rats treated with nano-sized and fine particles showed moderate alveolar infiltration with particle-laden macrophages (alveolar histiocytosis) at all three recovery time points (3, 28, and 90 days). In both treatment groups, a few particle-laden macrophages were seen intra-luminally and sub-epithelially in bronchi and bronchioli. Nano- and fine-particle agglomerates were rarely found in bronchiolar epithelium, in type-I pneumocytes, or as free particles in alveoli. In addition, a single fine particle-laden macrophage was detected in a parenchymal vessel and in the lung. In both treatment groups, minimal interstitial infiltration with mononuclear cells and minimal alveolar infiltration with neutrophilic granulocytes were observed, with a few animals in both groups showing minimal bronchioloalveolar hyperplasia. The lowest dose of 25/10 mg/m^3 (with/or without buffer) was a minimal LOAEL.

Leppanen and coworkers (2011) investigated airflow limitation in the airways of male mice (outbred Crl:OF1) caused by irritation and inflammation from inhalation of nanosized TiO2 NPs (primary particle size 20 nm; geometric mean diameters of 91, 113, or 130 nm at mass concentrations of 0, 8, 20, or 30 mg/m^3, respectively; crystal phase anatase + brookite [(3:1]). Airflow limitation in the conducting airways occurred at each exposure concentration, however, the response was not concentration-related. Repeated exposures (1 h/d, 4 d/wk for 4 weeks) to TiO2 NPs at a mass concentration of 30 mg/m^3 caused an intense airflow limitation that

remained the same over the exposure days. Sensory irritation was fairly minor; pulmonary irritation was more pronounced during the latter part of the repeated exposures. Sensory and pulmonary irritation were observed also in the control group (filtered air), suggesting that the reaction by-products of carbon monoxide (CO), nitrogen dioxide (NO_2), and propene (C_3H_6) may have contributed to the irritant effects. TiO2 NPs accumulated mainly in the pulmonary macrophages, but did not cause nasal or pulmonary inflammation. The authors concluded that the irritation and inflammation potencies of the studied TiO2 were low. The unusual exposure pattern made determination of a NOAEL and LOAEL difficult.

The same laboratory (Leppanen et al., 2015a) conducted a similarly-designed 4-week repeat exposure study using commercially available pigmentary TiO2 NPs (less than 5 μm, rutile at specific surface area of 2 m^2/g) with female BALB/c mice at a mass concentration of 16 mg/m^3. Minor sensory irritation was observed as elongation of the break after the inhalation, which is typical in sensory irritation (caused by closure of the glottis inhibiting airflow from the lungs after inspiration). No pulmonary irritation, airflow limitation, nasal or pulmonary inflammation was observed. The authors concluded that the respiratory irritation and inflammation potencies of the studied pigmentary TiO2 particles seemed to be low and could serve as an ideal control exposure agent in short-term studies in mice. Subsequently, Leppanen and coworkers (2015b) used a commercially available silica-coated TiO2 nanoparticle (10 x 40 nm, rutile) with a specific surface area of 132 m^2/g in the same mouse models. Repeated 4-week exposures at a mass concentration of 30 mg/m^3 to silica-coated TiO2 induced first phase of pulmonary irritation, which was seen as rapid, shallow breathing. Pulmonary mRNA expression of chemokines and levels of the proinflammatory cytokines TNF-α and IL-6 were elevated after repeated exposures. These results indicate that silica-coated TiO2 NPs induce pulmonary and sensory irritation, and airflow limitation and pulmonary inflammation after repeated exposure. While the objective of these studies was apparently to compare coatings on TiO2 particles (pigmentary vs. silica-coated) and used the same design, exposure regimen and strain of mice, differences in surface area (2 m^2/g vs. 132 m^2/g) and concentration precludes a conclusion as to the effect of coating on irritation outcome. The unusual exposure pattern made determination of a NOAEL and LOAEL difficult.

6.4.2.1 Summary

The recent literature search conducted for this project, identified four additional inhalation studies in rats and mice with exposures from 21 days to 13 weeks. All four were by head- or nose-only inhalation. Eydner et al. (2012) conducted a 3-week nose-only inhalation study with rats under OECD Test Guideline 412 and GLPs using nano- or fine-sized TiO_2 (Aeroxide® P25) at 0, 25/10 (with/without buffer) or 45 mg/m^3, followed by 3, 28, and 90 day recovery time periods. The lungs of rats treated with nano-sized and fine particles showed moderate alveolar infiltration with particle-laden macrophages at all three recovery time points (3, 28, and 90 days) with minimal interstitial infiltration of mononuclear cells and minimal alveolar infiltration with neutrophilic granulocytes observed, and with a few animals in both groups showing minimal bronchiolo-alveolar hyperplasia. Leppanen et al. (2011) showed non-dose-related irritation and inflammation in airways of mice by inhalation of 20 nm TiO2 NPs at 8, 20, and 30 mg/m^3. TiO2 NPs accumulated mainly in the pulmonary macrophages, but did not cause nasal or pulmonary inflammation, indicating the irritation and inflammation potencies of the studied TiO2 was low. The same laboratory (Leppanen et al., 2015a) conducted two more similarly-designed 4-week

studies, using commercially available pigmentary TiO2 particles. The first study used less than 5 μm (rutile) and found respiratory irritation and inflammation to be low. Subsequently, they used silica-coated TiO2 NPs (10 x 40 nm, rutile) which induced pulmonary irritation (rapid, shallow breathing). Pulmonary chemokines and levels of proinflammatory cytokines were elevated after repeated exposures. The results indicate that silica-coated TiO2 NPs induce pulmonary and sensory irritation, and airflow limitation after repeated exposures.

6.4.3 Dermal Exposure

One dermal exposure study to TiO2 NPs was identified in the recent literature (Adachi et al. 2013), which showed focal alterations, but no dermal penetration. Older studies in hairless mice and pigs (Wu et al., 2009) reported histopathological alterations to the skin and liver and systemic effects in hairless mice, and pathological changes in the skin of pigs.

Adachi and coworkers (2013) applied an emulsion containing 10 wt percent uncoated anatase TiO2 NPs or control emulsion to the dorsal skin (4 mg/cm^2 to a 15 cm^2 area) of male Wistar Yagi hairless rats once per day for a maximum of 56 consecutive days. The average size of the primary particles from the Manufacturer Safety Data Sheet was 17 nm. After 2, 4 and 8 weeks, skin samples were taken from the exposed skin area. Histopathology and Ti content of the brain, lung, liver, spleen and kidney were evaluated. The NPs were located only in the stratum corneum layer of the epidermis and follicular epithelium. Focal parakeratosis (retention of nuclei in the stratum corneum) and spongiosis (intercellular edema) were observed in the epidermis. TEM with energy-dispersive X-ray spectrometry analysis failed to show TiO2 NPs in the viable skin areas, indicating there was no evidence of TiO2 penetration.

In the literature prior to 2010, Versar (2012) described studies conducted by Wu et al. (2009) in BALB/c *nu/nu* hairless mice with suspensions of 5 percent TiO2 NPs applied to dorsal skin for 60 days. The physical properties of the particles utilized were measured experimentally: 10 nm anatase TiO2 particles (99.5 percent pure) had a hydrophobic surface area of 160 m^2/g; 25 nm rutile TiO2 particles (99.6 percent pure) had a hydrophilic surface area of 80 m^2/g; Degussa P25 particles (99.5 percent pure) were ~21 nm in size, 25 percent rutile/75 percent anatase, and had a hydrophilic surface area of 50 m^2/g; and 60 nm rutile TiO2 particles (99.6 percent pure) had a hydrophobic surface with of 40 m^2/g. An additional group of mice was exposed to coarse TiO2 particles (300 to 500 nm in size). Based on decreased body weight gain, changes in relative weights of the liver and spleen, changes in the activities of SOD and hydroxyproline (HYP) in the liver and skin, and histopathological changes to the skin and liver, which occurred mainly in mice treated with TiO2 with primary particle sizes of 10, 21, and/or 25 nm, the test concentration of 5 percent TiO2 (about 6.7 mg/kg/d) is identified as a LOAEL; no NOAEL was identified. The stratum corneum of the hairless mouse is less than half as thick as that of the human and with lower barrier properties. The available information on comparative penetration studies in humans and hairless mouse is sometimes contradictory. Some agents will penetrate in a similar manner, whereas others differ in at least one logarithmic order, the human skin being the less permeable (Simon and Maibach, 1998). Thus, this animal model has been significantly criticized that it may well amplify the penetration of NPs (Jonaitis et al., 2010). Only one concentration was tested, limiting the usefulness of this study for toxicity assessment.

Wu et al. (2009; as cited in Versar, 2012) also dermally exposed domestic pigs to test

formulations containing 5 percent (w/w) TiO2 NPs with average diameters of 4 nm (anatase) or 60 nm (rutile). About 24 mg of the test formulation was applied daily to the right ear of three pigs for 30 consecutive days. Skins of untreated ears served as controls. No clinical signs of toxicity and no erythema or edema of the treated area were reported. TEM analyses of the epidermis showed pathological changes in pigs treated with nano-TiO2 (4 nm in size). Based on the histopathological changes in the skin, a free-standing LOAEL of 5 percent nano-TiO2 (the only concentration tested) was identified.

No other data regarding the dermal toxicity of TiO2 NPs were located in the literature searches conducted for this project.

6.4.4 Other Routes of Exposure

Fu et al. (2014), designed a study to evaluate the systemic immune effects after IT administration of nano-TiO2 in rats. In this study, male Sprague Dawley rats were treated with manufactured P25 nano-TiO2 particles (mean diameter of 21 nm) at 0.5, 4, and 32 mg/kg bw or micro-TiO2 particles, sized (1 to 2 μm) at 32 mg/kg bw in 0.9 percent NaCl. Exposures were conducted twice a week, for four consecutive weeks at a volume of 0.1 ml/100 g. Histopathological examination of the immune organs from exposed animals showed slight congestion in spleen and particulate deposition in cervical and axillary lymph nodes. Immune function response was characterized by increased proliferation of T cells and B cells following mitogen stimulation, enhanced natural killer cell killing activity in the spleen, accompanied by increased number of B cells in blood. No significant changes of cytokines were observed. The authors suggest that exposure to TiO2 may trigger systemic immune responses.

Subchronic studies by other routes that would be relevant or supportive for data gaps were not located in the literature search for this project.

6.5 Chronic Toxicity/Carcinogenicity

There is a lack of epidemiological data regarding TiO2 NPs (Versar, 2012; NIOSH, 2017). Several scientists have reported that there was no clear evidence of increased respiratory disease or lung cancer mortality ratios in workers occupationally exposed to TiO2 dusts (Boffetta et al., 2004; Fryzek at al., 2003, as cited in Boffetta et al., 2004; Chen and Fayerweather, 1988). Although workers were presumably exposed to both fine and ultrafine TiO2 particles, these studies were not designed to investigate the relationship between TiO2 particle size, surface area or crystalline state and health or mortality risk; specific exposures to nanosized particles were not estimated (Versar, 2012; IARC, 2010; NIOSH, 2011, 2017). The literature search conducted for this project showed that there have not been more recent studies published.

The World Health Organization (WHO), International Agency for Research on Cancer (IARC) Working Group found little evidence of an increased risk for cancer among humans based on epidemiological data, although relatively few studies were available (IARC, 2010). Three epidemiological cohort studies and one population-based case–control study were available for evaluation. The latter multi-country study of TiO2 production workers found a slightly increased risk for lung cancer compared with the general population. The two other cohort studies showed no increased risks for lung cancer. The Working Group considered pathways and mechanisms

by which TiO2 particles may cause cancer and reasoned that the available mechanistic evidence for TiO2 was not strong enough to warrant a classification other than Group 2B human carcinogen, based on inhaled or IT-administered nano- and fine-sized TiO2 induced lung cancer in rats.

6.5.1 Oral Exposure

Only one study that investigated the chronic toxicity/carcinogenicity of TiO2 via the oral route was identified in the current literature.

Bettini et al. (2017) treated groups of 11 to 12 adult male Wistar rats with 1,2-dimethylhydrazine (DMH) to initiate colon carcinogenesis; other groups were not treated with the initiator. The groups were then exposed to TiO2 E171 (a food-grade whitening pigment) or NM-105 (a reference NP) through their drinking water for 100 days. E171 batches showed broad size distributions of TiO2 primary particles size (diameters of 30 to 400 nm), with up to 36 percent of particles falling below 100 nm in one dimension. Control rats received water only. Increases in immune responses were noted and E171 treatment alone promoted colon micro-inflammation and initiated preneoplastic lesions, while fostering the growth of aberrant crypt foci (ACF). Rats were exposed to TiO2 NPs in the drinking water at 200 µg and 10 mg/kg/d for 100 days. The number and size of ACF and the number of total aberrant crypts per colon were examined double-blind. E171 treatment at 10 mg/kg/d significantly increased the total number of aberrant crypts per colon as well as the number of large ACF per colon (i.e., more than three aberrant crypts per ACF) relative to the control and 200 µg/kg/d groups. Despite an increasing trend at the highest dose, no significant difference in the number of ACF per colon was observed between the groups of rats. The forms of TiO2 used in this study were food grade. While these forms of TiO2 are not within the purview of CPSC, this study is reviewed to inform chronic toxicity/carcinogenicity hazard via the oral route as there are limited data on other available forms. This study is a non-guideline design for carcinogenicity with only one dose level for each TiO2 form, and is limited in usefulness for risk assessment due to the short duration of exposure for carcinogenicity (thereby affecting the potential for tumors to develop over time), small group sizes, one sex and species of animals, and examination of limited organs for tumors.

6.5.2 Inhalation Exposure

The only chronic duration toxicity/cancer bioassay identified in the literature, conducted by Heinrich et al. (1995) in rats and mice, is described in Versar (2012), summarized here, and presented in Table 31. The usefulness of Heinrich et al. (1995) for development of an ADI is limited due to use of only one exposure level, only one sex (females), one strain/species each of rats and mice, and evaluation of limited endpoints (i.e., mortality, clinical signs, body and lung weights, BALF parameters [rats only], and respiratory tract histopathology), and, retrospectively, changes in pathologic diagnostic criteria for the lung tumors reported.

Table 31. Chronic Toxicity Studies via Inhalation to TiO2 NPs

Species and study type (n/sex/group)	Exposure (report concentrations, frequency, duration)	Particle Characteristics	NOAEC (mg/m^3)	LOAEC (mg/m^3)	Responses at the LOAEC	Comments	Reference
Wistar rats females 100/group whole body exposure	0 or 10 mg/m^3 for 18 h/d, 5 d/wk for 24 months	80% anatase/ 20% rutile; 15 to 40 nm particle size; surface area = 48 m^2/g; uncoated Aerosols: MMAD 0.80 µm; σ_g 1.8	none	10 (systemic, lung)	Decreased lifespan, decreased body weight, changes in BALF parameters, increased lung weights, and histopathological changes in lung (e.g., interstitial fibrosis in nearly all exposed rats and increased incidence of rats with lung tumors)	Endpoints evaluated: mortality, clinical signs of toxicity, body wts, BALF parameters, lung weights, and histopathological examination of nasal and prenasal cavities, larynx, trachea, and lung. Lung tumor incidence was significantly increased in rats exposed to TiO2 (32/100) relative to controls (1/217) Only one concentration tested	Heinrich et al., 1995
NMRI mice females 80/group whole-body exposure	0 or 10 mg/m^3 for 18 h/d, 5 d/wk for 13.5 mo	Same as above for rats	none	10 (systemic)	Decreased lifespan and increased lung weights	Same endpoints as for rats except BALF. Lung tumor incidence was not significantly increased relative to controls in mice exposed to TiO2. Only one concentration tested	

No new carcinogenicity studies of TiO2 by the inhalation route were identified in the literature since 2010.

Female Wistar rats were whole-body exposed to TiO2 NPs as an aerosol to a target concentration of 0 (clean air control) or 10 mg/m^3 for 18 h/d, 5 d/wk for up to 2 years (Heinrich et al., 1995; as reviewed in Versar, 2012). Actual exposure concentrations were 7.2 mg/m^3 for the first 4 months, 14.8 mg/m^3 for 4 additional months, and 9.4 mg/m^3 for the remaining exposure period (16 months). TiO2 particles used as a starting material were 80 percent anatase/20 percent rutile, measured 15 to 40 nm in size, with a surface area of 48 m^2/g. The aerosols had a MMAD of ~1.5 µm. To increase deposition efficiency, particle size distribution was reduced via filtering of coarse particles to produce MMAD and GSDs of 0.80 and 1.80 µm, respectively.

Several groups of rats were exposed to TiO2 to evaluate different endpoints; 80, 66, and 28 rats/group were used to evaluate histology, particle mass/lung, and lung clearance, respectively (Time-weighted average [TWA] for 24 months = 9.2 mg/m^3). Animals in the histology group were sacrificed at 6, 12, 18, or 24 months (20 per time point). Lungs of sacrificed animals were lavaged and biochemical and cytological parameters evaluated. Lung weights (wet) were recorded at 3, 6, 12, 18, 22, or 24 months after the start of exposure (particle mass/lung group). Histopathological analyses of the nasal and paranasal cavities, larynx, trachea, and lung were performed on all animals. Mortality in TiO2-treated rats reached 60 percent by 24 months, compared to 42 percent in control rats. Body weight was decreased, wet lung weight increased, bronchiolar hyperplasia incidence increased (99/100) in the carcinogenicity group, and interstitial fibrosis and the detection of free particles and particle-laden macrophages in the alveolar region of the lungs increased in exposed rats relative to controls. The LOAEL in rats is identified as 10 mg/m^3 (the only exposure concentration tested) for up to 24 month exposure duration to uncoated TiO2 NPs (80 percent anatase, 20 percent rutile).

Additional groups of animals (100 TiO2-treated rats and 220 controls) were exposed to TiO2 for 24 months and observed for 6 months post-exposure to assess carcinogenicity. At the end of the observation period, mortality was 90 and 85 percent in treated and control groups, respectively. Compared with control rats, the mean lifespan of rats treated with TiO2 was significantly shorter. No explanation was provided for the high mortality in controls (albeit the animals would be ~30 months old). Lung tumors were observed in groups of treated rats (serial histology group) sacrificed after 18 months or more of exposure; at 18 months, the incidence of lung tumors (benign squamous-cell tumors, squamous cell-carcinomas, and adenocarcinomas) was significantly higher in TiO2-treated rats (5/20) than control rats (0/18). In rats sacrificed at 30 months, tumor incidence was 32/100 in exposed rats (some rats had multiple lung tumors) compared to 1/217 (0 percent) in control rats. Despite few findings of lung tumors in control rats, high mortality within this group may have contributed to a lower rate of lung tumor incidence than might be expected given a lower mortality rate, as early mortality decreases the number of animals at risk for late-developing tumors. Tumors in other tissues examined histologically were not reported. The benign keratinizing cystic squamous cell tumors observed were later recharacterized pathologically as proliferative keratinizing cysts, a lesion of questionable pathological significance to humans (Boorman et al., 1996; Fryzek et al., 2003; Dankovic et al., 2007).

As part of the same experiment, NMRI mice (80, 40, and 40 females in the carcinogenicity, serial histology, and serial particle mass/lung groups, respectively) were whole-body exposed to TiO2 NPs (exhibiting the same particle characteristics as reported above for rats) at an average exposure concentration of 10 mg/m^3 for 18 h/d, 5 d/wk, for 13.5 months (Heinrich et al., 1995; as reviewed in Versar, 2012). With the exception of BALF parameters, which were not evaluated in mice, the same endpoints were assessed in rats and mice. Actual exposure concentrations were 7.2 mg/m^3 for the first 4 months, 14.8 mg/m^3 for 4 additional months, and 9.4 mg/m^3 for the remaining exposure period (5.5 months). Controls were exposed to clean air and observed for up to 9.5 months post-exposure. Although it was not explicitly stated by the researchers that ~15 mg/m^3 was the targeted exposure concentration for the duration of the study, the researchers did state that the exposure concentration was reduced to ~10 mg/m^3 at 8 months after the initiation of exposure because mice exhibited increased mortality and showed clinical signs of toxicity. By the end of the exposure period (13.5 months), mortality reached 33 percent in the TiO2 treatment group, compared with 10 percent in the control group; the researchers did not indicate the cause of death in untreated or treated mice. Compared with control mice, the mean lifespan of mice treated with TiO2 was significantly shortened. A statistically significant decrease in the body weight of treated rats occurred at 8 months after the start of exposure, but then was similar to controls by the end of the exposure period. Lung weights were significantly increased in TiO2-treated mice compared with controls during the exposure period, but decreased slightly relative to the 12-month time point at the end of the exposure period. Non-neoplastic lesions in the histologically examined tissues were not mentioned in the published report. Based on clinical signs of toxicity, shortened life span, decreased body weight, and increased wet lung weights, 10 mg/m^3 (the only exposure concentration tested) is identified as a LOAEL in NMRI mice exposed for up to 13.5 months to uncoated TiO2 NPs (80 percent anatase, 20 percent rutile); no NOAEL was identified. The incidence of lung adenomas and adenocarcinomas (and combined tumor incidence) observed in TiO2-treated mice were not significantly different from control animals. The use of the NMRI mouse, which has a very high spontaneous lung tumor rate (historical control of ~30 percent), as well as the shortened life-span of exposed mice likely compromised detection of treatment-related lung tumors.

6.5.3 Dermal Exposure

Two skin carcinogenicity studies (initiation-promotion studies) were conducted in mice and rats. No dose-related increase in tumors was reported in either study.

Furukawa et al. (2011) examined the post-initiation (terminology used by authors) carcinogenic potential of coated and uncoated TiO2 NPs using a mouse skin carcinogenesis bioassay. Coated (CTND-coating not specified) and uncoated TiO2 NPs at 5, 10 or 20 mg/animal were applied at concentrations of 5 mg/0.1 g or 20 mg/0.1 g, twice weekly to the back skin of mice in the post-initiation phase (up to 20 weeks) in a two-stage skin carcinogenesis model using 7-week old CD-1 (ICR) female mice. 7,12-Dimethylbenz[a]anthracene (DMBA; 0.1 mg/0.1 ml acetone) and 12-o-tetradecanoyl-phorbol 13-acetate (4 µg/0.2 ml acetone) were used as the initiator and positive control promoter, respectively. Pentalan 408 served as a vehicle control. The industrial material-grade coated TiO2 NPs (79.2 percent) were spindle shape, with a long axis of 50 to 100 nm, and short axis of 10 to 20 nm. Uncoated TiO2 NPs (96.0 percent), were spindle shape, with

a long axis of 50 to 100 nm, and short axis of 10 to 20 nm. No changes in survival rate, general condition and body weight related to the test materials were observed. On macroscopic observation, 1 to 2 skin nodules were observed in each group treated with coated and uncoated TiO_2 NPs, as well as in the control group, after DMBA initiation (see Table 32). The nodules were histopathologically diagnosed as squamous cell hyperplasia, sebaceous gland hyperplasia, squamous cell papilloma, and keratoacanthoma. Coated and uncoated TiO2 NP application caused enlargement of the mandibular, pancreatic, lumbar region and inguinofemoral lymph nodes, and spleen and thymus in mice given 5 and 10 mg, but not 20 mg. The lack of dose-response suggests no biological significance of the increase in development of nodules when compared to the positive control promoter, indicating a lack of post-initiation potential (lack of promotion) of TiO2 for mouse skin carcinogenesis.

Table 32. Carcinogenicity Study Results from Furukawa et al. (2011)

Groups	**1**	**2**	**3**	**4**	**5**	**6**	7
Initiation	DMBA				Acetone		
Test Chemical	Pentalin 408	CTND (mg/mouse)			TPA - 4 µg/mouse	Pentalin 408	CTND (mg/mouse)
		5	10	20			
Incidence (percent)	2/20 (10)	0/20 (0)	1/20 (5)	2/20 (10)	20/20 (100)	0/20 (0)	0/20 (0)
Total Nodules	3	0	1	2	513	0	0
Mean ± SD	0.2±0.5	0.00	0.1±0.2	0.1±0.3	25.7 ± 13.1	0.0	0.0

Sagawa et al. (2012) evaluated the effects of dermally-applied silicone coated TiO2 (sTiO2) compared to non-coated TiO2 (ncTiO2) to the shaven backs (2 x 2 cm area) of mice and rats in a two-stage skin carcinogenesis assay. The TiO2 rutile NPs were manufactured to have a mean diameter of 35 nm for the coated and 20 nm for the uncoated, and were suspended in silicone oil or Pentalin 408, respectively. The concentrations applied were 0, 50 and 100 mg/mL for both particles. The animals were male transgenic rasH2 mice and male Hras128 rats, known to be highly sensitive to chemically-induced skin carcinogenesis, and their wild-type counterparts, CB6F1 mice and Sprague-Dawley, respectively. Sixty rasH2 mice and 60 Hras128 rats were painted in the application area with a single dose of 0.1 ml of the promotor DMBA. Two weeks later, the animals were divided into 3 groups and painted with DMBA alone or the silicone coated TiO2 at 0, 50 or 100 mg/mL, five times a week until termination. The rasH2 mice were killed at week 8 and the wild-type CB6F1 mice at week 40. For the rat study, 50 male Hras128 rats and 36 wild-type rats received 0.5 ml of DMBA applied to their shaven backs. Two weeks later the rats were divided into 3 groups and painted with Pentalin 408 alone or with ncTiO2 suspended in Pentalin 408 at 0, 50 or 100 mg/mL, five times per week until termination. The Hras128 rats were killed at week 28 and the wild-type rats at week 40. The mean length of sTiO2 suspended in saline and silicone oil was 0.16 ± 0.07 and 0.28 ± 0.22 µm, respectively. The mean length of ncTiO2 suspended in saline and Pentalin 408 was 3.18 ± 0.35 and 4.97 ± 0.50 µm, respectively. The incidence and multiplicity of skin tumors (squamous cell papilloma and carcinoma) in the rasH2 mice and Hras128 rats or the wild-type mice did not increase over

DMBA alone treated animals. Analysis of the rat skin indicated that neither sTiO2 nor ncTiO2 penetrated through healthy or damaged epidermal tissue.

6.5.4 Summary

There is a lack of epidemiological data regarding TiO2 NPs (Versar, 2012; NIOSH, 2017). The WHO, IARC Working Group found little evidence of an increased risk for cancer among humans based on epidemiological data, although relatively few studies were available (IARC, 2010).

Only one study that investigated the chronic toxicity/carcinogenicity of TiO2 via the oral route is a non-guideline design with only one dose level for each TiO2 form tested. It is limited in usefulness for risk assessment due to the short duration of exposure for a carcinogenicity study (thereby affecting the potential for tumors to develop over time), small group sizes, one sex and species of animals, and examination of limited organs for tumors.

The only chronic duration toxicity/cancer bioassay via inhalation identified in the literature was conducted by Heinrich et al. (1995) in rats and mice, and is described in Versar (2012). The usefulness of Heinrich et al. (1995) for development of an ADI is limited due to the use of only one exposure level, only one sex (females), one strain/species each of rats and mice, and evaluation of limited endpoints (i.e., mortality, clinical signs, body and lung weights, BALF parameters [rats only], and respiratory tract histopathology), and, retrospectively, changes in pathologic diagnostic criteria for the lung tumors reported. A chronic LOAEL in rats was identified as 10 mg/m^3 (the only exposure concentration tested) for up to a 24 month exposure duration to uncoated TiO2 NPs (80 percent anatase, 20 percent rutile). No new carcinogenicity studies of TiO2 by the inhalation route were identified in the literature since 2010.

Two skin carcinogenicity studies (initiation-promotion studies) were conducted in mice and rats. However, no dose-related increase in tumors was reported in either study.

6.6 Reproductive/Developmental Toxicity

6.6.1 Oral Exposure

Prior to 2010, there were no reproductive or developmental studies via oral exposure. Since that time, while human data were not located, there have been numerous studies via the oral exposure route in animals: two reproductive studies (one in mice and one in two strains of rats), two developmental studies (one each in mice and rats), three male reproductive studies (two in mice and one in rats) and one juvenile toxicity study in rats (summarized in Table 33).

Table 33. Summary of Reproductive and Developmental Toxicity Studies of TiO2 NPs via Oral Exposure

Species/Strain (n/sex/group)	Dose, frequency, duration	Particle Characteristics	NOAEL (mg/kg/d)	LOAEL (mg/kg/d)	LOAEL Responses	Comments	Reference
Sprague-Dawley and Wistar rats males and females 10/sex/group	0 or 1000 mg/kg/d by gavage; males: 2 wks prior to mating through 2 wks post-mating; females: 2 wks prior to mating, through day 4 following delivery.	Surface areas of pg and uf ranged from 7 to 17 m^2/g and 50 to 82 m^2/g, respectively; anatase and/or rutile.	1000	none		Reproduction screening study (OECD 421)	Warheit et al., 2015b
CD-1 (ICR) mice males and females 10/sex/group	0, 2.5, 5 or 10 mg/kg/d daily by gavage for 90 days	Anatase; average 5 to 6 nm; surface area = 174.8 m^2/g; mean hydro-dynamic diameter = 208 to 330 nm	none	2.5	Adverse ovarian findings; ↓ mating rate; ↓ fertility; ↓ pup number, weight and survival	No male toxicity parameters collected (see Gao et al., 2013)	Zhao et al., 2013
CD-1 (ICR) mice females	0, 10, 100, or 1000 mg/kg/d by gavage in tragacanth gum on GD 9 only	Rutile, 99,5% pure; 50 nm (61.5 ± 1.8; range 51 to 65 nm), in tragacanth gum, 472 ± 56.2 nm	1000 (parental)	none	↑ morphological defects and nonviable fetuses		Philbrook et al., 2011
Wistar rats females 6/group	0 or 100 mg/kg/d by gavage; daily; GD 2 to 21	Anatase; particle size of 10 nm, surface area greater than 150 m^2/g, and purity +99%	none	100	TiO2 transversed the blood brain barrier to the hippocampus; increased brain weight; and impaired passive avoidance, and learning and memory in Morris water maze on day 60	Half examined neonatal brains day 1; remainder males weaned for learning and memory	Mohammadipour et al., 2014
albino rats males 20/group	0 or 100 mg/kg/d by gavage daily; 8 weeks (interim sac after 4 weeks)	Commercially purchased Aeroxide® P25, Titania; 21 nm primary particle size, ≥ 99.5% pure anatase	none	100	↓ relative testis & epididymis wts after 8 wks; ↓sperm motility, concentration & viability after both 4 and 8 wks and ↑ sperm abnormalities		Morgan et al., 2015

Species/Strain (n/sex/group)	Dose, frequency, duration	Particle Characteristics	NOAEL (mg/kg/d)	LOAEL (mg/kg/d)	LOAEL Responses	Comments	Reference
CD-1 (ICR) mice males and females 10/sex/group	0, 2.5, 5 or 10 mg/kg/d by gavage daily for 90 days	Anatase; average 5 to 6 nm; surface area = 174.8 m^2/g; mean hydro-dynamic diameter = 208 to 330 nm	none	2.5	↓ body and testes weights; severe pathological changes in testis, including sperm breakage, Sertoli cell apoptosis, and necrosis of the seminiferous tubules	No female toxicity parameters collected (see Zhao et al., 2013)	Gao et al., 2013
CD-1 (ICR) mice males	0, 2.5, 5 or 10 mg/kg/d by gavage daily for 60 days	Anatase; average 5 to 6 nm; surface area = 174.8 m^2/g; mean hydro-dynamic diameter = 208 to 330 nm	none	2.5	↓ body and testes weights; ↓ sperm motility, concentration & viability; ↑ sperm abnormalities; ↓ testicular enzyme and ↑ oxidative stress markers		Hong et al., 2015

pg = pigment grade; uf= ultrafine

6.6.1.1 Reproductive and Developmental Toxicity

The results of an oral OECD TG421 reproduction screening study, designed to assess the effects of pigment-grade TiO2 particles on fertility and prenatal developmental toxicity (NIER, 2007) are reported by Warheit et al. (2015a, b). Six different commercial forms and sizes of TiO2 particles (Table 34) were tested in separate oral prenatal developmental toxicity studies (OECD Test Guideline 414). In all studies the three pigment-grade (pg) or 3 ultrafine (uf) /nanoscale (anatase and/or rutile) TiO2 particle-types were evaluated for potential maternal and developmental toxicity by OECD Test Guideline 414 in two different strains of pregnant rats (Sprague-Dawley and Wistar) by two different laboratories. All test materials were robustly characterized. The BET surface areas of the pigmented and nano-sized samples ranged from 7 to 17 m^2/g and 50 to 82 m^2/g, respectively.

Table 34. Physicochemical Characteristics of TiO2 in Warheit et al. (2015b)

Test Sample	Crystal Structure	BET Value (m^2/g)	Calculated Size (nm)
uf-1	89% anatase/11% rutile	50.4	43
uf-2	100% anatase	82	42
uf-3	100% rutile	59	47
pg-1	100% anatase	8.1	153
pg-2	100% rutile	7.1	195
pg-3	100% rutile	17.1	213

In the OECD Test Guideline 414 prenatal developmental toxicity study (Warheit et al., 2015b), the test substances uf-1, uf-3 and pg-1 were formulated in sterile water and were administered by oral gavage to time-mated Sprague-Dawley rats daily from GD 6 to 20. Test substances uf-2, pg-2 and pg-3 were formulated in sterile water and administered by oral gavage to time-mated Wistar rats daily from GD 5 to 19. The dose levels used in all studies were 0, 100, 300, or 1000 mg/kg/d. All live fetuses were sexed, weighed, examined externally then euthanized. Following euthanasia, gross necropsies included an examination and description of uterine contents including counts of corpora lutea, implantation sites, resorptions, and live and dead fetuses. Fresh visceral and head examinations were performed on selected fetuses, then the fetal carcasses were processed, stained and examined for skeletal alterations. There were no mortalities and no evidence of maternal (clinical observations, body weight, body weight gain, feed consumption values) or developmental (litter size, post-implantation losses, fetal visceral or skeletal malformations or variations) toxicity at any dose level in any of the studies. Fetal alterations occurred with low frequency across all groups tested and occurred with similar frequency to the test facility historical control database. Based on these results, the maternal and developmental NOAEL for both the ultra-fine and pigmented TiO2 was 1000 mg/kg/d, the highest administered dose, in both the Sprague-Dawley and Wistar rats.

In the OECD Test Guideline 421 reproduction screening study (NIER, 2007 and reported by Warheit et al., 2015b) male and female Sprague-Dawley rats were treated with pigment-grade TiO2 by oral gavage at doses of 0 or 1000 mg/kg/d. The vehicle was 1 percent methyl cellulose. Males (10 rats/group) were administered the test substance for a total of 40 days (i.e., 2 weeks

prior to mating, during the mating period and an additional 2 weeks post-mating period). Females (10 rats per group) were treated for two weeks prior to mating, throughout gestation and until day 4 following delivery. No treatment-related changes relative to controls were observed in clinical signs, body weight, food consumption values, necropsy findings or organ weights of the testis and epididymis. All of the (minor) histopathological findings were considered to be incidental and not treatment-related, as similar results were observed in the vehicle control group. No treatment-related effects were observed or measured in the TiO2-exposed group in: gestation length, number of corpora lutea, implantation sites, delivery index, body weight of pups in both sexes on Day 0 and 4 of lactation, and pre- and post-implantation losses. From an observation of live pups at birth, it was concluded there were no externally malformed pups in any of the groups. At necropsy of pups, no gross finding was observed in any groups. Oral administration of pigment-grade TiO2 particles to adult/parental animals resulted in no adverse effects on any of the parameters examined at 1000 mg/kg /d. Therefore, the NOAEL of this study was determined to be 1000 mg/kg/d (only dose tested) in both sexes for general toxicity, reproductive capability and development of F1 neonates.

Zhao and coworkers (2013) gavaged female CD-1 mice (100 per group) daily with 0, 2.5, 5, or 10 mg/kg/d nano-TiO2 for 90 consecutive days to study the effects of nanosized TiO2 on reproduction and fertility in mice. The average aggregate or agglomerate size of the TiO2 ranged from 5 to 6 nm. The surface area of the sample was 174.8 m^2/g, the mean hydrodynamic diameter ranged from 208 to 330 nm (mainly 294 nm), and the Zeta potential was 9.28 mV. To evaluate the effect of nano-TiO2 on the fertility and growth of newborns, 10 untreated control males and 10 untreated control or treated female mice from each group were mated after 90 days of treatment and the number of newborn from each pregnant mouse were counted and weighed. With increasing TiO2 doses, the body weights and relative weight of the ovaries were significantly decreased, the severity of which was dose-related, while Ti contents in the ovary were significantly increased. Hematological and biochemical analyses indicated that WBC count, lymphocytes, neutrophils, RBCs and HB parameters in the TiO2-treated female mice were statistically significantly reduced starting with the lowest dose, the severity of which was related to increasing dose. Nano-TiO2 exposure significantly increased the activities of ALT, AST, ALP, LDH, and the levels of creatinine (CR), and reduced uric acid (UA) and BUN in sera. These effects also occurred at the lowest dose with severity increasing with increasing dose. With regards to reproductive and development indices, the mating rate, pregnancy rate, number of newborn, and the weights of neonates were significantly reduced at the lowest dose, and the severity of these effects increased with higher TiO2 doses. In addition, TiO2 exposure led to reduced survival of young mice at 28 days post-parturition at all doses.

Histopathological evaluation revealed an increased atretic follicle, severe inflammation and necrosis in the ovary, which was associated with premature ovarian failure. The authors concluded the decreased mating capacity of female mice following exposure to TiO2 may be associated with an imbalance of sex hormone levels; serum estradiol (E2) levels gradually increased with dose, and P4 (progesterone), LH, FSH, and testosterone were significantly decreased in female mice treated with increased nano-TiO2 doses. The LOAEL of this study is 2.5 mg/kg/d.

The effects of oral TiO2 NPs on fetal development of CD-1 (ICR) mice was investigated by

Philbrook and coworkers (2011). The commercially-purchased TiO2 NPs (rutile) were untreated, 99.5 percent pure and supplied as 50 nm NPs. TEM images revealed the TiO2 NPs ranged from 51 nm to 65 nm with an average size of 61.5 ± 1.8 nm. In contrast, the size range of TiO2 NPs in tragacanth gum ranged from 262 nm to 660 nm with an average size of 472 ± 56.2 nm, suggesting that TiO2 NPs clumped together more in tragacanth gum. The developmental success of CD-1 mice was evaluated after a single 5 ml/kg oral gavage dose to the dams (each group resulted in 11 to 14 litters) of 0 percent, 0.2 percent, 2.0 percent or 20 percent w/v (0, 10, 100 or 1000 mg/kg) in a 0.5 percent tragacanth gum solution of water, only on GD 9. Dams were weighed and then euthanized on GD 18 and the uterus was examined for resorptions. All fetuses were counted, weighed, measured for length and examined for any external morphological defects. Placentas, fetal livers and fetal kidneys were processed, stained with H&E, embedded in paraffin and then histopathologically examined. Fetal skeletons were stained with Alcian Blue and Alizarin Red S for cartilage and bone visualization, respectively. There was no indication of maternal toxicity after TiO2 NP treatment (10 to 1000 mg/kg/d) throughout the 10-day post-exposure period and the dams' behavior appeared normal. There were no statistically significant differences between the litter size or the change in maternal weight from GD 9 to GD 19, resulting in a maternal NOAEL of 1000 mg/kg/d. There were no significant differences in fetal resorptions, mean fetal weights or lengths (fetal growth) from the control group. At the two highest doses, however, there was a statistically significant increase in total fetal deformities (based on the fetus and not the litter as the statistical unit of measure), including exencephaly (6 fetuses), open eyelids (7 fetuses), leg (2 fetuses) and tail defects (1 fetus), and fetal mortality (7.6 percent at 1000 mg/kg/d only). This resulted in a developmental NOAEL of 1000 mg/kg/d.

A non-guideline developmental exposure study was designed to determine the effects of exposure to TiO2 NPs during pregnancy on hippocampal cell proliferation and the learning and memory of offspring (Mohammadipour et al., 2014). Six pregnant Wistar rats received TiO2 NPs (100 mg/kg bw) by oral gavage daily from GD 2 to 21. TiO2 NPs were a type of anatase nanopowder, with a particle size of 10 nm, surface area greater than 150 m^2/g, purity greater than 99 percent anatase, and density of 3.9 g/m^3. After delivery, two male pups from each litter were randomly assigned to an experimental group; one pup was used for the determination of hippocampal Ti content, and another was used for a histological examination. Male offspring (12/ group) were weaned at PND 21, and housed until PND 60. The whole hippocampus from the day-1 non-selected neonates were weighed and analyzed for Ti content. The results indicated that Ti accumulated in the hippocampus of the TiO2 group, while in the unexposed rats, Ti was not detected. The relative wet brain weight to body weight ratio was significantly higher in the exposed group compared to the unexposed group. To elucidate the effect of TiO2-NPs on hippocampal cell proliferation, an immunoreactive proliferating cell marker (Ki-67) was examined in the hippocampus of the offspring. Immuno-stained Ki-67-positive cells were observed in the hippocampus of all offspring. After the administration of TiO2 NPs, the number of Ki-67-positive cells in the hippocampus declined sharply. Learning and memory in animals were evaluated using passive avoidance and Morris water maze tests, which showed, that exposure to TiO2 NPs significantly impaired learning and memory in offspring. To summarize, TiO2 NPs absorbed from oral exposure during pregnancy can cross the placenta and fetal blood–brain barrier, enter the fetal brain, and partially deposit in the hippocampus, reducing

hippocampal cell proliferation in rat neonates. An inhibitory effect on memory and learning was an outcome in offspring after maternal exposure of TiO2 NPs via oral administration. The results of this study are difficult to interpret since the overall number of animals is small, only one dose was used, and statistical analysis appear, at least in part, to be pup-based, not litter-based.

6.6.1.2 Male Reproductive Toxicity

A recent repeat oral toxicity study was designed to investigate the male reproductive toxicity of TiO2 in male albino rats (Morgan et al., 2015). Forty adult male albino rats were divided into two equal groups. Group 1 served as the control and group 2 received TiO2 at 100 mg/kg/d by daily gavage for 8 weeks. The TiO2 NPs were commercially purchased Aeroxide® P25, Titania; 21 nm primary particle size (TEM), greater than 99.5 percent pure anatase. Half of each group was sacrificed after 4 weeks of treatment and the remainder was sacrificed after 8 weeks. Blood samples and testis, epididymis, seminal vesicle and prostate gland of each rat were collected, weighed and saved for histopathological examinations. Spermatozoa were collected from the tail of epididymis and vasa deferentia and examined for sperm cell concentration, progressive motility, live and dead sperm, and sperm abnormalities. Serum testosterone level was measured in collected serum samples. TiO2 affected the male reproductive system as evidenced by significantly reduced relative testis and epididymis weights after 8 weeks of treatment. Sperm motility, concentration and viability percentage were also significantly reduced after both 4 and 8 weeks of exposure with increased incidences of sperm morphological abnormalities (deformed head, detached head, curved tail and coiled tail). Serum testosterone level was significantly decreased at 4 and 8 weeks, compared with controls. Marked, but non-significant, decreases in body weight and histopathological alterations in testis, epididymis, seminal vesicle and prostate gland were observed.

In another male reproductive toxicity study, testicular damage and alterations in gene expression profiles occurred in male CD-1 mice after being orally gavaged for 90 consecutive days with 0, 2.5, 5, or 10 mg/kg/d TiO2 NPs (Gao et al., 2013). Anatase TiO2 NPs were prepared in the investigators' laboratory via controlled hydrolysis of titanium tetrabutoxide. The average particle size of powdered TiO2 NPs was 5 to 6 nm with the surface area of 174.8 m^2/g. The mean hydrodynamic diameter of the TiO2 NPs in solvent was 294 nm (range, 208 to 330 nm) and the Zeta potential after 12 and 24 hrs incubation was 7.57 and 9.28 mV, respectively. A hydroxypropyl methylcellulose concentration of 0.5 percent was used as the suspending agent. All histopathological tissues were stained with H&E and examined blind to the pathologist. Sera samples were evaluated for sex hormone content of E2, P4, LH, FSH, prolactin, testosterone, and sex hormone binding globulin using commercial kits. Cauda epididymis sperm concentration and sperm movement were manually examined using a light microscope. After staining, sperm were observed and photographed. With increased TiO2 NP doses, the body weight and testes weights were significantly reduced and Ti accumulation was increased at all dose levels, whereas no Ti was detected in control tissues. Histopathological evaluation of the testis found severe pathological changes at all dose levels tested, including sperm breakage, Sertoli cell apoptosis and irregular arrangement of Sertoli cells, necrosis of the seminiferous tubules, and vacuolation. In addition, black agglomerates were observed in the seminiferous tubules of mice exposed to 10 mg/kg of TiO2 NPs, which were confirmed as deposits of TiO2 in the testis. Sperm collected

from the cauda epididymis showed statistically significant decreases in sperm numbers and sperm motility, and dose-related increased abnormal sperm in all the TiO2 NPs-exposed groups. Increased TiO2 dosages at all levels induced toxicity-related changes in sperm morphology indicated by numerous significant breakages from the head to the tail. The effects of TiO2 on serum hormones of male mice were (1) significantly increased E2 and P4 levels; and, (2) LH, FSH, and testosterone markedly decreased with increased dosages. These findings show that TiO2 NPs can cross the blood–testis barrier to reach the testis and bioaccumulate, resulting in testicular lesions, sperm malformations, and alterations in serum sex hormone levels. There were no paternal or reproductive NOAELs; the paternal or reproductive LOAELs were 2.5 mg/kg/d.

In a non-guideline male reproductive study, young male (~6 weeks old) CD-1 (ICR) mice were exposed to 0 (0.5 percent w/v hydroxypropyl methylcellulose), 2.5, 5, or 10 mg/kg anatase TiO2 NPs via oral gavage for 60 consecutive days (Hong et al., 2015). The anatase particles were prepared by the investigating laboratory and measured 5 to 6 nm for particle size, 174.8 m^2/g for surface area, mainly 294 nm for mean hydrodynamic diameter, and 9.28 mV for Zeta potential, respectively. All testicular and epididymal tissues were stained with H&E and histopathologically examined blind to the pathologist. Sera samples were evaluated for sex hormone content of estradiol, progesterone, LH, FSH, prolactin, testosterone, and sex hormone binding globulin using commercial kits. Fresh testes were weighed, cauda epididymal sperm concentration measured, and sperm movement manually assessed by observation using a light microscope. Sperm were observed and photographed. Daily food intake and water intake were decreased by 7.44 percent to 43.24 percent and by 3.82 percent to 16.41 percent, respectively. With increasing TiO2 NP dose, significant reductions in final body weight (~6, 15 and 20 percent from low to high dose), testicular weight (~13, 32, and 42 percent), and relative testicular weight (~7, 20, and 28 percent) were observed at all doses. Findings showed that TiO2 exposure resulted in lesions of testis and epididymis, reductions in sperm concentration and sperm motility, and an increase in the number of abnormal sperm in mice in all groups tested. With increasing TiO2 dose, sperm numbers and sperm motility were remarkably reduced by ~30 to 49 percent and by ~7 to 41 percent, respectively. Abnormal sperm were significantly elevated by 4- to 12-fold in all the TiO2 NP-exposed groups. TiO2 exposure caused decreased activities of some testicular enzymes markers, and elevation of oxidative stress markers in the testes of mice. In addition, TiO2 NP exposure caused excessive production of ROS, and increased malondialdehyde of lipid peroxidation product, carbonyl of protein oxidative product, and 8-hydroxy deoxyguanosine of DNA oxidative product in the testes. These findings suggest that spermatogenesis suppression caused by TiO2 NP exposure may be associated with alterations of testicular marker enzymes and oxidative stress in the testes. There were no paternal or reproductive NOAELs; the paternal or reproductive LOAEL was 2.5 mg/kg/d.

6.6.1.3 Juvenile Toxicity

Young (3-week old) and adult (8-week old) male Sprague-Dawley rats were gavaged with TiO2 NPs at doses of 0, 10, 50, or 200 mg/kg/d for 30 days (Wang et al., 2013). The particles were nearly spherical anatase crystals with a hydroxyl group on the surface. Purity was 99.90 percent, the average size was 75 ± 15 nm, and the specific surface area was 63.95 m^2/g. At necropsy, the liver, kidney, spleen, testis, lung, heart, brain, stomach and small intestine were excised and weighed. Liver function was evaluated with serum levels of total protein, albumin, globulin, albumin/globulin ratio, ALT, AST, ALT/AST ratio, and total bilirubin. Nephrotoxicity was determined by BUN and CR. Glycolipid metabolism was judged by the levels of fasting blood glucose, total cholesterol, triglycerides, HDL, and LDL cholesterol. The enzymes of creatine kinase, LDH, and alpha-hydroxybutyrate dehydrogenase were assayed to evaluate the occurrence of cardiac damage. All histopathological tissues were stained with H&E and examined blind to the pathologist. The results showed that TiO2 NPs induced different toxic effects on young and adult rats. Liver edema, heart injuries and non-allergic mast cell activation in stomach tissues were found in young rats. Only slight injury in the liver and kidney and decreased intestinal permeability and molybdenum contents were found in adult rats.

6.6.1.4 Summary

Limited *in vivo* studies in mammals provide conflicting results, with some studies suggesting that TiO2 NPs may exert developmental and reproductive toxicities by oral administration at doses as low as 2.5 mg/kg/d. This is contrasted by one series of studies that followed current guideline designs (OECD 414 and 421), used two strains of rats, and demonstrated no developmental and reproductive toxicities at 1000 mg/kg/d, the highest dose tested. It might be that these conflicting results are due to differences in NP size with smaller NPs resulting in more severe toxicity, or differing lengths of exposure, or exposure during different portions of the developmental or reproductive cycle.

6.6.2 Inhalation Exposure

Hougaard et al. (2010), as the only developmental study prior to the Versar (2012) review, was extensively reviewed in that report, and is summarized below and presented in Table 35. Since 2010, there have been no new studies of developmental or reproductive toxicity via inhalation located in the literature.

6.6.2.1 Reproductive and Developmental Toxicity

Hougaard et al. (2010) exposed time-mated (22-23/group) C57BL/6J mice by whole body inhalation, one hour per day from presumed GD 8 to 18, to 0 or 40 mg/m^3 of aerosolized powder of nano-particulates of UV-Titan L181 (TiO2 coated with alumina and dimethicone) or to filtered air (controls). Primary particle size was 20.6 ± 0.3 nm of rutile. In the exposure atmosphere, the particle number concentration was 1.7×10^6 particles/cm^3 and the major particle size mode was 97 nm. Assuming each animal inhaled 1.8 L/hr, during the 11 days of exposure, the animals were estimated to have inhaled a total dose of 840 µg/animal, of which 73 µg/animal

was estimated to be deposited in the lungs. Lungs from exposed female mice contained 38 mg Ti/kg on day 5 after the exposure and 33 mg Ti/kg on days 26 to 27. No Ti was detected in unexposed female lungs. The mice were allowed to deliver and wean their litters. The F1 generation was behaviorally tested and mated to another strain of mice (naïve CBA/J) to produce an F2 generation. Similar numbers of control and exposed females delivered litters, and none of the time-mated females without litters displayed implantations. Gestational and litter parameters were similar, apart from a slight decrease in pup viability (p=0.08) in TiO2 litters. However, the number of F1 pups that died during lactation was significantly higher in the TiO2-treated group than the control group. Lung inflammation was evaluated by cell counts of BALF. BALF from exposed non-pregnant females contained 19 times more neutrophils in BALF than did unexposed non-pregnant females (5 days after exposure). The exposed pregnant females displayed 3-fold more neutrophils compared to unexposed pregnant females (26 to 27 days after exposure). Exposure resulted in overall change in BALF macrophage and lymphocyte numbers in pregnant females compared to unexposed pregnant females, with macrophages decreasing and lymphocytes increasing. In nonpregnant females, fewer macrophages but more lymphocytes occurred in exposed, as compared to unexposed nonpregnant, females. In the Morris water maze, no change was observed in performance as a result of prenatal TiO2 exposure in either male or female offspring. In the open field, ambulation differed by gender, but not exposure. Analysis of acoustic startle demonstrated that exposed male offspring startled less than control males and were less inhibited by prepulse, whereas the opposite pattern was apparent for female offspring. At termination of behavioral testing, control and exposed C57BL offspring were cross-mated to naïve CBA/J mice. Time-to-first-delivery of F2 litter was similar in control and exposed female offspring. Based on evidence of lung inflammation and increased absolute and relative lung weights, 40 mg/m^3 (the only concentration tested) is identified as a maternal LOAEL; no NOAEL was identified. Based on increased pup mortality during lactation and altered performance of pups exposed during fetal life in neurobehavioral tests, 40 mg/m^3 (1 h/d on GDs 8 to 18) is identified as a free-standing LOAEL for developmental toxicity. No NOAEL for developmental toxicity was identified. The results of the cross-mating trials for the F1 offspring indicated that the exposure conditions did not adversely affect the ability of the F1 offspring to produce F2 litters.

To test whether mitochondrial dysfunction and subsequent oxidative stress mechanisms could be a possible link between a gestational environmental exposure and adult disease, Stapleton et al. (2015) exposed pregnant Sprague-Dawley rats by whole body inhalation to nanosized P25 TiO2 aerosols after implantation (GD 6). The powder was composed primarily of anatase (80 percent) and rutile (20 percent) TiO2, with a primary particle size of 21 nm and a surface area of 48.08 m^2/g. Pregnant animals (6-7/group) were exposed for five hours per day for an average of 6.8 ± 0.5 days at a final mass concentration of 10.6 ± 0.3 mg/m^3 or to filtered air (0 mg/m^3, control). Pups were delivered, and the progeny allowed to grow to adulthood. Microvascular reactivity, mitochondrial respiration and hydrogen peroxide production of the coronary and uterine circulations of the female offspring were evaluated. A lack of response to nitric oxide indicates that exposure compromised the normal microvascular dilation in fetal vasculature. While there were no significant differences within the maternal or litter characteristics, endothelium-dependent dilation and specific cellular responses in both coronary and uterine arterioles were significantly impaired. In addition, there was a significant reduction in maximal mitochondrial

respiration in the left ventricle and uterus. These results suggest that pre-natal TiO2 NP exposure impairs microvascular function in the offspring and may persist through multiple developmental stages.

Table 35. Summary of Reproductive and Developmental Toxicity Studies of TiO2 NPs via Inhalation Exposure

Species n/sex/group	Dose, frequency, duration	Particle Characteristics	NOAEL mg/kg/d	LOAEL mg/kg/d	LOAEL Responses	Comments	Reference
C57BL/6 mice females (22–23/group)	0 or 40 mg/m^3 for 1 h/d on GDs 8–18	Rutile; ~21 nm, 71% TiO2 by weight; residual mass composed of zirconium, silicon, aluminum; coated with polyalcohols; surface area = 108 m^2/g Aerosols: geometric mean mass diameter 3.2 µm; less than 1% of total particle mass less than 100 nm	Maternal: none Fetal: none	Maternal: 40 Fetal: 40	Maternal: Changes in BALF (increased dead cells and increased neutrophils), increased lung weight. Fetal: Increased number of dead F1 pups during lactation, but not at birth; neurobehavioral effects (deficits in open field tests and prepulse inhibition response). No effects on reproductive performance by F1 offspring in cross-mating trials with nonexposed partners.	Endpoints evaluated included maternal body weights, BALF (total and differential cell counts) and organ weights, number of litters, body weights and sex distribution of pups, neurobehavioral assessments (pups), and fertility of F1 offspring in cross-mating trial (time-to-first-delivery of F2 litter, litter size, and gender). The litter was considered the unit for statistical analyses.	Hougaard et al., 2010[a]
Sprague-Dawley rats females 6-7/group	0 (filtered air) or 10.6 ± 0.3 mg/m^3; 5 h/d for average of 6.8 days; started on GD 6	Anatase (80%) and rutile (20%), with a primary particle size of 21 nm and a surface area of 48.08 m^2/g.	Maternal: none Fetal: none	10.6 ± 0.3	Microvascular and mitochondrial dysfunction	No effect on maternal wt, # of implantations, litter size or F1 growth	Stapleton et al., 2015

[a]As described in Versar (2010)

In summary, due to very limited and nonstandard testing, the potential for developmental or reproductive toxicity via the inhalation route is uncertain. Concern is lessened based on the apparently limited absorption and translocation of TiO2 NPs from the respiratory tract to the systemic distribution, but the studies of absorption have been conducted primarily on a mass basis, and it is difficult to evaluate whether a sufficient amount on a surface area basis could be absorbed.

6.6.3 Dermal Exposure

No developmental or reproductive studies by the dermal exposure route were located in the literature searches conducted for this project. The located TiO2 dermal studies are with sunscreen formulations (see review by Crosera et al., 2009).

6.6.4 Other Routes of Exposure

The reproductive and developmental toxicity studies of TiO2 NPs by other routes of administration have demonstrated embryonic death, growth retardation, structural abnormalities and behavioral and functional abnormalities. However, most of these studies were performed on mice using a parenteral injection route of exposure (reviewed by Ema et al., 2010; 2016) and particle size, crystal structure, or coating was not provided. Therefore, these studies are not directly applicable to development of the ADI.

6.6.5 Summary

The reproductive and developmental toxicity studies of TiO2 NPs in animals included evaluation of reproductive parameters, as well as mortality, growth retardation, structural abnormalities and behavioral and functional abnormalities. Although experimental evidence shows that absorbed TiO2 NPs may be able to move across the placenta into fetal tissue, epidemiological studies have yet to establish whether human exposure to TiO2 NPs causes reproductive and developmental toxicities. Many animal studies have been performed using a parenteral injection route of exposure (reviewed by Ema et al., 2010; 2016), which are not directly applicable to development of the ADI. Limited oral and inhalation route studies suggest that TiO2 NPs (when evaluated on a mg/kg basis) may exert developmental and reproductive toxicities by oral administration, but in most studies, the exposures (i.e., not multiple, dose-response exposures) and group size were limited. However, one series of studies followed current guideline designs and demonstrated no developmental and reproductive toxicities at 1000 mg/kg/d, the highest dose tested. Evaluation of the data with another dosimetric (such as m^2/g) may yield further understanding of the dose response of TiO2 NPs and developmental/reproductive outcome.

It is accepted in the field of toxicology that the fetus may be more sensitive to chemical exposures than adults. The database on developmental toxicity of TiO2 NPs is very limited and remains insufficient as a basis for risk assessment (Hougaard et al., 2015). Furthermore, as long as NPs do not translocate from the portal of entry to the fetus, fetal effects are unlikely. For many consumer products for particles to reach the fetus, they need to translocate at the portal of entry (whether that is the respiratory or gastrointestinal system, or skin) to the systemic circulation, and then to traverse the barrier of the placenta. However, it may be possible for

particles to elicit inflammation and oxidative stress or other effects during pregnancy, inducing perturbations that can be detrimental for fetal development. Inflammation may potentially alter neuroendocrine regulation of maternal hormonal systems during pregnancy having consequences for fetal and postnatal development (Powers et al., 2013).

6.7 Mechanistic Data

6.7.1 Mutagenicity/Genotoxicity Studies

Results of short-term tests to assess the mutagenicity/genotoxicity of TiO2 NPs published prior to 2010 have been previously reviewed in Versar (2012).

A brief summary of the Versar review is provided here. More detailed information on the results of these studies (as reported in Versar, 2012) is provided in Appendix H. In the studies covered by the Versar report, two *in vitro* tests to assess the mutagenicity of TiO_2 NPs in bacteria showed negative results in standard *Salmonella typhimurium* strains in the presence or absence of metabolic activation. However, one study reported positive results using *Escherichia coli* WP2*uvr*A (oxidative stress sensitive) strain in the presence of metabolic activation. Positive results were reported with TiO2 NPs in two *in vitro* mammalian gene mutation assays (gpt-delta assay in mouse embryo fibroblasts and HPRT assay in human B-cell lymphoblastoid cells). Seven of eleven (Versar, 2012, stated nine of eleven) published *in vitro* studies were reported to induce micronuclei in mammalian cells, supporting the conclusion that TiO2 NPs may be clastogenic. Six of nine studies gave positive results in the comet assay. Two *in vitro* studies in human cell lines reported the formation of oxidized bases in DNA following treatment with TiO_2 NPs. These latter studies indicate that TiO2 NPs may induce oxidative damage to DNA indirectly via an increase in ROS leading to single strand breaks in DNA.

Only two publications reviewed in Appendix H reported results from *in vivo* mutagenicity/ genotoxicity studies of TiO2 NPs. One study reported increased HPRT mutant frequency in alveolar type II cells after IT instillation of 100 mg/kg TiO2 NPs in rats. The other publication reported positive results in both a MN assay and a comet assay in peripheral blood, as well as in an assay for double stranded DNA breaks in bone marrow in mice given a total dose of 500 mg/kg via drinking water. Pregnant mice administered this dose also showed evidence of DNA deletions in offspring. Although information on NP characteristics was available for some of the previously reviewed studies which suggests that factors such as particle size, coating, and phase (e.g., anatase vs. rutile) can influence results, no broad conclusions were drawn by the Versar report. The Versar review also included literature on TiO2 cytotoxicity, and concluded that TiO2 NPs induce inflammatory and oxidative effects on cells that can lead to DNA damage. The Versar review did not examine the correlation between evidence of oxidative stress and results from the mutagenicity/genotoxicity studies.

Since 2011, numerous additional *in vitro* and *in vivo* mutagenicity/genotoxicity studies have been published. These are summarized below and in Appendix I. A large number of both *in vitro* and *in vivo* mutagenicity/genotoxicity studies on TiO2 NPs have been conducted. Bacterial mutagenicity assays have typically shown negative results, and this has been suggested to be explained by lack of cell uptake of the NPs, rather than reflecting a lack of mutagenic potential.

Mammalian cell mutagenicity assays have given conflicting results which cannot be easily explained by inter-study differences in NP concentration or duration of exposure, lack of evidence of cell uptake, or lack of an oxidative stress response. Three *in vivo* mutagenicity assays, two in mice and one in *D. melanogaster*, have all shown negative results, despite evidence of target tissue exposure in all three studies.

Genotoxicity studies, both *in vitro* and *in vivo*, have typically been conducted using the MN assay or the comet assay. *In vitro* MN studies in cells from a variety of mammalian species, including human cell lines derived from a number of different tissues, have shown predominantly positive results. Numerous *in vitro* comet assays have been conducted and have also shown predominantly positive results. When measurement of ROS has been conducted in either MN assays or comet assays, the vast majority have shown an increase in ROS accompanying the positive genotoxicity response. Other measures of oxidative stress, such as GSH/oxidized glutathione (GSSG) ratio, have been less consistent. Some *in vitro* studies have included direct comparison of genotoxicity results with NP characteristics. However, no clear conclusions can be drawn regarding the influence of particle size, coating, surface area, degree of agglomeration, or TiO2 mineral form.

Among ten *in vivo* MN studies in rats or mice, one study showed an increase in MN formation and one study was negative despite evidence of cytotoxicity to the bone marrow. The remaining studies were also negative. A lack of evidence of target tissue cytotoxicity, indicating lack of adequate exposure may be the explanation for some of these eight negative studies, but cytotoxicity in the target tissue was not evaluated in all of these studies. Time of sacrifice after exposure could also explain the lack of a MN response in at least one study. Numerous *in vivo* comet assays have also been conducted looking for DNA damage in various target organs after exposure via various routes (oral, inhalation, IV, IT). These studies have given conflicting results. As with the *in vivo* MN assays, negative results are not adequately explained by a lack of evidence of target organ exposure or target organ toxicity.

In vivo studies involving all routes of exposure, including oral, inhalation, IP and IV routes have been included in this report for completeness. However, the IP and IV routes of exposure are generally not recommended for risk assessment for consumer products without specific scientific justification.

6.7.2 Mode of Action for NanoTiO2

6.7.2.1 Introduction

Mode/mechanism(s) of action (MOA) refers to the biochemical and physicochemical interactions through which substances produce their toxicological effects. The MOA of toxicity induced by metal NPs, TiO2 included, are not well understood. Through review of physical and chemical properties and toxicity studies of various durations and routes of exposure, some potential MOA can be identified, but the specific mechanism(s) of toxicity for TiO2 is not known.

There are likely several potential MOAs for TiO2. Collectively, investigations have indicated the MOA cascade of events for TiO2 includes sustained inflammation, impairment of cellular

defense mechanisms, production of ROS, oxidative DNA damage, cell proliferation, apoptosis, necrosis, depletion of antioxidants and ROS scavengers, and/or gene mutations (Boland et al., 2014).

The nature of the inflammatory response, cytotoxicity, cell proliferation and histopathology can be influenced by choice of animal model, surface modifications/coatings, particle aggregation/agglomeration, route of exposure (oral, inhalation and dermal are the most important for consumer products), and the crystalline form of TiO2 (Shakeel et al., 2016).

6.7.2.2 Sustained Inflammation

Some of the earliest investigations with TiO2 NPs in animal models suggested that particle size may be of central importance to pulmonary toxicity with NPs inducing a greater inflammatory response (on a mass basis) (neutrophil infiltration) than microparticles (Ferin et al., 1992; Warheit et al., 2005). The smaller size TiO2 particles were found to remain in pulmonary tissue longer, with slower clearance than larger particles (Shi et al., 2013). The inefficiency of alveolar macrophages to engage nanosized particles allowed the NPs longer time to interact with pulmonary epithelial cells. The NPs, with a greater surface area than the microparticles, exhibited greater toxicity than an equal mass of micro-sized particle TiO2 (Hussain et al., 2010). However, the difference in potency was not present when dose was normalized to particle surface area delivered to the lungs.

In vitro studies have demonstrated pro-inflammatory responses after exposure to TiO2 NPs that involve MAPK, NFκB (a protein complex that controls transcription of DNA, cytokine production and cell survival) and/or receptor activation to induce cytokine production (for review Shi et al., 2013; Donaldson et al., 2005). Lung fibroblast exposure to TiO2 NPs induced IL-1β secretion and subsequent matrix metalloproteinase-1 (MMP1) induction (Armand et al., 2013). The authors speculated that this may be due to the activation of the inflammasome, which allows the maturation of pro-IL-1β by caspase-1 activation. Cathepsin B has been shown to activate the inflammasome and release IL-1β in response to rutile and anatase TiO2 NP exposure and is dependent on active cathepsin B and caspase-1 (Morishige et al., 2010).

Inflammation after acute and subchronic instillation and inhalation studies of TiO2 NPs has been illustrated by Bermudez et al. (2002, 2004), Warheit et al. (2005, 2007), and Klein et al. (2012). TiO2 NPs induced similar lung inflammatory responses after 24 hours in short-term studies (4 h/d for 10 days) with the same pulmonary exposures (Grassian et al., 2007a; Sager and Castranova, 2009). Inflammation after subchronic inhalation of TiO2 has been often attributed to lung overload. However, short-term inhalation with less lung burden confirmed that the induction of inflammation by TiO2 NPs was not attributed to lung overload (Renwick et al., 2004; Klein et al., 2012).

6.7.2.3 Impairment of Cellular Defense Mechanisms

Immunomodulatory changes have also occurred with TiO2 NPs exposure (Hussain et al., 2012a). Low doses of TiO2 NPs induced epithelial damage and aggravated inflammatory and asthmatic responses in a mouse model for occupational asthma (Hussain et al., 2011). Also in mice, TiO2

NPs significantly increased the dermal sensitization potency of a known skin sensitizer (dinitrochlorobenzene) by skewing the immune response towards memory Th2 cells (Hussain et al., 2012b). It has been speculated that the immunomodulatory interaction could be due to activation of dendritic cells by TiO2 (Zhang and Sun, 2004).

6.7.2.4 Reactive Oxygen Species (ROS)

The literature for MOA for TiO2 indicates that NPs (and microparticles) induce cytotoxicity *in vitro* and *in vivo* (Shi et al., 2013). Many investigations have focused on oxidative stress that leads to ROS as being one pathway for cytotoxicity (for example, Buechter, 1988). However, it is not clear whether oxidative stress is an initiating event or the result of an upstream event that leads to the toxic effects of TiO2 NPs.

ROS consist of a group of partially reduced forms of molecular oxygen, such as hydroxyl radical, superoxide anion, singlet oxygen, hydrogen peroxide, lipid peroxides, and hypochlorous acid that can bind to DNA or RNA, oxidize fatty acids, oxidize amino acids in proteins, and deactivate specific enzymes (Waris and Ahsan, 2006). The capacity of NPs to produce ROS inside the cell is influenced by their surface reactivity as well as by the chemical composition of cellular components (Donaldson et al., 2005). It is likely that cells can mount an effective anti-oxidant defense against low concentrations of NPs; however, with higher concentrations of NPs or repeated exposures, oxidative stress may result in inflammation and cellular necrosis (Nel et al., 2006). The oxidant generating capacity of a TiO2 particle has been demonstrated to be dependent on its physicochemical properties (e.g., size, surface area and crystal phase of anatase or rutile) (Jiang et al., 2008).

It is not known whether the oxidative stress from TiO2 NP exposure that produces ROS is generated directly in or near the cell, or indirectly by the effects of internalized particles on mitochondrial respiration and/or the depletion of antioxidants in the cell (Cheng et al., 2013). NPs appear to trigger more generation of ROS than larger microsize and macrosize particles, in biological systems (Li et al., 2003). This size differential with respect to ROS generation and toxicity may explain the significant increase surface reactivity of the NPs with decreasing particle size (Oberdörster et al., 2005).

6.7.2.5 Interaction of NanoTiO2 with Proteins

Another potential mechanism through which TiO2 NPs may induce toxicity includes its tendency to interact with proteins. The attachment of proteins onto the surface of NPs in physiological conditions leads to the formation of a 'protein corona' that enshrouds the NP with a layer of biomolecules (Deng et al., 2014). This corona can impact the effect of NPs by influencing the aggregation state, biodistribution, cellular uptake and/or reactivity of the NPs. The interaction of nanomaterials with proteins can impact the activity of the protein, having important physiological consequences via inactivation either by conformational changes and/or denaturation. A variety of proteins are known to bind with TiO2 NPs, including cytokines. A comparative study showed TiO2 NPs adsorbed cytokines, but the binding was dependent on the nature of the cytokine as well as on the type of NP. Interactions of TiO2 NPs with the cytoskeleton can lead to retardation of cell migration due to destabilization of microtubule

networks (Tay et. al., 2003). Impairment of the cytoskeleton disturbs lysosomal trafficking leading to autophagy disturbances, which have been observed after NP exposures (Stern et al., 2012 for review).

6.7.2.6 Cell Death and Genotoxicity

TiO2 NPs can induce a variety of cell death modalities (e.g., apoptosis, necrosis, gene mutations). Uncontrolled cell death (necrosis) leads to inflammatory pathways, whereas controlled cell death (apoptosis) avoids inflammation. Autophagy (intracellular degradation system by lysosomes) is a process that bypasses both of these cell death pathways by eliminating damaged cell structures or organelles (for reviews: Stern et al., 2012; De Stefano et al., 2012). Cell signaling cascades for apoptosis induction by TiO2 NPs can also generate ROS under acellular conditions (Roller, 2009). Neither the initiating event nor the sequence of events is known, that is, it is not known whether ROS, inflammation, or apoptosis is an initiating event for cell death from TiO2 NP exposure.

Many studies have shown that TiO2 NPs (and microparticles) induce genotoxicity *in vitro* and *in vivo* (Roller, 2009). DNA strand breaks, mutations, chromosomal damage and cell transformation have been observed in some investigations (Toyooka et al., 2012; Li et al., 2010). Bacterial mutagenicity assays have usually demonstrated negative results, whereas, mammalian cell mutagenicity assays have given conflicting results (refer to Section 6.7.1). Investigators suggest the negative results may be explained by lack of cell uptake of the NPs, rather than reflecting a lack of mutagenic potential.

Genotoxicity studies, both *in vitro* and *in vivo*, from a variety of mammalian species, including human cell lines derived from a number of different tissues, have had chiefly positive results. The vast majority of *in vitro* studies have shown an increase in ROS accompanying the positive genotoxicity response. However, no clear conclusions have been drawn regarding the influence of particle size, coating, surface area, degree of agglomeration, or TiO2 mineral form. *In vivo* studies in rodents, have been mainly negative. A lack of evidence of target tissue cytotoxicity, indicating lack of adequate exposure may be an explanation. Numerous *in vivo* comet assays have looked for DNA damage in various target organs after exposure via various routes, with conflicting results.

6.7.2.7 Summary

There are several potential MOAs for TiO2 NP toxicity. These include sustained inflammation, impairment of cellular defense mechanisms, production of ROS, oxidative DNA damage, cell proliferation, apoptosis, necrosis, depletion of antioxidants and ROS scavengers, and/or gene mutations. However, the exact mechanisms and pathways of TiO2 NP-induced toxicity are not clear. Inadequate studies, inadequate description of physicochemical characteristics, and use of various forms of TiO2 NPs makes it challenging to evaluate a potential cause-effect relationship between speculated mechanisms of toxicity and real-world human exposure scenarios.

6.8 Derivation of ADI

6.8.1 Short-term Oral ADI (14-day)

6.8.1.1 Principal Study and Critical Effect

The oral toxicity database for TiO2 is varied and conflicting.

There are no studies of 14-day duration. However, there are five studies with duration of 60 days or less that are appropriate for consideration of the short-term oral ADI. High gavage doses for larger diameter (d50= 173 nm) preparations with a NOAEL of 24,000 mg/kg/d appear to be without significant toxicity (e.g., Warheit et al, 2015a). Lower gavage doses (~1 to 50 mg/kg/d) of generally smaller diameter (~5 to 25 nm) preparations show toxicity at much lower doses (e.g., Chen et al., 2015a; Hu et al., 2010). Other studies show less toxicity with smaller diameters (5 nm) with laboratory synthesized TiO2 (e.g., Duan et al., 2010), or no toxicity in a non-guideline study evaluating limited endpoints (Auttachoat et al., 2014). Some of these discrepancies may be attributed to differences in degree of response between mice and rats; other differences might be due to inconsistent endpoints monitored. The TiO2 preparation also may be contributing to these differing responses, since some preparations were purchased and others were made by the investigators.

It is difficult to determine the most robust of these studies. If all of these studies were to be considered as roughly equivalent, then the traditional way to determine a short-term ADI would be to consider mild cardiovascular disturbances from the 30-day Chen et al. (2015a) study to be the critical effect, the dose of 2 mg/kg/d (the lowest dose tested in this study), to be a minimal LOAEL.

Limited *in vivo* studies in mammals provide conflicting results with regard to developmental and reproductive toxicities by oral administration. Some show adverse effects at doses as low as 2.5 mg/kg/d, which support the choice of the systemic toxicity LOAEL of Chen et al. (2015a). However, other studies, that followed current OECD test guideline designs (OECD TG 414 and 421), demonstrated no developmental and reproductive toxicities at 1000 mg/kg/d, the highest dose tested. It might be that these conflicting results are due to differences in NP size with smaller NPs resulting in more severe toxicity, or differing lengths of exposure, or exposure during different portions of the developmental or reproductive cycle.

6.8.1.2 Adjustment to Human-Equivalent Exposure

No duration adjustment is needed as exposure was for 30-consecutive days. The Chen et al. (2015a) study duration of 30 days is longer than the 14 days for the short-term ADI, which likely leads to a more conservative value than if a 14-day study were available.

6.8.1.3 Uncertainty Factors

Uncertainty in the 14-day ADI was accounted for using the following UFs:

An UF of 10 is used for extrapolation of the LOAEL in rats to the expected LOAEL in humans (animal to human extrapolation).

An UF of 10 was used to account for inter-individual variation including that of sensitive subpopulations in response to ingested TiO2. The critical effect is mild cardiovascular toxicity and it is anticipated that the adverse response could occur more readily in those persons with preexisting cardiovascular disease, including those with high blood pressure.

An UF of 3 was used for extrapolation of LOAEL to NOAEL due to the mild nature of the critical effect at this LOAEL (LOAEL to NOAEL extrapolation).

These UFs are reasonable defaults in the absence of specific data.

A traditional NOAEL/LOAEL approach has been taken for derivation of the ADI. The lack of quality and consistency amongst the studies and in the critical effect data preclude benchmark dose modeling.

ADI = LOAEL/UF = (2 mg/kg/d) / (300) = 0.007 mg/kg/d

Another approach for derivation of the short-term ADI would be to consider that the studies collectively suggest that the overall toxicity appears to be absent in the range of 1 mg/kg/d, a collective database NOAEL. If this approach is taken, then the ADI would be 0.01 mg/kg/d, marginally higher than the more classic approach, since the UF for the use of a minimal LOAEL would not be needed.

6.8.2 Long-Term Oral ADI

6.8.2.1 Principal Study and Critical Effect

At 90 days or greater duration, there are five studies, three in rats and two in mice, with doses ranging from 2 to 1000 mg/kg/d. All of the studies administered TiO2 via gavage, except the study by Bettini et al. (2017), which used drinking water administration. Studies with larger particle diameter (145 to 294 nm) showed differing results. Sheng et al. (2014) showed toxicity at lower doses (2.5 mg/kg/d), whereas another study (Warheit et al., 2015a) showed no toxicity up to 1000 mg/kg/d. When TiO2 of 25 to 50 nm were administered, mild cardiovascular effects were reported at 2 mg/kg/d (Chen et al., 2015a), whereas Hu et al. (2015) reported adverse effects at a higher dose, 64 mg/kg/d. Bettini et al. (2017) reported alterations of immune function in the colon from NM-105; however, this study is limited by testing of only one dose level and evaluation of limited endpoints.

Given the limitations in the database, and the same minimal LOAEL reported by Chen et al. (2015a) at both 30 and 90 days, it seems reasonable to use this study as the basis for a long term ADI.

6.8.2.2 Adjustment to Human-Equivalent Exposure

No duration adjustment is needed as exposure was for 90 consecutive days.

6.8.2.3 Uncertainty Factors

Uncertainty in the long-term ADI was accounted for using the same UFs as for the short-term ADI, with the addition of an extra UF for subchronic to chronic duration extrapolation.

An UF of 10 for extrapolation of the LOAEL in rats to the expected LOAEL in humans (animal to human extrapolation).

An UF of 10 was used to account for inter-individual variation including that of sensitive subpopulations in response to ingested TiO2. The critical effect is mild cardiovascular toxicity and it is anticipated that the adverse response could occur more readily in those persons with preexisting cardiovascular disease, including those with high blood pressure.

An UF of 3 was used for extrapolation of LOAEL to NOAEL due to the mild nature of the critical effect at this LOAEL (LOAEL to NOAEL extrapolation).

An UF of 10 was used to extrapolate from a 90-day subchronic duration study to a long-term (such as several years or lifetime). While the LOAEL for the critical effect was the same in 30 and 90-day studies, the longest duration study in the database is 100 days. There is uncertainty as to the progression of the critical effect over time and to be protective of human health, an UF of 10 is applied.

These UFs are reasonable defaults in the absence of specific data.

A traditional NOAEL/LOAEL approach has been taken for derivation of the ADI. The lack of quality and consistency amongst the studies and in the critical effect data preclude benchmark dose modeling.

ADI = LOAEL/UF = (2 mg/kg/d) / (3000) = 0.0007 mg/kg/d

6.8.3 Short-Term Inhalation ADI (14-day)

6.8.3.1 Principal Study and Critical Effect

As shown in Table 30, the inhalation toxicity database for TiO_2 is varied with several unconventional exposure scenarios (e.g., Leppanen et al., 2011). However, the effects from these various studies are more or less consistent. For example, lung effects are routinely seen at doses greater than 10 mg/m^3. Some of the disparity among studies in the development of lung effects at variable concentrations may be attributed to heterogeneity in responses between mice and rats; while other variance might be due to differences in effects monitored or the TiO_2 preparation. If all of the studies with conventional, non-food-grade exposure scenarios were to be considered as roughly equivalent, then a classic way to determine a short-term inhalation ADI would be to consider mild lung inflammatory and histopathological lesions in female rats at 50 mg/kg/d/m^3 for 6 h/d, 5 d/wk for 13 weeks from Bermudez et al. (2002) to be the critical effect, the dose of 10 mg/m^3 to be an equivocal NOAEL. Toxicity in two other animal species (mouse and hamster) was evaluated in the same study, and NOAELs in these species were also 10

mg/m^3.

6.8.3.2 Adjustment to Human-Equivalent Exposure

Adjustment of intermittent exposure in rats to continuous exposure was undertaken by adjusting exposure duration. Exposure duration was adjusted from experimental intermittent (H = h/d and D = d/wk) to continuous exposure (24h/d, 7d/wk) using the following equation:

$$NOAEC_{Continuous} = NOAEC_{Experimental} \times H/24 \times D/7$$

Using values from the principal study gives the following:

$$NOAEC_{Continuous} = 10\ mg/m^3 \times 6hr/24hr \times 5d/7d$$

$$NOAEC_{Continuous} = 1.8\ mg/m^3$$

Cross-species dosimetric adjustment of the experimental NOAEC to a HEC was undertaken by calculating the regional deposited dose ratio (RDDR) between rat and human (U.S. EPA, 1994), using pulmonary surface area (PU) as a normalizing factor and minute volume (Ve) and regional deposition fraction (Fr) in the following equation:

$$RDDR = \frac{PU_{Human} \times Ve_{Rat} \times Fr_{Rat}}{PU_{Rat} \times Ve_{Human} \times Fr_{Human}}$$

Fr values for the extrathoracic regions were calculated in MPPD v3.04 software using the reported MMAD (1.44 μm, GSD=1.71). Breathing scenarios were whole-body exposure and oro-nasal normal augmented breathing for the rat and human models, respectively. ETSA and Ve values for rat and human were calculated in MPPD, using a 124g default body weight for the rat and resulting default breathing and tidal volumes. Plugging these values into the RDDR equation gave the following:

$$RDDR = \frac{54.0\ m^2 \times 169\ mL/min \times 0.20}{0.9\ m^2 \times 7.5\ L/min \times 0.05}$$

$$RDDR = 5.4$$

The RDDR was multiplied by the duration-adjusted NOAEC ($NOAEC_{Continuous}$) to give the HEC:

$$1.8\ mg/m^3 \times 5.4 = NOAEC_{HEC}$$

$$NOAEC_{HEC} = 9.7\ mg/m^3$$

6.8.3.3 Uncertainty Factors

Uncertainty in the short-term inhalation ADI was accounted for using UFs for inter-individual variation, animal-human extrapolation, and database completeness. No UFs were needed to account for study duration or presumed no-effect dose extrapolation because the POD is a no-effect concentration taken from a short-term study.

An UF of 10 was used to account for inter-individual variation in responses to inhaled TiO_2. This UF is needed to protect sensitive human subpopulations such as those with preexisting lung disease.

An UF of 3 was used to account for toxicodynamic differences between rat and human. Toxicokinetic differences are addressed above in the respiratory tract dosimetry adjustments.

No UF (i.e., UF of 1) was used to account for database completeness. This was because suitable data are available in several species (rat, mouse, and hamster), and the critical effect in the lung is a reasonable expectation. Moreover, reproductive and developmental toxicity studies do not show these toxicities as lower than the lung effects.

The resulting inhalation ADI would be 0.3 mg/m^3. As before, these UFs are reasonable defaults in the absence of specific data.

$ADI = NOAEC_{HEC} / UFs = (9.7\ mg/m^3) / (30) \sim 0.3\ mg/m^3$ or 300 $\mu g/m^3$.

6.8.4 Long Term Inhalation ADI

The inhalation chronic toxicity database for TiO2 is insufficient for developing a long-term ADI due to use of only one exposure level, only one sex (females), evaluation of only limited endpoints (i.e., mortality, clinical signs, body and lung weights, BALF parameters [rats only], and respiratory tract histopathology), and, retrospectively, changes in pathologic diagnostic criteria for the lung tumors reported.

In light of these limitations, an approach that could be applied is to use the short-term inhalation ADI developed in Section 6.8.3, with an additional safety factor to reflect the uncertainty of using short-term data to develop a chronic safe dose. As for the oral route of exposure, the default value of 10 for this safety factor is reasonable, given the general lack of data to suggest a more data-derived value. The ADI would be 30 $\mu g/m^3$ with the use of a 300-fold safety factor (10 for within human variation, 3 for extrapolation of the NOAEL in rats to the expected NOAEL in humans, and the additional 10-fold factor for the use of the short-term studies).

6.8.5 Short-Term Dermal ADI

The short-term dermal toxicity database for TiO2 is not sufficient to allow for the development of a dermal ADI. While studies in BALB/c *nu/nu* hairless mice show local and systemic toxicity at a high concentration and small NP size (e.g., Wu et al., 2009), other experimental animal models, which are likely to be more appropriate for determining human effects because of more

similarity in skin between humans and these species, show either no toxicity or only local effects at similar concentrations and particle sizes.

6.8.6 Long-Term Dermal ADI

Long-term dermal toxicity studies for TiO2 are lacking; therefore, the database is insufficient to allow the development of a dermal ADI. While there are two skin carcinogenicity studies (initiation-promotion studies) conducted in mice and rats, no dose-related increase in tumors was reported in either study.

6.9 Research Needs and Data Gaps

6.9.1 General Research Needs

Derivation of ADIs for TiO2 is challenging, with generally high uncertainty as the existent studies are limited by lack of reliable, quantitative dose-response data.

There is a lack of epidemiological data regarding TiO2 NPs (Versar, 2012; NIOSH, 2017). Several scientists have reported that there was no clear evidence of increased respiratory disease or lung cancer mortality ratios in workers occupationally exposed to TiO2 dusts, although exposure presumably occurred to both fine and ultrafine TiO2 particles. The existent human studies were not designed to investigate the relationship between TiO2 particle size, surface area or crystalline state and health or mortality risk; specific exposures to nanosized particles were not estimated.

The biological activity of TiO2 NPs depends on physicochemical properties, such as dissolution rates, (or solubility), particle size and distribution, agglomeration state (mass), shape, crystal structure, chemical composition, surface area, surface chemistry, surface charge, and porosity. There is a need to characterize these properties in toxicity studies and to research how these properties influence TiO2 NP toxicity.

Limited information from human and animal studies indicates that TiO2 NPs are absorbed to a small extent from the lungs and gastrointestinal tract via alveolar macrophages or systemic blood circulation, and then distributed to liver, kidneys, spleen and the brain, causing localized effects. The rate of translocation is uncertain. TiO2 NPs, however, can penetrate the blood-brain, blood-testis and blood-placenta barriers. Additional research is needed as to the toxicokinetics of TiO2 in humans and more extensive studies in animals via oral, inhalation, dermal routes as well as the rate and mechanisms of translocation within the body, particularly the brain and across skin and blood-organ barriers.

Studies of 14-day, 90-day and chronic duration by relevant routes, using the forms and size of TiO2 NPs expected for consumer product exposure, conducted by OECD Testing Guidelines and GLP guidelines using thoroughly characterized material are needed to develop ADIs with lower uncertainty for humans. While there are several subchronic studies, they are limited by lack of guideline protocols and material characterization to allow comparisons and synthesis of information. Robust, repeat-dose, multi-dose studies are lacking in more than two species for

oral and inhalation routes (mice and rats), and dermal (hairless mice and domestic pigs). The available information on comparative penetration studies in humans and hairless mouse is sometimes contradictory. Many of the existing animal studies have limitations in the animal number, dosing period, dosage levels, and number of groups.

Cardiovascular, immune and neurological toxicity have been noted in systemic toxicity studies, but there is significant uncertainty with regard to these endpoints, their dose response and mechanism of toxicity.

The WHO IARC Working Group found little evidence of an increased risk for cancer among humans based on epidemiological data, although relatively few studies were available (IARC, 2010). The Working Group considered pathways and mechanisms by which TiO2 particles may cause cancer and reasoned that the available mechanistic evidence for TiO2 was not strong enough to warrant a classification other than Group 2B human carcinogen, based on inhaled or IT-administered nano- and fine-sized TiO2 induced lung cancer in rats. The sole study that investigated the chronic toxicity/carcinogenicity of TiO2 via the oral route is a non-guideline design with only one dose level for each TiO2 form tested. This study is severely limited in usefulness for risk assessment and development of an ADI. No new carcinogenicity studies of TiO2 by the inhalation route were identified in the literature since 2010.

The TiO2 NP reproductive and developmental animal toxicity studies included evaluation of reproductive parameters, as well as mortality, growth retardation, structural abnormalities and behavioral and functional abnormalities. These studies suggest that TiO2 NPs (when evaluated on a mg/kg basis) may exert developmental and reproductive toxicities, but in most studies, the exposures (i.e., not multiple, dose-response exposures) and group size were limited. Although experimental evidence shows that absorbed TiO2 NPs may be able to move across the placenta into fetal tissue, epidemiological studies have yet to establish whether human exposure to TiO2 NPs causes reproductive and developmental toxicities. Evaluation of the data with another dosimetric (such as m^2/g) may yield further understanding of the dose response of TiO2 NPs and developmental/reproductive outcome. The database on developmental toxicity of TiO2 NPs is very limited and remains insufficient as a basis for risk assessment (Hougaard et al., 2015). It is not clear whether potential developmental effects are due to translocation to the fetus (and if so, how) or to indirect effects such as inflammation and oxidative stress during pregnancy, inducing hormonal perturbations that can be detrimental for fetal development. Further research is clearly needed in this area.

There are several potential MOAs for TiO2 NP toxicity. These include sustained inflammation, impairment of cellular defense mechanisms, production of ROS, oxidative DNA damage, cell proliferation, apoptosis, necrosis, depletion of antioxidants and ROS scavengers, and/or gene mutations. However, the exact mechanisms and pathways of TiO2 NP-induced toxicity are not clear. Inadequate studies, inadequate description of physicochemical characteristics and use of various forms of TiO2 NPs makes it challenging to evaluate a potential cause-effect relationship between speculated mechanisms of toxicity and real-world human exposure scenarios.

Lack of understanding of human exposure from consumer products, particularly via the oral and dermal routes, makes it unknown how applicable the derived ADIs are to the consumer

scenario(s)

6.9.2 Specific Research Needs

Determination of ADIs for TiO2 requires additional data in the following areas:

- Studies using the form and size of TiO2 NPs used in consumer products
- Research into human exposure to TiO2 NPs from consumer products
- Characterization of physicochemical properties in toxicity studies and research as to how these properties influence TiO2 NP toxicity
- Toxicokinetics of TiO2 NPs in humans and more extensive studies in animals via oral, inhalation, and dermal routes, as well as the rate and mechanisms of translocation within the body (particularly the brain and across the skin and blood-organ barriers)
- Epidemiological studies of TiO2 NPs, including sensitive subpopulations
- OECD guideline and GLP studies of 14-day, 90-day and chronic duration by relevant routes, using the forms and size of TiO2 NPs expected for consumer product exposure and thoroughly characterized material, are needed to develop ADIs with low uncertainty for humans.
- Studies on the impact various diseases (*e.g.*, cardiovascular) have on TiO2 toxicity
- Mechanistic studies on cardiovascular, immune and neurological toxicity of TiO2 NPs with regard to their dose response and mechanism of toxicity
- Studies as to the carcinogenicity of TiO2 in animals and humans
- Appropriate dosimetric for TiO2 toxicity (*e.g.*, mg/kg, m^2/g)
- Robust developmental and reproductive studies on TiO2 NPs
- Further studies on MOA for TiO2 NPs

7 REFERENCES

Adachi, K., Yamada, N., Yoshida, Y., Yamamoto, O. 2013. Subchronic exposure of titanium dioxide nanoparticles to hairless rat skin. Exp Dermatol. 22(4):278–83.

Ahamed, M., Karns, M., Goodson, M., Rowe, J., Hussain, S.M., Schlager, J.J., Hong, Y. 2008. DNA damage response to different surface chemistry of silver nanoparticles in mammalian cells. Toxicol Appl Pharmacol. 233(3):404–10.

Ahmad, J., Ahamed, M., Akhtar, M.J., Alrokayan, S.A., Siddiqui, M.A., Musarrat, J., Al-Khedhairy, A.A. 2012. Apoptosis induction by silica nanoparticles mediated through reactive oxygen species in human liver cell line HepG2. Toxicol Appl Pharmacol. 259(2):160–8.

Al Faraj, A., Bessaad, A., Cieslar, K., Lacroix, G., Canet-Soulas, E., Crémillieux, Y. 2010. Long-term follow-up of lung biodistribution and effect of instilled SWCNTs using multiscale imaging techniques. Nanotechnology. 21(17):175103.

Al Gurabi, M.A., Ali, D., Alkahtani, S., Alarifi, S. 2015. In vivo DNA damaging and apoptotic potential of silver nanoparticles in Swiss albino mice. Onco Targets Ther. 8:295–302.

Al-Jamal, K.T., Nunes, A., Methven, L., Ali-Boucetta, H., Li, S., Toma, F.M., Herrero, M.A., Al-Jamal, W.T., ten Eikelder, H.M., Foster, J., Mather, S. 2012. Degree of chemical functionalization of carbon nanotubes determines tissue distribution and excretion profile. Angew Chem Int Edit. 51(26):6389–93.

Al-Kattan, A., Wichser, A., Vonbank, R., Brunner, S., Ulrich, A., Zuin, S., Nowack, B. 2013. Release of TiO 2 from paints containing pigment-TiO 2 or nano-TiO 2 by weathering. Env Sci Process Impact. 15(12):2186–93.

Al-Kattan, A., Wichser, A., Zuin, S., Arroyo, Y., Golanski, L., Ulrich, A., Nowack, B. 2014. Behavior of TiO2 released from nano-TiO2-containing paint and comparison to pristine nano-TiO2. Environ Sci Technol. 48(12):6710–8.

Alarifi, S., Ali, D. 2015. Mechanisms of Multi-walled Carbon Nanotubes–Induced Oxidative Stress and Genotoxicity in Mouse Fibroblast Cells. Int J Toxicol. 34(3):25–65.

Albini, A., Pagani, A., Pulze, L., Bruno, A., Principi, E., Congiu, T., Gini, E., Grimaldi, A., Bassani, B., De Flora, S., de Eguileor, M. 2015. Environmental impact of multi-wall carbon nanotubes in a novel model of exposure: systemic distribution, macrophage accumulation, and amyloid deposition. Int J Nanomed. 10:6133–45.

Aldossari, A.A., Shannahan, J.H., Podila, R., Brown, J.M. 2015. Influence of physicochemical properties of silver nanoparticles on mast cell activation and degranulation. Toxicol In Vitro. 29(1):195–203.

American Chemistry Council. 2005. Titanium Dioxide. IARC Monograph. 93:193–276.

Arai, Y., Miyayama, T., Hirano, S. 2015. Difference in the toxicity mechanism between ion and nanoparticle forms of silver in the mouse lung and in macrophages. Toxicology. 328:84–92.

Armand, L., Dagouassat, M., Belade, E., Simon-Deckers, A., Le Gouvello, S., Tharabat, C., Duprez, C., Andujar, P., Pairon, J.C., Boczkowski, J., Lanone, S. 2013. Titanium dioxide nanoparticles induce matrix metalloprotease 1 in human pulmonary fibroblasts partly via an interleukin-1β–dependent mechanism. Am J Respir Cell Mol Biol. 48(3):354–63.

Armand, L., Tarantini, A., Beal, D., Biola-Clier, M., Bobyk, L., Sorieul, S., Pernet-Gallay, K., Marie-Desvergne, C., Lynch, I., Herlin-Boime, N., Carriere, M. 2016. Long-term exposure of A549 cells to titanium dioxide nanoparticles induces DNA damage and sensitizes cells towards genotoxic agents. Nanotoxicology. 10(7):913–23.

Arnoldussen, Y.J., Skogstad, A., Skaug, V., Kasem, M., Haugen, A., Benker, N., Weinbruch, S., Apte, R.N., Zienolddiny, S. 2015. Involvement of IL-1 genes in the cellular responses to carbon nanotube exposure. Cytokine. 73(1):128–37.

Arora, S., Jain, J., Rajwade, J.M., Paknikar, K.M. 2008. Cellular responses induced by silver nanoparticles: in vitro studies. Toxicol Lett. 179(2):93–100.

Arora, S., Jain, J., Rajwade, J.M., Paknikar, K.M. 2009. Interactions of silver nanoparticles with primary mouse fibroblasts and liver cells. Toxicol Appl Pharmacol. 236(3):310–8.

Arts, J.H., Hadi, M., Irfan, M.A., Keene, A.M., Kreiling, R., Lyon, D., Maier, M., Michel, K., Petry, T., Sauer, U.G., Warheit, D. 2015. A decision-making framework for the grouping and testing of nanomaterials (DF4nanoGrouping). Regul Toxicol Pharmacol. 71(2):S1–S27.

Asare, N., Instanes, C., Sandberg, W.J., Refsnes, M., Schwarze, P., Kruszewski, M., Brunborg, G. 2012. Cytotoxic and genotoxic effects of silver nanoparticles in testicular cells. Toxicology. 291(1):65–72.

Ashraf, A., Sharif, R., Ahmad, M., Masood, M., Shahid, A., Anjum, D.H., Rafique, M.S., Ghani, S. 2015. In vivo evaluation of the biodistribution of intravenously administered naked and functionalised silver nanoparticles in rabbit. IET Nanobiotechnol. 9(6):368–74.

ASTM (American Society for Testing and Materials. 1988. Standard Specification for Titanium Dioxide Pigments. In: Storer, R.A., Cornillit, J.L., Savini, D.F., et al., Eds., 1988 Annual Book of ASTM Standards: Paint-Pigments, Resins, and Polymers. American Society for Testing and Materials, Philadelphia. 100–1.

Austin, C.A., Hinkley, G.K., Mishra, A.R., Zhang, Q., Umbreit, T.H., Betz, M.W., Wildt, E.B., Casey, B.J., Francke-Carroll, S., Hussain, S.M., Roberts, S.M. 2016. Distribution and accumulation of 10 nm silver nanoparticles in maternal tissues and visceral yolk sac of pregnant

mice, and a potential effect on embryo growth. Nanotoxicology. 10(6):654–61.

Austin, C.A., Umbreit, T.H., Brown, K.M., Barber, D.S., Dair, B.J., Francke-Carroll, S., Feswick, A., Saint-Louis, M.A., Hikawa, H., Siebein, K.N., Goering, P.L. 2012. Distribution of silver nanoparticles in pregnant mice and developing embryos. Nanotoxicology. 6(8):912–22.

Auttachoat, W., McLoughlin, C.E., White Jr, K.L., Smith, M.J. 2014. Route-dependent systemic and local immune effects following exposure to solutions prepared from titanium dioxide nanoparticles. J Immunotoxicol. 11(3):273–82.

Ávalos, A., Haza, A.I., Drosopoulou, E., Mavragani-Tsipidou, P., Morales, P. 2015a. In vivo genotoxicity assesment of silver nanoparticles of different sizes by the Somatic Mutation and Recombination Test (SMART) on Drosophila. Food Chem Toxicol. 85:114–9.

Ávalos, A., Haza, A.I., Morales, P. 2015b. Manufactured silver nanoparticles of different sizes induced DNA strand breaks and oxidative DNA damage in hepatoma and leukaemia cells and in dermal and pulmonary fibroblasts. Folia Biol (Praha). 61(1):33–42.

Awasthi, K.K., John, P.J., Awasthi, A., Awasthi, K. 2013. Multi walled carbon nano tubes induced hepatotoxicity in Swiss albino mice. Micron. 44:359–64.

Azad, N., Iyer, A.K.V., Wang, L., Liu, Y., Lu, Y., Rojanasakul, Y. 2013. Reactive oxygen species-mediated p38 MAPK regulates carbon nanotube-induced fibrogenic and angiogenic responses. Nanotoxicology. 7(2):157–68.

Bachler, G., von Goetz, N., Hungerbühler, K. 2013. A physiologically based pharmacokinetic model for ionic silver and silver nanoparticles. Int J Nanomed. 8:3365–82.

Baggs, R.B., Ferin, J., Oberdörster, G. 1997. Regression of pulmonary lesions produced by inhaled titanium dioxide in rats. Vet Pathol. 34(6):592–7.

Bai, Y., Zhang, Y., Zhang, J., Mu, Q., Zhang, W., Butch, E.R., Snyder, S.E., Yan, B. 2010. Repeated administrations of carbon nanotubes in male mice cause reversible testis damage without affecting fertility. Nat Nanotechnol. 5(9):683–9.

Baisch, B.L., Corson, N.M., Wade-Mercer, P., Gelein, R., Kennell, A.J., Oberdörster, G., Elder, A. 2014. Equivalent titanium dioxide nanoparticle deposition by intratracheal instillation and whole-body inhalation: the effect of dose rate on acute respiratory tract inflammation. Part Fibre Toxicol. 11(1):5.

Bandyopadhyay, S., Peralta-Videa, J.R., Hernandez-Viezcas, J.A., Montes, M.O., Keller, A.A., Gardea-Torresdey, J.L. 2012. Microscopic and spectroscopic methods applied to the measurements of nanoparticles in the environment. Appl Spectrosc Rev. 47(3):180–206.

Barna, B.P., Huizar, I., Malur, A., McPeek, M., Marshall, I., Jacob, M., Dobbs, L., Kavuru, M.S.,

Thomassen, M.J. 2013. Carbon nanotube-induced pulmonary granulomatous disease: Twist1 and alveolar macrophage M1 activation. Int J Mol Sci. 14(12):23858–71.

Beamer, C.A., Girtsman, T.A., Seaver, B.P., Finsaas, K.J., Migliaccio, C.T., Perry, V.K., Rottman, J.B., Smith, D.E., Holian, A. 2013. IL-33 mediates multi-walled carbon nanotube (MWCNT)-induced airway hyper-reactivity via the mobilization of innate helper cells in the lung. Nanotoxicology. 7(6):1070–81.

Becker, H., Herzberg, F., Schulte, A., Kolossa-Gehring, M. 2011. The carcinogenic potential of nanomaterials, their release from products and options for regulating them. Int J Hyg Environ Health. 214(3):231–8.

Bergin, I.L., Wilding, L.A., Morishita, M., Walacavage, K., Ault, A.P., Axson, J.L., Stark, D.I., Hashway, S.A., Capracotta, S.S., Leroueil, P.R., Maynard, A.D. 2016. Effects of particle size and coating on toxicologic parameters, fecal elimination kinetics and tissue distribution of acutely ingested silver nanoparticles in a mouse model. Nanotoxicology. 10(3):352–60.

Bermudez, E., Mangum, J.B., Asgharian, B., Wong, B.A., Reverdy, E.E., Janszen, D.B., Hext, P.M., Warheit, D.B., Everitt, J.I. 2002. Long-term pulmonary responses of three laboratory rodent species to subchronic inhalation of pigmentary titanium dioxide particles. Toxicol Sci. 70(1):86–97.

Bermudez, E., Mangum, J.B., Wong, B.A., Asgharian, B., Hext, P.M., Warheit, D.B., Everitt, J.I. 2004. Pulmonary responses of mice, rats, and hamsters to subchronic inhalation of ultrafine titanium dioxide particles. Toxicol Sci. 77(2):347–57.

Bettini, S., Boutet-Robinet, E., Cartier, C., Coméra, C., Gaultier, E., Dupuy, J., Naud, N., Taché, S., Grysan, P., Reuger, S., Thieriet, N. 2017. Food-grade TiO2 impairs intestinal and systemic immune homeostasis, initiates preneoplastic lesions and promotes aberrant crypt development in the rat colon. Sci Rep. 7

Bhattacharya, K., Andón, F.T., El-Sayed, R., Fadeel, B. 2013. Mechanisms of carbon nanotube-induced toxicity: focus on pulmonary inflammation. Adv Drug Deliv Rev. 65(15):2087–97.

Bhol, K.C., Schechter, P.J. 2007. Effects of nanocrystalline silver (NPI 32101) in a rat model of ulcerative colitis. Dig Dis Sci. 52(10):2732–42.

Birch, M.E., Ruda-Eberenz, T.A., Chai, M., Andrews, R., Hatfield, R.L. 2013. Properties that influence the specific surface areas of carbon nanotubes and nanofibers. Ann Occup Hyg. 57(9):1148–66.

Boffetta, P., Soutar, A., Cherrie, J.W., Granath, F., Andersen, A., Anttila, A., Blettner, M., Gaborieau, V., Klug, S.J., Luce, D. 2004. Mortality among workers employed in the titanium dioxide production industry in Europe. Cancer Causes Control. 15(7):697–706.

Böhmert, L., Girod, M., Hansen, U., Maul, R., Knappe, P., Niemann, B., Weidner, S.M., Thünemann, A.F., Lampen, A. 2014. Analytically monitored digestion of silver nanoparticles and their toxicity on human intestinal cells. Nanotoxicology. 8(6):631–42.

Boland, S., Hussain, S., Baeza-Squiban, A. 2014. Carbon black and titanium dioxide nanoparticles induce distinct molecular mechanisms of toxicity. Wiley Interdiscip Rev Nanomed Nanobiotechnol. 6(6):641–52.

Boonstra, J., Post, J.A. 2004. Molecular events associated with reactive oxygen species and cell cycle progression in mammalian cells. Gene. 337:1–13.

Boorman, G.A., Brockmann, M., Carlton, W.W., Davis, J.M., Dungworth, D.L., Hahn, F.F., Mohr, U., Reichhelm, H.B., Turusov, V.S., Wagner, B.M. 1996. Classification of cystic keratinizing squamous lesions of the rat lung: report of a workshop. Toxicol Pathol. 24(5):564–72.

Bossa, N., Chaurand, P., Levard, C., Borschneck, D., Miche, H., Vicente, J., Geantet, C., Aguerre-Chariol, O., Michel, F.M., Rose, J. 2017. Environmental exposure to TiO 2 nanomaterials incorporated in building material. Environ Pollut. 220:1160–70.

Botelho, M.C., Costa, C., Silva, S., Costa, S., Dhawan, A., Oliveira, P.A., Teixeira, J.P. 2014. Effects of titanium dioxide nanoparticles in human gastric epithelial cells in vitro. Biomed Pharmacother. 68(1):59–64.

Boudreau, M.D., Imam, M.S., Paredes, A.M., Bryant, M.S., Cunningham, C.K., Felton, R.P., Jones, M.Y., Davis, K.J., Olson, G.R. 2016. Differential effects of silver nanoparticles and silver ions on tissue accumulation, distribution, and toxicity in the Sprague Dawley rat following daily oral gavage administration for 13 weeks. Toxicol Sci. 150(1):131–60.

Bouwmeester, H., Poortman, J., Peters, R.J., Wijma, E., Kramer, E., Makama, S., Puspitaninganindita, K., Marvin, H.J., Peijnenburg, A.A., Hendriksen, P.J. 2011. Characterization of translocation of silver nanoparticles and effects on whole-genome gene expression using an in vitro intestinal epithelium coculture model. ACS Nano. 5(5):4091–103.

Braakhuis, H.M., Cassee, F.R., Fokkens, P.H., de la Fonteyne, L.J., Oomen, A.G., Krystek, P., de Jong, W.H., van Loveren, H., Park, M.V. 2016. Identification of the appropriate dose metric for pulmonary inflammation of silver nanoparticles in an inhalation toxicity study. Nanotoxicology. 10(1):63–73.

Braakhuis, H.M., Gosens, I., Krystek, P., Boere, J.A., Cassee, F.R., Fokkens, P.H., Post, J.A., van Loveren, H., Park, M.V. 2014. Particle size dependent deposition and pulmonary inflammation after short-term inhalation of silver nanoparticles. Part Fibre Toxicol. 11(1):49.

Braun, J.H. 1997. Titanium dioxide: A review. J Coat Technol. 69(868):59–72.

Braydich-Stolle, L.K., Lucas, B., Schrand, A., Murdock, R.C., Lee, T., Schlager, J.J., Hussain, S.M., Hofmann, M.C. 2010. Silver nanoparticles disrupt GDNF/Fyn kinase signaling in spermatogonial stem cells. Toxicol Sci. 116(2):577–89.

Brown, D.M., Dickson, C., Duncan, P., Al-Attili, F., Stone, V. 2010. Interaction between nanoparticles and cytokine proteins: impact on protein and particle functionality. Nanotechnology. 21(21):215104.

Brunauer, S., Emmett, P.H., Teller, E. 1938. Adsorption of gases in multimolecular layers. J Am Chem Soc. 60(2):309–19.

Buechter, D.D. 1988. Free radicals and oxygen toxicity. Pharm Res. 5(5):253–60.

Bussy, C., Pinault, M., Cambedouzou, J., Landry, M.J., Jegou, P., Mayne-L'Hermite, M., Launois, P., Boczkowski, J., Lanone, S. 2012. Critical role of surface chemical modifications induced by length shortening on multi-walled carbon nanotubes-induced toxicity. Part Fibre Toxicol. 9(1):46.

Butler, K.S., Casey, B.J., Garborcauskas, G.V., Dair, B.J., Elespuru, R.K. 2014. Assessment of titanium dioxide nanoparticle effects in bacteria: association, uptake, mutagenicity, co-mutagenicity and DNA repair inhibition. Mutat Res Genet Toxicol Environ Mutagen. 768:14–22.

Butler, K.S., Peeler, D.J., Casey, B.J., Dair, B.J., Elespuru, R.K. 2015. Silver nanoparticles: correlating nanoparticle size and cellular uptake with genotoxicity. Mutagenesis. 30(4):577–91.

Caballero-Guzman, A., Nowack, B. 2016. A critical review of engineered nanomaterial release data: Are current data useful for material flow modeling?. Environ Pollut. 213:502–17.

Campagnolo, L., Massimiani, M., Palmieri, G., Bernardini, R., Sacchetti, C., Bergamaschi, A., Vecchione, L, Magrini, A., Bottini, M., Pietroiusti, A. 2013. Biodistribution and toxicity of pegylated single wall carbon nanotubes in pregnant mice. Part Fibre Toxicol. 10(1):21.

Card, J.W., Jonaitis, T.S., Tafazoli, S., Magnuson, B.A. 2011. An appraisal of the published literature on the safety and toxicity of food-related nanomaterials. Crit Rev Toxicol. 41(1):20–49.

Card, J.W., Magnuson, B.A. 2010. A method to assess the quality of studies that examine the toxicity of engineered nanomaterials. Int J Toxicol. 29(4):402–10.

Carlson, C., Hussain, S.M., Schrand, A.M., Braydich-Stolle, L.K., Hess, K.L., Jones, R.L., Schlager, J.J. 2008. Unique cellular interaction of silver nanoparticles: size-dependent generation of reactive oxygen species. J Phys Chem B. 112(43):13608–19.

Carmona, E.R., Escobar, B., Vales, G., Marcos, R. 2015. Genotoxic testing of titanium dioxide anatase nanoparticles using the wing-spot test and the comet assay in Drosophila. Mutat Res

Genet Toxicol Environ Mutagen. 778.12–21.

Carrero-Sanchez, J.C., Elias, A.L., Mancilla, R., Arrellin, G., Terrones, H., Laclette, J.P., Terrones, M. 2006. Biocompatibility and toxicological studies of carbon nanotubes doped with nitrogen. Nano Lett. 6(8):1609–16.

Cassel, S.L., Eisenbarth, S.C., Iyer, S.S., Sadler, J.J., Colegio, O.R., Tephly, L.A., Carter, A.B., Rothman, P.B., Flavell, R.A., Sutterwala, F.S. 2008. The Nalp3 inflammasome is essential for the development of silicosis. Proc Natl Acad Sci USA. 105(26):9035–40.

Castellini, C., Ruggeri, S., Mattioli, S., Bernardini, G., Macchioni, L., Moretti, E., Collodel, G. 2014. Long-term effects of silver nanoparticles on reproductive activity of rabbit buck. Syst Biol Reprod Med. 60(3):143–50.

Castranova, V. 2011. Overview of current toxicological knowledge of engineered nanoparticles. J Occup Env Med. 53:S14–S17.

Catalán, J., Järventaus, H., Vippola, M., Savolainen, K., Norppa, H. 2012. Induction of chromosomal aberrations by carbon nanotubes and titanium dioxide nanoparticles in human lymphocytes in vitro. Nanotoxicology, 6(8):825–36.

Catalán, J., Siivola, K.M., Nymark, P., Lindberg, H., Suhonen, S., Järventaus, H., Koivisto, A.J., Moreno, C., Vanhala, E., Wolff, H., Kling, K.I. 2016. In vitro and in vivo genotoxic effects of straight versus tangled multi-walled carbon nanotubes. Nanotoxicology. 10(6):794–806.

Cavallo, D., Fanizza, C., Ursini, C.L., Casciardi, S., Paba, E., Ciervo, A., Fresegna, A.M., Maiello, R., Marcelloni, A.M., Buresti, G., Tombolini, F. 2012. Multi-walled carbon nanotubes induce cytotoxicity and genotoxicity in human lung epithelial cells. J Appl Toxicol. 32(6):454–464.

Chairuangkitti, P., Lawanprasert, S., Roytrakul, S., Aueviriyavit, S., Phummiratch, D., Kulthong, K., Chanvorachote, P., Maniratanachote, R. 2013. Silver nanoparticles induce toxicity in A549 cells via ROS-dependent and ROS-independent pathways. Toxicol In Vitro. 27(1):330–8.

Champion, J.A., Mitragotri, S. 2009. Shape induced inhibition of phagocytosis of polymer particles. Pharm Res. 26(1):244–9.

Chang, C.C., Tsai, M.L., Huang, H.C., Chen, C.Y., Dai, S.X. 2012. Epithelial-mesenchymal transition contributes to SWCNT-induced pulmonary fibrosis. Nanotoxicology. 6(6):600–10.

Chappell, M.A., Miller, L.F., George, A.J., Pettway, B.A., Price, C.L., Porter, B.E., Bednar, A.J., Seiter, J.M., Kennedy, A.J., Steevens, J.A. 2011. Simultaneous dispersion–dissolution behavior of concentrated silver nanoparticle suspensions in the presence of model organic solutes. Chemosphere. 84(8):1108–16.

Charehsaz, M., Hougaard, K.S., Sipahi, H., Ekici, A.I.D., Kaspar, Ç., Culha, M., Bucurgat, Ü.Ü., Aydin, A. 2016. Effects of developmental exposure to silver in ionic and nanoparticle form: A study in rats. DARU. 24(1):24.

Chen, J.L., Fayerweather, W.E. 1988. Epidemiologic study of workers exposed to titanium dioxide. J Occup Env Med. 30(12):937–42.

Chen, R., Zhao, L., Bai, R., Liu, Y., Han, L., Xu, Z., Chen, F., Autrup, H., Long, D., Chen, C. 2016. Silver nanoparticles induced oxidative and endoplasmic reticulum stresses in mouse tissues: implications for the development of acute toxicity after intravenous administration. Toxicol Res. 5(2):602–8.

Chen, T., Nie, H., Gao, X., Yang, J., Pu, J., Chen, Z., Cui, X., Wang, Y., Wang, H., Jia, G. 2014a. Epithelial–mesenchymal transition involved in pulmonary fibrosis induced by multi-walled carbon nanotubes via TGF-beta/Smad signaling pathway. Toxicol Lett. 226(2):150–62.

Chen, X., Schluesener, H.J. 2008. Nanosilver: a nanoproduct in medical application. Toxicol Lett. 176(1):1–12.

Chen, Y.T., Wu, J.H., Tsai, F.J., Chang, Y.W., Hsu, S.H., Lin, J.J., Sue, H.L., Liao, J.W. 2015a. Genotoxicity tests of poly (styrene-co-maleic anhydride)-coated silver nanoparticles in vivo and in vitro. J Exp Nanosci. 10(6):449–57.

Chen, Z., Wang, Y., Ba, T., Li, Y., Pu, J., Chen, T., Song, Y., Gu, Y., Qian, Q., Yang, J., Jia, G. 2014b. Genotoxic evaluation of titanium dioxide nanoparticles in vivo and in vitro. Toxicol Lett. 226(3):314–9.

Chen, Z., Wang, Y., Zhuo, L., Chen, S., Zhao, L., Chen, T., Li, Y., Zhang, W., Gao, X., Li, P., Wang, H. 2015c. Interaction of titanium dioxide nanoparticles with glucose on young rats after oral administration. Nanomed Nanotechnol. 11(7):1633–42.

Chen, Z., Wang, Y., Zhuo, L., Chen, S., Zhao, L., Luan, X., Wang, H., Jia, G. 2015b. Effect of titanium dioxide nanoparticles on the cardiovascular system after oral administration. Toxicol Lett. 239(2):123–30.

Cheng, L.C., Jiang, X., Wang, J., Chen, C., Liu, R.S. 2013. Nano–bio effects: interaction of nanomaterials with cells. Nanoscale. 5(9):3547–69.

Cho, W.S., Duffin, R., Thielbeer, F., Bradley, M., Megson, I.L., MacNee, W., Poland, C.A., Tran, C.L., Donaldson, K. 2012. Zeta potential and solubility to toxic ions as mechanisms of lung inflammation caused by metal/metal oxide nanoparticles. Toxicol Sci. 126(2):469–77.

Cho, W.S., Kang, B.C., Lee, J.K., Jeong, J., Che, J.H., Seok, S.H. 2013. Comparative absorption, distribution, and excretion of titanium dioxide and zinc oxide nanoparticles after repeated oral administration. Part Fibre Toxicol. 10(1):9.

Choi, J., Reipa, V., Hitchins, V.M., Goering, P.L., Malinauskas, R.A. 2011. Physicochemical Characterization and In Vitro Hemolysis Evaluation of Silver Nanoparticles. Toxicol Sci. 123(1):133–43.

Choi, O., Hu, Z. 2008. Size dependent and reactive oxygen species related nanosilver toxicity to nitrifying bacteria. Environ Sci Technol. 42(12):4583–8.

Chou, C.C., Hsiao, H.Y., Hong, Q.S., Chen, C.H., Peng, Y.W., Chen, H.W., Yang, P.C. 2008. Single-walled carbon nanotubes can induce pulmonary injury in mouse model. Nano Lett. 8(2):437–45.

Cicchetti, R., Divizia, M., Valentini, F., Argentin, G. 2011. Effects of single-wall carbon nanotubes in human cells of the oral cavity: geno-cytotoxic risk. Toxicol In Vitro. 25(8):1811–9.

Clift, M.J., Raemy, D.O., Endes, C., Ali, Z., Lehmann, A.D., Brandenberger, C., Petri-Fink, A., Wick, P., Parak, W.J., Gehr, P., Schins, R.P. 2013. Can the Ames test provide an insight into nano-object mutagenicity? Investigating the interaction between nano-objects and bacteria. Nanotoxicology. 7(8):1373–85.

Colman, B.P., Arnaout, C.L., Anciaux, S., Gunsch, C.K., Hochella Jr, M.F., Kim, B., Lowry, G.V., McGill, B.M., Reinsch, B.C., Richardson, C.J., Unrine, J.M. 2013. Low concentrations of silver nanoparticles in biosolids cause adverse ecosystem responses under realistic field scenario. PLoS One. 8(2):e57189.

Comfort, K.K., Maurer, E.I., Hussain, S.M. 2014. Slow release of ions from internalized silver nanoparticles modifies the epidermal growth factor signaling response. Colloids Surf B. 123:136–42.

CPSC (Consumer Product Safety Commission). 2011. Consumer Product Safety Act. Available at: https://www.cpsc.gov/s3fs-public/pdfs/blk_media_cpsa.pdf?epslanguage=en

Crosera, M., Bovenzi, M., Maina, G., Adami, G., Zanette, C., Florio, C., Larese, F.F. 2009. Nanoparticle dermal absorption and toxicity: a review of the literature. Int Arch Occup Environ Health. 82(9):1043–55.

Crouzier, D., Follot, S., Gentilhomme, E., Flahaut, E., Arnaud, R., Dabouis, V., Castellarin, C., Debouzy, J.C. 2010. Carbon nanotubes induce inflammation but decrease the production of reactive oxygen species in lung. Toxicology. 272(1):39–45.

Cveticanin, J., Joksic, G., Leskovac, A., Petrovic, S., Sobot, A.V., Neskovic, O. 2009. Using carbon nanotubes to induce micronuclei and double strand breaks of the DNA in human cells. Nanotechnology. 21(1):015102.

Dallas, P., Sharma, V.K., Zboril, R. 2011. Silver polymeric nanocomposites as advanced antimicrobial agents: classification, synthetic paths, applications, and perspectives. Adv Colloid Interface Sci. 166(1):119–35.

Danish EPA (The Danish Environmental Protection Agency). 2013. Systemic absorption of Nanomaterials by Oral Exposure. Environmental Project No. 1505.

Danish EPA (The Danish Environmental Protection Agency). 2015a. Exposure Assessment of Nanomaterials in Consumer Products. Environmental Project No. 1636. Available at: https://www2.mst.dk/Udgiv/publications/2015/01/978-87-93283-57-2_appendix.pdf

Danish EPA (The Danish Environmental Protection Agency). 2015b. Consumer Risk Assessment for Nanoproducts on the Danish Market. Environmental Project No. 1730. Available at: https://www2.mst.dk/Udgiv/publications/2015/07/978-87-93352-48-3.pdf

Dankovic, D., Kuempel, E., Wheeler, M. 2007. An approach to risk assessment for TiO2. Inhal Toxicol. 19(Sup1):205–12.

David, R.M., Boverhof, D.R., Butala, J.H., Clancy, S., Lafranconi, M., Bramante, C.M., West, W.J. 2015. Comparative assessment of nanomaterial definitions and considerations for implementation. American Chemistry Council, Washington, DC, USA. Available at: https://nanotechnology.americanchemistry.com/Nanotechnology/Panel-Activities/Nanotechnology-Definitions/Nanotechnology-Panel-Presents-at-Society-of-Toxicology.pdf

de Andrade, L.R., Brito, A.S., de Souza Melero, A.M.G., Zanin, H., Ceragioli, H.J., Baranauskas, V., Cunha, K.S., Irazusta, S.P. 2014. Absence of mutagenic and recombinagenic activity of multi-walled carbon nanotubes in the Drosophila wing-spot test and Allium cepa test. EcotoxicolEnviron Saf. 99:92–7.

De Jong, W.H., Van Der Ven, L.T., Sleijffers, A., Park, M.V., Jansen, E.H., Van Loveren, H., Vandebriel, R.J. 2013. Systemic and immunotoxicity of silver nanoparticles in an intravenous 28 days repeated dose toxicity study in rats. Biomaterials. 34(33):8333–43.

De Matteis, V., Malvindi, M.A., Galeone, A., Brunetti, V., De Luca, E., Kote, S., Kshirsagar, P., Sabella, S., Bardi, G., Pompa, P.P. 2015. Negligible particle-specific toxicity mechanism of silver nanoparticles: the role of Ag+ ion release in the cytosol. Nanomed Nanotechnol. 11(3):731–9.

De Stefano, D., Carnuccio, R., Maiuri, M.C. 2012. Nanomaterials toxicity and cell death modalities. J Drug Deliv. 2012.

De Volder, M.F., Tawfick, S.H., Baughman, R.H., Hart, A.J. 2013. Carbon nanotubes: present and future commercial applications. Science. 339(6119):535–9.

Demir, E., Akça, H., Turna, F., Aksakal, S., Burgucu, D., Kaya, B., Tokgun, O., Vales, G., Creus, A., Marcos, R. 2015. Genotoxic and cell-transforming effects of titanium dioxide nanoparticles. Environ Res. 136:300–8.

Deng, Z.J., Butcher, N.J., Mortimer, G.M., Jia, Z., Monteiro, M.J., Martin, D.J., Minchin, R.F. 2014. Interaction of human arylamine N-acetyltransferase 1 with different nanomaterials. Drug Metab Dispos. 42(3):377–83.

Di Giorgio, M.L., Di Bucchianico, S., Ragnelli, A.M., Aimola, P., Santucci, S., Poma, A. 2011. Effects of single and multi walled carbon nanotubes on macrophages: cyto and genotoxicity and electron microscopy. Mutat Res Genet Toxicol Environ Mutagen. 722(1):20–31.

Dinarello, C.A. 1996. Biologic basis for interleukin-1 in disease. Blood. 87(6):2095 – 147.

Dobrzyńska, M.M., Gajowik, A., Radzikowska, J., Lankoff, A., Dušinská, M., Kruszewski, M. 2014. Genotoxicity of silver and titanium dioxide nanoparticles in bone marrow cells of rats in vivo. Toxicology. 315:86–91.

Donaldson, K., Aitken, R., Tran, L., Stone, V., Duffin, R., Forrest, G., Alexander, A. 2006. Carbon nanotubes: a review of their properties in relation to pulmonary toxicology and workplace safety. Toxicol Sci. 92(1):5–22.

Donaldson, K., Tran, L., Jimenez, L.A., Duffin, R., Newby, D.E., Mills, N., MacNee, W., Stone, V. 2005. Combustion-derived nanoparticles: a review of their toxicology following inhalation exposure. Part Fibre Toxicol. 2(1):10.

Dong, J., Ma, Q. 2015. Advances in mechanisms and signaling pathways of carbon nanotube toxicity. Nanotoxicology. 9(5):658–76.

Dong, J., Ma, Q. 2016. Suppression of basal and carbon nanotube-induced oxidative stress, inflammation and fibrosis in mouse lungs by Nrf2. Nanotoxicology. 10(6):699–709.

Dong, J., Porter, D.W., Batteli, L.A., Wolfarth, M.G., Richardson, D.L., Ma, Q. 2015. Pathologic and molecular profiling of rapid-onset fibrosis and inflammation induced by multi-walled carbon nanotubes. Arch Toxicol. 89(4):621–33.

Donner, E.M., Myhre, A., Brown, S.C., Boatman, R., Warheit, D.B. 2016. In vivo micronucleus studies with 6 titanium dioxide materials (3 pigment-grade & 3 nanoscale) in orally-exposed rats. Regul Toxicol Pharmacol. 74:64–74.

Duan, Y., Liu, J., Ma, L., Li, N., Liu, H., Wang, J., Zheng, L., Liu, C., Wang, X., Zhao, X., Yan, J. 2010. Toxicological characteristics of nanoparticulate anatase titanium dioxide in mice. Biomaterials. 31(5):894–9.

Dziendzikowska, K., Gromadzka-Ostrowska, J., Lankoff, A., Oczkowski, M., Krawczyńska, A.,

Chwastowska, J., Sadowska-Bratek, M., Chajduk, E., Wojewódzka, M., Dušinská, M., Kruszewski, M. 2012. Time-dependent biodistribution and excretion of silver nanoparticles in male Wistar rats. J Appl Toxicol. 32(11):920–8.

Dziendzikowska, K., Krawczyńska, A., Oczkowski, M., Królikowski, T., Brzóska, K., Lankoff, A., Dziendzikowski, M., Stępkowski, T., Kruszewski, M., Gromadzka-Ostrowska, J. 2016. Progressive effects of silver nanoparticles on hormonal regulation of reproduction in male rats. Toxicol Appl Pharmacol. 313:35–46.

EFSA (European Food Safety Authority). 2011. Guidance on the risk assessment of the application of nanoscience and nanotechnologies in the food and feed chain. EFSA Journal. 9(5):2140.

El Mahdy, M.M., Eldin, T.A.S., Aly, H.S., Mohammed, F.F., Shaalan, M.I. 2015. Evaluation of hepatotoxic and genotoxic potential of silver nanoparticles in albino rats. Exp Toxicol Pathol. 67(1):21–9.

Elder, A., Gelein, R., Finkelstein, J.N., Driscoll, K.E., Harkema, J., Oberdörster, G. 2005. Effects of subchronically inhaled carbon black in three species. I. Retention kinetics, lung inflammation, and histopathology. Toxicol Sci. 88(2):614–29.

Elgrabli, D., Abella-Gallart, S., Robidel, F., Rogerieux, F., Boczkowski, J., Lacroix, G. 2008. Induction of apoptosis and absence of inflammation in rat lung after intratracheal instillation of multiwalled carbon nanotubes. Toxicology. 253(1):131–6.

Ellinger-Ziegelbauer, H., Pauluhn, J. 2009. Pulmonary toxicity of multi-walled carbon nanotubes (Baytubes®) relative to α-quartz following a single 6h inhalation exposure of rats and a 3 months post-exposure period. Toxicology. 266(1):16–29.

Ema, M., Hougaard, K.S., Kishimoto, A., Honda, K. 2016. Reproductive and developmental toxicity of carbon-based nanomaterials: A literature review. J Nanotoxicology. 10(4):391-412.

Ema, M., Imamura, T., Suzuki, H., Kobayashi, N., Naya, M., Nakanishi, J. 2012. Evaluation of genotoxicity of multi-walled carbon nanotubes in a battery of in vitro and in vivo assays. Regul Toxicol Pharmacol. 63(2):188–95.

Ema, M., Imamura, T., Suzuki, H., Kobayashi, N., Naya, M., Nakanishi, J. 2013. Genotoxicity evaluation for single-walled carbon nanotubes in a battery of in vitro and in vivo assays. J Appl Toxicol. 33(9):933–9.

Ema, M., Kobayashi, N., Naya, M., Hanai, S., Nakanishi, J. 2010. Reproductive and developmental toxicity studies of manufactured nanomaterials. Reprod Toxicol. 30(3):343–52.

Eom, H.J., Choi, J. 2010. p38 MAPK activation, DNA damage, cell cycle arrest and apoptosis as mechanisms of toxicity of silver nanoparticles in Jurkat T cells. Eviron Sci Technol.

44(21):8337–42.

Erdely, A., Dahm, M.M., Schubauer-Berigan, M.K., Chen, B.T., Antonini, J.M., Hoover, M.D. 2016. Bridging the gap between exposure assessment and inhalation toxicology: Some insights from the carbon nanotube experience. J Aerosol Sci. 99:157–62.

Erdely, A., Hulderman, T., Salmen, R., Liston, A., Zeidler-Erdely, P.C., Schwegler-Berry, D., Castranova, V., Koyama, S., Kim, Y.A., Endo, M., Simeonova, P.P. 2009. Cross-talk between lung and systemic circulation during carbon nanotube respiratory exposure. Potential biomarkers. Nano Lett. 9(1):36–43.

Ernest, V., Doss, C.G.P., Muthiah, A., Mukherjee, A., Chandrasekaran, N. 2013. Genotoxicity assessment of low concentration AgNPs to human peripheral blood lymphocytes. Int J Pharm Sci. 5(2):377–81.

Esposito, E.X., Hopfinger, A.J., Shao, C.Y., Su, B.H., Chen, S.Z., Tseng, Y.J. 2015. Exploring possible mechanisms of action for the nanotoxicity and protein binding of decorated nanotubes: interpretation of physicochemical properties from optimal QSAR models. Toxicol Appl Pharmacol. 288(1):52–62.

Evanoff, D.D., Chumanov, G. 2005. Synthesis and optical properties of silver nanoparticles and arrays. ChemPhysChem. 6(7):1221–31.

Eydner, M., Schaudien, D., Creutzenberg, O., Ernst, H., Hansen, T., Baumgärtner, W., Rittinghausen, S. 2012. Impacts after inhalation of nano-and fine-sized titanium dioxide particles: morphological changes, translocation within the rat lung, and evaluation of particle deposition using the relative deposition index. Inhal Toxicol. 24(9):557–69.

Faedmaleki, F., Shirazi, F.H., Salarian, A.A., Ashtiani, H.A., Rastegar, H. 2014. Toxicity effect of silver nanoparticles on mice liver primary cell culture and HepG2 cell line. Iran J Pharm Res. 13(1):235–42.

Fatemi, M., Roodbari, N.H., Ghaedi, K., Naderi, G. 2013. The effects of prenatal exposure to silver nanoparticles on the developing brain in neonatal rats. J Biol Res-Thessalon. 20:233–42.

Fatemi Tabatabaie, S.R., Mehdiabadi, B., Mori Bakhtiari, N., Tabandeh, M.R. 2017. Silver nanoparticle exposure in pregnant rats increases gene expression of tyrosine hydroxylase and monoamine oxidase in offspring brain. Drug Chem Toxicol. 40(4):440–7.

Fatkhutdinova, L.M., Khaliullin, T.O., Vasil'yeva, O.L., Zalyalov, R.R., Mustafin, I.G., Kisin, E. R., Birch, M.E., Yanamala, N., Shvedova, A.A. 2016. Fibrosis biomarkers in workers exposed to MWCNTs. Toxicol Appl Pharmacol. 299:125–31.

Fenoglio, I., Aldieri, E., Gazzano, E., Cesano, F., Colonna, M., Scarano, D., Mazzucco, G., Attanasio, A., Yakoub, Y., Lison, D., Fubini, B. 2012. Thickness of multiwalled carbon

nanotubes affects their lung toxicity. Chem Res Toxicol. 25(1):74–82.

Fenoglio, I., Tomatis, M., Lison, D., Muller, J., Fonseca, A., Nagy, J.B., Fubini, B. 2006. Reactivity of carbon nanotubes: free radical generation or scavenging activity. Free Radic Biol Med. 40(7):1227–33.

Ferin, J., Oberdörster, G., Penney, D.P. 1992. Pulmonary retention of ultrafine and fine particles in rats. Am J Respir Cell Mol Biol. 6(5):535–42.

Filon, F.L., Bello, D., Cherrie, J.W., Sleeuwenhoek, A., Spaan, S., Brouwer, D.H. 2016. Occupational dermal exposure to nanoparticles and nano-enabled products: part I—factors affecting skin absorption. Int J Hyg Environ Health. 219(6):536 - 44.

Foldbjerg, R., Dang, D.A., Autrup, H. 2011. Cytotoxicity and genotoxicity of silver nanoparticles in the human lung cancer cell line, A549. Arch Toxicol. 85(7):743–50.

Foldbjerg, R., Irving, E.S., Hayashi, Y., Sutherland, D.S., Thorsen, K., Autrup, H., Beer, C. 2012. Global gene expression profiling of human lung epithelial cells after exposure to nanosilver. Toxicol Sci. 130(1):145–57.

Foldbjerg, R., Olesen, P., Hougaard, M., Dang, D.A., Hoffmann, H.J., Autrup, H. 2009. PVP-coated silver nanoparticles and silver ions induce reactive oxygen species, apoptosis and necrosis in THP-1 monocytes. Toxicol Lett. 190(2):156–62.

Franchi, L.P., Manshian, B.B., de Souza, T.A., Soenen, S.J., Matsubara, E.Y., Rosolen, J.M., Takahashi, C.S. 2015. Cyto-and genotoxic effects of metallic nanoparticles in untransformed human fibroblast. Toxicol In Vitro. 29(7):1319–31.

Frank, E.A., Birch, M.E., Yadav, J.S. 2015. MyD88 mediates in vivo effector functions of alveolar macrophages in acute lung inflammatory responses to carbon nanotube exposure. Toxicol Appl Pharmacol. 288(3):322–9.

Frenzilli, G., Bernardeschi, M., Guidi, P., Scarcelli, V., Lucchesi, P., Marsili, L., Fossi, M.C., Brunelli, A., Pojana, G., Marcomini, A., Nigro, M. 2014. Effects of in vitro exposure to titanium dioxide on DNA integrity of bottlenose dolphin (Tursiops truncatus) fibroblasts and leukocytes. Mar Environ Res. 100:68–73.

Froggett, S.J., Clancy, S.F., Boverhof, D.R., Canady, R.A. 2014. A review and perspective of existing research on the release of nanomaterials from solid nanocomposites. Part Fibre Toxicol. 11(1):17.

Fryzek, J.P., Chadda, B., Marano, D., White, K., Schweitzer, S., McLaughlin, J.K., Blot, W.J. 2003. A cohort mortality study among titanium dioxide manufacturing workers in the United States. J Occup Env Med. 45(4):400–9.

Fu, Y., Zhang, Y., Chang, X., Zhang, Y., Ma, S., Sui, J., Yin, L., Pu, Y., Liang, G. 2014. Systemic immune effects of titanium dioxide nanoparticles after repeated intratracheal instillation in rat. Int J Mol Sci. 15(4):6961–73.

Fujita, K., Fukuda, M., Endoh, S., Maru, J., Kato, H., Nakamura, A., Shinohara, N., Uchino, K., Honda, K. 2015. Size effects of single-walled carbon nanotubes on in vivo and in vitro pulmonary toxicity. Inhal Toxicol. 27(4):207–23.

Fujitani, T., Ohyama, K.I., Hirose, A., Nishimura, T., Nakae, D, Ogata, A. 2012. Teratogenicity of multi-wall carbon nanotube (MWCNT) in CD-1 mice. J Toxicol Sci. 37:81–9.

Furukawa, F., Doi, Y., Suguro, M., Morita, O., Kuwahara, H., Masunaga, T., Hatakeyama, Y., Mori, F. 2011. Lack of skin carcinogenicity of topically applied titanium dioxide nanoparticles in the mouse. Food Chem Toxicol. 49(4):744–9.

Gábelová, A., El Yamani, N., Alonso, T.I., Buliaková, B., Srančíková, A., Bábelová, A., Pran, E.R., Fjellsbø, L.M., Elje, E., Yazdani, M., Silva, M.J. 2017. Fibrous shape underlies the mutagenic and carcinogenic potential of nanosilver while surface chemistry affects the biosafety of iron oxide nanoparticles. Mutagenesis. 32(1):193–202.

Galandáková, A., Franková, J., Ambrožová, N., Habartová, K., Pivodová, V., Zálešák, B., Šafářová, K., Smékalová, M., Ulrichová, J. 2016. Effects of silver nanoparticles on human dermal fibroblasts and epidermal keratinocytes. Hum Exp Toxicol. 35(9):946–57.

Galano, A. 2008. Carbon nanotubes as free-radical scavengers. J Phys Chem C. 112(24):8922–7.

Gao, G., Ze, Y., Zhao, X., Sang, X., Zheng, L., Ze, X., Gui, S., Sheng, L., Sun, Q., Hong, J., Yu, X. 2013. Titanium dioxide nanoparticle-induced testicular damage, spermatogenesis suppression, and gene expression alterations in male mice. J Hazard Mater. 258:133–143.

Garcia, T., Lafuente, D., Blanco, J., Sánchez, D.J., Sirvent, J.J., Domingo, J.L., Gómez, M. 2016. Oral subchronic exposure to silver nanoparticles in rats. Food Chem Toxicol. 92:177–87.

Garcia, T.X., Costa, G.M., Franca, L.R., Hofmann, M.C. 2014. Sub-acute intravenous administration of silver nanoparticles in male mice alters Leydig cell function and testosterone levels. Reprod Toxicol. 45:59–70.

Gasse, P., Mary, C., Guenon, I., Noulin, N., Charron, S., Schnyder-Candrian, S., Schnyder, B., Akira, S., Quesniaux, V.F., Lagente, V., Ryffel, B. 2007. IL-1R1/MyD88 signaling and the inflammasome are essential in pulmonary inflammation and fibrosis in mice. J Clin Investig. 117(12):3786–99.

Ge, C., Meng, L., Xu, L., Bai, R., Du, J., Zhang, L., Li, Y., Chang, Y., Zhao, Y., Chen, C. 2012. Acute pulmonary and moderate cardiovascular responses of spontaneously hypertensive rats after exposure to single-wall carbon nanotubes. Nanotoxicology. 6(5):526–42.

Geiser, M., Casaulta, M., Kupferschmid, B., Schulz, H., Semmler-Behnke, M., Kreyling, W. 2008. The role of macrophages in the clearance of inhaled ultrafine titanium dioxide particles. Am J Respir Cell Mol Biol. 38(3):371–6.

Geiser, M., Rothen-Rutishauser, B., Kapp, N., Schürch, S., Kreyling, W., Schulz, H., Semmler, M., Im Hof, V., Heyder, J., Gehr, P. 2005. Ultrafine particles cross cellular membranes by nonphagocytic mechanisms in lungs and in cultured cells. Environ Health Perspect. 113(11):1555.

Geraets, L., Oomen, A.G., Krystek, P., Jacobsen, N.R., Wallin, H., Laurentie, M., Verharen, H.W., Brandon, E.F., De Jong, W.H. 2014. Tissue distribution and elimination after oral and intravenous administration of different titanium dioxide nanoparticles in rats. Part Fibre Toxicol. 11(1):30.

Gernand, J.M., Casman, E.A. 2014. A Meta-Analysis of Carbon Nanotube Pulmonary Toxicity Studies—How Physical Dimensions and Impurities Affect the Toxicity of Carbon Nanotubes. Risk Anal. 34(3):583–97.

Ghaderi, S., Tabatabaei, S.R.F., Varzi, H.N., Rashno, M. 2015. Induced adverse effects of prenatal exposure to silver nanoparticles on neurobehavioral development of offspring of mice. J Toxicol Sci. 40(2):263–75.

Ghanbari, F., Nasarzadeh, P., Seydi, E., Ghasemi, A., Taghi Joghataei, M., Ashtari, K., Akbari, M. 2017. Mitochondrial oxidative stress and dysfunction induced by single-and multiwall carbon nanotubes: A comparative study. J Biomed Mater Res Part A. 105(7):2047–55.

Ghosh, M., Bandyopadhyay, M., Mukherjee, A. 2010. Genotoxicity of titanium dioxide (TiO 2) nanoparticles at two trophic levels: plant and human lymphocytes. Chemosphere. 81(10):1253–62.

Ghosh, M., Chakraborty, A., Bandyopadhyay, M., Mukherjee, A. 2011. Multi-walled carbon nanotubes (MWCNT): induction of DNA damage in plant and mammalian cells. J Hazard Mater. 197:327–36.

Ghosh, M., Chakraborty, A., Mukherjee, A. 2013. Cytotoxic, genotoxic and the hemolytic effect of titanium dioxide (TiO2) nanoparticles on human erythrocyte and lymphocyte cells in vitro. J Appl Toxicol. 33(10):1097–110.

Ghosh, M., Manivannan, J., Sinha, S., Chakraborty, A., Mallick, S.K., Bandyopadhyay, M., Mukherjee, A. 2012. In vitro and in vivo genotoxicity of silver nanoparticles. Mutat Res Genet Toxicol Environ Mutagen. 749(1):60–9.

Ging, J., Tejerina-Anton, R., Ramakrishnan, G., Nielsen, M., Murphy, K., Gorham, J.M., Nguyen, T., Orlov, A. 2014. Development of a conceptual framework for evaluation of

nanomaterials release from nanocomposites: environmental and toxicological implications. Sci Total Environ. 473:9–19.

Girtsman, T.A., Beamer, C.A., Wu, N., Buford, M., Holian, A. 2014. IL-1R signalling is critical for regulation of multi-walled carbon nanotubes-induced acute lung inflammation in C57Bl/6 mice. Nanotoxicology. 8(1):17–27.

Gliga, A.R., Skoglund, S., Wallinder, I.O., Fadeel, B., Karlsson, H.L. 2014. Size-dependent cytotoxicity of silver nanoparticles in human lung cells: the role of cellular uptake, agglomeration and Ag release. Part Fibre Toxicol. 11(1):11.

Glover, R.D., Miller, J.M., Hutchison, J.E. 2011. Generation of metal nanoparticles from silver and copper objects: nanoparticle dynamics on surfaces and potential sources of nanoparticles in the environment. ACS Nano. 5(11):8950–7.

Golokhvast, K.S., Chaika, V.V., Kuznetsov, L.V., Elumeeva, K.V., Kusaikin, M.I., Zakharenko, A.M., Kiselev, N.N., Panichev, A.M., Reva, G.V., Usov, V.V., Reva, I.V. 2013. Effects of multiwalled carbon nanotubes received orally during 6 days on the gastrointestinal tract. Bull Exp Biol Med. 155(6):788.

Gorham, J.M., Rohlfing, A.B., Lippa, K.A., MacCuspie, R.I., Hemmati, A., Holbrook, R.D. 2014. Storage Wars: how citrate-capped silver nanoparticle suspensions are affected by not-so-trivial decisions. J Nanopart Res. 16(4):2339.

Grassian, V.H., Adamcakova-Dodd, A., Pettibone, J.M., O'shaughnessy, P.I., Thorne, P.S. 2007b. Inflammatory response of mice to manufactured titanium dioxide nanoparticles: comparison of size effects through different exposure routes. Nanotoxicology. 1(3):211–26.

Grassian, V.H., O'Shaughnessy, P.T., Adamcakova-Dodd, A., Pettibone, J.M., Thorne, P.S. 2007a. Inhalation exposure study of titanium dioxide nanoparticles with a primary particle size of 2 to 5 nm. Environ Health Perspect. 115(3):397.

Greulich, C., Kittler, S., Epple, M., Muhr, G., Köller, M. 2009. Studies on the biocompatibility and the interaction of silver nanoparticles with human mesenchymal stem cells (hMSCs). Langenbeck's Arch Surg. 394(3):495–502.

Grieger, K.D., Redmon, J.H., Money, E.S., Widder, M.W., van der Schalie, W.H., Beaulieu, S.M., Womack, D. 2015. A relative ranking approach for nano-enabled applications to improve risk-based decision making: a case study of Army materiel. Environ Syst Decis. 35(1):42–53.

Grissa, I., Elghoul, J., Ezzi, L., Chakroun, S., Kerkeni, E., Hassine, M., El Mir, L., Medhi, M., Cheikh, H.B., Haouas, Z. 2015. Anemia and genotoxicity induced by sub-chronic intragastric treatment of rats with titanium dioxide nanoparticles. Mutat Res Genet Toxicol Environ Mutagen. 794:25–31.

Gromadzka-Ostrowska, J., Dziendzikowska, K., Lankoff, A., Dobrzyńska, M., Instanes, C., Brunborg, G., Gajowik, A., Radzikowska, J., Wojewódzka, M., Kruszewski, M. 2012. Silver nanoparticles effects on epididymal sperm in rats. Toxicol Lett. 214(3):251–8.

Grosse, Y., Loomis, D., Guyton, K.Z., Lauby-Secretan, B., El Ghissassi, F., Bouvard, V., Benbrahim-Tallaa, L., Guha, N., Scoccianti, C., Mattock, H., Straif, K. 2014. Carcinogenicity of fluoro-edenite, silicon carbide fibres and whiskers, and carbon nanotubes. Lancet Oncol. 15(13):1427.

Guichard, Y., Schmit, J., Darne, C., Gaté, L., Goutet, M., Rousset, D., Rastoix, O., Wrobel, R., Witschger, O., Martin, A., Fierro, V. 2012. Cytotoxicity and genotoxicity of nanosized and microsized titanium dioxide and iron oxide particles in Syrian hamster embryo cells. Ann Occup Hyg. 56(5):631–44.

Guigas, C., Walz, E., Gräf, V., Heller, K.J., Greiner, R. 2017. Mutagenicity of silver nanoparticles in CHO cells dependent on particle surface functionalization and metabolic activation. J Nanopart Res. 19(6):207.

Guo, F., Ma, N., Horibe, Y., Kawanishi, S., Murata, M., Hiraku, Y. 2012. Nitrative DNA damage induced by multi-walled carbon nanotube via endocytosis in human lung epithelial cells. Toxicol Appl Pharmacol. 260(2):183–92.

Guo, X., Li, Y., Yan, J., Ingle, T., Jones, M.Y., Mei, N., Boudreau, M.D., Cunningham, C.K., Abbas, M., Paredes, A.M., Zhou, T. 2016. Size-and coating-dependent cytotoxicity and genotoxicity of silver nanoparticles evaluated using in vitro standard assays. Nanotoxicology. 10(9):1373–84.

Guo, Y.Y., Zhang, J., Zheng, Y.F., Yang, J., Zhu, X.Q. 2011. Cytotoxic and genotoxic effects of multi-wall carbon nanotubes on human umbilical vein endothelial cells in vitro. Mutat Res Genet Toxicol Environ Mutagen. 721(2):184–91.

Hackenberg, S., Friehs, G., Froelich, K., Ginzkey, C., Koehler, C., Scherzed, A., Burghartz, M., Hagen, R., Kleinsasser, N. 2010. Intracellular distribution, geno-and cytotoxic effects of nanosized titanium dioxide particles in the anatase crystal phase on human nasal mucosa cells. Toxicol Lett. 195(1):9–14.

Hackenberg, S., Friehs, G., Kessler, M., Froelich, K., Ginzkey, C., Koehler, C., Scherzed, A., Burghartz, M., Kleinsasser, N. 2011b. Nanosized titanium dioxide particles do not induce DNA damage in human peripheral blood lymphocytes. Environmen Mol Mutagen. 52(4):264–8.

Hackenberg, S., Scherzed, A., Kessler, M., Hummel, S., Technau, A., Froelich, K., Ginzkey, C., Koehler, C., Hagen, R., Kleinsasser, N. 2011a. Silver nanoparticles: evaluation of DNA damage, toxicity and functional impairment in human mesenchymal stem cells. Toxicol Lett. 201(1):27–33.

Hadrup, N., Loeschner, K., Bergström, A., Wilcks, A., Gao, X., Vogel, U., Frandsen, H.L., Larsen, E.H., Lam, H.R., Mortensen, A. 2012a. Subacute oral toxicity investigation of nanoparticulate and ionic silver in rats. Arch Toxicol. 86(4):543–51.

Hadrup, N., Loeschner, K., Mortensen, A., Sharma, A.K., Qvortrup, K., Larsen, E.H., Lam, H.R. 2012b. The similar neurotoxic effects of nanoparticulate and ionic silver in vivo and in vitro. Neurotoxicology. 33(3):416–23.

Hamilton, R.F., Wu, Z., Mitra, S., Shaw, P.K., Holian, A. 2013. Effect of MWCNT size, carboxylation, and purification on in vitro and in vivo toxicity, inflammation and lung pathology. Part Fibre toxicol. 10(1):57.

Hamzeh, M., Sunahara, G.I. 2013. In vitro cytotoxicity and genotoxicity studies of titanium dioxide (TiO 2) nanoparticles in Chinese hamster lung fibroblast cells. Toxicol In Vitro. 27(2):864–73.

Han, J.W., Jeong, J.K., Gurunathan, S., Choi, Y.J., Das, J., Kwon, D.N., Cho, S.G., Park, C., Seo, H.G., Park, J.K., Kim, J.H. 2016. Male-and female-derived somatic and germ cell-specific toxicity of silver nanoparticles in mouse. Nanotoxicology. 10(3):361–73.

Han, S.G., Andrews, R., Gairola, C.G. 2010. Acute pulmonary response of mice to multi-wall carbon nanotubes. Inhal Toxicol. 22(4):340–7.

Harper, S., Wohlleben, W., Doa, M., Nowack, B., Clancy, S., Canady, R., Maynard, A. 2015. Measuring nanomaterial release from carbon nanotube composites: review of the state of the science. Journal of Physics: Conference Series, IOP Publishing.

Hatipoglu, M.K., Keleştemur, S., Altunbek, M., Culha, M. 2015. Source of cytotoxicity in a colloidal silver nanoparticle suspension. Nanotechnology. 26(19):195103.

He, X., Young, S.H., Schwegler-Berry, D., Chisholm, W.P., Fernback, J.E., Ma, Q. 2011. Multiwalled carbon nanotubes induce a fibrogenic response by stimulating reactive oxygen species production, activating NF-κB signaling, and promoting fibroblast-to-myofibroblast transformation. Chem Res Toxicol. 24(12):2237–48.

Heinrich, U., Fuhst, R., Rittinghausen, S., Creutzenberg, O., Bellmann, B., Koch, W., Levsen, K. 1995. Chronic inhalation exposure of Wistar rats and two different strains of mice to diesel engine exhaust, carbon black, and titanium dioxide. Inhal Toxicol. 7(4):533–56.

Hendrickson, O.D., Klochkov, S.G., Novikova, O.V., Bravova, I.M., Shevtsova, E.F., Safenkova, I.V., Zherdev, A.V., Bachurin, S.O.., Dzantiev, B.B. 2016. Toxicity of nanosilver in intragastric studies: Biodistribution and metabolic effects. Toxicol Lett. 241:184–92.

Heshmati, M., ArbabiBidgoli, S., Khoei, S., Rezayat, S.M., Parivar, K. 2015. Mutagenic effects of nanosilver consumer products: a new approach to physicochemical properties. Iran J Pharm

Res. 14(4):1171–80.

Hext, P.M., Tomenson, J.A., Thompson, P. 2005. Titanium dioxide: inhalation toxicology and epidemiology. Ann Occup Hyg. 49(6):461–72.

Hirano, S., Fujitani, Y., Furuyama, A., Kanno, S. 2012. Macrophage receptor with collagenous structure (MARCO) is a dynamic adhesive molecule that enhances uptake of carbon nanotubes by CHO-K1 cells. Toxicol Appl Pharmacol. 259(1):96–103.

Hirano, S., Kanno, S., Furuyama, A. 2008. Multi-walled carbon nanotubes injure the plasma membrane of macrophages. Toxicol Appl Pharmacol. 232(2):244–51.

Hong, F., Si, W., Zhao, X., Wang, L., Zhou, Y., Chen, M., Ge, Y., Zhang, Q., Wang, Y., Zhang, J. 2015. TiO2 nanoparticle exposure decreases spermatogenesis via biochemical dysfunctions in the testis of male mice. J Agric Food Chem. 63(31):7084–92.

Hong, J.S., Kim, S., Lee, S.H., Jo, E., Lee, B., Yoon, J., Eom, I.C., Kim, H.M., Kim, P., Choi, K., Lee, M.Y. 2014. Combined repeated-dose toxicity study of silver nanoparticles with the reproduction/developmental toxicity screening test. Nanotoxicology. 8(4):349–62.

Hougaard, K.S., Campagnolo, L., Chavatte-Palmer, P., Tarrade, A., Rousseau-Ralliard, D., Valentino, S., Park, M.V., de Jong, W.H., Wolterink, G., Piersma, A.H., Ross, B.L. 2015. A perspective on the developmental toxicity of inhaled nanoparticles. Reprod Toxicol. 56:118–40.

Hougaard, K.S., Jackson, P., Jensen, K.A., Sloth, J.J., Löschner, K., Larsen, E.H., Birkedal, R.K., Vibenholt, A., Boisen, A.M., Wallin, H., Vogel, U. 2010. Effects of prenatal exposure to surface-coated nanosized titanium dioxide (UV-Titan). A study in mice. Part Fibre Toxicol. 7(1):16.

Hougaard, K.S., Jackson, P., Kyjovska, Z.O., Birkedal, RA., De Temmerman, P.J., Brunelli, A., Verleysen, E., Madsen, A.M., Saber, A.T., Pojana, G., Mast, J. 2013. Effects of lung exposure to carbon nanotubes on female fertility and pregnancy. A study in mice. Reprod Toxicol. 41:86–97.

HSDB (Hazardous Substances Data Bank). 2017a. Carbon Nanotubes. Available at: https://toxnet.nlm.nih.gov/cgi-bin/sis/search/a?dbs+hsdb:@term+@DOCNO+7673

HSDB (Hazardous Substances Data Bank). 2017b. Silver Nanoparticles. Available at: https://toxnet.nlm.nih.gov/cgi-bin/sis/search/a?dbs+hsdb:@term+@DOCNO+7715

HSDB (Hazardous Substances Data Bank). 2017c. Titanium Oxide Nanoparticles. Available at: https://toxnet.nlm.nih.gov/cgi-bin/sis/search/a?dbs+hsdb:@term+@DOCNO+7717

Hsieh, W.Y., Chou, C.C., Ho, C.C., Yu, S.L., Chen, H.Y., Chou, H.Y.E., Chen, J.J., Chen, H.W., Yang, P.C. 2012. Single-walled carbon nanotubes induce airway hyperreactivity and parenchymal injury in mice. Am J Respir Cell Mol Biol. 46(2):257–67.

Hsin, Y.H., Chen, C.F., Huang, S., Shih, T.S., Lai, P.S., Chueh, P.J. 2008. The apoptotic effect of nanosilver is mediated by a ROS-and JNK-dependent mechanism involving the mitochondrial pathway in NIH3T3 cells. Toxicol Lett. 179(3):130–9.

Hsu, L.Y., Chein, H.M. 2007. Evaluation of nanoparticle emission for TiO2 nanopowder coating materials. J Nanopart Res. 9(1):157–63.

Hu, R., Gong, X., Duan, Y., Li, N., Che, Y., Cui, Y., Zhou, M., Liu, C., Wang, H., Hong, F. 2010. Neurotoxicological effects and the impairment of spatial recognition memory in mice caused by exposure to TiO 2 nanoparticles. Biomaterials. 31(31):8043–50.

Hu, H., Guo, Q., Wang, C., Ma, X., He, H., Oh, Y., Feng, Y., Wu, Q., Gu, N. 2015. Titanium dioxide nanoparticles increase plasma glucose via reactive oxygen species-induced insulin resistance in mice. J Appl Toxicol. 35(10):1122–32.

Huang, X., Zhang, F., Sun, X., Choi, K.Y., Niu, G., Zhang, G., Guo, J., Lee, S., Chen, X. 2014. The genotype-dependent influence of functionalized multi-walled carbon nanotubes on fetal development. Biomaterials. 35:856–65.

Huizar, I., Malur, A., Patel, J., McPeek, M., Dobbs, L., Wingard, C., Barna, B.P., Thomassen, M. J. 2013. The role of PPARγ in carbon nanotube-elicited granulomatous lung inflammation. Respir Res. 14(1):7.

Huk, A., Izak-Nau, E., El Yamani, N., Uggerud, H., Vadset, M., Zasonska, B., Duschl, A., Dusinska, M. 2015. Impact of nanosilver on various DNA lesions and HPRT gene mutations–effects of charge and surface coating. Part Fibre Toxicol. 12(1):25.

Huo, L., Chen, R., Zhao, L., Shi, X., Bai, R., Long, D., Chen, F., Zhao, Y., Chang, Y.Z., Chen, C. 2015. Silver nanoparticles activate endoplasmic reticulum stress signaling pathway in cell and mouse models: The role in toxicity evaluation. Biomaterials. 61:307–15.

Hussain, S., Sangtian, S., Anderson, S.M., Snyder, R.J., Marshburn, J.D., Rice, A.B., Bonner, J.C., Garantziotis, S. 2014. Inflammasome activation in airway epithelial cells after multi-walled carbon nanotube exposure mediates a profibrotic response in lung fibroblasts. Part Fibre Toxicol. 11(1):28.

Hussain, S., Smulders, S., De Vooght, V., Ectors, B., Boland, S., Marano, F., Van Landuyt, K.L., Nemery, B., Hoet, P.H., Vanoirbeek, J.A. 2012b. Nano-titanium dioxide modulates the dermal sensitization potency of DNCB. Part Fibre Toxicol. 9(1):15.

Hussain, S., Thomassen, L.C., Ferecatu, I., Borot, M.C., Andreau, K., Martens, J.A., Fleury, J., Baeza-Squiban, A., Marano, F., Boland, S. 2010. Carbon black and titanium dioxide nanoparticles elicit distinct apoptotic pathways in bronchial epithelial cells. Part Fibre Toxicol. 7(1):10.

Hussain, S., Vanoirbeek, J.A., Hoet, P.H. 2012a. Interactions of nanomaterials with the immune system. Wiley Interdiscip Rev Nanomed Nanobiotechnol. 4(2):169–83.

Hussain, S., Vanoirbeek, J.A., Luyts, K., De Vooght, V., Verbeken, E., Thomassen, L.C., Martens, J.A., Dinsdale, D., Boland, S., Marano, F., Nemery, B. 2011. Lung exposure to nanoparticles modulates an asthmatic response in a mouse model. Eur Respir J. 37(2):299–309.

Hussain, S.M., Hess, K.L., Gearhart, J.M., Geiss, K.T., Schlager, J.J. 2005. In vitro toxicity of nanoparticles in BRL 3A rat liver cells. Toxicology In Vitro, 19(7):975–83.

Hussain, S.M., Javorina, A.K., Schrand, A.M., Duhart, H.M., Ali, S.F., Schlager, J.J. 2006. The interaction of manganese nanoparticles with PC-12 cells induces dopamine depletion. Toxicol Sci. 92(2):456–63.

Hwang, E.T., Lee, J.H., Chae, Y.J., Kim, Y.S., Kim, B.C., Sang, B.I., Gu, M.B. 2008. Analysis of the Toxic Mode of Action of Silver Nanoparticles Using Stress-Specific Bioluminescent Bacteria. Small. 4(6):746–50.

Hyun, J.S., Lee, B.S., Ryu, H.Y., Sung, J.H., Chung, K.H., Yu, I.J. 2008. Effects of repeated silver nanoparticles exposure on the histological structure and mucins of nasal respiratory mucosa in rats. Toxicol Lett. 182(1):24–8.

IARC (International Agency for Research on Cancer). 2010. Carbon Black, Titanium Dioxide, and Talc. IARC Monogr Eval Carcinog Risks Hum. 93: 193–276.

ICRP (International Commission on Radiological Protection) 1994. Human Respiratory Tract Model for Radiological Protection. Technical Report ICRP Publication 66, Oxford, UK.

Inoue, K.I., Takano, H., Koike, E., Yanagisawa, R., Sakurai, M., Tasaka, S., Ishizaka, A., Shimada, A. 2008. Effects of pulmonary exposure to carbon nanotubes on lung and systemic inflammation with coagulatory disturbance induced by lipopolysaccharide in mice. Exp Biol Med. 233(12):1583–90.

ISO (International Organization for Standardization). 2012. Nanotechnologies – Guidance on Physico-chemical Characterization of Engineered Nanoscale Materials for Toxicologic Assessment. ISO/TR 13014. Available at: https://webstore.ansi.org/RecordDetail.aspx?sku=ISO%2fTR+13014%3a2012

Ivani, S., Karimi, I., Tabatabaei, S.R.F. 2012. Biosafety of multiwalled carbon nanotube in mice: a behavioral toxicological approach. J Toxicol Sci. 37:1191–205.

Ivask, A., Voelcker, N.H., Seabrook, S.A., Hor, M., Kirby, J.K., Fenech, M., Davis, T.P., Ke, P.C. 2015. DNA melting and genotoxicity induced by silver nanoparticles and graphene. Chem Res Toxicol. 28(5):1023–35.

Jackson, P., Kling, K., Jensen, K.A., Clausen, P.A., Madsen, A.M., Wallin, H., Vogel, U. 2015. Characterization of genotoxic response to 15 multiwalled carbon nanotubes with variable physicochemical properties including surface functionalizations in the FE1-Muta (TM) mouse lung epithelial cell line. Environ Mol Mutagen. 56(2):183–203.

Jacobsen, N.R., Møller, P., Jensen, K.A., Vogel, U., Ladefoged, O., Loft, S., Wallin, H. 2009. Lung inflammation and genotoxicity following pulmonary exposure to nanoparticles in ApoE-/- mice. Part Fibre Toxicol. 6(1):2.

Jacobsen, N.R., Pojana, G., White, P., MÖller, P., Cohn, C.A., Smith Korsholm, K., Vogel, U., Marcomini, A., Loft, S., Wallin, H. 2008. Genotoxicity, cytotoxicity, and reactive oxygen species induced by single-walled carbon nanotubes and C60 fullerenes in the FE1-Muta™ Mouse lung epithelial cells. Envion Mol Mutagen. 49(6):476–87.

Janssen, Y.M., Marsh, J.P., Driscoll, K.E., Borm, P.J., Oberdörster, G., Mossman, B.T. 1994. Increased expression of manganese-containing superoxide dismutase in rat lungs after inhalation of inflammatory and fibrogenic minerals. Free Radic Biol Med. 16(3):315–22.

Jensen, K.A., Kembouche, Y., Christiansen, E., Jacobsen, N.R., Wallin, H. 2011. Final protocol for producing suitable manufactures nanomaterial exposure media. The generic NANOGENOTOX dispersion protocol, Standard Operation Procedure (SOP).

Jeong, G.N., Jo, U.B., Ryu, H.Y., Kim, Y.S., Song, K.S., Yu, I.J. 2010. Histochemical study of intestinal mucins after administration of silver nanoparticles in Sprague–Dawley rats. Arch Toxicol. 84(1):63–9.

Ji, J.H., Jung, J.H., Kim, S.S., Yoon, J.U., Park, J.D., Choi, B.S., Chung, Y.H., Kwon, I.H., Jeong, J., Han, B.S., Shin, J.H. 2007a. Twenty-eight-day inhalation toxicity study of silver nanoparticles in Sprague-Dawley rats. Inhal Toxicol. 19(10):857–71.

Ji, J.H., Jung, J.H., Yu, I.J., Kim, S.S. 2007b. Long-term stability characteristics of metal nanoparticle generator using small ceramic heater for inhalation toxicity studies. Inhal Toxicol. 19(9):745–51.

Jiang, J., Oberdörster, G., Elder, A., Gelein, R., Mercer, P., Biswas, P. 2008. Does nanoparticle activity depend upon size and crystal phase? Nanotoxicology. 2(1):33–42.

Jiang, L., Kondo, A., Shigeta, M., Endoh, S., Uejima, M., Ogura, I., Naito, M. 2014. Evaluation of particles released from single-wall carbon nanotube/polymer composites with or without thermal aging by an accelerated abrasion test. J Occup Environ Hyg. 11(10):658–64.

Jiang, W., Wang, Q., Qu, X., Wang, L., Wei, X., Zhu, D., Yang, K. 2017. Effects of charge and surface defects of multi-walled carbon nanotubes on the disruption of model cell membranes. Sci Total Environ. 574:771–80.

Jiang, X., Foldbjerg, R., Miclaus, T., Wang, L., Singh, R., Hayashi, Y., Sutherland, D., Chen, C., Autrup, H., Beer, C. 2013. Multi-platform genotoxicity analysis of silver nanoparticles in the model cell line CHO-K1. Toxicol Lett. 222(1):55–63.

Jiménez-Lamana, J., Laborda, F., Bolea, E., Abad-Álvaro, I., Castillo, J.R., Bianga, J., He, M., Bierla, K., Mounicou, S., Ouerdane, L., Gaillet, S. 2014. An insight into silver nanoparticles bioavailability in rats. Metallomics. 6(12):2242–9.

Jiravova, J., Tomankova, K.B., Harvanova, M., Malina, L., Malohlava, J., Luhova, L., Panacek, A., Manisova, B., Kolarova, H. 2016. The effect of silver nanoparticles and silver ions on mammalian and plant cells in vitro. Food Chem Toxicol. 96:50–61.

Johnston, H.J., Hutchison, G., Christensen, F.M., Peters, S., Hankin, S., Stone, V. 2010. A review of the in vivo and in vitro toxicity of silver and gold particulates: particle attributes and biological mechanisms responsible for the observed toxicity. Crit Rev Toxicol. 40(4):328–46.

Jomini, S., Labille, J., Bauda, P., Pagnout, C. 2012. Modifications of the bacterial reverse mutation test reveals mutagenicity of TiO 2 nanoparticles and byproducts from a sunscreen TiO 2-based nanocomposite. Toxicol Lett. 215(1):5 –61.

Jonaitis, T.S., Card, J.W., Magnuson, B. 2010. Concerns regarding nano-sized titanium dioxide dermal penetration and toxicity study. Toxicol Lett. 192(2):268–9.

Jones, K., Morton, J., Smith, I., Jurkschat, K., Harding, A.H., Evans, G. 2015. Human in vivo and in vitro studies on gastrointestinal absorption of titanium dioxide nanoparticles. Toxicol Lett. 233(2):95–101.

Juarez-Moreno, K., Gonzalez, E.B., Girón-Vazquez, N., Chávez-Santoscoy, R.A., Mota-Morales, J.D., Perez-Mozqueda, L.L., Garcia-Garcia, M.R., Pestryakov, A., Bogdanchikova, N. 2016. Comparison of cytotoxicity and genotoxicity effects of silver nanoparticles on human cervix and breast cancer cell lines. Hum Exp Toxicol. 36(9):931–48.

Jugan, M.L., Barillet, S., Simon-Deckers, A., Herlin-Boime, N., Sauvaigo, S., Douki, T., Carriere, M. 2012. Titanium dioxide nanoparticles exhibit genotoxicity and impair DNA repair activity in A549 cells. Nanotoxicology. 6(5):501–13.

Jung, J.H., Oh, H.C., Noh, H.S., Ji, J.H., Kim, S.S. 2006. Metal nanoparticle generation using a small ceramic heater with a local heating area. J Aerosol Sci. 37(12):1662–70.

Jung, W.K., Koo, H.C., Kim, K.W., Shin, S., Kim, S.H., Park, Y.H. 2008. Antibacterial activity and mechanism of action of the silver ion in Staphylococcus aureus and Escherichia coli. Appl Environ Micobiol. 74(7):2171–8.

Kaegi, R., Ulrich, A., Sinnet, B., Vonbank, R., Wichser, A., Zuleeg, S., Simmler, H., Brunner,

S., Vonmont, H., Burkhardt, M., Boller, M. 2008. Synthetic TiO 2 nanoparticle emission from exterior facades into the aquatic environment. Environ Pollut. 156(2):233–9.

Kaegi, R., Voegelin, A., Sinnet, B., Zuleeg, S., Hagendorfer, H., Burkhardt, M., Siegrist, H. 2011. Behavior of metallic silver nanoparticles in a pilot wastewater treatment plant. Environ Sci Technol. 45(9):3902–8.

Kagan, V.E., Konduru, N.V., Feng, W., Allen, B.L., Conroy, J., Volkov, Y., Vlasova, I.I., Belikova, N.A., Yanamala, N., Kapralov, A., Tyurina, Y.Y. 2010. Carbon nanotubes degraded by neutrophil myeloperoxidase induce less pulmonary inflammation. Nat Nanotechnol. 5(5):354–9.

Kasai, T., Umeda, Y., Ohnishi, M., Kondo, H., Takeuchi, T., Aiso, S., Nishizawa, T., Matsumoto, M., Fukushima, S. 2015. Thirteen-week study of toxicity of fiber-like multi-walled carbon nanotubes with whole-body inhalation exposure in rats. Nanotoxicology. 9(4):413–22.

Kasai, T., Umeda, Y., Ohnishi, M., Mine, T., Kondo, H., Takeuchi, T., Matsumoto, M., Fukushima, S. 2016. Lung carcinogenicity of inhaled multi-walled carbon nanotube in rats. Part Fibre Toxicol. 13(1):53.

Kato, T., Totsuka, Y., Ishino, K., Matsumoto, Y., Tada, Y., Nakae, D., Goto, S., Masuda, S., Ogo, S., Kawanishi, M., Yagi, T. 2013. Genotoxicity of multi-walled carbon nanotubes in both in vitro and in vivo assay systems. Nanotoxicology. 7(4):452–61.

Katwa, P., Wang, X., Urankar, R.N., Podila, R., Hilderbrand, S.C., Fick, R.B., Rao, A.M., Ke, P.C., Wingard, C.J., Brown, J.M. 2012. A Carbon Nanotube Toxicity Paradigm Driven by Mast Cells and the IL-33/ST2 Axis. Small, 8(18):2904–12.

Kawata, K., Osawa, M., Okabe, S. 2009. In vitro toxicity of silver nanoparticles at noncytotoxic doses to HepG2 human hepatoma cells. Environ Sci Technol. 43(15):6046–51.

Keka, I.S., Evans, T.J., Hirota, K., Shimizu, H., Kono, K., Takeda, S., Hirano, S. 2014. A novel genotoxicity assay of carbon nanotubes using functional macrophage receptor with collagenous structure (MARCO)-expressing chicken B lymphocytes. Arch Toxicol. 88(1):145–60.

Kermanizadeh, A., Gaiser, B.K., Hutchison, G.R., Stone, V. 2012. An in vitro liver model-assessing oxidative stress and genotoxicity following exposure of hepatocytes to a panel of engineered nanomaterials. Part Fibre Toxicol. 9(1):28.

Khaliullin, T.O., Shvedova, A.A., Kisin, E.R., Zalyalov, R.R., Fatkhutdinova, L.M. 2015. Evaluation of fibrogenic potential of industrial multi-walled carbon nanotubes in acute aspiration experiment. Bull Exp Biol Med. 158(5):684–7.

Khodashenas, B., Ghorbani, H.R. 2015. Synthesis of silver nanoparticles with different shapes. Arab J Chem.

Kim, H.R., Kim, M.J., Lee, S.Y., Oh, S.M., Chung, K.H. 2011b. Genotoxic effects of silver nanoparticles stimulated by oxidative stress in human normal bronchial epithelial (BEAS-2B) cells. Mutat Res Genet Toxicol Environ Mutagen. 726(2):129–35.

Kim, H.R., Park, Y.J., Da Young Shin, S.M.O., Chung, K.H. 2013b. Appropriate in vitro methods for genotoxicity testing of silver nanoparticles. Environ Health Toxicol. 28.

Kim, J.S., Lee, K., Lee, Y.H., Cho, H.S., Kim, K.H., Choi, K.H., Lee, S.H., Song, K.S., Kang, C.S., Yu, I.J. 2011a. Aspect ratio has no effect on genotoxicity of multi-wall carbon nanotubes. Archi Toxicol. 85(7):775–86.

Kim, J.S., Song, K.S., Sung, J.H., Ryu, H.R., Choi, B.G., Cho, H.S., Lee, J.K., Yu, I.J. 2013a. Genotoxicity, acute oral and dermal toxicity, eye and dermal irritation and corrosion and skin sensitisation evaluation of silver nanoparticles. Nanotoxicology. 7(5):953–60.

Kim, J.S., Song, K.S., Yu, I.J. 2015. Evaluation of in vitro and in vivo genotoxicity of single-walled carbon nanotubes. Toxicol Ind Health. 31(8):747–757.

Kim, J.S., Sung, J.H., Choi, B.G., Ryu, H.Y., Song, K.S., Shin, J.H., Lee, J.S., Hwang, J.H., Lee, J.H., Lee, G.H., Jeon, K. 2014. In vivo genotoxicity evaluation of lung cells from Fischer 344 rats following 28 days of inhalation exposure to MWCNTs, plus 28 days and 90 days post-exposure. Inhal Toxicol. 26(4):222–34.

Kim, J.S., Sung, J.H., Song, K.S., Lee, J.H., Kim, S.M., Lee, G.H., Ahn, K.H., Lee, J.S., Shin, J.H., Park, J.D., Yu, I.J. 2012a. Persistent DNA damage measured by comet assay of Sprague Dawley rat lung cells after five days of inhalation exposure and 1 month post-exposure to dispersed multi-wall carbon nanotubes (MWCNTs) generated by new MWCNT aerosol generation system. Toxicol Sci. 128(2):439–48.

Kim, S., Choi, J.E., Choi, J., Chung, K.H., Park, K., Yi, J., Ryu, D.Y. 2009. Oxidative stress-dependent toxicity of silver nanoparticles in human hepatoma cells. Toxicol In Vitro. 23(6):1076–84.

Kim, S., Ryu, D.Y. 2013. Silver nanoparticle-induced oxidative stress, genotoxicity and apoptosis in cultured cells and animal tissues. J Appl Toxicol. 33(2):78–89.

Kim, T.H., Kim, M., Park, H.S., Shin, U.S., Gong, M.S., Kim, H.W. 2012b. Size-dependent cellular toxicity of silver nanoparticles. J Biomed Mater Res A. 100(4):1033–43.

Kim, Y.J., Yang, S.I., Ryu, J.C. 2010b. Cytotoxicity and genotoxicity of nano-silver in mammalian cell lines. Mol Cell Toxicol. 6(2):119–25.

Kim, Y.S., Davis, R., Uddin, N., Nyden, M., Rabb, S.A. 2016. Quantification of nanoparticle release from polymer nanocomposite coatings due to environmental stressing. J Occup Environ

Hyg. 13(4):303–13.

Kim, Y.S., Kim, J.S., Cho, H.S., Rha, D.S., Kim, J.M., Park, J.D., Choi, B.S., Lim, R., Chang, H.K., Chung, Y.H., Kwon, I.H. 2008. Twenty-eight-day oral toxicity, genotoxicity, and gender-related tissue distribution of silver nanoparticles in Sprague-Dawley rats. Inhal Toxicol. 20(6):575–83.

Kim, Y.S., Song, M.Y., Park, J.D., Song, K.S., Ryu, H.R., Chung, Y.H., Chang, H.K., Lee, J.H., Oh, K.H., Kelman, B.J., Hwang, I.K. 2010a. Subchronic oral toxicity of silver nanoparticles. Part Fibre Toxicol. 7(1):20.

Kingston, C., Zepp, R., Andrady, A., Boverhof, D., Fehir, R., Hawkins, D., Roberts, J., Sayre, P., Shelton, B., Sultan, Y., Vejins, V. 2014. Release characteristics of selected carbon nanotube polymer composites. Carbon. 68:33–57.

Kisin, E.R., Murray, A.R., Keane, M.J., Shi, X.C., Schwegler-Berry, D., Gorelik, O., Arepalli, S., Castranova, V., Wallace, W.E., Kagan, V.E., Shvedova, A.A. 2007. Single-walled carbon nanotubes: geno-and cytotoxic effects in lung fibroblast V79 cells. J Toxicol Environ Health A. 70(24):2071–9.

Kisin, E.R., Murray, A.R., Sargent, L., Lowry, D., Chirila, M., Siegrist, K.J., Schwegler-Berry, D., Leonard, S., Castranova, V., Fadeel, B., Kagan, V.E. 2011. Genotoxicity of carbon nanofibers: are they potentially more or less dangerous than carbon nanotubes or asbestos? Toxicol Appl Pharmacol: 252(1):1–10.

Kiss, B., Bíró, T., Czifra, G., Tóth, B.I., Kertész, Z., Szikszai, Z., Kiss, Á.Z., Juhász, I., Zouboulis, C.C., Hunyadi, J. 2008. Investigation of micronized titanium dioxide penetration in human skin xenografts and its effect on cellular functions of human skin-derived cells. Exp Dermatol. 17(8):659–67.

Klein, C. L., Wiench, K., Wiemann, M., Ma-Hock, L., van Ravenzwaay, B., Landsiedel, R. 2012. Hazard identification of inhaled nanomaterials: making use of short-term inhalation studies. Arch Toxicol. 86(7):1137–51.

Klimisch, H.J., Andreae, M., Tillmann, U. 1997. A systematic approach for evaluating the quality of experimental toxicological and ecotoxicological data. Regul Toxicol Pharmacol. 25(1):1–5

Kobayashi, N., Naya, M., Ema, M., Endoh, S., Maru, J., Mizuno, K., Nakanishi, J. 2010. Biological response and morphological assessment of individually dispersed multi-wall carbon nanotubes in the lung after intratracheal instillation in rats. Toxicology. 276(3):143–53.

Kobayashi, N., Naya, M., Mizuno, K., Yamamoto, K., Ema, M., Nakanishi, J. 2011. Pulmonary and systemic responses of highly pure and well-dispersed single-wall carbon nanotubes after intratracheal instillation in rats. Inhal Toxicol. 23(13):814–28.

Korani, M., Rezayat, S.M., Bidgoli, S.A. 2013. Sub-chronic dermal toxicity of silver nanoparticles in guinea pig: special emphasis to heart, bone and kidney toxicities. Iran J Pharm Res. 12(3):511–9.

Korani, M., Rezayat, S.M., Gilani, K., Bidgoli, S.A., Adeli, S. 2011. Acute and subchronic dermal toxicity of nanosilver in guinea pig. Int J Nanomed. 6:855–62.

Kovvuru, P., Mancilla, P.E., Shirode, A.B., Murray, T.M., Begley, T.J., Reliene, R. 2015. Oral ingestion of silver nanoparticles induces genomic instability and DNA damage in multiple tissues. Nanotoxicology. 9(2):162–71.

Kreyling, W.G., Semmler, M., Erbe, F., Mayer, P., Takenaka, S., Schulz, H., Oberdörster, G., Ziesenis, A. 2002. Translocation of ultrafine insoluble iridium particles from lung epithelium to extrapulmonary organs is size dependent but very low. J Toxicol Environ Health Part A. 65(20):1513–30.

Kulthong, K., Maniratanachote, R., Kobayashi, Y., Fukami, T., Yokoi, T. 2012. Effects of silver nanoparticles on rat hepatic cytochrome P450 enzyme activity. Xenobiotica. 42(9):854–62.

Kumar, G., Degheidy, H., Casey, B.J., Goering, P.L. 2015. Flow cytometry evaluation of in vitro cellular necrosis and apoptosis induced by silver nanoparticles. Food Chem Toxicol. 85:45–51.

Kvitek, L., Panáček, A., Soukupova, J., Kolář, M., Večeřová, R., Prucek, R., Holecova, M., Zbořil, R. 2008. Effect of surfactants and polymers on stability and antibacterial activity of silver nanoparticles (NPs). J Phys Chem. 112(15):5825–5834.

Kwon, J.T., Minai-Tehrani, A., Hwang, S.K., Kim, J.E., Shin, J.Y., Yu, K.N., Chang, S.H., Kim, D.S., Kwon, Y.T., Choi, I.J., Cheong, Y.H. 2012. Acute pulmonary toxicity and body distribution of inhaled metallic silver nanoparticles. Toxicol Res. 28(1):25–31.

Lafuente, D., Garcia, T., Blanco, J., Sánchez, D.J., Sirvent, J.J., Domingo, J.L., Gómez, M. 2016. Effects of oral exposure to silver nanoparticles on the sperm of rats. Reprod Toxicol. 60:133–9.

Lam, C.W., James, J.T., McCluskey, R., Hunter, R.L. 2004. Pulmonary toxicity of single-wall carbon nanotubes in mice 7 and 90 days after intratracheal instillation. Toxicol Sci. 77(1):126–34.

Landsiedel, R., Ma-Hock, L., Van Ravenzwaay, B., Schulz, M., Wiench, K., Champ, S., Schulte, S., Wohlleben, W., Oesch, F. 2010. Gene toxicity studies on titanium dioxide and zinc oxide nanomaterials used for UV-protection in cosmetic formulations. Nanotoxicology. 4(4):364–81.

Lankveld, D.P.K., Oomen, A.G., Krystek, P., Neigh, A., Troost–de Jong, A., Noorlander, C.W., Van Eijkeren, J.C, Geertsma, R.E., De Jong, W.H. 2010. The kinetics of the tissue distribution of silver nanoparticles of different sizes. Biomaterials. 31(32):8350–61.

Larsen, S.T., Jackson, P., Poulsen, S.S., Levin, M., Jensen, K.A., Wallin, H., Nielsen, G.D., Koponen, I.K. 2016. Airway irritation, inflammation, and toxicity in mice following inhalation of metal oxide nanoparticles. Nanotoxicology. 10(9): 1254–62.

Lee, B.W., Kadoya, C., Horie, M., Mizuguchi, Y., Hashiba, M., Kambara, T., Okada, T., Myojo, T., Oyabu, T., Ogami, A., Morimoto, Y. 2013. Analysis of pulmonary surfactant in rat lungs after intratracheal instillation of short and long multi-walled carbon nanotubes. Inhal Toxcol. 25(11):609–20.

Lee, S., Khang, D., Kim, S.H. 2015. High dispersity of carbon nanotubes diminishes immunotoxicity in spleen. Int J Nanomed. 10:2697–710.

Lee, Y., Choi, J., Kim, P., Choi, K., Kim, S., Shon, W., Park, K. 2012a. A transfer of silver nanoparticles from pregnant rat to offspring. Toxicol Res. 28(3):139–41.

Lee, Y.J., Kim, J., Oh, J., Bae, S., Lee, S., Hong, I.S., Kim, S.H. 2012b. Ion-release kinetics and ecotoxicity effects of silver nanoparticles. Environ Toxicol Chem. 31(1):155–9.

Leppänen, M., Korpi, A., Miettinen, M., Leskinen, J., Torvela, T., Rossi, E.M., Vanhala, E., Wolff, H., Alenius, H., Kosma, V.M., Joutsensaari, J. 2011. Nanosized TiO2 caused minor airflow limitation in the murine airways. Arch Toxicol. 85(7):827–39.

Leppänen, M., Korpi, A., Mikkonen, S., Yli-Pirilä, P., Lehto, M., Pylkkänen, L., Wolff, H., Kosma, V.M., Alenius, H., Joutsensaari, J., Pasanen, P. 2015a. Inhaled silica-coated TiO2 nanoparticles induced airway irritation, airflow limitation and inflammation in mice. Nanotoxicology. 9(2):210–8.

Leppänen, M., Korpi, A., Yli-Pirilä, P., Lehto, M., Wolff, H., Kosma, V. M., Alenius, H., Pasanen, P. 2015b. Negligible respiratory irritation and inflammation potency of pigmentary TiO2 in mice. Inhal Toxicol. 27(8):378–86.

Li, J.G., Li, Q.N., Xu, J.Y., Cai, X.Q., Liu, R.L., Li, Y.J., Ma, J.F., Li, W.X. 2009. The pulmonary toxicity of multi-wall carbon nanotubes in mice 30 and 60 days after inhalation exposure. J Nanosci Nanotechnol. 9(2):1384–7.

Li, J.G., Li, W.X., Xu, J.Y., Cai, X.Q., Liu, R.L., Li, Y.J., Zhao, Q.F., Li, Q.N. 2007. Comparative study of pathological lesions induced by multiwalled carbon nanotubes in lungs of mice by intratracheal instillation and inhalation. Environ Toxicol. 22(4):415–21.

Li, N., Ma, L., Wang, J., Zheng, L., Liu, J., Duan, Y., Liu, H., Zhao, X., Wang, S., Wang, H., Hong, F. 2010. Interaction between nano-anatase TiO2 and liver DNA from mice in vivo. Nanoscale Res Lett. 5(1):108.

Li, N., Sioutas, C., Cho, A., Schmitz, D., Misra, C., Sempf, J., Wang, M., Oberley, T., Froines,

Nel, A. 2003. Ultrafine particulate pollutants induce oxidative stress and mitochondrial damage. Environ Health Perspect. 111(4):455–60.

Li, R., Wang, X., Ji, Z., Sun, B., Zhang, H., Chang, C.H., Lin, S., Meng, H., Liao, Y.P., Wang, M., Li, Z. 2013. Surface charge and cellular processing of covalently functionalized multiwall carbon nanotubes determine pulmonary toxicity. ACS Nano. 7(3):2352–68.

Li, Y., Bhalli, J.A., Ding, W., Yan, J., Pearce, M.G., Sadiq, R., Cunningham, C.K., Jones, M.Y., Monroe, W.A., Howard, P.C., Zhou, T. 2014. Cytotoxicity and genotoxicity assessment of silver nanoparticles in mouse. Nanotoxicology. 8(Supp1):36–45.

Li, Y., Chen, D.H., Yan, J., Chen, Y., Mittelstaedt, R.A., Zhang, Y., Biris, A.S., Heflich, R.H., Chen, T. 2012. Genotoxicity of silver nanoparticles evaluated using the Ames test and in vitro micronucleus assay. Mutat Res Genet Toxicol Environ Mutagen. 745(1):4–10.

Li, Y., Qin, T., Ingle, T., Yan, J., He, W., Yin, J.J., Chen, T. 2017. Differential genotoxicity mechanisms of silver nanoparticles and silver ions. Arch Toxicol. 91(1):509–19.

Lidén, G. 2011. The European commission tries to define nanomaterials. Ann Occup Hyg. 55(1):1–5.

Lim, D.H., Jang, J., Kim, S., Kang, T., Lee, K., Choi, I.H. 2012b. The effects of sub-lethal concentrations of silver nanoparticles on inflammatory and stress genes in human macrophages using cDNA microarray analysis. Biomaterials. 33(18):4690–9.

Lim, H.K., Asharani, P.V., Hande, M.P. 2012a. Enhanced genotoxicity of silver nanoparticles in DNA repair deficient mammalian cells. Front Genet 3.

Lim, J.H., Kim, S.H., Lee, I.C., Moon, C., Kim, S.H., Shin, D.H., Kim, H.C., Kim, J.C. 2011. Evaluation of maternal toxicity in rats exposed to multi-wall carbon nanotubes during pregnancy. Environ Health Toxicol. 26.

Lin, Z., Liu, L., Xi, Z., Huang, J., Lin, B. 2012. Single-walled carbon nanotubes promote rat vascular adventitial fibroblasts to transform into myofibroblasts by SM22-α expression. Int J Nanomed. 7:4199–206.

Linak, E., Schlag, S., Kishi, A. 2002. Chemical Economics Handbook: Titanium Dioxide. Menlo Park, CA. SRI Consulting.

Lindberg, H.K., Falck, G.C., Catalán, J., Koivisto, A.J., Suhonen, S., Järventaus, H., Rossi, E.M., Nykäsenoja, H, Peltonen, Y., Moreno, C., Alenius, H. 2012. Genotoxicity of inhaled nanosized TiO 2 in mice. Mutat Res Genet Toxicol Environ Mutagen. 745(1):58–64.

Lindberg, H. K., Falck, G. C. M., Singh, R., Suhonen, S., Järventaus, H., Vanhala, E., Catalán, J., Farmer, P.B., Savolainen, K.M., Norppa, H. 2013. Genotoxicity of short single-wall and multi-

wall carbon nanotubes in human bronchial epithelial and mesothelial cells in vitro. Toxicology. 313(1):24–37.

Lindberg, H.K., Falck, G.C.M., Suhonen, S., Vippola, M., Vanhala, E., Catalán, J., Savolainen, K., Norppa, H. 2009. Genotoxicity of nanomaterials: DNA damage and micronuclei induced by carbon nanotubes and graphite nanofibres in human bronchial epithelial cells in vitro. Toxicol Lett. 186(3):166–73.

Lippmann, M. 1990. Effects of fiber characteristics on lung deposition, retention, and disease. Environ Health Perspect. 88:311–7.

Liu, W., Wu, Y., Wang, C., Li, H.C., Wang, T., Liao, C.Y., Cui, L., Zhou, Q.F., Yan, B., Jiang, G.B. 2010. Impact of silver nanoparticles on human cells: effect of particle size. Nanotoxicology. 4(3):319–30.

Liu, Y., Zhao, Y., Sun, B., Chen, C. 2013. Understanding the toxicity of carbon nanotubes. Acc Chem Res. 46(3):702–13.

Liu, Z., Liu, Y., Peng, D. 2014. Hydroxylation of multi-walled carbon nanotubes reduces their cytotoxicity by limiting the activation of mitochondrial mediated apoptotic pathway. J Mater Sci Mater Med. 25(4):1033–44.

Loeschner, K., Hadrup, N., Qvortrup, K., Larsen, A., Gao, X., Vogel, U., Mortensen, A., Lam, H.R., Larsen, E.H. 2011. Distribution of silver in rats following 28 days of repeated oral exposure to silver nanoparticles or silver acetate. Part Fibre Toxicol. 8(1):18.

Louro, H., Tavares, A., Vital, N., Costa, P.M., Alverca, E., Zwart, E., Jong, W.H., Fessard, V., Lavinha, J., Silva, M.J. 2014. Integrated approach to the in vivo genotoxic effects of a titanium dioxide nanomaterial using LacZ plasmid-based transgenic mice. Environ Mol Mutagen. 55(6):500–9.

Lynch, I., Dawson, K.A. 2008. Protein-nanoparticle interactions. Nano Today. 3(1):40–7.

Ma, L., Liu, J., Li, N., Wang, J., Duan, Y., Yan, J., Liu, H., Wang, H., Hong, F. 2010. Oxidative stress in the brain of mice caused by translocated nanoparticulate TiO 2 delivered to the abdominal cavity. Biomaterials. 31(1):99–105.

Ma-Hock, L., Burkhardt, S., Strauss, V., Gamer, A.O., Wiench, K., van Ravenzwaay, B., Landsiedel, R. 2009b. Development of a short-term inhalation test in the rat using nano-titanium dioxide as a model substance. Inhal Toxicol. 21(2):102–18.

Ma-Hock, L., Strauss, V., Treumann, S., Küttler, K., Wohlleben, W., Hofmann, T., Gröters, S., Wiench, K., van Ravenzwaay, B., Landsiedel, R. 2013. Comparative inhalation toxicity of multi-wall carbon nanotubes, graphene, graphite nanoplatelets and low surface carbon black. Part Fibre Toxicol. 10(1):23.

Ma-Hock, L., Treumann, S., Strauss, V., Brill, S., Luizi, F., Mertler, M., Wiench, K., Gamer, A.O., Van Ravenzwaay, B., Landsiedel, R. 2009a. Inhalation toxicity of multiwall carbon nanotubes in rats exposed for 3 months. Toxicol Sci. 112(2):468–81.

Machado, N.M., Lopes, J.C., Saturnino, R.S., Fagan, E.B., Nepomuceno, J.C. 2013. Lack of mutagenic effect by multi-walled functionalized carbon nanotubes in the somatic cells of Drosophila melanogaster. Food Chem Toxicol. 62:355–60.

Mackevica, A., Foss Hansen, S. 2016. Release of nanomaterials from solid nanocomposites and consumer exposure assessment–a forward-looking review. Nanotoxicology. 10(6):641–53.

Mahabady, M.K. 2012. The evaluation of teratogenicity of nanosilver on skeletal system and placenta of rat fetuses in prenatal period. Afr J Pharm Pharmacol. 6(6):419–24.

Maneewattanapinyo, P., Banlunara, W., Thammacharoen, C., Ekgasit, S., Kaewamatawong, T. 2011. An evaluation of acute toxicity of colloidal silver nanoparticles. J Vet Med Sci. 73(11):1417–23.

Mangum, J.B., Turpin, E.A., Antao-Menezes, A., Cesta, M.F., Bermudez, E., Bonner, J.C. 2006. Single-walled carbon nanotube (SWCNT)-induced interstitial fibrosis in the lungs of rats is associated with increased levels of PDGF mRNA and the formation of unique intercellular carbon structures that bridge alveolar macrophages in situ. Part Fibre toxicol. 3(1):15.

Manke, A., Luanpitpong, S., Dong, C., Wang, L., He, X., Battelli, L., Derk, R., Stueckle, T.A., Porter, D.W., Sager, T., Gou, H. 2014. Effect of fiber length on carbon nanotube-induced fibrogenesis. Int J Mol Sci. 15(5):7444–61.

Manshian, B.B., Jenkins, G.J., Williams, P.M., Wright, C., Barron, A.R., Brown, A.P., Hondow, N., Dunstan, P.R., Rickman, R., Brady, K., Doak, S.H. 2013. Single-walled carbon nanotubes: differential genotoxic potential associated with physico-chemical properties. Nanotoxicology. 7(2):144-56.

Mantovani, A., Allavena, P., Sica, A., Balkwill, F. 2008. Cancer-related inflammation. Nature. 54(7203):436–44.

Martinon, F. 2010. Signaling by ROS drives inflammasome activation. Eur J Immunol. 40(3):616–9.

Mathias, F.T., Romano, R.M., Kizys, M.M., Kasamatsu, T., Giannocco, G., Chiamolera, M.I., Dias-da-Silva, M.R., Romano, M.A. 2015. Daily exposure to silver nanoparticles during prepubertal development decreases adult sperm and reproductive parameters. Nanotoxicology. 9(1):64–70.

Matsumoto, M., Serizawa, H., Sunaga, M., Kato, H., Takahashi, M., Hirata-Koizumi, M., Ono,

A., Kamata, E., Hirose, A. 2012. No toxicological effects on acute and repeated oral gavage doses of single-wall or multi-wall carbon nanotube in rats. J Toxicol Sci. 37(3):463–74.

Matthews, I.P., Gregory, C.J., Aljayyoussi, G., Morris, C.J., Mcdonald, I., Hoogendoorn, B., Gumbleton, M. 2013. Maximal extent of translocation of single-walled carbon nanotubes from lung airways of the rat. Environ Toxicol Pharmacol. 35(3):461–4.

Mavon, A., Miquel, C., Lejeune, O., Payre, B., Moretto, P. 2007. In vitro percutaneous absorption and in vivo stratum corneum distribution of an organic and a mineral sunscreen. Skin Pharmacol Physiol. 20(1):10–20.

McCunney, R.J. 1996. Particle overload in the rat lung and lung cancer: implications for human risk assessment. CRC Press.

McKinney, W., Jackson, M., Sager, T.M., Reynolds, J.S., Chen, B.T., Afshari, A., Krajnak, K., Waugh, S., Johnson, C., Mercer, R.R., Frazer, D.G. 2012. Pulmonary and cardiovascular responses of rats to inhalation of a commercial antimicrobial spray containing titanium dioxide nanoparticles. Inhal Toxicol. 24(7):447–57.

McNaught, A.D., Wilkinson, A. 1997. Compendium of Chemical Terminology: IUPAC. Blackwell Science, Oxford.

McShan, D., Ray, P.C., Yu, H. 2014. Molecular toxicity mechanism of nanosilver. J Food Drug Anal. 22(1):116–27.

Meena, R., Kajal, K., Paulraj, R. 2015. Cytotoxic and genotoxic effects of titanium dioxide nanoparticles in testicular cells of male wistar rat. Appl Biochem Biotechnol. 175(2):825–40.

Mei, N., Zhang, Y., Chen, Y., Guo, X., Ding, W., Ali, S.F., Biris, A.S., Rice, P., Moore, M.M., Chen, T. 2012. Silver nanoparticle-induced mutations and oxidative stress in mouse lymphoma cells. Environ Mol Mutagen. 53(6):409–19.

Melnik, E.A., Buzulukov, Y.P., Demin, V.F., Demin, V.A., Gmoshinski, I.V., Tyshko, N.V., Tutelyan, V.A. 2013. Transfer of silver nanoparticles through the placenta and breast milk during in vivo experiments on rats. Acta Naturae. 5(3):107–15.

Menzel, F., Reinert, T., Vogt, J., Butz, T. 2004. Investigations of percutaneous uptake of ultrafine TiO 2 particles at the high energy ion nanoprobe LIPSION. Nucl Instrum Methods Phys Res B. 219:82–6.

Mercer, R.R., Hubbs, A.F., Scabilloni, J.F., Wang, L., Battelli, L.A., Friend, S., Castranova, V., Porter, D.W. 2011. Pulmonary fibrotic response to aspiration of multi-walled carbon nanotubes. Part Fibre Toxicol. 8(1):21.

Mercer, R.R., Hubbs, A.F., Scabilloni, J.F., Wang, L., Battelli, L.A., Schwegler-Berry, D.,

Castranova, V., Porter, D.W. 2010. Distribution and persistence of pleural penetrations by multi-walled carbon nanotubes. Part Fibre Toxicol. 7(1):28.

Mercer, R.R., Scabilloni, J.F., Hubbs, A.F., Wang, L., Battelli, L.A., McKinney, W., Castranova, V., Porter, D.W. 2013. Extrapulmonary transport of MWCNT following inhalation exposure. Part Fibre Toxicol. 10(1):38.

Mercer, R.R., Scabilloni, J., Wang, L., Kisin, E., Murray, A.R., Schwegler-Berry, D., Shvedova, A.A., Castranova, V. 2008. Alteration of deposition pattern and pulmonary response as a result of improved dispersion of aspirated single-walled carbon nanotubes in a mouse model. Am J Physiol Lung Cell Mol Physiol. 294(1):L87–97.

Migliore, L., Saracino, D., Bonelli, A., Colognato, R., D'errico, M.R., Magrini, A., Bergamaschi, A., Bergamaschi, E. 2010. Carbon nanotubes induce oxidative DNA damage in RAW 264.7 cells. Environ Mol Mutagen. 51(4):294–303.

Miresmaeili, S.M., Halvaei, I., Fesahat, F., Fallah, A., Nikonahad, N., Taherinejad, M. 2013. Evaluating the role of silver nanoparticles on acrosomal reaction and spermatogenic cells in rat. Iran J Reprod Med. 11(5):423–30.

Mishra, A., Stueckle, T.A., Mercer, R.R., Derk, R., Rojanasakul, Y., Castranova, V., Wang, L. 2015. Identification of TGF-β receptor-1 as a key regulator of carbon nanotube-induced fibrogenesis. Am J Physiol Lung Cell Mol Physiol. 309(8):L821–33.

Mitchell, L.A., Gao, J., Wal, R.V., Gigliotti, A., Burchiel, S.W., McDonald, J.D. 2007. Pulmonary and systemic immune response to inhaled multiwalled carbon nanotubes. Toxicol Sci. 100(1):203–14.

Mitrano, D.M., Motellier, S., Clavaguera, S., Nowack, B. 2015. Review of nanomaterial aging and transformations through the life cycle of nano-enhanced products. Environ Int. 77:132–47.

Miura, N., Shinohara, Y. 2009. Cytotoxic effect and apoptosis induction by silver nanoparticles in HeLa cells. Biochem Biophys Res Commun. 390(3):733–7.

Mohammadipour, A., Fazel, A., Haghir, H., Motejaded, F., Rafatpanah, H., Zabihi, H., Hosseini, M., Bideskan, A.E. 2014. Maternal exposure to titanium dioxide nanoparticles during pregnancy; impaired memory and decreased hippocampal cell proliferation in rat offspring. Environ Toxicol Pharmacol. 37(2):617–25.

Monteiro-Riviere, N.A., Wiench, K., Landsiedel, R., Schulte, S., Inman, A.O., Riviere, J.E. 2011. Safety evaluation of sunscreen formulations containing titanium dioxide and zinc oxide nanoparticles in UVB sunburned skin: an in vitro and in vivo study. Toxicol Sci. 123(1):264–80.

Morgan, A.M., MI, A.E.H., Noshy, P.A. 2015. Reproductive toxicity investigation of titanium dioxide nanoparticles in male albino rats. World J Pharm Pharmaceut Sci. 4(10):34–49.

Morimoto, Y., Hirohashi, M., Kobayashi, N., Ogami, A., Horie, M., Oyabu, T., Myojo, T., Hashiba, M., Mizuguchi, Y., Kambara, T., Lee, B.W. 2012. Pulmonary toxicity of well-dispersed single-wall carbon nanotubes after inhalation. Nanotoxicology. 6(7):766–75.

Morishige, T., Yoshioka, Y., Tanabe, A., Yao, X., Tsunoda, S.I., Tsutsumi, Y., Mukai, Y., Okada, N., Nakagawa, S. 2010. Titanium dioxide induces different levels of IL-1β production dependent on its particle characteristics through caspase-1 activation mediated by reactive oxygen species and cathepsin B. Biochem Biophys Res Commun. 392(2):160–5.

Morrow, P.E. 1988. Possible mechanisms to explain dust overloading of the lungs. Fundam Appl Toxicol. 10(3):369–84.

Mühlfeld, C., Geiser, M., Kapp, N., Gehr, P., Rothen-Rutishauser, B. 2007. Re-evaluation of pulmonary titanium dioxide nanoparticle distribution using the" relative deposition index": Evidence for clearance through microvasculature. Part Fibre Toxicol. 4(1):7.

Mühlfeld, C., Poland, C.A., Duffin, R., Brandenberger, C., Murphy, F.A., Rothen-Rutishauser, B., Gehr, P., Donaldson, K. 2012. Differential effects of long and short carbon nanotubes on the gas-exchange region of the mouse lung. Nanotoxicology. 6(8):867–79.

Muller, J., Huaux, F., Fonseca, A., Nagy, J.B., Moreau, N., Delos, M., Raymundo-Piñero, E., Béguin, F., Kirsch-Volders, M., Fenoglio, I., Fubini, B. 2008. Structural defects play a major role in the acute lung toxicity of multiwall carbon nanotubes: toxicological aspects. Chem Res Toxicol. 21(9):1698–705.

Muller, J., Huaux, F., Moreau, N., Misson, P., Heilier, J.F., Delos, M., Arras, M., Fonseca, A., Nagy, J.B., Lison, D. 2005. Respiratory toxicity of multi-wall carbon nanotubes. Toxicol Appl Pharmacol. 207(3):221–31.

Munger, M.A., Hadlock, G., Stoddard, G., Slawson, M.H., Wilkins, D.G., Cox, N., Rollins, D. 2015. Assessing orally bioavailable commercial silver nanoparticle product on human cytochrome P450 enzyme activity. Nanotoxicology. 9(4):474–81.

Munger, M.A., Radwanski, P., Hadlock, G.C., Stoddard, G., Shaaban, A., Falconer, J., Grainger, D.W., Deering-Rice, C.E. 2014. In vivo human time-exposure study of orally dosed commercial silver nanoparticles. Nanomed Nanotechnol. 10(1):1–9.

Murphy, F.A., Poland, C.A., Duffin, R., Al-Jamal, K.T., Ali-Boucetta, H., Nunes, A., Byrne, F., Prina-Mello, A., Volkov, Y., Li, S., Mather, S.J. 2011. Length-dependent retention of carbon nanotubes in the pleural space of mice initiates sustained inflammation and progressive fibrosis on the parietal pleura. Am J Pathol. 178(6):2587–600.

Mutlu, G.M., Budinger, G.S., Green, A.A., Urich, D., Soberanes, S., Chiarella, S.E., Alheid, G.F., McCrimmon, D.R., Szleifer, I., Hersam, M.C. 2010. Biocompatible nanoscale dispersion of

single-walled carbon nanotubes minimizes in vivo pulmonary toxicity. Nano Lett. 10(5):1664–70.

Nagai, H., Okazaki, Y., Chew, S.H., Misawa, N., Yamashita, Y., Akatsuka, S., Ishihara, T., Yamashita, K., Yoshikawa, Y., Yasui, H., Jiang, L. 2011. Diameter and rigidity of multiwalled carbon nanotubes are critical factors in mesothelial injury and carcinogenesis. Proc Natl Acad Sci USA. 108(49):E1330–8.

Nallanthighal, S., Chan, C., Bharali, D.J., Mousa, S.A., Vásquez, E., Reliene, R. 2017. Particle coatings but not silver ions mediate genotoxicity of ingested silver nanoparticles in a mouse model. NanoImpact. 5:92–100.

Naya, M., Kobayashi, N., Ema, M., Kasamoto, S., Fukumuro, M., Takami, S., Nakajima, M., Hayashi, M., Nakanishi, J. 2012b. In vivo genotoxicity study of titanium dioxide nanoparticles using comet assay following intratracheal instillation in rats. Regul Toxicol Pharmacol. 62(1):1–6.

Naya, M., Kobayashi, N., Endoh, S., Maru, J., Honda, K., Ema, M., Tanaka, J., Fukumuro, M., Hasegawa, K., Nakajima, M., Hayashi, M., Nakanishi, J. 2012a. In vivo genotoxicity study of single-wall carbon nanotubes using comet assay following intratracheal instillation in rats. Regul Toxicol Pharnacol. 64(1):124–9.

Naya, M., Kobayashi, N., Mizuno, K., Matsumoto, K., Ema, M., Nakanishi, J. 2011. Evaluation of the genotoxic potential of single-wall carbon nanotubes by using a battery of in vitro and in vivo genotoxicity assays. Regul Toxicol Pharmacol. 61(2):192–8.

Nazarenko, Y., Lioy, P.J., Mainelis, G. 2014. Quantitative assessment of inhalation exposure and deposited dose of aerosol from nanotechnology-based consumer sprays. Environ Sci Nano. 1(2):161–71.

Nel, A., Xia, T., Mädler, L., Li, N. 2006. Toxic potential of materials at the nanolevel. Science. 311(5761):622–7.

NIER (National Institute of Environmental Research), Korea, 2007. Reproduction and Developmental Toxicity Screening Test of Titanium Dioxide (CAS No:13463-67-7) by Oral Administration in Rats (Study No: G07147). Tested by KIT.

NIOSH (National Institute for Occupation Safety and Health). 2011. Occupational Exposure to Titanium Dioxide. Current Intelligence Bulletin 63. Available at: https://www.cdc.gov/niosh/docs/2011-160/pdfs/2011-160.pdf

NIOSH (National Institute for Occupation Safety and Health). 2015. External Review Draft – Current Intelligence Bulletin. Health Effects of Occupational Exposure to Silver Nanomaterials. Available at: https://www.cdc.gov/niosh/docket/review/docket260a/pdfs/draft--niosh-cib-on-silver-nanomaterials-1_8_16.pdf

NIOSH (National Institute for Occupation Safety and Health). 2017. Nanotechnology Research Center Publication No. 2017-175. Available at: https://www.cdc.gov/niosh/docs/ppop/pdfs/NTRC-PPOP-2017.pdf

Noël, A., Charbonneau, M., Cloutier, Y., Tardif, R., Truchon, G. 2013. Rat pulmonary responses to inhaled nano-TiO 2: effect of primary particle size and agglomeration state. Part Fibre Toxicol. 10(1):48.

Noël, A., Maghni, K., Cloutier, Y., Dion, C., Wilkinson, K.J., Halle, S., Tardif, R., Truchon, G. 2012. Effects of inhaled nano-TiO2 aerosols showing two distinct agglomeration states on rat lungs. Toxicol Lett. 214(2):109–19.

Nowack, B., David, R.M., Fissan, H., Morris, H., Shatkin, J.A., Stintz, M., Zepp, R., Brouwer, D. 2013. Potential release scenarios for carbon nanotubes used in composites. Environ Int. 59:1–11.

NTP (National Toxicology Program). 2017. Testing Status of Nanoscale Silver M070067. Available at: https://ntp.niehs.nih.gov/testing/status/agents/ts-m070067.html

Nurkiewicz, T.R., Porter, D.W., Hubbs, A.F., Cumpston, J.L., Chen, B.T., Frazer, D.G., Castranova, V. 2008. Nanoparticle inhalation augments particle-dependent systemic microvascular dysfunction. Part Fibre Toxicol. 5(1):1.

Nymark, P., Catalán, J., Suhonen, S., Järventaus, H., Birkedal, R., Clausen, P.A., Jensen, K.A., Vippola, M., Savolainen, K., Norppa, H. 2013. Genotoxicity of polyvinylpyrrolidone-coated silver nanoparticles in BEAS 2B cells. Toxicology. 313(1):38–48.

O'Brien, R.W. 1990. Electroacoustic studies of moderately concentrated colloidal suspensions. Faraday Discuss Chem Soc. 90:301–12.

Oberdörster, G. 1988. Lung clearance of inhaled insoluble and soluble particles. J Aerosol Med. 1(4):289–330.

Oberdörster, G. 1996. Significance of particle parameters in the evaluation of exposure-dose-response relationships of inhaled particles. Inhal Toxicol. 8:73–89.

Oberdörster, G. 2002. Toxicokinetics and effects of fibrous and nonfibrous particles. Inhal Toxicol. 14(1):29–56.

Oberdörster, G., Ferin, J., Gelein, R., Soderholm, S.C., Finkelstein, J. 1992. Role of the alveolar macrophage in lung injury: studies with ultrafine particles. Environ Health Perspect. 97:193–9.

Oberdörster, G., Ferin, J., Lehnert, B.E. 1994. Correlation between particle size, in vivo particle persistence, and lung injury. Environ Health Perspect. 102(Supp5):173.

Oberdörster, G., Maynard, A., Donaldson, K., Castranova, V., Fitzpatrick, J., Ausman, K., Carter, J., Karn, B., Kreyling, W., Lai, D., Olin, S. 2005. Principles for characterizing the potential human health effects from exposure to nanomaterials: elements of a screening strategy. Part Fibre Toxicol. 2(1):8.

Oberdörster, G., Sharp, Z., Atudorei, V., Elder, A., Gelein, R., Kreyling, W., Cox, C. 2004. Translocation of inhaled ultrafine particles to the brain. Inhal Toxicol. 16(6-7):437–45.

OECD (Organisation for Economic Co-operation and Development). 2016a. Physical-Chemical Parameters: Measurements and Methods Relevant for the Regulation of Nanomaterials. OECD Workshop Report. Series on the Safety of Manufactured Nanomaterials. No. 63. ENV/JM/MONO(2016)2.

OECD (Organisation for Economic Co-operation and Development). 2016b. Single-walled Carbon Nanotubes: Summary of the Dossier. Series on Safety of Manufactured Nanomaterials. No. 70. ENV/JM/MONO(2016)22.

Ohba, T., Xu, J., Alexander, D.B., Yamada, A., Kanno, J., Hirose, A., Tsuda, H., Imaizumi, Y. 2014. MWCNT causes extensive damage to the ciliated epithelium of the trachea of rodents. J Toxicol Sci. 39(3):499–505.

Olabarrieta, J., Zorita, S., Peña, I., Rioja, N., Monzón, O., Benguria, P., Scifo, L. 2012. Aging of photocatalytic coatings under a water flow: long run performance and TiO 2 nanoparticles release. Appl Catal B Environ. 123:182–92.

Oyabu, T., Morimoto, Y., Izumi, H., Yoshiura, Y., Tomonaga, T., Lee, B.W., Okada, T., Myojo, T., Shimada, M., Kubo, M., Yamamoto, K. 2016. Comparison between whole-body inhalation and nose-only inhalation on the deposition and health effects of nanoparticles. Environ Health Prev Med. 21(1):42–8.

Paino, I.M.M., Zucolotto, V. 2015. Poly (vinyl alcohol)-coated silver nanoparticles: Activation of neutrophils and nanotoxicology effects in human hepatocarcinoma and mononuclear cells. Environ Toxicol Pharmacol. 39(2):614–21.

Pal, S., Tak, Y.K., Song, J.M. 2007. Does the antibacterial activity of silver nanoparticles depend on the shape of the nanoparticle? A study of the gram-negative bacterium Escherichia coli. Appl Environ Microbiol. 73(6):1712–20.

Palomäki, J., Sund, J., Vippola, M., Kinaret, P., Greco, D., Savolainen, K., Puustinen, A., Alenius, H. 2015. A secretomics analysis reveals major differences in the macrophage responses towards different types of carbon nanotubes. Nanotoxicology. 9(6):719–28.

Palomäki, J., Välimäki, E., Sund, J., Vippola, M., Clausen, P.A., Jensen, K.A., Savolainen, K., Matikainen, S., Alenius, H. 2011. Long, needle-like carbon nanotubes and asbestos activate the

NLRP3 inflammasome through a similar mechanism. ACS Nano. 5(9):6861–70.

Park, E.J., Bae, E., Yi, J., Kim, Y., Choi, K., Lee, S.H., Yoon, J., Lee, B.C., Park, K. 2010a. Repeated-dose toxicity and inflammatory responses in mice by oral administration of silver nanoparticles. Environ Toxicol Pharmacol. 30(2):162–8.

Park, E.J., Cho, W.S., Jeong, J., Yi, J., Choi, K., Park, K. 2009. Pro-inflammatory and potential allergic responses resulting from B cell activation in mice treated with multi-walled carbon nanotubes by intratracheal instillation. Toxicology. 259(3):113–21.

Park, E.J., Hong, Y.S., Lee, B.S., Yoon, C., Jeong, U., Kim, Y. 2016. Single-walled carbon nanotubes disturbed the immune and metabolic regulation function 13-weeks after a single intratracheal instillation. Environ Res. 148:184–95.

Park, E.J., Yi, J., Kim, Y., Choi, K., Park, K. 2010b. Silver nanoparticles induce cytotoxicity by a Trojan-horse type mechanism. Toxicol In Vitro, 24(3):872–8.

Park, K. 2013. Toxicokinetic differences and toxicities of silver nanoparticles and silver ions in rats after single oral administration. J Toxicol Environ Health Part A. 76(22):1246–60.

Park, M.V., Verharen, H.W., Zwart, E., Hernandez, L.G., van Benthem, J., Elsaesser, A., Barnes, C., McKerr, G., Howard, C.V., Salvati, A., Lynch, I. 2011. Genotoxicity evaluation of amorphous silica nanoparticles of different sizes using the micronucleus and the plasmid lacZ gene mutation assay. Nanotoxicology. 5(2):168–81.

Patlolla, A.K., Hackett, D., Tchounwou, P.B. 2015. Genotoxicity study of silver nanoparticles in bone marrow cells of Sprague–Dawley rats. Food Chem Toxicol. 85:52–60.

Patlolla, A.K., Hussain, S.M., Schlager, J.J., Patlolla, S., Tchounwou, P.B. 2010. Comparative study of the clastogenicity of functionalized and nonfunctionalized multiwalled carbon nanotubes in bone marrow cells of Swiss-Webster mice. Environ Toxicol. 25(6):608–21.

Patlolla, A.K., Patra, P.K., Flountan, M., Tchounwou, P.B. 2016. Cytogenetic evaluation of functionalized single-walled carbon nanotube in mice bone marrow cells. Environ Toxicol. 31(9):1091–102.

Pauluhn, J. 2010. Subchronic 13-week inhalation exposure of rats to multiwalled carbon nanotubes: toxic effects are determined by density of agglomerate structures, not fibrillar structures. Toxicol Sci. 113(1):226–42.

Pauluhn, J., Rosenbruch, M. 2015. Lung burdens and kinetics of multi-walled carbon nanotubes (Baytubes) are highly dependent on the disaggregation of aerosolized MWCNT. Nanotoxicology. 9(2):242–52.

Pele, L.C., Thoree, V., Bruggraber, S.F., Koller, D., Thompson, R.P., Lomer, M.C., Powell, J.J.

2015. Pharmaceutical/food grade titanium dioxide particles are absorbed into the bloodstream of human volunteers. Part Fibre Toxicol. 12(1):26.

Petersen, E.J., Reipa, V., Watson, S.S., Stanley, D.L., Rabb, S.A., Nelson, B.C. 2014. DNA damaging potential of photoactivated P25 titanium dioxide nanoparticles. Chem Res Toxicol. 27(10):1877–84.

Pettitt, M.E., Lead, J.R. 2013. Minimum physicochemical characterisation requirements for nanomaterial regulation. Environ Int. 52:41–50.

Peuschel, H., Sydlik, U., Grether-Beck, S., Felsner, I., Stöckmann, D., Jakob, S., Kroker, M., Haendeler, J., Gotić, M., Bieschke, C., Krutmann, J. 2012. Carbon nanoparticles induce ceramide-and lipid raft-dependent signalling in lung epithelial cells: a target for a preventive strategy against environmentally-induced lung inflammation. Part Fibre Toxicol. 9(1):48.

Pflücker, F., Wendel, V., Hohenberg, H., Gärtner, E., Will, T., Pfeiffer, S., Wepf, R., Gers-Barlag, H. 2001. The human stratum corneum layer: an effective barrier against dermal uptake of different forms of topically applied micronised titanium dioxide. Skin Pharmacol Physiol. 14(Supp1):92–7.

Philbrook, N.A., Walker, V.K., Afrooz, A.N., Saleh, N.B., Winn, L.M. 2011. Investigating the effects of functionalized carbon nanotubes on reproduction and development in Drosophila melanogaster and CD-1 mice. Reprod Toxicol. 32:442–8.

Pietroiusti, A., Massimiani, M., Fenoglio, I., Colonna, M., Valentini, F., Palleschi, G., Camaioni, A., Magrini, A., Siracusa, G., Bergamaschi, A., Sgambato, A. 2011. Low doses of pristine and oxidized single-wall carbon nanotubes affect mammalian embryonic development. ACS Nano. 5:4624–33.

Pirela, S.V., Lu, X., Miousse, I., Sisler, J.D., Qian, Y., Guo, N., Koturbash, I., Castranova, V., Thomas, T., Godleski, J., Demokritou, P. 2016b. Effects of intratracheally instilled laser printer-emitted engineered nanoparticles in a mouse model: A case study of toxicological implications from nanomaterials released during consumer use. NanoImpact, 1:1–8.

Pirela, S.V., Miousse, I.R., Lu, X., Castranova, V., Thomas, T., Qian, Y., Bello, D., Kobzik, L., Koturbash, I., Demokritou, P. 2016a. Effects of laser printer–emitted engineered nanoparticles on cytotoxicity, chemokine expression, reactive oxygen species, DNA methylation, and DNA damage: a comprehensive in vitro analysis in human small airway epithelial cells, macrophages, and lymphoblasts. Environ Health Perspect. 124(2):210.

Pirela, S.V., Sotiriou, G.A., Bello, D., Shafer, M., Bunker, K.L., Castranova, V., Thomas, T., Demokritou, P. 2015. Consumer exposures to laser printer-emitted engineered nanoparticles: a case study of life-cycle implications from nano-enabled products. Nanotoxicology. 9(6):760–8.

Polimeni, M., Gulino, G.R., Gazzano, E., Kopecka, J., Marucco, A., Fenoglio, I., Cesano, F.,

Campagnolo, L., Magrini, A., Pietroiusti, A., Ghigo, D. 2016. Multi-walled carbon nanotubes directly induce epithelial-mesenchymal transition in human bronchial epithelial cells via the TGF-β-mediated Akt/GSK-3β/SNAIL-1 signalling pathway. Part Fibre Toxicol. 13(1):27.

Porter, D.W., Hubbs, A.F., Mercer, R.R., Wu, N., Wolfarth, M.G., Sriram, K., Leonard, S., Battelli, L., Schwegler-Berry, D., Friend, S., Andrew, M. 2010. Mouse pulmonary dose-and time course-responses induced by exposure to multi-walled carbon nanotubes. Toxicology. 269(2):136–47.

Porter, D.W., Wu, N., Hubbs, A.F., Mercer, R.R., Funk, K., Meng, F., Li, J., Wolfarth, M.G., Battelli, L., Friend, S., Andrew, M. 2012. Differential mouse pulmonary dose and time course responses to titanium dioxide nanospheres and nanobelts. Toxicol Sci. 131(1):179–93.

Pothmann, D., Simar, S., Schuler, D., Dony, E., Gaering, S., Net, J.L., Okazaki, Y., Chabagno, J.M., Bessibes, C., Beausoleil, J., Nesslany, F. 2015. Lung inflammation and lack of genotoxicity in the comet and micronucleus assays of industrial multiwalled carbon nanotubes Graphistrength© C100 after a 90-day nose-only inhalation exposure of rats. Part Fibre Toxicol. 12(1):21.

Poulsen, S.S., Jackson, P., Kling, K., Knudsen, K.B., Skaug, V., Kyjovska, Z.O., Thomsen, B.L., Clausen, P.A., Atluri, R., Berthing, T., Bengtson, S. 2016. Multi-walled carbon nanotube physicochemical properties predict pulmonary inflammation and genotoxicity. Nanotoxicology. 10(9):1263–75.

Poulsen, S.S., Saber, A.T., Williams, A., Andersen, O., Købler, C., Atluri, R., Pozzebon, M.E., Mucelli, S.P., Simion, M., Rickerby, D., Mortensen, A. 2015. MWCNTs of different physicochemical properties cause similar inflammatory responses, but differences in transcriptional and histological markers of fibrosis in mouse lungs. Toxicol Appl Pharmacol. 284(1):16–32.

Powers, C.M., Badireddy, A.R., Ryde, I.T., Seidler, F.J., Slotkin, T.A. 2011. Silver nanoparticles compromise neurodevelopment in PC12 cells: critical contributions of silver ion, particle size, coating, and composition. Environ Health Perspect. 119(1):37–44.

Powers, C.M., Bale, A.S., Kraft, A.D., Makris, S.L., Trecki, J., Cowden, J., Hotchkiss, A., Gillespie, P.A. 2013. Developmental neurotoxicity of engineered nanomaterials: identifying research needs to support human health risk assessment. Toxicol Sci. 134(2):225–42.

Powers, K.W., Brown, S.C., Krishna, V.B., Wasdo, S.C., Moudgil, B.M., Roberts, S.M. 2006. Research strategies for safety evaluation of nanomaterials. Part VI. Characterization of nanoscale particles for toxicological evaluation. Toxicol Sci. 90(2):296–303.

Powers, C.M., Wrench, N., Ryde, I.T., Smith, A.M., Seidler, F.J., Slotkin, T.A. 2010. Silver impairs neurodevelopment: studies in PC12 cells. Environ Health Perspect. 118(1):73–9.

Prasad, R.Y., Wallace, K., Daniel, K.M., Tennant, A.H., Zucker, R.M., Strickland, J., Dreher, K., Kligerman, A.D., Blackman, C.F., DeMarini, D.M. 2013. Effect of treatment media on the agglomeration of titanium dioxide nanoparticles: impact on genotoxicity, cellular interaction, and cell cycle. ACS Nano. 7(3):1929–42.

Principi, E., Girardello, R., Bruno, A., Manni, I., Gini, E., Pagani, A., Grimaldi, A., Ivaldi, F., Congiu, T., De Stefano, D., Piaggio, G. 2016. Systemic distribution of single-walled carbon nanotubes in a novel model: alteration of biochemical parameters, metabolic functions, liver accumulation, and inflammation in vivo. Int J Nanomed. 11:4299–316.

PubChem. Last accessed 2017. Titanium Dioxide. Available at: https://pubchem.ncbi.nlm.nih.gov/compound/26042#section=Top

Pulskamp, K., Diabaté, S., Krug, H.F. 2007. Carbon nanotubes show no sign of acute toxicity but induce intracellular reactive oxygen species in dependence on contaminants. Toxicol Lett. 168(1):58–74.

Qi, W., Bi, J., Zhang, X., Wang, J., Wang, J., Liu, P., Li, Z., Wu, W. 2014. Damaging effects of multi-walled carbon nanotubes on pregnant mice with different pregnancy time. Sci Rep. 4:4352.

Qin, G., Tang, S., Li, S., Lu, H., Wang, Y., Zhao, P., Li, B., Zhang, J., Peng, L. 2017. Toxicological evaluation of silver nanoparticles and silver nitrate in rats following 28 days of repeated oral exposure. Environ Toxicol. 32(2):609–18.

Quadros, M.E., Marr, L.C. 2010. Environmental and human health risks of aerosolized silver nanoparticles. J Air Waste Manag Assoc. 60(7):770–81.

Rabolli, V., Lison, D., Huaux, F. 2016. The complex cascade of cellular events governing inflammasome activation and IL-1β processing in response to inhaled particles. Part Fibre Toxicol. 13(1):40.

Radziuk, D., Skirtach, A., Sukhorukov, G., Shchukin, D., Möhwald, H. 2007. Stabilization of silver nanoparticles by polyelectrolytes and poly (ethylene glycol). Macromol Rapid Commun. 28(7):848–55.

Rahman, M.F., Wang, J., Patterson, T.A., Saini, U.T., Robinson, B.L., Newport, G.D., Murdock, R.C., Schlager, J.J., Hussain, S.M., Ali, S.F. 2009. Expression of genes related to oxidative stress in the mouse brain after exposure to silver-25 nanoparticles. Toxicol Lett. 187(1):15–21.

Rajapakse, K., Drobne, D., Kastelec, D., Marinsek-Logar, R. 2013. Experimental evidence of false-positive Comet test results due to TiO2 particle-assay interactions. Nanotoxicology. 7(5):1043–51.

Rashno, M., Fatemi Tabatabaei, S.R., Khaksary Mahabady, M., Ghaderi, S. 2014. Maternal exposure to silver nanoparticles in mice: effects on dams' reproductive performance and pups'

neurobehavioral ontogeny. Anat Sci J. 11(1):41–52.

Recordati, C., De Maglie, M., Bianchessi, S., Argentiere, S., Cella, C., Mattiello, S., Cubadda, F., Aureli, F., D'Amato, M., Raggi, A., Lenardi, C. 2015. Tissue distribution and acute toxicity of silver after single intravenous administration in mice: nano-specific and size-dependent effects. Part Fibre Toxicol. 13(1)12.

Reddy, A., Reddy, Y.N., Krishna, D.R, Himabindu, V. 2012. Pulmonary toxicity assessment of multiwalled carbon nanotubes in rats following intratracheal instillation. Environ Toxicol. 27(4):211–9.

Reddy, A.R., Krishna, D.R., Reddy, Y.N., Himabindu, V. 2010. Translocation and extra pulmonary toxicities of multi wall carbon nanotubes in rats. Toxicol Mech Meth. 20(5):267–72.

Reddy, A.R.N., Rao, M.V., Krishna, D.R., Himabindu, V., Reddy, Y.N. 2011. Evaluation of oxidative stress and anti-oxidant status in rat serum following exposure of carbon nanotubes. Regul Toxicol Pharmacol. 59(2):251–7.

Reidy, B., Haase, A., Luch, A., Dawson, K.A., Lynch, I. 2013. Mechanisms of silver nanoparticle release, transformation and toxicity: a critical review of current knowledge and recommendations for future studies and applications. Materials. 6(6):2295–350.

Renwick, L.C., Brown, D., Clouter, A., Donaldson, K. 2004. Increased inflammation and altered macrophage chemotactic responses caused by two ultrafine particle types. Occup Environ Med. 61(5):442–7.

Rezazadeh-Reyhani, Z., Razi, M., Malekinejad, H., Sadrkhanlou, R. 2015. Cytotoxic effect of nanosilver particles on testicular tissue: Evidence for biochemical stress and Hsp70-2 protein expression. Environ Toxicol Pharmacol. 40(2):626–38.

Riebeling, C., Luch, A., Götz, M.E. 2016. Comparative modeling of exposure to airborne nanoparticles released by consumer spray products. Nanotoxicology. 10(3):343–51.

Rinna, A., Magdolenova, Z., Hudecova, A., Kruszewski, M., Refsnes, M., Dusinska, M. 2015. Effect of silver nanoparticles on mitogen-activated protein kinases activation: role of reactive oxygen species and implication in DNA damage. Mutagenesis. 30(1):59–66.

Rodriguez-Yañez, Y., Muñoz, B., Albores, A. 2013. Mechanisms of toxicity by carbon nanotubes. Toxicol Mech Meth. 23(3):178–95.

Roller, M. 2009. Carcinogenicity of inhaled nanoparticles. Inhal Toxicol. 21(Supp 1):144–57.

Rosas-Hernández, H., Jiménez-Badillo, S., Martínez-Cuevas, P.P., Gracia-Espino, E., Terrones, H., Terrones, M., Hussain, S.M., Ali, S.F., González, C. 2009. Effects of 45-nm silver nanoparticles on coronary endothelial cells and isolated rat aortic rings. Toxicol Lett.

191(2):305–13.

Rossi, E.M., Pylkkänen, L., Koivisto, A.J., Vippola, M., Jensen, K.A., Miettinen, M., Sirola, K., Nykäsenoja, H., Karisola, P., Stjernvall, T., Vanhala, E. 2010. Airway exposure to silica-coated TiO2 nanoparticles induces pulmonary neutrophilia in mice. Toxicolo Sci. 113(2):422–33.

Russier, J., Ménard-Moyon, C., Venturelli, E., Gravel, E., Marcolongo, G., Meneghetti, M., Doris, E., Bianco, A. 2011. Oxidative biodegradation of single-and multi-walled carbon nanotubes. Nanoscale. 3(3):893–6.

Rydman, E.M., Ilves, M., Vanhala, E., Vippola, M., Lehto, M., Kinaret, P.A., Pylkkänen, L., Happo, M., Hirvonen, M.R., Greco, D., Savolainen, K. 2015. A single aspiration of rod-like carbon nanotubes induces asbestos-like pulmonary inflammation mediated in part by the IL-1 receptor. Toxicol Sci. 147(1):140–55.

Ryman-Rasmussen, J.P., Cesta, M.F., Brody, A.R., Shipley-Phillips, J.K., Everitt, J.I., Tewksbury, E.W., Moss, O.R., Wong, B.A., Dodd, D.E., Andersen, M.E., Bonner, J.C. 2009a. Inhaled carbon nanotubes reach the subpleural tissue in mice. Nat Nanotechnol. 4(11):747–51.

Ryman-Rasmussen, J.P., Tewksbury, E.W., Moss, O.R., Cesta, M.F., Wong, B.A., Bonner, J.C. 2009b. Inhaled multiwalled carbon nanotubes potentiate airway fibrosis in murine allergic asthma. Am J Respir Cell Mol Biol. 40(3):349–58.

Rasmussen, K., Mast, J., De Temmerman, P. J., Verleysen, E., Waegeneers, N., Van Steen, F., Pizzolon, J.C., De Temmerman, L., Van Doren, E., Jensen, K.A., Birkedal, R. 2014. Titanium dioxide, NM-100, NM-101, NM-102, NM-103, NM-104, NM-105: characterisation and physico-chemical properties. JRC Science and Policy Reports.

Saber, A.T., Mortensen, A., Szarek, J., Koponen, I.K., Levin, M., Jacobsen, N.R., Pozzebon, M.E., Mucelli, S.P., Rickerby, D.G., Kling, K., Atluri, R. 2016. Epoxy composite dusts with and without carbon nanotubes cause similar pulmonary responses, but differences in liver histology in mice following pulmonary deposition. Part Fibre Toxicol. 13(1):37.

Sadiq, R., Bhalli, J.A., Yan, J., Woodruff, R.S., Pearce, M.G., Li, Y., Mustafa, T., Waatanabe, F., Pack, L.M., Biris, A.S., Khan, Q.M. 2012. Genotoxicity of TiO 2 anatase nanoparticles in B6C3F1 male mice evaluated using Pig-a and flow cytometric micronucleus assays. Mutat Res Genet Toxicol Environ Mutagen. 745(1):65–72.

Sadrieh, N., Wokovich, A.M., Gopee, N.V., Zheng, J., Haines, D., Parmiter, D., Siitonen, P.H., Cozart, C.R., Patri, A.K., McNeil, S.E., Howard, P.C. 2010. Lack of significant dermal penetration of titanium dioxide from sunscreen formulations containing nano-and submicron-size TiO2 particles. Toxicol Sci. 115(1):156–66.

Sagawa, Y., Futakuchi, M., Xu, J., Fukamachi, K., Sakai, Y., Ikarashi, Y., Nishimura, T., Suzui, M., Tsuda, H., Morita, A. 2012. Lack of promoting effect of titanium dioxide particles on

chemically-induced skin carcinogenesis in rats and mice. J Soxicol Sci. 37(2):317–27.

Sager, T.M., Castranova, V. 2009. Surface area of particle administered versus mass in determining the pulmonary toxicity of ultrafine and fine carbon black: comparison to ultrafine titanium dioxide. Part Fibre Toxicol. 6(1):15.

Sager, T.M., Kommineni, C., Castranova, V. 2008a. Pulmonary response to intratracheal instillation of ultrafine versus fine titanium dioxide: role of particle surface area. Part Fibre Toxicol. 5(1):17.

Sager, T.M., Porter, D., Castranova, V. 2008b. Pulmonary response to intratracheal instillation of fine or ultrafine carbon black or titanium dioxide: role of surface area. The Toxicologist. 102(1):305–6.

Sahu, S.C., Njoroge, J., Bryce, S.M., Yourick, J.J., Sprando, R.L. 2014b. Comparative genotoxicity of nanosilver in human liver HepG2 and colon Caco2 cells evaluated by a flow cytometric in vitro micronucleus assay. J Appl Toxicol. 34(11):1226–34.

Sahu, S.C., Njoroge, J., Bryce, S.M., Zheng, J., Ihrie, J. 2016a. Flow cytometric evaluation of the contribution of ionic silver to genotoxic potential of nanosilver in human liver HepG2 and colon Caco2 cells. J Appl Toxicol. 36(4):521–31.

Sahu, S.C., Roy, S., Zheng, J., Ihrie, J. 2016b. Contribution of ionic silver to genotoxic potential of nanosilver in human liver HepG2 and colon Caco2 cells evaluated by the cytokinesis-block micronucleus assay. J Appl Toxicol. 36(4):532–42.

Sahu, S.C., Roy, S., Zheng, J., Yourick, J.J., Sprando, R.L. 2014a. Comparative genotoxicity of nanosilver in human liver HepG2 and colon Caco2 cells evaluated by fluorescent microscopy of cytochalasin B-blocked micronucleus formation. J Appl Toxicol. 34(11):1200–8.

Sakamoto, Y., Nakae, D., Fukumori, N., Tayama, K., Maekawa, A., Imai, K., Hirose, A., Nishimura, T., Ohashi, N., Ogata, A. 2009. Induction of mesothelioma by a single intrascrotal administration of multi-wall carbon nanotube in intact male Fischer 344 rats. J of Toxicol Sci. 34(1):65-76.

Samberg, M.E., Oldenburg, S.J., Monteiro-Riviere, N.A. 2010. Evaluation of silver nanoparticle toxicity in skin in vivo and keratinocytes in vitro. Environ Health Perspect. 118(3):407–13.

Samberg, M.E., Orndorff, P.E., Monteiro-Riviere, N.A. 2011. Antibacterial efficacy of silver nanoparticles of different sizes, surface conditions and synthesis methods. Nanotoxicology. 5(2):244 – 53.

Saptarshi, S.R., Duschl, A., Lopata, A.L. 2013. Interaction of nanoparticles with proteins: relation to bio-reactivity of the nanoparticle. J Nanobiotechnology. 11(1):26.

Saquib, Q., Al-Khedhairy, A.A., Siddiqui, M.A., Abou-Tarboush, F.M., Azam, A., Musarrat, J. 2012. Titanium dioxide nanoparticles induced cytotoxicity, oxidative stress and DNA damage in human amnion epithelial (WISH) cells. Toxicol In Vitro. 26(2):351–61.

Sargent, L.M., Hubbs, A.F., Young, S.H., Kashon, M.L., Dinu, C.Z., Salisbury, J.L., Benkovic, S.A., Lowry, D.T., Murray, A.R., Kisin, E.R., Siegrist, K.J. 2012. Single-walled carbon nanotube-induced mitotic disruption. Mutat Res Genet Toxicol Environ Mutagen. 745(1):28–37.

Sargent, L.M., Porter, D.W., Staska, L.M., Hubbs, A.F., Lowry, D.T., Battelli, L., Siegrist, K.J., Kashon, M.L., Mercer, R.R., Bauer, A.K., Chen, B.T. 2014. Promotion of lung adenocarcinoma following inhalation exposure to multi-walled carbon nanotubes. Part Fibre Toxicol. 11(1):3.

Sargent, L.M., Shvedova, A.A., Hubbs, A.F., Salisbury, J.L., Benkovic, S.A., Kashon, M.L., Lowry, D.T., Murray, A.R., Kisin, E.R., Friend, S., McKinstry, K.T. 2009. Induction of aneuploidy by single-walled carbon nanotubes. Environ Mol Mutagen. 50(8):708–17.

Schäfer, B., Vom Brocke, J., Epp, A., Götz, M., Herzberg, F., Kneuer, C., Sommer, Y., Tenschert, J., Noll, M., Günther, I., Banasiak, U. 2013. State of the art in human risk assessment of silver compounds in consumer products: a conference report on silver and nanosilver held at the BfR in 2012. Arch Toxicol. 87(12):2249–62.

Schlagenhauf, L., Buerki-Thurnherr, T., Kuo, Y.Y., Wichser, A., Nüesch, F., Wick, P., Wang, J. 2015a. Carbon nanotubes released from an epoxy-based nanocomposite: quantification and particle toxicity. Environ Sci Technol. 49(17):10616–23.

Schlagenhauf, L., Chu, B.T., Buha, J., Nüesch, F., Wang, J. 2012. Release of carbon nanotubes from an epoxy-based nanocomposite during an abrasion process. Environ Sci Technol. 46(13):7366–72.

Schlagenhauf, L., Kianfar, B., Buerki-Thurnherr, T., Kuo, Y.Y., Wichser, A., Nüesch, F., Wick, P., Wang, J. 2015b. Weathering of a carbon nanotube/epoxy nanocomposite under UV light and in water bath: impact on abraded particles. Nanoscale. 7(44):18524–36.

Schulte, S., Sukhova, G.K., Libby, P. 2008. Genetically programmed biases in Th1 and Th2 immune responses modulate atherogenesis. Am J Pathol. 172(6):1500–8.

Senzui, M., Tamura, T., Miura, K., Ikarashi, Y., Watanabe, Y., Fujii, M. 2010. Study on penetration of titanium dioxide (TiO2) nanoparticles into intact and damaged skin in vitro. J Toxicol Sci.35(1):107–13.

Shahare, B., Yashpal, M., Gajendra. 2013. Toxic effects of repeated oral exposure of silver nanoparticles on small intestine mucosa of mice. Toxicol Mech Meth. 23(3):161–7.

Shakeel, M., Jabeen, F., Shabbir, S., Asghar, M.S., Khan, M.S., Chaudhry, A.S. 2016. Toxicity of nano-titanium dioxide (TiO2-NP) through various routes of exposure: a review. Biol Trace

Elem Res. 172(1):1–36.

Shandilya, N., Bihan, O.L., Bressot, C., Morgeneyer, M. 2014. Evaluation of the particle aerosolization from n-TiO 2 photocatalytic nanocoatings under abrasion. J Nanomater. 2014:6.

Shandilya, N., Le Bihan, O., Bressot, C., Morgeneyer, M. 2015. Emission of titanium dioxide nanoparticles from building materials to the environment by wear and weather. Environ Sci Technol. 49(4):2163–70.

Sheng, L., Wang, L., Sang, X., Zhao, X., Hong, J., Cheng, S., Yu, X., Liu, D., Xu, B., Hu, R., Sun, Q. 2014. Nano-sized titanium dioxide-induced splenic toxicity: a biological pathway explored using microarray technology. J Hazard Mater. 278:180–8.

Shi, H., Zhao, J., Magaye, R., Castranova, V. 2013. Titanium dioxide nanoparticles: a review of current toxicological data. Part Fibre Toxicol. 10(1):15.

Shinohara, N., Nakazato, T., Ohkawa, K., Tamura, M., Kobayashi, N., Morimoto, Y., Oyabu, T., Myojo, T., Shimada, M., Yamamoto, K., Tao, H. 2016. Long-term retention of pristine multi-walled carbon nanotubes in rat lungs after intratracheal instillation. J Appl Toxicol. 36(4):501–9.

Shukla, R.K., Kumar, A., Gurbani, D., Pandey, A.K., Singh, S., Dhawan, A. 2013. TiO2 nanoparticles induce oxidative DNA damage and apoptosis in human liver cells. Nanotoxicology. 7(1):48–60.

Shukla, R.K., Sharma, V., Pandey, A.K., Singh, S., Sultana, S., Dhawan, A. 2011. ROS-mediated genotoxicity induced by titanium dioxide nanoparticles in human epidermal cells. Toxicol In Vitro. 25(1):231–41.

Shvedova, A.A., Kapralov, A.A., Feng, W.H., Kisin, E.R., Murray, A.R., Mercer, R.R., Croix, C.M., Lang, M.A., Watkins, S.C., Konduru, N.V., Allen, B.L. 2012. Impaired clearance and enhanced pulmonary inflammatory/fibrotic response to carbon nanotubes in myeloperoxidase-deficient mice. PLoS ONE. 7(3):e30923.

Shvedova, A.A., Kisin, E., Murray, A.R., Johnson, V.J., Gorelik, O., Arepalli, S., Hubbs, A.F., Mercer, R.R., Keohavong, P., Sussman, N., Jin, J. 2008. Inhalation vs. aspiration of single-walled carbon nanotubes in C57BL/6 mice: inflammation, fibrosis, oxidative stress, and mutagenesis. Am J Physiol Lung Cell Mol Physiol. 295(4):L552–65.

Shvedova, A.A., Yanamala, N., Kisin, E.R., Tkach, A.V., Murray, A.R., Hubbs, A., Chirila, M.M., Keohavong, P., Sycheva, L.P., Kagan, V.E., Castranova, V. 2014. Long-term effects of carbon containing engineered nanomaterials and asbestos in the lung: one year postexposure comparisons. Am J Physiol Lung Cell Mol Physiol. 306(2):L170–82.

Siegrist, K.J., Reynolds, S.H., Kashon, M.L., Lowry, D.T., Dong, C., Hubbs, A.F., Young, S.H., Salisbury, J.L., Porter, D.W., Benkovic, S.A., McCawley, M. 2014. Genotoxicity of multi-walled

carbon nanotubes at occupationally relevant doses. Part Fibre Toxicol. 11(1):6.

Silva, R.M., Doudrick, K., Franzi, L.M., TeeSy, C., Anderson, D.S., Wu, Z., Mitra, S., Vu, V., Dutrow, G., Evans, J.E., Westerhoff, P. 2014. Instillation versus inhalation of multiwalled carbon nanotubes: exposure-related health effects, clearance, and the role of particle characteristics. ACS Nano. 8(9):8911–31.

Silva, R.M., TeeSy, C., Franzi, L., Weir, A., Westerhoff, P., Evans, J.E., Pinkerton, K.E. 2013. Biological response to nano-scale titanium dioxide (TiO2): role of particle dose, shape, and retention. J Toxicol Environ Health Part A. 76(16):953–72.

Simon, G.A., Maibach, H.I. 1998. Relevance of hairless mouse as an experimental model of percutaneous penetration in man. Skin Pharmacol Physiol. 11(2):80–6.

Skalska, J., Dąbrowska-Bouta, B., Strużyńska, L. 2016. Oxidative stress in rat brain but not in liver following oral administration of a low dose of nanoparticulate silver. Food Chem Toxicol. 97:307–15.

Sleiman, H.K., Romano, R.M., Oliveira, C.A.D., Romano, M.A. 2013. Effects of prepubertal exposure to silver nanoparticles on reproductive parameters in adult male Wistar rats. J Toxicol Environ Health Part A. 76(17):1023–32.

Smulders, S., Larue, C., Sarret, G., Castillo-Michel, H., Vanoirbeek, J., Hoet, P.H. 2015. Lung distribution, quantification, co-localization and speciation of silver nanoparticles after lung exposure in mice. Toxicol Lett. 238(1):1–6.

Smulders, S., Luyts, K., Brabants, G., Landuyt, K.V., Kirschhock, C., Smolders, E., Golanski, L., Vanoirbeek, J., Hoet, P.H. 2014. Toxicity of nanoparticles embedded in paints compared with pristine nanoparticles in mice. Toxicol Sci. 141(1):132–40.

Song, M.F., Li, Y.S., Kasai, H., Kawai, K. 2012. Metal nanoparticle-induced micronuclei and oxidative DNA damage in mice. J Clin Biochem Nutr. 50(3):211–6.

Sotiriou, G.A., Singh, D., Zhang, F., Chalbot, M.C.G., Spielman-Sun, E., Hoering, L., Kavouras, I.G., Lowry, G.V., Wohlleben, W., Demokritou, P. 2016. Thermal decomposition of nano-enabled thermoplastics: possible environmental health and safety implications. J Hazard Mater. 305:87–95.

Souza, T.A., Franchi, L.P., Rosa, L.R., da Veiga, M.A., Takahashi, C.S. 2016. Cytotoxicity and genotoxicity of silver nanoparticles of different sizes in CHO-K1 and CHO-XRS5 cell lines. Mutat Res Genet Toxicol Environ Mutagen. 795:70–83.

Srivastava, R.K., Rahman, Q., Kashyap, M.P., Singh, A.K., Jain, G., Jahan, S., Lohani, M., Pant, A.B. 2013. Nano-titanium dioxide induces genotoxicity and apoptosis in human lung cancer cell line, A549. Hum Exp Toxicol. 32(2):153–66.

Srivastava, R.K., Rahman, Q., Kashyap, M.P., Lohani, M., Pant, A.B. 2011. Ameliorative effects of dimetylthiourea and N-acetylcysteine on nanoparticles induced cyto-genotoxicity in human lung cancer cells-A549. PLoS ONE: 6(9):e25767.

Stapleton, P.A., Nichols, C.E., Yi, J., McBride, C.R., Minarchick, V.C., Shepherd, D.L., Hollander, J.M., Nurkiewicz, T.R. 2015. Microvascular and mitochondrial dysfunction in the female F1 generation after gestational TiO2 nanoparticle exposure. Nanotoxicology. 9(8):941–51.

Stearns, R.C., Paulauskis, J.D., Godleski, J.J. 2001. Endocytosis of ultrafine particles by A549 cells. Am J Respir Cell Mol Biol. 24(2):108–15.

Stensberg, M.C., Wei, Q., McLamore, E.S., Porterfield, D.M., Wei, A., Sepúlveda, M.S. 2011. Toxicological studies on silver nanoparticles: challenges and opportunities in assessment, monitoring and imaging. Nanomedicine. 6(5):879–98.

Stern, S.T., Adiseshaiah, P.P., Crist, R.M. 2012. Autophagy and lysosomal dysfunction as emerging mechanisms of nanomaterial toxicity. Part Fibre Toxicol. 9(1):20.

Sturm, R. 2016. A stochastic model of carbon nanotube deposition in the airways and alveoli of the human respiratory tract. Inhal Toxicol. 28(2):49–60.

Suliman, Y., Omar, A., Ali, D., Alarifi, S., Harrath, A.H., Mansour, L., Alwasel, S.H. 2015. Evaluation of cytotoxic, oxidative stress, proinflammatory and genotoxic effect of silver nanoparticles in human lung epithelial cells. Environ Toxicol. 30(2):149–60.

Sung, J.H., Ji, J.H., Park, J.D., Yoon, J.U., Kim, D.S., Jeon, K.S., Song, M.Y., Jeong, J., Han, B.S., Han, J.H., Chung, Y.H. 2009. Subchronic inhalation toxicity of silver nanoparticles. Toxicol Sci. 108(2):452–61.

Sung, J.H., Ji, J.H., Song, K.S., Lee, J.H., Choi, K.H., Lee, S.H., Yu, I.J. 2011. Acute inhalation toxicity of silver nanoparticles. Toxicol Ind Health. 27(2):149–54.

Sung, J.H., Ji, J.H., Yoon, J.U., Kim, D.S., Song, M.Y., Jeong, J., Han, B.S., Han, J.H., Chung, Y.H., Kim, J., Kim, T.S. 2008. Lung function changes in Sprague-Dawley rats after prolonged inhalation exposure to silver nanoparticles. Inhal Toxicol. 20(6):567–74.

Sur, I., Altunbek, M., Kahraman, M., Culha, M. 2012. The influence of the surface chemistry of silver nanoparticles on cell death. Nanotechnology. 23(37):375102.

Suresh, A.K., Pelletier, D.A., Wang, W., Morrell-Falvey, J.L., Gu, B., Doktycz, M.J. 2012. Cytotoxicity induced by engineered silver nanocrystallites is dependent on surface coatings and cell types. Langmuir. 28(5):2727–35.

Suzuki, T., Miura, N., Hojo, R., Yanagiba, Y., Suda, M., Hasegawa, T., Miyagawa, M., Wang, R.S. 2016. Genotoxicity assessment of intravenously injected titanium dioxide nanoparticles in gpt delta transgenic mice. Mutat Res Genet Toxicol Environ Mutagen. 802:30–7.

Sycheva, L.P., Zhurkov, V.S., Iurchenko, V.V., Daugel-Dauge, N.O., Kovalenko, M.A., Krivtsova, E.K., Durnev, A.D. 2011. Investigation of genotoxic and cytotoxic effects of micro- and nanosized titanium dioxide in six organs of mice in vivo. Mutat Res Genet Toxicol Environ Mutagen. 726(1):8-14.

Tabatabaei, S.R.F., Moshrefi, M., Askaripour, M. 2015. Prenatal exposure to silver nanoparticles causes depression like responses in mice. Indian J Pharm Sci. 77(6):681–6.

Tabet, L., Bussy, C., Setyan, A., Simon-Deckers, A., Rossi, M.J., Boczkowski, J., Lanone, S. 2011. Coating carbon nanotubes with a polystyrene-based polymer protects against pulmonary toxicity. Part Fibre Toxicol. 8(1):3.

Takenaka, S., Karg, E., Roth, C., Schulz, H., Ziesenis, A., Heinzmann, U., Schramel, P., Heyder, J. 2001. Pulmonary and systemic distribution of inhaled ultrafine silver particles in rats. Environ Health Perspect. 19(Supp4):547–551.

Tang, J., Xiong, L., Wang, S., Wang, J., Liu, L., Li, J., Yuan, F., Xi, T. 2009. Distribution, translocation and accumulation of silver nanoparticles in rats. J Nanosci Nanotechnol. 9(8):4924–32.

Tassinari, R., Cubadda, F., Moracci, G., Aureli, F., D'Amato, M., Valeri, M., De Berardis, B., Raggi, A., Mantovani, A., Passeri, D., Rossi, M. 2014. Oral, short-term exposure to titanium dioxide nanoparticles in Sprague-Dawley rat: focus on reproductive and endocrine systems and spleen. Nanotoxicology. 8(6):654–62.

Tavares, A.M., Louro, H., Antunes, S., Quarré, S., Simar, S., De Temmerman, P.J., Verleysen, E., Mast, J., Jensen, K.A., Norppa, H., Nesslany, F. 2014. Genotoxicity evaluation of nanosized titanium dioxide, synthetic amorphous silica and multi-walled carbon nanotubes in human lymphocytes. Toxicol In Vitro. 28(1):60–9.

Tay, C.Y., Cai, P., Setyawati, M.I., Fang, W., Tan, L.P., Hong, C.H., Chen X., Leong, D.T. 2013. Nanoparticles strengthen intracellular tension and retard cellular migration. Nano Lett. 14(1):83–8.

Taylor, A.J., McClure, C.D., Shipkowski, K.A., Thompson, E.A., Hussain, S., Garantziotis, S., Parsons, G.N., Bonner, J.C. 2014. Atomic layer deposition coating of carbon nanotubes with aluminum oxide alters pro-fibrogenic cytokine expression by human mononuclear phagocytes in vitro and reduces lung fibrosis in mice in vivo. PLoS ONE. 9(9):e106870.

Teeguarden, J.G., Hinderliter, P.M., Orr, G., Thrall, B.D., Pounds, J.G. 2007. Particokinetics in vitro: dosimetry considerations for in vitro nanoparticle toxicity assessments. Toxicol Sci.

95(2):300–12.

TERA (Toxicology Excellence for Risk Assessment). 2013. Report of a Letter Peer Review of CPSC's Toxicity Data and Assessment of Nanosilver, Nano Titanium Dioxide, and Carbon Nanotubes Document. Submitted to Consumer Product Safety Commission.

Thakur, M., Gupta, H., Singh, D., Mohanty, I.R., Maheswari, U., Vanage, G., Joshi, D.S. 2014. Histopathological and ultra structural effects of nanoparticles on rat testis following 90 days (Chronic study) of repeated oral administration. J Nanobiotechnol. 12(1):42.

Theodorou, I.G., Botelho, D., Schwander, S., Zhang, J., Chung, K.F., Tetley, T.D., Shaffer, M.S., Gow, A., Ryan, M.P., Porter, A.E. 2015. Static and dynamic microscopy of the chemical stability and aggregation state of silver nanowires in components of murine pulmonary surfactant. Environ Sci Technol. 49(13):8048–56.

Thiery, J.P. 2002. Epithelial–mesenchymal transitions in tumour progression. Nat Rev Cancer. 2(6):442–54.

Thompson, L.C., Frasier, C.R., Sloan, R.C., Mann, E.E., Harrison, B.S., Brown, J.M., Brown, D.A., Wingard, C.J. 2014. Pulmonary instillation of multi-walled carbon nanotubes promotes coronary vasoconstriction and exacerbates injury in isolated hearts. Nanotoxicology. 8(1):38–49.

Thongkam, W., Gerloff, K., van Berlo, D., Albrecht, C., & Schins, R.P. 2016. Oxidant generation, DNA damage and cytotoxicity by a panel of engineered nanomaterials in three different human epithelial cell lines. Mutagenesis. 32(1):105–15.

Tomankova, K., Horakova, J., Harvanova, M., Malina, L., Soukupova, J., Hradilova, S., Kejlova, K., Malohlava, J., Licman, L., Dvorakova, M.., Jirova, D. 2015. Cytotoxicity, cell uptake and microscopic analysis of titanium dioxide and silver nanoparticles in vitro. Food Chem Toxicol. 82:106–15.

Toyooka, T., Amano, T., Ibuki, Y. 2012. Titanium dioxide particles phosphorylate histone H2AX independent of ROS production. Mutat Res Genet Toxicol Environ Mutagen. 742(1):84–91.

Tran, C.L., Buchanan, D., Cullen, R.T., Searl, A., Jones, A.D., Donaldson, K. 2000. Inhalation of poorly soluble particles. II. Influence of particle surface area on inflammation and clearance. Inhal Toxicol. 12(12)1113–26.

Trickler, W.J., Lantz, S.M., Murdock, R.C., Schrand, A.M., Robinson, B.L., Newport, G.D., Schlager, J.J., Oldenburg, S.J., Paule, M.G., Slikker, Jr.W., Hussain, S.M. 2010. Silver nanoparticle induced blood-brain barrier inflammation and increased permeability in primary rat brain microvessel endothelial cells. Toxicol Sci. 118(1):160–70.

Trop, M., Novak, M., Rodl, S., Hellbom, B., Kroell, W., Goessler, W. 2006. Silver-coated

dressing acticoat caused raised liver enzymes and argyria-like symptoms in burn patient. J Trauma Acute Care Surg. 60(3):648–52.

Tulve, N.S., Stefaniak, A.B., Vance, M.E., Rogers, K., Mwilu, S., LeBouf, R.F., Schwegler-Berry, D., Willis, R., Thomas, T.A., Marr, L.C. 2015. Characterization of silver nanoparticles in selected consumer products and its relevance for predicting children's potential exposures. Int J Hyg Environ Health. 218(3):345–57.

Umeda, Y., Kasai, T., Saito, M., Kondo, H., Toya, T., Aiso, S., Okuda, H., Nishizawa, T., Fukushima, S. 2013. Two-week toxicity of multi-walled carbon nanotubes by whole-body inhalation exposure in rats. J Toxicol Pathol. 26(2):131–40.

U.S. EPA (United States Environmental Protection Agency). 1994. Methods for Derivation of Inhalation Reference Concentrations and Application of Inhalation Dosimetry. Environmental Criteria Assessment Office. Research Triangle Park, NC. EPA 600/8-90/066F.

U.S. EPA (United States Environmental Protection Agency). 2007. Nanotechnology White Paper. Science Policy Council. U.S. Environmental Protection Agency, Washington, DC. EPA 100/B-07/001.

U.S. EPA (United States Environmental Protection Agency). 2010a. Nanomaterial Case Studies: Nanoscale Titanium Dioxide in Water Treatment and in Topical Sunscreen. Office of Research and Development. U.S. Environmental Protection Agency, Research Triangle Park, NC. EPA/600/R-09/057F.

U.S. EPA (United States Environmental Protection Agency). 2010b. State of the Science Literature Review: Everything Nanosilver and More. U.S. Environmental Protection Agency Office of Research and Development Washington, DC 20460.

U.S. EPA (United States Environmental Protection Agency). 2017a. Integrated Risk Information System (IRIS). Chemical Assessment Summary for Silver (CASRN 7440-22-4). Oral Reference Dose (RfD) (last revised 12/01/1991). National Center for Environmental Assessment. Accessed 12/27/2017.

U.S. EPA (United States Environmental Protection Agency). 2017b. Integrated Risk Information System (IRIS). Chemical Assessment Summary for Silver (CASRN 7440-22-4). Carcinogenicity Assessment (last revised 06/01/1989). National Center for Environmental Assessment. Accessed 12/27/2017.

Ursini, C.L., Cavallo, D., Fresegna, A.M., Ciervo, A., Maiello, R., Buresti, G., Casciardi, S., Bellucci, S., Iavicoli, S. 2014. Differences in cytotoxic, genotoxic, and inflammatory response of bronchial and alveolar human lung epithelial cells to pristine and COOH-functionalized multiwalled carbon nanotubes. BioMed Res Int. 2014.

Ursini, C.L., Cavallo, D., Fresegna, A.M., Ciervo, A., Maiello, R., Buresti, G., Casciardi, S.,

Tombolini, F., Bellucci, S., Iavicoli, S. 2012a. Comparative cyto-genotoxicity assessment of functionalized and pristine multiwalled carbon nanotubes on human lung epithelial cells. Toxicol In Vitro. 26(6):831–40.

Ursini, C.L., Cavallo, D., Fresegna, A.M., Ciervo, A., Maiello, R., Casciardi, S., Tombolini, F., Buresti, G., Iavicoli, S. 2012b. Study of cytotoxic and genotoxic effects of hydroxyl-functionalized multiwalled carbon nanotubes on human pulmonary cells. J Nanomater. 2012:7.

Ursini, C.L., Maiello, R., Ciervo, A., Fresegna, A.M., Buresti, G., Superti, F., Marchetti, M., Iavicoli, S., Cavallo, D. 2016. Evaluation of uptake, cytotoxicity and inflammatory effects in respiratory cells exposed to pristine and-OH and-COOH functionalized multi-wall carbon nanotubes. J Appl Toxicol. 36(3):394–403.

USNNI (United States National Nanotechnology Initiative (2017). What's so Special about the Nanoscale? Available at: https://www.nano.gov/nanotech-101/special

Valdiglesias, V., Costa, C., Sharma, V., Kiliç, G., Pásaro, E., Teixeira, J.P., Dhawan, A., Laffon, B. 2013. Comparative study on effects of two different types of titanium dioxide nanoparticles on human neuronal cells. Food Chem Toxicol. 57:352–61.

van der Zande, M., Vandebriel, R.J., Van Doren, E., Kramer, E., Herrera Rivera, Z., Serrano-Rojero, C.S., Gremmer, E.R., Mast, J., Peters, R.J., Hollman, P.C., Hendriksen, P.J. 2012. Distribution, elimination, and toxicity of silver nanoparticles and silver ions in rats after 28-day oral exposure. ACS Nano. 6(8):7427–42.

van Ravenzwaay, B., Landsiedel, R., Fabian, E., Burkhardt, S., Strauss, V., Ma-Hock, L. 2009. Comparing fate and effects of three particles of different surface properties: nano-TiO 2, pigmentary TiO 2 and quartz. Toxicol Lett. 186(3):152–9.

Vance, M.E., Kuiken, T., Vejerano, E.P., McGinnis, S.P., Hochella Jr, M.F., Rejeski, D., Hull, M.S. 2015. Nanotechnology in the real world: Redeveloping the nanomaterial consumer products inventory. Beilstein J Nanotechnol. 6:1769–80.

Vecchio, G., Fenech, M., Pompa, P.P., Voelcker, N.H. 2014. Lab-on-a-Chip-Based High-Throughput Screening of the Genotoxicity of Engineered Nanomaterials. Small. 10(13):2721–34.

Versar Inc., 2012. Review of Toxicity Data and Assessment of Nanosilver, Nano Titanium Dioxide, and Carbon Nanotubes. Task Order 009 Final Report. Consumer Product Safety Commission, Bethesda, MD.

Vietti, G., Lison, D., van den Brule, S. 2016. Mechanisms of lung fibrosis induced by carbon nanotubes: towards an Adverse Outcome Pathway (AOP). Part Fibre Toxicol. 13(1):11.

Vippola, M., Falck, G.C.M., Lindberg, H.K., Suhonen, S., Vanhala, E., Norppa, H., Savolainen, K., Tossavainen, A., Tuomi, T. 2009. Preparation of nanoparticle dispersions for in-vitro toxicity

testing. Hum Exp Toxicol. 28(6-7):377–85.

Vlachou, E., Chipp, E., Shale, E., Wilson, Y.T., Papini, R., Moiemen, N.S. 2007. The safety of nanocrystalline silver dressings on burns: a study of systemic silver absorption. Burns. 33(8):979–85.

Vlasova, I.I., Sokolov, A.V., Chekanov, A.V., Kostevich, V.A., Vasilyev, V.B. 2011. Myeloperoxidase-induced biodegradation of single-walled carbon nanotubes is mediated by hypochlorite. Russ J Bioorg Chem. 37(4):453–63.

Völker, C., Oetken, M., Oehlmann, J. 2013. The biological effects and possible modes of action of nanosilver. In Reviews of Environmental Contamination and Toxicology. Vol 223(pp. 81-106). Springer New York.

von Goetz, N., Fabricius, L., Glaus, R., Weitbrecht, V., Günther, D., Hungerbühler, K. 2013. Migration of silver from commercial plastic food containers and implications for consumer exposure assessment. Food Addit Contam A. 30(3):612–20.

Wang, H., Wang, J., Deng, X., Sun, H., Shi, Z., Gu, Z., Liu, Y., Zhaoc, Y. 2004. Biodistribution of carbon single-wall carbon nanotubes in mice. J Nanosci Nanotechnol. 4(8):1019–24.

Wang, J., Che, B., Zhang, L.W., Dong, G., Luo, Q., Xin, L. 2017. Comparative genotoxicity of silver nanoparticles in human liver HepG2 and lung epithelial A549 cells. J Appl Toxicol. 37(4):495–501.

Wang, J., Chen, C., Liu, Y., Jiao, F., Li, W., Lao, F., Li, Y., Li, B., Ge, C., Zhou, G., Gao, Y. 2008a. Potential neurological lesion after nasal instillation of TiO 2 nanoparticles in the anatase and rutile crystal phases. Toxicol Lett. 183(1):72-80.

Wang, J., Liu, Y., Jiao, F., Lao, F., Li, W., Gu, Y., Li, Y., Ge, C., Zhou, G., Li, B., Zhao, Y. 2008b. Time-dependent translocation and potential impairment on central nervous system by intranasally instilled TiO 2 nanoparticles. Toxicology. 254(1):82-90.

Wang, J., Zhou, G., Chen, C., Yu, H., Wang, T., Ma, Y., Jia, G., Gao, Y., Li, B., Sun, J, Li, Y. 2007b. Acute toxicity and biodistribution of different sized titanium dioxide particles in mice after oral administration. Toxicol Lett. 168(2):176–85.

Wang, P., Nie, X., Wang, Y., Li, Y., Ge, C., Zhang, L., Wang, L., Bai, R., Chen, Z., Zhao, Y., Chen, C. 2013. Multiwall Carbon Nanotubes Mediate Macrophage Activation and Promote Pulmonary Fibrosis Through TGF-β/Smad Signaling Pathway. Small. 9(22):3799–811.

Wang, P., Wang, Y., Nie, X., Braïni, C., Bai, R., Chen, C. 2015a. Multiwall Carbon Nanotubes Directly Promote Fibroblast–Myofibroblast and Epithelial–Mesenchymal Transitions through the Activation of the TGF-β/Smad Signaling Pathway. Small. 11(4):446–55.

Wang, S., Hunter, L.A., Arslan, Z., Wilkerson, M.G., Wickliffe, J.K. 2011b. Chronic exposure to nanosized, anatase titanium dioxide is not cyto-or genotoxic to Chinese hamster ovary cells. Environ Mol Mutagen. 52(8):614–22.

Wang, W., Jiang, C., Zhu, L., Liang, N., Liu, X., Jia, J., Zhang, C., Zhai, S., Zhang, B. 2014. Adsorption of bisphenol A to a carbon nanotube reduced its endocrine disrupting effect in mice male offspring. Int J Mol Sci. 15(9):15981-93.

Wang, X., Deng, X.Y., Wang, H.F., Liu, Y.F., Wang, T.C., Gu, Y.Q., Jia, G. 2007a. Bio-effects of water-soluble taurine multi-wall carbon nanotubes on lungs of mice. Zhonghua Yu Fang Yi Xue Za. 41(2):85–90.

Wang, X., Katwa, P., Podila, R., Chen, P., Ke, P.C., Rao, A.M., Walters, D.M., Wingard, C.J., Brown, J.M. 2011a. Multi-walled carbon nanotube instillation impairs pulmonary function in C57BL/6 mice. Part Fibre Toxicol. 8(1):24.

Wang, X., Xia, T., Duch, M.C., Ji, Z., Zhang, H., Li, R., Sun, B., Lin, S., Meng, H., Liao, Y.P., Wang, M. 2012. Pluronic F108 coating decreases the lung fibrosis potential of multiwall carbon nanotubes by reducing lysosomal injury. Nano Lett. 12(6):3050–61.

Wang, X., Zang, J.J., Wang, H., Nie, H., Wang, T.C., Deng, X.Y., Gu, Y.Q., Liu, Z.H., Jia, G. 2010. Pulmonary toxicity in mice exposed to low and medium doses of water-soluble multi-walled carbon nanotubes. J Nanosci Nanotechnol. 10(12):8516–26.

Wang, Z., Xia, T., Liu, S. 2015b. Mechanisms of nanosilver-induced toxicological effects: more attention should be paid to its sublethal effects. Nanoscale. 7(17):7470–81.

Warheit, D.B., Boatman, R., Brown, S.C. 2015b. Developmental toxicity studies with 6 forms of titanium dioxide test materials (3 pigment-different grade & 3 nanoscale) demonstrate an absence of effects in orally-exposed rats. Regul Toxicol Pharmacol. 73(3):887–96.

Warheit, D.B., Brock, W.J., Lee, K.P., Webb, T.R., Reed, K.L. 2005. Comparative pulmonary toxicity inhalation and instillation studies with different TiO2 particle formulations: impact of surface treatments on particle toxicity. Toxicol Sci. 88(2):514–24.

Warheit, D.B., Brown, S.C., Donner, E.M. 2015a. Acute and subchronic oral toxicity studies in rats with nanoscale and pigment grade titanium dioxide particles. Food Chem Toxicol. 84:208–24.

Warheit, D.B., Laurence, B.R., Reed, K.L., Roach, D.H., Reynolds, G.A., Webb, T.R. 2004. Comparative pulmonary toxicity assessment of single-wall carbon nanotubes in rats. Toxicol Sci. 77(1):117–25.

Warheit, D.B., Webb, T.R., Reed, K.L., Frerichs, S., Sayes, C.M. 2007. Pulmonary toxicity study in rats with three forms of ultrafine-TiO 2 particles: differential responses related to surface

properties. Toxicology. 230(1):90–104.

Waris, G., Ahsan, H. 2006. Reactive oxygen species: role in the development of cancer and various chronic conditions. J Carcinog. 5(1):14.

Weir, A., Westerhoff, P., Fabricius, L., Hristovski, K., Von Goetz, N. 2012. Titanium dioxide nanoparticles in food and personal care products. Environ Sci Technol. 46(4):2242–50.

Wen, R., Yang, X., Hu, L., Sun, C., Zhou, Q., Jiang, G. 2016. Brain-targeted distribution and high retention of silver by chronic intranasal instillation of silver nanoparticles and ions in Sprague–Dawley rats. J Appl Toxicol. 36(3):445–53.

Wijnhoven, S.W.P., Dekkers, S., Hagens, W.I., De Jong, W.H. 2009. Exposure to nanomaterials in consumer products. RIVM letter report. 340370001/2009.

Williams, K., Milner, J., Boudreau, M.D., Gokulan, K., Cerniglia, C.E., Khare, S. 2015. Effects of subchronic exposure of silver nanoparticles on intestinal microbiota and gut-associated immune responses in the ileum of Sprague-Dawley rats. Nanotoxicology. 9(3):279–89.

Williams, M. 2012. Ions, not particles, make silver toxic to bacteria. Rice University. Available at: http://news.rice.edu/2012/07/11/ions-not-particles-make-silver-toxic-to-bacteria-3/

Wilson, M.S., Madala, S.K., Ramalingam, T.R., Gochuico, B.R., Rosas, I.O., Cheever, A.W., Wynn, T.A. 2010. Bleomycin and IL-1β–mediated pulmonary fibrosis is IL-17A dependent. J Exp Med. 207(3):535–52.

Windler, L., Lorenz, C., Von Goetz, N., Hungerbuhler, K., Amberg, M., Heuberger, M., Nowack, B. 2012. Release of titanium dioxide from textiles during washing. Environ Sci Technol. 46(15):8181–8.

Winkler, J .2003. Titanium Dioxide. Hannover: Vincentz Network. pp. 5. ISBN 3-87870-148-9.

Wohlleben, W., Meyer, J., Muller, J., Müller, P., Vilsmeier, K., Stahlmecke, B., Kuhlbusch, T.A. 2016. Release from nanomaterials during their use phase: combined mechanical and chemical stresses applied to simple and multi-filler nanocomposites mimicking wear of nano-reinforced tires. Environ Sci Nano. 3(5):1036–51.

Wohlleben, W., Meier, M.W., Vogel, S., Landsiedel, R., Cox, G., Hirth, S., Tomović, Ž. 2013. Elastic CNT–polyurethane nanocomposite: synthesis, performance and assessment of fragments released during use. Nanoscale. 5(1):369–80.

Wohlleben, W., Neubauer, N. 2016. Quantitative rates of release from weathered nanocomposites are determined across 5 orders of magnitude by the matrix, modulated by the embedded nanomaterial. NanoImpact. 1:39–45.

Wong, K.K., Liu, X. 2010. Silver nanoparticles—the real “silver bullet” in clinical medicine? MedChemComm. 1(2):125–31.

Woodruff, R.S., Li, Y., Yan, J., Bishop, M., Jones, M.Y., Watanabe, F., Biris, A.S., Rice, P., Zhou, T., Chen, T. 2012. Genotoxicity evaluation of titanium dioxide nanoparticles using the Ames test and Comet assay. J Appl Toxicol. 32(11):934–43.

Wu, J., Liu, W., Xue, C., Zhou, S., Lan, F., Bi, L., Xu, H., Yang, X., Zeng, F.D. 2009. Toxicity and penetration of TiO 2 nanoparticles in hairless mice and porcine skin after subchronic dermal exposure. Toxicol Lett. 191(1):1-8.

Xie, G., Lu, W., Lu, D. 2015. Penetration of titanium dioxide nanoparticles through slightly damaged skin in vitro and in vivo. J Appl Biomater Funct Mater. 13(4).

Xu, J., Alexander, D.B., Futakuchi, M., Numano, T., Fukamachi, K., Suzui, M., Omori, T., Kanno, J., Hirose, A., Tsuda, H. 2014. Size-and shape-dependent pleural translocation, deposition, fibrogenesis, and mesothelial proliferation by multiwalled carbon nanotubes. Cancer Sci. 105(7):763–9.

Xu, J., Shi, H., Ruth, M., Yu, H., Lazar, L., Zou, B., Yang, C., Wu, A., Zhao, J. 2013. Acute toxicity of intravenously administered titanium dioxide nanoparticles in mice. PLoS ONE. 8(8):e70618.

Xue, Y., Zhang, S., Huang, Y., Zhang, T., Liu, X., Hu, Y., Zhang Z., Tang, M. 2012. Acute toxic effects and gender-related biokinetics of silver nanoparticles following an intravenous injection in mice. J Appl Toxicol. 32(11):890–9.

Yang, P., Lu, C., Hua, N., Du, Y. 2002. Titanium dioxide nanoparticles co-doped with Fe 3+ and Eu 3+ ions for photocatalysis. Mater Lett. 57(4):794–801.

Yang, X., Gondikas, A.P., Marinakos, S.M., Auffan, M., Liu, J., Hsu-Kim, H., Meyer, J.N. 2012. Mechanism of silver nanoparticle toxicity is dependent on dissolved silver and surface coating in Caenorhabditis elegans. Environ Sci Technol. 46(2):1119–27.

Yu, K.N., Kim, J.E., Seo, H.W., Chae, C., Cho, M.H. 2013. Differential toxic responses between pristine and functionalized multiwall nanotubes involve induction of autophagy accumulation in murine lung. J Toxicol Environ Health Part A. 76(23):1282–92.

Yu, W.J., Son, J.M., Lee, J., Kim, S.H., Lee, I.C., Baek, H.S., Shin, I.S., Moon, C., Kim, S.H., Kim, J.C. 2014. Effects of silver nanoparticles on pregnant dams and embryo-fetal development in rats. Nanotoxicology. 8(Supp1):85–91.

Zhang, A.P., Sun, Y.P. 2004. Photocatalytic killing effect of TiO2 nanoparticles on Ls-174-t human colon carcinoma cells. World J Gastroenterol. 10(21):3191–93.

Zhang, Q., Zhou, H., Yan, B. 2010. Reducing nanotube cytotoxicity using a nano-combinatorial library approach. Methods Mol Biol. 625:95–107.

Zhang, X.F., Liu, Z.G., Shen, W., Gurunathan, S. 2016. Silver nanoparticles: synthesis, characterization, properties, applications, and therapeutic approaches. Int J Mol Sci. 17(9):1534.

Zhang, X.F., Park, J.H., Choi, Y.J., Kang, M.H., Gurunathan, S., Kim, J.H. 2015. Silver nanoparticles cause complications in pregnant mice. Int J Nanomed. 10:7057–71.

Zhao, X., Ze, Y., Gao, G., Sang, X., Li, B., Gui, S., Sheng, L., Sun, Q., Cheng, J., Cheng, Z., Hu, R. 2013. Nanosized TiO2-induced reproductive system dysfunction and its mechanism in female mice. PLoS ONE. 8(4):e59378.

Zhao, Y., Allen, B.L., Star, A. 2011. Enzymatic degradation of multiwalled carbon nanotubes. J Phys Chem A. 115(34):9536–44.

Zhao, Z., Liu, M., Jia, X., Wang, H., Liu, Z., Zhang, J., Sun, L., Zhang, M. 2014. Toxicity Effect of Carbon Nanotubes. Nano LIFE. 4(3):1441009.

Zook, J.M., Halter, M.D., Cleveland, D., Long, S.E. 2012. Disentangling the effects of polymer coatings on silver nanoparticle agglomeration, dissolution, and toxicity to determine mechanisms of nanotoxicity. J Nanopart Res. 14(10):1165.

TERA

INDEPENDENT
NON-PROFIT
SCIENCE
FOR PUBLIC HEALTH PROTECTION

Literature Review on Nanomaterials – Carbon Nanotubes, Nano Silver, and Nano Titanium Dioxide

Appendices

Task Order 20
Contract Number
CPSC-D-12-0001

6/29/18
FINAL REPORT
Volume 2

Prepared by:
Toxicology Excellence for Risk Assessment (TERA):

Authors:
Patricia M. McGinnis
Julie A. Skare
Raymond G. York
Evan A. Frank
Chijioke G. Onyema
Michael L. Dourson

Contact:
Patricia McGinnis mcginnis@tera.org

CONTENTS

Appendix A*

LIST OF TIER 2 SECONDARY WEBSITES

*References for Appendices are located in Section 7 of Volume 1 report. Abbreviations for Appendices are located in Abbreviation list, Volume 1 report.

Table A-1. Tier 2 Secondary Authoritative Sources (Websites)

Secondary Authoritative References[a,b]		
Country	**Office**	**Website (n = 32)**
Australia	Dept. of Health	http://www.nicnas.gov.au/home
	NICNAS	http://www.nicnas.gov.au/industry/aics/search.asp
Canada	Canadian Centre for Occupational Health and Safety - RTECS	http://www.ccohs.ca/search.html
	Environment Canada	http://www.ec.gc.ca/default.asp?lang=En&n=ECD35C36
	Health Canada	http://www.hc-sc.gc.ca/index-eng.php
	Health Canada First Priority List Assesssments	http://www.hc-sc.gc.ca/ewh-semt/pubs/contaminants/psl1-lsp1/index-eng.php
	Health Canada Second Priority List Assesssments	http://www.hc-sc.gc.ca/ewh-semt/pubs/contaminants/psl2-lsp2/index-eng.php
	Risk Management Reports - Final Assessments	http://www.ec.gc.ca/lcpe-cepa/default.asp?lang=En&xml=09F567A7-B1EE-1FEE-73DB-8AE6C1EB7658
Europe	ECHA	http://echa.europa.eu/
	ECHA	http://echa.europa.eu/en/search?p_p_id=echasearch_WAR_echaportlet&p_p_lifecycle=0&p_p_state=normal&p_p_mode=view&p_p_col_id=column-
	REACH Database	http://echa.europa.eu/information-on-chemicals
	EFSA	http://www.efsa.europa.eu/en/press/news/170118-0
Denmark	Danish EPA	http://eng.mst.dk/topics/chemicals/consumers--consumer-products/danish-surveys-on-consumer-products/
United States	ACGIH	http://www.acgih.org/
	CPSC	http://www.cpsc.gov/
	Federal Docket	http://www.regulations.gov/#!home
	NNI	https://www.nano.gov/
	OSHA	https://www.osha.gov/dts/chemicalsampling/toc/toc_chemsamp.html
U.S. NIH	HSDB	http://toxnet.nlm.nih.gov/newtoxnet/hsdb.htm
	NTP	http://ntp.niehs.nih.gov/index.cfm
U.S. CalEPA	Draft Assessments	http://www.ec.gc.ca/lcpe-cepa/default.asp?lang=En&xml=6892C255-5597-C162-95FC-4B905320F8C9
	OEHHA	http://www.oehha.ca.gov/
	OEHHA Toxicity Criteria Database	http://www.oehha.ca.gov/tcdb/index.asp
	Office of Environmental Health Hazard Assessment	http://www.oehha.ca.gov/risk.html
	Toxic Substances Managed under CalEPA	http://www.ec.gc.ca/toxiques-toxics/Default.asp?lang=En&n=98E80CC6-1
U.S. CDC	ATSDR	http://www.atsdr.cdc.gov/substances/index.asp

Secondary Authoritative References[a,b]		
	NIOSH	http://www.cdc.gov/niosh/topics/
U.S. EPA	EPA Science Inventory	http://cfpub.epa.gov/si/
	IRIS Track/New Assessments & Reviews/NSCEP	http://www.epa.gov/ncepihom/
	National Service Center for Environmental Publications (NSCEP)	http://www.epa.gov/nscep/
U.S. HHS	U.S. FDA	https://www.fda.gov/
WHO	IARC	http://monographs.iarc.fr/ENG/Monographs/PDFs/index.php

[a]NICNAS – National Industrial Chemicals Notification and Assessment Scheme; RTECS – Registry of Toxic Effects of Chemical Substances; ECHA – European Chemicals Agency; EFSA – European Food Safety Authority; Danish EPA - Danish Environmental Protection Agency; ACGIH – American Conference of Governmental Industrial Hygienists; CPSC – Consumer Product Safety Commission; NNI – National Nanotechnology Initiative; OSHA – Occupational Safety and Health Administration; HSDB – Hazardous Substances Data Bank; NIH – National Institutes of Health; NTP – National Toxicology Program; CalEPA – California Environmental Protection Agency; OEHHA – Office of Environmental Health Hazard Assessment; CEPA – Canadian Environmental Protection Act; U.S. CDC – U.S. Center for Disease Control; ATSDR – Agency for Toxic Substances and Disease Registry; NIOSH – National Institute for Occupational Safety and Health; U.S. EPA – U.S. Environmental Protection Agency; IRIS – Integrated Risk Information System; NSCEP – National Service Center for Environmental Publications; U.S. HHS – U.S. Department of Health and Human Services; U.S. FDA – U.S. Food and Drug Administration; WHO – World Health Organization; IARC – International Agency for Research on Cancer

[b]Shaded sites (n=10) indicate the sites for which the search results were similar/same to the ones obtained from the website immediately above them.

Appendix B*

IT OR OPA SWCNT STUDIES

*References for Appendices are located in Section 7 of Volume 1 report. Abbreviations for Appendices are located in Abbreviation list, Volume 1 report.

Table B-1. Toxicity of SWCNTs via Intratracheal Instillation (IT) and Oropharyngeal Aspiration (OPA)[a]

Animal (species, strain, sex, group size)	Exposure	Endpoints examined	Nanotube description[c]	Results	Notes	Reference
Intratracheal instillation						
Male Crl:CD rats (8 wks old, 240–255 g), group size not specified	0, 1, or 5 mg/kg	Survival, lung weights, BALF analysis and lung pathology at 24 h, 1 wk, and 3 mo post-instillation	SWCNTs (5% Ni, 5% Co), referred to as "soot", 30 nm dia (usually existing as agglomerated ropes)[b]	Significant increases in lung wt at high dose up to 1 mo, but comparable to controls by 3 mo. BALF analysis revealed transient inflammatory and cell injury effects. Non-dose dependent multifocal granuloma formation, not progressive beyond 1 mo post-instillation.	15% mortality at high dose may be due to treatment rather than toxicity.	Warheit et al., 2004[b]
Male B6C3F1 mice (8 wks old), 9/group	0, 0.1, or 0.5 mg (estimated doses of 0, 3, or 17 mg/kg based on average body weight of 30 g)	Clinical signs, survival, and lung pathology at 7 and 90d post-instillation	Three SWCNTs with varying metal contents were tested: I: 0.53% Fe, 26% Ni, 5% Y; II: 26.9% Fe, 0.78% Ni, 0% Y III: 2.14% Fe, 0% Ni, 0% Y. Length and size distributions were not reported.[b]	Test compound I caused mortality at high dose (5/9) that occurred between d4 and 7, preceded by lethargy, inactivity, and bw loss. II and III caused no deaths. All SWCNT forms caused time- and dose-related increase in pulmonary granulomas and interstitial inflammation. These lesions were detected at 7d and persisted through 90d (more pronounced at 90d).	IT with carbon black at equivalent doses caused no deaths and no granulomas or inflammation in lung tissue.	Lam et al., 2004[b]
Male C57BL/6 mice (8–12 wks old), group size not reported	0, 10, or 40 μg/mouse (approximately 0, 0.4, or 1.8 mg/kg based on an average bw of 22.5 g)	BALF analysis, histology of the trachea, lungs and heart at 30 and 90d post-instillation	Dispersed SWCNTs or aggregated SWCNTs (8.5% Fe), 1 to 2 nm dia, 100 to 2,000 nm length[b]	Mild increases in lung collagen and granulomas and mild fibrosis in the large airways of mice treated with aggregated SWCNTs; these changes not observed in mice treated with dispersed SWCNTs.	Aggregates observed in the mid- to small-sized airways following exposure to aggregated SWCNTs; uptake of dispersed SWCNTs by macrophages with gradual clearance over time.	Mutlu et al., 2010[b]

Animal (species, strain, sex, group size)	Exposure	Endpoints examined	Nanotube description[c]	Results	Notes	Reference
Rats, sex and strain not specified, 3–4/group (only one control rat per observation time point)	0, 0.4, 2, or 4 mg/kg	Body weights, MRI image analysis of lungs, and lung pathology at 1, 7, 30, and 90d post-instillation	SWCNTs (10% Fe), size characteristics not reported[b]	No effect on weight gain, alveolar thickening at 7d post-instillation accompanied by cell infiltration, multifocal granulomatous lesions containing macrophages, lymphocytes, fibroblasts, and collagen deposition formed around the sites of SWCNT deposition by 30d, similar changes observed at 90d with membrane thickening and alveolar collapse.	Although sonication and albumin were used to obtain a homogenous distribution, SWCNTs tended to aggregate into clumps in bronchioles and alveoli.	Al Faraj et al., 2010[b]
Apolipoprotein E knockout mice (ApoE-/-) Sex and number of animals not reported	0 or 54 μg (estimated dose of 2 mg/kg assuming bw of 30 g)	Protein concentration in BALF, mRNA cytokine expression at 3 and 24 h post-instillation	SWCNTs, data on purity and size could not be obtained[b]	Significant increases in total protein in BALF indicative of lung cell injury and significant increases in IL-6 and monocyte chemoattractant protein-1 (Mcp-1) messenger ribonumcleic acid (mRNA) at 3 and 24 h		Jacobsen et al., 2009[b]
Male ICR mice (6 wks old), 20–25/group	4 mg/kg alone or following exposure to lipoolysaccharide (LPS)	BALF analysis and lung pathology at 24 h post-instillation	SWCNTs, 1.2 to 1.4 nm dia, 2 to 5 μm length[b]	SWCNTs significantly increased the number of neutrophils, total cells and protein levels in BALF and lung wt. Moderate infiltration of neutrophils in lungs. Chemokines and coagulatory parameters were significantly elevated.	Purity not reported; moderate enhancement of effects by LPS.	Inoue et al., 2008[b]
ICR mice, sex and group size not specified	0 or 0.5 mg/kg	Inflammatory responses evaluated at 3 and 14d post-instillation	SWCNTs characteristics not specified[b]	At 3d, foamy-like macrophages loaded with SWCNTs accumulated in alveoli to give rise to multifocal macrophage-containing granulomas around the sites of SWCNT aggregation by 14d.		Chou et al., 2008[b]

Animal (species, strain, sex, group size)	Exposure	Endpoints examined	Nanotube description[c]	Results	Notes	Reference
Male Sprague-Dawley rats, 6 /group	0.04, 0.2, or 1.0 mg/kg bw	BALF analyses and histology of trachea, lung, liver, kidney, spleen, and cerebrum taken 3, 7, 28, 91, or 182 d post-exposure.	Nat'l Institute of Advanced Industrial Science and Technology, Japan; 3.0 ± 1.1 nm dia., <1200 µm length; 1064 ± 37 m^2/g surface area; 99.95% pure; dispersed with Tween-80 as bundles 12.0 ± 6.5 nm dia.	SWCNT increased BALF cells at 0.2 mg/kg-bw and above. In lung histology, all doses caused macrophage accumulation and granuloma was seen at 1.0 mg/kg bw and higher. Alveolar epithelial hypertrophy was seen at 2.0 mg/kg bw.		Kobayashi et al., 2011
Male ICR mice, number per group not specified	0, 0.3, 1.5, 3, 15, 30, 100, or 500 µg	Airway hyperresponsiveness by methacholine challenge 7d post-exposure	CarboLex, Inc.; ~1.3 nm dia.; surface area not given; >95% purity; morphology not given.	Exposure to 100 or 500 µg caused increased airway resistance at 7d		Hsieh et al., 2012
Male ICR mice, 20/group	0, 50, 100, or 200 µg/kg bw	Hematology, blood biochemistry, BALF analyses, lung histology, and immunophenotyping of splenocytes was performed 90 d post-exposure	Hanwha Nanotech; dimensions not given; surface area not given; 15.2% Zn,3.5% Al, 2.6% Fe, 2.3% Co, 0.8% Ni, 0.5% Cu; Dispersed as fibers, ropes, and bundles using Pluronic F127 and "Gamble's solution" (not clear what was used in exposures)	All doses increased BALF cells and various cytokines, mostly skewed toward a Th1 immune response. Apoptosis in BALF cells was increased in all treatment groups. Lung pathology was not different between control and exposed groups but vehicle-treated lungs showed mild/moderate foamy macrophage accumulation and alveolar cell hyperplasia. BUN, glucose, lactate, alanine, creatine, and scyllo-insulin were decreased in the 200 µg/kg bw group, while acetate, 3-HB, acetoacetate, low-density lipoprotein (LDL), glycerophoshocholine (GPC), and lipids increased.		Park et al., 2016

Oropharyngeal Aspiration						
Female C57BL/6 mice (8–10 wks old at exposure), 12/group	0, 5, 10, or 20 µg/mouse suspended in phosphate buffered saline (PBS). Average bw of 20.0 g. Calculated doses were ~0, 0.25, 0.5, or 1.0 mg/kg.	Pulmonary inflammation assessed (BALF analysis, lung homogenates analysis for collagen, and lung histopathology) in mice killed on 1, 7, and 28d post-exposure.	SWCNTs had 82% elemental carbon and 17.7% Fe. The dia was 0.8 to 1.2 nm and length was 100 to 1,000 nm[b] Surface area and morphology not reported. SWCNTs were not processed (i.e., acid treated) to remove metal contaminants[b]	Significant dose-related inflammatory response was detected at 1d and appeared to be maximal at this time. Inflammation persisted at the 7 and 28d time points.	Comparison of aspiration vs. inhalation exposure showed that the inhalation was more potent than aspiration of an equivalent mass of SWCNTs.	Shvedova et al., 2008[b]
Female F344 rats (6 wks old) (number not specified)	0 or 2 mg/kg suspended in 0.1% Pluronic F-68 in PBS.	Lung histopathology, cell proliferation, and growth factor mRNA evaluated at 1 and 21d after exposure.	SWCNT particles had external dias of <2 nm, and 0.5 to 40 µm length. Purity was >90%.[b] Metal concentrations, surface area, and morphology not reported.[b]	SWCNTs caused no overt inflammatory response at 1 or 21d, but induced focal interstitial fibrosis in the alveolar region of the lung at 21d. SWCNTs also induced formation of unique carbon bridge structures between macrophages *in situ*.	The carbon bridge structures linking macrophages could serve as biomarkers of SWCNT exposure.	Mangum et al., 2006[b]
Male C57BL/6 mice (25 wks old at time of exposure), 6/group	0 or 10 µg/mouse of dispersed SWCNT in PBS. Average bw were not reported. Assuming a body weight of 0.02 kg, a dose of 0.5 mg/kg is calculated.[b]	Initial deposition pattern, inflammatory response, chronic fibrotic response, fate of the CNTs, connective tissue, and alveolar responses were evaluated at 1 hr and 1, 7, and 30d after aspiration.	Dispersed SWCNTs prepared from purified SWCNTs with <2% contaminants; mean dia was 0.69 µm.[b] Length, surface area, and morphology were not given.	Electron microscopy showed highly dispersed, interstitial distribution of dispersed SWCNT deposits on 1 d. Macrophage phagocytosis of dispersed SWCNTs was rarely observed. Lung sections and lavage cells showed early transient inflammation that resolved by 30d (dispersed SWCNTs). Granulomas apparent at 7 and 30d with nondispersed, but not with dispersed SWCNTs. Thickness of connective tissue in alveolar regions progressively increased between 1 and 30d.	Dispersed SWCNTs caused more interstitial collagen accumulation (evidence of fibrosis) than nondispersed SWCNTs. Dispersed SWCNTs caused pulmonary inflammation and interstitial fibrosis, but no granulomas.	Mercer et al., 2008[b]

Male C57BL/6 mice (10 wks old at time of exposure) Group size not given	40 µg SWCNTs dispersed in 0.3 mg/mL mouse serum albumin and 5 µg/mL 1,2-DPPC. Average bw were not reported.	Mice sacrificed 4 hrs postexposure. Blood collected for antigen analysis and whole blood gene expression. Gene expression changes in lung, aorta, and blood measured with a microarray including genes involved in inflammation (37%), oxidative stress (21%), growth factors (17%), tissue remodeling (12%), endothelial function (8%), and coagulation (5%).	SWCNTs with 8.8% iron content; 0.8 to 1.2 nm dia; 0.1 to 1 µm in length.[b]	Numbers of genes upregulated in lung by MWCNT was greater than the number upregulated by SWCNTs; both types upregulated genes involved in coding mediators of inflammation, oxidative stress, remodeling, and thrombosis. Upregulation of genes involved in inflammation and coagulation found in blood. Also, activation of inflammatory genes in aorta, heart, liver, and kidney.	CNT induced activation of an endothelial specific cell adhesion molecule ("E-selectin") in aorta that facilitates recruitment of leukocytes into the vessel wall. All genes upregulated in blood and aorta were confirmed by RT-PCR.	Erdely et al., 2009[b]

[a]Instillations and aspirations are administered as a single bolus dose, unless otherwise specified.
[b]As reported in Versar (2012)
[c] NT characterization data are stated, if reported: source, diameter and length, surface area, purity and impurities, and state of aggregation; shape (bundles, tangles, ropes)

Appendix C*

IT OR OPA MWCNT STUDIES

*References for Appendices are located in Section 7 of Volume 1 report. Abbreviations for Appendices are located in Abbreviation list, Volume 1 report.

Table C-1. Summary of Dose-response Studies of Animals exposed to MWCNTs by IT and OPA[a]

Animal (gender, strain, group size)	Exposure	Endpoints examined	Nanotube description[c]	Results	Notes	Reference
Intratracheal instillation						
Female Sprague-Dawley rats (200–250 g) group size not specified	0, 0.5, 2, or 5 mg (estimated doses of 0, 2.2, 8.9, or 22 mg/kg based on an average bw of 225 g)	BALF analysis at 3 and 15 d post-instillation, soluble collagen and hydroxyproline (HYP) levels and lung pathology at 60 d post-instillation	Intact MWCNTs (97.8% pure), 5.2 nm inner dia, 9.7 nm outer dia, 5.9 μm length; or, ground MWCNTs (98% pure), 5.1 nm inner dia, 11.3 nm outer diameter, 0.7 μm length[b]	Dose-related increase in LDH release, which was more marked with ground MWCNTs, increased total protein levels in BALF, accumulation of granulocytes, neutrophils, and eosinophils at both time points. Significant elevation HYP and collagen at the highest dose. Collagen-rich granulomas in the bronchi which blocked, partially or completely, the bronchial lumen. Ground MWCNTs exhibited greater dispersal in the parenchyma and induced granulomas in the interstitial tissue. Significant increases in TNF-α at 9 mg/kg for intact MWCNTs and at 2 and 9 mg/kg for ground MWCNTs.	The fibrotic response induced by 22 mg/kg of ground MWCNTs was equivalent to that induced by 9 mg/kg intact MWCNTs.	Muller et al., 2005[b]
Male Sprague-Dawley rats (180–220 g), 6/group	0, 1, 10, or 100 μg dispersed (estimated doses of 0, 0.005, 0.05, or 0.5 mg/kg based on an average bw of 200 g)	Body weights, plethysmography, collagen deposition, cytokine expression, and lung pathology at 1, 7, 30, 90, and 180 post-instillation	MWCNTs, 20 to 50 nm dia, 0.5–2 μm length, purity not reported[b]	No effect on bw or plethysmography parameters, increase in total numbers of alveolar cells at 100 μg at 7 and 180 d, no significant pathological changes in the lungs, apoptosis of alveolar macrophages after 30, 90, and 180 d with 100 μg and after 30 and 90 d with 10 μg, significant induction of caspase 3 protein at 100 μg	Phagocytosis of CNT agglomerate was also observed by alveolar macrophages.	Elgrabli et al., 2008[b]
Male ICR mice (6 wks old, 28–33 g), 20–25/group	4 mg/kg MWCNTs alone or following exposure to LPS	BALF analysis and lung pathology at 24 h post-instillation	MWCNTs, 2 to 20 nm dia, 100 nm to several micrometers length[b]	MWCNTs significantly increased lung weight and the number of neutrophils in BALF. Moderate infiltration of neutrophils in lungs. Chemokines and coagulatory parameters were significantly elevated. The level of MCP-1 was significantly increased by MWCNTs	Purity not reported; moderate enhancement of effects by LPS. This was a comparison study with SWCNTs (see Inoue et al., 2008 results in Appendix B))	Inoue et al., 2008[b]

Animal (gender, strain, group size)	Exposure	Endpoints examined	Nanotube description[c]	Results	Notes	Reference
Male Kunming mice (7 wks old, 30 g), 18/group	0, 6.67, 2.67, or 9.34 mg/kg of PBS, MWCNTs, benzene, or MWCNT-benzene combination, respectively	BALF analysis and lung pathology at 3 and 7 d post-instillation	MWCNTs (>95% pure, 1.25% Ni, 0.07% Fe, 0.01% Co, 0.005% Cu), 50 nm dia, 5 to 15 μm length[b]	Significant dose-related increase of total protein and LDH in BALF, and slight increase in ALP and acid phosphatase (ACP) in BALF at 3-d, but no obvious changes in BALF at 7 d. At 3 d, inflammatory cells surrounded the MWCNT aggregations in the alveolar area and the alveolar netted structure was destroyed. At 7 d, the alveolar netted structure around MWCNT aggregations was almost integrated. MWCNT aggregations adsorbed to inner wall of bronchi at 3 d and some thinner bronchi were almost blocked; quantity of aggregations significantly decreased by 7 d.	Benzene alone did not induce pulmonary toxicity, but enhanced MWCNT toxicity.	Li et al., 2009[b]
Male ICR mice, 10–12/group	0, 5, 20, or 50 mg/kg	BALF analysis, cytokine analysis and immunophenotyping on splenocytes, and lung pathology at 1, 3, 7, and 14 d	MWCNTs (>90% pure), 110 to 170 nm outer dia, 5 to 9 μm length[b]	Significant increase in the total numbers of immune cells in BALF at all doses and increased distribution of neutrophils at all time points. Dose-related increase in pro-inflammatory cytokines (IL-1, TNF-α, IL-6, IL-4, IL-5, IL-10, IL-12, and IFN-γ) in BALF and in blood (highest levels at d 1 post-instillation decreasing with time). Increased distribution of B cells in spleen and blood. Dose-related increase in granuloma formation in lungs that peaked at 3 d, persisting through to 14 d.	MWCNT found in the bronchiole and alveoli at d 1; number of MWCNTs in fibrous tissues decreased slightly with time; some MWCNTs found in the cytoplasm of alveolar macrophages, in the alveolar epithelial cells and interstitium of the alveoli.	Park et al., 2009[b]

Animal (gender, strain, group size)	Exposure	Endpoints examined	Nanotube description[c]	Results	Notes	Reference
Male Wistar albino rats, (8 wks old, 200–225 g) group size not specified	0.2, 1, or 5 mg/kg (controls not reported)	Serum biochemistry and histopathology of liver, kidney, and heart at 24 h, 1 wk, 1 mo, and 3 mo post-instillation	MWCNT produced by chemical vapor deposition, 60 to 80 nm dia; or, MWCNT produced by electric arc, 90 to 150 nm dia; both well-dispersed in PBS+Tween 80 solution[b]	Liver: dose-related increase in serum alanine aminotransferase (ALT) activities (significant increases at ≥1 mg/kg at all time points), dose-related periportal lymphocytic infiltration, congestion of sinusoids, and hemorrhage; ballooning foamy degeneration of hepatocytes, fatty changes, focal inflammation, and necrosis at all post-installation time periods. Kidney: dose-related increase in creatinine levels (significant increases at 5 mg/kg at 1 mo post-installation), "significant" tubular necrosis and interstitial nephritis with 5 mg/kg at 1 mo post-installation Heart: No significant pathological changes	Purity of MWCNTs and metal content were not reported. Histopathology findings were presented qualitatively with representative photomicrographs. Incidence data and severity scores not presented. Apparently, no controls.	Reddy et al., 2010[b]
Male CD-1 mice, (4 wks old), 10/group	0, 1, 2.5, or 5 mg/kg in PBS	Gross and microscopic evaluation of lung, heart, liver, spleen, and intestines, at 24 h, 48 h, 72 h, 7 d, and 30 d post treatment and serum biochemistry 1 d prior to sacrifice	Acid-functionalized MWCNT, 2–2.5% Fe, dia up to 50 nm, length up to 450 µm. Acid treatment conferred dispersability in PBS, and reported to introduce hydrophilic hydroxyl, carboxyl, and sulfate groups.[b]	Mortality (30, 60, and 90% at 1, 2.5, and 5 mg/kg, respectively), signs of pulmonary distress (dyspnea) in dead mice; time and dose-dependent increases in lung changes: granulomas in the lung interstitium and goblet cell hyperplasia, granulomatous inflammatory reaction in lumen of the bronchi, atypical hyperplasia of bronchiolar epithelium	Lung deposition observed at all doses, with level of deposition proportional to dose; clumps of MWCNTs observed in bronchi, aggregates observed to have broken the bronchiolar wall and infiltrated interstitium.	Carrero-Sanchez et al. 2006[b]

Animal (gender, strain, group size)	Exposure	Endpoints examined	Nanotube description[c]	Results	Notes	Reference
Male CD-1 mice (4 wks old), 10/group	0, 1, 2.5, or 5 mg/kg in PBS	Gross and microscopic evaluation of lung, heart, liver, spleen, and intestines, at 24 h, 48 h, 72 h, 7 d, and 30 d post treatment and serum biochemistry 1 d prior to sacrifice.	Nitrogen-doped, acid functionalized MWCNTs, 2–4% nitrogen, 2–2.5% Fe, 20–40 nm dia, 100–300 μm length. Pristine MWCNTs treated to introduce N atoms into the hexagonal carbon network, either as pyridine-type N (each N bound to two C atoms) or as substitutional N (each N atom bound to three C atoms). These were then acid treated before instillation into mice.[b]	No mortality; no effect on bw, external appearance, or behavior; no significant histological changes in heart, liver, spleen, or intestines; high-dose mice exhibited a time-dependent increase in lung inflammation (cuboidal or flattened epithelial cells, absence of epithelial cells in bronchiolar wall), lung lesions (extensive papillomatous hyperplasia with hyperchromatic nuclei and pleomorphic cells), and granulomatous reaction containing macrophages, lymphocytes, fibroblasts, and collagen deposition (also abundant in the peribronchiolar interstitium), hyperplastic lymph nodes (without deposition), reactive fibrosis in the peribronchiolar interstitium.	Lung deposition observed at ≥2.5 mg/kg, small aggregates in bronchioles. N-doped MWCNTs did not cause the acute lethality observed with acid functionalized MWCNTs at the same dose levels. Pulmonary responses to MWCNTs were more severe than responses to N-doped MWCNTs.	Carrero-Sanchez et al., 2006[b]
Kunming mice, 5/group (sex not specified)	0, 0.125, 0.25, 0.5, or 1 mg/kg	Serum biochemistry and lung pathology at 1, 7, 14, and 28 d post-instillation	MWCNTs functionalized with taurine (tau-MWCNTs)[b]	All exposed groups showed elevations in serum ALP and LDH 1 and 7 d after instillation Significant elevation in LDH at 28 d only in high-dose group. No significant exposure-related changes in angiotensin converting enzyme. Histopathology revealed a significant increase in pulmonary inflammation and lung cell proliferation in all groups.	Chinese study, English abstract. Many tau-MWCNTs were found in some alveolar macrophages and bronchial epithelial cells.	Wang et al., 2007a[b]

Animal (gender, strain, group size)	Exposure	Endpoints examined	Nanotube description[c]	Results	Notes	Reference
Male Sprague-Dawley rats, 5/group	0, 0.04, 0.2 or 1 mg/kg-bw	BALF and lung, liver, kidney, and cerebrum histology at 3, 7, 28, and 91 d post-exposure	Mitsui & Co. (MWNT-7); dia. not given, length ~2 µm; 23.0 m^2/g surface area; 99.79% pure; dispersed as individual fibers in Tween-80	MWCNTs caused macrophage accumulation and mild leukocyte infiltration in the lungs at 0.2 and 1 mg/kg. Limited granulomatous effects were seen at high dose. Significant changes in BALF analyses only at 1 mg/kg bw		Kobayashi et al., 2010
Male ICR mice, 5/group	0, 0.125, 0.25, 0.5, or 1 mg/kg-bw	Serum biochemistry, histology of lungs, liver, kidneys, heart, and spleen, oxidative stress and collagen in lung tissue 0, 7, 14, 21, and 28 d post-exposure	Shenzhen Nanoharbor; 10-20 nm dia., 300-600 nm length; 133.7 m^2/g surface area; Ni (0.85%), Fe (0.62%), Co (0.38%). Morphology not given. Study used pristine and taurine-functionalized (tau-) MWCNTs	Lung pathology (alveolar cell hyperplasia, septal thickening, neutrophil and macrophage infiltration) was reported at all doses for both MWCNT forms, but data not presented. Pristine MWCNT caused oxidative stress in lung tissue (responses in reduced glutathione [GSH] and malondialdehyde [MDA]), but not tau-MWCNTs.		Wang et al., 2010

Animal (gender, strain, group size)	Exposure	Endpoints examined	Nanotube description[c]	Results	Notes	Reference
Male Wistar rats, 6/group	0, 0.2, 1.0, or 5.0 mg/kg	Antioxidant enzymes and lipid peroxidation products measured in blood/serum at 1, 7, 28, or 90 d post-exposure. Lung histology and BALF also analyzed 1, 7, 28, or 90 d post-exposure.	Center for Environment, Institute of Science and Technology, JNTU, Hyderabad; ARC (electric arc discharge) MWCNT: 90 to 150 nm dia.; 197 m^2/g surface area. CVD (chemical vapor deposition) MWCNT: 60 to 80 nm dia.; 252 m^2/g surface area Purity not reported, morphology not reported. Both MWCNTs dispersed using Tween-80	All doses of both MWCNTs decreased serum GSH and catalase levels, increased lipid peroxidation products, and decreased antioxidant buffering capacity. All doses of both MWCNTs increased cells and enzymes in BALF. Analysis of histology not documented.	These data drawn from two companion studies describing the same experiment	Reddy et al., 2011, 2012
Male Sprague-Dawley rats, 6-10/group	0, 1, 10, or 100 µg	Cardiac ischemia/reperfusion injury (prevalence of premature ventricular contractions and cardiac infarct sizes) in *ex vivo* hearts 24 h post-exposure	NanoTechLabs, Inc.; 12.5-25 nm dia.; 113.1 m^2/g surface area; ~5% Fe; dispersed in clinical surfactant (Infasurf) and morphology not given	Hearts subjected to 20 mins ischemia showed significantly increased premature ventricular contractions in the 100 µg exposure group and showed a similar but non-significant trend in the 10 µg group. Infarct size was increased in the 100 µg group. Ending left ventricular develop pressure was impaired in all dose groups. Coronary flow was depressed in the 100 µg group.		Thompson et al., 2014

Animal (gender, strain, group size)	Exposure	Endpoints examined	Nanotube description[c]	Results	Notes	Reference
Female C57Bl/6 mice, 6/group	0, 18, 54, or 162 µg	Plasma acute phase response proteins, plasma lipids, hepatic cholesterol and liver histology collected 1, 3, and 28 d post-exposure	'Small' MWCNTs: Nanocyl; 847±102 nm long and 6-17 nm dia.; 245.8 m2/g; 15% Al_2O_3, 0.29% Fe_2O_3; dispersed as tangled agglomerates in 2% serum. 'Large' MWCNTs: EU Joint Research Centre; 4048±366 long and 24 to 138 nm dia; 14.6 m^2/g surface area; 0.14% P_2O_5.; dispersed as fibers in 2% serum.	Serum amyloid protein was increased in plasma on day 3 at all dose levels for MWCNT-small and 54 and 162 µg for MWCNT-large. Plasma haptoglobin and plasma cholesterol (both LDL and HDL) was increased 3 d in the 162 µg groups of both CNTs, and cholesterol was increased in 162 µg group for MWCNT-large. No MWCNTs were observed in liver but vacuolar degeneration, granulomas, and hypertrophy of Kupffer cells was seen in MWCNT-exposed groups with no observed dose-dependence.		Poulsen et al., 2015
Female C57Bl/6 mice, 7/group	0, 6, 18, or 54 µg	BALF analyses and lung histology at 1, 28, and 92 d post-exposure	10 stocks of MWCNTs sourced from Cheaptubes; ranging from 13-32 nm dia, 500-1600 nm length; 74-223 m^2/g surface area; >99% pure (all); dispersed with normal mouse serum into agglomerated tangles and bundles.	Nearly all doses of all MWCNTs increased BALF neutrophils on day 1. By 28 d only 54 µg groups showed cell increases, but 18 µg groups for higher surface area MWCNTs showed sustained increases. Granulomas and focal alveolitis were seen in lung tissue in 54 µg groups, while alveolar cell hyperplasia (reported as septal thickening) was increased after 18 µg exposure and above. Authors noted that BALF cell increases were correlated with MWCNT surface area.	This study meant to compare pristine, -OH, and –COOH MWCNTs of different dimensions ('thin', 'thick', and 'small'), but materials did not match manufacturer descriptions and were overall indistinct in these aspects.	Poulsen et al., 2016

Animal (gender, strain, group size)	Exposure	Endpoints examined	Nanotube description[c]	Results	Notes	Reference
Female C57Bl/6 mice, 5-7/group	0, 18, 54, or 162 µg	BALF analyses, liver histology at 1, 3, and 28 d post-exposure	Nanocyl; 11 ± 4 nm dia., 4 ± 0.4 µm length; 246 m^2/g surface area; 87% pure with >3% Fe and/or Al; dispersed with normal mouse serum and morphology not specified.	All MWCNTs doses increased BALF cells. In liver, necrotic foci, vascular degeneration, granuloma, and hyperplasia of Kupffer cells and bile duct epithelium occurred at all doses. Parenchymatous degeneration seen in 54 and 162 µg dose groups.	This study compared a reference CNT to particles generated by sanding of CNT-containing epoxies. CNT-epoxies were less toxic but it is not clear if dosing of free vs. epoxy CNT was equivalent.	Saber et al., 2016
Oropharyngeal Aspiration						
Female C57BL mice (8 wks old at time of exposure), 8/group	0, 20, or 40 µg in 40 µL PBS. Average bw were not reported.	BALF, serum, and lung tissues were analyzed for inflammatory and oxidative stress markers 1 and 7 d after treatment.	Mean outer and inner dia of acid-treated MWCNTs 31 and 6 nm, respectively; mean length 20 µm; surface area 50 m^2/g. MWCNTs formed bundles with dia 30 to 300 nm.[b]	MWCNTs induced acute inflammation in the lung greater at 1d and began to resolve at 7 d. Effects generally dose-related.	Indicators of localized oxidative stress in the lung were not significantly altered.	Han et al., 2010[b]
Male C57BL/6J mice (7 wks old), 4/group Average bws not reported.	0, 10, 20, 40, or 80 µg well-dispersed MWCNTs in Ca+2- and Mg+2-free PBS, pH 7.4, with 5.5 mM D-glucose, 0.6 mg/mL mouse serum albumin, and 0.01 mg/mL 1,2-DSCP.	BALF was examined 1, 7, 28, and 56 d post-dosing. Lung histopathology examined 7 and 28 d post-exposure. Mice in the 20 and 80 µg groups also examined at 56 d.	Number of walls in the MWCNTs ranged from 20 to 50. Na (0.41%) and Fe (0.32%) were the major metal contaminants. Median length of MWCNTs was 3.86 µm and count mean dia 49 nm.[b]	Pulmonary inflammation and damage markers in BALF increased with dose and peaked 7 d post-exposure and almost totally recovered by 56 d. Histopathology showed rapid development of pulmonary inflammation and fibrosis by 7 d (all doses, dose-related) which persisted until 56 d after aspiration. At each sampling, inflammation extended to the pleura in over half of the CNT-exposed mice.	Inflammation in pleura is consistent with companion morphometric study showing movement of MWCNT particles into intrapleural space and subpleural tissue (Mercer et al., 2010).	Porter et al., 2010[b]

Animal (gender, strain, group size)	Exposure	Endpoints examined	Nanotube description[c]	Results	Notes	Reference
Male C57Bl/6 mice, 8/group	0, 10, 20, 40, or 80 µg	Morphometric measurement of Sirius Red staining (assessment of fibrosis) at 1, 7, 28, 56 d post-exposure	Mitsui & Co. (MWNT-7); 49±13.4 nm mean dia, 3.86 µm median length; 26 m^2/g surface area; 0.32% Fe; dispersed as fibers with albumin and phosphocholine (DPPC)	Increased septal thickness was seen in 40 and 80 µg dose groups.	Comparison to SWCNTs in a companion study suggested that SWCNTs are roughly 10-fold more potent in inducing fibrosis	Mercer et al., 2011
Male C57Bl/6 mice, 6-8/group	0, 1, 2, or 4 mg/kg-bw	Pulmonary function, lung histology, BALF analyses, soluble collagen in lung at 30 d post-exposure	NanoTechLabs, Inc.; 12.5-25 nm dia; 113.1 m2/g surface area; ~5% Fe; dispersed in clinical surfactant (Infasurf), morphology not given	All doses increased cells in BALF. 4 mg/kg-bw dose increased lung collagen and caused significant perturbation of lung function as assessed using spirometry.		Wang et al., 2011a
Male C57Bl/6 mice, 6-8/group	0, 5, 20, or 40 µg	Lung histology (incl. special stains for fibrosis) at 7 d post-exposure	Mitsui & Co. (MWNT-7); 49 ± 13.4 nm mean dia., 3.86 µm median length; 26 m^2/g surface area; 99.22% purity, 0.32% Fe; dispersed as fibers with albumin and phosphocholine (DPPC)	Inflammatory foci were detectable in lung at 5 µg exposure, but were significant only at 20 µg and above. Fibrotic response only detected at 40 µg. Histology data only described, and not presented quantitatively.	Study focused on response differences in Nrf2-/- mice from wild-type following 40 µg exposure	Dong and Ma, 2016

[a]IT and OPA exposures are administered as a single bolus dose unless otherwise specified

[b]As reported by Versar (2012)

[c] NT characterization data are stated, if reported: source, diameter and length, surface area, purity and impurities, and state of aggregation; shape (bundles, tangles, ropes)

Appendix D*

DEVELOPMENTAL TOXICITY OF SWCNT VIA IV INJECTION

*****References for Appendices are located in Section 7 of Volume 1 report. Abbreviations for Appendices are located in Abbreviation list, Volume 1 report.

1 Developmental Toxicity of SWCNT via IV Injection.

Three studies evaluating developmental endpoints using IV injection of pristine or functionalized SWCNT in were located in the literature since 2010. These are described below and included in the Volume 1 report in Table 13.

Pietroiusti et al. (2011) administered, via IV injection, pristine, oxidized, or ultra-oxidized SWCNTs to CD-1 female mice (from 10 ng to 30 μg/mouse) on GD 5.5. Controls received vehicle only. The pristine and oxidized SWCNT were purchased and the ultra-oxidized SWCNTs were prepared by the laboratory. High percentages of early miscarriages and fetal malformations were observed in dams exposed to either of the oxidized SWCNTs while lower percentages were found in control animals and animals exposed to the pristine (unoxidized) material. Increased reactive oxygen species were detected in malformed fetuses and placentas of malformed fetuses, but not in normally developing fetuses or in maternal tissues. The lowest adverse dose was 100 ng/mouse.

Campagnolo et al. (2013) investigated the toxicity of single or multiple IV doses of vehicle or 0.1-30 μg/mouse of commercially available amino-functionalized (PEG) SWCNT during CD-1 mouse pregnancy. A single injection of doses up to 10 μg/mouse on GD 5.5 or 14.5 resulted in no adverse effects on embryos or dams. No comparison with non-functionalized SWCNT was provided in the study. At 30 μg/mouse, occasional teratogenic effects, associated with placental damage, were detected both when administered as a single bolus or as multiple doses (on days 5.5 and 14.5).

Huang et al. (2014) reported that IV tail vein injections of vehicle or amine-functionalized SWCNT (1-2 nm x 0.5-2 μm) into p53 (+/-) heterozygous pregnant transgenic mice at 2 mg/kg/d on GD 0.5, 12.5 and 15.5, did not cause maternal or fetotoxicity.

Appendix E*

MUTAGENICITY/GENOTOXICITY STUDIES OF SWCNTS AND MWCNTS

*References for Appendices are located in Section 7 of Volume 1 report. Abbreviations for Appendices are located in Abbreviation list, Volume 1 report.

Table E-1. Summary of Genotoxicity Data for SWCNTs (Versar, 2012)[a]

Endpoint	Assay	Test System	Exposure	Particle data	Result	Comments	Reference
Mutation	Reverse mutations	*S. typhimurium* YG1024 and YG1029	0, 60, 120, or 240 µg/plate for 48 h	SWCNTs (99.7% pure, 0.23% Fe), 0.4–1.2 nm dia, 1–3 µm length	Negative	No metabolic activation provided	Kisin et al., 2007
	Mutation at *cII* locus	FE1 Muta™ Mouse lung epithelial cells	0 or 100 µg/mL for 576 h	SWCNTs (95% carbon), 0.9–1.7 nm dia, <1 µm length	Negative		Jacobsen et al., 2008
	Micronuclei induction	Chinese hamster lung fibroblast (V79) cells	0, 12, 24, 48, or 96 µg/cm^2 for 24 h	SWCNTs (99.7% pure, 0.23% iron), 0.4–1.2 nm dia, 1–3 µm length	Equivocal	Micronuclei increased at 96 µg/cm^2, but not statistically significant	Kisin et al., 2007
	Micronuclei induction	Human lymphocyte cells	0, 0.25–150 µL per 5 mL of total cell culture volume	SWCNTs (70% pure) and functionalized SWCNTs (composition not reported	Positive	functionalized SWCNTs > SWCNTs	Cveticanin et al., 2010
	Micronuclei induction	RAW 264.7 cells	0, 0.01–100 µg/mL for 2 or 24 h	SWCNTs (96.7% carbon), 0.7–1.2 nm dia, 0.5–100 µm length; MWCNTs (>98% carbon), 110–170 nm dia, 5–9 µm length	Positive	SWCNTs and MWCNTs positive at ≥1 µg/mL	Migliore et al., 2010
	Micronuclei induction	Human bronchial epithelial BEAS 2B cells	3.8–380 µg/mL for 24, 48, or 72 h	CNTs (>50% SWCNTs, ~40% other CNTs), 1.1 nm dia, 0.5–100 µm length	Positive	Positive at 10 and 20 µg/cm^2 at 48 h, not at other time points	Lindberg et al., 2009
DNA repair	γH2AX foci induction (DS DNA break repair)	Human fibroblasts	0, 0.5–30 µL/mL for 24 h	SWCNTs (70% pure), amide-SWCNTs, and pristine MWCNTs (99% pure), 20–40 nm dia, 1–5 µm length	Positive	All three CNTs induced γH2AX foci to similar magnitudes at similar doses	Cveticanin et al., 2010
DNA Damage	DNA damage, Comet assay	Chinese hamster lung fibroblast (V79) cells	0, 24, 48, or 96 µg/cm^2 for 3 or 24 h	SWCNTs (99.7% pure, 0.23% Fe), 0.4–1.2 nm dia, 1–3 µm length	Positive		Kisin et al., 2007

Endpoint	Assay	Test System	Exposure	Particle data	Result	Comments	Reference
	DNA damage, Comet assay	RAW 264.7 cells: mouse macrophage cell line	0, 0.01–100 µg/mL for 2 or 24 h	SWCNTs (96.7% carbon), 0.7–1.2 nm dia, 0.5–100 µm length; MWCNTs (>98% carbon), 110–170 nm dia, 5–9 µm length	Positive	SWCNTs and MWCNTs positive at ≥10 and ≥1 µg/mL with 24-h exposure	Migliore et al., 2010
	DNA damage, Comet assay	Human bronchial epithelial BEAS 2B cells	3.8–380 µg/mL for 24, 48, or 72 h	CNTs (>50% SWCNTs, ~40% other CNTs), 1.1 nm dia, 0.5–100 µm length	Positive	Positive at all times tested	Lindberg et al., 2009
	DNA damage, Comet assay	FE1 Muta™ Mouse lung epithelial cells	0 or 100 µg/mL for 3 h	SWCNTs (95% carbon), 0.9–1.7 nm dia, <1 µm length	Negative	3-h exposure; other positive studies used 24 or 48 h	Jacobsen et al., 2008
	DNA damage, Comet assay	Human alveolar carcinoma epithelial cells (A549)	0 or 50 µg/mL for 3 h	SWCNTs, <2 nm dia and 5–15 µm length; 3 MWCNTs: M1: 20–60 nm dia, 5–15 µm length M2: 60–100 nm dia, 1–2 µm length; M3: <10 nm dia, 1–2 µm length	Positive, M1 or M2 MWCNTs Negative, M3 MWCNTs, SWCNTs	Thicker diameters were associated with DNA damage at the tested concentration	Yamashita et al., 2010

Source: Versar, 2012

[a]All references cited in Versar (2012).

dia = diameter; DS-DNA = double-stranded DNA

Table E-2. Summary of Genotoxicity Data for MWCNTs (Versar, 2012)[a]

Endpoint	Assay	Test System	Exposure	Particle data	Result	Comments	Reference
Mutation	Reverse mutations	*S. typhimurium* TA98 and 100; *E. coli* WP2*uvr*A	0, 0.01–9.0 µg/plate, ± metabolic activation for 48 h	MWCNTs (90% pure, <0.1% metal impurities), 110–170 nm dia, 5–9 µm length	Negative, ± metabolic activation		Di Sotto et al., 2009
	Reverse mutations	*S. typhimurium* TA98,100, 102, 1535, and 1537	0, 50–5,000 µg/plate, ± metabolic activation for 48 h	Baytubes® - agglomerates of MWCNTs (95% pure), 0.2–1 µm length	Negative, ± metabolic activation		Wirnitzer et al., 2009
	Mutation at hgprt locus	Chinese hamster lung cells	0, 6.3–100 µg/mL for 48 h	MWCNT (4,400 ppm iron, 48 ppm Cr, and 17 ppm Ni)	Negative	MWCNTs had 5 µm L, 88 nm D	Asakura et al., 2010
	Mutation at Aprt locus	Mouse embryonic stem cells, Aprt+/- 3C4 Aprt deficient	0, 5, or 100 µg/mL for 2 or 4 h	MWCNTs purified to remove catalyst residues	Positive	Further properties of MWCNTs were not reported	Zhu et al., 2007
	Micronuclei induction	Chinese hamster lung cells	0, 0.02–5.0 µg/mL for 48 hrs	MWCNT (4,400 ppm Fe, 48 ppm Cr and 17 ppm Ni), 5 µm length, 88 nm dia	Equivocal	Induction of bi- and multi-nucleated cells was clearly exposure-related	Asakura et al., 2010
	Micronuclei induction	Rat lung epithelial cells or Human breast cancer cells (MCF-7)	0, 10, 25, or 50 µg/mL for 12 h	Ground MWCNTs (98% pure), 11.3 nm dia, 0.7 µm length	Positive	Positive in both cell types	Muller et al., 2008b

Endpoint	Assay	Test System	Exposure	Particle data	Result	Comments	Reference
	Micronuclei induction	Rat lung epithelial cells	0 or 25 µg/mL for 12 h	Ground MWCNTs, ground MWCNTs modified at 600°C, ground MWCNTs modified at 2,400°C; size dimensions not reported	Positive with ground MWCNT ± 600°C Negative with ground MWCNTs modified at 2,400°C	Modification at 600°C resulted in loss of oxygen and metal oxides; modification at 2,400°C resulted in elimination of metal clusters and ablation of carbon framework defects	Muller et al., 2008a
	Micronuclei induction	Human lymphocyte cells	0, 0.25–150 µL per 5 mL of total cell culture volume	pristine MWCNTs (99% pure), 20–40 nm dia, 1–5 µm length	Positive		Cveticanin et al., 2010
	Chromosome aberrations	Chinese hamster lung fibroblast (V79) cells	0, 2.5, 5, or 10 µg/mL for 4 or 18 h	Baytubes® - agglomerates of MWCNTs (95% pure)	Negative, ± metabolic activation	MWCNTs had 0.2–1 µm L	Wirnitzer et al., 2009
	Chromosome aberrations	Chinese hamster lung cells	0, 0.078–80 µg/mL for 24 or 48 h	MWCNT (4,400 ppm Fe, 48 ppm Cr, and 17 ppm Ni)	Negative	MWCNTs had 5 µm L, 88 nm D	Asakura et al., 2010
	Polyploidy induction	Chinese hamster lung cells	0, 0.078–80 µg/mL for 24 or 48 h	MWCNT (see previous row)	Positive		Asakura et al., 2010
DNA repair	γH2AX foci induction (DS DNA break repair)	Human mesothelial cells, normal and malignant	0, 12.5, 25, or 50 µg/mL for 24 h	Pristine MWCNTs (99.5% pure), 81 nm dia, 8 µm length	Positive	Positive in both cell types	Pacurari et al., 2008
	DS-DNA break repair induction	Mouse embryonic stem cells J11	0, 5, or 100 µg/mL for 2 or 4 h	MWCNTs purified to remove catalyst residues	Positive	Proteins induced: Rad 51, XRCC4; exposure also ↑ γH2AX foci	Zhu et al., 2007

Endpoint	Assay	Test System	Exposure	Particle data	Result	Comments	Reference
	DNA repair induction	Mouse embryonic stem cells J11	0, 5, or 100 µg/mL for 2 or 4 h	MWCNTs purified to remove catalyst residues	Positive	8-oxoguanine-DNA glycoslase 1; and p53 were induced	Zhu et al., 2007
DNA Damage	DNA damage, Comet assay	Human dermal fibroblast cells	0, 40, 200, or 400 µg/mL for 48 h	Functionalized MWCNTs (2–7% carboxyl groups), 15–30 nm dia, 15–20 µm length	Positive		Patlolla et al., 2010
	DNA damage, Comet assay	Human mesothelial cells, normal or malignant	0, 25, or 50 µg/cm^2 for 24 h	Pristine MWCNTs (99.5% pure), 81 nm dia, 8 µm length	Positive	Positive in both cell types	Pacurari et al., 2008

Source: Versar, 2012
[a]References cited in Versar (2012)
dia = diameter; DS-DNA = double-stranded DNA

1 Single-walled CNTs

1.1 *In Vitro* Mutagenicity Studies

In vitro mutagenicity tests in bacteria (Naya et al., 2011; Ema et al., 2013; Clift et al., 2013; Kim et al., 2015) have confirmed the previous reports of negative results for SWCNTs in the standard Ames test in *S. typhimurium* strains as well as in the *E. coli* strain (WP2*uvr*A), the strain more sensitive to oxidative damage. Negative Ames test results have been generally attributed to the inability of nanomaterials to penetrate the bacterial cell wall. However, Clift et al. (2013) used TEM to study the interaction of SWCNTs with *S. typhimurium* TA98 and found that SWCNTs and other nanofibers (NFs) did penetrate the bacterial cells. This finding suggests that the lack of a mutagenic response for SWCNTs in the Ames test may not be due solely to a lack of cell uptake.

Results from only a single *in vitro* mammalian cell HPRT mutation assay were found (Manshian et al., 2013). This study evaluated the influence of SWCNT length on mutagenic potential and found that 1 to 3 μm length SWCNT induced a dose-related increase in mutation frequency while SWCNT test materials with lengths of either 400 to 800 nm or 5 to 30 μm did not. The SWCNTs used in this study were described as high purity samples, suggesting that the observed increase in MN was related to the SWCNT themselves rather than metal contaminants. ROS measurements were made in this study and revealed significant increases for the 1 to 3 μm and 400 to 800 nm SWCNTs, but not 5 to 30 μm SWCNTs. The 1 to 3 μm length SWCNTs induced the largest increase in ROS. Manshian et al. (2013) also studied the expression profile of a variety of oxidative stress and antioxidant defense-responsive genes, and they found that the 1 to 3 μm SWCNT sample induced the most striking change in gene expression. The increase in ROS and changes in gene expression observed suggested that oxidative stress may be associated with the mutagenicity of this test material.

1.2 *In Vitro* Genotoxicity Studies

1.2.1 Chromosomal Aberrations

Four chromosome aberration assays have produced mixed results. Two studies in a Chinese hamster lung fibroblast cell line (CHL/IU) showed no increase in the frequency of chromosomal aberrations and no evidence of cytotoxicity even when SWCNTs were evaluated at concentrations of up to 1000 μg/mL (Naya et al., 2011; Ema et al., 2012). SWCNTs in both of these studies were dispersed in CMC, but precipitation was reported in both studies. In contrast, Di Giorgio et al. (2011) reported an increase in chromosomal aberrations as well as dose-related cytotoxicity in a transformed mouse macrophage cell line treated with low concentrations (1 to 10 μg/mL) of a SWCNT test material reported to contain ~1.5% Ni as an impurity. Evidence of both clastogenic and aneugenic effects were observed. The macrophages were reported to take up the SWCNTs by phagocytosis. The SWCNT test material was reported to be well dispersed despite being suspended in serum free media without dispersant (no data shown). ROS production increased after SWCNT exposure at a dose higher than the highest test concentration.

Catalan et al. (2012) reported a significant increase in chromosomal aberrations in cultured

human peripheral blood lymphocytes only at the highest concentration scored (300 μg/mL). Higher concentrations were reported to exceed the acceptable limits of cytotoxicity. The test material was reported to consist of a mixture of SWCNTs (>50%) and MWCNTs (<50%), and agglomerates in culture media ranging from nanosized to a few μm in size were expected based on previously published work.

1.2.2 Micronucleus Formation

In vitro MN assay results were reported in five publications. Four of these studies reported positive results (Di Giorgio et al., 2011; Kisin et al., 2011; Cicchetti et al., 2011; Manshian et al., 2013), and one study reported negative results (Lindberg et al., 2013). Di Giorgio et al. (2011) observed a dose-related increase in MN and cytotoxicity at low doses (1 to 10 μg/mL) in the same mouse macrophage cell line used for the chromosomal aberration assay (see above). An increase in ROS was observed in cultures exposed to 50 μg/mL SWCNTs, but ROS was not measured at all the concentrations used in the MN assay. No inflammatory response was detected by quantification of TNF-α.

Manshian et al. (2013) tested three SWCNTs of differing lengths (400 to 800 nm, 1 to 3 μm, and 5 to 30 μm) in two different human cell lines. In both cell lines, SWCNTs were internalized regardless of length, and all of the test materials showed a time- and dose-related increase in MN frequency in the absence of cytotoxicity. The relative potency of the SWCNTs for MN induction was 400 to 800 nm > 5 to 30 μm > 1 to 3 μm. The increase in MN frequency reached a plateau for all three SWCNTs at a concentration of > 20 μg/mL. As noted above, only the 1 to 3 μm SWCNT test material induced HPRT mutations in this study, and mutation induction appeared to correlate with induction of oxidative stress. However, since MN induction was most prominent with the 400 to 800 nm SWCNT test material (and not the 1 to 3 μm test material), induction of oxidative stress was unlikely to be the primary mode of action for chromosomal damage. Further study is needed to clarify the mode of action of genotoxicity.

Cicchetti et al. (2011) studied both MN induction and ROS induction in human gingival fibroblasts. Information on the metal contaminants of the SWCNT test material was not provided. The test material was described as having a negligible degree of –COOH surface modification. A significant dose-related increase in MN frequency was observed up to a concentration of 100 μg/mL, followed by significant decreases at 125 and 150 μg/mL. A dose-related decrease in cell viability was also observed. Cell uptake was reported to occur, although data were not shown. As the response in the comet assay showed a consistent dose-related increase in DNA damage even at the higher doses, one possible explanation for the lack of a MN response at high doses is a failure of the cells to survive at least one mitotic cycle. There was also an increase in ROS and induction of heat shock protein Hsp70 at all test concentrations. The role of ROS induction in the genotoxicity leading to MN induction was unclear, but induction of Hsp70 appeared to play a protective role because inhibition of Hsp70 expression increased the comet response.

Kisin et al. (2011) reported an increase in MN frequency in Chinese hamster lung fibroblasts (V79 cells) treated with purified SWCNTs (0.23 wt% iron) at doses also showing evidence of cytotoxicity based on decreased cell viability. No other data providing insight on mode of action

for MN induction in this study were presented.

Lindberg et al. (2013) conducted a MN assay in a human bronchial epithelial cell line treated with SWCNTs (reported length of 1-5 μm and metal contaminant levels of <0.5 wt%). This test material contained >50% SWCNTs and ~40% other CNTs. TEM analyses showed that the test material was taken up by the cells and found in the cytoplasm, usually in lysosome-like organelles. Although cytotoxicity was reported, no increase in MN frequency was observed. However, an increase in M_1dG DNA adducts was observed.

1.2.3 Mitotic Spindle Analysis and FISH Analysis for Aneuploidy

Sargent et al. (2012) observed a significant dose-dependent increase in mitotic spindle damage in a human bronchial epithelial cell line and a significant dose-dependent increase in aneuploidy in primary cultures of human respiratory epithelium each exposed to low doses (0.024 – 24 μg/mL) of a purified SWCNT test material containing 0.23% iron. Laser scanning confocal microscopy showed nanotubes associated with the microtubules of the mitotic spindle apparatus, the DNA, and the centrosome fragments. These results support a mode of action involving a direct effect of the SWCNT on the mitotic spindles with resulting induction of aneuploidy.

1.2.4 Comet Assay

SWCNTs were evaluated in four *in vitro* comet assays, and all of them reported an increase in % tail DNA and/or tail moment as well as evidence of cytotoxicity (Cicchetti et al., 2011; Di Giorgio et al., 2011; Kisin et al., 2011; Lindberg et al., 2013). The test systems included cell lines derived from human gingival fibroblasts (Cicchetti et al., 2011), transformed mouse macrophages (Di Giorgio et al., 2011), and Chinese hamster lung fibroblasts (Kisin et al., 2011). Lindberg et al., (2013) evaluated SWCNTs in two human cell lines and results were considered "slightly positive" for DNA damage in bronchial epithelial cells and clearly positive in the mesothelial cells. These four publications also evaluated the same SWCNT test materials in *in vitro* MN assays, thus allowing a comparison of MN and comet results in the same studies. Positive results were observed in both MN and comet assays for all studies except for the Lindberg et al. (2013) study. Lindberg et al. (2013) measured MN induction only in human bronchial epithelial cells and found no increase in MN frequency (see above), while the comet assay was considered only slightly positive in this cell line.

Cell uptake occurred in studies where it was evaluated (Cicchetti et al., 2011; Lindberg et al., 2013). ROS was measured in two studies and shown to be increased in both (Cicchetti et al., 2011; Di Giorgio et al., 2011). None of these comet assays employed the fpg-modified protocol that would be informative on the presence of oxidative DNA damage and would help clarify the role of ROS in SWCNT-induced DNA damage.

1.2.5 DNA Adducts

Lindberg et al. (2013) measured the level of malondialdehyde DNA adducts (M_1dG) in a human bronchial epithelial cell line and a human mesothelioma cell line treated with SWCNTs (same material as used in MN and comet assays) using an immunoblot assay and reported a significant

increase after a 48 hr exposure. Malondialdehyde is an end product of lipid peroxidation. The M_1dG DNA adduct is formed by a condensation reaction between guanosine nucleotides and malondialdehyde. This finding is suggestive of SWCNT-induced oxidative effects leading to DNA damage. The level of M_1dG decreased to below control after a 72 hr exposure. The SWCNT used in the Lindberg et al. (2013) experiments was described as a purified sample with <0.5 wt% catalyst metals.

1.3 *In Vivo* Mutagenicity Studies

A search of published literature identified no in *vivo* mutagenicity studies with SWCNTs published subsequent to Versar (2013).

1.4 *In Vivo* Genotoxicity Studies

1.4.1 Micronucleus Formation

Three *in vivo* bone marrow MN assays in male mice have been published, and all have shown negative results. Two of these studies involved administration of the SWCNT test material by oral gavage (Ema et al., 2012; Naya et al., 2011), and the third study administered the test material by IP (Kim et al., 2015). The exposures involved doses from 5 to 200 mg/kg bw/d for two days in the oral gavage studies and a single dose ranging from 25 to 100 mg/kg bw in the intraperitoneal study. None of these studies showed evidence of bone marrow toxicity based on measurement of % polychromatic (PCE) or PCE/(PCE + normocytic erythrocyte [NCE]) ratio. The lack of an effect on these parameters suggests a lack of sufficient exposure in the bone marrow for the evaluation of *in vivo* genotoxic potential. None of the *in vivo* studies evaluated in the Versar review (2012) involved an evaluation of the genotoxicity of SWCNTs in MN or comet assays. However, *in vivo* studies involving other endpoints (oxidative DNA damage, K*ras* mutations, mitochondrial DNA damage) have shown positive results with SWCNTs by either oral gavage, inhalation, or pharyngeal aspiration. These observations suggest that the potential for SWCNTs to induce genotoxicity *in vivo*, especially in relevant target tissues (i.e., respiratory tract) after inhalation exposure may not be adequately evaluated by conducting a bone marrow MN assay.

1.4.2 Comet Assay

Results from an *in vivo* comet assay were reported by Naya et al. (2012a). In this study, rats were exposed by intratracheal instillation to once weekly doses for five weeks or a single dose of a SWCNT test material containing 0.365% (3650 ppm) iron. DNA damage was measured in the lung. Despite histopathological findings of hemorrhage in the alveolus and infiltration of alveolar macrophages and neutrophils after both single and repeated instillation, there was no increase in % tail DNA observed in lung cells. The lack of DNA damage with lung exposure to SWCNTs is different than the response observed in *in vivo* comet assays involving direct lung exposure to MWCNTs, which clearly show an increase in DNA damage (see Section 4.8.3). The reason for the difference in outcomes in not clear.

2 Multi-walled CNTs

2.1 *In Vitro* Mutagenicity Studies

In vitro mutagenicity tests in bacteria (Kim et al., 2011a; Ema et al., 2012; Clift et al., 2013; Kim et al., 2015) have confirmed the previous reports of negative results for MWCNTs in the standard Ames test in *S. typhimurium* strains as well as in the *E. coli* strain (WP2*uvr*A), the more sensitive strain to oxidative damage. These studies all involved testing up to concentrations that led to significant precipitation and aggregation. These negative results have been generally attributed to the inability of MWCNTs to penetrate the bacterial cell wall. In contrast, Clift et al. (2013) used TEM to study the interaction of MWCNTs with *S. typhimurium* TA98, the most commonly used *S. typhimurium* strain, and found that MWCNTs and other NFs penetrated the bacterial cells. This finding suggests that the lack of a mutagenic response for MWCNTs in the Ames test is independent of cell uptake.

No additional *in vitro* mutagenicity studies of MWCNTs in mammalian cells have been identified in the literature published subsequent to Versar (2012). Thus, no further data are available to clarify the conflicting findings of the two previously reviewed mammalian cell mutagenicity assays.

2.2 *In Vitro* Genotoxicity Studies

2.2.1 Chromosomal Aberrations

Four chromosome aberration assays with MWCNTs have been reported in the published literature (Di Giorgio et al., 2011; Kim et al., 2011a; Ema et al., 2012; Catalan et al., 2012). Similar to their results with SWCNTs, Di Giorgio et al. (2011) reported an increase in chromosomal aberrations as well as dose-related cytotoxicity in a transformed mouse macrophage cell line treated with low concentrations (1 to 10 μg/mL) of a MWCNT test material reported to contain ~1.5% of Ni as an impurity. Evidence for both clastogenic and aneugenic effects were observed. The macrophages were reported to take up the MWCNT by phagocytosis. ROS production increased after MWCNT exposure at a dose higher than the highest test concentration.

Catalan et al. (2012) reported a significant increase in chromosomal aberrations in cultured human peripheral blood lymphocytes after 48 hrs of exposure to 300 μg/mL MWCNTs, but not after 24 or 72 hrs. A significant increase in chromosomal aberrations was also observed after 48 hrs of exposure to 50 μg/mL of a purified short MWCNT test material, but overall there was no evidence of a dose response. Catalan et al. (2012) reported that metal catalyst levels were low in their test material, and their review of previously published genotoxicity studies did not suggest a pattern of positive responses with MWCNT test materials containing metal catalyst impurities. These observations indicate that the role of CNT metal catalyst impurities in the induction of genotoxicity remains unconfirmed.

Ema et al. (2012) observed no increase in structural chromosome aberrations in Chinese hamster lung cells treated with either of two MWCNTs, but both test materials caused an increase in the

number of aneuploid cells, one slightly and the other distinctly.

Kim et al. (2011a) evaluated two MWCNT test materials that had the same diameter (10-15 nm) but differed in their aspect ratio with one having a length of ~10 μm (high-aspect-ratio MWCNT) and the other having a length of ~150 nm (low-aspect-ratio MWCNT). Although the high-aspect-ratio test material was more cytotoxic than the low-aspect-ratio test material, no increase in the frequency of chromosomal aberrations was observed in Chinese hamster ovary cells after treatment with either of the two MWCNTs.

2.2.2 Micronucleus Formation

In vitro MN assay results were reported in five publications. Three of these studies showed positive results (Di Giorgio et al., 2011; Kato et al., 2013; Tavares et al., 2014), whereas two studies reported negative results (Lindberg et al., 2013; Catalan et al., 2016).

Di Giorgio et al. (2011) observed a dose-related increase in MN and cytotoxicity in the same mouse macrophage cell line used for the chromosomal aberration assay (see above). An increase in ROS was measured in cultures exposed to 50 μg/mL MWCNTs. No inflammatory response was detected by quantification of TNF-α at concentrations up to 50 μg/mL.

Kato et al. (2013) reported that clear growth inhibition and a significant dose-related increase in MN frequency occurred at all doses in a human lung carcinoma cell line treated with MWCNT. They also reported an increase in SCE frequency in Chinese hamster ovary cells. No additional data to address the mode of action were provided.

Tavares et al. (2014) studied a group of six different MWCNT test materials and found an increase in MN frequency at one or more of the test concentrations for three of six MWCNTs. Because there was no evidence of a dose response for any of the test materials and the increases in MN frequency were small, the results of this study are considered equivocal.

Lindberg et al. (2013) conducted a MN assay in a human bronchial epithelial cell line treated with a purified MWCNT reported to have a length of 1 to 2 μm and nickel levels <0.5 wt%. TEM analyses showed that the MWCNTs were taken up by the cells. The MWCNTs appeared as cut fibers or bundles of fibers apparently free in the cytoplasm. This intracellular distribution of MWCNTs was different than that observed for the SWCNT test material used in this study, the SWCNT was reported to be present in lysosome-like organelles (see above). MWCNTs were less cytotoxic than SWCNTs in this study. Similar to the SWCNT test material, no increase in MN frequency was observed.

Catalan et al. (2016) studied two distinct forms of MWCNTs referred to as straight or tangled. Neither test material was found to induce an increase in the frequency of MN. The *in vitro* MN assay results from this study provided no insight into possible mode of action.

2.2.3 Mitotic Spindle Analysis and FISH Analysis for Aneuploidy

Siegrist et al. (2014) observed a significant dose-related increase in mitotic spindle damage in a human bronchial epithelial cell line and a significant dose-dependent increase in aneuploidy in

primary cultures of human respiratory epithelium exposed to low doses (0.024 to 24 μg/mL) of a MWCNT test material. The increase observed with MWCNTs was greater than that observed with SWCNT in the same two cell lines (Sargent et al., 2012; see above). Location of the MWCNTs within the cell was determined by laser scanning confocal microscopy and TEM. MWCNTs were observed in association with microtubules of the mitotic spindle apparatus, the DNA, and the centrosome. These results support a mode of action involving a direct effect of the MWCNT on the mitotic spindles with resulting induction of aneuploidy.

2.2.4 Comet Assay

Results of nine *in vitro* comet assays have been published. All of these involved experiments conducted under alkaline conditions to detect single strand breaks. Four studies also employed a fgp-modified assay under conditions that specifically detect oxidative DNA damage. Overall, the results were positive in six studies (Di Giorgio et al., 2011; Cavallo et al., 2012; Ursini et al., 2012a; Ursini et al., 2012b; Ursini et al., 2014; Catalan et al., 2016) and weakly positive or equivocal in three studies (Lindberg et al., 2013; Jackson et al., 2015; Ghosh et al., 2011).

In Di Giorgio et al. (2011), significant increases in tail moment were observed at all doses tested, but a clear dose response was not observed as the response decreased in magnitude at the two highest doses. ROS was measured only at the highest dose tested in the comet assay and found to be increased. The comet response was different than the response seen in assays for clastogenicity in this same study, which showed a dose-related increase in MN frequency and chromosomal aberrations. No explanation was offered for the differences in dose response.

In three studies published by the same investigators (Ursini et al., 2012a; Ursini et al., 2012b; Ursini et al., 2014), the genotoxicity of MWCNTs was evaluated in the human A549 lung epithelial cell line using the alkaline comet assay and the fgp-modified assay for oxidative DNA damage. The MWCNTs tested in these studies included both pristine as well as –OH or –COOH functionalized MWCNTs. Oxidative DNA damage was not observed for any of the MWCNTs tested (Ursini et al, 2012a; Ursini et al., 2012b; Ursini et al. 2014). The failure to observe evidence of oxidative DNA damage in the fgp-modified assay suggests that the mode of action for DNA damage detected in the alkaline comet assay was not related to oxidative stress. In the alkaline comet assay, MWCNT-OHs showed higher and earlier genotoxicity than pristine MWCNTs (Ursini et al., 2012a) and MWCNT-COOHs (Ursini et al., 2014). However, in a different human epithelial cell line (BEAS-2B bronchial epithelial cells), pristine MWCNTs and MWCNT-COOHs induced similar dose-related increases in tail moment, although MWCNT-COOHs may have been slightly more potent. The reason for the differing results in the two cell lines for pristine and –COOH modified MWCNTs is not clear, but may be related to differences in agglomeration of the test material due to the use of different culture media for the two cell lines. This possible explanation is suggested by differences in dispersion of pristine and –COOH modified MWCNTS, observed by TEM, in the different culture media. Based on various measures of cytotoxicity, membrane integrity and inflammatory response, different modes of action for cytotoxicity appear to be important in A549 cells for pristine MWCNTs (membrane damage as measured by LDH), MWCNT-OH (apoptosis as measured by nuclear condensation visualization by fluorescence microscopy) and MWCNT-COOH (pro-inflammatory response as measured by cytokine release).

Cavallo et al. (2012) found an increase in DNA damage in an alkaline comet assay conducted in a human bronchial epithelial cell line. No evidence of oxidative DNA damage was observed in a fgp-modified assay. Cytoxicity measurements, including the LDH assay, suggested that MWCNTs damage the cell membrane.

Catalan et al. (2016) studied both straight (MWCNT-S) and tangled (MWCNT-T) test materials in a comet assay in a human bronchial epithelial cell line. MWCNT-S induced DNA damage only at the lowest two doses without a linear dose response, possibly due to an increase in agglomeration at higher concentrations preventing entry into the cells. MWCNT-T induced DNA damage only at the highest dose tested which showed ~60% cytotoxicity. As noted above, these test materials did not increase the frequency of MN in this study, suggesting that the primary DNA damage measurable by the comet assay did not give rise to chromosomal breaks or was efficiently repaired.

Jackson et al. (2015) studied fifteen MWCNTs with varying physicochemical properties in a mouse lung epithelial cell line for their cytotoxicity and genotoxicity as measured by the comet assay. Test materials differed in length, diameter, surface area, metal impurities, and surface functionalization (pristine, -OH functionalized, or –COOH functionalized). None of the MWCNTs were cytotoxic. Marginally increased levels of DNA single strand breaks as measured by % tail DNA were observed only for the group of MWCNTs with large diameters and high iron oxide and nickel content, but only one of these MWCNTs showed a statistically significant increase at the highest dose tested. ROS generation was also measured and shown to be increased for some MWCNTs, but the comet results did not correlate with the ROS results. The degree of functionalization of the MWCNTs was limited, precluding a meaningful analysis of its influence on genotoxicity potential.

Ghosh et al. (2011) did not observe a dose-dependent increase in % tail DNA in an alkaline comet assay in cultured human lymphocytes. Values of % tail DNA were higher than control at 2, 5, and 10 μg/mL but the increase was statistically significant only at 2 μg/mL. The decrease in response at 5 and 10 μg/mL relative to 2 μg/mL may be due to MWCNT agglomeration reducing cell uptake or affecting intracellular distribution.

Lindberg et al. (2013) found no increase in DNA damage in an alkaline comet assay in a human bronchial epithelial cell line. An increase in % tail DNA was observed in a human mesothelial cell line at the three highest concentrations, although two of these test concentrations produced >50% cytotoxicity.

2.2.5 γ-H2AX Assay for Double Strand Breaks

Guo et al. (2011) treated human umbilical vein endothelial cells with a MWCNT test material containing 3.38% nickel as well as other metals and observed a significant dose-related increase in % γ-H2AX positive cells, indicating the generation of DNA double strand breaks. An increase in ROS levels, glutathione peroxidase activity and superoxide dismutase activity were also observed. The addition of N-acetyl-L-cysteine as a free radical scavenger reduced both the γ-H2AX and ROS responses, indicating a mode of action involving oxidative damage.

2.2.6 DNA Adducts

Lindberg et al. (2013) measured malondialdeyde (M_1dG) DNA adducts in the same human cell lines used for their MN and comet assays. Treatment with MWCNTs produced a dose-dependent decrease in (M_1dG) DNA adducts in both cell lines to below control levels. As noted above, Lindberg et al. (2013) reported a significant increase in (M_1dG) DNA adducts in the same cell line after treatment with SWCNT. The reason for the difference in response was not explored.

2.3 *In Vivo* Mutagenicity Studies

Kato et al. (2013) measured *gpt* and Spi^- mutant frequency in lung tissue of *gpt* delta transgenic mice after intratracheal instillation of MWCNTs. They observed an increase in *gpt* mutant frequency after four weekly doses, but not after one or two doses, and no increase in Spi^- mutant frequency. Mutations scored by the *gpt* assay consist primarily of base pair substitution mutations, frameshift mutations and small insertions/deletions while large deletions are exclusively detected with the Spi^- assay. Lung tissue showed evidence of histopathology. *In vivo* assays for DNA damage (comet) and DNA adducts related to oxidative stress (8-oxodG, HεdA, and HεdC but not HεdG) were positive in lung after a single dose of MWCNT. The reason for the lack of a mutagenic response in the *gpt* assay after a single or double dose despite evidence of genotoxicity in these assays is unclear.

Two *in vivo* somatic mutation and recombination tests (SMART) in *Drosophila melanogaster* have been published (Machado et al., 2013; de Andrade et al., 2014). The MWCNT test material used by Machado et al. (2013) was functionalized by reflux with HNO_3 resulting in surface modification with –COOH (extent not reported) and contained 1.5% residual iron oxide. de Andrade et al. (2014) studied a purified MWCNT test material containing lower levels of metal contaminants. Neither of these studies showed evidence of a treatment-related increase in somatic mutation. Little or no evidence of cytotoxicity was reported. Although low levels of NTs were observed in the gut in both studies, systemic uptake appeared to be very low.

2.4 *In Vivo* Genotoxicity Studies

2.4.1 Chromosomal Aberrations

Patlolla et al. (2010) evaluated both nonfunctionalized and functionalized/oxidized MWCNTs containing 2-7 wt% -COOH in a bone marrow chromosomal aberration assay in mice. Both test materials caused an increase in chromosomal aberrations, but the response was greater with the functionalized MWCNTs. ROS was determined in bone marrow homogenates and shown to be increased, with a greater response in functionalized MWCNTs than nonfunctionalized MWCNTs. This difference may be due to better dispersion of the less hydrophobic functionalized MWCNTs in aqueous solution leading to higher concentrations of MWCNTs capable of being taken up by cells.

2.4.2 Micronucleus Formation

Results of five *in vivo* MN assays in mice have been reported. Three of these studies were bone marrow assays involving intraperitoneal (i.p.) injection of the test material (Patlolla et al., 2010; Ghosh et al., 2011; Kim et al., 2011a). Patlolla et al. (2010) tested both nonfunctionalized MWCNTs and functionalized/oxidized MWCNT-COOHs at IP doses of 0.25 – 0.75 mg/kg bw/d for five days, and reported a significant dose-related increase in MN for both test materials, although the increase was greater for MWCNT-COOH. Ghosh et al. (2011) administered MWCNTs to mice by IP injection at doses of 2, 5, or 10 mg/kg bw/d for two days, and reported an increase in MN frequency in bone marrow at all doses, although the degree of MN induction decreased with increasing dose. These investigators saw a similar pattern of decreasing genotoxicity with increasing dose in an *in vivo* comet assay. An inverse dose response for bone marrow cytotoxicity (% PCE) was also observed. Agglomeration of the test material is a likely explanation for the inverse dose response.

In the study by Kim et al. (2011a), MWCNTs were administered to mice as a single IP dose of 12.5 to 50 mg/kg bw. Two MWCNT test materials having the same diameter (10-15 nm) but differing in their aspect ratio were evaluated, with one having a length of ~10 μm (high-aspect-ratio MWCNT) and the other having a length of ~150 nm (low-aspect-ratio MWCNT). Neither of the test materials showed an increase in MN frequency in bone marrow. No evidence of bone marrow cytotoxicity as measured by PCE/(PCE+NCE) ratio was observed. These test materials also failed to increase chromosomal aberrations in an *in vitro* assay.

In a study published by Ema et al. (2012), two MWCNT test materials were administered to mice by oral gavage at 5, 10, or 20 mg/kg bw/day for two days. No evidence of an increase in MN frequency in bone marrow was observed with either test material, and no change in % immature erythrocytes was observed as a measure of bone marrow toxicity.

Catalan et al. (2016) evaluated a straight MWCNT test material (MWCNT-S) that had been studied *in vitro* in human bronchial epithelial cells and in an *in vivo* MN assay involving inhalation exposure. Although MWCNT-S did not induce an increase in the frequency of MN in the *in vitro* assay, an increase in MN was measured *in vivo* in lung alveolar type II cells after inhalation exposure. Lung inflammation was also observed. The pro-inflammatory response in the lung may have contributed to the MN response. However, because no measures of oxidative stress were included in the *in vitro* study lacking a MN response, this hypothesis remains untested. No increase in MN frequency was observed in peripheral blood PCEs or bone marrow PCEs in the *in vivo* study. The lack of a response in systemic tissues suggests a lack of sufficient exposure.

2.4.3 Comet Assay

All six of the *in vivo* comet assays produced positive results (Patlolla et al., 2010; Ghosh et al., 2011; Kato et al., 2013; Kim et al., 2012; Kim et al., 2014; Catalan et al., 2016). Three of these studies involved inhalation exposure, and DNA damage in lung cells was measured with the alkaline comet assay. Significant increases in Olive tail moment were reported in rats at the high dose (0.95 mg/m^3) after inhalation exposure for 5 days (6 h/d) (Kim et al., 2012) and at 0.17,

0.49, or 0.96 mg/m^3 after 28 days (6 hrs/day) (Kim et al., 2014). In both studies, DNA damage persisted 90 days post-exposure and MWCNT deposited in the lung were still present 90 days post-exposure.

Catalan et al. (2016) exposed mice by inhalation to either straight (MWCNT-S) or tangled (MWCNT-T) test materials and measured DNA damage by alkaline comet assay in cells prepared from lung tissue or cells recovered by BALF. MWCNT-S induced a significant increase in % tail DNA in both cells prepared from lung and cells recovered from BALF. No increase in % tail DNA was observed with MWCNT-T in either cell preparation. An additional experiment involving pharyngeal aspiration showed a significant increase in % tail DNA for MWCNT-S only at the highest dose tested. MWCNT-T did not increase % tail DNA after pharyngeal aspiration; instead it induced a significant trend for a decreasing dose response. Factors that may have contributed to these variable findings may include differences in agglomeration status, differences in cell type found in cells prepared from lung vs. those recovered from BALF, or differences in the exposure regimen. The results from this comet assay, as well as the results from the MN assay in lung alveolar type II cells also presented in this publication, suggest that straight MWCNTs are more genotoxic after inhalation exposure than tangled MWCNTs.

One study in mice involved intratracheal instillation, and a significant dose-related increase in % tail DNA in lung cells was observed (Kato et al., 2013). These investigators also observed an increase in oxidative and lipid peroxide-related DNA adducts in these cells, suggesting a mode of action involving oxidative stress.

Two *in vivo* comet assays in mice exposed to MWCNTs by IP injection showed positive responses. One study showed a significant increase in % tail DNA in isolated lymphocytes after 5 daily doses of either a functionalized (MWCNT-COOH) or nonfunctionalized test material (Patlolla et al., 2010). The other study (Ghosh et al., 2011) reported an increase % tail DNA in bone marrow cells at all doses, although the magnitude of the effect decreased with increasing dose. A similar pattern of decreasing genotoxicity effect with increasing dose was observed in an *in vivo* MN assay. An inverse dose response for bone marrow cytotoxicity (% PCE) was also observed in this study. Increasing agglomeration with increasing dose is a likely explanation for the inverse dose response.

2.4.4 DNA Adducts

In the same study in mice in which DNA damage was observed in the lung after intratracheal instillation using the comet assay, an increase was also observed in DNA adducts indicative of oxidative and lipid peroxide-related DNA damage (8-oxodG, HεdA, and HεdC but not HεdG) (Kato et al., 2013).

Table E-3. Summary of Mutagenicity/Genotoxicity data for SWCNTs

Assay	Test system	Exposure	NT Characterization[a]	Result	Comments	Reference
Mutation *In Vitro*						
Reverse mutation assay	*Salmonella typhimurium* strains TA97, TA98, TA100, TA1535, and *Eschericha coli* WP2*uvr*A/pKM101; pre-incubation assay	0, 12.5, 25, 50, 100, 200, or 500 µg/plate with and without S9 for 48 hrs. Dispersed in 0.1% sodium carboxymethyl cellulose.	1. National Institute of Advanced Industrial Science and Technology, Japan 2. dia. 3.0 nm; Max. length 1200 nm 3. 1064 m^2/g 4. Impurities: amorphous carbon <2.3 %, total metal impurity 0.051 %, Fe 145 ppm, Ni 103 ppm, Cr 34 ppm, Mn 2 ppm, Al 12 ppm 5. Bundled CNTs with some individual fibers, dia and length of bundles were 12 nm and 0.51 µm, respectively.	Negative	Precipitation observed at 50 µg/plate and above; no evidence of cytotoxicity.	Naya et al., 2011
Reverse mutation assay	*Salmonella typhimurium* strains TA98, TA100, TA1535, TA1537 and *Eschericha coli* WP2*uvr*A; pre-incubation assay	0, 0.78, 1.56, 3.13, 6.25, 12.5, 25, 50, or 100 µg/plate with S9; 0, 1.56, 3.13, 6.25, 12.5, 25, or 50 µg/plate without S9. Dispersed with 0.3% sodium carboxy methyl cellulose.	1. Nikkiso Co., Ltd. 2. dia 1.8 nm 3. 878 m^2/g 4. Impurities: Fe 4.4% 5. NR	Negative	Precipitation observed at 25 µg/plate in all strains with or without S9 and at 12.5 µg/plate in TA98 with S9. Slight growth inhibition with S9 in some strains at concentrations as low as 12.5 µg/plate.	Ema et al., 2013
Reverse mutation assay	*Salmonella typhimurium* strains TA100, TA98, TA1535, and TA1537; pre-incubation assay	0, 0.005, 0.01, 0.02, 0.03, or 0.04 mg/mL without S9 for 48 hrs. Suspended in 'bacterial exposure medium'	1. Yangtze Nanotechnology, China 2. dia 20 nm, Length 0.5-3 µm 3. NR 4. 5.5% Ni, 0.7% Y	Negative	No evidence of cytotoxicity. TA98 strain was used to evaluate SCWNT/bacterial cell inter-action and SWCNTs were shown to penetrate cells.	Clift et al., 2013

Assay	Test system	Exposure	NT Characterization[a]	Result	Comments	Reference
		(Xenometrix, CH)	5. "Fibrous bundles" (not clear whether CNTs were assessed in medium)			
Reverse mutation assay	*Salmonella typhimurium* strains TA98, TA100, TA1535, TA1537 and *Eschericha coli* WP2uvrA	0, 31.3, 62.5, 125, 250, or 500 µg/plate with and without S9 for 44 to 48 hrs. Dispersed in albumin/DPPC-based medium.	1. Hanwha Nano-tech, Korea 2. Dia 1-1.2 nm; length ~20 µm 3. NR 4. Purity: ~91% Impurities: Co <3.0 wt%, Ni <3.0 wt%, Fe < 1.5 wt%, S <1.5 wt% 5. "Tangled shape"	Negative	Precipitation and aggregation of SWCNTs were observed at 250 µg/plate and above.	Kim et al., 2015
HPRT assay	MCL-5 (human lymphoblastoid B cells)	0, 1, 5, 10, 15, 20, 25, 50, or 100 µg/mL for 48 hrs. Dispersed in cell culture media with 10% serum.	1. Synthesized by collaborators: 400-800 nm SWCNT and 1-3 µm SWCNT; Cheap Tubes: 5-30 µm SWCNT 2. Dia. of the 3 test materials is as stated in item 1 above 3. 400-800 nm SWCNT: 585 m^2/g; 1-3 µm SWCNT: 337 m^2/g; 5-30 µm SWCNT: 310 m^2/g 4. Purity: 400-800 nm SWCNT: 99% 1-3 µm SWCNT: 97%; 5-30 µm, SWCNT: 99% Impurities: trace metals <0.5%; Fe content: 400-800 nm SWCNT: 0.11%; 1-3 µm SWCNT: 1.18%;	400-800 nm and 5-30 µm length SWCNTs did not cause a treatment-related increase in mutant frequency. 1-3 µm length SWCNTs induced a dose-related increase in mutant frequency at 25, 50, and 100 µg/mL.	No significant increase in cytotoxicity for 400-800 nm length SWCNTs. A decrease to 80% viability observed at 1 and 5 µg/mL for 1-3 and 5-30 µm length SWCNTs, respectively, which was maintained at concentrations up to 25 µg/mL. Significant increase in ROS at 5 µg/mL and above for 1-3 µm length SWCNTs at 4 hrs. 400-800 nm SWCNTs increased ROS at 50 and 100 µg/mL. No significant effect on ROS for 5-30 µm length SWCNs.	Manshian et al., 2013

Assay	Test system	Exposure	NT Characterization[a]	Result	Comments	Reference
			5-30 µm SWCNT: 0.3% 5. 400-800 nm and 1-3 µm variants: ropes and individual fibers forming tangled agglomerates up to several µm. 5-30 µm variant: Dense flocculates of up to 1 µm			
Clastogenicity *In Vitro*						
Chromosomal aberrations	RAW 264.7 (a leukemia virus-transformed mouse macrophage cell line)	0, 1, 3, or 10 µg/mL for 24, 48 or 72 hrs. No dispersants used, CNTs suspended in serum-free culture media.	1. Sigma-Aldrich 2. Dia. 1.2-1.5 nm; length 2-5 µm (supplier data) 3. 400 m^2/g 4. Purity: >96% Impurities: Ni ~1.5% 5. No dispersant used; authors chose to allow some aggregation, although no TEM photomicrographs were shown.	Positive: increase in chromosome aberrations at all doses.	Dose-related cytotoxicity was observed. An increase in ROS was observed in cells treated with 50 µg/mL for 5 hrs and 24 hrs. No increase in TNF-α was observed in cells treated with 10 or 50 µg/mL for 5 hrs or 24 hrs.	Di Giorgio et al., 2011
Chromosomal aberrations	CHL/IU (Chinese hamster lung fibroblast cell line)	0, 300, 500, or 1000 µg/mL for 12 or 24 hrs with and without S9. Dispersed in 1% sodium carboxymethyl cellulose.	See above entry for Naya et al., 2011	Negative: no increase in structural or numerical chromosomal aberrations.	Precipitation observed at all concentrations. No evidence of cytotoxicity.	Naya et al., 2011

Assay	Test system	Exposure	NT Characterization[a]	Result	Comments	Reference
Chromosomal aberrations	Human peripheral blood lymphocytes	0, 6.25, 50, 100, 150, or 300 μg/mL for 24, 48, or 72 hrs. Dispersed in culture medium with 15% serum.	1. SES Research, Houston 2. Dia <2 nm; Length 1-5 μm; described as short purified SWCNTs 3. 436 m^2/g 4. Purity: >90% CNTs (~ >50% SWCNTs, <50% MWCNTs) Impurities: <5% amorphous carbon, <0.2% ash, traces of Co 5. Bundles and tangles forming agglomerates with sizes ranging from nanosized to a few μm (Vippola, et al., Hum. Exp. Toxicol. 28:377-385, 2009)	Significant increase in chromosomal aberrations only at the highest dose after 48 hrs and 72 hrs. No dose response.	Highest dose selected based on 50% cytotoxicity at 450 μg/mL for 72 hrs.	Catalan et al., 2012
Chromosomal aberrations	CHL/IU (Chinese hamster lung fibroblast cell line)	0, 6.25, 12.5, 25, 50, or 100 μg/mL for 6 hrs (with and without S9) or 24 hrs (without S9). Dispersed in 0.3% sodium carboxymethyl cellulose.	See above entry for Ema et al., 2013	Negative: no increase in structural or numerical chromosomal aberrations.	Precipitation observed at 25 and above regardless of metabolic activation and duration of exposure. No evidence of cytotoxicity.	Ema et al., 2013
Chromosomal aberrations	CHO-k1 (Chinese hamster ovary cell line)	0, 12.5, 25, or 50 μg/mL for 24 hrs. Dispersed in albumin/DPPC-based medium.	See above entry for Kim et al., 2015	Negative: no increase in structural or numerical chromosomal aberrations.	Test substance precipitation observed at 50 μg/mL.	Kim et al., 2015

Assay	Test system	Exposure	NT Characterization[a]	Result	Comments	Reference
MN formation	BEAS-2B cells (human bronchial epithelial cells)	0, 5, 10, 20, 40, 80, 120, 160, or 200 μg/cm^2 (corresponding to 0, 25, 50, 100, 200, 400, 600, 800 or 1000 μg/mL) for 48 and 72 hrs. Dispersed in cell culture medium containing serum.	1. SES Research 2. Dia. 2 nm; Length 1-5 μm 3. 436 m^2/g 4. Purity: >90% CNT (>50% Single-walled, ~40% other nanotubes), <5% amorphous carbon, <2% ash, <0.5 wt% catalyst metals 5. Bundles and tangles forming agglomerates several hundred nm in size (based on data from Vippola et al., Hum. Exp. Toxicol. 28:377-385, 2009)	Negative	Cytotoxicity observed at 200 μg/mL and above. SWCNTs were found in cytoplasm by TEM.	Lindberg et al., 2013
MN formation	RAW 264.7 (a leukemia virus-transformed mouse macrophage cell line)	0, 1, 3, or 10 μg/mL for 48 hrs. No dispersants used, CNTs suspended in serum-free culture media.	See above entry for Di Giorgio et al., 2011	Positive: significant dose-related increase in MN frequency.	Dose-related cytotoxicity was observed. An increase in ROS was observed in cells treated with 50 μg/mL for 5 hrs and 24 hrs. No increase in TNF-α.	Di Giorgio et al., 2011
MN formation	V79 cells (Chinese hamster lung fibroblasts)	0, 3, 12, or 48 μg/cm^2 for 24 hrs. The authors do not report using dispersants.	1. CNI, Houston 2. Dia. 1-4 nm; Aspect ratio 1000 3. 1040 m^2/g 4. Purity: >95% Impurities: Fe 0.23 wt% 5. Aggregated into ropes	Positive: significant increase in MN frequency at 12 and 48 μg/cm^2.	Some cytotoxicity at 12 and 48 μg/cm^2 based on decreases in cell viability.	Kisin et al., 2011

Assay	Test system	Exposure	NT Characterization[a]	Result	Comments	Reference
MN formation	BEAS-2B cells (human bronchial epithelial cells); MCL-5 (human lymphoblastoid B cells)	0, 1, 5, 10, 15, 20, 25, 50, or 100 μg/mL for 24 or 48 hrs in BEAS-2B cells and for 24 hrs in MCL-5 cells. Dispersed in cell culture media with 10% serum.	See above entry for Manshian et al., 2013	BEAS-2B cells: Positive, significant increase in MN frequency at 5 μg/mL and above for 400-800 nm length SWCNTs exposed for 24 hrs, but only at doses of 15 μg/mL and above for 1-3 and 5-30 μm length SWCNTs. MN frequency reached a plateau at >20 μg/mL for all three SWCNTs. 48 hr exposure showed increased MN frequency at 15 μg/mL and above for all three SWCNTs with relative potency of 400-800 nm > 5-30 μm ≥ 1-3 μm. MCL-5 cells: Similar MN response as BEAS-2B cells; relative potency 400-800 nm > 5-30 μm > 1-3 μm.	BEAS-2B cells: No significant cytotoxicity for either 24 or 48 hr exposures for any of the SWCNTs. A large time- and dose-related increase in ROS was observed for 1-3 μm length SWCNTs, but only at 20 μg/mL and above. 400-800 nm length SWCNTs increased ROS at doses up to 20 μg/mL, but ROS not increased at higher doses. 5-30 μm length SWCNTs did not increase ROS. Oxidative stress gene expression profiling showed the greatest alterations for 1-3 μm length SWCNTs at 100 μg/mL. MCL-5 cells: See Mansion et al., (2013) HPRT assay entry above for information on cytotoxicity and ROS increases.	Manshian et al., 2013
MN formation	Human gingival fibroblasts	0, 50, 75, 100, 125, or 150 μg/mL for 24 hrs. Cell culture medium with 1% fetal bovine serum	1. CheapTubes 2. Dia. 1.58 nm; Length 0.76 μm 3. 407 m^2/g 4. Purity >90 wt%; MWCNT content: <5 wt%, amorphous carbon <3 wt%,	Positive: significant increase in MN frequency at 50 – 100 μg/mL, but a significant decrease at 125 and 150 μg/mL	Cell uptake reported to occur (data not shown). Dose-related decrease in viability was observed. Significant increase in ROS and heat shock protein Hsp70 expression at all concentrations.	Cicchetti et al., 2011

Assay	Test system	Exposure	NT Characterization[a]	Result	Comments	Reference
			oxygen 2.7 % (w/w) (amount of attached –COOH groups considered negligible) 5. NR			
Clastogenicity *In Vivo*[b]						
MN assay	Bone marrow assay in male Crlj:CD1 mice	0, 5, 10, or 20 mg/kg bw/d for 2 days by oral gavage; animals sacrificed 25 hrs after the last dose. Dispersed with 0.3% sodium carboxy methyl cellulose.	See above entry for Ema et al., 2012	Negative	20 mg/kg bw/d was determined to be the practical upper limit (basis for this not stated). No evidence of bone marrow toxicity based on no significant decrease in % immature erythrocytes.	Ema et al., 2012
MN assay	Bone marrow assay in male Crlj:CD1 (ICR) mice	0, 60, or 200 mg/kg bw/d for 2 days by oral gavage; animals sacrificed 24 hrs after the last dose. Dispersed in 0.1% sodium carboxymethyl cellulose.	See above entry for Naya et al., 2011	Negative	200 mg/kg bw was the upper limit that could be administered by oral gavage. No evidence of bone marrow toxicity based on no significant decrease in % PCE.	Naya et al., 2011
MN assay	Bone marrow assay in male ICR mice	0, 25, 50, or 100 mg/kg single dose by IP adminstration.	See above entry for Kim et al., 2015	Negative	No evidence of bone marrow toxicity as measured by PCE/(PCE+ NCE) ratio.	Kim et al., 2015
DNA Damage *In Vitro*						
Comet assay	Human gingival fibroblasts	0, 50, 75, 100, 125, or 150 µg/mL for 24 hrs. Cell culture medium with 1% fetal bovine serum.	See above entry for Cicchetti et al., 2011	Positive: significant increase in tail moment at all concentrations.	Cell uptake reported to occur (data not shown). Cytotoxicity was observed. Significant increase in ROS at all concentrations.	Cicchetti et al., 2011
Comet assay	RAW 264.7 (a leukemia virus-transformed mouse	0, 1, 3, 10 or 50 µg/mL for 24 hrs.	See above entry for Di Giorgiio et al., 2011	Positive: increase in tail moment at 10 and 50 µg/mL.	Dose-related cytotoxicity was observed. An increase in ROS was observed in	Di Giorgio et al., 2011

Assay	Test system	Exposure	NT Characterization[a]	Result	Comments	Reference
	macrophage cell line)				cells treated with 50 μg/mL for 5 hrs and 24 hrs.	
Comet assay	V79 cells (Chinese hamster lung fibroblasts)	0, 3 or 48 μg/cm^2 for 3 and 24 hrs. The authors do not report using dispersants.	See above entry for Kisin et al., 2011	Positive: significant increase in % migrated DNA, tail length, and Olive tail moment at 48 μg/cm^2 for 24 hrs but not 3 hrs.	Some cytotoxicity at 48 μg/cm^2 at both 3 and 24 hrs.	Kisin et al., 2011
Comet assay	BEAS 2B cells (human bronchial epithelial cells) and MET-5A cells (human mesothelial cells)	0, 5, 10, 20, 40, 80, 120, 160, or 200 μg/cm^2 (corresponding to 0, 19, 38, 76, 152 304, 456, 608, or 760 μg/mL) for 3 and 24 hrs. Dispersed in cell culture media containing 0.06% bovine serum albumin.	See above entry for Lindberg et al., 2013	Positive: slightly positive for BEAS 2B cells due to significant increase in % tail DNA only at 80 and 120 μg/mL with no dose dependency. Positive in MET-5A cells due to significant dose-related increase in % tail DNA at 40 and 80 μg/mL. Results at higher doses not shown for MET-5A cells.	Cytotoxicity observed at doses of 40 μg/mL and above and SWCNTs were found in cytoplasm by TEM for both cell lines.	Lindberg et al., 2013
Assays for mitotic spindle damage and chromosome number (aneuploidy)	BEAS-2B (human respiratory epithelial cell line) for mitotic spindle damage and SAEC (primary human respiratory epithelial cells) for chromosome number (by FISH analysis)	0, 0.024, 0.24, 2.4, or 24 μg/cm^2 for 24 hrs and 72 hrs. CNTs were dispersed in culture medium with 10% fetal bovine serum.	1. CNI Inc., Houston 2. Dia 1-4 nm, Length 0.5-1 μm 3. 1040 m^2/g 4. Purity: 99% elemental carbon, 0.23% Fe 5. NR	Positive: significant dose-related increase in mitotic spindle damage at all doses in BEAS-2B cells. Positive: significant dose-related increase in aneuploidy at all doses in SEAC cells	No evidence of decrease in cell viability in BEAS-2B cells. Dose-related reduction in cell viability in SEAC cells; significant at 2.4 and 24 μg/cm^2. Laser scanning confocal microscopy showed nanotubes associated with the microtubules of the mitotic spindle apparatus, the DNA, and the	Sargent et al., 2012

Assay	Test system	Exposure	NT Characterization[a]	Result	Comments	Reference
					centrosome fragments.	
DNA Damage *In Vivo*[b]						
Comet assay	Male Crl:CD Sprague Dawley rats Tissue: lung	0, 0.04, or 0.2 mg/kg bw once per wk for 5 wks or a single dose of 0.2 or 1.0 mg/kg by IT instillation; animals sacrificed 3 hrs after last treatment (for repeated instillation), or 3 and 24 hrs after treatment (for single instillation). CNTs dispersed using 1% Tween-80.	1. Nikkiso Co., Ltd. 2. Dia. 1.8 nm 3. 878 m^2/g 4. Impurities: Fe 3,650 ppm, Cu 10 ppm, Zn 22 ppm, Ga 12 ppm, Rb 56 ppm 5. Dispersed rope-like aggregates	Negative: no increase in % tail DNA after either single instillation or repeated intermittent instillation.	Lung histopathology showed hemorrhage in the alveolus and infiltration of alveolar macrophages and neutrophils after both doses for both single and repeated instillation.	Naya et al., 2012a
DNA Adducts *In Vitro*						
Quantification of malondialdehyde (M_1dG) DNA adducts by immunoblot assay	BEAS 2B cells (human bronchial epithelial cells) and MET-5A cells (human mesothelial cells)	0, 1, 5, 10, 20, 40, 80, or 160 μg/cm^2 (corresponding to 0, 5, 25,50, 100, 200, 400, or 800 μg/mL) for 48 and 72 hrs. Dispersed in cell culture media with bovine serum albumin (BEAS-2B) or fetal bovine serum (MET-5A).	See above entry for Lindberg et al., 2013	Positive: in BEAS 2B cells significant increase in M_1dG DNA adducts at 5 μg/cm^2 after 48 hrs and at 10 and 40 μg/cm^2 after 72 hrs. In MeT-5A cells significant increase in M_1dG DNA adducts at 1, 5, 10, and 40 μg/cm^2 after 48 hrs, but significant decrease at 5 μg/cm^2 and above at 72 hrs.	Cytotoxicity observed at doses of 40 μg/mL and above and SWCNTs were found in cytoplasm by TEM for both cell lines.	Lindberg et al., 2013

FISH = fluorescence *in situ* hybridization; MN = micronucleus; NCE = normochromic erythrocytes; NR = Not reported; PCE = polychromic erythrocytes; ROS = reactive oxygen species; TEM = transmission electron microscopy

[a] NT characterization data are itemized as follows: 1. Source 2. Diameter and length 3. Surface area 4. Purity and impurities 5. State of aggregation; shape (bundles, tangles, ropes)

[b] *In vivo* studies in mammalian species involving all routes of exposure, including oral, inhalation, IP and IV routes are included in this table, although the IP and IV routes of exposure are generally not recommended for risk assessment without specific scientific justification.

Table E-4. Summary of Mutagenicity/Genotoxicity Data for MWCNTs

Assay	Test system	Exposure	NT Characterization[a]	Result		Comments	Reference
Mutation *In Vitro*							
Reverse mutation assay	*Salmonella typhimurium* strains TA98, TA100, TA1535, TA1537, and *Escherichia coli* WP2*uvr*A	0, 12, 37, 111, 333, 1000 µg/plate with and without S9 for 44-48 hrs. CNTs dispersed using serum albumin and DPPC-supplemented medium.	Hanwha Nanotech Low aspect ratio MWCNT: dia 10-15 nm, length 150 nm; High aspect ratio MWCNT: dia 10-15 nm, length ~10 µm Low aspect ratio MWCNT: 195.29 m^2/g; High aspect ratio 177.57 m^2/g Purity: Low aspect ratio MWCNT 99%; High aspect ratio MWCNT 95% Tangled agglomerates with dispersed fibers	Negative		Precipitation and aggregation observed at 333 µg/plate and above; no evidence of cytotoxicity. 'Low aspect ratio' CNTs were subjected to treatment expected to oxidize (functionalize) tube surface.	Kim et al., 2011a
Reverse mutation assay	*Salmonella typhimurium* strains TA98, TA100, TA1535, TA1537, and *Escherichia coli* WP2*uvr*A; pre-incubation assay	0, 1.56, 3.13, 6.25, 12.5, 25, 50, or 100 µg/plate without S9 for 48 hrs. CNTs were dispersed in 0.3% sodium carboxymethyl cellulose.	Nikkiso Co., Ltd.: N-MWCNT; Mitsui & Co., Ltd.: MWNT-7 N-MWCNT: dia. 44 nm; MWNT-7: dia. 70 nm N-MWCNT: 69 m^2/g; MWNT-7: 23 m^2/g N-MWCNT: 89 ppm Al, 16 ppm Cd, 53 ppm Fe MWNT-7: 3600 ppm Fe, 14 ppm Cr "Well-dispersed" (no visual documentation)	Negative for both test materials, N-MWCT and MWNT-7.		Precipitation observed at 50 and 100 µg/plate. No evidence of cytotoxicity.	Ema et al., 2012

Assay	Test system	Exposure	NT Characterization[a]	Result		Comments	Reference
Reverse mutation assay	*Salmonella typhimurium* strains TA100, TA98, TA1535, and TA1537; pre-incubation assay	0, 0.005, 0.01, 0.02, 0.03, or 0.04 mg/mL without S9 for 48 hrs. CNTs dispersed in 'bacterial exposure medium' (Xenomatrix, CH)	Cheap Tubes, Inc. Dia. 100 nm, Length 1-10 µm NR 0.12% Ni, 0.05% Fe "Fibrous bundles" (not clear whether CNTs were assessed in medium)	Negative		No evidence of cytotoxicity. TA98 strain was used to evaluate MWCNT/bacterial cell interaction and MWCNTs were shown to penetrate cells.	Clift et al., 2013
Mutation *In Vivo*[b]							
gpt and Spi$^-$ mutation assays	Male *gpt* delta transgenic mice; target tissue: lung	0 or 0.2 mg/animal single dose, two doses at 2 wk intervals, or once weekly for 4 wks by intratracheal instillation. CNTs dispersed using 0.05% Tween-80.	Mitsui & Co., Ltd. Dia. 90 nm (range 70-110); length 2 µm (range 1 – 4 µm) NR Reported in a previous paper (Sakamoto et al., J. Tox. Sci. 34:65-76 (2009) Mostly individual dispersed fibers Sakamoto et al., 2009	No increase in Spi$^-$ mutant frequency; increase in gpt mutant frequency only in the group receiving 0.2 mg/animal once weekly for 4 wk		Evidence of histopathology in lung.	Kato et al., 2013
SMART assay	*Drosophila melanogaster*	0, 50, 100, 150, 200, or 250 mg/mL; larvae were fed on medium at these concentrations for 48 hrs. Suspension information not given.	CNT Co., Ltd. (Korea) Dia. 10-40 nm; length 1-2 µm 298 m^2/g Purity 98.5%, 1.5% iron oxide, functionalized Loose, tangled agglomerates of fibers and ropes/bundles (dry powder)	Negative: no significant effect on mutant frequency.		Low but uniform dispersion of NTs in the gut of treated larvae were observed.	Machado et al., 2013
SMART assay	*Drosophila melanogaster*	0, 64, 160, 400, or 1000 mg/mL; larvae were fed on medium at these concentrations for 48 hrs. CNTs were suspended in	Synthesized by Laboratory of Nanoengineering at State University of Campinas, Brazil NR NR Purity: 98.95%; Impurities:Ni 0.11 wt%, Cu 0.94 wt%	Negative: no significant effect on mutant frequency.		NTs observable in intestine of treated larvae, but decreased over time suggesting possible excretion and low bioavailability.	de Andrade et al., 2014

Assay	Test system	Exposure	NT Characterization[a]	Result		Comments	Reference
		aqueous media without dispersants.	Tangled agglomerate (dry form)				
Clastogenicity *In Vitro*							
Chromo-somal aberrations	RAW 264.7 (a leukemia virus-transformed mouse macrophage cell line)	0, 1, 3, or 10 µg/mL for 24, 48 or 72 hrs. CNTs suspended in cell culture media without dispersants (cell cultures contained serum during experiments).	Sigma-Aldrich Dia 10-30 nm; length 0.5-50 µm (supplier data) 400 m^2/g Purity: >96% Impurities: ~1.5% Ni, ~0.2% Yttrium Agglomerates 2.4-3 µm in size	Positive: increase in chromosome aberrations at all doses.		Dose-dependent cytotoxicity was observed. An increase in ROS was observed in cells treated with 50 µg/mL for 5 hrs and 24 hrs. No increase in TNF-α was observed in cells treated with 10 or 50 µg/mL for 5 hrs or 24 hrs.	Di Giorgio et al., 2011
Chromo-somal aberrations	CHO-k1 (Chinese hamster ovary) cells	0, 1.563, 3.125, or 6.25 µg/mL without S9; 0, 6.25, 12.5, 25, or 50 µg/mL for 6 and 24 hrs with and without S9. CNTs dispersed using serum albumin and DPPC-supplemented medium.	See above entry for Kim et al., 2011a	Negative for both high- and low-aspect ratio MWCNTs.		Both high- and low-aspect ratio MWCNTs showed evidence of cytotoxicity; cytotoxicity was greater for high-aspect-ratio MWCNTs. Aggregation and precipitation reported at doses ≥ 50 µg/mL.	Kim et al., 2011a

Assay	Test system	Exposure	NT Characterization[a]	Result		Comments	Reference
Chromo-somal aberrations	Human peripheral blood lymphocytes	0, 6.25, 50, 100, 150, or 300 µg/mL for 24, 48, or 72 hrs. CNTs were dispersed in cell culture medium with 15% fetal bovine serum.	SES Research, Houston Dia. 10-30 nm; length 1-2 µm; described as short purified MWCNTs 60 m^2/g Purity: >95% CNTs Impurities: <2% amorphous carbon, <0.2% ash, traces of Ni Dense agglomerates up to several µm in size	Significant increase in chromosomal aberrations at the highest dose and at 50 µg/mL after 48 hrs. No dose response.		Highest dose selected based on 50% cytotoxicity at 600 µg/mL for 72 hrs.	Catalan et al., 2012
Chromo-somal aberrations	CHL/IU (Chinese hamster lung fibroblast cell line	0, 0.78, 1.56, 3.13, 6.25, 12.5, 25, 50, or 100 µg/mL for 6 hrs (with and without S9) and 24 hrs (without S9). CNTs were dispersed in 0.3% sodium carboxymethyl cellulose.	See above entry for Ema et al., 2012	Negative for structural aberrations: both test materials, N-MWCNT and MWNT-7; positive for numerical aberrations: slightly increased at 100 µg/mL for 6 hrs but not 24 hrs without S9 for N-MWCNT and strongly increased without S9 for MWNT-7 after both 6 and 24 hrs.		No evidence of growth inhibition	Ema et al., 2012
MN formation	RAW 264.7 (a leukemia virus-transformed mouse macrophage cell line)	0, 1, 3, or 10 µg/mL for 48 hrs. CNTs suspended in cell culture media without dispersants (cell cultures contained serum during experiments).	See above entry for Di Giorgio et al., 2011	Positive: significant dose-dependent increase in MN frequency.		Dose-dependent cytotoxicity was observed. An increase in ROS was observed in cells treated with 50 µg/mL for 5 hrs and 24 hrs. No increase in TNF-α was observed in cells treated with 10 or 50 µg/mL for 5 hrs or 24 hrs.	Di Giorgio et al., 2011

Assay	Test system	Exposure	NT Characterization[a]	Result		Comments	Reference
MN formation	A549 human lung carcinoma cell line	0, 20, 100, or 200 μg/mL for 48 hrs with and without S9. CNTs dispersed in 0.05% Tween-80.	See above entry for Kato et al., 2013	Positive: significant dose-dependent increase in MN at all doses.		Inhibition of cell growth to ~70% of controls at ≥ 20 μg/mL.	Kato et al., 2013
MN formation	BEAS-2B cells (human bronchial epithelial cells)	0, 5, 10, 20, 40, 80, 120, 160, or 200 μg/cm^2 (corresponding to 0, 25, 50, 100, 200, 400, 600, 800, or 1000 μg/mL) for 48 and 72 hrs. CNTs were dispersed in cell culture media supplemented with 0.06% bovine serum albumin.	SES Research (Houston) Dia. 10-30 nm; length 1-2 μm 60 m^2/g Purity: >95% CNTs Impurities: <0.2% ash, Dispersion techniques used produced evenly distributed CNT agglomerates of moderate size (based on data from Vippola et al., Hum. Exp. Toxicol. 28:377-385, 2009)	Negative		Some cytotoxicity; only 250 μg/cm^2 consistently decrease living cells by >50%. MWCNTs were found in cytoplasm by TEM.	Lindberg et al., 2013
MN formation	Human peripheral blood lymphocytes	Concentrations for the 6 MWCNTs tested included 0, 2.5, 5, 7.5, 15, 45, 60, 125, or 250 μg/mL. Each MWCNT was not tested at all of these concentrations. CNTs were dispersed in cell culture medium with 15-20% fetal bovine serum.	Joint Research Centre: NM-400, NM-201, NM-402, NM-403, Mitsui & Co., Ltd.: NRCWE-006, Cheap Tubes: NRCWE-007 Diam: NM-400 108 nm, NM-401 62.8 nm, NM-402 10.7 nm, NM-403 11.1 nm, NRCWE-006 69.4 nm, NRCWE-007 15.3 nm. Length: NM-400 726 nm, NM-401 3366 nm, NM-402 1141 nm, NM-403 394 nm, NRCWE-006 4424 nm, NRCWE-007 369 nm Aspect Ratio: NM-400 67.3, NM-401 53.6, NM-402 107.2, NM-403	Significant increase in MN frequency at all doses except 125 μg/mL for NM-403 (but no dose-response); at 2.5 and 15 μg/mL but not higher doses for NRCWE-006; and at 15 μg/mL only for NM-402.		Cytotoxicity data not reported.	Tavares et al., 2014

Assay	Test system	Exposure	NT Characterization[a]	Result		Comments	Reference
			35.6 nm, NRCWE-006 63.7, NRCWE-007 24.1 NM-400 280 m^2/g, NM-401 300 m^2/g, NM-402 250 m^2/g, NM-403 NR, NRCWE-006 24-28 m^2/g, NRCWE-007 233 m^2/g NR Degree of dispersion NM-400>NM-402>NM-403> NRCWE-007; Coarsest dispersions were for NM-401 and NRCWE-006. Deaggregation and disen-tanglement were less efficient for NM-401 and NRCWE-006 and moderate for NM-403				
MN formation	BEAS-2B cells (human bronchial epithelial cells)	MWCNT-S: 0, 2.5, 5, 10 or 20 $\mu g/cm^2$ (corresponding to 12.5, 25, 50 or 100 µg/mL) for 48 hrs MWCNT-T: 0, 5, 12.5, 25, 50, or 100 $\mu g/cm^2$ (corresponding to 25, 50, 250 or 500 µg/mL) for 48 hrs. CNTs were dispersed in cell culture media supplemented with 0.06 % bovine serum albumin.	Mitsui & Co., Ltd.: MWCNT-S, Cheap Tubes: MWCNT-T Dia: MWCNT-S 60 or 71 nm (two analyses at different conc.); MWCNT-T 21 nm (two analyses at different conc.) Length: MWCNT-S 7 µm. MWCNT-T 0.37 µm (from a previous publictation) MWCNT-S 22-29 m^2/g (range cited from 3 different publications), MWCNT-T 130-233 m^2/g (range cited from 2 different publications) Residues of Ni and Fe; <0.5 wt% Ni, Na, Fe, Al, Mg, Mn State of dispersion: MNCNT-S: minor fraction of MWCNTs fully dispersed; dominated by open-structured	Negative for both MWCNT-S and MWCNT-T.		Evidence of cytotoxicity. Higher doses could not be tested due to fibers compromising the analysis for MN. Highest dose for both MWCNT-S and MWCNT-T were at or above acceptable cytotoxicity limits.	Catalan et al., 2016

Assay	Test system	Exposure	NT Characterization[a]	Result		Comments	Reference
			agglomerates/ aggregates. MNCNT-T: very minor fraction of MWCNTs fully dispersed; dominated by dense agglomerates/ aggregates. Sedimentation: MWCNT-S: Rapid MWCNT-T: Rapid although <MWCNT-S				
Clastogenicity *In Vivo*[b]							
Chromo-somal aberrations	Bone marrow assay in male Swiss-Webster mice	0, 0.25, 0.5, or 0.75 mg/kg bw/d for 5 days by IP injection; animals sacrificed 24 hrs after last dose. CNTs were dispersed using a 1% Tween-80 medium.	NanoLab Non-functionalized MWCNT dia. 15-30 nm; length 15-20 µm; functionalized MWCNT dia. 11.5 nm 41 m^2/g and 42 m^2/g for purified and non-purified MWCNTs Purity >95%; functionalized MWCNT 2-7 wt% -COOH Dense agglomerates with hydrodynamic dia of >~1 µm	Positive: significant dose-related increase in chromosome aberrations for both functionalized and non-functionalized MWCNTs. No significant difference in response between functionalized and nonfunctionalized MWCNTs.		Dose-related increase in ROS for both functionalized and non-functionalized MWCNTs. Response greater in functionalized MWCNT.	Patlolla et al., 2010
MN assay	Bone marrow assay in male Swiss-Webster mice	0, 0.25, 0.5, or 0.75 mg/kg bw/d for 5 days by IP injection; animals sacrificed 24 hrs after last dose. CNTs were dispersed using a 1% Tween-80 medium.	See above entry for Patlolla et al., 2010	Positive: significant dose-related increase in MN frequency for both functionalized and non-functionalized MWCNTs. Response greater in functionalized MWCNT.		Dose-related increase in ROS for both functionalized and non-functionalized MWCNTs. Response greater in functionalized MWCNT.	Patlolla et al., 2010
MN assay	Bone marrow assay in male Swiss-Webster mice	0, 2, 5, or 10 mg/kg bw/d by IP injection for 2 days; animals sacrificed 24 hrs after last dose	Sigma-Aldrich Mean dia 22.55 nm, length 0.5-200 µm NR Bundles/ropes and agglomerates with mean	Positive: significant increase in MN frequency at all doses which was inversely related to dose.		Some evidence of bone marrow cytotoxicity: a dose-related decrease in % PCE was observed but was not statistically significant and was inversely related to dose.	Ghosh et al., 2011

Assay	Test system	Exposure	NT Characterization[a]	Result		Comments	Reference
		CNTs were suspended in aqueous medium without dispersants.	hydrodynamic dia. of 1895 nm.				
MN assay	Bone marrow assay in male ICR mice	0, 12.5, 25, or 50 mg/kg-bw by single IP injection; animals sacrificed 24 hrs after dosing. CNTs dispersed using serum albumin and DPPC-supplemented medium.	See above entry for Kim et al., 2011a	Negative: no signficant increase in MN frequency for either high- or low-aspect ratio MWCNTs.		No evidence of bone marrow toxicity based on no significant effect on PCE/ (PCE+NCE) ratio.	Kim et al., 2011a
MN assay	Bone marrow assay in male Crlj: CD1 (ICR) mice	0, 5, 10, or 20 mg/kg bw/d by oral gavage for 2 days; animals sacrificed 24 hrs after the last dose. CNTs were dispersed in 0.3% sodium carboxymethyl cellulose.	See above entry for Ema et al., 2012	Negative for both MWCNT test materials		No evidence of bone marrow toxicity as measured by % immature erythrocytes.	Ema et al., 2012
MN assay	Female C57Bl/6 mice evaluated for MN in bone marrow PCEs, peripheral blood PCEs, and lung alveolar type II cells.	Inhalation exposure to 10.8 mg/m^3 4 hrs per day for 4 days	See above entry for Catalan et al., 2016. State of dispersion for *in vivo* studies differed from *in vitro* studies; MWCNT-S was less dispersed with only a very minor fraction of fully dispersed MWCNTs. Dominated by dense to open-structured agglomerates/aggregates.	Alveolar type II cells: MWCNT-S positive Bone marrow PCEs: MWCNT-S: negative. Peripheral blood PCEs: MWCNT-S negative; MWCNT-T decreased MN frequency in bone marrow PCEs.		No evidence of bone marrow cytotoxicity based on % PCEs; uptake of both MWCNT-S and MWCNT-T by macro-phages; MWCNT-S also associated, to a lesser extent, with alveolar epithelial cells; evidence of lung inflammation with MWCNT-S.	Catalan et al., 2016

Assay	Test system	Exposure	NT Characterization[a]	Result		Comments	Reference
			MWCNT-T appeared more aggregated than in the *in vitro* dispersions. Very minor fraction fully dispersed. Dominated by dense agglomerates/aggregates.				
	DNA Damage *In Vitro*						
Comet assay	RAW 264.7 (a leukemia virus-transformed mouse macrophage cell line)	0, 1, 3, 10 or 50 μg/mL for 24 hrs. CNTs suspended in cell culture media without dispersants (cell cultures contained serum during experiments).	See above entry for Di Giorgio et al., 2011	Positive: increase in tail moment at all doses; greatest response at 3 μg/mL		Dose-dependent cytotoxicity was observed. An increase in ROS was observed in cells treated with 50 μg/mL for 5 hrs and 24 hrs. No increase in TNF-α was observed in cells treated with 10 or 50 μg/mL for 5 hrs or 24 hrs.	Di Giorgio et al., 2011
Comet assay	Human peripheral blood lymphocytes	0, 1, 2, 5, or 10 μg/mL for 3 hrs CNTs were suspended in aqueous medium without dispersants.	.	No dose-dependent effect on % tail DNA. Significant increase in % tail DNA only at 2 μg/mL. Decrease in % tail DNA proposed to be due to formation of crosslinks.		No significant effect on cell viability (trypan blue exclusion).	Ghosh et al., 2011
Comet assay	BEAS 2B cells (human bronchial epithelial cells) and MET-5A cells (human mesothelial cells)	0, 5, 10, 20, 40, 80, 120, 160, or 200 μg/cm^2 (corresponding to 0, 19, 38, 76, 152 304, 456, 608, or 760 μg/mL) for 24 and 48 hrs. CNTs were dispersed in cell culture media supplemented with 0.06% bovine	See above entry for Lindberg et al., 2013	BEAS 2B cells: negative. No significant increase in % tail DNA. MET-5A cells: positive due to increase in % tail DNA at 80, 120, and 160 μg/cm^2 after 48 hrs but no dose response; excessive cytotoxicity (>50%) at 120 and 160 μg/cm^2.		Cytotoxicity observed only at 250 μg/cm^2 in BEAS 2B cells. In MET-5A cells cytotoxicity at 40 μg/cm^2 and above. MWCNTs were found in cytoplasm by TEM for both cell lines.	Lindberg et al., 2013

Assay	Test system	Exposure	NT Characterization[a]	Result		Comments	Reference
		serum albumin.					
Comet assay	BEAS 2B cells (human bronchial epithelial cells)	0, 5, 10, 40, or 100 μg/mL for 2, 4, and 24 hrs. CNTs were suspended in aqueous medium without dispersants.	HeJi, Inc. (Hong Kong) Outside dia. 20-40 nm (manufacturer's data), mean 32 (range 3-66) nm (measured during study); Inside dia. 5-15 nm (manufacturer's data); Length 0.5-200 μm (manufacturer's data), range 70 nm to 7.8 μm (measured during study) NR Purity: 93.7% Impurities: Cl 0.20%, Fe 0.55%, Ni 1.86%, S 0.02% Tangled, loose agglomerates with extensive knotting and bundling	Std. comet assay: positive. Significant dose-related increase in % tail DNA at all doses at one or more time points. Fpg-modified comet assay: no evidence of oxidative DNA damage.		Cytotoxic effects included decreased cell viability (MTT assay), loss of cell membrane integrity (LDH assay), and surface morphological changes (SEM). MWCNT agglomerates entered cells at all doses and time points.	Cavallo et al., 2012
Comet assay	A549 human lung carcinoma cell line	MWCNT: 0, 5, 10, or 40 μg/mL for 2, 4, and 24 hrs MWCNT-OH: 0, 1, 5, 10, 20, or 40 μg/mL for 2, 4, and 24 hrs TEM was performed on CNTs suspended without dispersants, but for experiments CNTs were dispersed in cell culture medium with 10% fetal bovine serum.	HeJi (China): MWCNT and MWCNT-OH MWCNT: dia 32 nm, length 0.07-7.8 μm MWCNT-OH: dia. 18 nm, length 0.02-1.70 μm MWCNT: 106.7 m^2/g MWCNT-OH: 129.8 m^2/g Purity:97.37% Impurities: Cl 0.20%, Fe 0.55%, Ni 1.86% S 0.02%; functionalized NTs (MWCNT-OH) have –OH> 5 wt% Extensive bundling and supercoiling into high-aspect ratio aggregates forming larger agglomerates. Bundling more extensive in pristine	Std. comet assay: MWCNT: slight dose-dependent increase in tail moment at 2 and 4 hrs, becoming more pronounced at 24 hrs. MWCNT-OH: significant increase in tail moment at 5 μg/mL and above for all exposure times. Fpg-modified assay: no evidence of oxidative DNA damage.		Fpg-modified Comet assay also used to detect oxidative DNA base damage. Different cytotoxicity mechanisms for MWCNT (membrane damage) and MWCNT-OH (apoptosis).	Ursini et al., 2012a

Assay	Test system	Exposure	NT Characterization[a]	Result		Comments	Reference
			CNTs (~600 nm dia bundles/ropes vs ~300 nm for oxidized CNTs). (TEM done on non-wetted CNTs)				
Comet assay	A549 human lung carcinoma cell line	0, 10, 20, 40, or 100 µg/mL for 24 hrs. TEM was performed on CNTs suspended without dispersants, but for experiments CNTs were dispersed in cell culture medium with 10% fetal bovine serum.	HiJi, Inc. (China): MWCNT-OH Dia. mean 18 nm (range 10-60 nm), length 20 nm to 1.7 µm NR Purity: 97.37% Impurities: Cl 0.20%, Fe 0.55%, Ni 1.86%, S 0.02%; functionalized MWCNT-OH has –OH> 5 wt% Extensive bundling of non-wetted CNTs forming rope-like aggregates up to 60 nm dia and several µm length, which agglomerated as tangles. Individual CNTs were self-coiled into short bundles.	Positive: significant dose-related increase in tail moment at all doses. Fpg: no evidence of oxidative DNA damage in the fpg-modified assay.		Fpg-modified Comet assay also used to detect oxidative DNA base damage. Evidence of cytotoxicity through reduction in cell viability (MTT assay), induction of apoptosis, but no evidence of cell membrane damage (LDH assay).	Ursini et al., 2012b
Comet assay	A549 human lung carcinoma cell line; BEAS-2B cells (human bronchial epithelial cells)	0, 1, 5, 10, 20, or 40 µg/mL for 24 hrs; A549 cells cultured in RPMI with 10% FBS, BEAS-2B cells cultured in BEGM TEM was performed on CNTs suspended without dispersants, but for experiments CNTs were dispersed in cell culture	HeJi (China): MWCNT and MWCNT-COOH MWCNT: Dia. 32 nm; Length 0.70-7.80 µm MWCNT-COOH: Dia. 24.5 nm; Length 0.029-1.56 µm MWCNT: 106.7 m^2/g MWCNT-COOH; 139.1 m^2/g MWCNT: Purity: 97.37% Impurities: Cl 0.20%, Fe 0.55%, Ni 1.86%, S 0.02% MWCNT-COOH: Purity: 97.46% Impurities: Al 0.19%, Cl 1.02%, Co 1.09%, S 0.04% Extensive bundling and self-coiling of non-wetted CNTs	Std Comet assay: A549 cells, MWCNT: positive, significant dose-related increase in tail moment. MWCNT-COOH: negative, no significant increase in tail moment. BEAS-2B cells: positive for both MWCNT and MWCNT-COOH, significant dose-related increase in tail moment. Fpg-modified comet assay: no evidence of oxidative DNA damage for either MWCNT or		Fpg-modified Comet assay also used to detect oxidative DNA base damage. Viability (WST-1 assay): A549 cells, slight decrease in viability for both MWCNT and MWCNT-COOH; BEAS-2B cells, significant dose-dependent decrease in viability. Membrane integrity (LDH assay): A549 cells, significant dose-dependent decrease in membrane integrity; BEAS-2B cells, significant dose-dependent decrease in membrane integrity. Response greater than in A549 cells. Cell uptake (adherence to cell membrane or intra-cellular): rapid	Ursini et al., 2014

Assay	Test system	Exposure	NT Characterization[a]	Result		Comments	Reference
		medium with 10% fetal bovine serum.	into ropes and high-aspect-ratio aggregates. Non-aggregated CNTs were more common in oxidized form. Ropes and aggregates formed tangled agglomerates several µm across.	MWCNT-COOH.		increase in uptake starting at 8 hrs; significantly higher uptake for MWCNT-COOH than MWCNT, and higher uptake of both in A549 cells than in BEAS-2B cells. Cytokine release: A549 cells more susceptible to MWCNT-OOH and BEAS-2B cells to MWCNT.	
Comet assay	MML cells (FEI-Muta™ mouse lung epithelial cell line	0, 7.1, 14.1, 28.3, 56.6, or 113.2 µg/cm^2 (corresponding to 0, 12.5, 25, 50, 100, or 200 µg/mL) for 24 hrs. CNTs were dispersed in aqueous media with 2% murine serum.	Confidential: NRCWE-026 Standard; OECD WPMNM: NM-401, NM-402, NM-403; Misui/Hadoga: NRCWE-006; Cheaptubes: NRCWE-040, NRCWE-041, NRCWE-042, NRCWE-043, NRCWE-044, NRCWE-045, NRCWE-046, NRCWE-047, NRCWE-048, NRCWE-049 Dia. and Length (supplier data) NRCWE-026: dia. 9.5 nm, length 1.5µm; NM-401: dia. 10-30 nm, length 5-15 µm; NM-402: dia. NR, length NR; NM-403: dia. 10-15 nm, length 0.1-10 µm; NRCWE-006: dia. 40-90 nm, length NR; Group I (NRCW-040 NRCWE-041 and NRCWE-042): dia. 8-15 nm, length 10-50 µm; Group II (NRCWE-043, NRCWE-044, and NRCWE-045): dia.60 nm, length 10-20 µm; Group III (NRCWE-046, NRCWE-047, NRCWE-048 and NRCWE-049): dia. 13-18 nm, length 1-12 µm	Weakly positive for Group II test materials (MWCNTs with large dias and high Fe_2O_3 and Ni content). based on tail length. MWCNT-042 increased % tail DNA at 200 µg/mL)		No evidence of cytotoxicity.	Jackson et al., 2015

Assay	Test system	Exposure	NT Characterization[a]	Result		Comments	Reference
			Surface Area (Measured in study) NRCWE-026: 245 m^2/g, NM-401: 18 m^2/g, NM-402 226 m^2/g, NM-403: 135 m^2/g, NRCWE-006: 26 m^2/g, NRCWE-040: 150 m^2/g NRCWE-041: 152 m^2/g, NRCWE-042: 141 m^2/g, NRCWE-043: 82 m^2/g, NRCWE-044: 74 m^2/g, NRCWE-045: 119 m^2/g, NRCWE-046: 223 m^2/g, NRCWE-047: 216 m^2/g, NRCWE-048: 185 m^2/g, NRCWE-049: 199 m^2/g Purity: NRCWE-026 and NM-403 >90%; NM-401, Group I, and Group II: >95%; Group III: .99%; NM-402 NR Functionaliza-tion: NRCWE-041, NRCWE-044, and NRCWE-047: -OH functionalized; NRCWE-042, NRCWE-045, and NRCWE-048: -COOH functionalized; NRCWE-049: $-NH_2$ functionalized; all others pristine Dispersed CNTs were not assessed.				
Comet assay	BEAS-2B cells (human bronchial epithelial cells)	MWCNT-S: 0, 5, 10, 50 or 100 $\mu g/cm^2$ (corresponding to 0, 19, 38, 190, or 380 µg/mL) for 24 hrs. MWCNT-T: 0,	See above entry for Catalan et al., 2016	MWCNT-S: positive based on significant increase in % tail DNA at 5 and 10 $\mu g/cm^2$; % tail DNA also increased at 50 and 100 $\mu g/cm^2$ but not statistically significant;		Highest doses for both MWCNT-S and MWCNT-T were based on cytotoxicity	Catalan et al., 2016

Assay	Test system	Exposure	NT Characterization[a]	Result		Comments	Reference
		5, 50, 100, or 200 μg/cm^2 (corresponding to 0, 19, 38, 170, 380, or 760 μg/mL) for 24 hrs. CNTs dispersed in cell culture media supplemented with 0.06% bovine serum albumin.		no dose response. MWCNT-T: positive based on significant increase in % tail DNA at 200 μg/cm^2 and some evidence of dose response.			
γ-H2AX assay for double-stranded breaks	HUVEC cells (human umbilical vein endothelial cells)	0, 0.5, 5, or 20 μg/mL for 6, 12 or 24 hrs. CNTs were dispersed in cell culture medium with 10% fetal bovine serum.	Lawrence Berkeley National Laboratory Dia. 30 nm; Length <1 μm NR Purity: >95% Impurities: Ni 3.38%, Yttrium 0.67%, Fe 0.13% Thin ropes up to several μm in length, occasional dispersed fibers	Positive: significant dose-related increase in % γ-H2AX positive cells at all three time points, peaking at 12 hrs. Response reduced by pre-treatment with NAC.		Dose- and time- dependent decrease in cell viability (trypan blue) observed. ROS increased at 20 μg/mL, MDA at 5 and 20 μg/mL. ROS response reduced by pre-treatment with NAC. Increased GSH-Px and SOD activity at 0.5 and 5 μg/mL.	Guo et al., 2011
Assays for mitotic spindle damage and chromo-some number (aneuploidy)	BEAS-2B (human respiratory epithelial cell line) for mitotic spindle damage and SAEC (primary respiratory epithelial cells) for chromosome number (by FISH analysis)	0, 0024, 0.24, 2.4, or 24 μg/cm^2 for 24 hrs. CNTs were suspended in aqueous medium without dispersants, but exposures occurred in cell cultures with 10% fetal bovine serum.	Nanolab Inc. Ave. dia. 15 nm; Ave. length 825 nm NR Composition of acid washed MWCNT: Carbon 91.86 wt%, Oxygen 6.58 wt%, Fe 0.81 wt %, Cu 0.28 wt%, S 0.26 w%, Si 0.22 wt% (from supplemental material) Oxygen content is due to –COOH func-tionalization AFM was not well-represented, but CNTs appeared to be dispersed with some bundling	Positive for both endpoints based on dose dependent increases in mitotic spindle damage (BEAS-2B cells) and aneuploidy (SAEC cells).		Cytotoxicity not reported. Laser scanning confocal microscopy showed nanotubes associated with the microtubules of the mitotic spindle apparatus, the DNA, and the centrosome.	Siegrist et al., 2014

Assay	Test system	Exposure	NT Characterization[a]	Result		Comments	Reference
SCE	CHO (Chinese hamster ovary) AA8 cells	0, 0.1, 1.0, or 2.0 μg/mL for 1 hr CNTs dispersed in 0.05% Tween-80.	See above entry for Kato et al., 2013	Positive: significantly increased frequency of SCE.		Cytotoxicity not reported.	Kato et al., 2013
	DNA Damage *In Vivo*[b]						
Comet assay	Male Swiss-Webster mice target tissue: lymphocytes	0, 0.25, 0.5, or 0.75 mg/kg bw/d for 5 days by intraperitoneal injection; time of sacrifice after last dose NR. CNTs were dispersed using a 1% Tween-80 medium.	See above entry for Patlolla et al., 2010	Positive: significant dose-related increase in % tail DNA for both functionalized and non-functionalized MWCNT test materials. DNA damage greater with functionalized MWCNT.			Patlolla et al., 2010
Comet assay	Male Swiss Webster mice tissues evaluated: bone marrow cells	0, 2, 5, or 10 mg/kg bw/d by intraperitoneal injection for 2 days; animals sacrificed 24 hrs after last dose. CNTs were suspended in aqueous medium without dispersants.	See above entry for Ghosh et al., 2011	Significant increase in % tail DNA at 2 and 5 mg/kg bw/day, but not at 10 mg/kg bw/day. Increase in % tail DNA was inversely related to dose.		Some evidence of bone marrow cytotoxicity: a dose-related decrease in % PCE was observed but was not statistically significant.	Ghosh et al., 2011
Comet assay	Male ICR mice tissues evaluated: lung	Single dose of 0.05 or 0.2 mg/mouse by intratracheal instillation; animals sacrificed 3 hrs after dosing. CNTs dispersed in 0.05% Tween-80.	See above entry for Kato et al., 2013	Positive: significant dose-dependent increase in % tail DNA.			Kato et al., 2013
Comet	Male and	Nose only	Hanwha Nanotech	Positive: Significant		MWCNTs were deposited in the	Kim et al., 2014

Assay	Test system	Exposure	NT Characterization[a]	Result		Comments	Reference
assay	female F344 rats, tissues evaluated: lung	inhalation exposure at 0, 0.17, 0.49, or 0.96 mg/m^3 for 6 h/d, 5 d/wk for 28 days. Animals sacrificed on day 0, day 28 or day 90 post-exposure	Dia 10-15 nm; Mean length 330 nm (range 68-1517 nm) 224.9 m^2/g Purity: >95% Impurities: Fe <2 wt%, Co < wt%, Al_2O_3 <4 wt% Dispersed fibers	increase in Olive tail moment at all exposure groups at day 0 post-exposure. High dose males and middle and high dose females also showed significant increases in Olive tail moment at 90 days post-exposure.		lung. H_2O_2 was measured in BALF as a marker for ROS. In males, H_2O_2 was increased on day 0 and day 28 post-exposure. In females, H_2O_2 was not significantly affected. No significant change in inflammatory cytokines in BALF.	
Comet assay	Male Sprague Dawley rats tissues evaluated: lung	Inhalation chamber exposure to 0, 0.16, 0.34, or 0.94 mg/m^3 for 6 h/d for 5 days. Animals sacrificed on day 0 and 1 month post-exposure.	Hanwha Nanotech Dia 10-15 nm; mean length 2.57 µm (range0.5-20 µm) 224.9 m^2/g Purity: >95% Impurities: Fe <2 wt%; Co <2 wt%, Al_2O_3 <4 wt% Dispersed fibers, with frequent self-coiling or bundling with other single fibers	Positive: significant increase in Olive tail moment after high dose exposure on day 0 and 1 month post-exposure.		H_2O_2 in BALF was measured in BALF as a marker for ROS, and showed a significant increase at 1 month post-exposure in the high dose group. Dark field light microscopy showed MWCNT deposition in alveolar epithelium and alveolar macrophages on day 0 post-exposure and at 1 month post-exposure.	Kim et al., 2012
Comet assay	Female C57Bl/6 mice target tissue: lung and BALF cells	Inhalation: 0 or 8.2 mg/m^3 for MWCNT-S and 0 or 17.5 mg/m^3 for MWCNT-T 4 hrs per day for 4 days. Animals sacrificed 24 hrs after last exposure. Pharyngeal aspiration: 0 50, 100 or 200 µg/mouse. Animals sacrificed 24 hrs after exposure.	See above entry for Catalan et al., 2016. State of dispersion for *in vivo* studies differed from *in vitro* studies; MWCNT-S was less dispersed with only a very minor fraction of fully dispersed MWCNTs. Dominated by dense to open-structured agglomerates/aggregates. MWCNT-T appeared more aggregated than in the *in vitro* dispersions. Very minor fraction fully dispersed.	Inhalation: MWCNT-S, significant increase in % tail DNA in both BALF and lung cells. MWCNT-T, no increase in % tail DNA. Pharyngeal aspiration: MWCNT-S - significant increase in % tail DNA in lung cells only at 200 µg/mouse. MWCNT-T, no increase in % tail DNA.		Lung histopathology showed hemorrhage in the alveolus and infiltration of alveolar macrophages and neutrophils after both doses for both single and repeated instillation.	Catalan et al., 2016

Assay	Test system	Exposure	NT Characterization[a]	Result		Comments	Reference
		For aspiration, CNTs were dispersed in aqueous medium with 0.06% bovine serum albumin.					
γ-H_2AX assay for double-stranded breaks	Female C57Bl/6 mice target tissue: lung cells and blood mononuclear leukocytes	Inhalation: 0 or 8.2 mg/m^3 for MWCNT-S and 0 or 17.5 mg/m^3 for MWCNT-T 4 hrs per day for 4 days; animals sacrificed 24 hrs after exposure. Pharyngeal aspiration: 0 50, 100 or 200 μg/mouse. For aspiration; animals sacrificed 24 hrs after exposure. CNTs were dispersed in aqueous medium with 0.06% bovine serum albumin.	See above entry for Catalan et al., 2016. State of dispersion for *in vivo* studies differed from *in vitro* studies; MWCNT-S was less dispersed with only a very minor fraction of fully dispersed MWCNTs. Dominated by dense to open-structured agglomerates/aggregates. MWCNT-T appeared more aggregated than in the *in vitro* dispersions. Very minor fraction fully dispersed.	Inhalation: MWCNT-S and MWCNT-T. Negative: no significant increase in γ-H_2AX positive cells in lung or in blood leukocytes by either inhalation or pharyngeal exposure. .		Inhalation: Both MWCNT materials distributed mainly in alveolar lung tissue. MWCNT-S showed evidence of an inflammatory response. Pharyngeal aspiration: Dose-dependent distribution of both MWCNT materials mainly in bronchi and, to a lesser extent, in alveolar lung tissue.	Catalan et al., 2016
	DNA Adducts *In Vitro*						
Quantitation of malon-dialdehyde (M_1dG) DNA adducts by immunoblot assay	BEAS 2B cells (human bronchial epithelial cells) and MET-5A cells (human mesothelial cells)	0, 1, 5, 10, 20, 40, 80, or 160 μg/cm^2 (corresponding to 0, 5, 25,50, 100, 200, 400, or 800 μg/mL) for 48 and 72 hrs. CNTs were dispersed in cell	See entry above for Lindberg et al., 2013	Positive: in BEAS 2B cells, significant increase in M_1dG DNA adducts at 5 μg/cm^2 after 48 hrs and at 10 and 40 μg/cm^2 after 72 hrs. In MeT-5A cells significant increase in M_1dG DNA adducts at 1, 5, 10, and 40 μg/cm^2 after		Cytotoxicity observed at doses of 40 μg/mL and above and MWCNTs were found in cytoplasm by TEM for both cell lines.	Lindberg et al., 2013

Assay	Test system	Exposure	NT Characterization[a]	Result		Comments	Reference
		culture media supplemented with 0.06% bovine serum albumin.		48 hrs but significant decrease at 5 μg/cm^2 and above at 72 hrs.			
DNA Adducts *In Vivo*[b]							
Quanti-tation of oxidative and lipid peroxide-related DNA adducts by LC-MS/MS	Male *gpt* delta mice; target tissue - lung	Single dose of 0.2 mg/mouse; by intratracheal instillation; animals sacrificed at 3, 24, 72 or 168 hrs after dosing CNTs dispersed in 0.05% Tween-80.	See above entry for Kato et al., 2013	Positive: DNA adducts related to oxidative stress and lipid peroxidation (8-oxodG, HεdA, HεdC) were increased up to 72 hrs, then slightly less so at 168 hrs.		Evidence of histopathology in lung.	Kato et al.,2013

[a]NT characterization data are itemized as follows: 1. Source 2. Diameter and length 3. Surface area 4. Purity and impurities 5. State of aggregation; shape (bundles, tangles, ropes)
[b]*In vivo* studies in mammalian species involving all routes of exposure, including oral, inhalation, intraperitoneal and intravenous routes are included in this table, although the intraperitoneal and intravenous routes of exposure are generally not recommended for risk assessment without specific scientific justification.
BALF = bronchial alveolar lavage fluid; FISH = fluorescence *in situ* hybridization; *gpt* = guanine phosphoribosyltransferase; GSH-Px = glutathione peroxidase; HεdA = heptanone etheno-2'-deoxyadenine HεdC = heptanone etheno-2'-deoxycytidine; LDH = lactate dehydrogenase; M_1dG = malondialdehyde DNA adduct; MN = micronucleus; NAC = N-acetylcysteine; NCE = normochromic erythrocytes; NR = Not reported; 8-oxo-dG = 8-oxo-7,8-dihydro-2'-deoxyguanosine; PCE = polychromic erythrocytes; ROS = reactive oxygen species; SCE = sister chromatid exchange; SEM = scanning electron microscopy; SMART = somatic mutation and recombination test; SOD = superoxide dismutase; TEM = transmission electron microscopy

Appendix F

Developmental and Reproductive Toxicity (DART) Studies of Ag NPs via Parenteral Routes of Exposure

*References for Appendices are located in Section 7 of Volume 1 report. Abbreviations for Appendices are located in Abbreviation list, Volume 1 report.

1 Reproductive Toxicity

Synthesized Ag NPs (~ 45 nm in diameter) were administered by a single IV injection into the marginal ear vein at 0 (physiological saline) or 0.6 mg/kg bw at a volume of 2.0 mL/kg to eight NZW male rabbits per group and evaluated for up to 126 days (Castellini et al., 2014). The Ag NPs produced higher seminal ROS, less motile sperm, and lower curvilinear velocity and oxygen consumption in ejaculated sperm after 21, 42, 63, 84, 105 and 126 days of exposure, than control animals. Serum testosterone, sperm concentration, semen volume and morphology of the testes were not affected by treatment. Ag NPs, however, were visible (via TEM) in spermatids and ejaculated sperm. Results show that Ag NPs can cross the blood-testes barrier to reach the testes via IV administration and compromise sperm motility, speed, and acrosome and mitochondria shape and function.

Han et al. (2016) demonstrated the adverse effects of Ag NPs (20 nm in diameter) on germ cells using male and female CD-1 (ICR) mice. Six/sex/group mice were IV injected (tail vein) with a single bolus of 0 (saline), 0.5, or 1.0 mg/kg Ag NPs. Two groups were injected with 0.5 or 1.0 mg/kg $AgNO_3$ (Ag+) as a comparative control. For fertility testing, four additional groups (6/sex/group) of CD-1 (ICR) mice were injected once with either: 0 (vehicle) for both males and females; 1.0 mg/kg Ag NPs in males and 0 (vehicle) in females; 0 (vehicle) in males and 1.0 mg/kg Ag NPs in females, or 1.0 mg/kg Ag NPs in males and females. Each group was mated after 4 weeks and sacrificed at GD 8.5 to harvest oviducts and evaluate the morphology of the implants. Ag NP-treated mice at 1.0 mg/mL showed a significant loss of male and female germ cells. In addition, Ag NP-treated males and females could fertilize and implantation resulted; however, a significant number of the GD 8.5 implants were arrested, indicating that treatment resulted in subfertility or infertility. A similar toxicity trend was observed between Ag NPs and $AgNO_3$ concentrations, with dosages of Ag+ showing more cytotoxicity to germ cells. The authors speculated this could be due to the faster release of Ag+ from $AgNO_3$ than from Ag NPs.

Purchased Ag particles (20 nm Ag NPs or 200 nm Ag sub-micron particles) were administered via tail vein as a single bolus IV injection to male Wistar rats at 0 (0.9% NaCl solution), 5 or 10 mg/kg of body weight (Dziendzikowska et al., 2016). After 1, 7 and 28 days of exposure to Ag NPs and 200 nm Ag sub-micron particles, depending on the dose and particle size, adverse effects on hormonal regulation were observed: altered luteinizing hormone concentration in the plasma and the sex hormone concentration in the plasma and testes, and decreased 5α-reductase type 1 and the aromatase protein level in the testes. Plasma and testicular levels of testosterone and dihydrotestosterone were significantly decreased at both 7 and 28 days after treatment. No change in the prolactin and sex hormone-binding globulin concentration was observed.

Doses of 1 mg/kg of citrate-coated 10 nm Ag NPs were IV injected into the tail vein of 36 male CD1 mice every 3 days (5 times total) over 12 days (Garcia et al., 2014), with another 36 male mice being injected with vehicle (PBS). One group of treated mice (n = 12 per group) were then used for breeding assessment beginning on days 15, 60, or 120 post-initial treatment (36 total). Two untreated female mice were mated with each of the treated males and sacrificed on day 17 post-mating with pregnancy status and number of fetuses determined. The second group of treated males (n = 36) were sacrificed on day 15 (half of them) and the remaining half on day 120. There were no significant changes in body and testes weights, sperm concentration and

motility, fertility indices, or FSH and LH serum concentrations; however, serum and intra-testicular testosterone concentrations were significantly increased 15 days after initial treatment. Histologic evaluation of testicular sections revealed significant changes in epithelium morphology, germ cell apoptosis, and Leydig cell size.

Ninety-six male Wistar rats were administered a single IV bolus dose of Ag NPs to examine any acute adverse effect on spermatogenesis and seminiferous tubule morphology (Gromadzka-Ostrowska et al., 2012). The uncoated Ag NPs were purchased in 20 ± 5 nm and 200 ± 50 nm sizes. The rats were divided into 4 groups of 24 and injected (tail vein) with 5 or 10 mg/kg of the 20 nm Ag NPs or 5 mg/kg of the 200 nm Ag NPs; the fourth group was injected with 0.9% NaCl solution. Eight rats from each group were necropsied after 1, 7 and 28 days and the testes and sperm evaluated. There were no significant differences in body, epididymal or testicular weights at any time point. A statistically significant decrease in epididymal sperm count was reported for both treatment groups at all time points; there were no differences in the number of abnormal sperm. Morphological measurement of the seminiferous tubules in the testes showed a statistically significant increase in tubular area, circumference and diameter after 28 days for the rats treated with 5 mg/kg of the 200 nm Ag NPs.

Coated Ag NPs (50 to 60 nm) were administrated IP at 0 (saline), 0.5, 1, or 5 mg/kg for 35 days to male albino rats (Rezazadeh-Reyhani et al., 2015). The Ag NPs resulted in dose-related enhanced germinal cells degeneration, necrosis, seminiferous tubules atrophy and decreased serum levels of LH, FSH and testosterone.

Hormone levels for male reproductive regulation were shown to be altered with IV administration of Ag NPs (Gromadzka-Ostrowska et al., 2012; Garcia et al., 2014; Dziendzikowska et al., 2016).

2 Developmental Toxicity

Synthesized Ag NPs were administered to pregnant CD-1 (ICR) mice (20/group) via a single IV infusion (site not specified) at 0 (phosphate buffered saline) or 1.0 mg/kg doses on GD 6.5 (Zhang et al., 2015). The Ag NPs were spherical in shape with an average size of 8 nm (range 4-24 nm). At GDs 13.5, 15.5, or 17.5 the pregnant mice were euthanized, and the embryo and placenta isolated to determine the meiotic status of oocytes in the fetus and to determine progression of female germ cells. DNA methylation studies were performed on fetal, placental, and postnatal development. Quantitative real-time polymerase chain reaction analysis and Western blot were used to analyze regulation of expression of various genes. Ag NP exposure increased the meiotic progression of female germ cells in the fetal mouse ovaries, and maternal Ag NPs exposure significantly disrupted imprinted gene expression in GD 15.5 embryos and placentas. The results from this study indicate that early exposure to Ag NPs has the potential to disrupt fetal and postnatal development through epigenetic changes in the embryo and abnormal development of the placenta.

Ag NPs (99.9% pure) were purchased as 10 nm spheres, measuring to be 32 ± 6.6 nm (by TEM). They were injected SC at 0 (sodium citrate suspension), 5, or 50 µg/mouse every 3 days during pregnancy into female NMRI mice (10/group) (Rashno et al., 2014). Pups were assessed for growth and neurobehavioral development until PND 28. There were delays in development of

some neurobehavioral reflexes but no adverse effects on the dam, their reproductive performance, or pup growth and attainment of physical landmarks (except for delayed fur development at 50 µg/mouse).

The same laboratory dosed female NMRI mice (10/group) SC with 32 nm Ag NPs by SEM at 0 (sodium citrate suspension), 0.2, or 2.0 mg/kg body weight every 3 days from initiation of mating until delivery (Ghaderi et al., 2015). The offspring were not further treated, and were tested at PND 44 to 49 for spatial memory, passive avoidance learning, stress, anxiety-like behaviors and locomotor activities. Prenatal exposure of Ag NPs significantly impaired cognitive behavior in the Morris water maze on PNDs 44 to 49. There was no indication that anxiety behaviors in the elevated water maze, open field, or light/dark box were affected in the Ag NP exposed groups.

Tabatabaei and coworkers (2015), also in the same laboratory as above, and using the same strain of mice, group size, dosages, route of administration and same purchased Ag NPs, measured offspring behavior. Depression behaviors were assessed by tail suspension tests and forced swimming tests in 45-day-old male and female progeny (6 groups, n = 10/group). In males, both the 0.2 and 2.0 doses of Ag NPs significantly decreased mobility and increased immobility time in the forced swimming test, but in the female offspring, no effects were observed in mobility and immobility time. In the tail suspension test, 2 mg/kg of Ag NPs led to significantly decreased mobility time and significantly increased immobility times in female offspring, but in males no significant effect was observed on mobility and immobility times. The authors concluded that the prenatal exposure to 10 nm Ag NPs at 2 mg/kg caused gender-specific depression-like behaviors in offspring.

Female Wistar rats, 5/group, were SC injected equal volumes of 0.2 mL of suspension on days 1, 4, 7, 10, 13, 16 and 19 of pregnancy with 0, 0.2, or 2.0 mg/kg/day of synthesized Ag NPs (16 ± 4.6 nm) (Tabatabaei et al., 2017). Gene expression of tyrosine hydroxylase and monoamine oxidase A was analyzed in the brain of male and female offspring on days of 1, 7, 14 and 21 after parturition. Ag NP exposure during pregnancy resulted in increases in the expression levels of tyrosine hydroxylase in the brain of male and female pups in a time- and dose-dependent manner at all tested days. Ag NPs had stimulatory effect on monoamine oxidase A mRNA expression in pups only at the age of 7 and 14 days. Female pups showed a higher level of these enzymes compared to male pups. Results demonstrated that the exposure of pregnant rats to Ag NPs increased the expression of genes involved in dopamine metabolism in the brain of offspring.

Table F-1. Summary of DART Studies of Ag NPs via Other Routes of Exposure

Species n/sex/group	Exposure concentrations frequency, duration	Particle characteristics	Route	Responses	Comments	Reference
Male NZW rabbits 8/group	0.6 mg/kg bw	Synthesized ~45 nm in diameter	IV	TEM analysis showed no morphological damage in testes; however, Ag NPs were visible in spermatids and ejaculated sperm.	Reproductive study. Ag can reach testes and compromise sperm motility and speed	Castellini et al., 2014
Male and female CD-1 mice 12/sex/group	0 or 1 mg/kg/day; every 3 days for 5 times	Purchased citrate-coated 10 nm in diameter	IV	Testosterone concentrations were significantly increased	Reproductive study. Ag NP affect Leydig cell function, yielding increasing testicular and serum testosterone levels	Garcia et al., 2014
Male albino rats 6/group	0, 0.5, 1, or 5 mg/kg/d; 35 days	Purchased 50-60 nm coated	IP	Adverse male repro effects (hormonal and histological) at 0.5, 1, and 5 mg/kg/day	Reproductive study. Effects via antioxidant and endocrine pathways	Rezazadeh-Reyhani et al., 2015
Male and female CD-1 mice 6/sex/group	0, 0.5, or 1.0 mg/kg/d; 4 weeks	Synthesized 20 nm (range 2-26 nm)	IV	Treated mice could mate, resulting in implantation, most implants were arrested at GD 8.5, indicating subfertility or infertility	Reproductive study. Histopathology of treated mice shows significant ↓ of male and female germ cells	Han et al., 2016
Male Wistar rats 21, 24, 24 and 24/group	0, 5, or 10 mg/kg of 20 nm or 5 mg/kg of 200 nm; 28 days	Purchased 20 ± 5 nm and 200 ± 50 nm in diameter	IV	Plasma and testicular levels of testosterone and dihydrotestosterone were significantly decreased.	Reproductive study - adverse effect on the hormonal regulation of male reproductive function	Dziendzikowska et al., 2016
Male Wistar rats 24/group	0, 5, or 10 mg/kg of 20 nm or 5 mg/kg of 200 nm; 1 bolus	Purchased 20 ± 5 nm and 200 ± 50 nm in diameter	IV	5 and 10 mg/kg of 20 nm and 5 mg/kg of 200 nm decreased epididymal sperm counts	Reproductive study. 20 nm NPs were more toxic than 200 nm particles	Gromadzka-Ostrowska et al., 2012
Female NMRI mice 10/group	0, 5, or 50 µg/mouse every 3 days of pregnancy	Purchased 10 nm; measured 32 ± 6.6 nm	SC	Delayed development of some neuro-behavioral reflexes in pups	No adverse effects on pup growth	Rashno et al., 2014
Female NMRI mice 10/group	0, 0.2, or 2.0 mg/kg; every 3 days GD 3 to 17	Purchased 32 ± 6.6 nm; ranged 5-70 nm in diameter	SC	Ag NPs significantly impaired cognitive behavior in Morris water maze in offspring of treated dams	Deficits in various neurobehavioral tests	Ghaderi et al., 2015

Species n/sex/group	Exposure concentrations frequency, duration	Particle characteristics	Route	Responses	Comments	Reference
NMRI mice 10/group	0, 0.2, or 2.0 mg/kg/d every 3 days GDs 3 to 17	Purchased 10 nm	SC	Gender-specific depression-like behaviors in offspring of 0.2 or 2.0 mg/kg/d groups	Assessed by tail suspension test and forced swimming test, in 45-day-old progenies	Tabatabaei et al., 2015
Female Wistar rats; 5/group	0, 0.2, or 2.0 mg/kg/d; GDs 1 and every 3rd day	Synthesized 16 ± 4.6 nm (range 5-75 nm)	IP	Both dosages (0.2, or 2.0 mg/kg/d) adversely affect gene expression pup brains for dopamine metabolism	Exposure during pregnancy ↑ genes for dopamine metab-olism in brain of pups	Tabatabaei et al., 2017
Female CD-1 mice; 20/group	0 or 1.0 mg/kg/d GD 6.5	Synthesized spherical 8 nm average; range 4-24 nm in diameter	IV	Increased meiotic progression germ cells in fetal ovaries and disrupted imprinted gene expression in embryos	Early exposure has potential to disrupt development through epigenetic changes	Zhang et al., 2015

3 Summary

It is not likely that humans would be exposed to NPs from consumer products via IP or IV routes. However, these routes may provide insight for data gaps for more common routes. SC or IV studies may provide an indication of potential reproductive/developmental effects should there be dermal exposure to damaged skin. These routes also provide information as to kinetics, such as transfer across the blood-brain barrier, blood-testes barrier, and transplacental transfer.

Several IV and IP studies (Gromadzka-Ostrowska et al., 2012; Castellini et al., 2014; Garcia et al.,2014; Rezazadeh-Reyhani et al., 2015; Han et al., 2016; Dziendzikowska et al., 2016) support the adverse male reproductive effects of Ag NPs reported in oral studies. They provide a clear indication that Ag NPs can cross the blood-testes barrier and suggest they influence hormonal regulation.

Several IV, IP, and SC developmental studies (Rashno et al., 2014; Ghaderi et al., 2015; Tabatabaei et al., 2015, 2017) fill data gaps for developmental neurobehavioral testing and indicate neurochemical alterations. These endpoints were not evaluated via the oral or inhalational routes. Zhang et al. (2015) may indicate that early exposure has the potential to disrupt development through epigenetic changes. This was not evaluated by oral, dermal or inhalation routes and requires further investigation.

Appendix G*

Mutagenicity/Genotoxicity Studies of Ag NPs

*References for Appendices are located in Section 7 of Volume 1 report. Abbreviations for Appendices are located in Abbreviation list, Volume 1 report.

G. Mutagenicity/Genotoxicity Studies of Ag NPs

1 *In Vitro* Mutagenicity Studies

Seven i*n vitro* mutagenicity tests in bacteria (Li et al., 2012; Kim et al., 2013a, b; Butler et al., 2015; Chen et al., 2015a; Heshmati et al., 2015; and Guo et al., 2016) have not shown any evidence of mutagenicity for Ag NP test materials that varied in size and surface coating or lack thereof. No uptake of Ag NPs into the bacterial cells was reported in studies where this was evaluated by TEM (Butler et al., 2015; Guo et al., 2016). The lack of uptake by bacterial cells, as well as the significant anti-bacterial properties of Ag, suggest that bacterial mutagenicity tests such as the Ames test are not well-suited for the evaluation of Ag NP mutagenicity.

Results of *in vitro* mammalian cell mutation assays have included mouse lymphoma $tk^{+/-}$ assays (Kim et al., 2010a; Mei et al., 2012; Gabelova et al., 2017; Guo et al., 2016), HPRT assays in either B79 or CHO cells (Huk et al., 2015; Guigas et al., 2017) and a LacZ mutation assay in mouse embryonic fibroblasts isolated from transgenic C57BL/6 mice carrying the lacZ gene (Park et al., 2011).

The mouse lymphoma assays gave mixed results, with positive responses in two studies (Mei et al., 2012; Guo et al., 2016) and negative responses in two studies (Kim et al., 2010a; Gabelova et al., 2017). The six Ag NP test materials studied by Guo et al. (2016) varied in particle size (20, 50, and 100 nm) and coating (either PVP- or citrate-coated). The test materials varied in mutagenic potency by 12-fold. Citrate-coated 20 nm Ag NPs were more potent than PVP-coated 20 nm Ag NPs. The smaller Ag NPs had a higher mutagenic potency per unit weight than the larger Ag NPs. Mei et al. (2012) tested a 5 nm uncoated Ag NP and also observed an increase in mutation frequency at the tk locus. HPRT mutation assays conducted by two groups of investigators have both shown positive results (Huk et al., 2015; Guigas et al., 2017).

Gabelova et al. (2017) observed no increase in mutant frequency in a mouse lymphoma assay of a 14 nm Tween 20/PEG-coated Ag NPs. These investigators also tested a Ag NP test material with a nanorod/wire shape rather than spherical or spheroid shape, and this test material was positive in the mouse lymphoma assay. It should be noted that when information on particle shape was provided, all other Ag NPs studied in the mutagenicity/genotoxicity studies included in this Appendix were described as spherical or spheroid. Lastly, a 100 nm Ag NP test material with no information provided about coating was tested by Kim et al. (2010) and did not induce mutations at the tk locus.

An *in vitro* assay utilizing mouse embryo fibroblasts isolated from embryos of transgenic mice containing the bacterial lacZ gene as a reporter gene was published by Park et al. (2011). Three Ag NP test materials that differed in particle size (20, 80 and 113 nm) were evaluated, and the results were equivocal. For the 20 nm Ag NPs, no increase in mutation frequency was observed at lower doses (up to 3 μg/ml), and higher concentrations were too cytotoxic to evaluate. For the 80 nm Ag NPs a dose-related increase in mutation frequency was observed, but the increases were not statistically significant. For the 113 nm Ag NPs, an increase in mutation frequency was observed, but it was neither dose-related nor statistically significant. All doses that showed an increase in mutation frequency were cytotoxic, showing a greater than 20 percent decrease in metabolic activity. NP size influenced cytotoxicity. The 20 nm Ag NPs could not be tested at concentrations higher than 3 μg/ml, while 80 and 113 nm Ag NPs were tested up to 50 μg/ml.

Although Ag NPs have shown mixed results in mutagenicity assays in mammalian cells, the data suggest that at least some Ag NPs are mutagenic. Small size and citrate-coated Ag NPs appear to have greater mutagenic potency.

2 *In Vitro* Genotoxicity Studies

2.1 Chromosomal Aberrations

Four chromosomal aberration assays with Ag NPs have produced mixed results. Two studies produced positive results, and particle characteristics of the test materials were different. Ernest et al. (2013) tested uncoated less than 100 nm Ag NPs and reported chromosomal aberrations at 15 and 25 μg/ml but not 5 μg/ml in human peripheral blood lymphocytes, while Chen et al. (2015a) reported chromosomal aberrations with an 8.6 nm poly(styrene-comaleic anhydride)-grafting poly(oxyalkylene)-coated-(SMA-Ag NP) test material at doses as low as 1.875 μg/ml in Chinese hamster ovary (CHO-K1) cells. However, Kim et al. (2013a) reported no evidence of chromosomal aberrations in CHO-K1 cells exposed to 10 nm citrate-coated Ag NPs at doses comparable to and higher than those tested by Chen et al. (2015a). This test material was also negative in a MN assay in CHO-K1 cells (see below). Nymark et al. (2013) reported no increase in chromosomal aberrations in a human bronchial epithelial cell line (BEAS 2B) treated with 42.5 nm PVP-coated Ag NPs. As discussed below, this test material was also negative when tested by these investigators in BEAS 2B cells in a MN assay, although DNA damage was observed in an alkaline comet assay. The reason for the mixed results in these four chromosomal aberration assays is unclear. None of these investigators compared Ag NPs varying in particle size and coating in the same test system, thus precluding an evaluation of the influence of these characteristics on clastogenicity in the chromosome aberration assay.

2.2 Micronucleus Formation

In vitro MN assay results were reported in 18 publications. Positive results were reported in 15 of them, one study showed positive results with one cell line but not in another, and two studies showed negative results.

Most of the *in vitro* MN studies involved human cell lines as a test system. Human cell lines showing an increase in MN included those derived from bronchial epithelial cells (BEAS 2B), lymphoblastoid cells (TK6), spleen B lymphocytes (WIL2-NS), T lymphocytes (Jurkat), monocytes (THP-1), lung alveolar cells (A549), glioblastoma cells (M059K and M059J), hepatoblastoma cells (HepG2), colon carcinoma cells (CaCo2), and keratinocytes (HaCaT). Primary cultures of human lymphocytes also showed positive results (Vecchio et al., 2014; Ivask et al., 2015).

One study showed both positive and negative results depending on cell type (Sahu et al., 2016a). These authors reported that 50 nm citrate-coated Ag NPs showed a positive response in HepG2 cells, but not in CaCo2 cells when MN frequency was measured by a flow cytometry method. These investigators found that this test material gave negative results in both cell types when MN frequency was measured using the standard cytochalasin B blocked MN (CBMN) assay with measurement by fluorescent microscopy (Sahu et al., 2016b). These investigators also found that 20 nm citrate-coated Ag NPs showed an increased frequency of MN in both HepG2 and CaCo2 cells in the standard CBMN

assay with HepG2 cells more sensitive, while in the flow cytometric MN assay, only HepG2 cells showed a positive response (Sahu et al., 2014a, b). The difference in results for 20 nm vs. 50 nm Ag NPs suggests that particle size influences genotoxic potential in the MN assay. These studies also demonstrate that sensitivity to MN induction by Ag NPs can differ between cell types and that MN assay methodology can influence study outcomes.

Besides Sahu et al. (2016b), one other negative result in an *in vitro* MN assay was observed. Nymark et al. (2013) reported no increase in MN frequency in BEAS 2B cells, and these negative results are in contrast to the positive results observed by Kim et al. (2011) in the same cell line. Both groups of investigators tested Ag NPs of roughly similar size [(42.5 nm for Nymark et al. (2013) and 58.9 nm for Kim et al. (2011)]. The Ag NPs tested by Nymark et al. (2013) were reported to be PVP-coated, while data on coating were not reported by Kim et al. (2011), making it unclear whether the test material was coated or uncoated (but possibly suggesting the latter). Kim et al. (2011) reported positive results at doses lower than those showing negative results in the Nymark et al. (2013) study. No other investigators have published studies using BEAS 2B cells, and the difference in results remains unexplained.

A few studies have evaluated Ag NP test materials differing in particle characteristics such as size and coating under the same experimental conditions (Vecchio et al., 2014; Butler et al., 2015; Ivask et al., 2015; Souza et al., 2016; Guo et al., 2016). Vecchio et al. (2014) compared citrate coated Ag NPs (either 10 or 70 nm) and PVP-coated Ag NPs (either 10 or 70 nm) and found that all of them induced an increase in MN frequency. The Ag NPs differed in potency with 10 nm citrate-coated Ag NP causing the most induction followed, in decreasing order of potency, by 10 nm PVP-coated , 70 nm citrate-coated, and 70 nm PVP-coated. Guo et al. (2016) also compared citrate-coated and PVP-coated Ag NPs, each with particle sizes of 20, 50, or 100 nm. They also found that smaller particle sized Ag NPs showed a greater MN response. The coatings had less effect on the relative genotoxicity of Ag NPs than the particle size in their study. Butler et al. (2015) also found that the response in the MN assay was strongly dependent upon particle size when testing citrate-coated Ag NPs of 10, 20 and 50 nm, with a stronger response for smaller particle sizes.

One study contradicts these observations on the influence of particle size on potency. Souza et al. (2016) reported a greater MN response in 100 nm Ag NPs compared to 10 nm Ag NPs. However, these investigators also reported a greater stability, i.e., less agglomeration, of the 100 nm particles in culture medium, while formation of small aggregates was indicated for the 10 nm Ag NPs in this study. Information was not provided on what type of coating of the Ag NP test material was used. Ivask et al. (2015) evaluated citrate-coated Ag NPs and a branched PEI-coated Ag NP, both ~20 nm. Both increased MN frequency, but only the branched PEI-coated Ag NPs induced a MN response at low concentrations that were not cytotoxic.

2.3 Comet Assay

Results of 26 *in vitro* comet assays have been published; positive results were reported in 24 studies. Most of these were conducted under alkaline conditions that detect single strand breaks. In addition to the alkaline comet assay, some investigators also employed modified assays that detect oxidative DNA damage. Positive results in alkaline comet assays were reported in 23 studies; one of these reported Ag NP-induced DNA damage in only one of three cell types evaluated (Asare et al., 2012). One

positive study reported results only for a modified comet assay and showed evidence of oxidative DNA damage (Rinna et al., 2015). One study reported positive results in three different modified comet assays detecting various types of oxidative DNA damage, but showed negative results in the alkaline assay (Mei et al., 2012). One study reported negative results in an alkaline comet assay (Galandakova et al., 2016).

Most of the *in vitro* comet assays involved human cell lines as a test system. Human cell lines showing an increase in Ag NP-induced DNA damage in the comet assay included those derived from bronchial epithelial cells (BEAS 2B), lymphoblastoid cells (TK6), T lymphocytes (Jurkat), monocytes (THP-1), leukemia cells (HL60), lung alveolar cells (A549), hepatoblastoma cells (HepG2), breast cancer cells (MDA-MB-731 and MCF7), glioblastoma cells (M059K and M069J), pulmonary fibroblasts (HPF), keratinocytes (SVK), foreskin fibroblasts (BJ), normal human fibroblasts (GM07492), embryonic epithelial cells (EUE) and testicular embryonic carcinoma cells (NT2). Normal human dermal fibroblasts and primary cultures of human lymphocytes also showed positive results. Several cell lines derived from animals (L5178Y, CHO K1, NIH3T3) have also shown positive comet results.

One study reported negative results for 20 uncoated Ag NPs in primary cultures of normal human epidermal fibroblasts and normal human epidermal keratinocytes when tested at non-cytotoxic concentrations (Galandakova et al., 2016). Silver nitrate was also tested at non-cytotoxic concentrations and gave negative results. The method of scoring was unconventional (visual scoring and categorization of nuclei on a 0 to 5 breakage scale). Two other studies in CHO K1 cells (Kim et al., 2013b) and in three different human cell types (Avalos et al., 2015b) have shown positive results in comet assays even at concentrations that are non-cytotoxic. Given the large number of studies showing positive findings, the study by Galandakova et al. (2016) that showed negative results can be given little weight in the overall evaluation of *in vitro* comet results.

In one study evaluating a 5 nm uncoated Ag NP, negative results were reported in L5178 mouse lymphoma cells in the alkaline comet assay, but positive results were observed in three modified comet assays that measure different oxidative lesions to DNA bases (EndoIII, fpg, hOOG1) (Mei et al., 2012). However, four other studies in human cell lines reported results of studies where both the alkaline comet assay and a modified assay for oxidative DNA damage were conducted (Asare et al., 2012; Avalos et al., 2015b; Franchi et al., 2015; Huk et al., 2015), and all reported positive results in the alkaline comet assay. Huk et al. (2015) reported positive results in the fpg-modified assay in addition to the alkaline assay. Avalos et al. (2015b) reported positive results in both the fpg-modified and the EndoIII-modified assay as well as the alkaline assay with both PEI+PVP-coated and uncoated test materials. In the Franchi et al. (2015) study, positive results were obtained in both the alkaline comet assay and the OGG1-modified assay that detects 8-oxoguanine oxidative lesions in DNA. The test material evaluated was a 50 to 82 nm PVP-coated Ag NP. One study evaluating a 20 nm Ag NP (coating status not reported) was negative in the fpg-modified assay, although positive in the alkaline comet assay (Asare et al., 2012). Although three of these studies suggest that some Ag NPs have the capacity to induce DNA damage *in vitro* that arises from oxidative lesions in the DNA, further study of the characteristics of Ag NPs that are associated with this capacity is warranted since the Asare et al. (2012) study did not support such a mode of action.

The capacity of Ag NPs to induce ROS or other measures of oxidative responses were evaluated in nine of the comet studies (Kim et al., 2011b; Suliman et al., 2013; Gliga et al., 2014; Paino and Zucolotto, 2015; Rinna et al., 2015; Tomankova et al., 2015; Jiravova et al., 2016; Juarez-Moreno et al., 2016; Thongkam et al., 2017), and all except one (Gliga et al., 2014) showed an effect. However, Tomankova et al. (2015) observed that, while ROS were increased by all three Ag NPs evaluated, the ROS responses across three different cell lines did not correlate with increases in percent tail DNA. The role of ROS in the mode of action of Ag NP-induced DNA damage requires further evaluation.

Characterization of the test materials evaluated in these assays indicates that, when reported, the shape of the Ag NPs was spherical or spheroid. The one exception to this was Gabelova et al. (2017), who tested both spherical Ag NPs and Ag NPs with a nanorod/wire shape. The Ag NPs tested included a wide range of particle sizes from 5 to 100 nm. Coated Ag NPs were used in many of the studies, but uncoated test materials were evaluated in some studies. In some publications, information on coating was not reported. Thus, the experimental evidence indicates that Ag NPs of diverse characteristics are capable of inducing DNA damage *in vitro* as measured by the comet assay.

Several of the *in vitro* comet studies included more than one type of Ag NP test material with the objective of allowing a direct comparison of results across samples with different characteristics The test materials varied with respect to particle size (Asare et al., 2012; Butler et al., 2015; Souza et al., 2016), coating (Sur et al., 2012; Huk et al., 2015) or both particle size and coating (Gliga et al., 2014; Avalos et al., 2015b).

Conflicting information on the influence of particle size was reported. Asare et al. (2012) reported that 200 nm Ag NPs showed a greater comet response than 20 nm Ag NPs (coating not reported for either test material). Butler et al. (2015) reported that citrate-coated Ag NPs of smaller size (10 and 20 nm) were positive in the comet assay while 50 and 100 nm citrate-coated Ag NPs were negative. Souza et al. (2016) reported that the magnitude of the comet response was similar for 10 and 100 nm Ag NPs (coating not reported for either test material). Similar to the results for *in vitro* MN studies, smaller citrate-coated Ag NPs are more potent in inducing a comet response than larger ones on a mass basis. In studies where coating is not reported, perhaps because the particles are uncoated, the impact of particle size disappears or reverses, which is also consistent with the MN findings (see above for a possible explanation).

The two studies evaluating the influence of particle coating of Ag NPs independent of size both showed that citrate-coated Ag NPs showed the greatest response in *in vitro* comet assays (Sur et al., 2012; Huk et al., 2015). This is also consistent with the findings for MN results discussed above. Gliga et al. (2014) studied five different Ag NP test materials, 10 nm citrate-coated, 10 nm PVP-coated, 40 nm citrate-coated, 75 nm citrate-coated, and 50 nm uncoated, and found that all of them increased percent tail DNA to a comparable extent independent of size and coating. Avalos et al. (2015b) reported that a 4.7 nm PEI + PVP-coated Ag NP showed a greater comet assay response than a 42 nm uncoated Ag NP. The influence of size vs. coating on the comet assay outcome in this study could not be determined.

2.4 Other DNA Damage Assays

Positive findings in a γ-H_2AX assay that measures DNA double strand breaks were observed in three studies (Franchi et al., 2015; Awasthi et al., 2013; Lim et al., 2012a). These results are consistent with the γ-H_2AX assay results reported in the Kim and Ryu (2013) review discussed above.

2.5 DNA Adducts

One *in vitro* study utilizing ^{32}P-post-labeling methodology to DNA adducts after treatment of CHO cells with Ag NPs reported a dose-related increase in bulky DNA adducts (Jiang et al., 2013). When tested at identical concentrations of Ag, $AgNO_3$ induced a two-fold greater increase in bulky adducts than Ag NPs. The formation of bulky DNA adducts with Ag NP treatment observed in this study is consistent with the previous study of these investigators (Foldbjerg et al., 2011) reviewed by Kim and Ryu (2013). In the previous study it was noted that the Ag NP-induced bulky DNA adducts showed a similar migration pattern to endogenously formed adducts (I-compounds) and therefore appear to arise via interaction of DNA with endogenous reactants formed during metabolism (e.g., ROS).

2.6 Comparative Effects of Silver NPs and Silver Salts in *In Vitro* Mutagenicity/Genotoxicity Studies

Kim and Ryu (2013) noted that Ag+ ions are released by the surface oxidation of Ag NPs in the presence of water and that studies have demonstrated Ag+ genotoxicity, although the role of Ag+ release in the mode of action of Ag NPs was unclear. Subsequent to the Kim and Ryu (2013) review, several investigators have compared the relative mutagenic, genotoxic, and cytotoxic potency of Ag salts and Ag NPs. Nearly all of the published studies have consistently reported that Ag salts such as $AgNO_3$ and Ag acetate are more cytotoxic than Ag NPs and are more potent in *in vitro* assays for mutagenicity (Guo et al., 2016), MN induction (Jiang et al., 2013; Butler et al., 2015; Sahu et al., 2016a, b; Guo et al., 2016; Li et al. 2017) and DNA damage (comet assay) (Butler et al., 2015).

However, a few studies have shown results that conflict with these findings. Galandakova et al. (2016) reported that, although $AgNO_3$ was extremely cytotoxic, neither this form of Ag nor Ag NPs were positive in a comet assay. Jiravova et al. (2016) reported that at concentrations producing equivalent high cytotoxicity (IC75 concentration) Ag NPs showed a greater increase in percent tail DNA in a comet assay than did Ag+ dosed in the form of a Ag salt.

Experiments with Ag salts and Ag NPs conducted by Gliga et al. (2014) showed that Ag+ release by the Ag NPs in the culture medium was not correlated with cytotoxicity, but that intracellular release of Ag+ may be involved in the cytotoxic mode of action of Ag NPs. However, Guo et al. (2016) found that addition of N-acetyl cysteine, an Ag+ chelator, had no effect on Ag NP-induced MN or ROS induction. These results are consistent with the previous finding reported in the Kim and Ryu (2013) review, that in an *in vitro* MN study, the increase in MN frequency was only partially eliminated by cysteine, a strong Ag+ ligand. This finding suggests that the genotoxicity of Ag NPs was not fully accounted for by Ag+ release. The role of Ag+ release, either extracellularly or intracellularly, in the mode of action of Ag NP mutagenicity/genotoxicity is not clear.

3 *In Vivo* Mutagenicity Studies

Only two published *in vivo* mutagenicity studies conducted with Ag NPs have been identified. Both of them showed negative results. Li et al. (2014) conducted a *Pig-a* assay in mice and observed no increase in mutant frequency in reticulocytes or total red blood cells when measured on day 2 or weeks 2, 4 and 6 after an IV injection of up to 20 mg/kg bw of either of two PVP-coated Ag NP test materials (sizes 5 nm and 15 to 100 nm) or a 10 to 80 nm silicon-coated Ag NP test material. These investigators also studied these test materials in *in vivo* genotoxicity assays and the results are discussed below.

Avalos et al. (2015a) tested one 4.7 nm Ag NP test material coated with PEI plus PVP and a second 42 nm uncoated Ag NP in a *Drosophila melanogaster* Somatic Mutation and Recombination Test (SMART). The test materials did not exhibit any mutagenic or recombinogenic activity in this assay. The test materials did induce pigmentation defects and reduction in locomotor ability in adult flies after ingestion during the larval stage. Developmental abnormalities including reduction in locomotor ability have been linked to pigmentation defects by other investigators, but the mode of action of Ag NPs in producing these effects is unknown.

The results of these two studies suggest a lack of *in vivo* mutagenicity for the Ag NPs evaluated under the conditions of these assays. However, the data are too limited to make definitive conclusions concerning the overall *in vivo* mutagenicity of Ag NPs as a class of materials.

4 *In Vivo* Genotoxicity Studies

4.1 Chromosome Aberrations

Three groups of investigators have published results of *in vivo* bone marrow chromosomal aberration assays in rats or mice. In contrast to the *in vitro* studies discussed above, which have shown mixed results, the *in vivo* assays have all shown positive results after either IP injection in mice (Ghosh et al., 2012) or rats (El Mahdy et al., 2014) or in rats by oral gavage (Patlolla et al., 2015). The oral gavage study involved daily doses of 0, 5, 25, 50 or 100 mg/kg/d for 5 days (Patlolla et al., 2015). One of the IP studies involved a single injection of 0, 10, 20, 40 or 80 mg/kg bw/d and the other involved doses of 0, 1, 2, or 4 mg/kg/d for 28 days. All three studies showed a significant dose-related increase in the frequency of chromosomal aberrations. The test materials varied in particle size from 8.7 and 10 nm (El Mahdy et al., 2014 and Patlolla et al., 2015, respectively) to less than 100 nm (Ghosh et al., 2012). Particles were coated with PVP plus citrate in one study (El Mahdy et al., 2014) and coating information was not reported in the other two studies (Ghosh et al., 2012; Patlolla et al., 2015). Ghosh et al. (2012) and Patlolla et al. (2015) also reported increases in ROS in bone marrow cells after *in vivo* treatment. These results indicate genotoxic potential for Ag NPs following *in vivo* exposure, including exposure via the oral route.

4.2 Micronucleus Formation

Results of seven *in vivo* MN assays conducted in bone marrow or peripheral blood reticulocytes or erythrocytes from either rats or mice have been reported. Five of these studies reported positive results, and two showed negative findings. The route of administration in the positive studies was by

oral gavage in three studies (Kovvuru et al., 2015; Patlolla et al., 2015; Nallanthighal et al., 2017), IP injection in one study (Song et al., 2012) and IV injection in one study (Dobrzynska et al., 2014).

In one of the three positive oral gavage studies, the exposure was quite high (500 mg/kg/d for five days) (Kovvuru et al., 2015). However, other studies have shown positive results at lower doses. Patlolla et al. (2015) reported a clear dose-related increase in MN frequency in bone marrow cells at oral gavage doses of 5, 25, 50, and 100 mg/kg/d for five days, and the increase was statistically significant at greater than or equal to 50 mg/kg bw/d. Nallanthighal et al. (2017) observed an increase in MN frequency in peripheral blood erythrocytes in mice dosed by oral gavage at 4 mg/kg/day for 7 days with a 20 nm citrate-coated Ag NP, but not with a 20 nm PVP-coated Ag NP.

While the results of Nallanthighal et al. (2017) suggest that citrate-coated Ag NPs may be more genotoxic than PVP-coated Ag NPs after oral exposure, the reason for this observation is unclear. Higher agglomeration of citrate-coated Ag NPs compared to PVP-coated Ag NPs in synthetic gastric juice was observed by Nallanthighal et al. (2017). However, agglomeration was partially reversed in synthetic intestinal juice, suggesting that both test materials are present as both nanoscale and larger particles in the intestine after oral gavage. Neither of the other two positive oral gavage studies evaluated a citrate-coated Ag NP. The Ag NP test material evaluated at a high dose by Kovvuru et al. (2015) was PVP-coated, and information about coating was not provided in the study published by Patlolla et al. (2015).

In the positive MN assay involving IP injection of a single dose of 3 mg/kg bw of a less than100 nm Ag NP, with no reported information on coating, was shown to increase MN frequency in peripheral reticulocytes in mice (Song et al., 2012). In this study, the level of 8-OH-dG in 24 hr urine samples was increased after Ag NP treatment, but not when corrected by creatinine. 8-OH-dG levels in bone marrow target tissue were not measured, but 8-OH-dG levels in liver DNA 24 hrs after treatment were not increased. Dobrzynska et al. (2014) dosed rats with a single IV injection of either 5 or 10 mg/kg bw of 20 nm uncoated Ag NPs or 5 mg/kg bw of 200 nm uncoated Ag NPs and reported a significant increase in MN frequency in bone marrow polychromatic erythrocytes for both test materials. No evidence of bone marrow cytotoxicity was reported as measured by the percentage of polychromatic erythrocytes in bone marrow.

Regarding the two negative *in vivo* MN assays, one IV study in mice reported no increase in MN frequency in peripheral blood reticulocytes after a single dose of up to 20 mg/kg bw of 5 nm PVP-coated Ag NPs, 15 to 100 nm PVP-coated Ag NPs, or 10 to 80 nm silicon-coated Ag NPs (Li et al., 2014). Three daily IV doses of up to 20 mg/kg bw of the latter two test materials also showed no increase in MN frequency. Ag NPs were confirmed to accumulate in the bone marrow by TEM. A higher Ag level in bone marrow was detected in animals treated with PVP-coated Ag NPs compared to silicon-coated Ag NPs. The 5 nm PVP-coated Ag NPs, at all doses, were associated with a significant decrease in percent reticulocytes indicating bone marrow toxicity. The 15 to 100 nm PVP-coated Ag NPs also showed significant reductions in percent reticulocytes after single or repeat dose treatment. No decrease in percent reticulocytes was observed for silicon-coated Ag NPs. These results suggest that particle coating (PVP vs. silicon) may have an influence of *in vivo* distribution of Ag NPs or of Ag to tissues and on target tissue toxicity following IV dosing.

In the other negative study, a single IP dose of either 0.25 or 1 mg/kg bw of an 8.6 nm poly(styrene-comaleic anhydride)-grafting poly(oxyalkylene)-coated (SMA-Ag NP) test material did not result in

an increase in MN frequency in peripheral blood reticulocytes in mice (Chen et al., 2015a). There was evidence of target tissue cytotoxicity based on an increase in percent reticulocytes in peripheral blood at 1 mg/kg bw, suggesting that an adequate exposure to the target tissue was achieved.

To summarize the *in vivo* MN results, five positive studies indicate genotoxic potential for Ag NPs following *in vivo* exposure by the oral, IP, or IV routes. However, negative results have also been reported in one IV study and one IP study. The lack of a MN response does not appear to be explained by inadequate target tissue exposure. Further study of the factors that may influence the outcome of *in vivo* MN assays with Ag NPs, such as dosing regimens, Ag NP characteristics such as particle size and coating, effect of dispersion method on aggregation, assay methodology, vehicle used, and route-specific differences in biokinetics and protein corona surrounding the NP would be useful.

4.3 Comet Assay

Results from five *in vivo* comet assays have been published. Three of these reported positive results in the alkaline comet assay in either the bone marrow or peripheral lymphocytes of mice after either a single IP injection in the range of 10 to 80 mg/kg bw (Ghosh et al., 2012; Al Gurabi et al., 2015) or in rat bone marrow after dosing by oral gavage at 50 and 100 mg/kg/d for 5 days (Patlolla et al., 2015). Significant increases in ROS were observed in the bone marrow by both Ghosh et al. (2012) and Patlolla et al. (2015). The Ag NP reported size was 10 nm (Patlolla et al., 2015), 43 nm (Al Gurabi et al., 2015), and less than 100 nm (Ghosh et al., 2012). The synthesis description provided by Al Gurabi et al. (2015) indicated that the Ag NP was uncoated. No information on coating was provided for the other two studies.

Dobrzynska et al. (2014) observed no significant increase in percent tail DNA in bone marrow in rats administered a single IV dose of 5 or 10 mg/kg bw of 20 or 200 nm Ag NP (coating information not provided). Small, but non-significant, increases in percent tail DNA were observed at 10 mg/kg bw. The negative results in this study may be attributable to lack of adequate exposure. As noted above, an increase in MN frequency was observed in bone marrow with both 20 and 200 nm Ag NPs in this study. The reason for the differing outcomes in the MN and comet assays is unclear, although the low level of exposure may be a factor since the investigators reported that the percentage of polychromatic erythrocytes (PCEs) in bone marrow was not significantly increased, indicating an absence of significant bone marrow toxicity.

Li et al. (2014) dosed mice with either 15 to 100 nm PVP-coated or 10 to 80 nm silicon-coated Ag NPs at 25 mg/kg/d for three days by IV injection and found no increase in percent tail DNA in the liver with the alkaline comet assay. However, positive results were obtained with the PVP-coated test material, but not the silicon-coated test material, in both the EndoIII- and hOOG1-modified comet assays, indicating the induction of oxidative DNA damage.

In summary, Ag NPs have been shown to cause DNA damage as measured in the comet assay in bone marrow following exposure by either the oral or IP route. An analysis of the influence of Ag NP test material characteristics on the outcome of *in vivo* comet assays was not undertaken given the complexity introduced by the varying routes and durations of exposure, and target tissues analyzed.

4.4 Other DNA Damage Assays

Other less common types of DNA damage assays have also been used to evaluate DNA damage induced by Ag NPs in some *in vivo* studies. Using the γH2AX assay, Kovvuru et al. (2015) observed double strand DNA breaks in peripheral blood cells and in bone marrow following oral gavage of PVP-coated Ag NPs (average size 33.6 nm, range 5 to 150 nm) at 500 mg/kg/d for five days. These investigators also observed an increase in 8-oxodG in peripheral blood cells as well as a positive result in a P^{un} reversion/DNA deletion assay. In the latter assay, pregnant female C57BL/6J p^{un}/p^{un} mice were subjected to the same dosing regimen on days 9.5 to 13.5 post-conception. The assay measures the frequency of homologous recombination between two repeats in the p^{un} locus, resulting in deletion that reverts the pun allele to a functional p gene, allowing black pigment accumulation in the eye of developing pun/pun mice *in utero*, visualized after birth. Nallanthighal et al. (2017) also observed increases in double strand DNA breaks measured in a γH2AX assay and 8-oxoG oxidative DNA damage in peripheral blood cells following oral gavage dosing of 20 nm citrate-coated Ag NPs (4 mg/kg/d for 7 days) but not with PVP-coated Ag NPs under the same exposure conditions.

Table G-1 shows the studies described above.

Table G-1. Summary of Mutagenicity/Genotoxicity Data for Ag NPs

Assay	Test system	Exposure	Particle data[a]	Result	Comments	Reference
Mutation *In Vitro*						
Reverse mutation assay	*Salmonella typhimurium* strains TA102, TA100, TA1537, TA98, and TA1535; pre-incubation assay	0, 0.15, 0.3, 0.6, 1.2, 2.4, 4.8, 9.6, 19.2, 38.4, or 76.8 µg/plate without S9	6. Novacentrix 7. NR 8. 5 nm (range 2-12 nm) 9. NR 10. Spherical 11. NR 12. NR	Negative	Test material clearly antibacterial. Frank toxicity for TA98 and TA100 at 4.8 µg/plate and higher, for TA1535 and TA1537 at 9.6 µg/plate and higher, and for TA102 at 76.8 µg/plate.	Li et al., 2012
Reverse mutation assay	*Salmonella typhimurium* strains TA98, TA100, TA1535, TA1537 and *Escherichia coli* WP2*uvr*A; pre-incubation assay	0, 7.813, 15.625, 31.25, 62.5, 125, 250, or 500 µg/plate with S9; 0, 0.977, 1.953, 3.906, 7.813, 15.625, 31.25, 62.5, or 125 µg/plate without S9	6. ABC Nanotech Co., Ltd. 7. Dispersed in 1% citric acid 8. 10.0 nm 9. 54.88 m^2/g 10. NR 11. NR 12. NR	Negative	Without S9 cytotoxicity was observed beginning at 31.25 or 62.5 µg/plate. With S9 cytotoxicity was observed beginning at 125 or 250 µg/plate. Precipitation and aggregation was observed at doses above 125 µg/plate.	Kim et al., 2013a
Reverse mutation assay	*Salmonella typhimurium* strains TA98, TA100, TA1535, and TA1537; pre-incubation assay	0, 100, 200, 300, 400, or 500 µg/plate with and without S9	1. Sigma-Aldrich 2. None 3. 40-59 nm 4. NR 5. Spherical 6. 43-315 nm by DLS due to aggregation 7. NR	Negative	Growth inhibition observed with or without S9 at 500 µg/plate.	Kim et al., 2013b
Reverse mutation assay	*Salmonella typhimurium* strains TA100, TA98, T102 and *Escherichia coli* WP2 *pKM101* and	0, 0.5,1, 5, 10, 50, 100, 500, 1000, or 5000 µg/plate without S9	1. NanoComposix 2. Citrate-coated 3. 10, 20, 50 or 100 nm 4. NR 5. Spherical	Negative	No AgNPs were identified within the bacterial cells using TEM. 5000 µg/plate is the upper limit for testing in the Ames test.	Butler et al., 2015

	WP2 *uvrA pKM101*; pre-incubation assay		6. Minimal aggregation based on TEM micrographs 7. NR			
Reverse mutation assay	*Salmonella typhimurium* strains TA98, TA100, and TA1535, plate incorporation method	TA98: 0, 0.05, 0.10, 0.20, 0.40, or 0.80 µg/plate; TA100: 0, 0.10, 0.20, 0.40, 0.80, 1.60 µg/plate; TA1535: 0, 0.02, 0.04, 0.08, 0.16, or 0.32 µg/plate. All assays conducted with and without S9 for 48 hrs	1. Synthesized by investigator 2. Poly(styrene-comaleic anhydride)-grafting poly (oxyalkylene) (SMA)-AgNP 3. 8.6 nm 4. NR 5. Spherical 6. NR 7. 19.6% Ag, 80.4% SMA	Negative	In the preliminary cytotoxicity study, no toxicity was reported at up to 0.8 µg/plate (TA98), 1.6 µg/plate (TA100) and 0.32 µg/plate (TA1535).	Chen et al., 2015a
Reverse mutation assay	*Salmonella typhimurium* strains TA98, TA100 and YG1029 (derived from TA100 with enzymatic activity for O-acetyltrans-ferase)	0, 0.0015, 0.003, 0.006, 0.012, 0.024, 0.048, 0.097, 0.195, 0.39, 0.78, 1.56, or 3.12 µg/plate, with and without S9.	6. A-AgNP: local manufacturer in Tehran, Iran; B-AgNP: local manufacturer in Isfahan, Iran; C-AgNP: US Research Nanomaterials Co., Ltd. 7. A-AgNP: uncoated; B-AgNP; coated, coating unspecified; C-AgNP: NR; all three test materials were water-based colloids 8. A-AgNP: 19.6 nm; B-AgNP: 21.8 nm; C-AgNP 15 nm	Negative; No increase in number of revertant colonies/plate for any of the 3 test materials. All 3 test materials showed a dose-related reduction in Mutagenicity Index (ratio of the number of revertants induced per plate for test sample to spontaneous revertants for negative control).	Concentrations above 0.39 µg/plate (TA98) or above 0.78 µg/plate (TA100 and G1029) were considered cytotoxic. Authors propose that significant microbial inhibitory effects of all 3 test materials suggests possible anti-mutagenic effects.	Heshmati et al., 2015

			(determined by TEM) 9. NR 10. A-AgNP; stated as "different"; B-AgNP: spherical; C-AgNP: spherical 11. NR 12. NR			
Reverse mutation assay	*Salmonella typhimurium* strains TA98 and TA100; preincubation assay	0 to 4.8 μg/plate, without S9	1. NanoComposix 2. PVP- or citrate-coated 3. 20, 50, and 100 nm, each in PVP- or citrate-coated form 4. NR 5. Spherical 6. Minimal agglomeration in cell culture medium (PDI of 0.1) 7. NR	Results described as inconclusive due to the high toxicity of Ag to the test bacteria and lack of entry of the NPs into cells.	No AgNPs found inside cells by TEM.	Guo et al., 2016
Mouse lymphoma ($tk^{+/-}$) assay	Mouse lymphoma L5178Y cells	0, 313, 625, 1250, or 2500 μg/ml without S9 and 0, 313, 615, 12500, 2500, or 3750 μg/ml with S9 for 3 hrs.	1. Aldrich 2. NR 3. < 100 nm 4. NR 5. NR 6. NR 7. 99.5%	Negative: No increase in mutant frequency at any test concentration. However, small colonies were slightly more frequent than large colonies both with and without S9. Investigators suggested that AgNPs may have potential for damage at the chromosomal level.	Dose-related cytotoxicity was observed that was more pronounced without S9.	Kim et al., 2010a

Mouse lymphoma ($tk^{+/-}$) assay	Mouse lymphoma L5178Y cells; both microwell and soft-agar versions of the assay	0 μg/ml and seven concentrations ranging from 3 to 6 μg/ml for 4 hrs	1. Novacentrix Inc. 2. Uncoated 3. 5 nm 4. NR 5. Spherical 6. Average diameter: In PBS – 1965.8 nm; In culture medium – 1608.7 nm 7. NR	Positive: Dose-related increase in mutant frequency in both assay versions	Dose-related cytotoxicity measured as decrease in relative total growth. Loss of heterozygosity analysis of the Tk mutants showed that AgNPs induced mainly chromosomal alterations spanning less than 34 megabase pairs.	Mei et al., 2012
Mouse lymphoma ($tk^{+/-}$) assay	Mouse lymphoma L5178Y cells	0, 1, 3, 10, 30, 50, or 100 $\mu g/cm^3$ for 24 hrs for both test materials	1. Fraunhofer Institute 2. AgNM300 and AgNM302: both Tween 20/PEG-coated 3. AgNM300: 14 nm; AgNM302: 50 x 3000 nm 4. NR 5. AgNM300: spherical; AgNM302: nanorod 6. Size distribution after 24 hrs in cell culture media: AgNM300: 66 or 88 nm depending on type of medium; AgNM302: 199 or 184 nm depending on type of medium 7. NR	Negative for spherical AgNM300. Positive for AgNM302 nanorods/wires	Dose-related cytotoxicity for both test materials.	Gabelova et al., 2017
Mouse lymphoma ($tk^{+/-}$) assay	Mouse lymphoma L5178Y/$Tk^{+/-}$ 3.7.2 cell line	Ag NPs: 1 to 60 μg/ml for 4 hrs. $AgNO_3$ and Ag acetate: 0, 0.4, 0.45,	1. NanoComposix 2. PVP- or citrate-coated	Positive: Dose-related increase in mutant frequency for all 6 AgNPs. Lowest concentration	Dose related cytotoxicity was observed. Acceptable levels of cytotoxicity were observed at doses of 5 to 60 μg/ml. Smallest NPs had	Guo et al., 2016

		0.5, 0.55 or 0.6 µg/ml for 4 hrs.	3. 20, 50, and 100 nm, each in PVP- or citrate-coated form 4. NR 5. Spherical 6. Minimal agglomeration in cell culture medium (PDI of 0.1) 7. NR	showing a positive MF response was 4, 7, 20, 25, 30, and 50 µg/ml for 20 nm citrate-, 20 nm PVP-, 50 nm citrate-, 50 nm PVP, 100 nm citrate- and 100 NM PVP-coated AgNPs, respectively. Mutagenic potencies (mutants per µg/ml) among the AgNP types varied in potency by 12 fold. Citrate-coated 20 nm AgNPs> PVP-coated 20 nm. Smaller AgNPs had a higher mutagenic potency than larger AgNPs. Ag NO_3 and Ag acetate had much higher mutagenic potency than any of the AgNPs.	the greatest toxicity. TEM showed AgNPs inside cells. $AgNO_3$ and Ag acetate both much more cytotoxic than AgNPs.	
HPRT assay	V79-4 cells	0, 0.3, 0.6, or 2.5 µg/ml for 24 hrs	1. Synthesized by investigator 2. Six AgNP test materials each with a different surface coating. Anionic	Positive: All test materials increased mutation frequency. Mutagenic potential was surface-coating related but not		Huk et al., 2015

			coatings: Citrate- and SDS-coated; Neutral coatings: Disperbyk- and Tween-coated; Cationic coatings: Byk- and Chitosan-coated 3. All six test materials were 5-10 nm 4. NR 5. All six test materials were spherical/quasi-spherical 6. Agglomerate size as measured by DLS: Ag-Citrate: 133 nm; Ag-SDS: 137.4 nm; Ag-Disperbyk: 391.5 nm; Ag-Tween: 49.73 nm; Ag-Byk: 34.83 nm; Ag-Chitosan: 763.7 nm 7. NR	charge-related. Highest MF was observed with Ag-_Byk. Ag_SDS, Ag_Dispebyk and Ag_Chitosan were weakly mutagenic. Ag_Tween and Ag_Citrate were considered false positives due to strong mutagenic effects of the Ag ENM stabilizers alone.		
HPRT mutation assay	CHO (Chinese hamster ovary) cells	0, 5, 10, or 20 ppm with or without S9 for 4 hrs for all three test materials	1. W10 (AgPure): RAS GmbH Regensburg, Germany; Citrate-Ag: NanoComposix; PVP-Ag: Synthesized by study investigators 2. AgPure: poloxethylene glycerol trioleate and Tween 20-	Positive: Significant increases in mutation frequency at 10 and 20 ppm (AgPure and PVP-Ag) or at 20 ppm (Citrate-Ag) without S9; Significant increases in mutation frequency at 5, 10, and 20 ppm (PVP-Ag and Citrate-Ag) or at	Cytotoxicity was greater for PVP-Ag than for AgPure and Citrate-Ag. Cytotoxicity was observed both with and without S9.	Guigas, et al., 2017

			coated; Citrate-Ag: citrate coated; PVP-Ag: PVP coated 3. AgPure: 15-20 nm; Citrate-Ag: 20 nm; PVP-Ag: NR but described as similar to AgPure and PVP-AG 4. NR 5. Spherical; tendency for AgNPs to agglomerate in medium was Citrate-Ag > PVP-Ag > AgPure 6. Approximately 90% of the number-based size distribution was <30 nm for each AgNP preparation. Degree of agglomeration was Citrate-Ag>PVP-Ag>AgPure 7. NR	10 and 20 ppm (AgPure) with S9.		
LacZ mutation assay	Mouse embryonic fibroblasts isolated from 15 day old embryos from transgenic mice containing the lacZ reporter gene in their genome (MEF-*LacZ* cells)	0, 0.1, 0.3, 1, 3, 10, 30, or 50 μg/ml for 16 hrs	1. NanoComposix, Inc. 2. None 3. 20, 80 and 113 nm 4. 20 nm AgNPs: 1.31 x 10^3 nm^2/particle; 80 nm AgNPs: 2.01 x 10^4 nm^2/particle; 113 nm AgNPs: 4.00 x 10^4 nm^2/particle 5. Spherical 6. NR	Negative or equivocal: 20 nm AgNPs: no increase in mutation frequency up to 3 μg/ml, higher concentrations too cytotoxic to evaluate; 80 nm AgNPs: dose-related increase in mutation frequency but not statistically significant; 113 nm	Metabolic activity measurement for 80 nm AgNPs using the WST-1 Cell Proliferation Reagent (Roche) showed that all doses inducing an increase in mutation frequency were cytotoxic (≥20% decrease in metabolic activity).	Park et al., 2011

			7. <0.001 mg/L formaldehyde	AgNPs: an increase in mutation frequency was observed but it was neither dose-related nor statistically significant.		
Mutation *In Vivo*[c]						
Pig-a assay	Male B6C3F1 mice-*Pig-a* mutant frequency monitored in reticulotyces and total RBCs	0, 0.5, 1.0, 2.5, 5.0, 10.0, or 20.0 mg/kg bw single dose by IV injection; Pig-a mutant frequency monitored by blood draws on day 2 and weeks 2, 4, and 6	1. NanoComposix 2. Two PVP-coated AgNP test materials and one silicon-coated AgNP 3. 5 nm PVP-coated AgNP: mean 5.4 nm (range 3-8 nm); 15-100 nm PVP-coated AgNP: mean 51.4 nm; 10-80 nm silicon-coated AgNP: mean 45.5. nm 4. NR 5. Spherical 6. Investigators report that agglomeration seldom occurred 7. NR	Negative: No increase in mutant frequencies in reticulocytes or RBCs.	Accompanying bone marrow MN assay indicated a reduction in % reticulocytes indicating treatment-related cytotoxicity. AgNPs were observed by TEM in bone marrow.	Li et al., 2014
SMART assay	*Drosophila melanogaster*	0, 25, 30, or 50 µg/ml (AgNP 4.7 nm) and 0, 250, 500 or 1000 µg/ml (AgNP 42 nm); larvae were fed on medium at these	1. Nanogap Subparticles 2. 4.7 nm AgNP: PEI plus PVP- coated; 42 nm AgNP: uncoated 3. 4.7 nm and 42 nm	Negative: while characterized as inconclusive based on statistical analysis, the study authors concluded that both test	Doses chosen based on previous viability experiments (results not shown). Both test materials reduced locomotor ability and induced melanization (pigmentation) defects in	Avalos et al., 2015a

		concentrations for 48 hrs.	4. NR 5. NR 6. NR 7. NR	materials appeared to be non-mutagenic.	adult flies after larval exposure.	
Clastogenicity *In Vitro*						
Chromosomal aberrations	Human peripheral blood lymphocytes	0, 5, 15, or 25 µg/ml for 24 hrs	1. Sigma Aldrich 2. None 3. <100 nm (supplier specification), 46 nm as measured by investigators 4. 5.0 m^2/g 5. NR 6. 200-700 nm in aqueous solution 7. 99.5% trace metals basis AgNPs	Positive: Tri-radial chromosomes observed at 15 µg/ml and chromosome breaks and gaps at 25 µg/ml.		Ernest et al., 2013
Chromosomal aberrations	CHO-K1 (Chinese hamster ovary) cells	0, 0.488, 0.977, or 1.953 µg/ml without S9 for 24 hrs; 0, 0.977, 1.953, or 3.906 µg/ml without S9 for 6 hrs; 0, 7.813, 15.625, or 31.25 µg/ml with S9 for 6 hrs	1. ABC Nanotech Co., Ltd. 2. Dispersed in 1% citric acid 3. 10.0 nm 4. 54.88 m^2/g 5. NR 6. NR 7. NR	Negative: No significant increase in the number of cells with aberrations at any dose with or without S9.	Cytotoxiciy (decrease in RCC) observed without S9 at 6 and 24 hrs at doses above 15.625 µg/ml and no metaphase chromosomes observed at 3.906 µg/ml; Cytotoxicity (decrease in RCC) observed with S9 at 6 hrs at doses above 31.25 µg/ml.	Kim et al., 2013a
Chromosomal aberrations	BEAS 2B cells (human bronchial epithelial cell line)	0, 2, 4, 8, 16, 24, or 48 µg/cm^2 (corresponding to 0, 10, 20, 40, 80, 120	1. NANOGAP Milladoiro, Spain 2. PVP-coated 3. 42.5 nm	Negative: No significant increase in chromatid-type, chromosome-type or	Dose-related decrease in cell viability by Trypan Blue assay; only a slight cytotoxic effect in the	Nymark et al., 2013

		or 240 μg/ml) for 24 hrs; 0, 0.5, 1, 2, 4, 6, or 8 μg/cm^2 (corresponding to 2.5, 5, 10, 20, 30, or 40 μg/ml) for 48 hrs	4. 0.03 m^2/g as measured by analysis of the powdered sample 5. Micron-scale irregular shaped aggregates with AgNPs embedded in an organic matrix as supplied in dry powder; when dispersed in EtOH the sample spread out into spherical AgNs consistent with 42.5 nm size 6. See above 7. Ag constituted 80 wt% of the aggregates	total aberrations at any dose or time point.	luminescent cell viability assay.	
Chromosomal aberrations	CHO-k1 (Chinese hamster ovary) cells	0, 1.875, 3.75, or 7.5 μg/ml for 18 to 21 hrs with S9	1. Synthesized by investigator 2. Poly(styrene-comaleic anhydride)-grafting poly (oxyalkylene) (SMA)-AgNP 3. 8.6 nm 4. NR 5. Spherical 6. NR 7. 19.6% Ag, 80.4% SMA	Positive: Significant increase in percent of cells with chromosomal aberrations at all three doses.	Cell survival rate decreased to 80% at 7.5 μg/ml.	Chen et al., 2015a
MN formation	BEAS-2B (human bronchial epithelial cell line)	0, 0.01, 0.1, 1, or 10 μg/ml for 24 hrs	1. Sigma-Aldrich 2. NR 3. 58.9 nm 4. NR 5. Spherical	Positive: Significant dose-related increase in MN frequency in both CBMN and MN assays; response greater with MN	ROS increased at all doses. TEM images showed AgNP aggregates wrapped within endocytic vesicle within the cytoplasm and nucleus.	Kim et al., 2011b

			6. Size distribution by DLS ranged from 43 to 260 nm 7. NR	assay (without cytochalasin B). Co-treatment with AgNPs (10 μg/ml) and scavengers for OH radicals (mannitol), H_2O_2 (catalase and sodium selenite), and superoxide radicals (SOD) showed that all of them reduced the magnitude of MN frequency induction with SOD being most effective.		
MN formation	TK6 human lymphoblastoid cells	0, 10, 15, 20, 25, or 30 μg/ml for 28 hrs	1. Novacentrix 2. NR 3. 5 nm (range 2 to 12 nm) 4. NR 5. Spherical 6. NR 7. NR	Positive: Dose-related increase in MN frequency with significant increases at 25 and 30 μg/ml.	Major increase in cytotoxicity at concentra-tions above 20 μg/ml.	Li et al., 2012
MN formation	IMR-90 (normal human fibroblasts), M059K and M059J (human glioblastoma cells), CHO AA8 and CHO V33 (Chinese hamster ovary cells)	0 or 100 μg/ml for 48 hrs	1. Synthesized by investigators 2. PVP-coated 3. 20 nm 4. NR 5. Spherical 6. NR 7. 15.24 wt % Ag	Positive: Significant increases in MN frequency in all cell types.	The different cell types were used to explore the impact of DNA protein kinase (DNA-PKcs) sufficiency vs. deficiency on MN frequency. The results suggested that cells lacking functional DNA PKcs are more sensitive.	Lim et al., 2012a
MN formation	CHO-k1 (Chinese hamster ovary) cells;	0, 1, 5, or 10 μg/ml for 24 hrs	1. Synthesized by investigataors 2. BSA-coated 3. Mean 15.9 nm	Positive: Significant dose-related increase in MN frequency for both AgNPs and	Cell uptake into endosomes and lysosomes but not nuclei or mitochondria was shown by TEM. Increased	Jiang et al., 2013

	flow cytometry based MN assay		Other characterization information was not provided in this publication but Foldbjerg et al., Tox. Sci. 130:145-157 (2012) was cited.	$AgNO_3$. Ag^+ (administered as $AgNO_3$) induced 1.7 fold more micronuclei at 10 µg/ml of Ag than AgNPs.	cytotoxicity (MTT assay, apoptosis, necrosis) and increased ROS observed for both AgNPs and Ag^+.	
MN formation	CHO-K1 (Chinese hamster ovary) cells	CBMN Assay: 0, 0.01, 0.10, 1.0 or 10 µg/ml for 24 hrs with and without S9 MN Assay without CB: 0, 0.01, 0.10, 1.0 or 10 µg/ml for 24 hrs without S9	See above entry for Kim et al., 2013b	Positive: In the CBMN assay significant dose-related increase in MN frequency both with and without S9. Presence or absence of S9 had significant influence on the results. Positive: In the MN assay without CB significant dose-related increase in MN frequency. Response was significantly greater for MN assay without CB vs. CBMN (both assays without S9).	No evidence of cytotoxicity based on no reductions in % binucleated cells, cytokinesis block-proliferation index, or relative increase in cell counts.	Kim et al., 2013b
MN formation	BEAS-2B (human bronchial epithelial cell line)	0, 2, 4, 8, 16, 24, 36 or 48 µg/cm^2 (corresponding to 0, 10, 20, 40, 80, 120, 180, or 240 µg/cm^2) for 48 hrs	See above entry for Nymark et al., 2013	Negative	Dose-related decrease in cell viability by Trypan Blue assay; only a slight cytotoxic effect in the luminescent cell viability assay.	Nymark et al., 2013

MN formation (fluorescent microscopy in CBMN assay)	HepG2 (human hepatoblastoma cell line) and CaCo2 (human colon carcinoma cell line)	HepG2 cells: 0, 5, 10, or 15 μg/ml for 4 hrs or 0, 0.5, 1.0 or 2.5 μg/ml for 24 hrs; CaCo2 cells: 0, 5, 10, or 15 μg/ml for 4 and 24 hrs	1. NanoComposix 2. Citrate-coated 3. 20 nm 4. NR 5. NR 6. TEM images showed no noticeable aggregation or agglomeration 7. NR	Positive in both HepG2 and CaCo2 cells HepG2: Significant increase in MN frequency at 10 and 15 μg/ml after 4 hrs and at 0.5, and 2.5 but not 1.0 after 24 hrs. No dose response. CaCo2: Signifiant increase in MN frequency at 10 and 15 μg/ml after 4 hrs and at 15 μg/ml after 24 hrs. No dose response.	Cytotoxic to both HepG2 and CaCo2 cells. Concentrations used in the 4 hr exposure in HepG2 cells were too cytotoxic to use in the 24 hr exposure. Cell uptake in these cell lines was confirmed by TEM in a previous study by these investigators.	Sahu et al., 2014a
MN formation (flow cytometry in MN assay)	HepG2 (human hepatoblastoma cell line) and CaCo2 (human colon carcinoma cell line); both cell lines were assayed as attached cells and as suspended cells	0, 1.0, 2.0, 5.0, or 10.0 μg/ml for 48 hrs for attached cells and 0, 5, 10, or 15 μg/ml for 4 hrs for suspended cells for both cell lines	1. Nanocomposix 2. Citrate-coated 3. 20 nm 4. NR 5. NR 6. TEM images showed no noticeable aggregation or agglomeration 7. NR	Positive: Significant dose-related increase in MN frequency in attached HepG2 cells but not attached CaCo2 cells. Negative: No significant increase in MN frequency in suspended HepG2 or CaCo2 cells	Cytotoxic to both attached HepG2 and attached CaCo2 cells. Cytotoxicity in suspended cells not reported. Cell uptake in these cell lines was confirmed by TEM in a previous study by these investigators.	Sahu et al., 2014b
MN formation (HTS modification	Human primary lymphocytes and WIL2-NS cells	0 or 12.5 μg/ml for 24 hrs in WIL2-NS cells; 0, 0.1, 1.0, or	1. NanoComposix 2. Citrate-coated 3. Ag10-cit: 8.8 nm; Ag10-PVP: 11.8	Positive in WIL2-NS cells: All four AgNP test materials showed a significant increase	Dose- related cytotoxicity in all primary lymphocyte subtypes for 10 nm AgNPs and particularly pronounced	Vecchio et al., 2014

of CBMN assay)	(human spleen B lymphocyte cell line)	10 μg/ml in primary human lynphocytes	nm: Ag70-cit: 68.5 nm; Ag70-PVP: 69.9 nm 4. NR 5. NR 6. NR 7. NR	in MN frequency; Ag10-cit > Ag10-PVP > Ag70-cit > Ag70-PVP. Positive in primary human lymphocytes: All four AgNP test materials showed a significant increase in MN frequency at 10 μg/ml. Lymphocyte sorted by subtype differed in genotoxic response; CD2+ and CD4+ were more sensitive than CD8+ and CD20+. Same order of AgNP potency as indicated above for WIL2-NS cells.	at 50 ug/ml; cytotoxicity observed at 10 μg/ml with 70 nm AgNPs only for unsorted lymphocytes and for sorted CD2, CD4 and CD45.	
MN formation	Jurkat Clone E6-1 (a human T lymphocyte cell line) and THP-1 (a human monocyte cell line)	For 10 nm and 20 nm AgNPs: 0, 1, 2.5, 5, 10, 15, 20, or 25 μg/ml for 24 hrs. For 50 and 100 nm AgNPs: 0, 1, 5, 10, 25, or 50 μg/ml for 24 hrs. For $AgNO_3$: 0, 1, 1.5, 2.0, 2.5, or 5.0 μg/ml for 24 hrs.	See entry above for Butler et al., 2015	Positive: Significant dose-related increase in MN frequency for AgNPs of all four sizes. MN induction was strongly size-dependent; 10 nm AgNPs > 20 nm AgNPs > 50 nm AgNPs >100 nm AgNPs. $AgNO_3$ produced the greatest MN induction.	Both cell lines showed dose-related cytotoxicity for 10 and 20 nm AgNPs. Jurkat cell line was more sensitive than THP-1 cell line. 50 and 100 nm Ag NPs were not cytotoxic The strongest cytotoxicity in both cells lines was seen with $AgNO_3$.	Butler et al., 2015

MN formation	Jurkat (ATCC TIB-152), a human T lymphocyte cell line; WIL2-NS (ATCC CRL-8155), human B lymphocyte cell line; Primary cultures of human lymphocytes	Citrate-coated AgNPs (c-AgNPs): 0, 0.2, 0.4, 0.8, 1.5, 3.1, 6.2, or 12.5 µg/ml for ~72 hrs. Branched polyethylene-imine-coated (bPEI) AgNPs (b-AgNPs): 0, 0.1, 0.2, 0.4, 0.8, 1.5, 3.l, or 6.2 µg/ml for ~72 hrs.	1. NanoComposix 2. Citrate- and branched PEI (bPEI)-coated 3. Citrate-coated AgNP: 18.8 nm; b-PEI-coated AgNP: 18.6nm 4. NR 5. Spherical 6. In cell culture medium, hydrodynamic diameter measured by Z-potential was 41.8 nm for citrate-coated and 323 nm for bPEI-coated AgNPs, respectively. The difference was likely due to formation of coronas around the NPs by the amino acids and proteins in culture medium. 7. NR	Positive; Both AgNP test materials induced a significant increase in MN frequency in both cell lines and in primary cultures of human lymphocytes.	Decrease in cell viability. MN were observed at doses producing significant decreases in cell viability.	Ivask et al., 2015
MN formation	HepG2 cells (human hepato-blastoma) and CaCo2 cells (human colon carcinoma cell line)	50 nm AgNPs: 0, 1.0 ,3.0, 5.0, 10.0, or 20.0 µg/ml for 40 to 44 hrs for both cell lines Ag acetate: 0, 0.2, 0.5, 1.0, or 2.0 µg/ml for 40 to 44	1. NanoComposix 2. Citrate-coated 3. 50 nm 4. NR 5. Spherical 6. No noticeable aggregation or agglomeration reported 7. NR	50 nm AgNPs: HepG2 cells: Positive – Dose-related increase in MN frequency. CaCo2 cells: Negative –No increase in MN frequency.	Highest test concentrations for AgNPs and Ag acetate were based on preliminary cytotoxicity assays and chosen to produce approximately 50% cytotoxicity. Ionic Ag exposure was more cytotoxic to CaCo2 cells than HepG2 cells.	Sahu et al., 2016a

		hrs for both cell lines		Ag acetate: HepG2 cells: Negative – No increase in MN frequency. CaCo2 cells: Increase in MN frequency only at highest dose that also showed only 46% cell survival.		
MN formation	HepG2 cells (human hepato-blastoma) and CaCo2 cells (human colon carcinoma)	50 nm AgNPs: 0, 10, 25, 50, 75, or 100 µg/ml for 4 hrs and 0, 2.5, 5, 10, 15, or 25 µg/ml for 24 hrs for both cell lines Ag acetate: 0, 0.1, 0.2, 0.5, 1.0, 2.5, or 5.0 µg/ml for 4 hrs and 0, 0.5, 1.0, 2.0, 4.0, or 5.0 µg/ml for 24 hrs for both cell lines	1. NanoComposix 2. Citrate-coated 3. 50 nm 4. NR 5. Spherical 6. No noticeable aggregation or agglomeration reported 7. NR	50 nm AgNPs: Negative for both cell lines Ag acetate: HepG2 cells – Increase in MN frequency at 2.5 µg/ml after 4 hrs and 2.0 µg/ml after 24 hrs. CaCo2 cells – Increase in MN frequency at 0.5 µg/ml after 4 hrs and 2.0 µg/ml after 24 hrs.	50 nm AgNPs: Significantly cytotoxic to both cell lines at 10 to 50 µg/ml after 4 hrs. After 24 hrs 50 nm AgNPs are significantly cytotoxic at 5 to 50 µg/ml in HepG2 cells and at 10 to 50 µg/ml in CaCo2 cells (i.e., CaCo2 cells less susceptible) Ag acetate: Much more cytotoxic to both cell lines than 50 nm AgNPs. Cytotoxic at 0.5 to 3.0 µg/ml after 4 hrs but at a lower concentration (0.2 to 3.0 µg/ml) after 24 hrs.	Sahu et al., 2016b
MN formation	CHO-K1 cells and CHO-XRS5 cells (both Chinese hamster ovary cell lines). CHO-XRS5 cells are deficient in the repair of DNA double strand breaks	0, 0.025, 0.25, 1.25, or 2.5 µg/ml for 24 hrs for both 10 nm and 100 nm AgNPs	1. Sigma-Aldrich 2. NR 3. 10 and 100 nm 4. NR 5. Spherical 6. Formation of small agglomerates based on hydrodynamic diameter	Positive: Both 10 nm and 100 nm AgNPs increased MN frequency at the highest dose tested in both cell lines. Response was greater for CHO-XRS5 than CHO-K1. Nucleoplasmic	CHO-XRS5 cells had a higher baseline frequency of MN in negative controls. Nucleoplasmic bridges evaluated as an indicator of genomic instability. Cytotoxicity was observed for both 10 and 100 nm Ag NPs,but was greater for 100 nm AgNPs. TEM indicated	Souza et al., 2016

			measurements and PDI values 7. NR	bridges in binucleated cells were greater in all treatments in both cell types compared to negative controls. Greatest number of nucleoplasmic bridges observed in CHO-XRS5 cells treated with 100 nm AgNPs.	localization of AgNPs in endosomal compartments.	
MN formation	HaCaT (human keratinocyte) cell line	0, 10, or 40 µg/ml for 24 and 48 hrs	1. Nanocomposix Europe 2. NR 3. Hydrodynamic diameter 43.3 nm in water and 64.8 in cell culture medium 4. NR 5. NR 6. NR 7. NR	Positive: Significant increase in MN frequency at 40 µg/ml; response somewhat more pronounced at 48 vs. 24 hrs. No significant increase in nucleoplasmic bridges or nuclear buds.	Dose-related cytotoxicity at both 24 and 48 hrs.	Bastos et al., 2017
MN formation	Mouse lymphoma L5178Y/Tk$^{+/-}$ 3.7.2 cell line and TK6 cells (human lymphoblastoid cell line)	Ag NPs: 1 to ~50 µg/ml for 4 hrs in mouse lymphoma L5178Y/Tk$^{+/-}$ 3.7.2 cell line and 1 to 400 µg/ml for 4 hrs in TK6 cells. $AgNO_3$ and Ag acetate: 0, 0.4, 0.45, 0.5, 0.6, or 0.65 µg/ml for 4 hrs in mouse lymphoma L5178Y/Tk$^{+/-}$ 3.7.2	1. NanoComposix 2. PVP- or citrate-coated 3. 20, 50, and 100 nm, each in PVP- or citrate-coated form 4. NR 5. Spherical 6. Minimal agglomeration in cell culture medium (PDI of 0.1) 7. NR	AgNPs: Positive in L5178Y/Tk$^{+/-}$ 3.7.2 – A dose related increase in MN frequency was observed for all test materials; greatest response was observed with 20 nm citrate-AgNPs. $AgNO_3$ and Ag acetate: Both positive and much	AgNPs induced a size related cytotoxicity (20 nm-citrate > 20 nm PVP- > 50 nm citrate- > 50 nm PVP- > 100 nm citrate > 100 nm PVP-coated AgNPs). TEM showed AgNPs inside cells. $AgNO_3$ and Ag acetate both much more cytotoxic than AgNPs.	Guo et al., 2016

		cell line and 0, 1.25, 1.5, 2.0, 2.25, 2.5, 2.75, or 3.0 μg/ml in TK6 cell line		more potent than AgNPs for induction of MN.		
MN formation	TK6 cells (human lymphoblastoid cells)	0, 1, 1.25, or 1.5 μg/ml for 28 hrs for both AgNPs and $AgNO_3$	1. Nanocomposix 2. PVP-coated 3. 5 nm 4. NR Other characteristics not reported but same as described in Li et al., Nanotoxcology 8:36-45 (2014)	Positive: Dose-related increases in MN frequency for both AgNPs and $AgNO_3$. Increase was significant at 1.5 μg/ml for both AgNPs and $AgNO_3$. Addition of Trolox (free radical scavenger) significantly decreased MN response and ROS induction by both AgNPs and $AgNO_3$. Addition of NAC (an Ag^+ chelator) had no significant effect on AgNP-induced MN or ROS response.	Both AgNPs and AgNO3 induced dose-related cytotoxicity in a similar concentration range. Expression of oxidative stress genes, ROS generation, release of Ag+ from AgNPs in cell culture medium, and ESR analysis of hydroxyl radicals, and effects of NAC and Trolox on cytotoxicity and MN and ROS induction were evaluated. Results indicate that Trolox abolished the MN response, NAC signifi-cantly reduced the MN response to $AgNO_3$, but not to AgNPs. The amount of Ag^+ released from AgNPs into culture medium was not genotoxic. AgNPs, but not $AgNO_3$, produced hydroxyl radicals directly.	Li et al., 2017
MN formation	HepG2- and A549-luciferase cells	0, 12.5, 25, 50, 100, or 200 μg/ml for 24 hrs for both cell lines	1. Sigma-Aldrich 2. NR 3. 20-50 nm 4. NR 5. Spherical 6. Change in charge when the AgNPs were added to	Positive in HepG2-luciferase cells: Significant dose-related increase in MN frequency up to 50 μg/ml; no further increase with increasing dose.	Dose related cytotoxicity in both cell lines. HepG2-luciferase cells more sensitive than A549-luciferase cells. These cells contained a GADD45a promoter-driven luciferase reporter system. GADD45a	Wang et al., 2017

			culture medium containing 10% FBS indicated possible presence of a NP-protein complex 7. NR	Magnitude of the increase was greater than A549-luciferase cells. Positive in A549-luciferase cells: Significant and comparable increase in MN frequency at 50 and 100 μg/ml, but not at other doses.	is a growth arrest and DNA-damage-inducible protein. A significant dose-related increase in luciferase activity was observed for HepG2-luciferase cells. Small but significant increases in luciferase activity was seen at 12.5 to 100 μg/ml but not at 200 μg/ml for A546-luciferase cells.	
Clastogenicity *In Vivo*[c]						
Chromosomal aberrations	Bone marrow assay in Swiss albino male mice	0, 10, 20, 40, or 80 mg/kg bw; single dose by IP injection; animals sacrificed 18 hrs after dosing.	1. Sigma-Aldrich 2. NR 3. ≤ 100 nm (supplier specification); measured mean: 125 nm (range 75-130 nm) 4. 5.0 m^2/g 5. Roughly spherical 6. Agglomeration reported; size of agglomerates not quantitated 7. 99.5% (supplier specification)	Positive: Significant increase in chromosomal aberrations at all doses. Dose-related increase from 10 to 40 mg/kg bw. Response at 80 mg/kg bw lower than at 40 mg/kg bw but still significantly increased relative to negative control.	Significant increase in ROS generation in bone marrow cells at 10 and 20 mg/kg bw. ROS generation at higher doses was comparable to negative control.	Ghosh et al., 2012
Chromosomal aberrations	Bone marrow assay in female albino rats (strain not specified)	0, 1, 2, or 4 mg/kg/d for 28 days by IP injection	1.Synthesized by investigators 2. PVP and citrate 3. 8.7 nm 4. NR 5. Spherical 6. NR 7. NR	Positive: Significant dose-related increase in total structural aberrations at all doses; no increase in numerical aberrations.	Significant increase in liver weight at all dose levels. Liver MDA levels: Significant increase at 2 mg/kg/day; significant	El Mahdy et al., 2014

					decrease at 4 mg/kg/day compared to control. Liver GSH levels: Significant increase at 1 and 2 mg/kg/d but not at 4 mg/kg/d	
Chromosomal aberrations	Bone marrow assay in male Sprague-Dawley rats	0, 5, 25, 50, or 100 mg/kg/d for 5 days by oral gavage; animals sacrificed 24 hrs after last dose	1. Ocean Nanotech 2. NR 3. 10 nm 4. 2.0 m^2/g 5. Mainly spherical 6. DLS analysis showed some agglomeration of NPs to more than their primary size 7. 99.5% trace metal basis	Positive: Significant dose-related increase in chromosomal aberrations	Dose-related increase in ROS in bone marrow; statistically significant at 50 and 100 mg/kg/day. Decrease in mitotic index in bone marrow, but no significant dose-response; most likely associated with AgNPs toxicity.	Patlolla et al., 2015
MN assay	Peripheral blood reticulocyte assay in female ICR mice mice	0 or 3 mg/mouse by a single IP injection; animals sacrificed 48 hrs after dosing	1. Sigma-Aldrich 2. NR 3. <100 nm 4. 5 m^2/g 5. NR 6. NR 7. NR	Positive: Significant increase in MN frequency	No evaluation of target organ toxicity was reported. Other metal NPs (CuO, Fe_2O_3, Fe_3O_4 and TiO_2) were also tested at 3 mg/mouse and increased MN frequency, but the CuO NP response was greatest. Urinary 8-OH-dG in 24 hr urine samples was increased AgNP treatment, but not at 24, 48 or 72 hrs when corrected by creatinine. 8-OH-dG levels in liver DNA 24 hrs after treatment were not increased. CuO NPs did show an increase in OH-dG levels in liver DNA and in	Song et al., 2012

					creatinine corrected urinary 8-OH-dG.	
MN assay	Peripheral blood reticulocyte assay in male B6C3F1 mice	5 nm PVP-coated AgNPs: 0, 0.5, 1.0, 2.5, 5.0, 10.0, or 20.0 mg/kg bw single dose by IV injection; animals sacrificed 48 hrs after treatment. 15 to 100 nm PVP- and 10 to 80 nm silicon-coated AgNPs: single IV injection of 0 or 25 mg/kg bw or 25 mg/kg/d for 3 days; animals sacrificed 48 hrs after last treatment.	See above entry for Li et al., 2014	5 nm PVP-coated AgNPs: Negative in single IV injection study. 15 to 100 nm PVP-coated and 10 to 80 nm silicon-coated AgNPs: Negative in both single and three-day treatment studies.	AgNPs were confirmed to accumulate in the bone marrow by TEM. A higher Ag level in bone marrow was detected for PVP-coated AgNPs. The 5 nm PVP-coated AgNPs caused a significant decrease in % reticulocytes indicating bone marrow toxicity at all doses. 15 to 100 nm PVP-coated AgNPs also caused significant reductions in % reticulocytes after single or repeat dose treatment. No decrease in % reticulocytes was observed for silicon-coated AgNPs.	Li et al., 2014
MN assay	Assay in male Wistar rats in both bone marrow polychromatic erythrocytes and bone marrow reticulocytes	20 nm AgNPs: 0, 5 or 10 mg/kg bw single dose by IV injection; animals sacrificed at 24 hrs, 1 week, and 4 weeks after injection 200 nm AgNPs: 0 or 5 mg/kg bw single dose by IV injection; animals sacrificed at 24 hrs, 1 week, and 4	1. Plasmachem 2. None 3. 20 nm AgNP and 200 nm AgNP 4. NR 5. NR 6. PDI[b]- 20 nm AgNP: 0.295; 200 nm AgNP: 0.328 7. NR	Polychromatic erythrocytes: Positive Significant non-dose-related increase in MN frequency for both AgNPs in polychromatic erythrocytes at 24 hrs and at 1 week after dosing. At 4 weeks, only animals dosed with 10 mg/kg bw 20 nm AgNPs had a significantly higher MN frequency.	No evidence of bone marrow cytotoxicity as measured by % PCE in bone marrow.	Dobrzynska et al., 2014

		weeks after injection		Reticulocytes: Negative for both AgNPs.		
MN assay	Peripheral blood reticulocyte assay in male ICR mice	0, 0.25, or 1 mg/kg bw single dose by IP injection; animals sacrificed at 48 and 72 hrs.	Poly(styrene-co-maleic anhydride)-coated AgNPs (SMA-AgNPs)	Negative	Evidence of cytotoxicity based on an increase in % reticulocytes at 1 mg/kg bw.	Chen et al., 2015a
MN assay	Bone marrow and peripheral blood erythrocytes in C57BL/6J p^{un}/p^{un} male and female mice; both wild type and $Myh^{-/-}$ [deficient in BER (base excision repair)]	0 or 500 mg/kg/d for 5 days by oral gavage; peripheral blood drawn after 1 and 5 days of treatment (24 hrs after dosing); animals sacrificed for bone marrow assay 24 hrs after last dose	1. Sigma-Aldrich 2. PVP-coated 3. 33.6 nm (range 5-150 nm) 4. NR 5. Spherical 6. Both monomers and agglomerates were observed by TEM 7. NR	Positive: Significant increase in MN frequency in both peripheral erythrocytes and bone marrow after both 1 and 5 days. Increase was greater after 5 days. BER deficient $Myh^{-/-}$ mice showed a greater increase in MN frequency than wild type at both time points.	Cytotoxicity to bone marrow was not evaluated. Gene expression of DNA repair genes was measured in liver, and AgNP treatment down-regulated BER gene expression. This endpoint was not evaluated in assay target tissue.	Kovvuru et al., 2015
MN assay	Bone marrow assay in male Sprague-Dawley rats	0, 5, 25, 50, or 100 mg/kg/d for 5 days; animals sacrificed 24 hrs after last dose	See above entry for Patlolla et al., 2015	Positive: Significant dose-related increase in MN frequency.	Dose-related increase in ROS in bone marrow; statistically significant at 50 and 100 mg/kg/day. Decrease in mitotic index in bone marrow, but no significant dose-response; most likely associated with AgNPs toxicity.	Patlolla et al., 2015

MN assay	Peripheral blood erythrocyte assay in male and female C57BL/6J p^{un}/p^{un} mice	0 or 4 mg/kg/d for 7 days by oral gavage; peripheral blood sampled at 24 hrs after last dose and on days 7 and 14 post-treatment	1. NanoComposix 2. Citrate- and PVP-coated 3. 20 nm 4. NR 5. NR 6. Narrow size distribution reported. PDI was 0.15 for citrate-coated and 0.2 for PVP-coated AgNPs, respectively 7. NR	Citrate-coated AgNPs: Positive – significant increase in MN frequency at all sampling times. PVP-coated AgNPs: Negative – no increase in MN frequency at any sampling time. Ag acetate: Negative - no increase in MN frequency at any sampling time.	Target tissue toxicity was not evaluated. AgNP behavior in synthetic gastric juice and synthetic intestinal juice. Higher agglomeration of citrate-coated AgNPs compared to PVP-coated AgNPs in synthetic gastric juice was observed. However, agglomeration was partially reversed in synthetic intestinal juice, suggesting that both test materials are present as both nanoscale and larger particles in the intestine after oral gavage.	Nallanthighal et al., 2017
DNA Damage *In Vitro*						
Comet assay	Mouse lymphoma L5178Y cells and BEAS-2B (human bronchial epithelial cells line)	L5178Y Cells: 0, 942.38, 1884.77, or 3769.53 µg/ml for 24 hrs with S9; 0, 449.22, 898.22, or 1796.88 µg/ml for 24 hrs without S9 BEAS-2B Cells: 0, 292.97, 582.94, or 1171.88 µg/ml for 24 hrs with S9; 0, 190.43, 380.86, or 761.72 µg/ml for 24 hrs without S9	1. Aldrich 2. NR 3. < 100 nm 4. NR 5. NR 6. NR 7. NR	Positive: Significant increase in tail moment at all concentrations in both cell lines with and without S9.	Dose-related cytotoxicity was observed that was more pronounced without S9 in both cell lines.	Kim et al., 2010a

Comet assay	BEAS-2B (human bronchial epithelial cell line)	0, 0.01, 0.1, 1, or 10 μg/ml for 24 hrs	1. Sigma-Aldrich 2. NR 3. 58.9 nm 4. NR 5. Spherical 6. Size distribution by DLS ranged from 43 to 260 nm 7. NR	Positive: Significant dose-related increase in Olive tail moment at all doses; Fgp- and Endo III-modified assays both showed oxidative DNA damage; Fgp-modified assay showed greater oxidative DNA damage than Endo III-modified assay indicating more significant oxidative damage at purines. Co-treatment with AgNPs (10 μg/ml) and scavengers for OH radicals (mannitol), H_2O_2 (catalase and sodium selenite), and superoxide radicals (SOD) showed that all of them reduced the magnitude of the increase in Olive tail moment with SOD being most effective.	ROS increased at all doses. TEM images showed AgNP aggregates wrapped within endocytic vesicles within the cytoplasm and nucleus; Fpg- and Endo III-modified comet assays also conducted to measure oxidative DNA damage.	Kim et al., 2011b
Comet assay	NT2 cells (human testicular embryonic carcinoma cell line), KO, mOgg1$^{-/-}$ cells (primary testicular cells obtained from 8-oxoguanine DNA glycosylase knockout	0, 12.5, 50, or 100 μg/ml for 24 hrs	1. Plasmachem GmbH 2. NR 3. 20 nm, 200 nm 4. NR 5. NR 6. Hydrodynamic size by DLS was 154/6 nm; tendency to	NT2 cells: Positive - Dose-related increase in % tail DNA; 200 nm AgNPs showed a greater increase than 20 nm AgNPs.	A submicron (200 nm size) Ag test material was also evaluated. KO, mOgg1$^{-/-}$ cells were used as a model for human testicular cells which have been reported to be less efficient at repairing oxidative DNA damage	Asare et al., 2012

	mice derived from C57Bl/6 mice), and WT cells (primary testicular cells obtained from C57Bl/6 mice)		agglomerate in suspension was acknowledged and attempted to be minimized by fresh preparation of suspensions before exposure 7. NR	KO, mOgg1$^{-/-}$ cells: negative – no increase in % tail DNA. WT cells: Negative – no increase in % tail DNA. None of the test systems showed an increase in % tail DNA in the fpg-modified comet assay, indicating a lack of evidence of oxidative purine base damage to DNA.	than rodent testicular cells. Cytotoxic effects as measured by MTT were observed in both WT and KO, mOgg1$^{-/-}$ cells at very low concentrations (10 μg/ml), but were not observed until higher concentrations (50 and 100 μg/ml) in NT2 cells.	
Comet assay	Human peripheral blood cells	0, 50, or 100 μg/ml for 3 hrs; 0, 50, or 100 μg/ml for 5 minutes with or without H_2O_2.	1. Synthesized by investigators 2. None 3. 40-60 nm 4. NR 5. Spherical 6. Described as slightly agglomerated when diameter of 40-60 nm was stated 7. NR	Positive: Significant increase in DNA migration (arbitrary units) and in distribution of cells into higher DNA damage categories (arbitrary units) after treatment with both 50 and 100 μg/ml for 3 hrs. However, treatment with 50 or 100 μg/ml AgNPs with H_2O_2 reduced the degree of DNA damage to a level indistinguishable	The experiment with and without H_2O_2 was conducted to evaluate whether AgNPs could react with or trap other free radicals and thus quench their activity.	Flower et al., 2012

				from the untreated control.		
Comet assay	Human peripheral blood lymphocytes	0, 25, 50, 100, 150, or 200 μg/ml for 3 hrs	See above entry for Ghosh et al., 2012	Positive: Increase in % tail DNA at all concentrations, but no dose response. Statistically significant at 25, 50 and 200 μg/ml.	Dose-related cytotoxicity at all concentrations. AgNP uptake observed by flow cytometry analysis.	Ghosh et al 2012
Comet assay	IMR-90 (normal human fibroblasts), M059K and M059J (human glioblastoma cells), CHO AA8 and CHO V33 (Chinese hamster ovary cells)	0 or 100 μg/ml for 48 hrs	1. Synthesized by investigators 2. PVP-coated 3. 20 nm 4. NR 5. Spherical 6. NR 7. 15.24 wt% Ag	Positive: Significant increases in tail moment in all cell types except IMR-90 where the increase was minimal.	The different cell types were used to explore the impact of DNA-PKcs sufficiency vs. deficiency on comet assay results. The results suggest a role DNA PKcs in the repair of AgNP-induced DNA damage.	Lim et al., 2012a
Comet assay (alkaline as well as EndoIII-, hOGG1- and fpg-modified assays)	Mouse lymphoma L5178Y cells	0, 4, 4.5, 5, 5.5, or 6 μg/ml for 4 hrs	1. Novacentrix Inc. 2. Uncoated 3. 5 nm 4. NR 5. Spherical 6. Average diameter: In PBS – 1965.8 nm; In culture medium – 1608.7 nm 7. NR	Alkaline assay: Negative- no significant increase in % tail DNA; EndoIII-modified assay: Positive – dose-related increase in % tail DNA, significant at all doses except 4 μg/ml. hOOG1-modified assay: Positive – dose-related increase in % tail DNA, significant at all doses except 4 μg/ml.	Dose-related cytotoxicity based on similar range of doses as reported for the mouse lymphoma assay mutation assay (see entry above); EndoIII-, hOGG1- and fpg-modified assays measure oxidative DNA damage.	Mei et al., 2012

				Fgp-modified assay: Positive – dose-related increase in % tail DNA, significant at 5.5 and 6 μg/ml.		
Comet assay	HDF cells (primary human dermal fibroblasts) and A549 cells (human alveolar adenocarcinoma cell line)	0, 12.5, 25, 50, or 100 μg/ml for 24, 48 and 72 hrs	1. Synthesized by investigators 2. C-AgNPs: citrate-coated; L-AgNPs: lactose-coated; O-AgNPs: coated with a 12-base long oligonucleotide 3. 50 nm 4. NR 5. NR 6. Almost no aggregation observed in cell culture medium 7. NR	Positive: Surface chemistry-concentration-time related DNA damage for both HDF and A549 cells based on increases in tail moment. C-AgNPs showed the greatest DNA damage in both cell types. DNA damage in HDF cells was greater for O-AgNPs than L-AgNPs. In A549 cells DNA damage was comparable for O-AgNPs and L-AgNPs at higher concentrations and longer exposures.	C-AgNPs were more cytotoxic than O-AgNPs or L-AgNPs for both cell types. O-AgNPs were less cytotoxic than L-AgNPs in A549 cells with higher concentration and longer exposure. After 72 hrs of exposure L-AgNPs were less toxic than O-AgNPs at lower concentrations, but showed comparable toxicity at 100 μg/ml. C-AgNPs caused apoptosis in both cell types and a significant necrosis response in HDF cells, but not A549 cells. O-AgNPs and L-AgNPs caused lower levels of necrosis and apoptosis than C-AgNPs in both cell types, but the relative effects on these endpoints differed between cell types. p53 gene expression was upregulated in C-AgNPs to the greatest extent when compared with O-AgNPs and L-AgNPs in both cell types. Up regulation of p53 for O-AgNPs and L-AgNPs	Sur et al., 2012

					was greater in A549 cells compared to HDF cells.	
Comet assay	CHO-K1 (Chinese hamster ovary) cells	0, 0.01, 0.10, 1.0, or 10 μg/ml for 24 hrs	See above entry for Kim et al., 2013b	Positive: Significant dose-related increase in Olive tail moment.	Concentrations tested were referred to as non-cytotoxic (data not shown).	Kim et al., 2013b
Comet assay	BEAS-2B (human bronchial epithelial cell line)	0, 2, 4, 8, 16, 24, 36, or 48 μg/cm^2 (corresponding to 0, 7.6, 15.2, 30.4, 60.8, 91.2, 136.8, or 182.4 μg/ml) for 4 and 24 hrs	See above entry for Nymark et al., 2013	Positive: Dose-related increase in % tail DNA after both 4 and 24 hrs. Significant effect at 16 μg/cm^2 that did not increase further with increasing dose.	Dose-related decrease in cell viability by Trypan Blue assay; only a slight cytotoxic effect in the luminescent cell viability assay.	Nymark et al., 2013
Comet assay	A549 cells (human alveolar adenocarcinoma cell line)	0, 10, 25, or 50 μg/ml for 24 and 48 hrs	1. Sigma-Aldrich 2. NR 3. Mean 56.4 nm 4. NR 5. Spheroid 6. Mean hydrodynamic diameter in cell culture medium was 252 nm 7. NR	Positive: Significant dose-related increase in % tail DNA.	Dose-related increase in cytotoxicity as measured by MTT and LDH assays. Dose-related depletion of GSH and induction of ROS, LPO, SOD, and catalase. Activities of caspases and level of proinflammatory cytokines were also increased. NAC (antioxidant) completely abolished AgNP-induced cytotoxicity (effect on comet was not evaluated). Vitamin C or vitamin C plus vitamin E also abolished cytotoxicity.	Suliman et al., 2013
Comet assay	BEAS 2B cells (human bronchial epithelial cell line)	0 to 50 μg/ml for 4 and 24 hrs	1. 10 nm OECD PVP BioPure™ Ag, 10 nm Citrate BioPure™ Ag, 40 nm Citrate Citrate	Positive: Significant increase in % tail DNA for all AgNPs independent of size	Cytotoxicity was observed only for 10 nm AgNPs independent of surface coating and only at 20 or 50 μg/ml, a dose higher than	Gliga et al., 2014

			BioPure™ Ag and 75 nm OECD BioPure™ Ag: NanoComposix, Inc. Uncoated AgNPs: EV NANO Technology Co. Ltd. 2. PVP-coated and citrate-coated 10 nm AgNPs, citrate-coated 40 nm AgNPs, citrate-coted 75 nm AgNPs, and uncoated 40-650 nm AgNPs 3. See item 2 4. NR 5. NR 6. Size distribution in cell culture medium was evaluated by DLS and PCCS. All the AgNPs agglomerated in cell medium. All but the 10 nm PVP coated AgNPs sedimented significantly over time. 7. NR	and coating at 24 hrs but not 4 hrs.	used in the comet assay. No increase in ROS for any AgNP at doses up to 20 μg/ml. No evidence of difference in uptake or intracellular localization for citrate- or PVP-coated AgNPs despite different agglomeration patterns. 10 nm AgNPs released significantly more Ag following 24 hrs in cell culture medium, but Ag released in medium did not induce cytotoxicity, thus implying intracellular Ag release is responsible for cytotoxicity.	
Comet assay	HL-60 cells (human leukemia cell line); HepG2 (human hepatoma cell line); HPF cells (human pulmonary	0, 0.1, 0.5, 0.8, 1.6 or 6.7 μg/ml for 24 hrs	1. Nanogap Subparticles 2. 4.7 nm AgNP: PEI plus PVP coated; 42 nm AgNP: uncoated 3. 4.7 nm and 42 nm	Positive: Significant dose-related increase in % tail DNA in all cell types for both AgNP test materials. 4.7 nm AgNPs were	4.7 nm and 42 nm AgNPs were cytotoxic at concentra-tions as low as 0.1 ug/ml in several cell lines. Concentrations for comet	Avalos et al., 2015b

	fibroblasts); NHDF cells (normal human dermal fibroblasts)		4. NR 5. NR 6. NR 7. NR	generally more genotoxic than 42 nm AgNPs in all cell types. Fpg-modified and Endo III-modified comet assays showed that pryimidines and purines in DNA were oxidatively damaged by both AgNPs in all cell types except NHDF. Oxidative damage was not size-dependent.	assay were selected to be non-cytotoxic. Fpg-modified and Endo III-modified comet assays were used to evaluate oxidative DNA damage.	
Comet assay	Jurkat Clone E6-1 (a human T lymphocyte cell line) and THP-1 (a human monocyte cell line)	Jurkat Cells - 10 nm AgNPs: 0, 2.5, 5, 7.5, 10, or 20 μg/ml for 24 hrs; 20 nm AgNPs: 0, 5, 10, 15, 20, or 25 μg/ml for 24 hrs; 50 nm and 100 nm AgNPs: 0, 10, 25, or 50 μg/ml for 24 hrs THO-1 Cells -10 nm AgNPs: 0, 1, 5, 10, or 25 μg/ml for 24 hrs; 20 nm AgNPs: 0, 5, 10, 20, 25, or 40 μg/ml for 24 hrs; 50 nm and 100 nm AgNPs: 0, 10, 25, or 50 μg/ml for 24 hrs	1. NanoComposix 2. Citrate-coated 3. 10, 20, 50, or 100 nm 4. NR 5. Spherical 6. Minimal aggregation based on TEM micrographs 7. NR	Positive: Significant increase in % tail DNA in both cell lines for 10 nm and 20 nm AgNPs. No significant increase in % tail DNA for 50 or 100 nm AgNPs. $AgNO_3$ induced more DNA damage than any of the AgNPs.	Both cell lines showed dose-related cytotoxicity for 10 and 20 nm AgNPs. Jurkat cell line was more sensitive than THP-1 cell line. 50 and 100 nm Ag NPs were not cytotoxic. The strongest cytotoxicity in both cells lines was seen with $AgNO_3$.	Butler et al., 2015

		$AgNO_3$: 0, 0.5, 1, 1.5, 2.0, or 2.5 μg/ml for 24 hrs (Jurkat cells) and 0, 1, 2.5, 5, or 10 μg/ml for 24 hrs (THP-1 cells)				
Comet assay (alkaline assay and OGG1-modified assay)	GM07492 (human normal untransformed fibroblasts)	0, 0.01, 0.1, 1, or 10 μg/ml for 24 hrs	1. Sigma-Aldrich 2. PVP-coated 3. 50 to 82 nm 4. NR 5. Spherical 6. Small agglomerates of AgNPs and serum proteins formed based on hydrodynamic size much higher than primary size 7. NR	Positive: Significant increase in % tail DNA in alkaline comet assay and OGG1-modified assay only at 10 μg/ml.	Little or no significant decrease in cell viability at doses up to 10 μg/ml. Substantial cytotoxicity at 100 μg/ml (dose not tested in comet assay). Intracellular localization in vesicular structures. AgNP increased expression of GADD45a (a growth arrest and DNA-damage-inducible protein.	Franchi et al., 2015
Comet assay	TK6 cells (human lymphoblastoid cells)	0, 0.31, 0.63, 1.25, or 2.5 $\mu g/cm^2$ (corresponding to 0, 1, 2, 4, 8, or 10 μg /ml) for 2 or 24 hrs	See above entry for Huk et al., 2015	Positive: Ag_Citrate and Ag_SDS: both positive at 24 hrs, Ag_Citrate positive at 2 hrs; Ag_Dispebyk and and Ag_Tween: positive at 24 hrs; Ag_Chitosan and Ag_Byk: positive at 2 hrs; could not be evaluated at 24 hrs due to excessive toxicity.	Cationic (positively charged) AgNPs were the most cytotoxic, strongly affecting cell membrane and cell morphology, inhibiting proliferation and inducing cell death. Fpg-modified comet assay used to assess oxidative DNA damage. TEM showed greater uptake of cationic AgNPs and greater presence in nucleus and mitochondria. Full extent of intracellular localization of AgNPs could not be evaluated due to high	Huk et al., 2015

				Strongest effects were observed for positively charged AgNPs. Ag_SDS showed the weakest genotoxicity. Almost all AgNPs induced DNA oxidation; level of DNA oxidation based on fpg-modified assay was similar to the level of strand breaks.	toxicity, necrosis and apoptosis.	
Comet assay	HepG2 (human hepatocellular carcinoma cell line) and primary human peripheral blood mononuclear cells	0, 1.0, or 50 μM for 24 hrs	1. Synthesized by study investigators 2. PVA-coated 3. 4 nm 4. NR 5. Spherical 6. In cell culture medium 11.7 nm as measured by DLS 7. NR	Positive: Significant increase in DNA damage index (a non-conventional measurement) at both doses for both AgNPs in both test systems	An increase in ROS in human isolated neutrophils was induced by both AgNPs. Cell uptake of AgNP was increased as evaluated by flow cytometry using SSC (side-scattered light) measurement.	Paino and Zucolotto, 2015
Comet assay (OGG1 modified assay)	EUE cells (human epithelial embryonic cell line)	0, 1, 25, or 100 μg/ml for 30 min or 2 hrs	1. Plasmachem GmbH 2. NR 3. 20 nm 4. NR 5. Spherical 6. Immediately after dispersion in cell culture medium, three populations of particles: single particles (mean diam. 33.9 nm) and medium and large agglomerates (mean diam. of 225.9 and	Positive: Significant dose-related increase in % tail DNA in OGG1 modified assay that detects oxidative damage (8-oxoG) after 30 min, but not 2 hrs. Lack of response at 2 hrs was suggestive of DNA repair. Incubation with U0126 (inhibitor of ERK activation) followed by AgNP showed	Increase in ROS and NOX-dependent superoxide formation. ROS dependent ERK and JNK activation was observed. Data show that AgNP genotoxicity is mainly mediated by ROS production and that a ROS-engaged ERK pathway is critical for the	Rinna et al., 2015

			4050 nm, respectively). TEM image showed AgNPs ranging from 20 to 100 nm, although agglomerates were also observed. 7. NR	increased % tail DNA at 2 hrs suggesting a role for ERK in the DNA repair response. Incubation with DPI followed by AgNP exposure completely inhibited the increase in % tail DNA in the OGG1 modified assay, suggesting that DNA oxidation was dependent on AgNP induced O2· formation.	cytoprotection against AgNP toxicity.	
Comet assay	NIH3T3 cell line, SVK14 (human keratinocytes) and BJ (human foreskin fibroblasts)	KCRulc 14 IC50s: 2.7, 2.53, and 1.9 mg/l for SVK14, BJ and NIH3T3 cell, respectively. KC Rulc 20 IC50s: 2.1, 2.2 and 1.3 mg/l for SK 14, BJ and NIH3T3 cells, respectively; Vintr IC50s: 2.2, 2.3 and14 mg/l for SVK14, Bj and NIH3T3 cells, respectively	1. KC Rulc 14 and KC Rulc 20: KC Rulc Company; Vintr: Lakshmi-Narayan Company 2. NR 3. KC Rulc 14: two Ag NP populations, one with diameter 1793 nm (80%) and one with diameter 0.75 nm (20%), average value 986.1 nm, median 10.2 nm; KC Rulc 20: NP populations of diameter 162.5 nm (91.4%), 19.4 nm (4.8%) and 4 nm (3.8%), median 24.4 nm; Vintr: 131.5 nm by DLS, primary	Positive: Significant increase in % tail DNA for all three AgNPs. Response was greatest in BJ cells with KC Rule20 and Vintr test materials.	All three AgNPs increased ROS, but the ROS responses across cell lines did not correlate with increases in % tail DNA. The investigators concluded that ROS production was not a major mechanism of cell damage. AgNP penetration was studied in SVK14 cells and confirmed for all three AgNPs.	Tomankova et al., 2015

			particle size 48.4 nm 4. NR 5. NR 6. Largest size values reported in item 3 suggest agglomerates 7. NR			
Comet assay	Primary cultures of NHDF (normal human dermal fibroblasts)	AgNPs: 0, 1, 10, or 25 μg/ml for 24 hrs $AgNO_3$: 0, 0.1, 0.5, or 1 μg/ml for 24 hrs	1. Nano-Trade 2. None 3. Mean 10.43 nm (range 5-40 nm) 4. NR 5. Spherical 6. NR 7. NR	Negative: Neither AgNPs nor AgNO3 were reported to increase the number of damaged nuclei.	Non-conventional method of evaluating extent of DNA damage in this comet assay (visual scoring using a 4 point scale ranging from no discernible tail to almost all DNA in tail). AgNPs were not cytotoxic in the concentration range tested. $AgNO_3$ was extremely cytotoxic at >10 μg/ml.	Galandakova et al., 2016
Comet assay	SVK14 (human keratinocyte cell line) and NIH3T3 (mouse fibroblast cell line)	AgNPs: SVK14: 0, 30.1, 60.1, or 90.1 mg/l AgNP (representing the IC25, IC50 or IC75, respectively). NIH3T3: 0, 25.4, 50.7, or 76.1 mg/l AgNP (representing the IC25, IC50 or IC75, respectively). Ag^+: SVK14: 0, 1.8, 3.6, or 5.4 mg/l Ag^+ (representing the IC25, IC50 or IC75, respectively). NIH3T3: 0, 1.3, 2.5 or 5 mg/l Ag^+	1. Synthesized by study investigators. 2. 27 nm Other characteristics were described as being detailed in other publications (Kvitek et al,. J. Phys. Chem..C 112:5825-5834 (2008); Panacek et al. Biomaterials 30:6333-6340 (2009); Panacek et al. Molecules 21:26 (2015); Panacek et al. Colloids Surfaces B Biointerfaces 142:392-399 (2016)).	Positive: Significant dose-related increase in % tail DNA at all AgNP doses in NIH3T3 cells but not in SVK15 cells. Ag^+ also showed a dose-related increase in % tail DNA, but the effect was seen only in NIH3T3 cells. AgNPs showed a much greater effect at IC75 than Ag^+.	Cytotoxicity was observed for both AgNPs and Ag+, but was greater for Ag^+. NIH3T3 cells were more sensitive to cytotoxicity than SVK14 cells. Ag^+ increased ROS in both cell lines at all doses, but the effect was greater in NIH3T3 cells. AgNPs increased ROS in NIH3T3 cells (IC50 and IC75) and in SVK14 cells (IC75). AgNPs accumulated in the nucleus of NIH3T3 cells and in the cytoplasm of SVK14 cells. Significant increases in lipid	Jiravova et al., 2016

		(representing the IC25, IC50 or IC75, respectively).			peroxidation were seen with AgNPs (IC50 and IC75) in both cell lines and with Ag^+ (IC75) in SVK14.	
Comet assay	HeLa (human cervical carcinoma cell line), MDA-MB-231 (human breast cancer cell line), and MCF7 (human breast cancer cell line)	0, 1.25, 2.5, 3.5, 5, or 10 μg/ml for 12 and 24 hrs	1. Donated by V. Burmistrov from the Scientific and Productuion Center Vector-Vita (Russia) 2. PVP-coated 3. 35 nm 4. NR 5. Spheroid 6. NR 7. 1.2 wt% metallic Ag; 18.8 wt% PVP	Positive: While exposure to the IC50 dose, which ranged from 2.62 to 3.43 μg/ml across the 3 cell lines, did not increase % tail DNA, significant increases were observed at 5 and 10 μg/ml in all 3 cell lines at 12 and 24 hrs.	Dose- and time-related cytotoxicity was observed in all cell lines. Dose-related increase in ROS was observed in all cell lines, with significant responses at 5 and 10 μg/ml at 24 hrs in all cell lines, and at 12 hrs in MCF7 cells.	Juarez-Moreno et al., 2016
Comet assay	CHO-K1 cells and CHO-XRS5 cells (both Chinese hamster ovary cell lines). CHO-XRS5 cells are deficient in the repair of DNA double strand breaks	0, 0.025, 0.25, 1.25, or 2.5 μg/ml for 24 hrs for both 10 nm and 100 nm AgNPs.	1. Sigma-Aldrich 2. NR 3. 10 and 100 nm 4. NR 5. Spherical 6. Formation of small agglomerated based on hydrodynamic diameter measurements and PDI values 7. NR	Positive: In both cell lines significant increases in % tail DNA at 1.25 and 2.5 μg/ml for both 10 nm and 100 nm AgNPs and at 0.25 μg/ml for 10 nm AgNPs in CHO-K1 cells. Magnitude of comet response similar for both 10 and 100 nm AgNPs.	Cytotoxicity was observed for both 10 and 100 nm AgNPs, but was greater for 100 nm AgNPs. TEM indicated localization of AgNPs in endosomal compartments.	Souza et al., 2016
Comet assay	HaCaT (human keratinocyte) cell line	0, 10, or 40 μg/ml for 24 and 48 hrs	1. Nanocomposix Europe 2. NR 3. Hydrodynamic diam. 43.3 nm in water and 64.8 nm	Positive: Significant dose-related increase in GDI (genetic damage indicator) (a non-conventional measurement) at both 10 and 40 μg/ml.		Bastos et al., 2017

			in cell culture medium 4. NR 5. NR 6. NR 7. NR	Effects were more pronounced after 48 vs. 24 hrs.		
Comet assay	A549 (human alveolar adenocarcinoma cell line), HepG2 (human hepatocellular carcinoma cell line), and HK-2 (human proximal tubule epithelial cell line)	0, 0.625, 2.5, 10, or 40 μg/cm^2 for NM402; 0, 0.625, 2.5, or 10 μg/cm^2 for NM300	1. JRC repository/RAS GmbH 2. Polyethylene glycerol trioleate and 4% Tween 20 coated 3. <20 nm 4. NR 5. NR 6. NR 7. NR	Positive: Significant dose-related increase in % tail DNA for NM300 in all three cell lines, but considerable variability was observed among experimental replicates and doses were cytotoxic. A notable increase in % tail DNA in the absence of cytotoxicity was also observed for the NM300 dispersant control.	Dose-related cytotoxicity. Oxidant generation as measured by ESR spectroscopy capacity was increased was not affected by NM300 or NM300 dispersant.	Thongkam et al., 2017
Comet assay	HepG2- and A549-luciferase cells	0, 12.5, 25, 50, 100, or 200 μg/ml for 24 hrs for both cell lines	See above entry for Wang et al., 2017	Positive: Significant dose-related increases in Olive tail moment, % tail DNA, and tail length. Response was greater in HepG2-luciferase cells vs. A549-luciferase cells.	Dose related cytotoxicity in both cell lines. HepG2-luciferase cells more sensitive than A549-luciferase cells. These cells contained a GADD45a promoter-driven luciferase reporter system. A significant dose-related increase in luciferase activity was observed for HepG2-luciferase cells. Small but significant increases in luciferase	Wang et al., 2017

					activity was seen at 12.5 to 100 μg/ml but not at 200 μg/ml for A546-luciferase cells.	
γH2AX foci immunofluor-escence assay for DNA double strand breaks	IMR-90 (normal human fibroblasts), M059K and M059J (human glioblastoma cells), CHO AA8 and CHO V33 (Chinese hamster ovary cells)	0 or 100 μg/ml for 48 hrs	1. Synthesized by investigators 2. PVP-coated 3. 20 nm 4. NR 5. Spherical 6. NR 7. 15.24 wt% Ag	Positive: Significant increases in γH2AX foci in all cell types.	The different cell types were used to explore the impact of DNA-PKcs sufficiency vs. deficiency on DNA damage induced by AgNPs. The overall results suggested that cells lacking functional DNA PKcs are more sensitive.	Lim et al., 2012a
γH2AX foci immunofluor-escence assay for DNA double strand breaks	BEAS 2B cells (human bronchial epithelial cell line)	0 or 10 μg/ml for 4 and 24 hrs	See above entry for Gliga et al. 2014	Negative: No γH2AX foci formation for any of the AgNPs.	Cytotoxicity was observed only for 10 nm AgNPs independent of surface coating and only at 50 μg/ml, a dose higher than used in the comet assay. No increase in ROS for any AgNP at doses up to 20 μg/ml. No evidence of difference in uptake or intracellular localization for citrate- or PVP-coated AgNPs despite different agglomeration patterns. 10 nm AgNPs released significantly more Ag+ following 24 hrs in cell culture medium, but Ag+ released in medium did not induce cytotoxicity, thus implying intracellular Ag release is responsible for cytotoxicity.	Gliga et al., 2014

γH2AX and assays for DNA double strand breaks	GM07492 (human normal untransformed fibroblasts)	0 or 10 μg/ml for 24 hrs	See above entry for Franchi et al., 2015	Positive: Increase in γH2AX but not ATM phosphorylation at 10 μg/ml. Both assays measure DNA double strand breaks. Investigators did not address the difference in response.	Little or no significant decrease in cell viability at doses up to 10 μg/ml. Substantial cytotoxicity at 100 μg/ml (dose not tested in comet assay). Intracellular localization in vesicular structures. AgNP increased expression of GADD45a.	Franchi et al., 2015
DNA Damage *In Vivo*[c]						
Comet assay	Swiss albino male mice Tissue: bone marrow	0, 10, 20, 40, or 80 mg/kg bw; single dose by IP injection; animals sacrificed 18 hrs after dosing.	1. Sigma-Aldrich 2. NR 3. ≤100 nm (supplier specification); mean ~125 nm (range 75 to 130 nm) (investigator's analysis by TEM) 4. 5.0 m^2/g (supplier's specification) 5. Roughly spherical 6. Agglomeration reported; size of agglomerates not quantitated 7. 99.5% (supplier specification)	Positive: Significant increase in % tail DNA at 10 and 20 mg/kg bw. Increase in % tail DNA was not significant at 40 and 80 mg/kg bw.	Significant increase in ROS generation in bone marrow cells at 10 and 20 mg/kg bw. ROS generation at higher doses was comparable to negative control.	Ghosh et al 2012
Comet assay	Male B6C3F1 mice Tissue: liver	0 or 25 mg/kg/d by IV injection for 3 days; animals sacrificed 3 hrs after last dose	See above entry for Li et al., 2014	Negative: No increase in % tail DNA for either AgNP test material. Positive: Significant increases in % tail DNA for both AgNPs in both the	Only 15 to 100 nm PVP- and 10 to 80 nm silicon-coated AgNPs tested. Additional AgNPs were tested in an *in vivo* MN assay (see Li et al., 2014 entry above). EndoIII- and hOOG1-modified comet assays used to measure	Li et al., 2014

				EndoIII- and hOOG1-modified comet assays indicating oxidative DNA damage.	oxidative DNA damage. AgNPs were confirmed to accumulate in the bone marrow by TEM.	
Comet assay	Male Wistar rats Tissue: bone marrow	20 nm AgNPs: 0, 5 or 10 mg/kg bw single dose by IV injection; animals sacrificed at 24 hrs, 1 week, and 4 weeks after injection 200 nm AgNPs: 0 or 5 mg/kg bw single dose by IV injection; animals sacrificed at 24 hrs, 1 week, and 4 weeks after injection	1. Plasmachem 2. NR 3. 20 nm AgNP and 200 nm Ag test material 4. NR 5. NR 6. PDI[b] – 20 nm AgNP: 0.295; 200 nm Ag test material: 0.328 7. NR	Negative: Values for % tail DNA or tail moment were sometimes slightly enhanced compared to controls, but results were not statistically significant	No evidence of bone marrow cytotoxicity as measured by % PCE in bone marrow.	Dobrzynska et al., 2014
Comet assay	Swiss albino mice (sex not specified) Tissue: Peripheral lymphocytes	0, 26, 52, or 78 mg/kg bw; single dose by IP injection; animals sacrificed 24 and 72 hrs after dosing	1. Synthesized by investigators 2. None 3. 43 nm 4. NR 5. Spherical 6. Small agglomerates in aqueous suspension with	Positive: Significant dose-related increase in % tail DNA at all doses at both time points.	Increase in serum ALP, ALT, and AST. Histopathologic evaluation of the liver showed severe damage.	Al Gurabi et al., 2015

			hydrodynamic size of ~189 nm 7. NR			
Comet assay	Male Sprague-Dawley rats Tissue: bone marrow	0, 5, 25, 50, or 100 mg/kg/d for 5 days; animals sacrificed 24 hrs after last dose	See above entry for Patlolla et al., 2015	Positive: Significant dose-related increase in % tail DNA. The % tail DNA increases were statistically significant at 50 and 100 mg/kg/d for 5 days	Dose-related increase in ROS in bone marrow; statistically significant at 50 and 100 mg/kg/day. Decrease in mitotic index in bone marrow but no significant dose-response; most likely associated with AgNPs toxicity.	Patlolla et al., 2015
γH2AX immunofluor-escence assay for DNA double strand breaks	Bone marrow and peripheral blood erythrocytes in C57BL/6J p^{un}/p^{un} male and female mice; both wild type and $Myh^{-/-}$ [deficient in BER (base excision repair)]	0 or 500 mg/kg/d for 5 days by oral gavage; peripheral blood drawn after 1 and 5 days of treatment (24 hrs after dosing) animals sacrificed for bone marrow assay 24 hrs after last dose	See above entry for Kovvuru et al., 2015	Positive: Significant increase in % γH2AX positive cells in peripheral blood on both days 1 and 5 in both wild type and $Myh^{-/-}$ mice. Percentage of γH2AX positive cells was also increased in bone marrow in both wild type and $Myh^{-/-}$ mice.	Cytotoxicity to bone marrow was not evaluated. Gene expression of DNA repair genes was measured in liver, and AgNP treatment down-regulated BER gene expression. This endpoint was not evaluated in assay target tissue.	Kovvuru et al., 2015
γH2AX immunofluor-escence assay for DNA double strand breaks	Peripheral blood leukocyte assay in male and female C57BL/6J p^{un}/p^{un} mice	0 or 4 mg/kg/day for 7 days by oral gavage; peripheral blood sampled at 24 hrs after last dose and on days 7 and 14 post-treatment	See above entry for Nallanthighal et al., 2017	Positive for citrate-coated AgNPs: Significant increase in % γH2AX positive cells on days 7 and 14. Negative for PVP-coated AgNPs:	See above entry for Nallanthighal et al., 2017	Nallanthighal et al., 2017

				Negative for Ag acetate		
P^{un} reversion/ DNA deletion assay	Pregnant female C57BL/6J p^{un}/p^{un} mice, both wild type and $Myh^{-/-}$ [deficient in BER (base excision repair)]	0 or 500 mg/kg/d for 5 days by oral gavage from 9.5 dpc to 13.5 dpc	See above entry for Kovvuru et al., 2015	Positive: Significant increase in the number of eye spots per retinal pigment epithelium in offspring of both wild type and and $Myh^{-/-}$ mice, demonstrating that maternal dosing of AgNPs during gestation induces large-scale genome rearrangements in developing embryos.	This assay measures frequency of homologous recombination between two repeats in the p^{un} locus, resulting in deletion that reverts the P^{un} allele to a functional p gene, allowing black pigment accumulation in the eye of developing p^{un}/p^{un} mice *in utero*, visualized after birth.	Kovvuru et al., 2015
DNA Adducts *In Vitro*						
1. ^{32}P post-labeling method for bulky DNA adducts 2. 8-oxodG analysis by LC/MS/MS	CHO-k1 (Chinese hamster ovary)	0, 1, 5, or 10, µg/ml for 24 hrs	1. Synthesized b5:743-750 (by investigators) 2. BSA-coated 3. Mean 15.9 nm Other characterization information was not provided in this publication, but Foldbjerg et al., Tox. Sci. 130:145-157 (2012) was cited.	Positive: Significant dose-related increase in bulky DNA adducts with both AgNPs and $AgNO_3$. Comparing identical Ag concentrations $AgNO_3$ induced a 2-fold higher increase in bulky DNA adducts than AgNPs. Significant dose-related increase in 8-oxodG (marker of oxidative DNA damage) with both AgNPs and $AgNO_3$.	Cell uptake into endosomes and lysosomes but not nuclei or mitochondria was shown by TEM. Increased cytotoxicity (MTT assay, apoptosis, necrosis) and increased ROS observed for both AgNPs and Ag^{+}.	Jiang et al., 2013

				Increase was greater for AgNPs compared to $AgNO_3$ at identical Ag concentration. Results suggest a quantitative and qualitative difference in DNA damage induced by Ag^+ vs. AgNPs.		
DNA Adducts *In Vivo*[c]						
8-oxoG quantitation by immunofluor-escence	Peripheral blood leukocyte assay in male and female C57BL/6J p^{un}/p^{un} mice	0 or 4 mg/kg/d for 7 days by oral gavage; peripheral blood sampled at 24 hrs after last dose and on days 7 and 14 post-treatment	See above entry for Nallanthighal et al., 2017	Citrate-coated AgNPs: Positive – significant increase in 8-oxoG levels 24 hrs after last dose and also on days 6 and 14 post-treatment. Since 8-oxoG is repaired within a short period of time, elevated 8-oxoG at 7 and 14 days post-treatment suggests that citrate-coated AgNPs persist in the body. PVP-coated AgNPs: Negative - no increase 8-oxoG levels at any time point. Ag acetate: Negative - no increase 8-oxoG	See above entry for Nallanthighal et al., 2017	Nallanthighal et al., 2017

				levels at any time point.		

[a] Particle characterization data are itemized as follows: 1. Source 2. Coating 3. Primary size 4. Surface area 5. Shape 6. Aggregation/agglomeration 7. Purity

[b]Polydispersity index (PDI) is a unitless number ranging from 0-0.1 for monodisperse and up to 0.5-0.7 for varying degrees of agglomeration; value of >0.7 represent very broad size distribution. The PDI = M_w/M_n, i.e., weight average molecular weight/number average molecular weight

[c]*In vivo* studies in mammalian species involving all routes of exposure, including oral, inhalation ,IP and intravenous routes are included in this table, although the IP and intravenous routes of exposure are generally not recommended for risk assessment without specific scientific justification.

ALP = alkaline phosphatase; ALT = alanine amino transferase; AST = aspartate amino transferase; bPEI = branched polyethylene imine; BSA = bovine serum albumin; CB = cytochalasin B; CBMN = cytochalasin B micronucleus assay; DLS = dynamic light scattering; dpc = days post conception; DPI = diphenyleneiodonium; ENM = engineered nanomaterials; ESR = electron spin resonance; FBS = fetal bovine serum; GADD45a = growth arrest and DNA damage-inducible protein; GDI = genetic damage indicator; GSH = glutathione; HTS = high throughput screening; IC25, IC50 and IC75 = inhibitory concentration where viability is reduced by 25, 50 and 75%, respectively; LDH = lactate dehydrogenase; LPO = lipid peroxidase; MTT = 3-(4,5-dimethylthiazol-2-yl)-2,5-diphenyltetrazolium bromide; NAC = N-acetyl cysteine; NR = not reported; PDI = polydispersity index; PEI = polyethyleneimine; PKcs = protein kinase C's; PVP = polyvinylpyrrolidone; RBCs = red blood cells; RCC = relative cell count; ROS = reactive oxygen species; SMA = styrene-comaleic anhydride; SOD = superoxide dismutase

Appendix H*

Genotoxicity Studies of TiO2 Nanoparticles (Versar, 2012)

*References for Appendices are located in Section 7 of Volume 1 report. Abbreviations for Appendices are located in Abbreviation list, Volume 1 report.

Table H.1 Summary of Genotoxicity Data for TiO2 Nanoparticles (Versar, 2012)a,b

Endpoint	Assay	Test system	Exposure	Particle data	Result	Comments	Reference
Mutation	Reverse mutation assay	*Salmonella typhimurium* strains TA97a and TA100 and *Escherichia coli* WP2*uvr*A	0, 10, 100, or 1,000 µg/plate for 72 hrs	<100 nm in size	Negative, with or without metabolic activation (*S. typhimurium*); positive in WP2 with activation		Pan et al., 2010
	Reverse mutation assay	*S. typhimurium* strains TA 98, TA100, TA1535, and TA1537 and *E. coli* WP2*uvr*A	0, 100, 333, 1,000, or 5,000 µg/plate	Median primary particle size of 140 nm (in water); 79% rutile/21% anatase; surface area = 38.5 m^2/g	Negative, with or without metabolic activation		Warheit et al., 2007
	Gpt-delta assay	MEF cells	0, 0.1, 1, 10, or 30 µg/mL for 24 hrs	Anatase particles with average primary particle dia of 5 or 40 nm and surface areas of 114 and 38 m^2/g, respectively; and -325 mesh TiO2 (fine) with a surface area of 9 m^2/g	Positive for 5 and 40 nm particles (all doses); negative for -325 mesh TiO2		Xu et al., 2009
	HPRT assay	WIL2-NS (human B-cell lymphoblastoid) cells	0, 26, 65, or 130 µg/mL for 6, 24, or 48 hrs	Particles 99% pure	Positive results reported at 130 µg/mL for 24 hrs (data not shown)	Particle size distribution: by volume 6.57 nm (100%); by intensity 8.2 nm (80%) and 196 nm (19%)	Wang et al., 2007
	HPRT assay	Alveolar type II cells (rats)	0, 10, or 100 mg/kg via IT	Anatase; median dia 180 nm; surface area of 8.8 m^2/g	Positive at 100 mg/kg		Driscoll et al., 1997

Endpoint	Assay	Test system	Exposure	Particle data	Result	Comments	Reference
Clastogenicity	SCE	CHO-K1 cells	0, 5,10, or 25 µg/mL for 24 hrs	Average particle size 20 ± 7 nm; surface area of 142 m^2/g	Positive at 1–5 µg/mL	Cytotoxicity was apparent at 10 and 25 µg/mL	Di Virgilio et al., 2010
	SCE	CHO-K1 cells	1–20 µM (0.08–1.6 µg/mL) for 24 hrs	No data available	Positive	Phase and particle size not reported	Lu et al., 1998, as cited in Di Virgilio et al., 2010
	Chromosomal aberrations	CHO-WBL cells	Concentrations up to 5,000 µg/mL or that resulted in ≥50% toxicity (whichever was lowest)	Eight test particles (coated, doped, and uncoated), various crystal types, particle sizes ranging from 14 to 60 nm	Negative (in the presence or absence of UV light)		Theogaraj et al., 2007
	DNA deletions	C57B1/6Jp^{un}/p^{un} mice	500 mg/kg in drinking water during pregnancy	75% anatase, 25% rutile particles; purity 99.5%, primary particle size 21 nm	Positive	Offspring were sacrificed at PND 20 and assessed for deletions	Trouiller et al., 2009
	MN formation	V79 cells (hamster lung fibroblasts)	0, 1, 5, 10, 15, or 25 µg/cm^3 for 24, 48, or 72 hrs	Anatase with a diameter of 30 to 50 nm, uncoated or coated with V_2O_5	Negative (uncoated particles); positive (coated particles) at 2 µg/cm^3 for 24 or 48 hrs	Pure V_2O_5 alone did not induce genotoxic effects in V79 cells at the applied concentrations	Bhattacharya et al., 2008

Endpoint	Assay	Test system	Exposure	Particle data	Result	Comments	Reference
	MN formation	CHO cells	0, 750, 1,250, or 2,500 µg/mL without activation (4 hrs), 0, 62.5, 125, or 250 µg/mL with activation (4 hrs), 0, 25, 50, or 100 µg/mL without activation (20 hrs)	Median primary particle size of 140 nm (in water); 79% rutile/21% anatase; surface area = 38.5 m^2/g	Negative		Warheit et al., 2007
	MN formation	CHO-K1 cells	0, 0.6, 1, 6, or 10 µg/mL for 24 hrs	Average particle size 20 ± 7 nm; surface area of 142 m^2/g	Positive at 0.5 and 1 µg/mL	Cytotoxicity was apparent at 10 µg/mL	Di Virgilio et al., 2010
	MN formation	CHO-K1 cells	1–20 µM (0.08 to 1.6 µg/mL) for 24 hrs		Positive	Phase and particle size not reported	Lu et al., 1998 (as cited in Di Virgilio et al., 2010)
	MN formation	SHE cells	0, 0.5, 1.0, 5, or 10 µg/cm^2 for 12, 24, 48, 66, or 72 hrs	Particle size ≤20 nm	Positive at 1.0 µg/cm^2 for 24, 48, 66, or 72 hrs; at 5.0 µg/cm^2 for 24 hrs		Rahman et al., 2002
	MN formation	RLE cells	0, 5, 10, or 20 µg/cm^2 for 21 hrs	Anatase particles, 20 nm in size	Negative		Linnainmaa et al., 1997
	MN formation	BEAS-2B (human bronchial) cells	0, 1, 5, 10, 20, 40, 60, 80, or 100 µg/cm^2 (or 0, 3.8, 19, 38, 76, 114, 228, 304, or 380 µg/mL) for 24, 48 or 72 hrs	Uncoated anatase (<25 nm); rutile (10 × 40 nm) coated in SiO_2	Positive for anatase particles at 10 or 60 µg/cm^2 for 72 hrs Negative for coated rutile particles	Average agglomerate sizes were 5.5 and 4.5 µm for anatase and coated rutile particles, respectively	Falck et al., 2009

Endpoint	Assay	Test system	Exposure	Particle data	Result	Comments	Reference
	MN formation	BEAS-2B (human bronchial) cells	10 µg/mL for 24 hrs	Anatase particles, 10 nm in diameter	Positive		Gurr et al., 2005
	MN formation	Human peripheral blood lymphocytes	0, 20, 50, or 100 µg/mL for 48 hrs	70 to 85% anatase, 15 to 30% rutile particles, ~30 nm in size	Positive at ≥50 µg/mL		Kang et al., 2008
	MN formation	L-02 (human embryo) hepatocytes	0, 0.01, 0.1, or 1 µg/L for 24 hrs	The anatase: rutile ratio of particles was 8:2; primary particle diameter ~25 nm	Negative		Shi et al., 2010
	MN formation	WIL2-NS (human B-cell lymphoblastoid) cells	0, 26, 65, or 130 µg/mL for 6, 24, or 48 hrs	Particles 99% pure	Positive at 26 µg/mL (48 hrs), 65 µg/mL (all time points), and 130 µg/mL (6 hrs)	Particle size distribution: by volume 6.57 nm (100%); by intensity 8.2 nm (80%) and 196 nm (19%) Cytotoxicity (>60%) was observed at 130 µg/mL in cells treated ≥24 hrs	Wang et al., 2007
	MN formation	C57B1/6Jp^{un}/p^{un} mice (erythrocytes from peripheral blood)	50, 100, 250, or 500 mg/kg in drinking water	75% anatase, 25% rutile particles; purity 99.5%, primary particle size 21 nm	Positive at 500 mg/kg		Trouiller et al., 2009

Endpoint	Assay	Test system	Exposure	Particle data	Result	Comments	Reference
DNA damage	Comet assay	Bottlenose dolphin leukocytes	0, 20, 50, or 100 µg/mL for 4, 24, or 48 hrs	Anatase (<25 nm) or rutile (<5,000 nm) particles	Positive for anatase particles at 50 µg/mL for 24 or 48 hrs; positive for rutile particles at ≥50 µg/mL for 48 hrs	In solution, both particle types showed aggregation. The size frequency distribution was similar for both particles; limited numbers of single particles or small aggregates (<100 nm in size) and a large number of aggregates in the µm range were observed	Bernardeschi et al., 2010
	Comet assay	BEAS-2B or IMR-90 (human bronchial) cells	0, 2, 5, 10, or 50 µg/cm^2 for 24 hrs	Particles with an average dia of 91 nm; composed of 56% titanium, 41% oxygen, and 3% carbon	Negative		Bhattacharya et al., 2009
	Comet assay	BEAS-2B (human bronchial) cells	0, 1, 5, 10, 20, 40, 60, 80, or 100 µg/cm^2 (or 0, 3.8, 19, 38, 76, 114, 228, 304, or 380 µg/mL) for 24, 48, or 72 hrs	Uncoated anatase (<25 nm); rutile (10 × 40 nm) coated in SiO_2	Positive for anatase particles at 10–80 µg/cm^2 for 24 hrs, 60 to 100 µg/cm^2 for 48 hrs, or 40, 80, or 100 µg/cm^2 for 72 hrs Positive for coated rutile particles at 80 µg/cm^2 for 24 hrs or ≥80 µg/cm^2 for 72 hrs	Average agglomerate sizes were 5.5 and 4.5 µm for anatase and coated rutile particles, respectively	Falck et al., 2009

Endpoint	Assay	Test system	Exposure	Particle data	Result	Comments	Reference
	Comet assay	BEAS-2B (human bronchial) cells	10 µg/mL for 1 hr	Anatase particles, 10, 20, or ≥200 nm in size; rutile TiO_2 (200 nm in size)	Positive for 10 or 20 nm anatase and 200 nm rutile particles; negative for ≥200 nm anatase particles		Gurr et al., 2005
	Comet assay	Human nasal epithelial cells	0, 10, 25, 50, or 100 µg/mL for 24 hrs	Anatase, <25 nm in size	Negative	Mean size of aggregated particles was 285 ± 52 nm	Hackenberg et al., 2010
	Comet assay	Human peripheral blood lymphocytes	20, 50, or 100 µg/mL for 0, 6, 12, or 24 hrs	70 to 85% anatase, 15 to 30% rutile particles, ~30 nm in size	Positive (all concentrations and time points)		Kang et al., 2008
	Comet assay	A549 (human lung epithelial) cells	1, 20, or 40 µg/cm^2 (2, 40, or 80 µg/mL) for 4 hrs	Mixture of anatase and rutile, average particle size 63 nm	Positive at ≥20 µg/cm^2	Aggregations (typically 10 larger than the primary particle size) were noted	Karlsson et al., 2008
	Comet assay	L-02 (human embryo) hepatocytes	0, 0.01, 0.1, or 1 µg/L for 24 hrs	The anatase: rutile ratio of particles was 8:2; primary particle diameter ~25 nm	Negative		Shi et al., 2010
	Comet assay	WIL2-NS (human B-cell lymphoblastoid) cells	0, 26, 65, or 130 µg/mL for 6, 24, or 48 hrs	Particles 99% pure	Positive results reported at 65 µg/mL for 24 hrs (data not shown)	Particle size distribution: by volume 6.57 nm (100%); by intensity 8.2 nm (80%) and 196 nm (19%)	Wang et al., 2007

Endpoint	Assay	Test system	Exposure	Particle data	Result	Comments	Reference
	Comet assay	C57B1/6Jp^{un}/p^{un} mice (peripheral blood)	500 mg/kg in drinking water	75% anatase 25% rutile particles; purity 99.5%, primary particle size 21 nm	Positive		Trouiller et al., 2009
	Double-stranded breaks	C57B1/6Jp^{un}/p^{un} mice (bone marrow)	50, 100, 250, or 500 mg/kg in drinking water	75% anatase 25% rutile particles; purity 99.5%, primary particle size 21 nm	Positive (all doses)		Trouiller et al., 2009
	Damage to DNA fragments in test tube	DNA fragments incubated with TiO_2 nanoparticles in presence of UVA light	0, 4, 8, or 16 µg/mL, ± Cu II	Photo-irradiated anatase or rutile NPs (50 to 300 nm; commercial products)	Positive	Anatase was more potent than rutile; DNA damage was dependent on UVA irradiation and stimulated by Cu II	Hirakawa et al., 2004
	DNA adduct formation	IMR-90 (human bronchial) cells	5 or 10 µg/cm^3 for 24 hrs	Particles with an average dia of 91 nm; composed of 56% titanium, 41% oxygen, and 3% carbon	Positive		Bhattacharya et al., 2009
	DNA adduct formation	L-02 (human embryo) hepatocytes	0, 0.01, 0.1, or 1 µg/L for 24 hrs	The anatase:rutile ratio of particles was 8:2; primary particle dia ~25 nm	Positive at 1 µg/L		Shi et al., 2010

[a]Source: Versar (2012)
[b]Refernces cited are in Versar (2012)
CHO = Chinese hamster ovary; MEF = mouse embryo fibroblast; MN = micronucleus; RLE = rat liver epithelial; SCE = sister chromatid exchange; SHE = Syrian hamster embryo

Appendix I*

Mutagenicity/Genotoxicity Studies of Nano TiO2

*References for Appendices are located in Section 7 of Volume 1 report. Abbreviations for Appendices are located in Abbreviation list, Volume 1 report.

I Mutagenicity/Genotoxicity Studies of Nano TiO2

1 *In Vitro* Mutagenicity Studies

In vitro mutagenicity tests in bacteria (Butler et al., 2014; Woodruff et al., 2012; Landsiedel et al., 2010) have confirmed the previous reports of negative results in the standard Ames test in *S. typhimurium* strains. These studies did not corroborate previous results showing a positive response in the *E. coli* strain (WP2*uvr*A), the more sensitive strain to oxidative damage, nor was a mutagenic result observed in TA102, a *S. typhimurium* strain also sensitive to oxidative effects, even when tested to the maximum recommended test concentration. These negative results have been generally attributed to the lack of uptake of TiO2 NPs by bacterial cells. Consistent with this hypothesis, the use of the fluctuation test procedure with *S. typhimurium* strains TA97a, TA98, TA100, and TA102 resulted in negative results except under conditions where a pre-incubation step was included to improve interaction of the NPs with bacterial cells. In this study, a positive response was seen only with TA102 (Jomini et al., 2012).

Results of *in vitro* mammalian cell HPRT mutation assays have been mixed, with Chen et al. (2014) reporting a positive response in V79 cells after a two hr exposure to 20 or 100 μg/mL and Wang et al. (2011) reporting a negative response in CHO-K1 cells after exposures of either 24 hrs, 48 hrs, or 60 days to concentrations of up to 40 μg/mL. In the latter study, TEM documented internalization of NPs in cells exposed for 60 days, and both the short term and 60-day exposures resulted in increases in reactive oxygen species (ROS).

There does not appear to be enough information to determine a cause for the conflicting results between these studies. Reasons for the different results could include duration of exposure, cell uptake, oxidative stress response, particle size distribution, agglomeration, or unmeasured characteristics of the administered TiO2.

2 *In Vitro* Genotoxicity Studies

2.1 Chromosomal Aberrations

In one chromosome aberration assay in cultured human peripheral blood lymphocytes conducted using test concentrations ranging from 6.25 to 300 μg/mL, a significant increase in chromosome aberrations was noted after 48 hrs but not after 24 hrs or 72 hrs. A significant increase was observed at 100 and 300 μg/mL, but there was no evidence of a dose response (Catalan et al., 2012).

2.2 Micronucleus Formation

In vitro MN assay results were reported in 12 publications. Two of the publications involved cell lines derived from laboratory animals, nine involved human cell lines or primary human cell cultures, and one evaluated both human and animal cell lines. Four studies reported negative results in human cells (Jugan et al., 2012; Armand et al., 2016) or animal cells (Landsiedel et al., 2010; Guichard et al., 2012). One study with negative results involved coated rutile TiO2 NPs and showed no evidence of cytotoxicity at the highest concentration tested (75 μg/mL)

(Landsiedel et al., 2010). These results might suggest that rutile form and/or the presence of a coating decreases the potential for cytotoxicity and genotoxicity of TiO2 NPs. In the other three negative studies, TiO2 NPs of various types were tested, including anatase, rutile, and anatase:rutile mixtures, and none of the forms tested increased MN frequency when tested up to cytotoxic concentrations (Jugan et al., 2012; Guichard et al., 2012) and/or at concentrations that increased ROS (Jugan et al., 2012; Guichard et al., 2012; and Armand et al., 2016). However, these three studies with negative results for MN induction were all positive in the *in vitro* comet assay (see below), whereas Landsiedel et al. (2010) did not conduct a comet assay. The negative results in the four *in vitro* MN assays might be due to a lower sensitivity of the assay compared to the comet assay or to the efficient completion of DNA repair before DNA damage is fixed into a clastogenic event.

Eight *in vitro* MN studies reported positive results in human cells (Shukla et al., 2011; Srivastava et al., 2011; Prasad et al., 2013; Shukla et al., 2013; Srivastava et al., 2013; Valdiglesias et al., 2013; Tavares et al., 2014) and one study reported positive results in both human and mammalian cells (Demir et al., 2015). Human cell lines showing an increase in MN included an epidermal cell line (Shukla et al., 2011), a bronchial epithelial cell line (Prasad et al., 2013), a liver cell line (Shukla et al., 2013), a neuroblastoma cell line (Valdiglesias et al., 2013), an embryonic kidney cell line (Demir et al., 2015), and a human lung carcinoma cell line (A549 cells). In the studies with positive results in A549 cells, there was evidence of cytotoxicity and increased ROS (Srivastava et al., 2013; Srivastava et al., 2011) as well as cell uptake of TiO2 NPs (Srivastava et al., 2013). Srivastava et al. (2011) also demonstrated that administration of antioxidant decreased both the MN response and the ROS response. However, two other studies in A549 cells reported negative MN results, and both also reported cytotoxicity, an increase in ROS, and evidence of cell uptake of the NPs (Jugan et al., 2012; Armand et al., 2016).

Among the other MN studies in human cells, several included measurement of ROS, and they all showed an increase in this parameter. One study did not show a change in the glutathione-glutathione disulfide (GSH/GSSG) ratio, a marker of oxidative stress, but did not measure ROS (Valdiglesias et al., 2013). In general, the concentrations showing positive MN responses were in the range of 8 to 80 μg/mL, although one study showed a response at 0.8 μg/mL (Shukla et al., 2011), and one did not show a response at 100 μg/mL but did at 1000 μg/mL (Demir et al., 2015). Most of these MN studies involved TiO2 NPs of the anatase or ~80:20 anatase to rutile type. Information on the presence or absence of NP coating was rarely reported. One study compared results across experiments using three different culture media and reported that positive results for MN formation were observed only with the medium with the least extensive agglomeration of NPs (Prasad et al., 2013). One MN study conducted with primary cultures of human peripheral blood lymphocytes tested four types of TiO2 NPs, including coated and uncoated, anatase, rutile and a mixture of anatase/rutile, and a range of particle sizes. Results were positive for all samples except one that was uncoated, was a mix of anatase/rutile, and had particle dimensions of 200 x 30 nm (Tavares et al., 2014).

2.3 Comet Assay

Results of 22 *in vitro* comet assays have been published. Most of these were conducted under alkaline conditions which detect single strand breaks. Some studies also employed a modified

assay that detects oxidative DNA damage. One neutral comet assay measuring double strand breaks was also reported. Overall, the results were positive in 17 studies (16 alkaline comet assays and one neutral comet assay) and negative in five studies [four alkaline comet assays (Hackenberg et al., 2010; Hackenberg et al., 2011; Wang et al., 2011; Woodruff et al., 2012) and one modified assay for a specific type of oxidative DNA damage (Valdiglesias et al., 2013)].

In two of the negative alkaline comet assays there was no evidence of concomitant cytotoxicity although low to moderate uptake of NPs was reported (Hackenberg et al., 2010; Hackenberg et al., 2011). In two other negative studies, evidence of cytotoxicity (Woodruff et al., 2012) or cell uptake and increased ROS (Wang et al., 2011) was reported. One study reported negative results in a modified comet assay to detect oxidative DNA damage and positive results in the alkaline comet assay. No evidence of cytotoxicity was observed although cell uptake was reported (Valdiglesias et al., 2013). Several studies reporting positive responses in comet assays also measured ROS and all reported ROS increases (Shukla et al., 2011; Wang et al., 2011; Guichard et al., 2012; Kermanizadeh et al., 2012; Jugan et al., 2012; Saquib et al., 2012; Botelho et al., 2014; Ghosh et al., 2013; Shukla et al., 2013; Armand et al., 2016), but when other measures of oxidative stress (GSH, GSH/GSSG ratio, antioxidant enzyme activity, lipid peroxidation) were evaluated, they were affected in some cases (Shukla et al., 2011; Saquib et al., 2012; Botelho et al., 2014), but not in others (Kermanizadeh et al., 2012; Jugan et al., 2012; Valdilesias et al., 2013; Armand et al 2016). A positive response in one alkaline comet assay was concluded to be due to an assay-related artifact (Rajapakse et al., 2013).

Several of the *in vitro* comet studies included more than one type of TiO2 NP test material, allowing a direct comparison of results across samples with different characteristics (Guichard et al., 2012; Kermanizadeh et al., 2012; Jugan et al., 2012; Hamzeh and Sunahara 2013; Valdiglesias et al., 2013). In two of these studies, all TiO2 NP test material results were positive, despite differences in particle diameter, surface area, shape (spherical vs. elongated or rod) and form (anatase vs. rutile) (Guichard et al., 2012; Jugan et al., 2012). Valdiglesias et al. (2013) reported similar positive responses in two TiO2 NP test materials that, while having the same particle diameter (25 nm), were reported to have significantly different surface areas (35 to 45 m^2/g vs. 200 to 220 m^2/g) and different forms (anatase/rutile mixture vs. anatase).

Only two studies found notable differences between TiO2 NP test materials in the degree of DNA damage as indicated by comet results (Kermanizadeh et al., 2012; Hamzeh and Sunahara, 2013). Kermanizadeh et al. (2012) reported that DNA damage was most evident with two of the five TiO2 NP test materials. These two test materials were similar only in primary particle size (9 to 10 nm). They differed in mineral form (anatase vs. rutile), surface area (322 vs. 84 m^2/g), and coating/surface charge (uncoated vs. positively charged). Two other TiO2 NP test materials in this study showed less DNA damage at the same concentrations. They were both rutile form, but differed in particle size (10 vs. 100 nm). One was uncoated and had a surface area of 99 m^2/g; information on these particle characteristics was not provided for the other test material. The fifth test material did not produce a positive comet response. This test material was rutile form and differed from the most DNA-damaging rutile test material only in that it had a negatively charged surface. Hamzeh and Sunahara (2013) reported results for several TiO2 NP test materials and found that the comet response was greatest for a NP reported to be 5.9 nm in size with a surface area of 281 m^2/g, anatase in form, and appeared to be uncoated. One test

material showing no response in the comet assay was reported to be coated (coating not specified). Although its nominal size was 1 to 10 nm, in culture media it had a very broad size distribution and may have contained large aggregates that could slowly sediment. From these limited data, it appears that the determination of particle characteristics associated with a genotoxicity response is plagued by inconsistencies in findings, lack of complete reporting of particle characteristics, especially presence or absence of coating and surface area, and a paucity of studies where direct comparisons across NPs have been made.

2.4 Other DNA Damage Assays

Other less commonly used types of *in vitro* DNA damage assays such as the γ-H_2AX assay and the 53BP1 foci assay, which both measure double strand breaks, have given conflicting results, with negative findings in two γ-H_2AX assays (Jugan et al., 2012; Valdiglesias et al., 2013) and positive results in one 53BP1 foci assay (Armand et al., 2016). Two *in vitro* studies quantitating DNA adducts after treatment of either cells or calf thymus DNA with TiO2 NPs both reported an increased level of oxidized bases using HPLC-MS/MS or GC-MS/MS detection methods (Jugan et al., 2012; Petersen et al., 2014).

3 *In Vivo* Mutagenicity Studies

Sadiq et al. (2012) conducted a Pig-a assay in mice with a TiO2 NP test material and reported no increase in mutant frequency in either reticulocytes or red blood cells after IV injection of doses of up to 50 mg/kg bw/day for three days. Titanium was detected in the bone marrow using an assay that did not provide information on TiO2 presence or particle size, and a decrease in percent reticulocytes provided evidence of cytotoxicity. In a LacZ mutation assay in transgenic mice, Louro et al. (2014) observed no increase in mutant frequency in either liver or spleen of mice after IV injection of 10 or 15 mg/kg bw/day for two days, despite evidence of an inflammatory response in the liver at 15 mg/kg bw/day. In a wing spot test in *Drosophila melanogaster*, no evidence of somatic mutation was observed in larvae treated up to cytotoxic doses (Carmona et al., 2015). These three studies involved TiO2 NPs of anatase form with particle dimensions less than 25 nm. Negative results in these studies suggest a lack of *in vivo* mutagenicity for TiO2 NPs with these characteristics.

4 *In Vivo* Genotoxicity Studies

4.1 Micronucleus Formation

Results of ten *in vivo* MN assays conducted in bone marrow or peripheral blood reticulocytes with either rats or mice have been reported, and only one study (Grissa et al., 2015) showed an increase in MN formation. In this rat study, a test material consisting of spherical anatase NPs of 5 to 12 nm size showed an increase in MN formation in bone marrow after a single oral gavage dose of either 100 or 200 mg/kg bw/day. Three other oral gavage studies did not show a response in rats after treatment with up to 200 mg/kg bw/day for 30 days (Chen et al., 2014), up to 1000 mg/kg bw/day for seven days (Sycheva et al., 2011), or after a single dose of up to 2000 mg/kg bw (Donner et al., 2016). In one of these studies (Donner et al., 2016), no increase in blood Ti levels were observed indicating a lack of exposure to the bone marrow. In the study by

Chen et al. (2014) there was no evidence of cytotoxicity in the bone marrow. However, this study was positive for an increase in γ-H2AX foci, suggesting that TiO2 NPs did reach the bone marrow at a biologically effective dose and that γ-H2AX foci was a more sensitive endpoint for detecting a genotoxic effect than MN induction. Furthermore, while Sycheva et al. (2011) did not observe an increase in bone marrow MN following oral gavage dosing of TiO2 NPs, they did observe a positive response in bone marrow in the comet assay. This may have been due to a lower sensitivity for the MN assay or to the efficient completion of DNA repair before DNA damage was fixed into a clastogenic event.

Five *in vivo* MN studies involving a single IV injection or multiple injections of TiO2 NPs in mice all failed to show an increase in MN in either bone marrow or peripheral blood reticulocytes (Sadiq et al., 2012; Xu et al., 2013; Dobrynska et al., 2014; Louro et al., 2014; Suzuki et al., 2016). A lack of evidence of target tissue cytotoxicity indicating lack of adequate exposure even with IV administration may be the explanation for some of these negative studies (Dobrynska et al., 2014; Louro et al., 2014; Suzuki et al., 2016). However, one negative IV injection study in mice (Sadiq et al., 2012) did report a reduction in percent reticulocytes indicating treatment-related cytotoxicity. One study in mice exposed via inhalation also failed to show an increase in MN formation, and there was no evidence of cytotoxicity to the bone marrow (Lindberg et al., 2012). In one MN study, animals were sacrificed 14 days after the last exposure, which may explain the negative results (Xu et al., 2013). An analysis of the influence of TiO2 NP test material characteristics on the outcome of *in vivo* MN assays was not undertaken given the complexity introduced concerning adequacy of target tissue exposure and differences in dosing regimen.

4.2 Comet Assay

Results of nine *in vivo* comet assays in rats or mice have been reported which employed different routes of exposure (two oral gavage studies, four IV injection studies, two inhalation studies, and one IT study) and evaluated a variety of tissues. Two studies involving oral gavage reported evidence of DNA damage. Sycheva et al. (2011) observed DNA damage in the bone marrow and liver, but not in the brains of mice dosed by oral gavage with up to 200 mg/kg/day for seven days. Grissa et al. (2015) also reported DNA damage in peripheral blood leukocytes in rats dosed by oral gavage at 100 or 200 mg/kg/day for 60 days.

Meena et al. (2015) reported that in a comet study in rats injected IV with up to 50 mg/kg/day weekly for 30 days, DNA damage was observed in sperm cells. However, the other studies involving IV injection reported no evidence of DNA damage in the liver of mice that received up to 50 mg/kg bw once per week for four weeks (Suzuki et al., 2016), in the liver or spleen of mice dosed with up to 15 mg/kg/day for two days (Louro et al., 2014) or in bone marrow of mice given a single injection of 5 mg/kg bw (Dobrynska et al., 2014). Despite the failure to detect DNA damage in the liver as measured by percent tail DNA, one of these studies did show evidence of NP accumulation in the liver, mainly in Kupffer cells (Suzuki et al., 2016).

The three comet studies involving exposure by inhalation or IT followed by evaluation of lung tissue all showed negative results. Exposure was documented in each of these studies by evidence of lung toxicity (Landsiedel et al., 2010), dose-related deposition of Ti in the lung

(Lindberg et al., 2012), or histopathological evidence of lung infiltration by macrophages laden with NPs and/or neutrophils (Naya et al., 2012b).

An analysis of the influence of TiO2 NP test material characteristics on the outcome of *in vivo* comet assays was not undertaken given the complexity introduced by the varying routes and durations of exposure, and target tissues analyzed.

Table I-1 shows the studies described above.

Table I-1. Summary of Mutagenicity/Genotoxicity Data for Nano TiO2

Assay	Test system	Exposure	Particle Data[a]	Result	Comments	Reference
Mutation *In Vitro*						
Reverse mutation assay	*Salmonella typhimurium* strains TA100, TA98, TA102, and *E. coli* WP2 and WP2*uvrApKM101*	0, 0.000056, 0.00056, 0.0056, 0.056, 0.56, 5.6, or 56 µg/plate without S9 for 28 hrs	1. DeGussa AG W740x 2. NR 3. 20 nm 4. NR 5. NR 6. 8:2 ratio of anatase:rutile 7. NR 8. NR	Negative with and without FBS	Assay also conducted with TiO_2 + FBS. No enhanced association of NM with bacteria by FBS as assessed by flow cytometry	Butler et al., 2014
Reverse mutation assay	*Salmonella typhimurium* strains TA98, TA100, TA1535, TA1537, and TA102; pre-incubation assay	0, 38.4, 76.8, 153.6, 307.2, 614.4, 1228.8, 2457.6 or 4915.2 µg/plate without S9 for 48 hrs	1. synthesized at Nanotechnology Center, Univ. of Arkansas 2. NR 3. 10 x 30 nm 4. NR 5. slight ellipsoid 6. anatase 7. 130 to 170 nm in culture medium 8. NR	Negative	No NPs identified within bacterial cells as assessed by TEM. Highest concentration tested was near maximum recommended (5000 µg/plate)	Woodruff et al., 2012
Reverse mutation assay	*Salmonella typhimurium* strains TA98, TA100, TA102, TA1535, and TA1537; plate incorporation and pre-incubation assays	0, 20, 100, 500, 2500, or 5000 µg/plate with or without S9 for 48 hrs	1. BASF, T-Lite™ SF and T-Lite™ MAX 2. T-Lite™ SF: $Al(OH)_3$ and dimethicone/ methicone copolymer T-Lite™ MAX: dimethoxydiphenylsilane, triethoxycaprylylsilane crosspolymer, hydrated silica and $Al(OH)_3$ 3. 10 x 50 nm 4. 100 m^2/g 5. acicular 6. rutile 7. mean ~200 nm 8. $\geq$99%	Negative	Highest concentration tested was maximum recommended	Landsiedel et al., 2010

Assay	Test system	Exposure	Particle Data[a]	Result	Comments	Reference
Fluctuation test for reverse mutation	*Salmonella typhimurium* strains TA97a, TA98, TA100, and TA102	Conventional fluctuation test: 0, 0.875, 8.75, or 87.5 mg/L for 5 days. Modified fluctuation test: 0,0.025, 0.25, or 2.5 mg/L for 5 days	1. A) Evonik Degussa GmbH, AEROXIDE® P45 (TiO_2-P25); B) Nanostructural and Amorphous Materials, Inc., TiO_2-NA; C) CEREGE Laboratory, byproduct of accelerated aging of T-Lite™ SF (TiO_2-TLB) 2. TiO_2-P25 and TiO_2-NA: NR, TiO_2-TLB: most of PDMS layer removed and remaining Al in solid form at surface 3. TiO_2-P25: 23 nm, TiO_2-NA: 5.7 nm, TiO_2-TLB: NR 4. TiO_2-P25: 50 m^2/g, TiO_2-NA: 200 to 220 m^2/g, TiO_2-TLB: NR 5. NR 6. TiO_2-P25: 84:16 ratio of anatase:rutile; TiO_2-NA: 86:14 ratio of anatase:brookite; TiO_2-TLB: NR 7. Avg. hydrodynamic dia. TiO_2-P25: 800 nm (SS media) and 700 nm (AM media); TiO_2-NA: 67 nm (SS media) and 3800 nm (AM media); TiO_2-TLB: 730 nm (SS media) and 1300 nm (AM media) 8. TiO_2-NA: >99.5%	Conventional fluctuation test: Negative Modified fluctuation test: Increased number of revertants with TA102 at all concentrations for all 3 test materials; increased number of revertants with TA98 at highest concentration only for TiO2-P25 (all pre-incubation times) and TiO2-TLB (20 min pre-incubation)	Conventional fluctuation assay conducted in Ames media. Modified fluctuation assay conducted by including 0.1, 10, or 20 hr pre-exposure step in SS. Ames media-induced aggregation was reduced by SS pre-incubation	Jomini et al., 2012
HPRT assay	Chinese hamster lung fibroblasts (V79 cells)	0, 5, 20, or 100 μg/mL for 2 hrs without S9	1. Shanghai Aladdin Reagent Co. Ltd. 2. hydroxyl groups on surface 3. 75 nm 4. 64 m^2/g 5. nearly spherical 6. anatase 7. 473.6 nm and 486.8 nm in H_2O and DMEM 8. 99.9%	Positive: Significant dose-related increase in mutation frequency at 20 and 100 μg/mL	Data on cytotoxicity not reported	Chen et al., 2014

Assay	Test system	Exposure	Particle Data[a]	Result	Comments	Reference
HPRT assay	CHO-K1 cells	0, 10, 20, or 40 µg/mL for 1 day (24 hrs), 2 days (48 hrs), or for 60 days without S9	1. Same source as used in studies by the Finnish Inst. of Occup. Health 2. NR 3. <25 nm 4. NR 5. NR 6. anatase 7. aggregated in culture medium but size NR 8. 99.7%	Negative	TEM showed aggregates internalized by cells chronically exposed. Both acute and chronic exposures increased ROS. No cytotoxicity observed	Wang et al., 2011
Mutation *In Vivo*						
Pig-a assay	Male B6C3F1 mice Pig-a mutant frequency monitored in reticulocytes and total RBCs	0, 0.5, 5.0, or 50 mg/kg bw/day by IV injection for 3 days; Pig-a mutant frequency monitored in reticulocytes and total RBCs at 1, 2, 4, and 6 wks after last treatment	1. Synthesized at Nanotechnology Center, Univ. of Arkansas 2. slight ellipsoid 3. 12.1 minor axis, aspect ratio ~1.4 4. NR 5. NR 6. anatase 7. 130 to 70 nm in treatment solution 8. NR	Negative: No increase in mutant frequency in either reticulocytes or RBCs	Ti detected in bone marrow of animals sacrificed 4, 24, or 48 hrs after last IV injection. Treatment-related cytotoxicity based on reduction in % reticuloctyes	Sadiq et al., 2012
LacZ Mutation Assay	C57Bl/6 LacZ transgenic mice; mutant frequency measured in liver and spleen	0, 10 or 15 mg/kg bw/day for 2 days by IV injection; animals sacrificed 28 days after last injection	1. Provided by the Joint Research Center 2. none 3. 22 nm avg diameter 4. NR 5. spheroid 6. anatase 7. NR 8. NR	Negative: No increase in LacZ mutant frequency in either liver or spleen	Low inflammatory response in liver by histopathology at 15 mg/kg bw/day	Louro et al., 2014
Wing-Spot test	*Drosophila melanogaster*	0, 0.08, 0.40, 0.80, or 1.60 mg/mL; larvae were fed on medium at these concentrations for 48 hrs	1. Sigma-Aldrich 2. NR 3. <25 nm 4. 45 to 50 m^2/g 5. spherical 6. anastase 7. Average hydrodynamic dia in water 85.88 (12.9- to 85.6) nm 8. NR	Negative	Test measures somatic mutation and recombination activity. Evidence of cytotoxicity in larvae confirmed exposure	Carmona et al., 2015

Assay	Test system	Exposure	Particle Data[a]	Result	Comments	Reference
Clastogenicity *In Vitro*						
Chromosomal aberrations	Human peripheral blood lymphocytes	0, 6.25, 12.5, 25, 50, 100, 150, or 300 µg/mL for 24, 48, or 72 hrs without S9	1. Sigma Aldrich #637254 2. NR 3. <25 nm 4. 222 m^2/g 5. NR 6. anatase 7. agglomeration size not given 8. 99.7%	Increase in chromosomal aberrations only at 6.25 µg/mL after 24 hrs and at 100 and 300 µg/mL after 48 hrs. No dose response. No increase in chromosomal aberrations after 72 hrs	Response was greatest after 48 hrs exposure	Catalan et al., 2012
MN formation	Chinese hamster lung fibroblasts (V79 cells)	0, 75, 150, or 300 µg/mL for 4 hrs or 0, 18.8, 37.5, or 75 µg/mL for 24 hrs	See above entry for Landsiedel et al., 2010	Negative	Only T-Lite™ SF was tested. No cytotoxicity observed up to highest concentrations tested. Higher concentrations were not scorable due to precipitate	Landsiedel et al., 2010
MN formation	Human epidermal cell line (A431)	0, 0.008, 0.08, 0.8, 8, or 80 µg/mL for 6 hrs	1. Sigma Chemical Co. 2. NR 3. NR 4. NR 5. NR 6. anatase 7. avg hydrodynamic dia 124.9 nm in water, 171.4 nm in culture medium 8. 99.7%	Positive: Significant induction of MN formation at 0.8, 8, and 80 µg/mL	Mild cytotoxic response. Flow cytometry and TEM indicated cell uptake. ROS and oxidative stress were induced	Shukla et al., 2011
MN formation	A549 human lung carcinoma cell line	0, 10, or 50 µg/mL for 24 hrs	1. Sigma-Aldrich 2. none 3. 5 to 20 nm 4. 200 to 220 m^2/g 5. spherical 6. NR 7. avg hydrodynamic dia	Positive: Significant dose-related induction of MN formation.	Dimethylthiourea (DMTU) or N-acetylcysteine (NAC) exposure for 30 minutes prior	Srivastava et al., 2011

Assay	Test system	Exposure	Particle Data[a]	Result	Comments	Reference
			417.7 nm 8. 99.7%	Both DMTU and NAC reduced the response	to TiO2 was also studied. TiO2 increased ROS, and this response was reduced by both DMTU and NAC	
MN formation	A549 human lung carcinoma cell line (CCL-185)	0, 50, 100, or 200 µg/mL for 24 hrs	1. A) Degussa, AEROXIDE® P45 (TiO_2-A25); B) Sigma Aldrich, TIO_2-R68, and TIO_2-A140; C) Laboratoire Francis Perrin, TiO_2-A12 and TiO_2-R20 2. NR 3. TiO_2-A12: 12 nm, TiO_2-A25: 24 nm; TiO_2-A140: 142 nm, TiO_2-R68: 68 x 9 nm, TiO_2-R20: 21 nm 4. TiO_2-A12: 92 m^2/g, TiO_2-A25:46 m^2/g, TiO_2-A140: 10 m^2/g, TiO_2-R68: 118 m^2/g, TiO_2-R20: 73 m^2/g 5. TiO_2-A12, TiO_2-A25, TiO_2-A140, and TiO_2-R20: spherical; TiO_2-R68: elongated 6. TiO_2-A12: 95% anatase, TiO_2-A25: 86% anatase, TiO_2-A140: 100% anatase, TiO_2-R20: 100% rutile, TiO_2-R20: 90% rutile 7. NR 8. NR	Negative	Micrometric TiO_2 (TiO_2-A140, particle diameter 142 nm and SSA 10 m^2/g) was also studied. All TiO_2 NPs and TiO_2-A140 increased ROS; ROS remained elevated longer in TiO_2 NP-treated cells. TiO_2 NPs induced more pronounced cytotoxicity than TiO_2-A140. TEM evaluation showed TiO_2-A12, TiO_2-A25, and TiO_2-R20 in cytoplasm and nucleus (TiO_2-A12 only). No effect on GSH/GSSG	Jugan et al., 2012
MN formation	SHE cells	0, 5, 10 or 50 µg/cm^2 for 24 hrs	1. A) Sigma-Aldrich, TiO_2 A and TiO_2 R, B) Evonik- Degussa, TiO_2 P25 2. NR 3. TiO_2 A: 14 nm, TiO_2	Negative	TiO_2 A micro and TiO_2 R micro were also evaluated. Nanometric	Guichard et al., 2012

Assay	Test system	Exposure	Particle Data[a]	Result	Comments	Reference
			R: 62x10 nm, TiO_2 P25: 25 nm 4. TiO_2 A: 149 m^2/g, TiO_2 R: 177 m^2/g, TiO_2 P25: 58 m^2/g 5. TiO_2 A and TiO_2 P25: spherical, TiO_2 R: rod 6. TiO_2 A: anatase and nanopowder, TiO_2R: rutile and nanopowder, TiO_2 P25: 80:20 anatase: rutile 7. ~300 to 700 nm 8. TiO_2 A: >99.5% , TiO_2 R: impurities - 11% SiO_2, 1% NaO, 1% SO_4, TiO_2 P25: >99.5%		TiO_2 samples were all more cytotoxic than micrometric TiO_2. TEM showed that all TiO_2 nano- and microparticles penetrated cells. ROS were measured at 1, 5, or 10 µg/cm^2 for 72 hrs. ROS induction was greatest for anatase TiO_2 NPs. Micrometric TiO2 induced ROS only at the highest dose	
MN formation	BEAS-2B human bronchial epithelial cell line	0, 10, 20, 50, or 100 µg/mL for 24 hrs	1. Degussa, AEROXIDE P25 2. NR 3. 14.2 to 64.6 nm 4. 49 m^2/g 5. spherical 6. 86:14 anatase: rutile 7. concentration-dependent agglomeration in media; at 100 µg/mL, avg hydrodynamic dia 1580 nm in KB, 927 nm in DM, and 360 nm in KF 8. 95.1%	Positive: Significant dose- related increase in MN formation in KF media. No increase in DM or KB media.	Effect of media (KF, KB, and MN) on TiO2 agglomeration and impact on genotoxicity were evaluated. Effect of media on agglomera-tion was as follows: KF<DM<KB. No cytotoxicity reported at any concentration. Flow cytometry showed NP interaction with cells, confirmed by SEM	Prasad et al., 2013
MN formation	HEPG2 cells	0, 1, 10, 20, 40, or 80 µg/mL for 6 hrs	1. Sigma Chemical Co. 2. NR 3. 30 to 70 nm 4. NR 5. NR	Positive: Significant induction of MN at 10	No significant cytotoxicity after 6 hrs (time of MN assay), only	Shukla et al., 2013

Assay	Test system	Exposure	Particle Data[a]	Result	Comments	Reference
			6. anatase 7. avg hydrodynamic dia 124.9 nm in water, 192.5 nm in culture medium 8. 99.7%	µg/mL and above; response peaked at 20 µg/cm^2 and decreased at 40 and 80 µg/mL	after 24 and 48 hrs at 40 and 80 µg/mL. Cell uptake of NP (flow cytometry), confirmed by TEM showing NPs in cytoplasm TiO_2 NPs increased ROS and oxidative stress.	
MN formation	A549 human lung carcinoma cell line	0, 1, 10, or 50 µg/mL for 24 hrs	1. Sigma Chemical Co. 2. none 3. <25 nm 4. 200 to 220 m^2/g 5. NR 6. NR 7. avg hydrodynamic dia 34.1 nm 8. NR	Positive: Significant induction of MN at 10 and 50 µg/mL	Evidence of cytotoxicity at 10 µg/mL and above. TiO_2 NPs increased ROS and decreased GSH levels. TEM confirmed internalization of NPs	Srivastava et al., 2013
MN formation	Human neuroblastoma SHSY5Y cell line	0, 80, 120, or 150 µg/mL for 3 or 6 hrs	1. Degussa Evonik, TiO_2D; Sigma-Aldrich, TiO_2S 2. NR 3. 25 nm for both NMs 4. TiO_2D: 35 to 45 m^2/g, TiO_2S: 200 to 220 m^2/g 5. NR 6. TiO_2D:80:20 anatase:rutile, TiO_2S: anatase 7. NR 8. NR	Positive: Significant dose-related induction of MN at all doses after 6 hrs but not after 3 hrs of exposure for both NPs	No decrease in cell viability at any dose. Evidence of cellular uptake by flow cytometry. No effect on GSH/GSSG ratio	Valdiglesias et al., 2013
MN formation	Human peripheral blood lymphocytes	0, 5, 15, 45, 125, or 250 µg/mL for 6 hrs	1. Provided by the Joint Research Centre 2. NM-102: NM-103: dimethicone 2%, NM-104: glycerine, NM-105: none 3. NM-102: 20.8x33.0 nm NM-103: 21.9x37.9 nm NM-104: 19.0x25.8 nm, NM-105: 200x29.6	Positive: Significant induction of MN at 125 µg/mL for NM-102, at 5 and 45 µg/mL for NM-103, at 15 and 45 µg/mL for	Cytotoxicity data not reported	Tavares et al., 2014

Assay	Test system	Exposure	Particle Data[a]	Result	Comments	Reference
			nm 4. NM-102: 90 m^2/g, NM-103: 60 m^2/g, NM-104: 60 m^2/g, NM-105: 61 m^2/g 5. polyhedral 6. NM-102: anatase NM-103 and NM-104: rutile, NM-105: 15:85 rutile:anatase 7. median hydrodynamic dia NM-102: 54 nm, NM-103: 67 nm, NM-104: 60 nm, NM-105: 90 nm 8. NR	NM-104. No evidence of a dose-response. No evidence of MN induction in NM-105		
MN formation	Human embryonic kidney (HEK293) and mouse embryonic fibroblast (NIH/3T3) cell lines	0, 10, 100, or 1000 µg/mL for 48 hrs	1. Sigma Chemical Co. 2. NR 3. Two different sizes: 21.01 nm and 50.72 nm 4. NR 5. spherical 6. NR 7. avg hydrodynamic dia 22.94 nm 8. >99.5%	Positive: Significant induction of MN at 1000 µg/mL in both HEK293 and NIH/3T3 cells	Cytotoxicity was observed. Micrometric TiO_2 was also tested and was negative in the MN assay and showed no evidence of cytotoxicity	Demir et al., 2015
MN formation	A549 human lung carcinoma cell line	0, 1, 2.5, 5, 10, or 50 µg/mL for 24 hrs, 1 wk, 2 wks, 1 month, or 2 months	1. Joint Research Center, Ispra Italy – TiO_2 Aeroxide P25 See data for TiO_2 A25 cited in Jugan et al., 2012 entry above	Negative	Intracellular accumulation of NPs was observed. Increase in ROS, but no effect on GSH/GSSG or antioxidant enzyme activity	Armand et al., 2016

Assay	Test system	Exposure	Particle Data[a]	Result	Comments	Reference
Clastogenicity *In Vivo*						
MN formation	Bone marrow assay in CBAxB6 mice	0, 40, 200, or 1000 mg/kg/day for 7 days by oral gavage; animals sacrificed 24 hrs after last dose	1. Sensient Cosmetic Technologies 2. NR 3. 33.2 nm 4. NR 5. nearly spherical 6. anatase 7. NR 8. NR	Negative	Evidence of bone marrow toxicity not reported. Micrometric TiO_2 was also studied and an increase in MN frequency was seen at 1000 mg/kg	Sycheva et al., 2011
MN formation	Peripheral blood reticulocyte assay in male B6C3F1 mice	0, 0.5, 5.0, or 50 mg/kg bw/day by IV injection for 3 days; animals sacrificed on day 4	See above entry for Sadiq et al., 2012	Negative	Ti detected in bone marrow of animals sacrificed 4, 24, or 48 hrs after last IV injection. Treatment-related cytotoxicity based on reduction in % reticuloctyes	Sadiq et al., 2012
MN formation	Peripheral blood reticulocyte assay in male C57Bl/6J mice	0, 0.8, 7.2, or 28.5 mg/m^3 inhalation exposure for 4 hrs/day for 5 consecutive days; blood samples collected 48 hrs after last exposure	1. Sigma-Aldrich 2. NR 3. anatase: 41 nm, brookite: 7 nm 4. 61 m^2/g 5. NR 6. 74:26 anatase:brookite 7. 10 to 60 nm 8. 97%	Negative	No evidence of cytotoxicity in bone marrow as measure by % PCE	Lindberg et al., 2012
MN formation	Bone marrow assay in male and female ICR mice	0, 140, 300, 645, or 1387 mg/kg bw by single IV injection; animals sacrificed 14 days after	1. Hangzhou Wanjing Co. Ltd. 2. hydrophilic surface 3. 40 nm 4. NR 5. spherical 6. anatase 7. NR 8. 99.99%	Negative	Cytotoxicity to bone marrow not reported, but histopathology in brain, lung, spleen, liver, and kidneys	Xu et al., 2013

Assay	Test system	Exposure	Particle Data[a]	Result	Comments	Reference
		treatment			was reported.	
MN formation	Bone marrow assay in male Sprague-Dawley rats	0, 10, 50, or 200 mg/kg/day by oral gavage for 30 days; timing of animal sacrifice relative to last dose not specified	See above entry for Chen et al., 2014	Negative	No evidence of cytotoxicity as measured by PCE/NCE ratio	Chen et al., 2014
MN formation	Bone marrow assay in male Wistar rats	0 or 5 mg/kg bw by single IV injection; animals sacrificed 24 hrs, 1 wk, or 4 wks after dosing	1. Evonik Aeroxide TiO_2 P25 2. NR 3. 21 nm 4. NR 5. NR 6. anatase/rutile 7. maximum reported hydrodynamic dia 129 nm 8. NR	Negative	No evidence of bone marrow cytotoxicity based on % PCE	Dobrynska et al., 2014
MN formation	Peripheral blood reticulocyte assay in C57Bl/6 LacZ transgenic mice	0, 10, or 15 mg/kg bw/day for 2 days by IV injection; animals sacrificed 42 hrs after last dose	See above entry for Louro et al., 2014	Negative	No evidence of cytotoxicity as measured by % reticulocytes	Louro et al., 2014
MN formation	Bone marrow assay in male Wistar rats	0, 50, 100, or 200 mg/kg/day by oral gavage for 60 days; animals sacrificed 24 hrs after the last dose	1. AZ Tech 2. NR 3. 5 to 12 nm 4. NR 5. nearly spherical 6. anatase 7. NR 8. NR	Positive: Significant dose-related increase in MN at 100 and 200 mg/kg	Evidence of bone marrow cytotoxicity as measured by PCE/NCE ratio	Grissa et al., 2015
MN formation	Peripheral blood reticulocyte assay in male and female Sprague Dawley	0, 500, 1000, or 2000 mg/kg bw single oral gavage	1. NR 2. coating mentioned only for pg-3 but not identified 3. uf-1: 23 nm, uf-2: 19	Negative	No significant increase in blood TiO_2 indicating lack of bone	Donner et al., 2016

Assay	Test system	Exposure	Particle Data[a]	Result	Comments	Reference
	rats	dose; animals sacrificed 48 or 72 hrs after dosing	nm, uf-3: 22 nm, pg-1:120 nm, pg-2: 165 nm, pg-3:132 nm 4. uf-1: 50.4 m^2/g, uf-2: 82 m^2/g, uf-3: 58.8 m^2/g, pg-1: 8.1 m^2/g, pg-2: 7.1 m^2/g, pg-3:17.1 m^2/g 5. uf-1 and uf-2: irregular, uf-3: rod-like, pg-1, pg-2, pg-3: irregular 6. uf-1: 83.5:16.5 anatase:rutile, uf-2: anatase, uf-3: rutile, pg-1: anatase, pg-2: rutile, pg-3: rutile 7. hydrodynamic dia uf-1: 43 nm, uf-2: 42 nm, uf-3: 47 nm, pg-1: 153 nm, pg-2: 195 nm, pg-3: 213 nm 8. NR		marrow exposure	
MN formation	Peripheral blood reticulocyte assay in male C57BL/6J*gpt* Delta transgenic mice	0, 2, 10, or 50 mg/kg bw by IV injection once per week for 4 weeks; peripheral blood collected 2 days and 9 days after final injection	1. Sigma-Aldrich, Aeroxide® P25 (TiO_2-P25) 2. NR 3. 21 nm 4. 50 m^2/g 5. NR 6. 80:20 anatase:rutile 7. NR 8. NR	Negative	Percent reticulocytes in high dose group significantly higher than controls. Unclear whether this was a treatment-related effect	Suzuki et al., 2016
DNA Damage *In Vitro*						
Comet assay	Primary cultures of human nasal epithelial cells	0, 10, 25, 50, or 100 µg/mL for 24 hrs	1. Sigma-Aldrich 2. NR 3. 15 to 30 nm 4. NR 5. spherical 6. anatase 7. mean aggregate size 285 nm 8. NR	Negative: No increase in tail DNA, tail length, or Olive tail moment	NP observed in cytoplasm in 11% of cells and in nucleus in 4% of cells. No evidence of cytotoxicity	Hackenberg et al., 2010

Assay	Test system	Exposure	Particle Data[a]	Result	Comments	Reference
Comet assay	Human peripheral blood lymphocytes	0, 0.25, 0.5, 0.75, 1, 1.25, 1.50, or 1.75 mM for 3 hrs	See above entry for Ghosh et al., 2010	Positive: Significant increase in % tail DNA only at 0.25 mM	Cytotoxicity was observed with TiO_2 NPs. Study also evaluated bulk TiO_2. The latter showed a dose-related increase in % tail DNA at doses above 1 mM	Ghosh et al., 2010
Comet assay	Human peripheral blood lymphocytes	0, 20, 50, 100, or 200 µg/mL for 24 hrs	1. Sigma-Aldrich 2. NR 3. 15 to 30 nm 4. NR 5. spherical 6. anatase 7. mean aggregate size 285 nm	Negative: No increase in tail DNA, tail length, or Olive tail moment	No significant cytotoxicity observed. Only 5% of cells showed intracellular NPs by TEM	Hackenberg et al., 2011
Comet assay	Human epidermal cell line (A431)	0, 0.008, 0.08, 0.8, 8, or 80 µg/mL for 6 hrs	See above entry for Shukla et al., 2011	Positive: significant increase in Olive tail moment and % tail DNA with and without Fpg treatment at 0.8, 8, and 80 µg/mL	Fpg-modified Comet assay also used to detect oxidative DNA base damage. Mild cytotoxic response to NPs. Flow cytometry and TEM indicated cell uptake. ROS, GSH and lipid peroxidation were increased	Shukla et al., 2011
Comet assay	CHO-K1 cells	0, 10, 20, or 40 µg/mL for 1 day (24 hrs), 2 days (48 hrs), or 60 days without S9	See above entry for Wang et al., 2011	Negative: No increase in tail length	See comments above for Wang et al., 2011	Wang et al., 2011
Comet assay	SHE cells	0, 10, 25, or 50 µg/mL for 24 hrs	See above entry for Guichard et al., 2012	Positive: Significant increase in % tail DNA at 50 µg/mL for nano	See comments above for Guichard et al., 2012	Guichard et al., 2012

Assay	Test system	Exposure	Particle Data[a]	Result	Comments	Reference
				TiO_2 A and TiO_2 P25 but not nano TiO_2 R;.Significant increase in % tail DNA also for micro TiO_2 A (response similar to nano) and for micro TiO_2 R		
Comet assay	Human hepatoblastoma C3A cell line	0, 5, 10, or 20 μg/mL for 4 hrs	1. Joint Research Centre, NM101; NanoAmor, NRCWE101; NaBond, NRCWE104; NRCWE102 and NRCWE103 produced from NRCWE101 2. NM101: none NRCWE101: none NRCWE102: positive charge, NRCWE103: negative charge, NRCWE104: NR 3. NM101: 9 nm NRCWE101: 10 nm NRCWE102: 10 nm NRCWE103: 10 nm NRCWE104: ~100 nm 4. NM101: 322 m^2/g NRCWE101: 99 m^2/g NRCWE102: 84 m^2/g NRCWE103: 84 m^2/g NRCWE104: NR 5. NM101: 2 structure types reported, shape not specified; NRCWE101, RCWE102 and NRCWE103: irregular euhedral, NRCWE104: mixture of five different shapes 6. NM101: anatase;	Positive: Significant increase in % tail DNA most evident for NM 101, and NRCWE 102 without fpg, which was further increased with fpg. No increase for NRCWE103	Fpg-modified Comet assay also used to detect oxidative DNA base damage. Evidence of oxidative DNA damage in the fpg modified assay. No effect on total glutathione or GSH. Dose-related increase in ROS for all TiO_2 NPs. Pre-treatment with a vitamin E derivative antioxidant inhibited the ROS response	Kermanizadeh et al., 2012

Assay	Test system	Exposure	Particle Data[a]	Result	Comments	Reference
			NRCWE101, RCWE102, NRCWE103, and NRCWE104: rutile 7. Size in culture medium NM101: 185, 742 nm NRCWE101: 203 nm NRCWE102: 287 nm NRCWE103: 240, 1487 nm, NRCWE104: 339 nm 8. NR			
Comet assay	A549 human lung carcinoma cell line (CCL-185)	0 or 100 µg/mL for 4, 24, or 48 hrs	See above entry for Jugan et al., 2012	Positive: Significant increase in % tail DNA during first 24 hrs of treatment observed with strongest responses mostly for spherical NPs with diameter <68 nm (TiO2-A12, –A25, and –R20)	See comments above for Jugan et al., 2012	Jugan et al., 2012
Neutral Comet assay	Human amnion epithelial (WISH) cells	0, 0.625, 1.25, 2.5, 5, 10, or 20 µg/mL for 6 hrs	1. Synthesized from bulk TiO_2 2. NR 3. 13 nm 4. NR 5. crystallites with polyhedral morphology 6. rutile 7. 152 nm in media 8. NR	Positive: Significant increase in Olive tail moment, tail length and % tail DNA at 20 µg/mL	Neutral Comet assay measures DNA double strand breaks. Dose-related cytotoxicity observed. Increase in ROS and decrease in catalase activity and.GSH	Saquib et al., 2012
Comet assay	TK6 human lymphoblastoid cells	0, 50, 100, 150, or 200 µg/mL for	See above entry for Woodruff et al., 2012	Negative: No increase in % tail	Endonuclease III and 8-hydroxy-guanine DNA-	Woodruff et al., 2012

Assay	Test system	Exposure	Particle Data[a]	Result	Comments	Reference
		24 hrs		DNA in any of the Comet assays	glycosylase modified Comet assays also used. Cell uptake of NPs seen by TEM. No evidence of oxidative damage in modified assays. Evidence of cytotoxicity was reported	
Comet assay	*Tetrahymena thermophila* in suspension (i.e., "*in vivo"*) or embedded in gel (i.e.,"*in vitro"*) with either alkaline lysis (single strand breaks) or neutral lysis (double strand breaks), or embedded nuclei (i.e., "acellular") with alkaline lysis	0, 0.1, or 100 µg/mL for 4 hrs	1. Sigma-Aldrich 2. NR 3. 15 nm 4. 190 to 290 m^2/g 5. elongated spheroid 6. anatase 7. hydrodynamic radius 820 nm 8. 99.7%	Positive: Significant increase in % tail DNA for alkaline lysis at all concentrations for *in vivo*, *in vitro*, and acellular assays except acellular assay at 100 µg/mL. Negative for neutral lysis assay (no double strand breaks)	*Tetrahymena thermophila* is a unicellular eukaryotic organism. Bulk TiO_2 was also tested and was positive in alkaline assay. Comet results for both NP and bulk TiO2 were independent of effects on ROS. Authors conclude results are an artifact of *post festum* interactions of TiO2 with DNA	Rajapakse et al., 2013
Comet assay	AGS (gastric epithelial cancer) cells	0 or 150 µg/mL for 3 hrs	1. Degussa Corp., Aeroxide TiO_2 P25; Sigma-Aldrich, TiO_2 637254 2. NR 3. TiO_2 P25: 21 nm; Sigma-Aldrich TiO_2: <25 nm 4. NR 5. NR 6. TiO_2 P25 80:20 anatase:rutile Sigma	Positive: Significant increase in % tail DNA. Results for the two types of NPs not reported separately	TiO_2 NP induced in-crease in ROS and GSSG. TiO_2 NP in-duced increase in cell proliferation and decrease in apoptosis was referred to as "tumor-like	Botelho et al., 2014

Assay	Test system	Exposure	Particle Data[a]	Result	Comments	Reference
			TiO_2: anatase 7. TiO_2 P25: avg hydrodynamic dia 160.5 nm Sigma TiO_2: 420.7 nm 8. NR		phenotypes" by authors	
Comet assay	Human peripheral lymphocytes	0, 25, 50, or 100 μg/mL for 3 hrs	1. Sigma-Aldrich 2. NR 3. 50.93 nm 4. NR 5. spherical 6. anatase/rutile, ratio not given 7. avg hydrodynamic dia ~6000 nm 8. NR	Positive: Significant increase in % tail DNA at 25 μg/mL but not at 50 or 100 μg/mL	Significant cytotoxicity. Significant increase in ROS	Ghosh et al., 2013
Comet assay	Chinese hamster lung fibroblasts (V79 cells)	0, 10, or 100 mg/L for 25 hrs	1. MTI Corporation, MT15; Evonik Industries, P25; Sigma-Aldrich, nanofilament rutile; Vive Nano Inc., Vive Nano Titania (-) 2. Vive Nano Titania coated (coating not specified) 3. MT15: 5.9 nm, P25: 34.1 nm, Nanofilament: 10 x 40 nm, Vive Nano Titania: 1 to 10 nm 4. MT15: 280.9 m^2/g P25: 48.9 m^2/g Nanofilament: 107.4 m^2/g Vive Nano Titania: NR 5. NR 6. MT15: anatase, P25: 83:17 anatase:rutile, Nanofilament: rutile, Vive Nano Titania:NR 7. MT15: 460 nm, P25: 400 nm, Nanofilament: 420 nm, Vive Nano Titania: 600 nm 8. 99.5%	Positive: Significant increase in Olive tail moment and % tail DNA at 100 mg/L. Response greatest in MT15	All NPs tested induced cytotoxicity, but the polyacrylate-coated NP was cytotoxic only at higher concentrations	Hamzeh and Sunahara, 2013
Comet assay	BEAS-2B human bronchial	0, 10, 20, 50, or 100 μg/mL for	See above entry for Prasad et al., 2013	Positive: Small but	See comments above for Prasad et al.,	Prasad et al., 2013

Assay	Test system	Exposure	Particle Data[a]	Result	Comments	Reference
	epithelial cell line	24 hrs		statistically significant dose- related increase in % tail DNA	2013	
Comet assay	HEPG2 cells	0, 1, 10, 20, 40, or 80 µg/mL for 6 hrs	See above entry for Shukla et al., 2013	Positive: Significant dose-related increase in % tail DNA (20 µg/mL and above) and Olive tail moment (10 µg/mL and above); response greater in fpg-modified assay indicating significant oxidative DNA damage	Fpg-modified Comet assay was used for detection of oxidative DNA base damage. See comments above for Shukla et al., 2013	Shukla et al., 2013
Comet assay	Human neuroblastoma SHSY5Y cell line	0, 80, 120, or 150 µg/mL for 3 or 6 hrs	See above entry for Valdiglesias et al., 2013	Positive: Significant increase in % tail DNA after both 3 and 6 hrs with NP prepared from Sigma TiO_2; significant dose-related increase in % tail DNA only after 6 hrs with NP prepared from Degussa TiO_2	See above comments for Valdiglesias et al., 2013	Valdiglesias et al., 2013

Assay	Test system	Exposure	Particle Data[a]	Result	Comments	Reference
Comet assay	Chinese hamster lung fibroblasts (V79 cells)	0, 5, 20, or 100 µg/mL for 6 and 24 hrs without S9	See above entry for Chen et al., 2014	Positive: Significant increase in % tail DNA but not Olive tail moment at 100 µg/mL after 24 hrs	Dose-related cytotoxicity observed at both 6 and 24 hrs	Chen et al., 2014
Comet assay	Skin fibroblasts and leukocytes from bottlenose dolphin, murine fibroblasts (3T3 cells), human skin fibroblasts, and human leukocytes	0, 20, 50, or 100 µg/mL for 4, 24, and 48 hrs	1. Sigma-Aldrich 2. none 3. 20 to 50 nm 4. 101.0 m^2/g 5. elongated 6. anatase 7. NR 8. 99.7% Rutile micrometric TiO_2 (1-5 µm) was also studied	Positive for nano-anataseTiO_2: Increase in % tail DNA in human skin fibroblasts only at 4 hrs; negative in dolphin and mouse fibroblasts. Negative in dolphin and human lymphocytes . Micro-rutile TiO_2: Increase in % tail DNA in 3T3 cells and dolphin leukocytes	Anatase nanometric TiO_2 was compared with rutile micrometric TiO_2. TiO_2 (both forms) reported as only slightly cytotoxic	Frenzelli et al., 2014
Comet assay	Human embryonic kidney (HEK293) and mouse embryonic fibroblast (NIH/3T3) cell lines	0, 10, 100, or 1000 µg/mL for 1 hr	See above entry for Demir et al., 2015	Positive: Significant increase in % tail DNA at 1000 µg /mL in both HEK293 and NIH/3T3 cells. No evidence of	Micrometric TiO2 was also tested, showed no evidence of genotoxicity in the same dose range	Demir et al., 2015

Assay	Test system	Exposure	Particle Data[a]	Result	Comments	Reference
				oxidative DNA damage in FPG-modified Comet assay		
Comet assay	A549 human lung carcinoma cell line	0, 1, 2.5, 5, 10, or 50 µg/mL for 24 hrs, 1 wk, 2 wks, 1 month, or 2 months	See above entry for Armand et al., 2016	Positive: Increase in % tail DNA at 10 µg/mL after 1 or 2 months and at 50 µg/mL regardless of exposure time; in Fpg-modified assay increases in % tail DNA at all doses and clear exposure time/dose response	Fpg-modified Comet assay for oxidative DNA base damage was also used. See above comments for Armand et al., 2016	Armand et al., 2016
OGG1-modified Comet assay	Human neuroblastoma SHSY5Y cell line	0, 80, 120, or 150 µg/mL for 3 or 6 hrs	See above entry for Valdiglesias et al., 2013	Negative	OGG1-modified Comet assay evaluates oxidative DNA damage, specifically the presence of 8-oxoguanine. See above comments for Valdiglesias et al., 2013	Valdiglesias et al., 2013
γ-H_2AX assay for double-stranded breaks	A549 human lung carcinoma cell line (CCL-185)	0, 50, 100, or 200 µg/mL for 24 hrs	See above entry for Jugan et al., 2012	Negative	See above comments for Jugan et al., 2012	Jugan et al., 2012
γ-H_2AX assay for double-stranded	Human neuroblastoma SHSY5Y cell	0, 80, 120, or 150 µg/mL for 3	See above entry for Valdiglesias et al., 2013	Negative	See above comments for Valdiglesias et	Valdiglesias et al., 2013

Assay	Test system	Exposure	Particle Data[a]	Result	Comments	Reference
breaks	line	or 6 hrs			al., 2013	
53BP1 foci assay for double-stranded breaks	A549 human lung carcinoma cell line	0, 1, 2.5, 5, 10, or 50 µg/mL for 24 hrs, 1 wk, 2 wks, 1 month, or 2 months	See above entry for Armand et al., 2016	Positive: Increase in nuclear 53BP1 foci at 2.5 and 5 µg/mL (1 month exposure) and at 10 and 50 µg/mL (2 month exposure)	See above comments for Armand et al., 2016	Armand et al., 2016
DNA Damage *In Vivo*						
Comet assay	Male Wistar Crl:WI Han rats Tissues evaluated: lung – alveolar lavage cells	0 or 10 mg/m^3 dust aerosol nose only inhalation exposure, 6 hrs per day for five consecutive days; animals sacrificed 23 days after last exposure	1. BASF, T-Lite™ SF and T-Lite™ MAX 2. T-Lite™ SF, aluminium hydroxide and dimethicone/ methicone co-polymer; T-Lite™ MAX, dimethoxydi-phenylsilane, triethoxycaprylsilane cross-polmer, hydrated silica and aluminium hydroxide 3. 10 x 50 m 4. 100 m^2/g 5. acicular-shaped 6. rutile 7. mean agglomerates ~200 nm (range 90 to 460 nm) 8. ≤99%	Negative: No significant changes in tail intensity, tail length, or tail moment	The Comet assay was performed on recovery animals. Evidence of lung toxicity was partly reversible within the 23 day recovery time	Landsiedel et al., 2010
Comet assay	Male CBAxB6 mice Tissues evaluated: Bone marrow, brain, and liver	0, 40 or 200 mg/kg /day for 7 days by oral gavage; animals sacrificed 24 hrs after last dose	See above entry for Sycheva et al., 2011	Positive: Significant increases in % tail DNA in bone marrow (40 and 200 mg/kg/day) and liver (200	Toxicity not evaluated in these organs	Sycheva et al., 2011

Assay	Test system	Exposure	Particle Data[a]	Result	Comments	Reference
				mg/kg/day)		
Comet assay	Male C57Bl/6J mice Tissues evaluated: Lung (alveolar type II cells and Clara cells)	0, 0.8, 7.2, or 28.5 mg/m^3 inhalation exposure for 4 hrs per day for 5 consecutive days; animals sacrificed immediately after last exposure	See above entry for Lindberg et al., 2012	Negative: No increase in % tail DNA in alveolar type II or Clara cells	Dose- related deposition of Ti in lung	Lindberg et al., 2012
Comet assay	Male Sprague Dawley rats Tissues evaluated: Lung	0, 1, or 5 mg/kg bw (single dose) or 0, 0.2, or 1 mg/kg bw (repeat dose once weekly for 5 wks) by IT; animals sacrificed 3 or 24 hrs post-instillation (single dose) or 3 hrs after the last dose (repeat dose)	1. Ishihara Sangyo Kaisha, Ltd. 2. none 3. 5 nm primary dia; 10 nm secondary dia 4. 316 m^2/g 5. elongated 6. anatase 7. NR 8. 99.99%	Negative	Histopathology of the lung revealed infil-tration of alveolar macrophages laden with NPs and/or neutrophils	Naya et al., 2012b
Comet assay	Male Wistar rats Tissues evaluated: Bone marrow	0 or 5 mg/kg bw by single IV injection; animals sacrificed 24 hrs, 1 wk, and 4 wks after dosing	1. Evonik Aeroxide TiO_2 P25 2. NR 3. 21 nm 4. NR 5. NR 6. anatase/rutile 7. maximum reported hydrodynamic dia 129 nm 8. NR	Negative: No increase in % tail DNA or tail moment	No evidence of bone marrow cytotoxicity based on % PCE	Dobrynska et al., 2014
Comet assay	C57Bl/6 LacZ transgenic mice Tissues	0, 10, or 15 mg/kg bw/day for 2 days by IV injection;	See above entry for Louro et al., 2014	Negative: No increase in % tail DNA or		Louro et al., 2014

Assay	Test system	Exposure	Particle Data[a]	Result	Comments	Reference
	evaluated: Liver and spleen	animals sacrificed 28 days after last dose		Olive tail moment in liver or spleen		
Comet assay	Male Wistar rats Tissues evaluated: Sperm cells	0, 5, 25, or 50 mg/kg weekly for 30 days by IV injection	1. Sigma-Aldrich 2. NR 3. 10 to 20 nm 4. NR 5. Spherical 6. NR 7. NR 8. NR	Positive: Significant increases in tail length, tail movement, and tail migration at 25 and 50 mg/kg/week	Dose-related increase in Ti in the testis. Dose-related decrease in antioxidative enzyme activity	Meena et al., 2015
Comet assay	Male Wistar rats Tissues evaluated: Peripheral blood leukocytes	0, 50, 100, or 200 mg/kg/day by oral gavage for 60 days; animals sacrificed 24 hrs after the last dose	See above entry for Grissa et al., 2015	Positive: Significant increase in tail moment at 100 and 200 mg/kg bw	See above comments for Grissa et al., 2015	Grissa et al., 2015
Comet assay	*Drosophila melanogaster* Tissues evaluated: Hemocytes (blood cells)	0, 0.08, 0.40, 0.80, or 1.60 mg/mL; larvae were fed on medium at these concentrations for 24 hrs	See above entry for Carmona et al., 2015	Positive: Significant dose-related increase in % tail DNA at 0.40 mg/mL and above	Evidence of cytotoxicity in larvae confirmed exposure	Carmona et al., 2015
Comet assay	Male C57BL/6J*gpt* Delta transgenic mice Tissues evaluated: Liver	0, 2, 10, or 50 mg/kg bw by IV injection once a week for 4 consecutive weeks; animals sacrificed 3 days after final	See above entry for Suzuki et al., 2016	Negative: No increase in tail intensity (% TI)	TEM showed evidence of accumulation of TiO2 NPs in the liver, mainly in Kupffer cells	Suzuki et al., 2016

Assay	Test system	Exposure	Particle Data[a]	Result	Comments	Reference
		injection				
Poly-organ karyological assay	CBAxB6 mice Tissues evaluated: Forestomach epithelial cells, colon epithelial cells, spermatids	0, 200, or 1000 mg/kg/day for 7 days by oral gavage; animals sacrificed 24 hrs after last dose	See above entry for Sycheva et al., 2011	Negative	Genotoxicity endpoints included MN, nuclear protrusions, and atypical nuclei. Cytotoxic effects reported included in-creased mitotic index in fore-stomach and colon epithelia, increased apoptotic index in testis	Sycheva et al., 2011
γ-H_2AX assay for double-stranded breaks	Bone marrow assay in male Sprague-Dawley rats	0, 10, 50, or 200 mg kg/day by oral gavage for 30 days	See above entry for Chen et al., 2014	Positive: Significant increase in γ-H_2AX positive cells at 50 and 100 mg/kg/day	See comments above for Chen et al., 2014	Chen et al., 2014
DNA Adducts *In Vitro*						
Quantitation of 8-oxodGuo and other oxidized bases by HPLC-MS/MS	A549 human lung carcinoma cell line (CCL-185)	0 or 100 µg/mL for 4, 24, or 48 hrs	See above entry for Jugan et al., 2012	Positive: Increased level of 8-oxo-dGuo at 4, 24, and 48 hrs for TiO_2-A12 and –A25, at 24 and 48 hrs for TiO_2-R68, and at 48 hrs for TiO_2 R20.	See comments above for Jugan et al., 2012	Jugan et al., 2012
Quantitation of five different oxidized bases by	Calf thymus DNA	0, 0.5, 5, or 50 mg/mL in the dark for 3 or 24 hrs, using	1. Evonik Degussa GmbH, AEROXIDE TiO_2 P25 2. NR 3. ~25 inferred from	Positive: Ambient light conditions:	Oxidative DNA damage observed only with photoactivation	Petersen et al., 2014

Assay	Test system	Exposure	Particle Data[a]	Result	Comments	Reference
stable isotope-dilution GC-MS/MS		ambient light for 24 hrs, or using UVA irradiation for 30 min	product name 4. 55.55 m^2/g 5. NR 6. 76:24 anatase: rutile 7. mean particle size ranged from 59.8 to 83.0 nm	significant increase in all five oxidized bases at 50 mg/mL; and also in 8-OH-Guanine at 5 mg/mL UVA irradiation: Significant increase in all five oxidized bases at 5 and 50 mg/mL	. Potential for assay artifacts from laboratory light	
Cell Transformation						
Soft-agar colony assay	Human embryonic kidney (HEK293) and mouse embryonic fibroblast (NIH/3T3) cell lines	0, 10, 100, or 1000 µg/mL for 3 weeks	See entry above for Demir et al., 2015	Positive: Significant increase in anchorage-independent colonies at 1000 µg /mL in both HEK293 and NIH/3T3 cells		Demir et al., 2015

[a]Particle data are itemized as follows: 1. Source 2. Coating 3. Primary particle size 4. Surface area 5. Shape/morphology 6. Mineral form 7. Aggregation 8. Purity

CHO = Chinese hamster ovary; FBS = fetal bovine serum; GSH = reduced glutathione; GSSG = oxidized glutathione; MN = micronucleus; NCE = normochromic erythrocytes; NM= nanomaterial; NP= nanoparticle; NR = Not reported; OGG1 = 8-oxoguanine DNA glycosylase; PDMS = polydimethyl siloxane; PCE = polychromic erythrocytes; RBC = red blood cell; ROS = reactive oxygen species; SEM = scanning electron microscopy; SHE = Syrian hamster embryo; SS = saline solution; TEM = transmission electron microscopy